Reliability-Based Fatigue Assessment of Mast-Arm Sign Support Structures

Joseph A. Diekfuss
Marquette University

RELIABILITY-BASED FATIGUE ASSESSMENT OF MAST-ARM SIGN SUPPORT STRUCTURES

by

Joseph A. Diekfuss, B.S., M.S.

A Dissertation submitted to the Faculty of the Graduate School,
Marquette University,
in Partial Fulfillment of the Requirements for
the Degree of Doctor of Philosophy

Milwaukee, Wisconsin

May 2013

ABSTRACT

RELIABILITY-BASED FATIGUE ASSESSMENT OF
MAST-ARM SIGN SUPPORT STRUCTURES

Joseph A. Diekfuss, B.S., M.S.

Marquette University, 2013

Over the past few decades, there have been issues of poor fatigue performance (the main failure mechanism) of the welded, tube-to-transverse plate connections within sign support structures. Review of the literature has indicated that a considerable amount of research has been devoted to identifying the structural response characteristics of these signs. Others have tried to identify how these connections may be repaired, retrofitted or simply better designed to sustain longer fatigue lives. However, little attention has been given to using a systematic reliability-based approach to assess the risk of fatigue-induced fracture in these structures.

Using a reliability-based approach to solve structural engineering problems requires a fundamental knowledge of the uncertainty associated with three variables: resistance, demand and modeling error. The present research effort has focused on systematically quantifying this uncertainty. The procedure utilizes statistical parameters determined from probability frequency distributions generated for each of the three variables. Resistance is defined by the fatigue life of the connection, demand is defined by the wind loading (buffeting-type only) and modeling error is evaluated using high-fidelity finite element analysis (FEA) with comparison to measured data from a field monitoring system.

This research effort develops a reliability-based approach for prescribing inspection intervals corresponding to user-specified levels of fatigue-induced fracture risk. The resulting level of risk for a particular structure is dependent upon its geographical location, the type of connection it contains, the orientation of its mast-arm relative to north and the number of years it has been in service. The results of this research effort indicate that implementation of state-of-the-art reliability-based assessment procedures can contribute very valuable procedures for assigning inspection protocols (*i.e.* inspection intervals) that are based upon probabilities of finding fatigue-induced cracking in these structures. The engineering community can use the results of this research effort to establish inspection intervals based upon risk and thereby better align inspection needs with limited fiscal and human resources.

ACKNOWLEDGMENTS

Joseph A. Diekfuss, B.S., M.S.

This dissertation is the culmination of many years of dedication, determination and hard work. There are many individuals who have guided and encouraged me along the way. I would like to recognize those who have been truly instrumental in the successful completion of this work.

First of all, I would like to thank the Wisconsin Highway Research Program, Federal Highway Administration and the Marquette University Department of Civil, Construction and Environmental Engineering for the financial support throughout my graduate career. I would also like to thank all of the individuals from these groups for their invaluable expertise and input on the project.

I would like to extend a special thank you to Dr. Christopher Foley. I am very proud to call Dr. Foley my mentor, fellow researcher and friend. Dr. Foley's capacity of patience while sharing his knowledge, enthusiasm and guidance is truly remarkable and inspirational – thank you.

I would like to thank Dr. Raymond Fournelle, Dr. Stephen Heinrich, Dr. Saeed Karshenas and Dr. Baolin Wan for reading this dissertation, sharing their expertise and providing invaluable input along the way. I also want to thank David Newman, Thomas Silman and Anthony Senger for their contributions to the experimental portions of this work.

I want to thank both my family and my wife's family for their support and encouragement throughout this effort. I want to especially thank my parents, John and Margaret Diekfuss and my wife's parents, Gregory and Susan Kummer. Mom and Dad, your example of principled values, hard work and dedication was my inspiration and source of continual

motivation whenever I felt discouraged – I can never repay you for what you have done for me, I only hope I can live up to your example. Greg and Sue, you have always treated me like your own son and have given me constant encouragement and support throughout this effort – thank you.

To my best friend, Becky, I cannot put into words how much I appreciate your love, loyalty and sacrifice. You have been the epicenter of support and encouragement throughout this work. I am so proud to be your husband – thank you.

Lastly and not so easily conveyed through words, I want to thank God. His blessings are countless and the only reason I am able to do what I do. Thank you, Lord.

TABLE OF CONTENTS

LIST OF TABLES

LIST OF FIGURES

CHAPTER 1 – INTRODUCTION AND LITERATURE REVIEW

1.1 – Introduction

Wisconsin has encountered problems with the connections contained in, and the in-service performance of, several cantilevered mast-arm sign support structures. In one case, a structure was taken down because of excessive mast-arm deflections. After detailed inspection, it was discovered that recently installed bolts were loose, which may have led to premature fatigue failure. In a second case, a routine inspection discovered a welded tube-to-plate connection that exhibited cracking on over 50% of its circumference since the last scheduled inspection. A third case occurred during completion of the present research effort. Sign support structures S-61-0001 and S-61-0002 in Osseo, Wisconsin were decommissioned in the fall of 2011 after cracking was found at the weld-toe in the mast-arm-to-plate connection.

A forensic analysis of the most recent failure was conducted as part of the present research effort to set the stage for evaluating the validity and usefulness of the reliability analysis procedures developed. It is important to demonstrate that this failure was driven by fatigue and therefore, an overview of the forensic study reaching this conclusion is provided in Appendix A. A photo of S-61-0001 is provided in Figure 1.1.

Figure 1.1. S-61-0001: most recent fatigue failure of mast-arm sign support structure in Osseo, Wisconsin (note: a detailed failure analysis is provided for this structure in Appendix A).

The latest edition of the AASHTO design specifications (AASHTO 2009) includes provisions for fatigue design. However, many structures presently in service were designed before fatigue provisions were part of the design specifications. Furthermore, the fatigue design procedures that are now included in these specifications do not address the variability in fatigue life that is likely for structures in service, nor do these provisions allow an engineer to quantify the risk of fatigue-induced fracture for structures that have been in service. As a result, Wisconsin undertook a research effort designed to assess the risk of fatigue-induced fracture in its existing

sign support structures that were designed before these latest AASHTO specification revisions. This was done to develop procedures that can be used to assign inspection protocols for mast-arm sign support structures.

The objectives of the research effort were to implement state-of-the-art fatigue reliability analysis and current knowledge regarding fatigue lives of connections in a systematic assessment of fatigue-induced fracture risk in mast-arm sign support structures within Wisconsin, and assign inspection cycle frequencies for these structures and their components. There are very clear benefits to the proposed research effort. First and foremost, there is an unknown probability of future failures in mast-arm-to-pole connections typical of sign support structures in Wisconsin. This research will result in guidelines for inspection cycles, retrofit measures, or other changes in inspection or maintenance policy to assure the safety of the traveling public. Application of the results of the effort will reduce inconvenience to the motoring public through establishing rational inspection intervals for these structures. Furthermore, these relatively innocuous structures are sources of relatively severe failure consequences. To mitigate this risk, inspections are necessary. By defining reliability-based inspection frequencies, the present research effort will allow better use of public funds for ancillary structure inspection and maintenance.

1.2 – Literature Review

Sign support structures have been studied extensively over the past four decades. In fact, there is an almost overwhelming amount of literature regarding these types of structures. This is not without good reason though. When one considers the entire life span of a sign support structure (from design to decommission), a significant amount of uncertainty exists: statistical scatter in the basic fatigue data; the equations used to describe fatigue crack growth under random stresses; weld fabrication issues (*e.g.* undercut severity varies tremendously); wind speeds and direction defining the loading demand; expressions used to migrate wind speed to pressures for structural

analysis; equations used to conduct detailed stress analysis at the joints in these structures (*e.g.* stress concentration factors); ability of inspection tools (*e.g.* visual inspection, dye penetrant, magnetic particle) to detect cracks; and environmental conditions like corrosion and reduced material toughness (Foley et al. 2008).

In order to meet the objectives outlined in the introduction to this chapter, this uncertainty must be quantified. As indicated by Byers et al. (1997a), a fatigue reliability assessment consists of: (1) stress-range distributions from field monitored or simulated data; (2) the use of the Palmgren-Miner damage accumulation rule in conjunction with fatigue detail categories that define the stress-range-to-cycles until failure (S_R-N) relationship for fatigue critical locations within structural systems; and (3) a performance function which describes the reliability of a particular component and its corresponding fatigue life.

Given the problems (*i.e.* premature fatigue lives) discussed in the introduction to this chapter, it is no wonder why many have spent so much time and effort studying these structures. There are thousands of these structures throughout the state of Wisconsin alone, and many more throughout the United States and the world.

This literature review will be compartmentalized into three categories: (1) sign structure response characteristics and wind demand; (2) experimental fatigue testing; and (3) reliability-based fatigue evaluations. Extensive literature reviews pertaining to the first two categories have already been completed (Foley et al. 2008; Ginal 2003). Therefore, the literature review conducted as part of the present research effort was focused on reliability-based fatigue evaluations. The following sections will first provide a brief overview of the first two categories and then finish with more in-depth coverage of some of the reliability studies performed over the past few decades.

1.2.1 – Sign Structure Response Characteristics and Wind Demand

Ginal (2003) conducted an exhaustive literature review of previous research efforts aimed at quantifying the structural response characteristics of sign support structures. The reviewed literature provided insight regarding: truck-induced wind gusts, wind tunnel studies of support structures, field experimentation and analytical finite element analysis (Ginal 2003). The reader is encouraged to read this literature review as it provides a thorough synthesis of the research conducted through the year 2003.

Since 2003, additional research pertinent to sign support structures has been completed and will be referenced frequently throughout this dissertation. The literature to-date (including that synthesized by Ginal (2003)) has addressed a number of issues as they pertain to sign support structures. This section provides a brief overview of what has been studied thus far.

Several researchers have spent time reevaluating naturally occurring wind speeds which has resulted in modifications to design wind speed maps, development of wind speed statistical distributions, evaluation of superstations or simulation-based wind studies (ASCE 2005; Atadero et al. 2007; Beaupuits et al. 2004; Diekfuss and Foley 2012; Ellingwood and Tekie 1999; Foley et al. 2004; Foley et al. 2008; Ginal 2003; Iannuzzi and Spinelli 1987; Kaimal 1972; Levy 1996; Liu 1991; Peterka 1992; Peterka and Shahid 1998; Phares et al. 2007; Shinozuka and Jan 1972; Simiu et al. 1980; Simiu and Scanlon 1996; Simiu et al. 2003).

The susceptibility of sign, traffic signal or high-mast luminaire support structures to aero-elastic phenomena of galloping and vortex shedding has been considered (Foley et al. 2004; Ginal 2003; Irwin and Peeters 1980; Johns and Dexter 1998; McDonald et al. 1995; Phares et al. 2007). Furthermore, structures have been studied for their response to truck-induced or natural gust-pressures as measured by field or experimental investigations (Cook et al. 1996; Creamer et al. 1979; Foley et al. 2004; Ginal 2003; Johns and Dexter 1999; South 1994).

Finite element (FE) models of sign support structures have been developed and subjected to time-history analyses to quantify vibrational response characteristics or accumulated fatigue damage via stress-range cycle counting when subjected to natural wind or truck-induced gusts (Edwards and Bingham 1984; Foley et al. 2004; Ginal 2003). Further FE analysis on sign structures has been conducted to quantify stress concentration effects present within the connections they contain (Foley et al. 2004; Foley et al. 2008; Gilani et al. 1997; Ocel et al. 2006; Richman 2009; Roy et al. 2011).

Finally, fatigue detail categories with constant amplitude fatigue limits (CAFLs) have been established for design purposes (AASHTO 2009; Fisher et al. 1981; Fouad et al. 1998; Kaczinski et al. 1998) and used during fatigue damage accumulation assessments in conjunction with Miner's rule (DeSantis and Haig 1996; Foley et al. 2004; Ginal 2003; South 1994).

It should be noted that the research work conducted in the studies previously listed were vital to the successful completion of the present effort. These studies provided valuable information necessary for the development of wind speed probabilities, simulation procedures for estimating stress-ranges and quantification of modeling error; therefore, many of these studies will be referenced frequently throughout the dissertation.

1.2.2 – Experimental Fatigue Testing

A significant number of fatigue tests have been performed on connections typically found in sign support structures over the past three decades. A previous research effort provided a review of the most pertinent experimental efforts conducted on mast-arm to pole connections (Foley et al 2008). This review became the foundation for quantifying the uncertainty associated with fatigue life (number of load cycles until crack initiation).

The literature reviewed for experimental fatigue testing on connections typically used in sign support structures included unreinforced/untreated connections (Alderson 1999; Archer and Gurney 1970; Chen et al. 2002; Deschamp 2002; Fisher et al. 1981; Koenigs et al. 2003; Machietto 2002; Ocel et al. 2006; Rios 2007; South 1997) and reinforced/treated connections (Koenigs et al. 2003; Machietto 2002; Ocel et al. 2006). The experimental results from additional studies conducted after the completion of the first phase of the present research effort were also evaluated for use within the present study (Anderson 2007; Puckett et al. 2010; Richman 2009; Roy et al. 2012; Roy et al. 2011). The results from these previous efforts provide the foundational fatigue life data for statistical analysis conducted in chapter three of this dissertation.

1.2.3 – Reliability-Based Fatigue Evaluations

This section will introduce studies which incorporate state-of-the-art reliability methods to assess risk in structural systems. More often than not, the *risk* in these studies was considered the probability of finding a fatigue-induced crack or the probability of growing a fatigue-induced crack to a critical state (*e.g.* fracture). It should be noted that reliability-based fatigue evaluations have deep roots in the offshore structure industry. Nearly all fatigue reliability studies performed to-date (regardless of the structural system being assessed) give reference to studies performed by the offshore structure industry in the early to mid- 1980's.

The following review will illustrate the importance of the present study as well as its novelty in structural engineering. Reliability-based fatigue evaluations have been performed by a number of researchers over the years. This review will be conducted in chronological order with the exception of some of the earliest work. Wirsching (1983) conducted a reliability-based fatigue evaluation for offshore structures. At that time, reliability-based fatigue studies were in their infancy. However, this work resulted in the completion of several technical reports and numerous other seminal publications which are referenced by nearly all studies conducted since. The

reliability formulation used in the present study will use the work conducted by Wirsching (1983) as a foundational framework. Therefore, exhaustive details regarding this reliability framework will be discussed toward the end of the chapter. Quantification of statistical and deterministic parameters needed to utilize this foundational work, as it applies to mast-arm sign support structures, will serve as the motivation for the present study.

Sommer et al. (1993)

This study developed a probability-based procedure for specifying inspection intervals for bridge girders. Three main failure modes are considered in the procedure: (1) bending failure of the girders; (2) shear failure of the web plates; and (3) bearing failure of the stiffened web at supports. The paper indicates that current inspection authorities prefer regular inspection intervals; however, recommends that bridges with higher failure probabilities be inspected more frequently. Intervals are selected to minimize the number of inspections, repairs and failures. The results indicate that bending failure controls in the first ten years of service for bridge girders. After the first ten years, shear failure becomes the dominant mode of failure. It should be noted that if a constant inspection frequency is desired, the results from this paper indicate that an optimal solution would be an interval somewhere between five and ten years, which is longer than the two-year interval mandated by the Federal Highway Administration for fracture-critical components.

Zhao et al. (1994a)

This paper evaluated the fatigue reliability of steel-bridge components. The limit-state (performance function) equation and the uncertainty associated with all basic random variables are quantified. Two approaches are considered: (1) AASHTO approach and (2) LEFM (linear elastic fracture mechanics) approach. The LEFM approach retains the simplicity of the AASHTO

approach but allows updating of reliability indices which is discussed in the companion paper (Zhao et al. 1994b). The LEFM approach was recommended because it can incorporate information on crack size when determining fatigue reliability. However, when employing this method it was noted that additional uncertainties are introduced via crack detectability and inspection accuracy.

Zhao et al. (1994b)

This paper employs the LEFM approach described in its companion paper (Zhao et al. 1994a). Information from non-destructive inspections (NDI) is incorporated into the fatigue-reliability approach in order to update the resulting reliability indices. Three example cases which consider various inspection results are described: (1) no crack detection; (2) crack detection without size measurement; and (3) crack detection with size measurement. If no crack is detected, the reliability index is not dramatically affected; however, if a crack is detected, the reliability index for a particular detail would decrease. If the reliability index decreases below a critical value (user-defined), the bridge would need to be repaired or replaced. If the bridge is repaired, the initial crack size returns to the original assumed magnitude but the number of fatigue cycles is preserved for damage estimates. If the bridge is replaced, the reliability procedure starts over.

Assakkaf and Ayyub (1999)

The objective of this paper is to develop design methods for fatigue of structural details for conventional displacement-type surface monohull ships. The methods followed four requirements: (1) they used spectral analysis of wave loads for demand; (2) they are built upon existing codes; (3) they used nominal strength and load values; and (4) they achieved target reliability levels. The paper systematically describes what is needed and provides two methods for satisfying these requirements. The first method recommended was a load and resistance factor

design (LRFD) approach. Like any LRFD approach, this first method employed partial safety factors to be attached to loads and resistance. The first-order reliability method is used to quantify these safety factors. A direct reliability-based design for fatigue of marine structures was the second method recommended. This method requires spectral analysis for fatigue loads generated by demand characteristics of a ship in the sea. In this method, reliability indices are checked against specified target values and safety is defined when the computed indices are greater than or equal to specified target reliability indices.

Deoliya and Datta (2001)

This paper describes a fatigue reliability analysis performed on Microwave Antenna Towers subjected to gusty wind. Gustiness of wind is assumed to be a stationary random process and was quantified using standard modal spectral analyses. Wind is assumed to act perpendicular to the members of the example antenna towers. Fatigue damage estimation considered several modeling techniques: exact distribution assumption, wide band assumption, narrow band assumption, wide band approximation, Weibull distribution, lognormal distribution, and determination of expected annual fatigue damage. Fatigue failure is classified as crack initiation and the S_R-N approach is used to classify fatigue life. The failure probabilities (p_f) are then computed using two different procedures: (1) full distribution procedure which utilizes the Weibull distribution; and (2) first-order second-moment (FOSM) technique. A numerical study was performed on an antenna tower while considering the effects of: distribution of stress peaks, surrounding terrain conditions, spatial correlation parameters, number of storm events, duration of storm events, and distribution of wind speeds.

The results from this study provided several important conclusions: (1) the FOSM method generated higher failure probabilities than the full distribution method; (2) the peak stress distribution used to classify fatigue life has a significant effect on the probability of fatigue

failure; (3) terrain conditions have significant influence on resulting failure probabilities – p_f for towers situated in cities are many times greater than similar towers situated in open terrain; (4) p_f increases when wind velocities are highly correlated; (5) beyond a certain number of storm events, the p_f increases sharply as the duration and number of events increase; (6) highly peaked distributions of wind speed with long tail ends generate higher probabilities of fatigue failure.

Chung et al. (2003)

The goal of this study was to optimize the inspection program for steel bridge members as they tend to be a significant portion of a DOT's maintenance budget. The study utilized experimental fatigue testing results from Fisher et al (1970). The fatigue results provided the required statistical parameters for input into an optimization function which prescribes an inspection interval.

This procedure relies on being able to define an expected stress-range. This study explored three options for defining an expected stress-range: (1) stress spectrum analysis; (2) an assumed stress Rayleigh distribution analysis; and (3) a fatigue truck analysis. The stress spectrum analysis required the acquisition and extrapolation of measured strain gage data. The assumed stress Raleigh distribution analysis simply estimated the expected stress-range distribution using a probability density function.

The fatigue truck analysis provided an ability to generate a moment influence line. Using the moment influence line in conjunction with the AASHTO importance factor (I) and appropriate distribution factors (DF), an expected stress-range could be computed.

This study optimizes an inspection program through the use of an event tree analysis. The reliability of a particular detail decreases over time. Once a specified level of reliability is reached, the structure is inspected. If the detail being inspected is found to have no cracks or an

acceptable amount of cracking (*i.e.* cracks that do not need repair) then the connection is classified as new. If repair is needed, then the detail is first repaired and then classified as new.

van de Lindt and Goode (2006) & Goode and van de Lindt (2007)

The objective of this report and subsequent paper was to develop a reliability-based design procedure for high-mast lighting (HML) structural supports based upon fatigue life. The procedure is a semiprescriptive approach that is based upon several hundreds of thousands of time-domain finite element analysis simulations. The simulations are specified with varying types of support design and varying wind loading conditions. The motion of the structure was monitored during these simulations and the resulting stresses were computed at the base of the structures using basic mechanics. After a time history of stresses was obtained for a given wind loading condition, the Palmgren-Miner rule was used to determine the expected fatigue damage as a result of that particular loading. Completing this process for a range of input parameters and over a spectrum of wind speeds, it was determined that the fatigue life for an HML structure is most sensitive to pole thickness, pole diameter and variations in wind velocity distributions.

Ni et al. (2010)

Strain measurements were recorded from a permanently installed structural health monitoring system on a bridge in Hong Kong. The strains were used to determine the nominal stress-range seen over a period of one year. Global and local finite element models were utilized to determine the stress concentration factor (*SCF*) for typical details within the structure. Miner's damage accumulation rule was used to sum damage from various magnitudes of stress-range. Both nominal stress-range and *SCF* were modeled using probability distribution functions (PDFs). The *SCF* was modeled using a normal PDF with a mean value obtained from FEM experiments and a *CV* of 0.021 (Ye 2010). Normal, lognormal and Weibull PDFs were used to model the nominal

stress-range (all looked very similar and appropriate). A joint PDF of *SCF* and nominal stress-range (*i.e.* joint PDF of hot spot stress-range) was developed. The predicted fatigue life from monitoring, and without incorporating any *SCF*, was 927 years. If the joint PDF is used (*i.e.* one that incorporates *SCF*), the predicted fatigue life was 716 years, a reduction of approximately 23%.

Wang et al. (2012)

This paper focuses on using non-destructive inspection (NDI) techniques to evaluate the fatigue-reliability of existing steel bridges in China. The NDI methods for crack detection considered in this study include: visual inspection, eddy current, radiography, magnetic particle inspection, acoustic emission, and ultrasonic testing. The study incorporates the probability of detection (POD) for the NDI techniques to assess the effectiveness of each at finding flaws within members. It is mentioned that POD will increase with flaw size to a maximum value; however, non-detection probabilities can also increase depending on factors such as human error during inspection. The study shows for various NDI techniques, the reliability of a bridge member that is inspected can increase or decrease depending upon whether or not a crack or flaw is found. The degree to which reliability increases or decreases depends on the POD for the NDI method considered. The study found that NDI methods are a viable way to effectively update crack growth models and can be employed to evaluate the fatigue life and safe service life for existing steel bridges.

Other Recent Efforts

Several additional (and fairly recent) reliability studies have been performed on steel bridges (Guo et al. 2012; Kwon and Frangopol 2010; Kwon et al. 2012; Liu et al. 2012) and suspension bridges (Chen et al. 2012). It should be noted that all of these studies incorporate real-time field

monitoring data to either predict or update the reliability of the structural systems to improve or enhance inspection and maintenance of these structures.

Synthesis of Past Work

All previous studies in the area of reliability-based fatigue rely on the ability to accurately quantify the uncertainty associated with specific variables that are needed to carry out reliability-based optimization and maintenance intervention. The common thread between all of these previous efforts is trying to maintain the safe, effective and efficient use of existing structural systems while also seeking to improve how engineers may move forward with better design procedures. The benefits of using state-of-the-art reliability techniques to assess risk in structural systems are clear. It is also clear that no such study exists for mast-arm sign support structures. It is prudent to extend these methodologies to these types of structures given their prevalence in society.

The present research effort will build off of the previous studies and expand reliability-based analysis into a suitable form for mast-arm sign support structures. Developing a sound reliability-based framework for assessing the fatigue-induced fracture risk of sign support structures requires a fundamental knowledge of the uncertainty associated with three variables: resistance, demand and modeling error. As indicated earlier, there are a large number of parameters that contribute to the uncertainty present within each of the three variables (Foley et al. 2008).

The remaining sections of the chapter will provide the mathematical derivation for the reliability-based formulation that will be used as the foundation of this dissertation. The derivation will bring to surface the exact parameters (statistical and deterministic) which are required to implement a reliability-based procedure for assessing fatigue-induced fracture risk in sign support structures. The required parameters will be defined throughout the derivation;

however, specific details of each parameter will be provided after the entire derivation is given for clarity.

1.3 – Reliability Framework

To begin the reliability formulation, the fatigue life for a specific detail category will be assumed to be characterized by,

$$N \cdot \left(S_R\right)^m = A \tag{1.1}$$

where the following are defined;

N	=	fatigue life of the detail, number of stress-range cycles accumulated at failure (initial crack formation);
S_R	=	constant stress-range cycle magnitude;
A	=	fatigue detail constant, x-intercept of fatigue life curve;
m	=	exponent describing the slope of the S_R - N curve for the specific detail category.

Stress-range cycles are rarely, if ever, applied at constant magnitude in real structural systems; therefore, models for accumulated damage resulting from variable-amplitude stress-ranges are needed. The Palmgren-Miner linear damage accumulation rule (Miner's rule) is a commonly accepted accumulated damage model and it can be written as (Miner 1945),

$$D = \sum_{i=1}^{n} \frac{n_i}{N_i} = \sum_{i=1}^{n} \frac{n_i \left(S_{R,i}\right)^m}{A} = \frac{n_1 \left(S_{R,1}\right)^m + n_2 \left(S_{R,2}\right)^m + \ldots + n_n \left(S_{R,n}\right)^m}{A} \tag{1.2}$$

where the following additional terms are defined,

n_i = number of constant-amplitude cycles applied at stress-range magnitude *i*;

N_i = the fatigue life of the detail at stress-range magnitude *i*.

The difficulty in applying Miner's rule for accumulated damage as posed in equation (1.2) is that the applied stress-range cycle magnitudes are highly variable and these cycle magnitudes comprise a spectrum of stress-range cycle magnitudes. Therefore, this spectrum must be considered and a characteristic stress-range cycle magnitude for the spectrum needs to be defined.

Schilling et al. (1978) proposed the following simple procedure for defining a single stress-range cycle magnitude that characterizes the stress-range spectrum. This process uses an equivalent expected stress-range,

$$D = \frac{N_T}{A} \cdot \sum_{i=1}^{n} \frac{n_i \left(S_{R,i}\right)^m}{N_T} = \frac{N_T}{A} \cdot S_{RE}^m \geq \Delta \tag{1.3}$$

where N_T is the total number of applied stress-range cycles and S_{RE} is the equivalent expected single stress-range cycle magnitude which has been defined as,

$$S_{RE} = \left[\sum_{i=1}^{n} \frac{n_i \left(S_{R,i}\right)^m}{N_T} \right]^{1/m} \tag{1.4}$$

When Δ is exceeded, the fatigue life of the detail is considered exhausted. The magnitude of Δ is commonly taken to be 1.0 for deterministic fatigue studies. The critical number of stress-range cycles resulting in crack initiation, N_c, can then be written as,

$$N_c = \frac{A \cdot \Delta}{S_{RE}^m} \tag{1.5}$$

The equivalent stress-range magnitudes will be utilized in later sections of this dissertation to develop a spectrum of stress-range magnitudes for various levels of wind loading (speed). The remaining portions of this derivation will assume that fatigue life is non-deterministic and will be devoted to developing the foundation for the reliability-based approach for assessing fatigue-induced fracture risk within sign-support structures.

The derivation continues here by defining a limit-state or performance function for reliability-based fatigue analysis. Equation (1.5) can be used to write the performance function as,

$$Y = g(\mathrm{X}) = \frac{N_c}{N_T} = \frac{A \cdot \Delta}{S_{RE}^m N_T} \tag{1.6}$$

where X is a vector of random variables (A and Δ), and N_c is the critical number of applied stress-range cycles resulting in crack initiation.

Crack initiation is defined as $Y \le 1.0$. If the performance function contains lognormal random variables, then it too is a lognormal random variable. Since Y is lognormal, the probability of failure can be determined using the standard normal cumulative distribution function (CDF) as (Nowak and Collins 2000),

$$p_F = P[Y \le 1.0] = \Phi\left[\frac{\ln(1.0) - \mu_{\ln Y}}{\sigma_{\ln Y}}\right] = \Phi\left[-\frac{\mu_{\ln Y}}{\sigma_{\ln Y}}\right] = \Phi[-\beta] \tag{1.7}$$

where β is commonly known as the reliability index.

Taking the natural logarithm of the performance function is done to begin the process,

$$\ln Y = \ln\left(\frac{A \cdot \Delta}{S_{RE}^m \cdot N_T}\right) \tag{1.8}$$

Using standard procedures (Swokowski 1979), the natural logarithm of the performance function can be written as,

$$\ln Y = \ln A + \ln \Delta - m \ln S_{RE} - \ln N_T \tag{1.9}$$

which is essentially a linear combination of random variables (Nowak and Collins 2000).

The mean and variance of the natural logarithm of the performance function can be written as (Nowak and Collins 2000),

$$\mu_{\ln Y} = \mu_{\ln A} + \mu_{\ln \Delta} - m \ln S_{RE} - \ln N_T \tag{1.10}$$

$$\sigma^2_{\ln Y} = \sum_{i=1}^{n} \sigma^2_{\ln X_i} \tag{1.11}$$

where;

$$\sigma^2_{\ln X_i} = \ln\left(1 + \frac{\sigma^2_{X_i}}{\mu^2_{X_i}}\right) = \ln\left(1 + CV^2_{X_i}\right) \tag{1.12}$$

$$\mu_{\ln X_i} = \ln \mu_{X_i} - \frac{1}{2}\sigma^2_{\ln X_i} = \ln \mu_{X_i} - \frac{1}{2}\ln\left(1 + CV^2_{X_i}\right) \tag{1.13}$$

and CV_{X_i} is the coefficient of variation; $\sigma^2_{X_i}$ is the variance; and μ_{X_i} is the mean of the lognormally distributed random variable, X_i. Equations (1.12) and (1.13) generate the following for the random variables;

$$\mu_{\ln A} = \ln \mu_A - \frac{1}{2}\ln\left(1 + CV^2_A\right) \tag{1.14}$$

$$\mu_{\ln \Delta} = \ln \mu_\Delta - \frac{1}{2}\ln\left(1 + CV^2_\Delta\right) \tag{1.15}$$

$$\sigma_{\ln A}^2 = \ln\left(1+CV_A^2\right) \tag{1.16}$$

$$\sigma_{\ln \Delta}^2 = \ln\left(1+CV_\Delta^2\right) \tag{1.17}$$

Plugging equations (1.14) and (1.15) into equation (1.10) gives,

$$\mu_{\ln Y} = \left(\ln \mu_A - \frac{1}{2}\ln\left(1+CV_A^2\right)\right) + \left(\ln \mu_\Delta - \frac{1}{2}\ln\left(1+CV_\Delta^2\right)\right) - m\ln S_{RE} - \ln N_T$$

which simplifies to,

$$\mu_{\ln Y} = \ln\left(\mu_A \cdot \mu_\Delta\right) - \frac{1}{2}\ln\left[\left(1+CV_A^2\right)\left(1+CV_\Delta^2\right)\right] - m\ln S_{RE} - \ln N_T \tag{1.18}$$

Plugging equations (1.16) and (1.17) into equation (1.11) gives,

$$\sigma_{\ln Y}^2 = \ln\left(1+CV_A^2\right) + \ln\left(1+CV_\Delta^2\right)$$

which simplifies to,

$$\sigma_{\ln Y} = \sqrt{\ln\left[\left(1+CV_A^2\right)\left(1+CV_\Delta^2\right)\right]} \tag{1.19}$$

The reliability index defining the probability of the performance function being less than one (*i.e.* a crack initiating and failure resulting) can be written by plugging equations (1.18) and (1.19) into equation (1.7) resulting in,

$$\beta = \frac{\mu_{\ln Y}}{\sigma_{\ln Y}} = \frac{\ln\left(\mu_A \cdot \mu_\Delta\right) - \frac{1}{2}\ln\left[\left(1+CV_A^2\right)\left(1+CV_\Delta^2\right)\right] - m\ln S_{RE} - \ln N_T}{\sqrt{\ln\left[\left(1+CV_A^2\right)\left(1+CV_\Delta^2\right)\right]}} \tag{1.20}$$

Additional sources of uncertainty may now be considered and incorporated within the present approach. The stress-range cycles are often determined using predictive mechanisms

(*e.g.* finite element analysis). As a result, there is uncertainty associated with the modeling and the prediction of the stress-range magnitude.

This uncertainty can be handled through a bias factor (*B*) attached to the stress-range magnitude (Wirsching 1983). Miner's rule must be slightly adjusted to account for this and equation (1.2) can be rewritten as,

$$D = \sum_{i=1}^{n} \frac{n_i \left(B \cdot S_{R,i} \right)^m}{A} \tag{1.21}$$

Expanding equation (1.21) gives,

$$D = \frac{1}{A} \cdot \left(n_1 B^m S_{R,1}^m + n_2 B^m S_{R,2}^m + \cdots + n_n B^m S_{R,n}^m \right) = \frac{1}{A} \cdot B^m \cdot \sum_{i=1}^{n} n_i S_{R,i}^m \tag{1.22}$$

Using equation (1.22) and the concept of the equivalent expected stress-range as described in equation (1.3), the cumulative damage rule can be rewritten as,

$$D = \frac{N_T}{A} \cdot B^m \cdot \sum_{i=1}^{n} \frac{n_i \left(S_{R,i} \right)^m}{N_T} = \frac{N_T B^m S_{RE}^m}{A} \geq \Delta \tag{1.23}$$

This alternate form (equation (1.23)) can be used to introduce an expected service time interval until the initiation of a crack, *T*. This allows an average frequency of stress-range cycles occurring in the time interval to be defined as,

$$f_o = \frac{N_T}{T} \tag{1.24}$$

Equation (1.23) can now be rewritten as,

$$D = \frac{N_T B^m}{A} \cdot \frac{T}{T} \cdot \sum_{i=1}^{n} \frac{n_i}{N_T} S_{R,i}^m = \frac{T B^m}{A} \cdot f_o \sum_{i=1}^{n} \frac{n_i}{N_T} S_{R,i}^m \geq \Delta \tag{1.25}$$

Wirsching (1983) defines a deterministic stress parameter as,

$$\Omega = f_o \sum_{i=1}^{n} \zeta_i S_{R,i}^m \tag{1.26}$$

where the following is defined,

$$\zeta_i = \frac{n_i}{N_T}$$

This allows equation (1.23) (adjusted Miner's rule) to be written as,

$$D = \frac{T \cdot B^m \cdot \Omega}{A} \geq \Delta \tag{1.27}$$

Equation (1.27) can be solved for the critical time interval expected at crack initiation,

$$T_c = \frac{\Delta \cdot A}{B^m \cdot \Omega} \tag{1.28}$$

A performance function for reliability-based fatigue analysis can now be formulated in a manner similar to that done in equation (1.6),

$$Y = g(\mathbf{X}) = \frac{T_c}{T} = \frac{\Delta \cdot A}{B^m \cdot \Omega \cdot T} \tag{1.29}$$

where T is the specified, expected service life. The random variables in equation (1.29) are A, B, and Δ. Again, fatigue failure occurs when $Y \leq 1.0$ (*i.e.* when the specified, expected service life is greater than or equal to the critical time interval expected at crack initiation).

The natural logarithm of the performance function can be written in a similar manner as that done in equation (1.9),

$$\ln Y = \ln A + \ln \Delta - m \ln B - \ln \Omega - \ln T \tag{1.30}$$

The mean of the natural logarithm of the performance function can be written as,

$$\mu_{\ln Y} = \mu_{\ln A} + \mu_{\ln \Delta} - m\mu_{\ln B} - \ln \Omega - \ln T \tag{1.31}$$

Expanding using equations (1.14) and (1.15) and a similar equation for the additional random variable gives,

$$\mu_{\ln Y} = \left(\ln \mu_A - \frac{1}{2} \ln\left(1 + CV_A^2\right) \right) + \left(\ln \mu_\Delta - \frac{1}{2} \ln\left(1 + CV_\Delta^2\right) \right) - m\left(\ln \mu_B - \frac{1}{2} \ln\left(1 + CV_B^2\right) \right) - \ln \Omega - \ln T$$

Simplifying considerably gives,

$$\mu_{\ln Y} = \ln\left(\frac{\mu_A \mu_\Delta}{\mu_B^m} \right) - \frac{1}{2} \ln\left[\frac{\left(1 + CV_A^2\right)\left(1 + CV_\Delta^2\right)}{\left(1 + CV_B^2\right)^m} \right] - \ln \Omega - \ln T \tag{1.32}$$

The standard deviation of the natural logarithm of the performance function is,

$$\sigma_{\ln Y} = \sqrt{\ln\left[\left(1 + CV_A^2\right)\left(1 + CV_\Delta^2\right)\left(1 + CV_B^2\right) \right]} \tag{1.33}$$

The reliability index, modified to incorporate modeling uncertainty and a stress parameter, defining the probability of the performance function being less than one (*i.e.* a crack initiating and failure resulting) can now be written,

$$\beta = \frac{\mu_{\ln Y}}{\sigma_{\ln Y}} = \frac{\ln\left(\frac{\mu_A \mu_\Delta}{\mu_B^m} \right) - \frac{1}{2} \ln\left[\frac{\left(1 + CV_A^2\right)\left(1 + CV_\Delta^2\right)}{\left(1 + CV_B^2\right)^m} \right] - \ln \Omega - \ln T}{\sqrt{\ln\left[\left(1 + CV_A^2\right)\left(1 + CV_\Delta^2\right)\left(1 + CV_B^2\right) \right]}} \tag{1.34}$$

Finally, the probability of failure may be determined by plugging equation (1.34) into equation (1.7) restated as follows,

$$p_F = P\left[Y \le 1.0\right] = \Phi\left[\frac{\ln(1.0) - \mu_{\ln Y}}{\sigma_{\ln Y}}\right] = \Phi\left[-\frac{\mu_{\ln Y}}{\sigma_{\ln Y}}\right] = \Phi\left[-\beta\right] \tag{1.7}$$

A procedure for developing a performance function that defines the probability that a given sign-support structure will have a fatigue-induced crack has been described. This framework consists of both random variables (A, B, and Δ) and semi-deterministic parameters (m and Ω). In order to gain an understanding of the parameters used within this procedure, a careful examination of uncertainty associated with each one was conducted.

1.4 – Objectives of Dissertation

The remaining sections of this chapter will address each of the three random variables and both of the semi-deterministic parameters found in equation (1.7). Each section will begin by providing a brief outline of the methods that will be used to quantify each of them and end with references to the reliability formulation which will indicate exactly what deliverables are sought. These outlines may then act as a roadmap for navigating through the remaining chapters of this dissertation.

1.4.1 – Stress Parameter: Ω

The stress parameter is far and above the most involved portion of the reliability derivation. Its formulation draws on results from chapters two, three, four, five and six of the dissertation. Wirsching (1983) outlines three methods used to evaluate the stress parameter: (a) the deterministic method; (b) the spectral method; and (c) the Weibull model.

All three methods outlined by Wirsching (1983) require statistical models for the stress-range, which in turn require statistical models for loading demand (in this case, wind). Because of readily available computational power, familiarity with finite element software (ANSYS 14.0) and work conducted in earlier research efforts (Foley et al. 2004; Foley et al. 2008), it was decided to move forward with the deterministic approach.

If the deterministic method is employed to characterize the stress parameter, Ω, then damage may be found by summing blocks of constant amplitude stress-range cycles. The deterministic approach, as it pertains to offshore structures, was presented in equation (1.26) and is provided again here for convenience (Wirsching 1983),

$$\Omega = f_o \sum_{i=1}^{n} \zeta_i S_{R,i}^m \tag{1.26}$$

To migrate from wave loading on offshore structures to wind loading on sign support structures, equation (1.26) was reformulated. Ginal (2003) and Foley et al. (2004) used intersecting probabilistic wind models for speed and direction to recast equation (1.26) into the following form (Foley et al. 2008),

$$\Omega = n_{5-\text{sec}/\,year} \sum_j \sum_i P\left[\bar{V}_{5-\text{sec}} = v_j\right] \cdot P\left[D = d \,|\, \bar{V}_{5-\text{sec}} = v_j\right] \cdot \left(S_i^m\right)_{v_j} \tag{1.35}$$

where: $n_{5-\text{sec}/\,year}$ is the number of 5-second intervals in the given time period (one year in this former effort); $P\left[\bar{V}_{5-\text{sec}} = v_j\right]$ is the probability that the 5-second averaged wind speed will be the user-defined magnitude, v_j; and $P\left[D = d \,|\, \bar{V}_{5-\text{sec}} = v_j\right]$ is the probability that the wind speed is in a user-defined direction, d, (taken as direction perpendicular to sign face) given the 5-second averaging time is equal to the user-defined magnitude; and $\left(S_i\right)_{v_j}$ is the *i*th stress cycle magnitude

for a given 5-second wind speed, v_j. It should be noted that 5-second wind speeds were taken as 5, 10, 15, 20, 25, 30, 35, 40, 45, and 50 mph (Foley et al. 2008).

This procedure requires simulation of wind speeds at each of the magnitudes previously listed. The wind speed simulations for each of the magnitudes may then be converted to pressure using procedures outlined in AASHTO (2009), ASCE (2005) and Simiu and Scanlon (1996). The wind pressure simulation may then be subjected onto the elements of a finite element model of the sign support structure at an orientation perpendicular to the sign face. Transient analyses of the sign provide corresponding stress histories for any location within the sign structure. The expected stress-range magnitude for any given wind speed can be found using the rainflow counting technique (Matsuishi and Endo 1968).

There is one shortcoming of the stress parameter as presented in equation (1.35). If the stress cycle magnitude for a given 5-second wind speed, v_j, is determined by applying wind pressure (corresponding to wind speed magnitude, v_j) perpendicular to the signs supported by the structure, then only wind acting out of perpendicular directions will contribute to the demand.

To ensure that all wind demand (*i.e.* wind acting out of every direction) was being accounted for within the stress parameter, equation (1.35) was modified as follows,

$$\Omega = n_{1-hr/yr} \cdot \sum_i \sum_j \left[P(U = u_i \bigcap D = d_j) \cdot n_{cycles/hr,i} (S_{RE}^m)_i \cdot \cos\theta_j \right] \tag{1.36}$$

where: $n_{1-hr/year}$ is the number of 1-hour intervals in a year (8,760); $P(U = u_i \cap D = d_j)$ is the probability that a 1-hour averaged wind speed of user-defined magnitude, u_i, will be intersected with a 1-hour averaged wind direction of user-defined orientation, d_j; $n_{cycles/hr,i}$ is the number of stress cycles occurring in one hour resulting from the application of a wind pressure simulation

corresponding to a mean wind speed magnitude, u_i (applied perpendicular to sign face); $\left(S_{RE}^{m}\right)_i$ is the expected stress-range magnitude from the 1-hour stress history results (corresponding to mean wind speed magnitude, u_i); and θ_j is the angle between the axis of the mast-arm and the centroidal axis of the *j*th cardinal direction.

Similar to the previous stress parameter formulation, it should be noted that 1-hour wind speeds were taken as 5, 10, 15, 20, 25, 30, 35, 40, 45, and 50 mph. Details regarding the change in averaging time from five seconds to one hour are provided in chapter two of the dissertation. The simulation of wind speed and generation of simulated expected stress-range magnitudes are provided in chapter five of the dissertation.

1.4.2 – Fatigue Parameters: *A* and *m*

The reliability-based framework presented earlier in this chapter classifies resistance as the fatigue life (*i.e.* length of time or number of cycles of stress-range until crack initiation) of the most fatigue-critical location of a sign support structure. This location is most often found to be on the mast-arm wall at the weld-toe of the welded tube-to-plate connection.

In some cases, when stiffeners are used for reinforcement, the fatigue-critical location remains on the mast-arm wall but moves to the weld-toe of the stiffener (at its termination point). However, this is largely dependent upon the stress concentration effect at the fatigue-critical locations. Typically, the most fatigue-critical location coincides with the location of the largest stress-concentration factor (*SCF*).

Classifying finite fatigue life is most often conducted with the use of an S_R - N diagram where S_R is defined as stress-range and N is defined as the number of cycles to fatigue failure. AASHTO (2009) provides an S_R - N diagram which is broken down into fatigue detail categories.

Each detail category is provided in the form of a single straight line on the S_R - N diagram. Associated with each straight line is a slope, *m*, and an x-intercept referred to as the fatigue constant for a particular detail category, *A*. The mathematical representation of the S_R - N diagram was provided in equation (1.1) which is restated below for convenience,

$$N \cdot (S_R)^m = A \tag{1.1}$$

The values of *A* and *m* depend upon the specific detail category chosen. The values provided by AASHTO (2009) are the results from statistical analysis performed on data obtained from a significant number of experimental fatigue tests performed on various connection details.

Right now, nearly all connections used in sign support structures are classified as the AASHTO E' fatigue detail category. This means that there is one value of μ_A, one value of CV_A, and one value of m used to define the fatigue life of most connections presently considered. However, examination of fatigue testing data for these connections has indicated that there is significant statistical scatter in the results. Statistical scatter needs to be quantified if an accurate estimate for fatigue life of these connections is to be made. Therefore, all fatigue test data relevant to connections contained within sign support structures were synthesized into categories to provide connection-specific statistical parameters for quantifying the fatigue life uncertainty. Details of this procedure and the results obtained for connection-specific values of μ_A, CV_A and m are provided in chapter three of the dissertation.

1.4.3 – Modeling Error Bias Factor: *B*

It should be anticipated that modeling error will be introduced when predictive methods are used to estimate expected stress-range magnitudes within sign support structures. The predictive methods include a number of simplifying assumptions and modeling techniques to make the

effort tractable. The following is a list of potential sources where modeling error may be introduced while using this method:

- Using a simplified finite element model (*i.e.* a "stick model" consisting of one-dimensional elements) to carry out simulations for obtaining stress-histories;
- Simulating natural wind speed using power spectral analyses;
- Using the rainflow cycle counting technique to provide an expected stress-range magnitude corresponding to a particular variable amplitude stress-history.

Modeling error must be included in the reliability procedure formulated earlier so that uncertainty in the simplifying assumptions may be taken into account. As previously noted, modeling error may be accounted for through the random variable B. The reliability procedure can be carried out with an expected value of B equal to 1.0 and a CV_B equal to 0.0. A value of $\mu_B = 1.0$ and $CV_B = 0.0$ requires the ability to model resistance and demand exactly. For the resistance to be modeled exactly, the finite element model for the sign support structure must incorporate accurate and precise geometry, material properties and dynamic response characteristics as well as appropriate element selection and resolution. For the demand to be modeled exactly, the power spectral density (PSD) for the simulated wind speed must align itself exactly with the PSD for the measured wind speed as well as provide an equivalent mean magnitude.

The requirements listed above are very unlikely to occur. Therefore, it should be expected that bias will be introduced in the procedure. That is to say, the results from the model will not be exactly equal to the physical reality of the sign being modeled. The random variable B provides an ability to quantify the amount of bias that is introduced when the method previously formulated is utilized. Finite element models used in this procedure are discussed in

chapter four. The methods used and results found for quantifying μ_B and CV_B are provided in chapter five of the dissertation.

1.4.4 – Damage Accumulation: Δ

The accumulation of fatigue damage, D, is calculated using Miner's rule. Miner's rule was provided in equation (1.2), and is restated below for convenience,

$$D = \sum_{i=1}^{n} \frac{n_i}{N_i} = \sum_{i=1}^{n} \frac{n_i \left(S_{R,i}\right)^m}{A} = \frac{n_1 \left(S_{R,1}\right)^m + n_2 \left(S_{R,2}\right)^m + \ldots + n_n \left(S_{R,n}\right)^m}{A} \tag{1.2}$$

When using the deterministic approach provided in equation (1.2), failure is defined when $D = 1.0$. However, Miner's rule is considered a fairly simplistic procedure used to estimate failure from fatigue, which is a complex phenomenon dependent upon many factors. Because of this, the predictions for fatigue failure are not always consistently accurate (Wirsching 1983). Therefore, inherent uncertainty is associated with the use of Miner's rule.

To account for the uncertainty associated with the use of Miner's rule, it has been suggested to define failure as $D = \Delta$, where Δ is a random variable denoting damage at failure (Wirsching 1983). It is recommended to use $\mu_\Delta = 1.0$ and $CV_\Delta = 0.30$. It should be noted that these recommendations are from studies conducted in the offshore structure industry, but will be directly used without modification in the present research effort.

1.4.5 – Process for Defining Inspection Frequencies

To describe how the previous formulation will be used to define inspection frequencies for sign support structures, consider the hypothetical example of a sign structure going into service in Milwaukee, Wisconsin. The methodology formulated in this research effort will allow probabilities of finding fatigue-induced cracking after any number of years of service. If the

probability of finding fatigue-induced cracking after 5 years is 5%, after 15 years is 20%, and after 25 years is 90%; the engineer can establish the first inspection at 15 years and then inspect in regular four-year intervals after that. The current WisDOT process is to inspect on four-year cycles. Therefore, the inspection cycle scenario described would save three inspections during its service life. An average estimate for cost per inspection was provided by WisDOT as around one thousand dollars. Given the number of mast-arm sign support structures around the State, the potential cost savings (or reallocation) is appreciable.

The methodology also allows targeted probabilities of finding a fatigue-induced crack to be defined with subsequent service lives meeting this threshold. Thus, if a 95% confidence level (*i.e.* 5% chance a fatigue-induced crack is initiated) is set as a target, then one can establish the first inspection at a service life corresponding to a 5% probability of failure. Depending upon the location within the State, the mast-arm detail configuration and the orientation of the mast-arm from north, this might be 30+ years. As a result, sign support structures that enter service in good condition may never need to be inspected. Furthermore, there are other sign support structures that may indeed need to be inspected more frequently than the current four-year interval; perhaps a two-year interval is necessary to meet this confidence level on in-service fatigue performance. Chapter six of the dissertation discusses the results of this study and recommends new inspection frequencies that are reliability-based.

CHAPTER 2 – QUANTIFYING WIND DEMAND UNCERTAINTY

2.1 – Introduction

Quantifying the uncertainty in wind loading demand is integral to assessing fatigue-induced fracture risk in mast-arm sign support structures and establishing inspection protocols for these structures. In order to accomplish this, one must understand and quantify daily wind speeds and directions in the location where the sign support structure is in service. This is often in conflict with established methods of carrying out design of these structures as maximum expected wind speeds during the service life (sometimes 50 years) of a sign support structure is needed.

The majority of past research conducted for modeling wind has been in the area of extreme winds (Ellingwood and Tekie 1999; Peterka 1992; Peterka and Shahid 1998; Simiu et al. 1980; Simiu et al. 2003). Engineering models for extreme winds have been based upon fifty-year recurrence interval speeds using averaging times corresponding to fastest mile winds or 3-second gusts (AASHTO 2009; ASCE 1998). Much of the fatigue-related research pertaining to sign and signal support structures has focused on quantifying structural response characteristics with regard to the aero-elastic phenomena of galloping and vortex shedding (Foley et al. 2004; Ginal 2003; Kaczinski et al. 1998; McDonald et al. 1995; South 1994). Statistical models of wind speeds (irrespective of direction) have been developed to gain understanding of what a sign structure might experience at a given location (Li et al. 2005); and probabilistic models of 5-second averaged wind speeds and directions for use in evaluating fatigue response of full-span sign support and high-mast luminaire support structures have been developed (Foley et al. 2004; Ginal 2003). The effect of truck-induced wind gusts has also been investigated (Edwards and Bingham 1984; Foley et al. 2004; Ginal 2003; Ocel et al. 2006).

The objective of this chapter is to provide a statistical modeling process for wind suitable for input into the reliability-based model for fatigue performance outlined in chapter one. As indicated in chapter one, the wind demand will be quantified through a semi-deterministic quantity identified previously as the stress parameter, Ω. For convenience, the equation for the stress parameter is restated as,

$$\Omega = n_{1-hr/yr} \cdot \sum_i \sum_j \left[P(U = u_i \bigcap D = d_j) \cdot n_{cycles/hr,i} (S_{RE}^m)_i \cdot \cos\theta_j \right] \quad (2.1)$$

Obtaining the combined probabilities (probability of intersection) of wind speed and wind direction, $P(U = u_i \cap D = d_j)$, in equation (2.1) for any location throughout the state of Wisconsin where a sign support structure is in service, will be the end goal of this chapter.

2.2 – Wind Speed Data Sources

Sign and signal support structures tend to be located more frequently in areas of higher population density. Wind speed and direction data from the southern half of Wisconsin was collected. The cities used in the collection process are shown in Figure 2.1. There is a fairly wide dispersion of data collection sites utilized. It was felt that the data collected would yield significant understanding of wind speed and direction variability throughout the areas of the state where there is a significant number of sign and signal support structures.

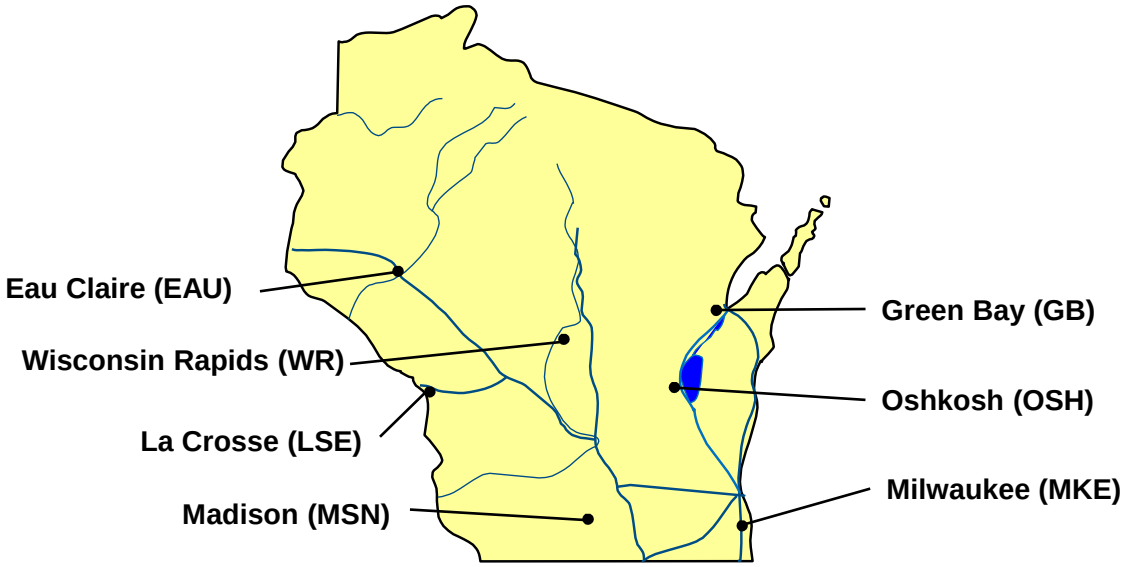

Figure 2.1. Map of Wisconsin listing the NCDC-ASOS wind data collection sites.

2.2.1 – NCDC-ASOS Sites

The National Climatic Data Center (NCDC) within the U.S. Department of Commerce maintains a weather data inventory as part of the National Oceanographic and Atmospheric Administration (NOAA) Satellite and Information Service. There are many U.S. controlled weather observation stations throughout the country continually collecting weather-related data. Many of these weather collection sites are called Automated Surface Observation System (ASOS) sites. The NCDC-ASOS sites are referenced by city and state as well as a Weather-Bureau-Army-Navy (WBAN) number. The city, WBAN number, and number of years of data collected for the seven cities considered in this research effort are given in Table 2.1.

Table 2.1. Cities used for NCDC wind speed and direction data collection.

City	WBAN #	Location	Years	Data Collection Years
Green Bay	14898	Austin Straubel International Airport	14	Jan. 1998 – Dec. 2011
La Crosse	14920	La Crosse Municipal Airport	14	Jan. 1998 – Dec. 2011
Eau Claire	14991	Eau Claire Regional Airport	14	Jan. 1998 – Dec. 2011
Madison	14837	Dane County Regional Airport	14	Jan. 1998 – Dec. 2011
Milwaukee	14839	Mitchell International Airport	14	Jan. 1998 – Dec. 2011
Oshkosh	94855	Oshkosh Wittman Airport	14	Jan. 1998 – Dec. 2011
Wisconsin Rapids	04826	Wisconsin Rapids Alexander Field	14	Jan. 1998 – Dec. 2011

Academic and government institutions can access the data at no cost through the following web-site: http://www.ncdc.noaa.gov/oa/climate/stationlocator.html. The user must specify the WBAN number and the time frame for which data is desired. Within minutes, spreadsheets containing an array of hourly climatic data are sent to the user via email. Upon receipt of the spreadsheets, the user may sift through and utilize any data of interest such as dew point, relative humidity, atmospheric pressure, visibility, wind speed, wind direction, etc. Given the present research effort, wind speed and corresponding direction were manually extracted and placed into blank Excel spreadsheets formatted for later access by MATLAB.

2.2.2 – Field Monitoring System

The sign chosen for monitoring in the present study was WisDOT S-40-703. This sign is a cantilevered mono-tube mast-arm structure designed and manufactured by Valmont Industries of Valley, NE. This structure represents the typical mast-arm-pole support structure configuration found in Wisconsin. The sign is located in Milwaukee, Wisconsin just south of the intersection of Walnut Street and Fond du Lac Avenue. This is an urban area that is relatively free of wind-

stream obstructions in the immediate vicinity, yet is still in the midst of buildings, overpasses and a varying topographical gradient. This location was ideal for instrumentation due to its proximity to the Marquette University campus.

The field monitoring system (FMS) provided two functions. First, it collected bi-axial bending strain using eight Vishay Micromeasurements 350-ohm weldable strain gages mounted to the sign at four diametrically opposite locations (top, bottom and both sides). Second, it collected wind speed and corresponding direction using a Gill Windsonic 2D sonic anemometer mounted to an aluminum weather station tower. The overall anemometer height was 33 feet (10 meters) above the ground with respect to the base elevation of S-40-703. Also mounted on the weather station tower was a solar panel for marine-battery charging, an enclosure for a battery and solar power regulator, and an enclosure for data acquisition software and hardware. A National Instruments (NI) CompactRIO data acquisition hardware chassis and National Instruments 9237 full-bridge conditioning card, operated through LabVIEW, made up the data acquisition system (Smith 2010). An aerial view of the sign and FMS location is provided in Figure 2.2.

Figure 2.2. Location of Milwaukee sign support structure S-40-703 and the field monitoring station used to collect site/sign-specific wind data and corresponding bending strain response.

The FMS was deployed in October 2009 and was operational between March 12, 2010 and November 24, 2010. However, wind data is only available between March 12, 2010 and September 5, 2010 due to a loss of anemometer functionality for unknown reasons on September

6, 2010. The Gill anemometer used as part of the FMS was capable of a sampling rate of 4 Hz. The manufacturer rates the accuracy of velocity at +/- 2% and the accuracy of direction at +/- 3 degrees. Given the present research focus, it should be noted that the readings of the anemometer used in this study were validated using wind tunnel experimentation within a Marquette University laboratory (Smith 2010). A single 24 hour period results in the FMS producing data files containing wind and strain information with sizes of approximately 45 Mb. Consequently, weekly visits to the FMS were necessary to collect data and free-up memory on the NI system in order to avoid overwriting of data. A more detailed discussion of the chosen sign, FMS components as well as data validation techniques of the data acquisition hardware and software deployed can be found elsewhere (Smith 2010).

2.3 – Wind Data Syntheses

There is a tremendous amount of wind speed and wind direction data that was synthesized as part of the present research effort. Data from two sources was digested. The first was the NCDC-ASOS sites. This data was used to formulate probabilities suitable for the reliability-analysis procedure developed. This included formulation and evaluation of an interpolation procedure for wind speed and wind direction combined probability models. The second data source was the FMS site deployed during the research effort. This data was used to evaluate topological effects at locations where sign structures are likely installed when compared to those locations where the data was collected (*e.g.* NCDC-ASOS sites). The FMS site data was also used to evaluate the interpolation procedure developed. This section outlines the wind data synthesis conducted as part of the present research effort.

2.3.1 – NCDC-ASOS Wind Data Synthesis

The NCDC wind data collected from ASOS sites was manipulated into a form suitable for subsequent statistical analysis. A two-minute averaged wind speed is one of many recorded parameters provided by NCDC-ASOS weather stations. This two-minute averaged wind speed is updated once every five seconds and reported to the database once per hour (ASOS 1998). This means that once, every hour, a two-minute averaged wind speed (and its corresponding direction) is extracted from the station and documented as the two-minute wind data for that hour. The value is representative of only the two minutes of time that contributed to the reported average. No additional information is given by the database of record between the hourly readings. Therefore, in order to obtain a pseudo-contiguous record of wind speed and corresponding direction over an extended period of time, extrapolation of this two-minute averaged wind speed, over its respective hour, is necessary.

It is prudent to provide discussion with regard to how the extrapolation procedure was conducted. With the mindset of performing a subsequent reliability study involving the fatigue evaluation of these structures, and with the goal of obtaining accumulated damage caused by fatigue, it was felt that one-hour averaged wind speeds would be more appropriate than two-minute averaged wind speeds. Also, if a single two-minute averaged wind speed was going to be used to represent an entire hour, then perhaps the averaging time should be adjusted to an hourly average.

It is widely known that averaging time has a direct impact on the magnitude of averaged wind speed. In general, as averaging time increases, the resulting averaged wind speed decreases (Simiu and Scanlon 1996). The extent to which various averaging times affect the magnitude of the resulting averaged wind speed can be quantified through the use of the Durst Curve (Figure 2.3). The curve shown in Figure 2.3 allows a wind speed magnitude of one averaging time to be

adjusted to the corresponding magnitude of a different averaging time. The curve provides ratios of specified averaged wind speed magnitudes to their equivalent one-hour averaged wind speed magnitudes.

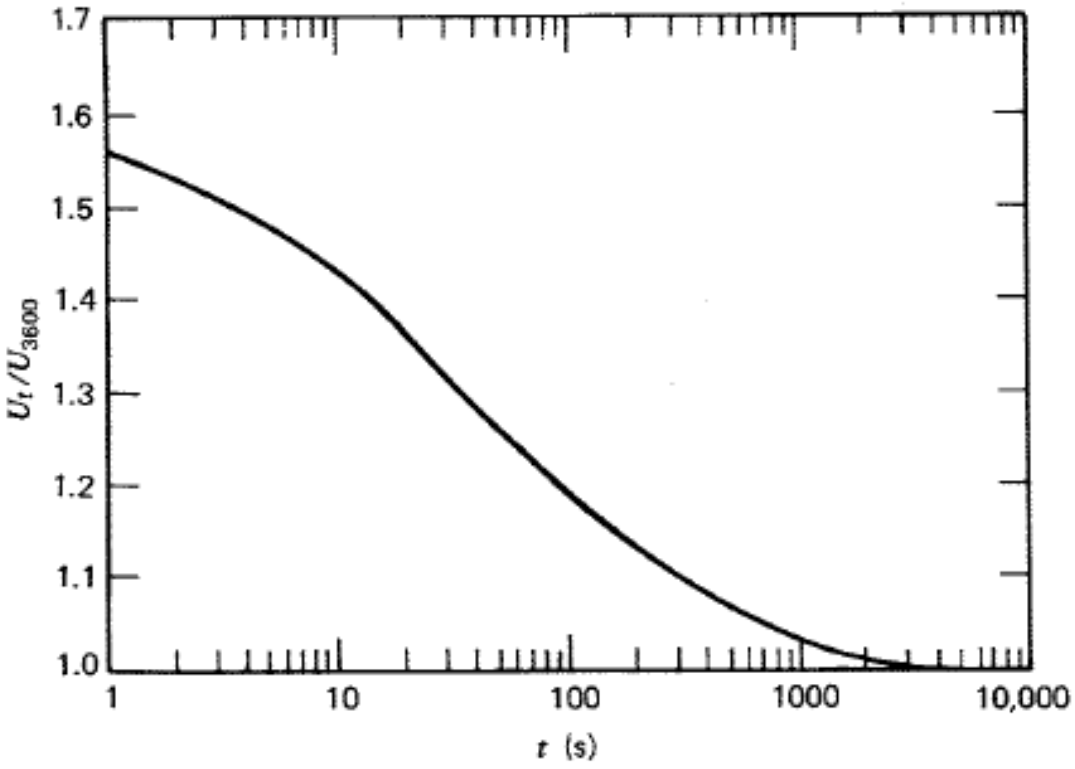

Figure 2.3. Wind speed variation with averaging time (Simiu and Scanlon 1996).

For example, consider a two-minute averaged wind speed, collected by one of the ASOS stations, having a magnitude of 10 mph. The averaging time for this wind speed corresponds to a value of *t* in Figure 2.3 equal to two minutes or 120 seconds (U_{120} = 10 mph). If the goal is to obtain the one-hour averaged equivalent (U_{3600}), then using Figure 2.3, the following averaging time conversion can be accomplished:

$$\frac{U_{120}}{U_{3600}} = 1.175 \text{ (taken from Figure 2.3)} \qquad (2.2)$$

$$U_{3600} = \frac{U_{120}}{1.175} = \frac{10 \text{ mph}}{1.175} = 8.51 \text{ mph} \quad (2.3)$$

Adjusting the averaging time from two minutes to one hour clearly reduces the magnitude of the averaged wind speed. Initial thoughts may consider this as a non-conservative approach to obtaining a suitable database of wind speed for later statistical analysis as this procedure will reduce all wind speeds by a factor of (1/1.175). However, the goal is not to be conservative, but rather to provide a realistic estimate of the level of demand sustained by mast-arm sign support structures throughout their service lives. If one were to consider a strength design procedure, a maximum expected wind speed in a 50-year service life might be more appropriate and 3-second, 5-second or another averaging time might be employed. ASCE 7 uses 5-second averaging times for the maximum considered wind events used in design of building systems (ASCE 2005). However, the present approach is felt to be the best method for generating a pseudo-contiguous record of wind speeds for fatigue life evaluation of these structures when single hourly two-minute averaged wind speeds are readily available.

As mentioned in the preceding sections, wind information was extracted from spreadsheets obtained from NCDC and placed into a single blank Excel spreadsheet. The spreadsheet was named *XXX_WindData.xlsx* where *XXX* was a prefix reserved for identifying the city where the contributing NCDC-ASOS site was located (*e.g. MKE_WindData.xlsx* contained the wind data extracted from the NCDC-ASOS site located in Milwaukee, WI at the Mitchell International Airport). Within the (*XXX_WindData.xlsx*) spreadsheets, all collected wind speed data was divided by 1.175 to adjust it from a two-minute averaging time to a one-hour averaging time while all collected wind direction data was left unadjusted. This was the first step in the NCDC data synthesis. Additional manual manipulation was required and will now be discussed.

In addition to adjusting the magnitude of the wind speed to account for a longer averaging time, further manipulation was required prior to stepping through the synthesis of wind

data. There were a number of cases where the wind speed was very, very small such that a wind direction could not be defined in the weather data. In these cases, a placeholder was found (*e.g.* *** was found in the database) in lieu of a numerical value. All entries containing this placeholder for the wind direction, as well as its corresponding wind speed, were set equal to zero.

There were other instances where the wind speed was very small, but a wind direction was specified. Wind directions corresponding to very small wind speeds were considered unreliable. For example, if the wind speed is zero, how can there be a wind direction present? It was this question that led to setting all wind speeds of 2.5 mph or less, and their accompanying directions, equal to zero. The lower limit of 2.5 mph was chosen because it is the value of the lower limit on the 5 mph bin of values described later in this section. It was important to preserve these "zero entries" so that an accurate total number of wind speed data entries could be used when determining probabilities of occurrence for wind speed and direction. Approximately 17% of all data entries obtained from the NCDC database were manually set equal to zero and preserved for later synthesis (161,769 "zero entries" out of 959,399 total wind data entries).

At this point, no further manipulation of the NCDC wind data was necessary. An example illustrating the manual adjustment of wind data up to this point in the discussion is provided in Figure 2.4. This figure illustrates that a single value of two-minute averaged wind speed recorded every hour is converted to a one-hour averaged wind speed that is then assumed to exist for the entire sixty-minute period for which the original two-minute averaged wind speed was recorded. The algorithms used and the procedure followed to further synthesize the wind data into appropriate bins for statistical analysis will now be discussed.

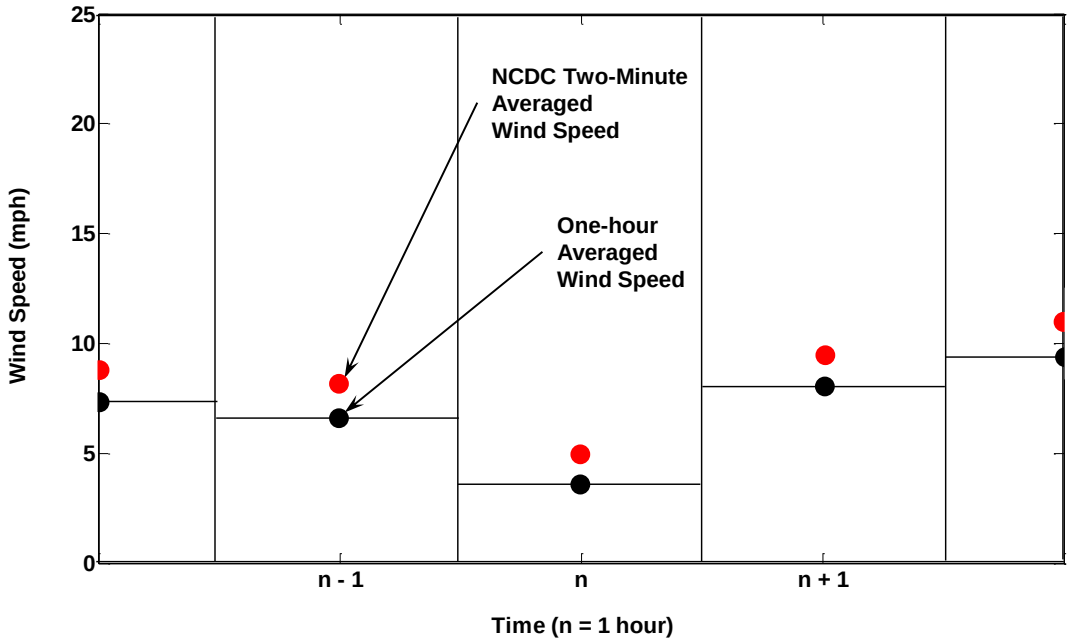

Figure 2.4. NCDC adjustment procedure utilized to obtain one-hour averaged wind speeds note: data shown is fabricated to illustrate the procedure – red markers indicate the data as it would be obtained from NCDC and black markers illustrate the reduction in magnitude (to scale) when averaging time increases from two minutes to one hour).

MATLAB programs created and used in previous research efforts (Foley et al. 2004; Foley et al. 2008; Smith 2010) were utilized as the basis for the following synthesis procedures. It should be noted that all MATLAB programs used for the synthesis of the NCDC-ASOS wind data are provided in Appendix B.

It will be helpful to define specific file types and extensions that will be used from this point forward to avoid confusion. Files that have "*.m*" extensions are MATLAB script files and are referred to as m-files. There were four m-files utilized during the synthesis of the NCDC wind data:

- *NCDC_sifter.m*
- *NCDC_analysis.m*

- *NCDC_speedonly.m*
- *NCDC_directiononly.m*

Files that have a "*.mat*" extension are MATLAB output files and are referred to as mat-files. Mat-files contain the results of executed tasks from m-files and are in a form that is MATLAB-friendly allowing MATLAB to process their information more efficiently. Mat-files can also be called and used by other m-files. There were two mat-files used during the synthesis of the NCDC data:

- *XXX_matfile_data.mat*
- *XXX_Speeds.mat*

The *XXX* is a prefix reserved for identifying the city where the contributing NCDC-ASOS site was located.

The process of synthesis beyond the point of initial data collection and manual manipulation was conducted as follows. *NCDC_sifter.m* was utilized to read in *XXX_WindData.xlsx*. Execution of *NCDC_sifter.m* resulted in the mat-file *XXX_matfile_data.mat* which was populated with three distinct arrays: SpeedOnly, DirectionOnly and SpeedDirection. The contents of each array are in their titles – a one-column array of wind speeds, a one-column array of wind directions, and a two-column array of wind speeds and corresponding directions, respectively. The remaining m-files rely on *XXX_matfile_data.mat* as their input and can be carried out in any order.

NCDC_analysis.m is a binning program that first separates occurrences of wind speeds into one of nine different columns based on their corresponding directions. The nine columns included eight cardinal directions (N, NE, E, SE, S, SW, W and NW) in addition to a not applicable (NA) column. The NA column was reserved for the "zero entries" as described

previously. After the appropriate column is specified, the wind speed data within each column is segregated according to magnitude. The wind speeds are broken into 5 mph bins in order to count the number of occurrences that a particular wind speed is 5 mph, 10 mph, 15 mph, all the way up to 80 mph. Each bin had a range of +/- 2.5 mph. For example, all wind speeds greater than 2.5 mph, but less than or equal to 7.5 mph, were considered a 5 mph wind speed and placed into the 5 mph bin. The results from this m-file are sent to the *XXX_Analysis.xlsx* spreadsheet.

The two remaining m-files are much simpler programs. *NCDC_speedonly.m* separates wind speeds, irrespective of direction, into the same 5 mph bins described in the previous paragraph. *NCDC_directiononly.m* separates wind directions, irrespective of wind speed, using one of two binning methods. The first method bins wind directions into one of the eight cardinal directions (N, NE, E, SE, S, SW, W and NW) or the NA column (same as direction binning procedure used in *NCDC_analysis.m*). The second method bins wind directions into a ten degree resolution. This provided higher resolution taxonomy of wind directions which simply counted the occurrences of wind directions since these values were obtained in 10-degree increments. The results from these m-files were sent to *XXX.Speed.xlsx* and *XXX.Direction.xlsx*, respectively.

2.3.2 – FMS Wind Data Synthesis

As noted previously, the FMS was capable of operating at a 4 Hz data acquisition rate. Therefore, the compactRIO DAQ system collected ten strain values (five strain values pertaining to bending about the horizontal axis and recorded through channel F1and five strain values pertaining to bending about the vertical axis and recorded through channel F2), one wind speed value and one corresponding wind direction value four times every second that the FMS was in operation. This was an important component of the present research effort. The simultaneous collection of mast arm bending strain, and wind information causing that bending strain, provides an ability to verify finite element models as discussed later in this thesis. In order to do this,

however, the FMS wind data needed to be synthesized into one-hour averages. The process by which data synthesis was conducted for the FMS will now be described.

The C-programming language was introduced to ensure that a concentrated and systematic approach was taken to deal with the massive amount of data collected by the FMS. Similar to MATLAB m-files mentioned in the NCDC wind data synthesis section, executable programs were written using the C-programming language and are denoted with a "*.c*" file extension (referred to as c-files). A single c-file (*HourlyAvg.c*) contains the entire averaging process utilized to properly synthesize the FMS dataset. *HourlyAvg.c* can be found in Appendix C for reference.

HourlyAvg.c creates text files containing one-hour averages for both strain and wind data collected by the compactRIO data acquisition system. As mentioned, the compactRIO collects ten strain values (five F1 strain values and five F2 strain values) and four wind values per second (4 Hz collection speed) and places them into text files named *cRIO_(timestamp).txt* where the timestamp includes the day, time of day, month and year that the data was collected. The *compactRIO(timestamp).txt* text file contains the following 15 column format:

F1_Strain_1 F1_Strain_2 F1_Strain_3 F1_Strain_4 F1_Strain_5 ...
F2_Strain_1 F2_Strain_2 F2_Strain_3 F2_Strain_4 F2_Strain_5 ...
Wind_Speed Wind_Direction Date Time AM/PM

This means that the strain values used for the one-hour averages were effectively obtained at 20 Hz (five strain values per 0.25 sec.), whereas the wind values were obtained at 4 Hz (1 wind value per 0.25 sec.). Therefore, *HourlyAvg.c* must average ten strain values (five F1 and five F2) to two values (one F1 and one F2) every 0.25 seconds. This is dealt with in the first section of *HourlyAvg.c* and provides a new text file named *RawData_(timestamp).txt* which contains the following four column format:

Avg_F1_Strain Avg_F2_Strain Wind_Speed Wind_Direction

The next step in the synthesis procedure is to read in the values within *RawData_(timestamp).txt* and calculate one-hour averages by selecting 14,400 contiguous values at a time [(1 hour) x (60 minutes/hour) x (60 seconds/minute) x (4Hz) = 14,400]. The one-hour averages are then written to two separate files per day, one file for strain *AvgStrain_(timestamp).txt* and one file for wind *AvgWind_(timestamp).txt*. Their respective formats are as follows:

AvgStrain_(timestamp).txt: 1HourAvg_F1_Strain 1HourAvg_F2_Strain

AvgWind_(timestamp).txt: 1HourAvg_Wind_Speed 1HourAvg_Wind_Direction

The strain values (both F1 and F2) as well as the wind speed values are simply one-hour averages (containing 14,400 contiguous values). The wind direction values, however, must be dealt with in a slightly more complicated manner due to the circular nature of wind direction. A good explanation can be provided within the context of an example. Consider the following eight wind directions (in degrees from true north) reported via the data acquisition system:

357 | 358 | 359 | 360 | 0 | 1 | 2 | 3

The average of the eight directions listed should be 0 or 360 degrees (both representing true north). However, the average of the numbers would give 180 degrees (representing true south). Each wind direction was thought of as a unit vector to prevent this from happening. The unit vectors were broken down into their x- and y-components using direction cosines. After breaking the wind directions into their components, averages of the components were calculated. Finally, the average x-component and average y-component over one hour was found. They were then combined and the resulting direction of the unit vector was used as the one-hour averaged wind direction.

Unlike the NCDC-ASOS wind data, there were no such occurrences where a resulting one-hour averaged wind speed did not have an accompanying direction present. Moreover, there were no occurrences where a one-hour average of "0" was found for either wind speed or wind direction. However, there were a relatively small number of instances (453 entries out of a total of 4,069 entries – approximately 11% of total) where the anemometer would provide a value of "999.99" for both wind speed and direction at a particular point in time. A wind speed of approximately 1000 mph and a wind direction of approximately 1000 degrees did not make sense. Therefore, it was decided to manually set these values equal to zero before *HourlyAvg.c* was employed. It was felt that clearly inaccurate readings would generate artificially high one-hour averaged wind values for both speed and direction.

After the entire averaging process was finished, one last step was taken to ensure the foundational datasets obtained from both the FMS and the NCDC-ASOS sites were of equivalent form. This last step was necessary because the FMS measured wind direction in a one-degree resolution while the NCDC-ASOS sites recorded wind direction in a ten-degree resolution. Therefore, prior to synthesizing the averaged FMS data into direction specific bins, all wind directions were rounded to the nearest ten-degree increment.

The wind speed synthesis procedure conducted for the dataset obtained at the FMS site is summarized in Figure 2.5. The figure illustrates the near-contiguous wind speed data stream and the dots represent the magnitude of the one-hour average. A comparison between Figures 2.4 and 2.5 illustrates the difference between the formats of the data as they were collected, and the procedures utilized for their respective wind speed syntheses. The field monitoring system provided wind speed and wind direction data samples at 4 Hz. This allowed 14,400 readings to be averaged each hour and thus, generates a more representative string of one-hour averaged wind speeds than the ASOS site data. The FMS data synthesis conducted as described led to wind data that was suitable for final synthesis in the same manner as the NCDC-ASOS data. The MATLAB

m- and mat-files, as well as all Excel files, are identical for synthesis between both datasets with the exception of the filenames. All "*NCDC_*" tags were removed and replaced with "*FMS_*" tags. All m- and mat-files used for synthesis of the FMS data are provided in Appendix D for reference.

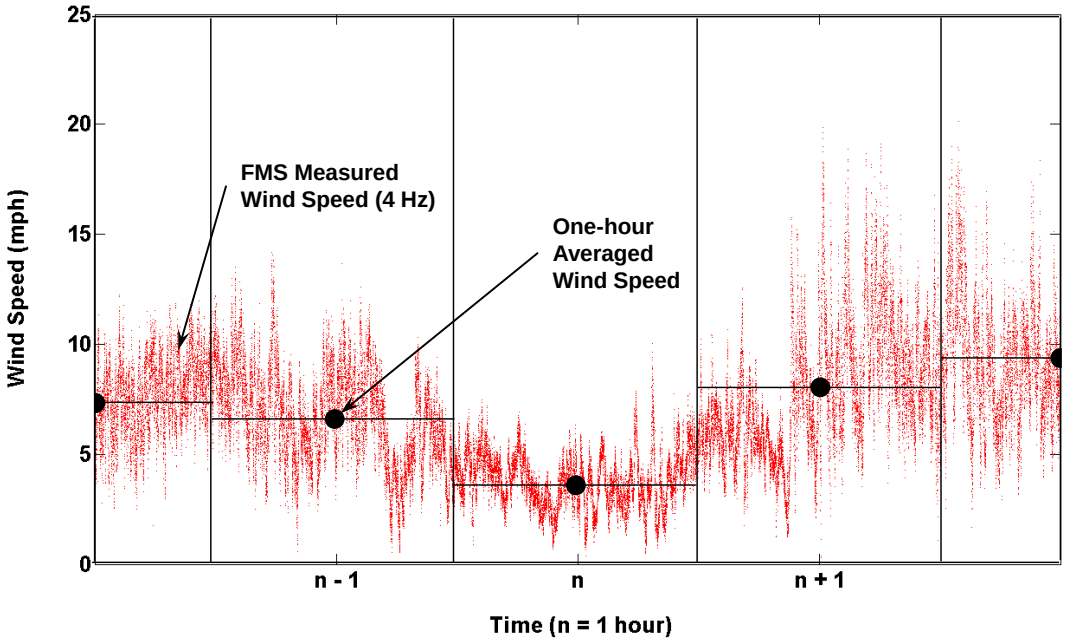

Figure 2.5. FMS averaging procedure utilized to obtain one-hour averaged wind speeds (note: data shown is a snippet of four hours of real measured data obtained by the FMS on April 1, 2010).

2.3.3 – Statistical Analysis and Discussion

The spreadsheets described in the previous sections contain the frequency of occurrences for each of the various binning procedures conducted. All spreadsheets for a particular site were consolidated into a final spreadsheet, *XXX_Probabilities.xlsx*. The synthesized data for each ASOS site and the FMS site in this spreadsheet were used to assemble individual probabilities of one-hour averaged wind speed and one-hour averaged wind direction events. From this point forward, one-hour averaged wind speed and one-hour averaged wind direction will be referred to as wind speed and wind direction, respectively.

Mean wind speed, *U*, and mean wind direction, *D*, are both continuous random variables with sample spaces of $\{0 \le U < \infty \text{ mph}\}$ and $\{0 \le D < 360 \text{ degrees}\}$, respectively. However, by virtue of the synthesis procedures carried out previously, wind speed and wind direction should be assumed to be discrete random variables. The binning procedure employed allowed discrete random variable models to provide individual probabilities for wind speed, individual probabilities for wind direction, conditional probabilities for wind speed *given* wind direction and combined (*i.e.* intersecting) probabilities of wind speed *and* wind direction to be determined. The equations used and results found for each of the probabilities outlined will now be discussed.

The individual probabilities for wind speed can be computed using the results generated through the *NCDC_speedonly.m* and *FMS_speedonly.m* m-files using,

$$P(U = u_i) = \frac{N_{u_i}}{N_{speed}} \qquad u_i \in \{5,10,15,...,70,75,80\} \tag{2.4}$$

where: N_{u_i} is the number of one-hour averaged wind speed u_i occurrences; N_{speed} is the total number of one-hour averaged wind speeds; and u_i is a wind speed (mph) in 5-mph increments. The individual probabilities for wind direction are computed using the synthesized wind direction data and the following,

$$P(D = d_j) = \frac{N_{d_j}}{N_{direct}} \qquad d_j \in \{0,10,20,30,...,340,350,360\} \tag{2.5}$$

if the 10-degree resolution binning procedure is used. If the eight cardinal directions are used in the binning procedure, the probabilities are computed using,

$$P(D = d_j) = \frac{N_{d_j}}{N_{direct}} \qquad d_j \in \{N, NE, E, SE, S, SW, W, NW\} \tag{2.6}$$

The total number of wind speed directions, N_{direct}, depends upon the binning procedure used and N_{d_j} is the number of occurrences for one-hour averaged wind direction d_j.

The resulting individual probabilities of wind speed and wind direction are provided in Appendix E for reference. The histograms for wind speed and wind rose histograms for wind direction are provided in Figure 2.6. A few notes about Figure 2.6 are warranted and will be discussed after presenting the results for the conditional and combined probabilities.

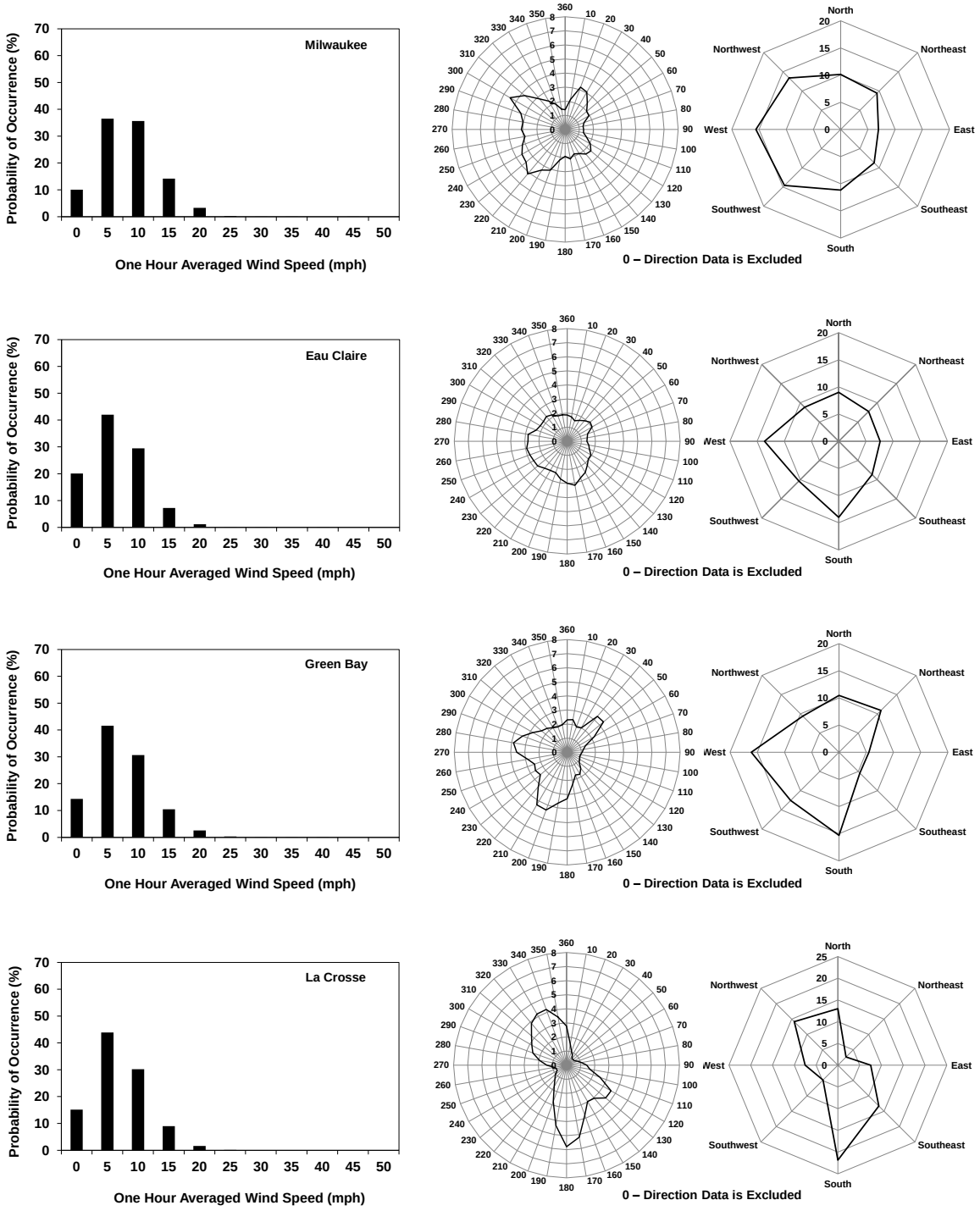

Figure 2.6. Individual one-hour wind speed histograms and wind rose histograms for Milwaukee, Eau Claire, Green Bay and La Crosse NCDC-ASOS sites.

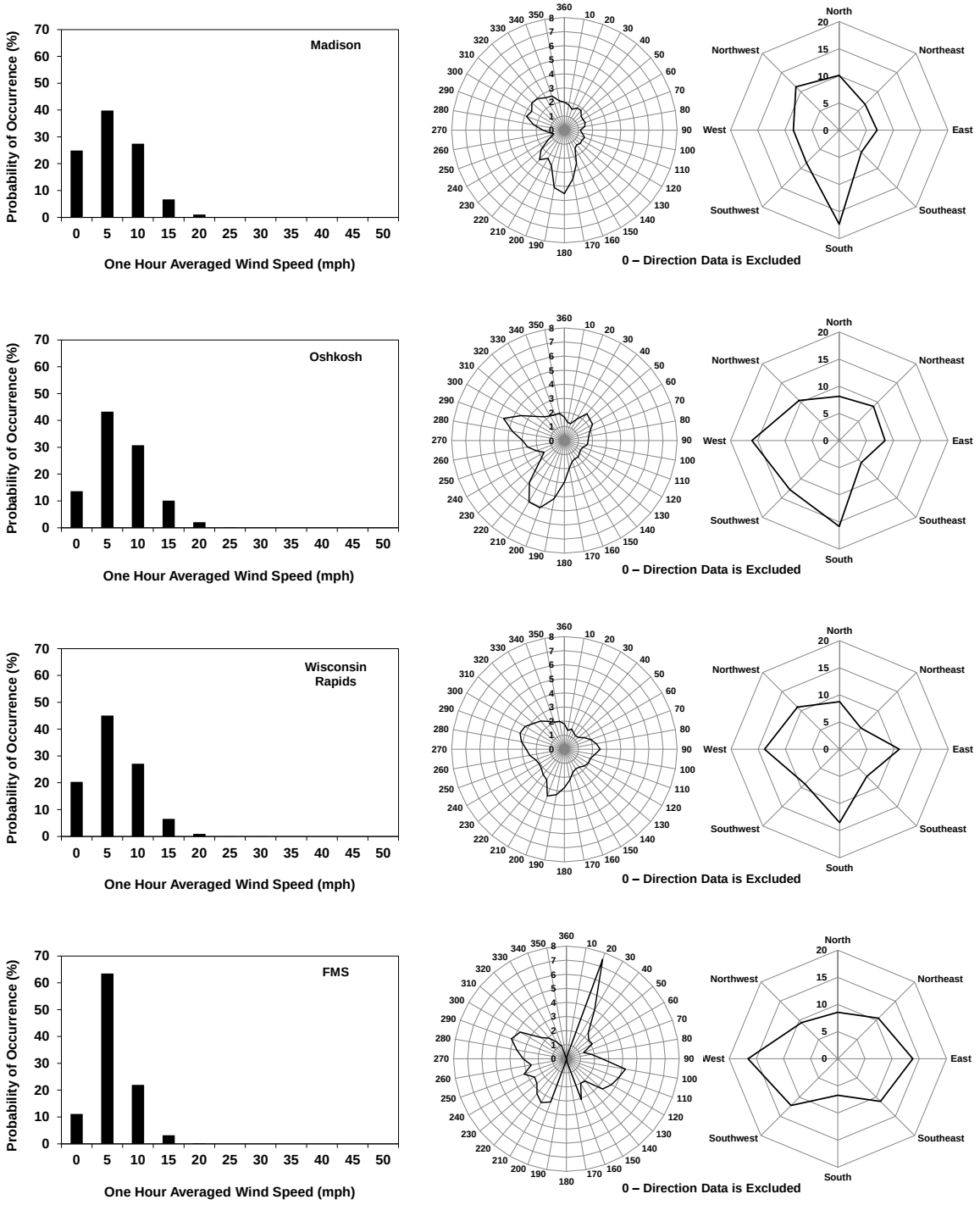

Figure 2.6. Continued… Individual one-hour wind speed histograms and wind rose histograms for Madison, Oshkosh and Wisconsin Rapids NCDC-ASOS sites and FMS site.

After the individual probabilities for wind speed and wind direction are found, the combined probabilities (*i.e.* the probability of intersection) of wind speed and wind direction can be determined. Because these two random variables are statistically dependent upon one another, probability theory dictates that the probability of their intersection must be determined as (Ginal 2003),

$$P\left(U=u_i \bigcap D=d_j\right)=P\left(D=d_j\right)\cdot P\left(U=u_i \middle| D=d_j\right) \tag{2.7}$$

In words, equation (2.7) says that the combined probability of a wind speed of magnitude u_i intersected with a wind direction of orientation d_j is equal to the individual probability that the wind direction will be orientation d_j multiplied by the conditional probability that the wind speed will be magnitude u_i given that the wind direction is already orientation d_j.

Equation (2.7) requires that the conditional probability of wind speed given wind direction be computed. This too was conducted within *XXX_Probabilities.xlsx*. The conditional probabilities may be computed as,

$$P\left(U=u_i \middle| D=d_j\right)=\frac{N'_{u_i}}{N_{d_j}} \tag{2.8}$$

where N'_{u_i} is the total number of one-hour averaged wind speeds with magnitude u_i that have one-hour averaged directions d_j and N_{d_j} is the total number of occurrences of one-hour averaged wind directions d_j.

The wind direction resolution for both conditional and combined probabilities was limited to the eight cardinal directions based upon the similarities seen in the wind rose histograms of Figure 2.6. The conditional probabilities for wind speed given direction are

provided in tabular form within Appendix E and schematically in Figure 2.7. The resulting combined probabilities of wind speed acting out of each cardinal direction are provided in Tables 2.2 through 2.9 and Figure 2.8.

The wind speed histograms from Figure 2.6 indicate that for all but one location (Green Bay), there were zero occurrences of one-hour averaged wind speeds, from any direction, with magnitudes larger than 50 mph. This is a reasonable result given the one-hour averaging time and the size of the bins used in the counting procedure. Comparisons between the wind rose histograms of Figure 2.6 indicate that there is some notable variation in the distribution of wind directions throughout the state. Some locations (Milwaukee, Eau Claire and Wisconsin Rapids) have distributions of wind direction that is fairly evenly spread across all bins that were considered. However, others (Green Bay, La Crosse, Madison and Oshkosh) have distributions of wind direction that appear to have heavier contributions from the northern and southern bins. Finally, it appears that lower-resolution modeling of wind direction (*i.e.* cardinal direction binning procedure) appears to be a suitable approach. The wind rose histograms for wind direction of Figure 2.6 show very similar trends when comparing the results of the two different binning procedures.

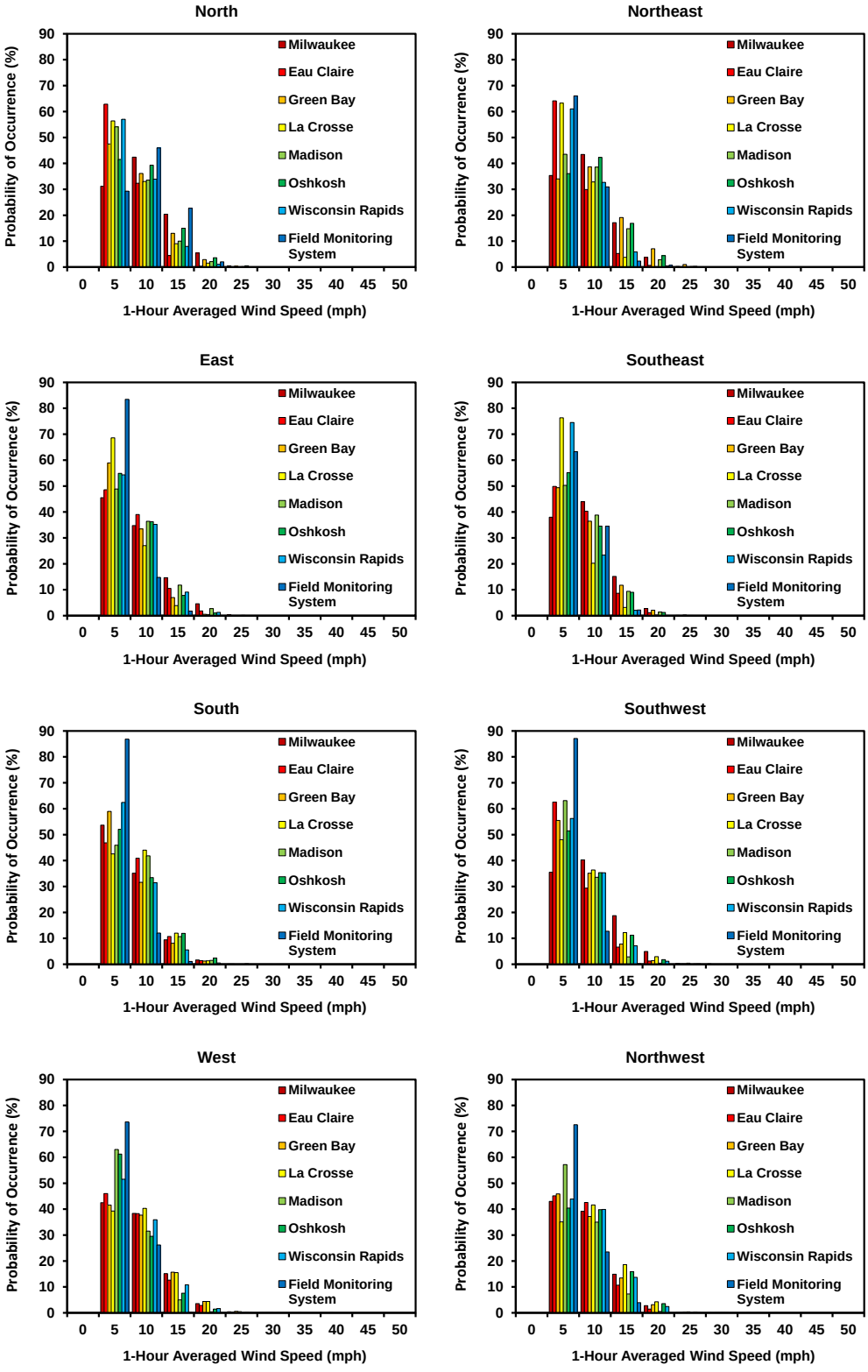

Figure 2.7. Conditional probabilities for all NCDC-ASOS sites and the FMS site – $P(U = u_i \mid D = d_j)$.

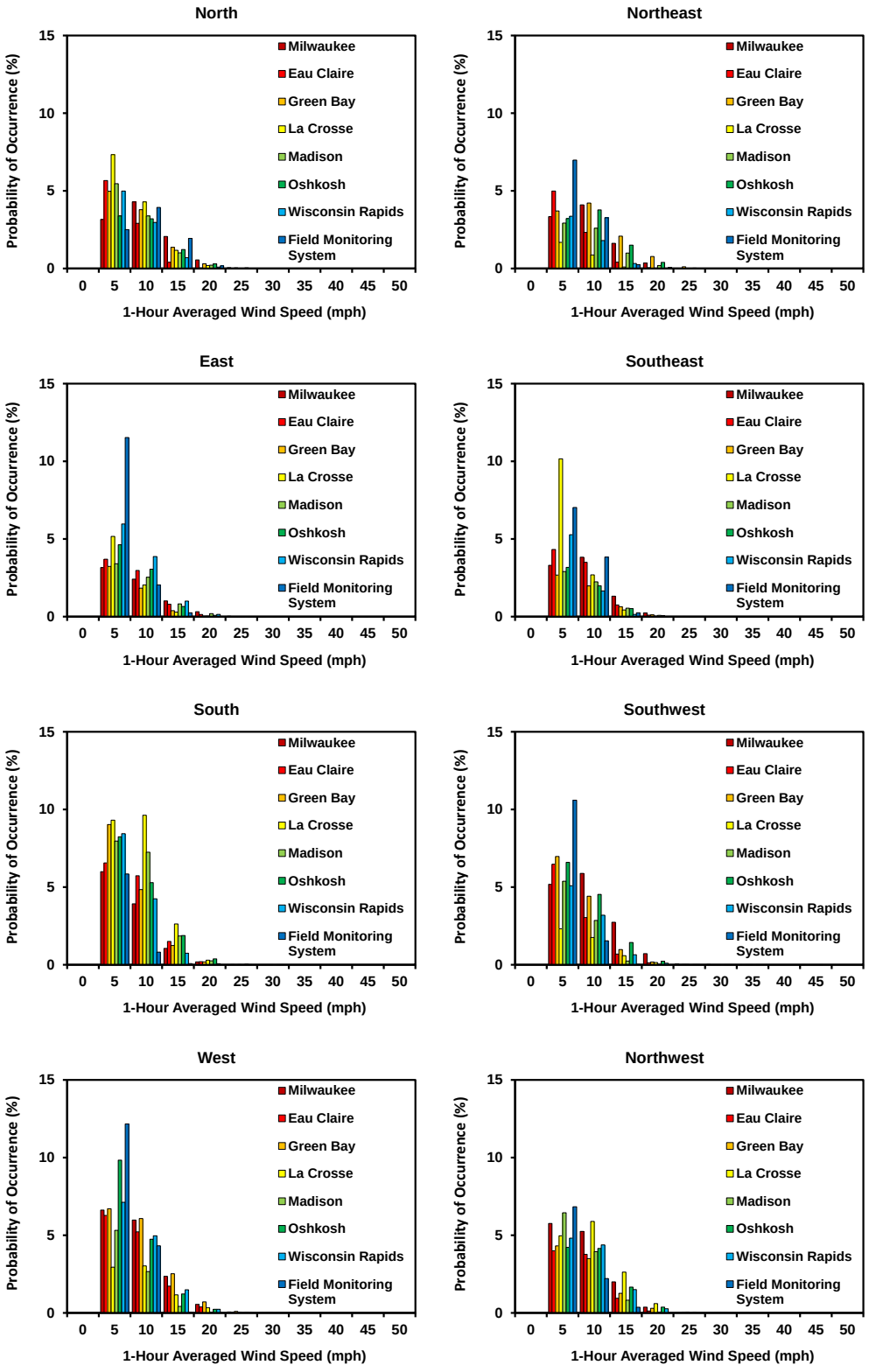

Figure 2.8. Combined probabilities for all NCDC-ASOS sites and the FMS site – $P(U = u_i \cap D = d_j)$.

Table 2.2. Combined probabilities for wind speed and wind direction from the Milwaukee NCDC-ASOS site – P ($U = u_i \cap D = d_j$).

		One-Hour Averaged Wind Direction - Probability of Occurrence									
		N/A	**North**	**Northeast**	**East**	**Southeast**	**South**	**Southwest**	**West**	**Northwest**	**SUM**
One-Hour Averaged Wind Speed (mph)	0	0.10061	0.00000	0.00000	0.00000	0.00000	0.00000	0.00000	0.00000	0.00000	0.10061
	5	0.00000	0.03158	0.03336	0.03158	0.03301	0.05995	0.05182	0.06621	0.05759	0.36510
	10	0.00000	0.04293	0.04099	0.02413	0.03825	0.03924	0.05880	0.05976	0.05251	0.35660
	15	0.00000	0.02063	0.01618	0.01015	0.01316	0.01055	0.02735	0.02362	0.01998	0.14163
	20	0.00000	0.00551	0.00355	0.00319	0.00241	0.00185	0.00720	0.00553	0.00374	0.03298
	25	0.00000	0.00053	0.00023	0.00026	0.00012	0.00010	0.00057	0.00064	0.00017	0.00263
	30	0.00000	0.00001	0.00004	0.00002	0.00000	0.00002	0.00022	0.00002	0.00001	0.00034
	35	0.00000	0.00000	0.00001	0.00005	0.00000	0.00000	0.00004	0.00000	0.00000	0.00010
	40	0.00000	0.00000	0.00000	0.00000	0.00000	0.00000	0.00000	0.00000	0.00000	0.00000
	45	0.00000	0.00000	0.00000	0.00000	0.00000	0.00000	0.00001	0.00000	0.00000	0.00001
	50	0.00000	0.00000	0.00000	0.00000	0.00000	0.00000	0.00000	0.00000	0.00000	0.00000
	55	0.00000	0.00000	0.00000	0.00000	0.00000	0.00000	0.00000	0.00000	0.00000	0.00000
	60	0.00000	0.00000	0.00000	0.00000	0.00000	0.00000	0.00000	0.00000	0.00000	0.00000
	65	0.00000	0.00000	0.00000	0.00000	0.00000	0.00000	0.00000	0.00000	0.00000	0.00000
	70	0.00000	0.00000	0.00000	0.00000	0.00000	0.00000	0.00000	0.00000	0.00000	0.00000
	75	0.00000	0.00000	0.00000	0.00000	0.00000	0.00000	0.00000	0.00000	0.00000	0.00000
	80	0.00000	0.00000	0.00000	0.00000	0.00000	0.00000	0.00000	0.00000	0.00000	0.00000
	SUM	0.10061	0.10119	0.09436	0.06939	0.08695	0.11171	0.14600	0.15579	0.13400	**1.00000**

Table 2.3. Combined probabilities for wind speed and wind direction from the Eau Claire NCDC-ASOS site – P ($U = u_i \cap D = d_j$).

		One-Hour Averaged Wind Direction - Probability of Occurrence									
		N/A	**North**	**Northeast**	**East**	**Southeast**	**South**	**Southwest**	**West**	**Northwest**	**SUM**
One-Hour Averaged Wind Speed (mph)	0	0.20084	0.00000	0.00000	0.00000	0.00000	0.00000	0.00000	0.00000	0.00000	0.20084
	5	0.00000	0.05660	0.04985	0.03697	0.04324	0.06559	0.06477	0.06275	0.03997	0.41975
	10	0.00000	0.02912	0.02325	0.02969	0.03497	0.05732	0.03039	0.05219	0.03770	0.29463
	15	0.00000	0.00402	0.00408	0.00801	0.00752	0.01502	0.00688	0.01725	0.00946	0.07224
	20	0.00000	0.00030	0.00051	0.00140	0.00100	0.00198	0.00130	0.00388	0.00128	0.01164
	25	0.00000	0.00001	0.00003	0.00002	0.00001	0.00012	0.00017	0.00033	0.00012	0.00080
	30	0.00000	0.00000	0.00000	0.00001	0.00001	0.00003	0.00001	0.00003	0.00000	0.00009
	35	0.00000	0.00000	0.00000	0.00000	0.00000	0.00000	0.00000	0.00000	0.00000	0.00000
	40	0.00000	0.00000	0.00000	0.00000	0.00000	0.00000	0.00000	0.00000	0.00001	0.00001
	45	0.00000	0.00000	0.00000	0.00000	0.00000	0.00000	0.00000	0.00000	0.00000	0.00000
	50	0.00000	0.00000	0.00000	0.00000	0.00000	0.00000	0.00000	0.00000	0.00000	0.00000
	55	0.00000	0.00000	0.00000	0.00000	0.00000	0.00000	0.00000	0.00000	0.00000	0.00000
	60	0.00000	0.00000	0.00000	0.00000	0.00000	0.00000	0.00000	0.00000	0.00000	0.00000
	65	0.00000	0.00000	0.00000	0.00000	0.00000	0.00000	0.00000	0.00000	0.00000	0.00000
	70	0.00000	0.00000	0.00000	0.00000	0.00000	0.00000	0.00000	0.00000	0.00000	0.00000
	75	0.00000	0.00000	0.00000	0.00000	0.00000	0.00000	0.00000	0.00000	0.00000	0.00000
	80	0.00000	0.00000	0.00000	0.00000	0.00000	0.00000	0.00000	0.00000	0.00000	0.00000
	SUM	0.20084	0.09005	0.07772	0.07610	0.08674	0.14005	0.10353	0.13642	0.08855	**1.00000**

Table 2.4. Combined probabilities for wind speed and wind direction from the Green Bay NCDC-ASOS site – P ($U = u_i \cap D = d_j$).

		One-Hour Averaged Wind Direction - Probability of Occurrence									
		N/A	**North**	**Northeast**	**East**	**Southeast**	**South**	**Southwest**	**West**	**Northwest**	**SUM**
One-Hour Averaged Wind Speed (mph)	0	0.14328	0.00000	0.00000	0.00000	0.00000	0.00000	0.00000	0.00000	0.00000	0.14328
	5	0.00000	0.04970	0.03706	0.03236	0.02678	0.09027	0.06969	0.06703	0.04316	0.41605
	10	0.00000	0.03783	0.04217	0.01838	0.01978	0.04842	0.04410	0.06072	0.03494	0.30633
	15	0.00000	0.01363	0.02081	0.00385	0.00638	0.01244	0.00977	0.02525	0.01265	0.10478
	20	0.00000	0.00303	0.00772	0.00030	0.00116	0.00190	0.00178	0.00708	0.00295	0.02593
	25	0.00000	0.00041	0.00110	0.00003	0.00015	0.00007	0.00021	0.00095	0.00032	0.00324
	30	0.00000	0.00008	0.00008	0.00000	0.00001	0.00002	0.00003	0.00011	0.00001	0.00034
	35	0.00000	0.00000	0.00000	0.00000	0.00000	0.00000	0.00001	0.00001	0.00002	0.00003
	40	0.00000	0.00000	0.00000	0.00000	0.00000	0.00000	0.00000	0.00001	0.00000	0.00001
	45	0.00000	0.00000	0.00000	0.00000	0.00000	0.00000	0.00000	0.00000	0.00000	0.00000
	50	0.00000	0.00000	0.00000	0.00000	0.00000	0.00000	0.00000	0.00000	0.00000	0.00000
	55	0.00000	0.00000	0.00000	0.00000	0.00000	0.00001	0.00000	0.00000	0.00000	0.00001
	60	0.00000	0.00000	0.00000	0.00000	0.00000	0.00000	0.00000	0.00000	0.00000	0.00000
	65	0.00000	0.00000	0.00000	0.00000	0.00000	0.00000	0.00000	0.00000	0.00000	0.00000
	70	0.00000	0.00000	0.00000	0.00000	0.00000	0.00000	0.00000	0.00000	0.00000	0.00000
	75	0.00000	0.00000	0.00000	0.00000	0.00000	0.00000	0.00000	0.00000	0.00000	0.00000
	80	0.00000	0.00000	0.00000	0.00000	0.00000	0.00000	0.00000	0.00000	0.00000	0.00000
	SUM	0.14328	0.10468	0.10895	0.05492	0.05426	0.15312	0.12559	0.16116	0.09405	**1.00000**

Table 2.5. Combined probabilities for wind speed and wind direction from the La Crosse NCDC-ASOS site – P ($U = u_i \cap D = d_j$).

		One-Hour Averaged Wind Direction - Probability of Occurrence									
		N/A	**North**	**Northeast**	**East**	**Southeast**	**South**	**Southwest**	**West**	**Northwest**	**SUM**
One-Hour Averaged Wind Speed (mph)	0	0.15155	0.00000	0.00000	0.00000	0.00000	0.00000	0.00000	0.00000	0.00000	0.15155
	5	0.00000	0.07332	0.01681	0.05167	0.10155	0.09310	0.02321	0.02947	0.04966	0.43878
	10	0.00000	0.04292	0.00872	0.02034	0.02692	0.09624	0.01757	0.03026	0.05890	0.30187
	15	0.00000	0.01171	0.00100	0.00293	0.00426	0.02625	0.00590	0.01165	0.02630	0.08999
	20	0.00000	0.00197	0.00004	0.00035	0.00030	0.00294	0.00143	0.00329	0.00602	0.01634
	25	0.00000	0.00008	0.00000	0.00003	0.00002	0.00012	0.00019	0.00036	0.00054	0.00133
	30	0.00000	0.00000	0.00000	0.00000	0.00000	0.00001	0.00002	0.00004	0.00005	0.00012
	35	0.00000	0.00000	0.00000	0.00000	0.00000	0.00000	0.00002	0.00000	0.00000	0.00002
	40	0.00000	0.00000	0.00000	0.00000	0.00000	0.00000	0.00000	0.00000	0.00000	0.00000
	45	0.00000	0.00000	0.00000	0.00001	0.00000	0.00000	0.00000	0.00000	0.00000	0.00001
	50	0.00000	0.00000	0.00000	0.00000	0.00000	0.00000	0.00000	0.00000	0.00000	0.00000
	55	0.00000	0.00000	0.00000	0.00000	0.00000	0.00000	0.00000	0.00000	0.00000	0.00000
	60	0.00000	0.00000	0.00000	0.00000	0.00000	0.00000	0.00000	0.00000	0.00000	0.00000
	65	0.00000	0.00000	0.00000	0.00000	0.00000	0.00000	0.00000	0.00000	0.00000	0.00000
	70	0.00000	0.00000	0.00000	0.00000	0.00000	0.00000	0.00000	0.00000	0.00000	0.00000
	75	0.00000	0.00000	0.00000	0.00000	0.00000	0.00000	0.00000	0.00000	0.00000	0.00000
	80	0.00000	0.00000	0.00000	0.00000	0.00000	0.00000	0.00000	0.00000	0.00000	0.00000
	SUM	0.15155	0.13000	0.02656	0.07533	0.13305	0.21866	0.04832	0.07506	0.14147	**1.00000**

Table 2.6. Combined probabilities for wind speed and wind direction from the Madison NCDC-ASOS site – P ($U = u_i \cap D = d_j$).

		One-Hour Averaged Wind Direction - Probability of Occurrence									
		N/A	**North**	**Northeast**	**East**	**Southeast**	**South**	**Southwest**	**West**	**Northwest**	**SUM**
One-Hour Averaged Wind Speed (mph)	0	0.24889	0.00000	0.00000	0.00000	0.00000	0.00000	0.00000	0.00000	0.00000	0.24889
	5	0.00000	0.05464	0.02925	0.03404	0.02901	0.07964	0.05377	0.05318	0.06446	0.39800
	10	0.00000	0.03388	0.02592	0.02536	0.02241	0.07249	0.02859	0.02659	0.03946	0.27470
	15	0.00000	0.01010	0.00997	0.00822	0.00543	0.01854	0.00242	0.00424	0.00820	0.06711
	20	0.00000	0.00211	0.00193	0.00192	0.00081	0.00258	0.00035	0.00037	0.00059	0.01066
	25	0.00000	0.00016	0.00014	0.00010	0.00004	0.00010	0.00003	0.00001	0.00000	0.00058
	30	0.00000	0.00002	0.00001	0.00001	0.00000	0.00000	0.00000	0.00000	0.00001	0.00004
	35	0.00000	0.00001	0.00000	0.00000	0.00000	0.00000	0.00000	0.00000	0.00000	0.00001
	40	0.00000	0.00001	0.00000	0.00000	0.00000	0.00000	0.00000	0.00000	0.00000	0.00001
	45	0.00000	0.00000	0.00000	0.00000	0.00000	0.00000	0.00000	0.00000	0.00000	0.00000
	50	0.00000	0.00000	0.00000	0.00000	0.00000	0.00000	0.00000	0.00000	0.00000	0.00000
	55	0.00000	0.00000	0.00000	0.00000	0.00000	0.00000	0.00000	0.00000	0.00000	0.00000
	60	0.00000	0.00000	0.00000	0.00000	0.00000	0.00000	0.00000	0.00000	0.00000	0.00000
	65	0.00000	0.00000	0.00000	0.00000	0.00000	0.00000	0.00000	0.00000	0.00000	0.00000
	70	0.00000	0.00000	0.00000	0.00000	0.00000	0.00000	0.00000	0.00000	0.00000	0.00000
	75	0.00000	0.00000	0.00000	0.00000	0.00000	0.00000	0.00000	0.00000	0.00000	0.00000
	80	0.00000	0.00000	0.00000	0.00000	0.00000	0.00000	0.00000	0.00000	0.00000	0.00000
	SUM	0.24889	0.10094	0.06722	0.06965	0.05770	0.17334	0.08515	0.08439	0.11272	**1.00000**

Table 2.7. Combined probabilities for wind speed and wind direction from the Oshkosh NCDC-ASOS site – P ($U = u_i \cap D = d_j$).

		One-Hour Averaged Wind Direction - Probability of Occurrence									
		N/A	**North**	**Northeast**	**East**	**Southeast**	**South**	**Southwest**	**West**	**Northwest**	**SUM**
One-Hour Averaged Wind Speed (mph)	0	0.13618	0.00000	0.00000	0.00000	0.00000	0.00000	0.00000	0.00000	0.00000	0.13618
	5	0.00000	0.03384	0.03214	0.04629	0.03170	0.08238	0.06596	0.09835	0.04218	0.43284
	10	0.00000	0.03202	0.03770	0.03057	0.01985	0.05291	0.04530	0.04746	0.04154	0.30735
	15	0.00000	0.01222	0.01504	0.00658	0.00519	0.01884	0.01436	0.01218	0.01660	0.10100
	20	0.00000	0.00295	0.00395	0.00086	0.00073	0.00380	0.00231	0.00234	0.00371	0.02065
	25	0.00000	0.00040	0.00028	0.00000	0.00001	0.00034	0.00017	0.00026	0.00032	0.00178
	30	0.00000	0.00006	0.00000	0.00000	0.00000	0.00002	0.00006	0.00002	0.00001	0.00015
	35	0.00000	0.00000	0.00000	0.00000	0.00000	0.00000	0.00002	0.00000	0.00001	0.00002
	40	0.00000	0.00000	0.00000	0.00000	0.00000	0.00000	0.00000	0.00000	0.00000	0.00000
	45	0.00000	0.00000	0.00000	0.00000	0.00000	0.00000	0.00001	0.00000	0.00000	0.00001
	50	0.00000	0.00000	0.00000	0.00000	0.00000	0.00000	0.00000	0.00000	0.00000	0.00000
	55	0.00000	0.00000	0.00000	0.00000	0.00000	0.00000	0.00000	0.00000	0.00000	0.00000
	60	0.00000	0.00000	0.00000	0.00000	0.00000	0.00000	0.00000	0.00000	0.00000	0.00000
	65	0.00000	0.00000	0.00000	0.00000	0.00000	0.00000	0.00000	0.00000	0.00000	0.00000
	70	0.00000	0.00000	0.00000	0.00000	0.00000	0.00000	0.00000	0.00000	0.00000	0.00000
	75	0.00000	0.00000	0.00000	0.00000	0.00000	0.00000	0.00000	0.00000	0.00000	0.00000
	80	0.00000	0.00000	0.00000	0.00000	0.00000	0.00000	0.00000	0.00000	0.00000	0.00000
	SUM	0.13618	0.08149	0.08911	0.08431	0.05748	0.15828	0.12817	0.16061	0.10437	**1.00000**

Table 2.8. Combined probabilities for wind speed and wind direction from the Wisconsin Rapids NCDC-ASOS site – P ($U = u_i \cap D = d_j$).

		One-Hour Averaged Wind Direction - Probability of Occurrence									
		N/A	North	Northeast	East	Southeast	South	Southwest	West	Northwest	SUM
One-Hour Averaged Wind Speed (mph)	0	0.20314	0.00000	0.00000	0.00000	0.00000	0.00000	0.00000	0.00000	0.00000	0.20314
	5	0.00000	0.04988	0.03368	0.05968	0.05277	0.08439	0.05087	0.07120	0.04815	0.45062
	10	0.00000	0.02968	0.01803	0.03868	0.01655	0.04249	0.03192	0.04963	0.04376	0.27074
	15	0.00000	0.00698	0.00322	0.01000	0.00146	0.00748	0.00646	0.01490	0.01505	0.06554
	20	0.00000	0.00094	0.00025	0.00143	0.00005	0.00069	0.00106	0.00232	0.00267	0.00940
	25	0.00000	0.00004	0.00002	0.00004	0.00000	0.00007	0.00014	0.00012	0.00010	0.00052
	30	0.00000	0.00000	0.00000	0.00000	0.00000	0.00002	0.00001	0.00000	0.00000	0.00003
	35	0.00000	0.00000	0.00000	0.00000	0.00000	0.00000	0.00000	0.00000	0.00000	0.00000
	40	0.00000	0.00000	0.00000	0.00000	0.00000	0.00000	0.00000	0.00000	0.00000	0.00000
	45	0.00000	0.00000	0.00000	0.00000	0.00000	0.00000	0.00000	0.00000	0.00000	0.00000
	50	0.00000	0.00000	0.00000	0.00000	0.00000	0.00000	0.00000	0.00000	0.00000	0.00000
	55	0.00000	0.00000	0.00000	0.00000	0.00000	0.00000	0.00000	0.00000	0.00000	0.00000
	60	0.00000	0.00000	0.00000	0.00000	0.00000	0.00000	0.00000	0.00000	0.00000	0.00000
	65	0.00000	0.00000	0.00000	0.00000	0.00000	0.00000	0.00000	0.00000	0.00000	0.00000
	70	0.00000	0.00000	0.00000	0.00000	0.00000	0.00000	0.00000	0.00000	0.00000	0.00000
	75	0.00000	0.00000	0.00000	0.00000	0.00000	0.00000	0.00000	0.00000	0.00000	0.00000
	80	0.00000	0.00000	0.00000	0.00000	0.00000	0.00000	0.00000	0.00000	0.00000	0.00000
	SUM	0.20314	0.08751	0.05520	0.10983	0.07082	0.13515	0.09045	0.13817	0.10973	**1.00000**

Table 2.9. Combined probabilities for wind speed and wind direction from the FMS site – P ($U = u_i \cap D = d_j$).

		One-Hour Averaged Wind Direction - Probability of Occurrence									
		N/A	North	Northeast	East	Southeast	South	Southwest	West	Northwest	SUM
One-Hour Averaged Wind Speed (mph)	0	0.11133	0.00000	0.00000	0.00000	0.00000	0.00000	0.00000	0.00000	0.00000	0.11133
	5	0.00000	0.02507	0.06980	0.11526	0.07029	0.05849	0.10592	0.12165	0.06832	0.63480
	10	0.00000	0.03932	0.03269	0.02040	0.03834	0.00811	0.01548	0.04325	0.02212	0.21971
	15	0.00000	0.01942	0.00246	0.00246	0.00246	0.00074	0.00025	0.00025	0.00369	0.03170
	20	0.00000	0.00172	0.00074	0.00000	0.00000	0.00000	0.00000	0.00000	0.00000	0.00246
	25	0.00000	0.00000	0.00000	0.00000	0.00000	0.00000	0.00000	0.00000	0.00000	0.00000
	30	0.00000	0.00000	0.00000	0.00000	0.00000	0.00000	0.00000	0.00000	0.00000	0.00000
	35	0.00000	0.00000	0.00000	0.00000	0.00000	0.00000	0.00000	0.00000	0.00000	0.00000
	40	0.00000	0.00000	0.00000	0.00000	0.00000	0.00000	0.00000	0.00000	0.00000	0.00000
	45	0.00000	0.00000	0.00000	0.00000	0.00000	0.00000	0.00000	0.00000	0.00000	0.00000
	50	0.00000	0.00000	0.00000	0.00000	0.00000	0.00000	0.00000	0.00000	0.00000	0.00000
	55	0.00000	0.00000	0.00000	0.00000	0.00000	0.00000	0.00000	0.00000	0.00000	0.00000
	60	0.00000	0.00000	0.00000	0.00000	0.00000	0.00000	0.00000	0.00000	0.00000	0.00000
	65	0.00000	0.00000	0.00000	0.00000	0.00000	0.00000	0.00000	0.00000	0.00000	0.00000
	70	0.00000	0.00000	0.00000	0.00000	0.00000	0.00000	0.00000	0.00000	0.00000	0.00000
	75	0.00000	0.00000	0.00000	0.00000	0.00000	0.00000	0.00000	0.00000	0.00000	0.00000
	80	0.00000	0.00000	0.00000	0.00000	0.00000	0.00000	0.00000	0.00000	0.00000	0.00000
	SUM	0.11133	0.08552	0.10568	0.13812	0.11108	0.06734	0.12165	0.16515	0.09413	**1.00000**

Dataset Length and Topography Effects

The field monitoring station data provided the opportunity to evaluate the impact of dataset length on resulting statistical analyses. The effects of topography at locations where sign support structures are likely to exist when compared to locations where wind speed data is likely to come from (*i.e.* the NCDC-ASOS sites) was also studied. The following discussion addresses dataset length and topography effects on the resulting wind models.

Three distinct datasets were isolated for a detailed comparison. Two datasets from the Mitchell International NCDC-ASOS site were considered. The first was composed of hourly weather data records for all years indicated in Table 2.1 and is signified by Milwaukee (1998-2011). The second includes data for the time period in which the FMS was in service and is signified by Milwaukee (2010). The last of the three datasets was that obtained from the field monitoring station signified by FMS. The probability mass functions for the natural wind speed data are shown in Figure 2.9 and the wind rose histograms for the natural wind direction data are shown in Figure 2.10.

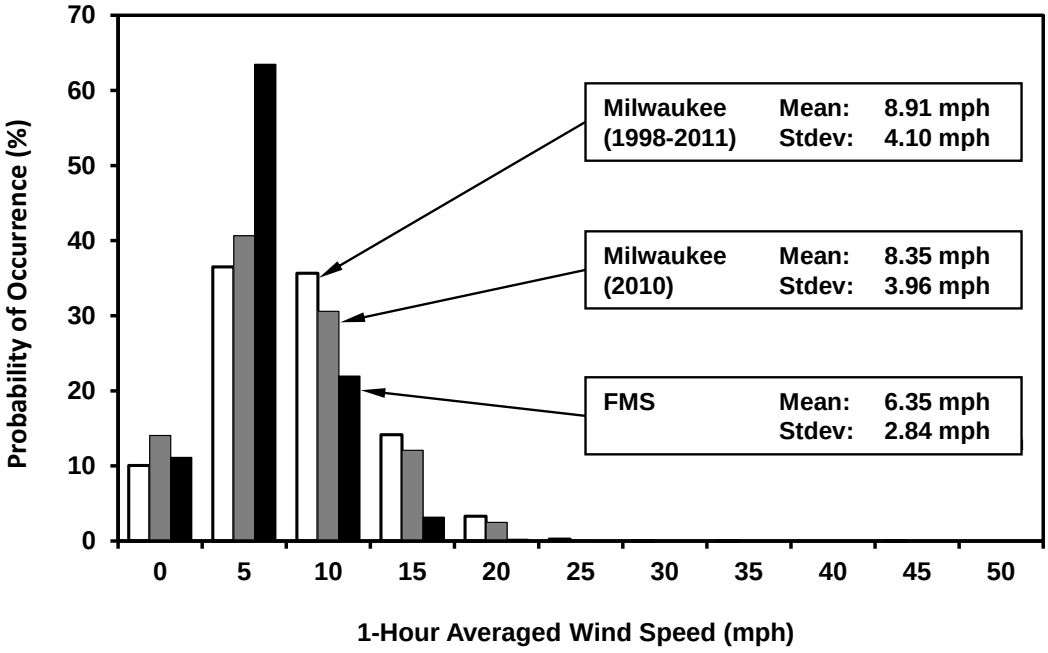

Figure 2.9. Individual one-Hour wind speed histograms from Milwaukee NCDC-ASOS site and the FMS site – P ($U = u_i$).

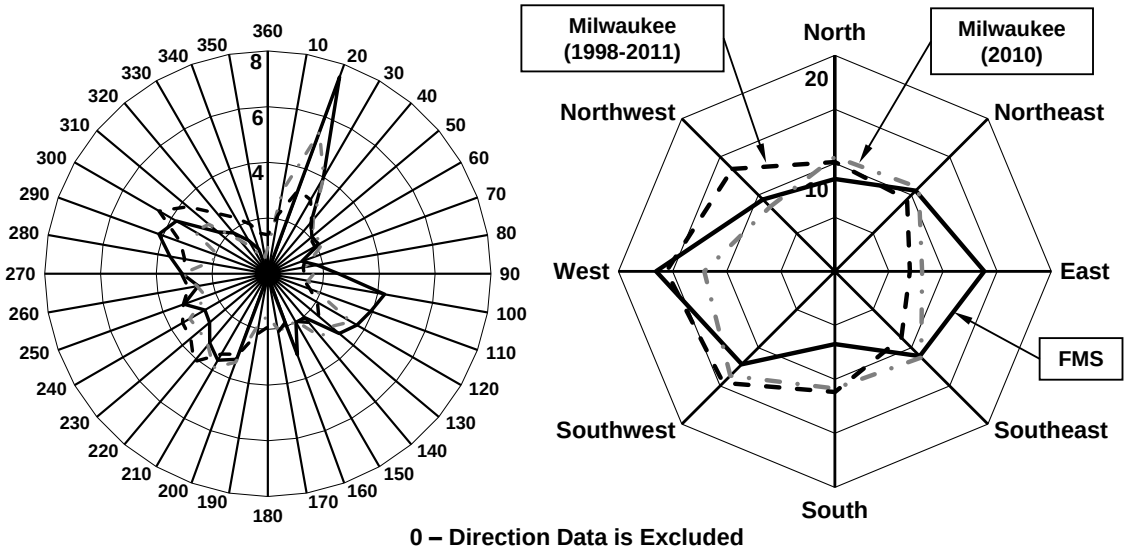

Figure 2.10. Individual one-hour wind rose histograms from Milwaukee NCDC-ASOS site and the FMS site (note: legends for both wind roses on right wind rose) – P ($D = d_j$).

The histograms in Figure 2.9 indicate a very similar distribution of wind speeds. The mean wind speed and standard deviation for the Milwaukee (1998-2011) data and the data in the 6-month sampling window Milwaukee (2010) are very similar to one another. This indicates that in just six months, a reasonable estimate for wind speed and direction variability can be approximated. However, it is recommended to use longer sampling periods to improve the model and provide the most accurate distributions of wind speed. The magnitude of the most frequently occurring wind speed at the field monitoring site is slightly less than the magnitude of the most frequently occurring wind speed at the NCDC-ASOS site. There is also a slightly smaller standard deviation in the sample data for the field monitored site.

It is widely known that topography has an effect on wind speed. Design provisions (ASCE 2005) require that topographical conditions be considered. Exposure categories with unique surface roughness characteristics have been defined to differentiate between flat, open terrain as seen at airports (Surface Roughness C) and that of terrain with many, closely spaced

obstructions as seen in urban and suburban areas (Surface Roughness B). Site topologies for all locations considered in the present study are provided in Figure 2.11 (note that the two sites being compared in the present discussion are at the top of Figure 2.11).

The differences in what is seen between the wind speed probability mass functions shown in Figure 2.9 can be evaluated by looking at them in conjunction with Figure 2.11. The apparently open grassy area in the middle of a city (Figure 2.2) has significantly different topography when compared to NCDC-ASOS sites that are often located at airports as seen in Figure 2.11. Figure 2.11 clearly indicates that the FMS site does not have the same surrounding topology as the NCDC-ASOS site at Mitchell International Airport (or any of the NCDC-ASOS sites for that matter) and therefore, differences are expected in the wind speed magnitude. It is clear that some locations where sign structures are in service (*e.g.* FMS site) will likely experience lower wind speed magnitudes when compared to locations where wind speed data is typically collected (*e.g.* NCDC-ASOS sites).

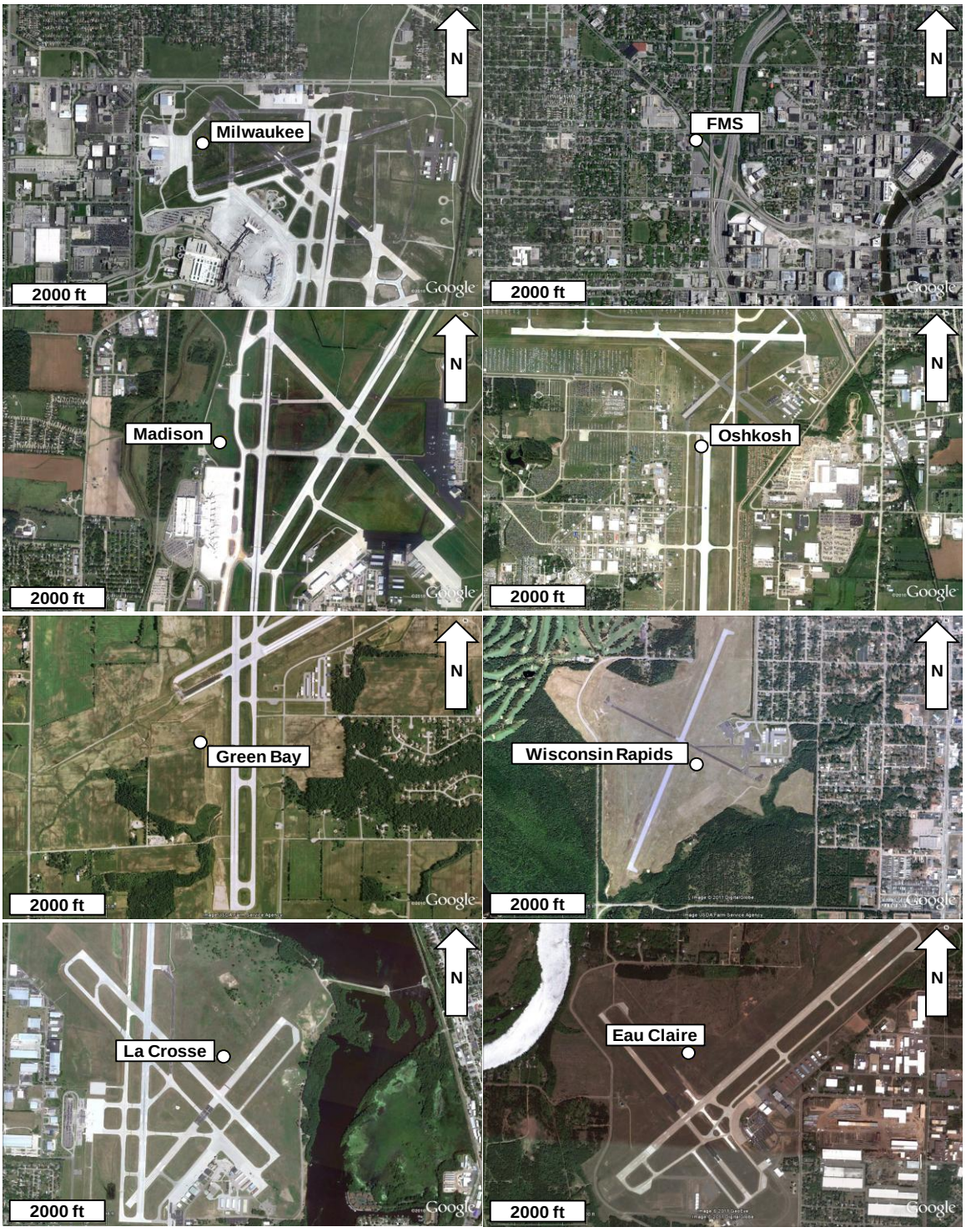

Figure 2.11. Aerial Photos of the Wisconsin NCDC-ASOS sites and the FMS site (Google 2012).

The wind rose histograms shown in Figure 2.10 illustrate that while the Milwaukee (2010) data tends to have larger peaks at some 10-degree orientations, the fundamental shape of the wind rose remains consistent. It is expected that if more data were collected at the FMS site, the wind roses with 10-degree resolutions would approach a similar configuration. When the eight cardinal directions are utilized, the wind roses take on slightly different shapes. The peaks and valleys seen in the 10-degree resolution wind roses are softened in favor of a more egalitarian distribution of wind directions among the eight possibilities. From this comparison, it is clear that neither sample size, nor surrounding site topology, have a significant effect on the resulting wind direction, but there is an effect on wind speeds.

A statement can be made based upon the results studied in this section. Wind speeds at a local site where a sign structure is typically in service (*e.g.* an FMS site in an urban environment with many closely-spaced surrounding obstructions to wind flow) will likely have a lower mean wind speed than the location where the wind speed data are collected (*e.g.* NCDC-ASOS site with flat, open terrain). It should be noted that this statement is heavily dependent upon the surrounding site characteristics. Furthermore, wind directions will not differ significantly from the location where the sign is in service when compared to the location where data is obtained.

The comparison between these three sample datasets was continued by looking at both conditional and combined probabilities in the form of probability mass functions. Figures 2.12 and 2.13 illustrate the variation among each of the designated cardinal directions for conditional and combined probabilities, respectively.

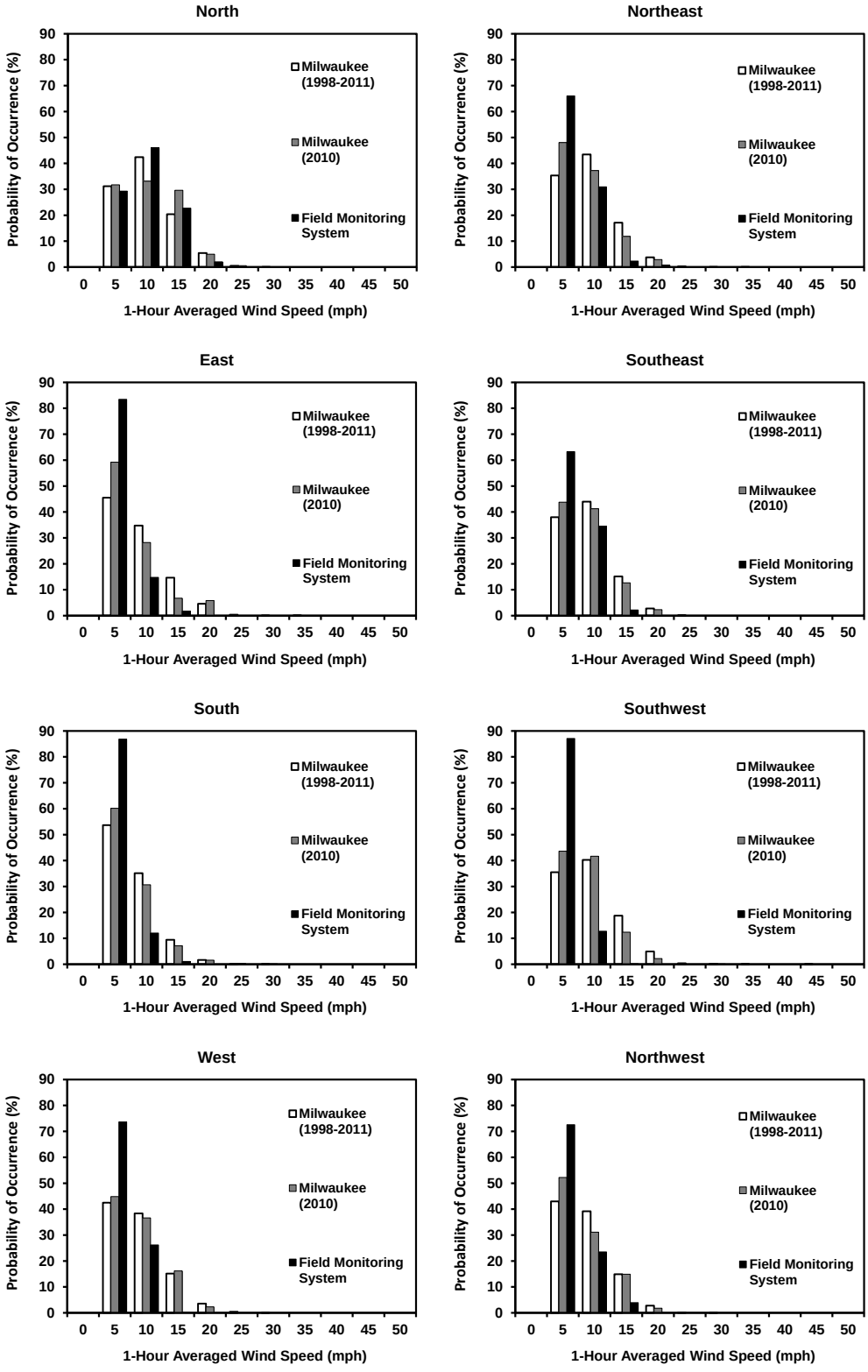

Figure 2.12. Variation between conditional probabilities of Milwaukee NCDC-ASOS site and the FMS site – P ($U = u_i \mid D = d_j$).

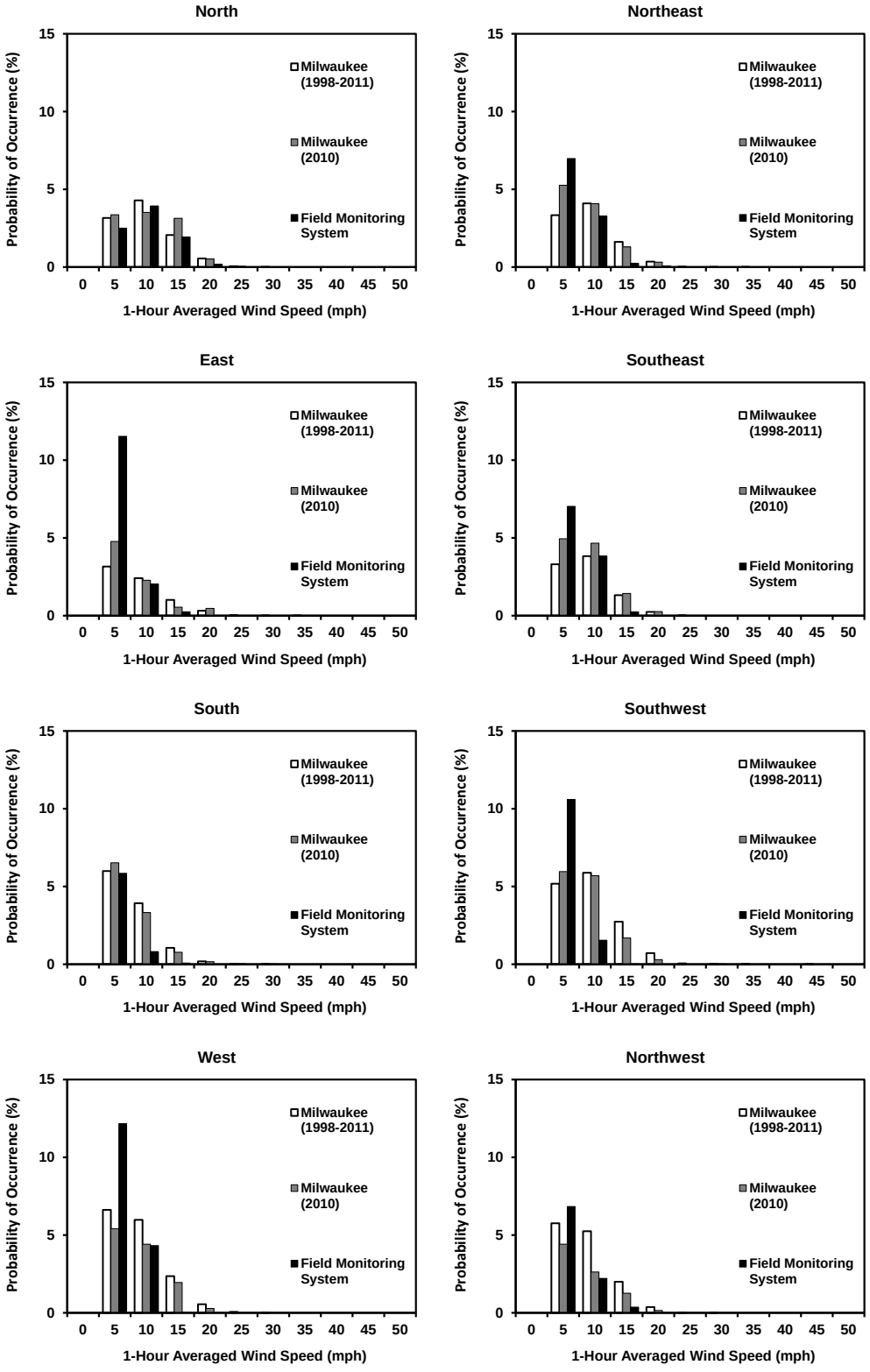

Figure 2.13. Variation between combined probabilities of Milwaukee NCDC-ASOS site and the FMS site – P ($U = u_i \cap D = d_j$).

Overall, the shapes of the probability mass functions for each type of probability and for each designated direction look very similar between the three sample datasets. There is a more notable difference between the Milwaukee NCDC-ASOS data (both sets) and that of the FMS. However, this can be attributed to the differences in surrounding topology between the two sites (as indicated by the top two aerial photos of Figure 2.11).

At this point, all statistical analysis regarding wind speed and direction variability has been conducted and the results have been synthesized into the form of combined probabilities for wind speed and wind direction. It is essential to note that the information provided thus far is specific to the discrete locations where either NCDC-ASOS stations or the FMS measured the wind data. With the exception of the FMS, all of the sites where wind data was obtained are at some distance away from surrounding sign support structures. If the goal is to determine what the wind demand uncertainty is at some location where a sign support structure exists, then a major question arises. Which table of combined probabilities should be used when the sign structure location of interest is remote from the locations of measured data? Should the combined probabilities from the closest NCDC-ASOS site be used, or perhaps, should the combined probabilities (*i.e.* probabilities of intersection) from multiple surrounding NCDC-ASOS sites be used? The following discussion will seek to answer these questions.

2.4 – Virtual Weather Station Probabilistic Model

This section seeks to present a methodology for creating tables of combined probabilities of wind speed and wind direction at locations away from NCDC-ASOS sites where data regarding wind speed and wind direction will be monitored and assembled. Previous research in the pavement arena has led to the development of an interpolation method used for determining climatic parameters at desired locations where such parameters are not measured. A version of this procedure has been presented in a paper by Diekfuss and Foley (2012). Since the presentation of

this paper, modifications have been made to the model and will be addressed in the subsequent sections.

The Enhanced Integrated Climatic Model (EICM) contained within the Mechanistic-Empirical Pavement Design Guide (MEPDG) provides users the ability to generate a virtual weather station (VWS) using selected data from automated weather stations (AWS) in surrounding areas (*i.e.* ASOS stations). The interpolation method establishes weights for the climatic parameters of a particular AWS based upon the distance it is away from the VWS being generated (Li et al. 2010),

$$U_m = \frac{\sum_{k=1}^{n}\left(\frac{U_{mk}}{R_k}\right)}{\sum_{k=1}^{n}\left(\frac{1}{R_k}\right)} \tag{2.9}$$

where: U_m is the calculated virtual weather data element (*e.g.* relative humidity, temperature, dew point, etc.) for day *m*; *n* is the number of weather stations for VWS interpolation; U_{mk} is the value of a data element on day *m* for weather station *k*; and R_k is the distance of weather station *k* from the virtual weather station. It was recommended that certain weather stations be omitted if they had surrounding topography that was much different than that expected at the VWS being generated, even if they are closer in proximity to the VWS than others (Li et al. 2010). Because the contributing combined probabilities of wind speed and wind direction are limited to the locations where wind data is collected (*i.e.* NCDC-ASOS sites) and since the sites where data is collected clearly does not have similar site topography/topology, this recommendation is ignored in the subsequent interpolation computations.

The results of the synthesis of wind data up to this point has yielded combined probabilities of wind speed and wind direction at several discrete locations around the state of

Wisconsin. In order to make the interpolation procedure given in equation (2.9) directly applicable within the present research effort, it needed to be modified to reflect the interpolation of combined probabilities rather than climatic parameters. Therefore, the combined probabilities of wind speed and wind direction at any remote location around the state of Wisconsin may be determined using,

$$P(U=u_i \cap D=d_j)_m = \frac{\sum_{k=1}^{n}\left(\frac{P(U=u_i \cap D=d_j)_k}{R_k}\right)}{\sum_{k=1}^{n}\left(\frac{1}{R_k}\right)} \tag{2.10}$$

where: $P(U=u_i \cap D=d_j)_m$ is a table of interpolated combined probabilities of wind speed and direction for remote location *m*; *n* is the number of weather stations used in the VWS interpolation; $P(U=u_i \cap D=d_j)_k$ is the table of combined probabilities from NCDC-ASOS site *k*; and R_k is the distance of NCDC-ASOS site *k* from remote location *m*.

Prior to the implementation of the MEPDG interpolation method, a systematic method for determining the vector distances between the ASOS sites and potential VWS sites needed to be defined. The distances utilized in this procedure were determined using the latitude and longitude coordinates from each ASOS site. In order to provide the most accurate measure of distance between the potential VWS and each of the NCDC-ASOS sites used for interpolation, consideration was given to the fact that the earth is spherical (approximately) in nature. Therefore, curvature must be accounted for in the distance measurement. The following section will describe the procedure used to determine the vector distances between the NCDC-ASOS sites and a potential VWS site within the context of an example.

Consider an example VWS site located northeast of the Wisconsin Rapids NCDC-ASOS site. Figure 2.14 shows a map of Wisconsin that provides the latitude and longitude coordinates

for each ASOS site, as well as the resulting vector distance for each ASOS site from the example VWS site.

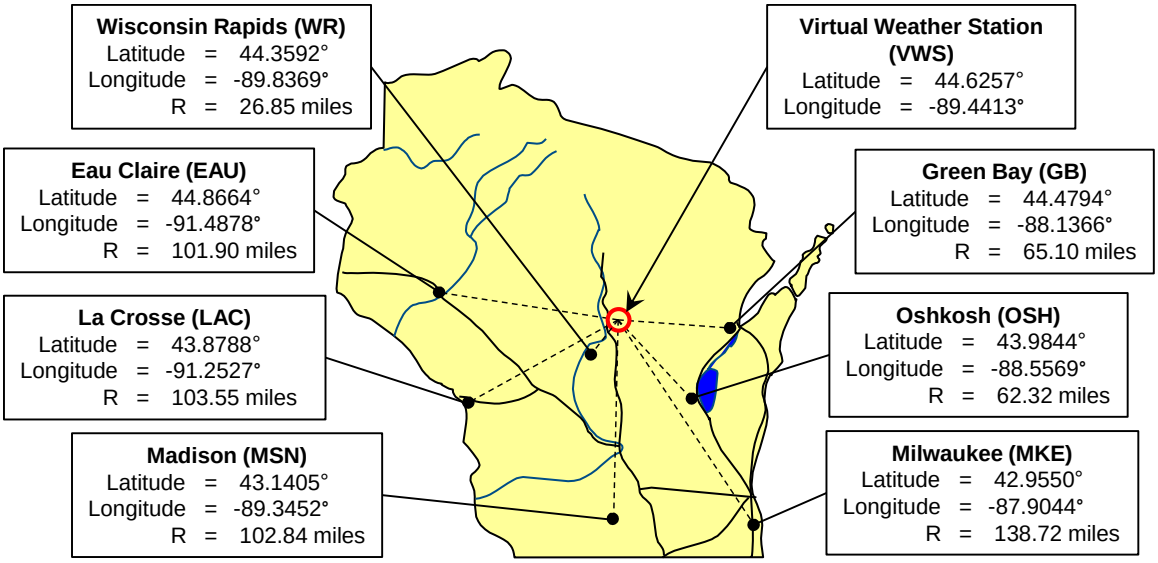

Figure 2.14. Map of Wisconsin listing the NCDC-ASOS wind data collection sites with corresponding latitudes and longitudes as well as their respective vector distance to the example VWS site.

The distance between any two points on the earth's surface is not a straight line, but rather a great-circle distance (Type 2012). Therefore, the spherical law of cosines should be employed to account for the curvature of the earth:

$$R_k = \cos^{-1}\left(\begin{array}{l}\sin\left(Lat_{VWS}\right)\cdot\sin\left(Lat_{ASOSk}\right)\\ +\cos\left(Lat_{VWS}\right)\cdot\cos\left(Lat_{ASOSk}\right)\cdot\cos\left(Lon_{ASOSk}-Lon_{VWS}\right)\end{array}\right)\cdot R_E \qquad (2.11)$$

where: R_E is the earth's radius (approximated as 3,693 miles); Lat_{VWS} and Lon_{VWS} are the latitude and longitude coordinates (in radians) for the VWS site, respectively; Lat_{ASOSk} and Lon_{ASOSk} are the latitude and longitude coordinates (in radians) for NCDC-ASOS site *k*, respectively. This procedure has two very important assumptions:

1. The earth is assumed to be a perfect sphere when in fact it is slightly ellipsoidal;

2. The end points, between which distance is determined, are assumed to be at an equal distance from the center of the spherical earth (*i.e.* there is no account for change in elevation between two points). It should be noted that differences in elevation between ASOS sites and VWS sites are accounted for in the simulation of site specific wind speed histories using the Power Law. This is discussed in chapter five of the dissertation.

The VWS interpolation procedure was assessed by comparing combined probabilities of wind speed and wind direction for each of the seven ASOS sites using the combined probabilities from the surrounding ASOS sites. Two interpolation cases were conducted for each site. Interpolation Case 1 applies the VWS procedure utilizing the combined probabilities from the single closest ASOS site. Carrying out the VWS procedure with combined probabilities from a single site will result in the exact combined probabilities that were input. Therefore, Interpolation Case 1 may be thought of as using the combined probabilities of the closest NCDC-ASOS site without modification, regardless of the actual distance between the remote location and the location where the data was measured. Interpolation Case 2 applies the VWS procedure utilizing the tables of combined probabilities from all surrounding ASOS sites (not including the combined probabilities from the ASOS site being assessed). The parameters for this interpolation case used the distance and combined probabilities from the other six cities.

Figures 2.15 through 2.21 provide the resulting combined probabilities in the form of direction-specific probability mass functions for each of the seven cities as well as the resulting interpolated models from both cases. Qualitatively, these figures indicate that the interpolation procedure works reasonably well for all wind directions. Looking at these figures in conjunction with Figure 2.11 illustrates that when NCDC-ASOS site topology is present at all locations where the virtual weather station is to be created, very good results occur.

Figure 2.22 illustrates application of the interpolation procedure to the field monitoring

station site. Recall, the FMS site recorded wind speed data for 6 months and this data allows the interpolation procedure to be evaluated for a site where data has been acquired, but is not an ASOS site. It should be emphasized that the FMS site has significantly different topology when compared to the sites from which the interpolated data originates (ASOS sites). Figure 2.22 illustrates that the interpolated combined probabilities provide greater wind speed density at higher wind speed magnitudes than should be expected. This should not be a problem, however, because providing greater probability density at higher wind speed magnitudes than will actually occur can be thought of as an estimate on the conservative side. It should be noted that these results are based upon comparisons to measured data from a single FMS site. It should be expected that FMS sites located in flat, open terrain will provide distributions of wind speed that approach those of the ASOS sites. However, most sign support structures are located in urban and suburban environments. Thus, the VWS procedure is suitable for generating the foundational wind speed probability models at a site where a sign structure is typically located. However, all of the Figures, 2.7 through 2.22, indicate that local topology effects should be considered.

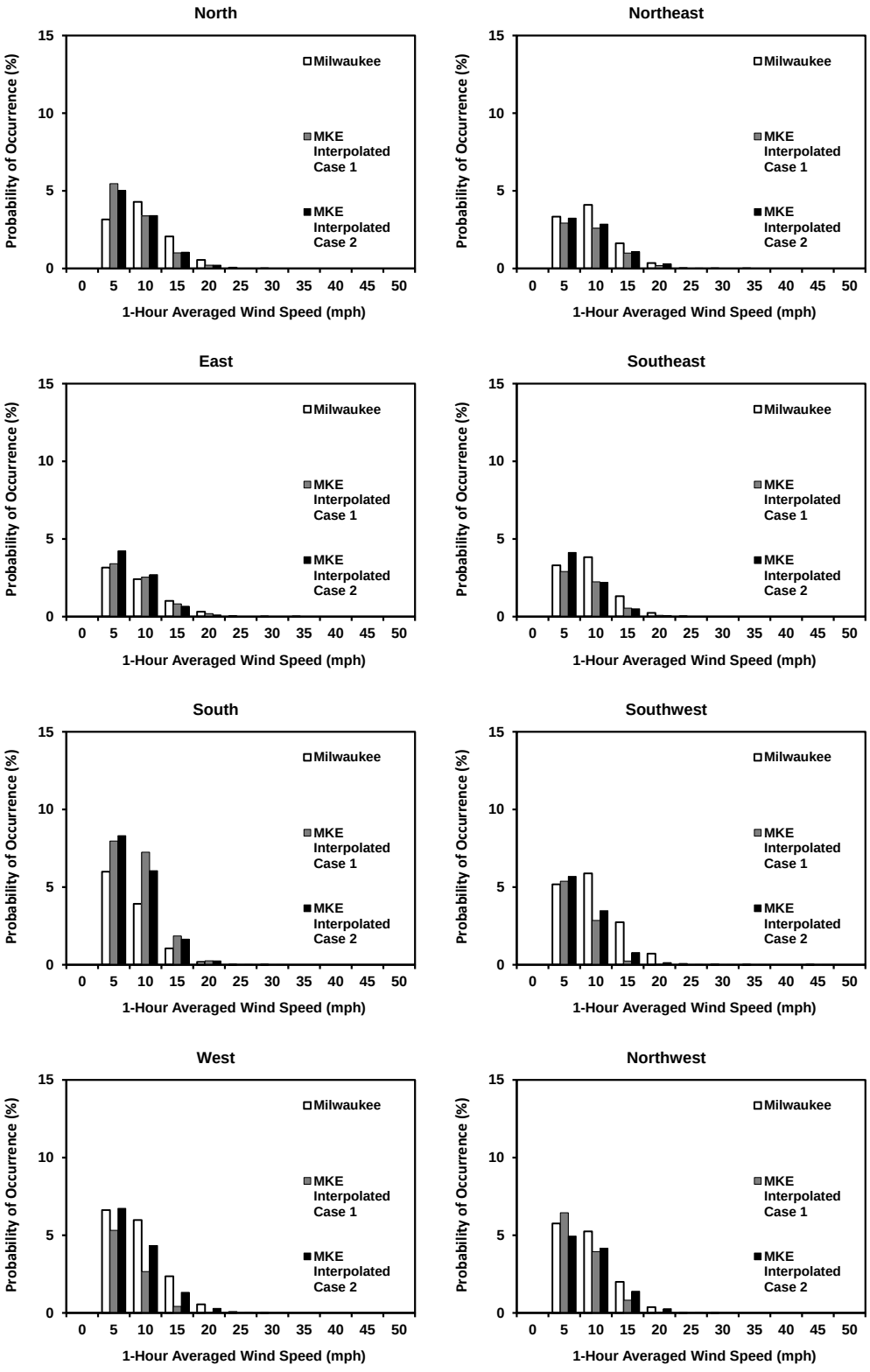

Figure 2.15. Comparison of combined probabilities for collected, Case 1 interpolated and Case 2 interpolated datasets for the MKE NCDC-ASOS site – $P(U = u_i \cap D = d_j)$.

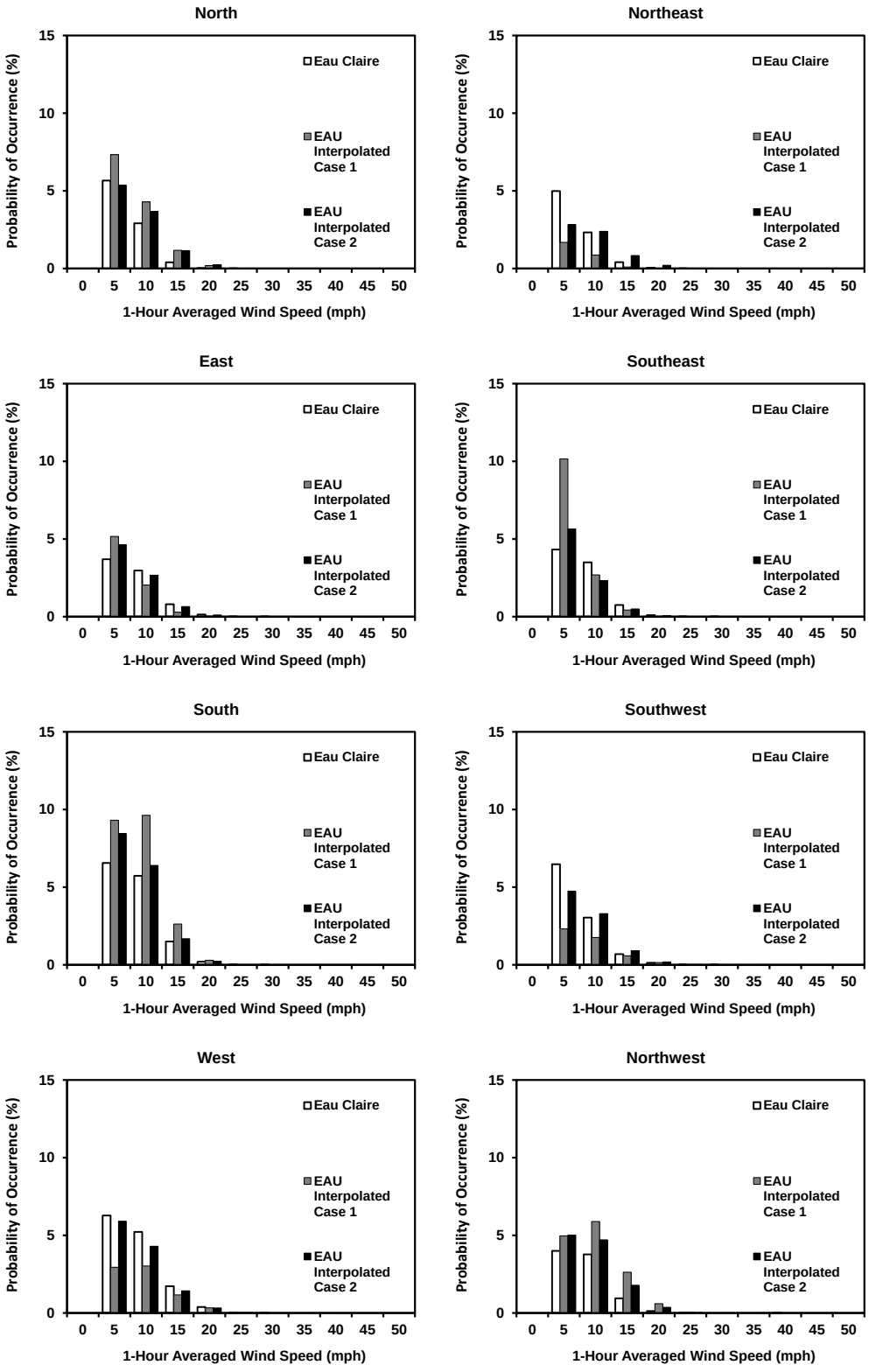

Figure 2.16. Comparison of combined probabilities for collected, Case 1 interpolated and Case 2 interpolated datasets for the EAU NCDC-ASOS site – $P(U = u_i \cap D = d_j)$.

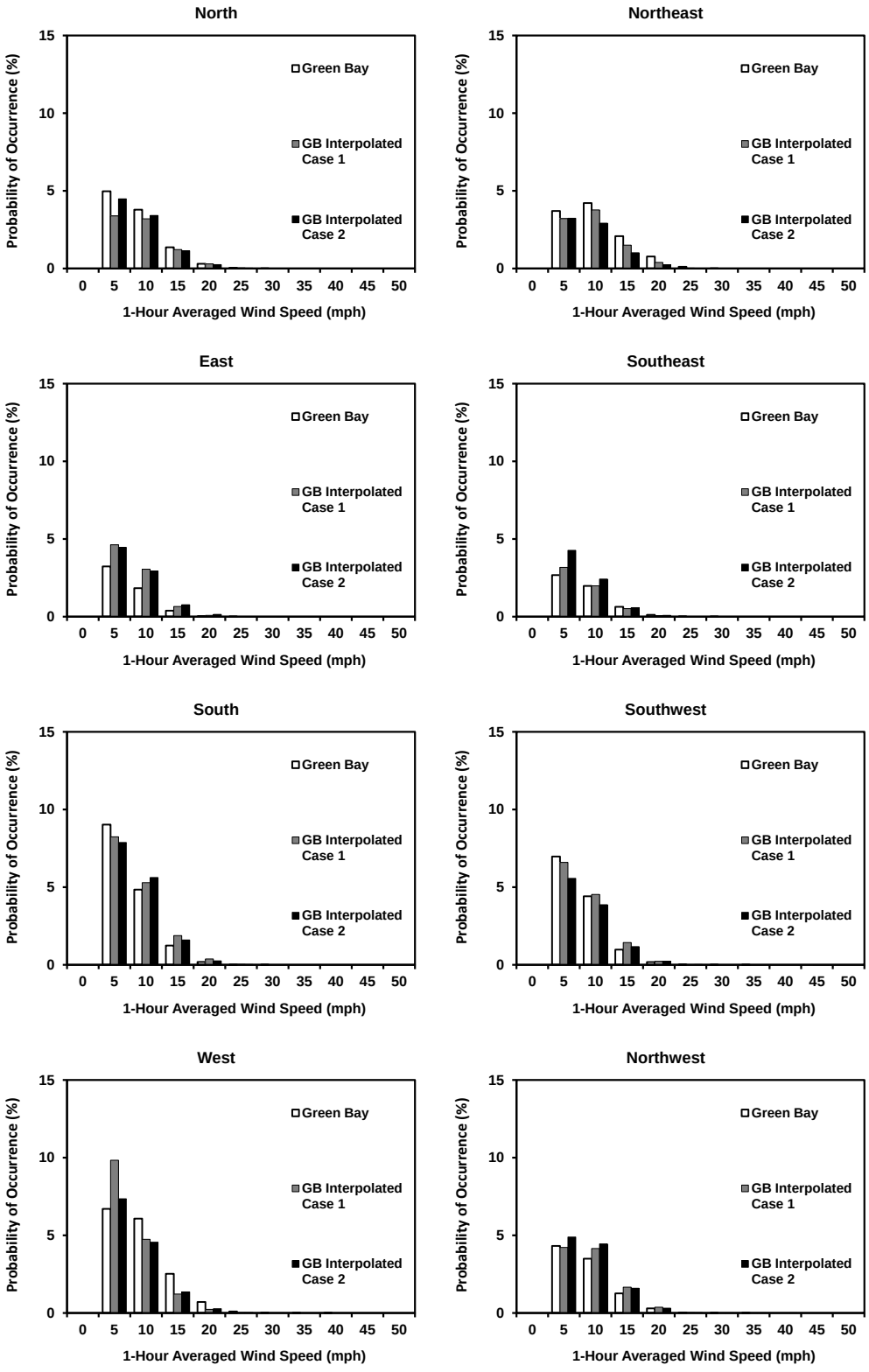

Figure 2.17. Comparison of combined probabilities for collected, Case 1 interpolated and Case 2 interpolated datasets for the GB NCDC-ASOS site – P ($U = u_i \cap D = d_j$).

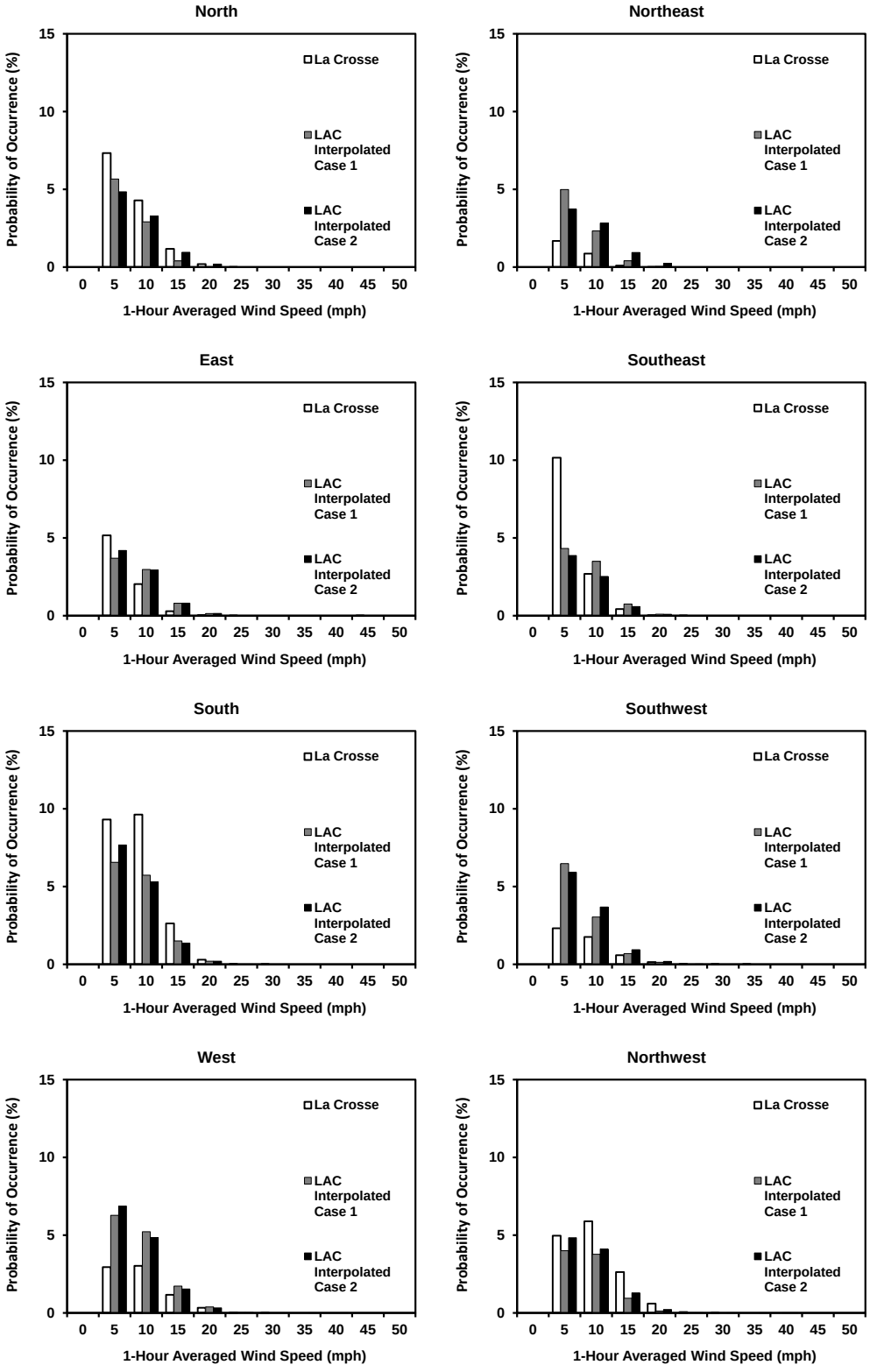

Figure 2.18. Comparison of combined probabilities for collected, Case 1 interpolated and Case 2 interpolated datasets for the LAC NCDC-ASOS site – P ($U = u_i \cap D = d_j$).

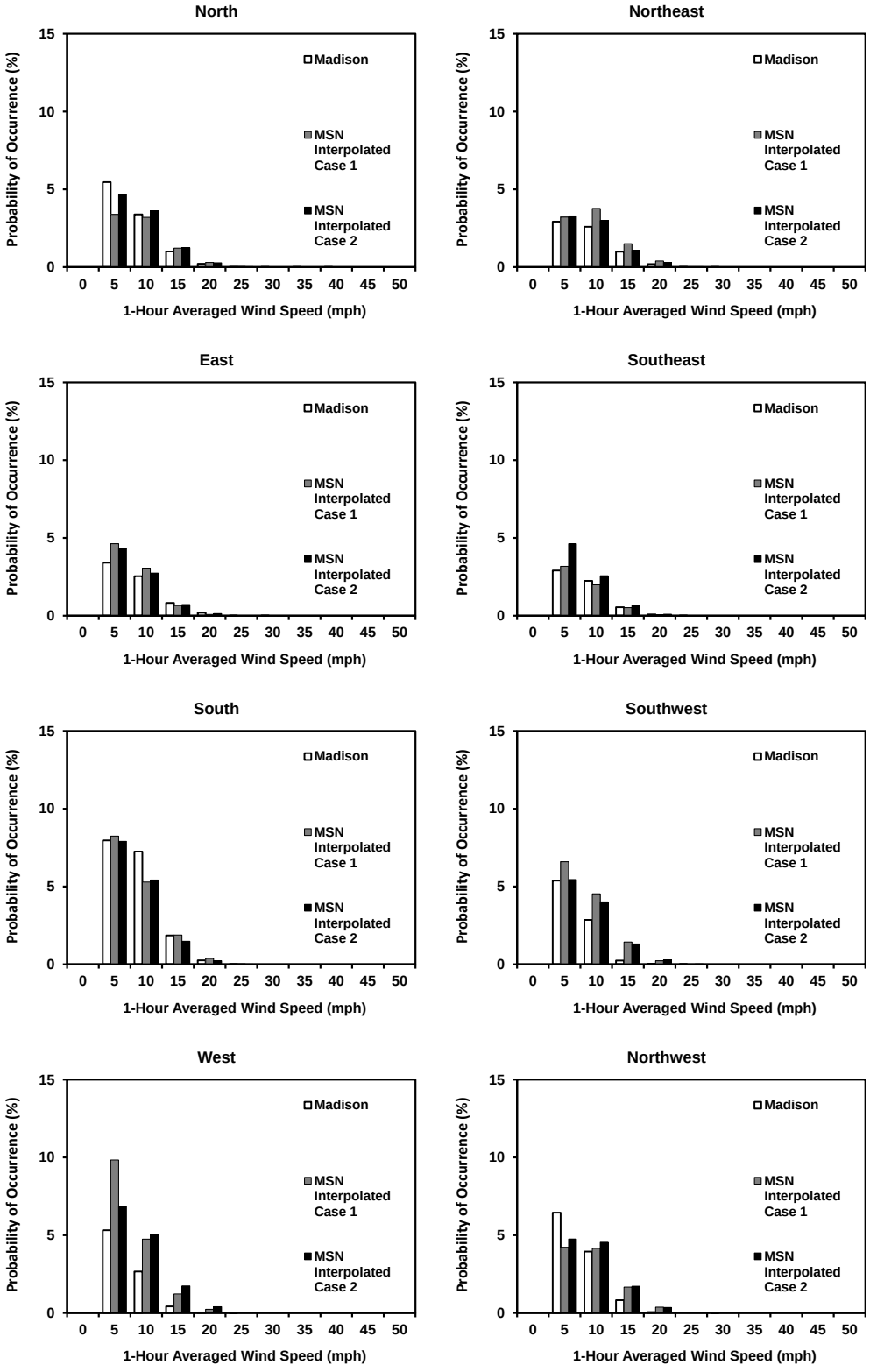

Figure 2.19. Comparison of combined probabilities for collected, Case 1 interpolated and Case 2 interpolated datasets for the MSN NCDC-ASOS site – $P(U = u_i \cap D = d_j)$.

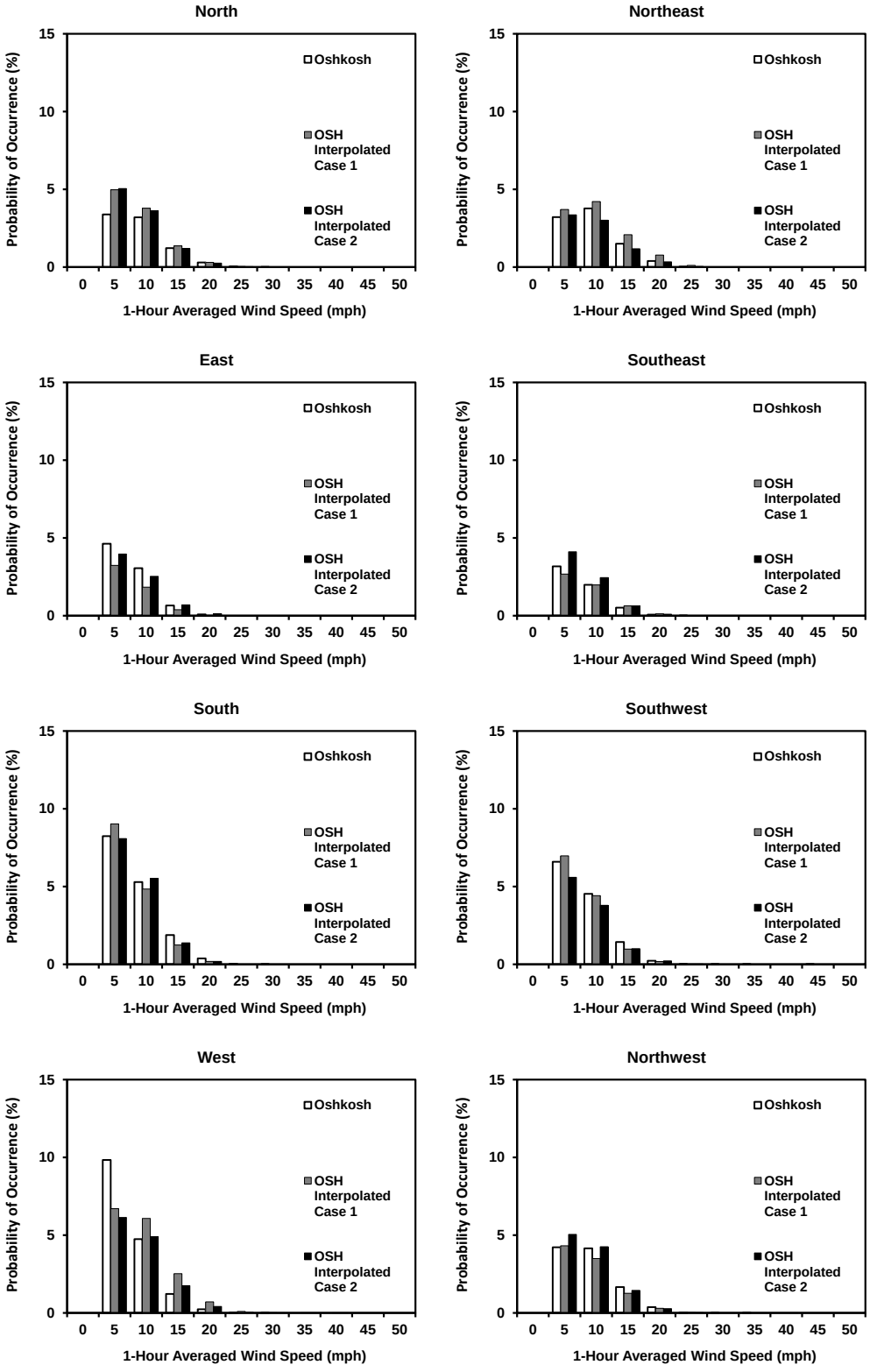

Figure 2.20. Comparison of combined probabilities for collected, Case 1 interpolated and Case 2 interpolated datasets for the OSH NCDC-ASOS site – $P(U = u_i \cap D = d_j)$.

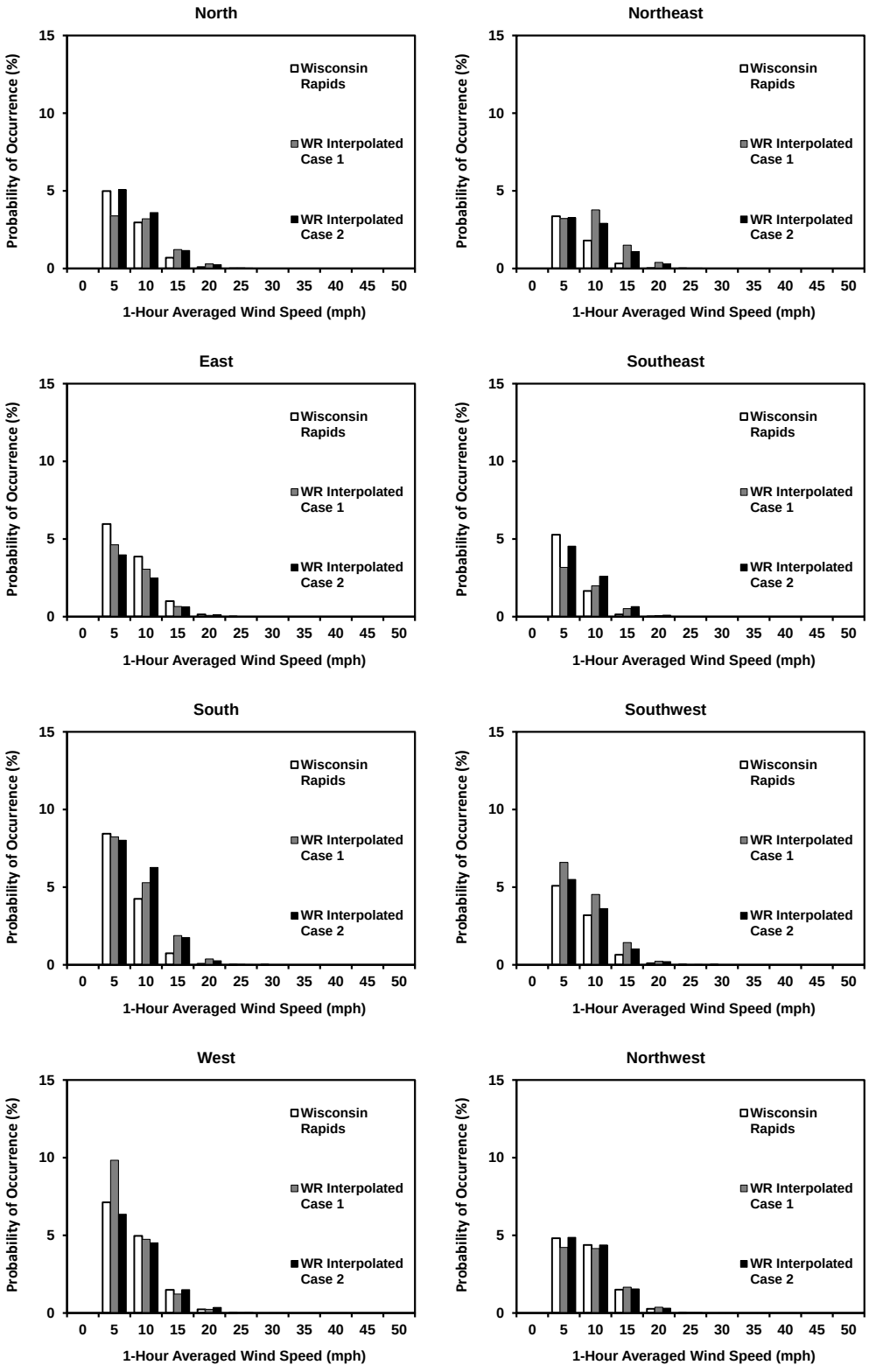

Figure 2.21. Comparison of combined probabilities for collected, Case 1 interpolated and Case 2 interpolated datasets for the WR NCDC-ASOS site – P ($U = u_i \cap D = d_j$).

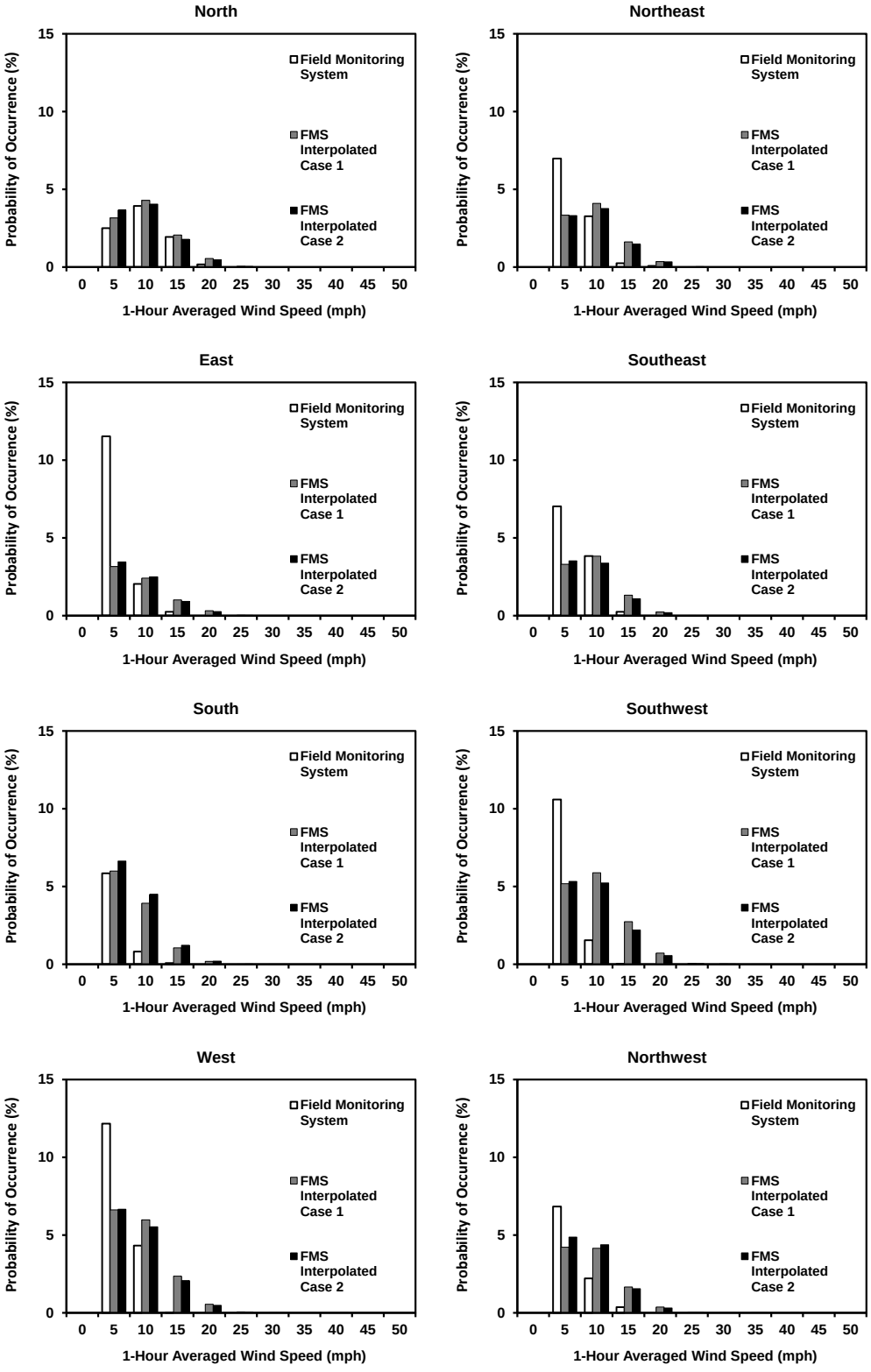

Figure 2.22. Comparison of combined probabilities for collected, Case 1 interpolated and Case 2 interpolated datasets for the FMS site – P ($U = u_i \cap D = d_j$).

2.5 – Concluding Remarks

A process through which wind speed and direction data was collected, synthesized and statistically analyzed has been described. Individual, conditional, and combined probabilities of one-hour averaged wind speed and one-hour averaged wind direction have been computed for discrete locations throughout the state of Wisconsin and at a field monitoring station designed, constructed and deployed as part of the present research effort. An interpolation procedure which allows for the computation of combined probabilities at any location throughout the state of Wisconsin has been presented.

A comparison between NCDC-ASOS site data for Milwaukee, Wisconsin and the data acquired at the FMS site indicates that local topography has a significant impact on mean one-hour average wind speed and one-hour wind speed standard deviation and a minor effect on wind direction. A lower mean and standard deviation in the wind speed appears to occur when the sign support structure site is in urban and suburban terrain compared to flat, open terrain like that found at airport ASOS sites. Therefore, use of ASOS sites will result in higher mean wind speeds and likely greater wind loading demand (from a fatigue point of view) than what will likely occur at a typical sign structure site.

An interpolation procedure for wind speed probability distributions for each of eight cardinal directions was evaluated using NCDC-ASOS site data and the FMS site data. This evaluation indicated that when interpolating combined probability distributions computed from wind speed and direction statistics gathered from NCDC-ASOS sites, the combined probability distributions in each of the eight cardinal directions appear to be conservative. Greater density of higher wind speed magnitudes result when the interpolation procedure is implemented. The wind speed variability is also likely to be slightly larger than the variability that can be expected at the sign structure location. It should be noted that these results are based upon comparisons to data

collected from a single FMS site, one that is located in an urban environment.

The synthesis of wind speed data conducted indicates that because sign support structures typically exist at locations that are remote from where wind data is measured (*i.e.* NCDC-ASOS sites), there is a need to develop a rational methodology for including topographical effects. It is recommended that additional field monitoring systems be deployed throughout the state at locations resembling similar site conditions as those typically found near sign support structures in areas that are less densely populated than those found at major cities (*e.g.* Milwaukee). This would allow further evaluation, confirmation and modification of the interpolation procedure proposed in this chapter so that combined probabilities of wind speed and wind direction can be accurately computed throughout the State. This would allow much greater understanding of the impact of topography and would facilitate modifications to the interpolation procedure that allow topography to be better incorporated in the procedure.

CHAPTER 3 – QUANTIFYING FATIGUE LIFE UNCERTAINTY

3.1 – Introduction

Typical design methods for considering the fatigue limit state are formulated in terms of defining an infinite life. In other words, ensuring that a specific connection will not see stress-range magnitudes above the constant amplitude fatigue limit (CAFL) for a predetermined fatigue detail category such as those found in the AASHTO specifications. AASHTO (2009) provides design stress-life curves that correspond to numerous detail categories. However, many (if not, all) of the connections used in mast-arm sign support structures typically land in the same detail category (E') corresponding to a severe fatigue condition. Because many connections are lumped into the same detail category that is independent of geometric dimension considerations (*i.e.* tube thickness, plate thickness, bolt pattern, etc.), there exists significant variability among their resulting fatigue lives.

The discussion in chapter one of this dissertation indicated that a number of statistical parameters are required before a reliability-based fatigue life assessment for these types of structures (and connections) may be carried out. Therefore, this chapter will seek to fill this void through accomplishing the following goals:

- Perform fatigue testing on connections typically used in highway mast-arm sign support structures to supplement the existing test database.
- Develop a comprehensive database of fatigue testing results for these types of connections that have been conducted to-date.
- Perform a complete, high-resolution taxonomy of these types of connections – one that synthesizes results from applicable fatigue tests into new detail categories. These detail categories can be thought of as sub-details of the existing AASHTO E' Detail Category.

- Conduct statistical analyses on the new details in order to quantify the fatigue life uncertainty associated with each of them.

3.2 – Background

It is important to provide background with regard to the current procedure that is followed when utilizing the specifications for the design of sign and luminaire support structures (AASHTO 2009). A designer must be able to distinguish their connection configuration within the context of detail schematics. When a designer finds a connection configuration that looks like the one (or one very close to that) under consideration, he/she is referred to a table which groups examples of connection configurations into fatigue detail categories. Some connection configurations can be classified into several fatigue detail categories depending upon the loading scenario that the connection will undergo. Once the fatigue detail category is chosen, a number of cycles of loading or tension stress-ranges (until fatigue failure) may be anticipated as long as the nominal stress-range at the detail is known (Fisher et al. 1998).

The procedure just described is founded on some very important assumptions. At its most basic level, it assumes the designer has chosen a detail category which very closely represents the detail under consideration. Next, it assumes that the nominal stress-range at the location of the detail (within the structure) was correctly determined. Finally, and perhaps most critically, this procedure assumes that the stress concentration factor for the detail under consideration, at its most fatigue-sensitive location, can be represented by the details used to create the fatigue detail category. This is because the procedure just described does not account for stress concentration effects directly. This effect is assumed to be embedded into the results of the fatigue tests used to generate these fatigue detail categories.

The difficulty with the existing AASHTO fatigue design procedure, as it relates to the present reliability study, is that it is better suited for *design*. It works reasonably well in design because curves that represent the statistical mean fatigue life curves are conservatively defined to provide approximately 95% confidence that a given connection will not fail by fatigue before the determined number of cycles for any nominal stress-range specified. When the goal is infinite fatigue life for expected loading demand, the process works reasonably well. However, the goal in this reliability study is *not* to determine what the *infinite* life of the connection is, but rather, what the *expected* life is and how much variability should be anticipated with that expected life.

In order to define when a fatigue crack is expected to initiate, statistical analysis on groupings of fatigue test data is required. A very important emphasis should be placed on the word groupings. As shown in the AASHTO specification (AASHTO 2009), connections composed of different geometric configurations and details will exhibit vastly different fatigue lives. Proper synthesis of fatigue testing data into appropriate categories for the reliability analysis conducted in this thesis will be crucial to the adequacy and accuracy of the subsequent reliability results.

3.3 – Experimental Program

The fatigue tests performed as part of this research effort were conducted in order to supplement the existing database of fatigue testing data found in the literature. Focus was given to socketed tube-to-transverse plate connections given their prevalence throughout the WisDOT transportation infrastructure network. A review of the literature revealed that all applicable fatigue tests for this type of connection were conducted at stress-range magnitudes that ranged from 4.9 ksi on the low end to 18.9 ksi on the high end. Earlier research work in this field indicates that there is a difference in variability at these stress-range magnitudes for welded connections (Little and Jebe 1975). Specifically, when stress-ranges applied to a connection are

high (*e.g.* 19 ksi), variability in the fatigue life is low and when stress-ranges applied to a connection are low (*e.g.* 5 ksi), variability in the fatigue life is high (Little and Jebe 1975).

Statistical analysis has been performed on fatigue test results of unreinforced (un-stiffened) mast-arm connections in an earlier research effort (Foley et al. 2008). It was recommended in that study that additional testing be conducted at stress-range magnitudes of 6 ksi and 15 ksi. New statistical analysis and additional synthesis has since been conducted in the present research effort and will be presented in subsequent sections of this chapter. However, based upon the previous recommendations, the experimental program in the present research effort will focus on conducting fatigue tests on un-stiffened mast arm connections at stress-range magnitudes of 6 ksi and 15 ksi.

3.3.1 – Test Setup and Procedure

A test arrangement similar to that used in previous research efforts (Koenigs 2003; Koenigs et al. 2003) was used to perform the full scale constant amplitude fatigue tests on round tube specimens. The arrangement consisted of bolting two specimens end-to-end utilizing what is referred to as a load box. A load may then be applied to this load box while providing end support fixturing consistent with that of a simply supported beam (*i.e.* double restraint fixture representing a pin support on one end and single restraint fixture representing a roller support on the opposite end). In this way, stresses measured by strain gages can be verified by simple statics.

This procedure enables both specimens to be tested simultaneously at the same constant amplitude stress-range. Each specimen can be thought of as a cantilever with fixed end located at the cross-section that is bolted to the load box and free end located at the cross-section bolted to the support fixture.

It should be noted that this testing arrangement is limited to the application of tensile loads and tensile stress-ranges. The fixtures utilized are incapable of supporting compressive loads due to a lack of lateral bracing. This enables the design of the test setup to be simplified, but prevents the application of fully-reversed cyclic loading (Koenigs 2003). Therefore, only the top half of each specimen was loaded in tension during each test conducted. Because only the top half of the cross-section was loaded in tension, the bottom half was assumed to remain in compression (*i.e.* not subjected to any fatigue loading) and considered as a new specimen for subsequent fatigue testing.

3.3.2 – Test Specimens

Two types of test specimens were utilized in the present study – round and multi-sided (faceted with 16 sides). The reason for two types of specimens was because the State of Wisconsin has both round and multi-sided mast-arm connection configurations throughout the state in its inventory. The following discussion will provide a complete description of both types of test specimens.

The two round specimens used for the fatigue tests conducted in the present effort were purchased from Valmont Industries, Inc. located in Valley, Nebraska. Each specimen consisted of a 97.75” round tube, with an outer diameter tapered from 11.0” to 9.9” and a wall thickness of 0.1793”. Each end of the specimens contained a socketed connection with unequal leg fillet welds (0.44” x 0.25”) on the outside of the connection socket and equal leg fillet welds (0.1793” x 0.1793”) on the inside of the connection socket. The socketed plates were 1.75” thick, 18.5” x 18.5” square and contained a center-to-center bolt hole spacing of 15.25”.

The two multi-sided specimens used for the fatigue tests conducted in the present effort were purchased from Millerbernd Manufacturing Company located in Winsted, Minnesota. Each

specimen consisted of a 97.75” multi-sided tube (16 sides), with an outer opposite flat-to-flat distance of 11.0” and a wall thickness of 0.1875”. Each end of the specimens contained a socketed connection with unequal leg fillet welds (0.44” x 0.25”) on the outside of the connection and equal leg fillet welds (0.1875” x 0.1875”) on the inside of the connection. The socketed plates were 1.75” thick, 18.5” x 18.5” square and contained a center-to-center bolt hole spacing of 15.25”.

3.3.3 – Fatigue Test Fixtures and Testing Protocol

The fixturing used in the present study was fabricated at Construction Supply & Erection, Inc. located in Germantown, WI. A photo of the overall test setup, including all fixturing, the two round specimens, the MTS control station and the data acquisition system is shown in Figure 3.1. Photos of the key individual components used in the experimental fixture are displayed in Figure 3.2.

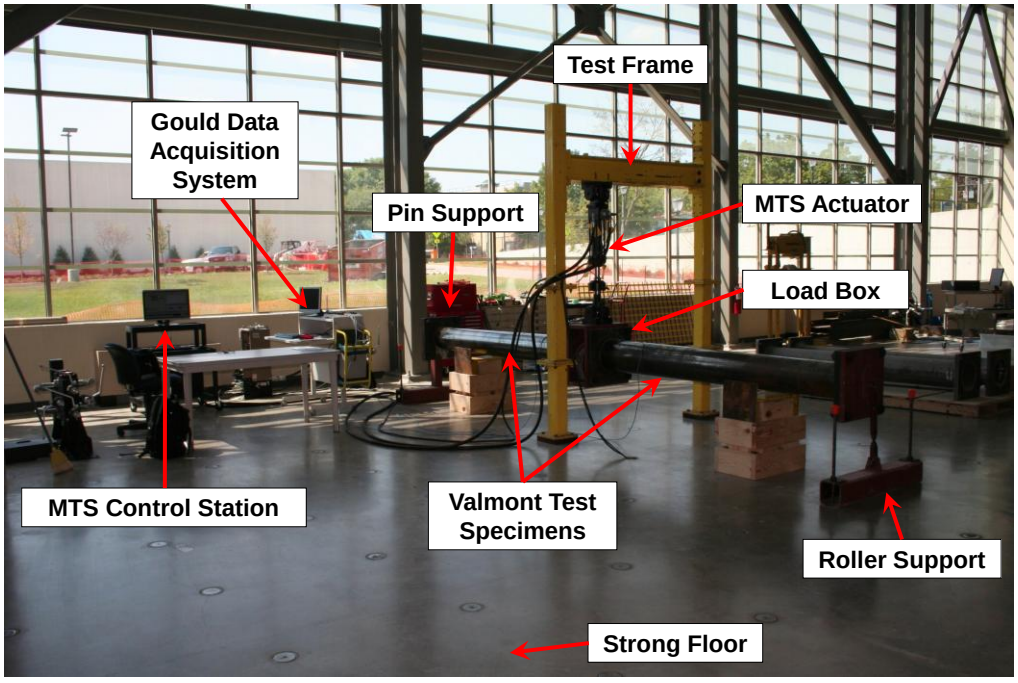

Figure 3.1. Test Setup inside Marquette University Engineering Materials and Structural Testing Laboratory (EMSTL).

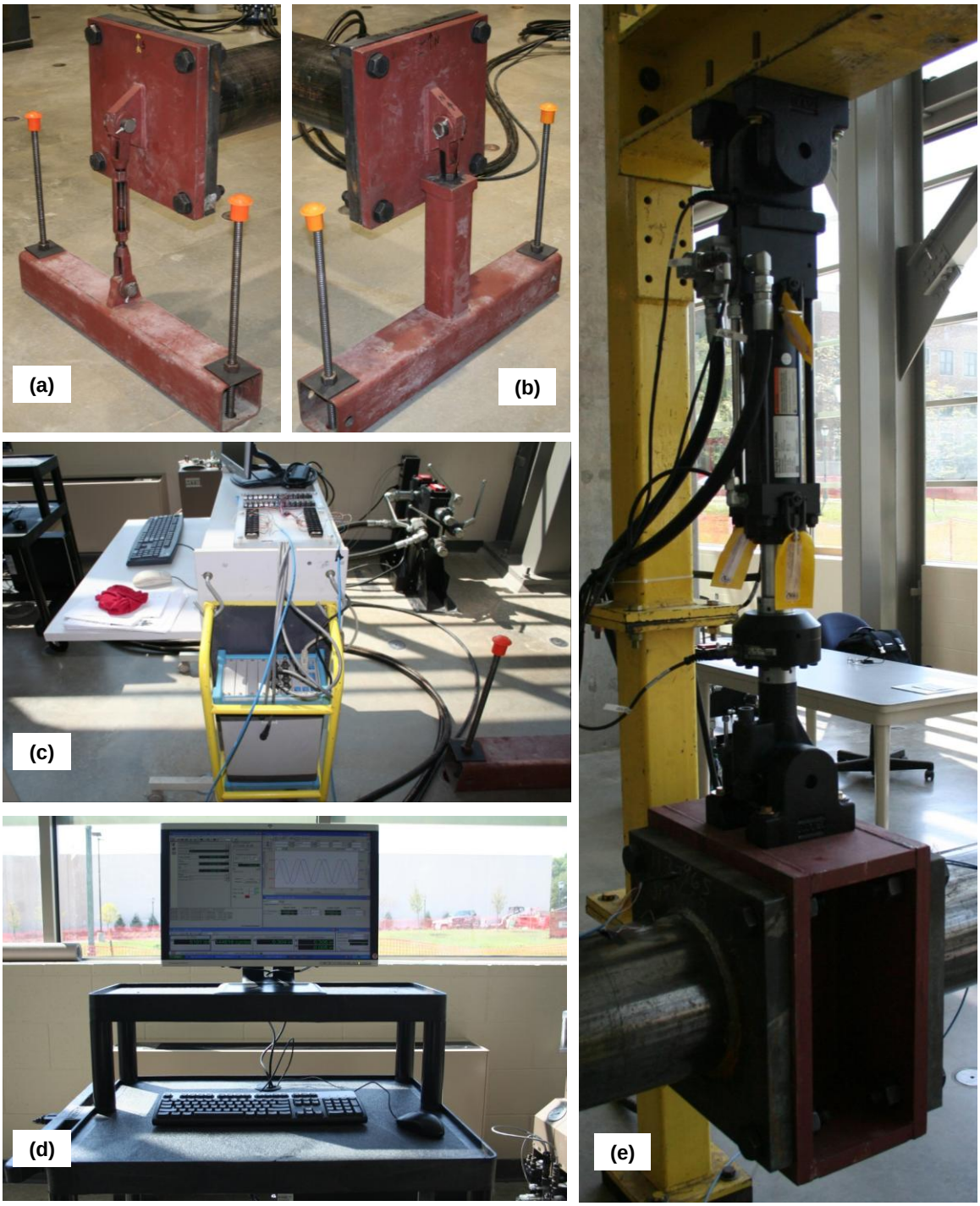

Figure 3.2. Test setup in EMSTL: (a) roller support, (b) pin support, (c) Gould data aquisition system, (d) MTS control station, (e) MTS actuator and load box.

All of the fatigue testing conducted as part of this study was done with the use of Vishay weldable strain gages so that stress-ranges could be monitored during testing. The strain gages were spot welded to the test specimens at the top most tension fiber two inches from the weld-toe. Although it is now known that the stress concentration effect on the tube wall extends beyond two inches from the weld-toe for the type of connection used in the test specimens, it was unknown in earlier phases of this research effort during which the real-time health monitoring system (discussed in chapter two) was implemented in Milwaukee, WI. Therefore, the stress concentration effects must be accounted for when making comparisons between measured stress data and stress data simulated using finite element models. This is dealt with in chapter five of the dissertation.

The test specimens were cleaned at the locations where they were to be gaged. The specimens were first cleaned with a wire brush and then rinsed with acetone. This procedure was conducted to ensure that the mill scale would not inhibit the accurate acquisition of strain readings and that good quality spot welds could be created for the gages. A photo of the strain gaged specimens, an up-close picture of a typical Vishay strain gage as well as a photo of the Vishay spot welder used to secure the gages onto the specimen is provided in Figure 3.3. It should be noted that two strain gages were used for the first set of specimens to verify the strain gages were in good working order.

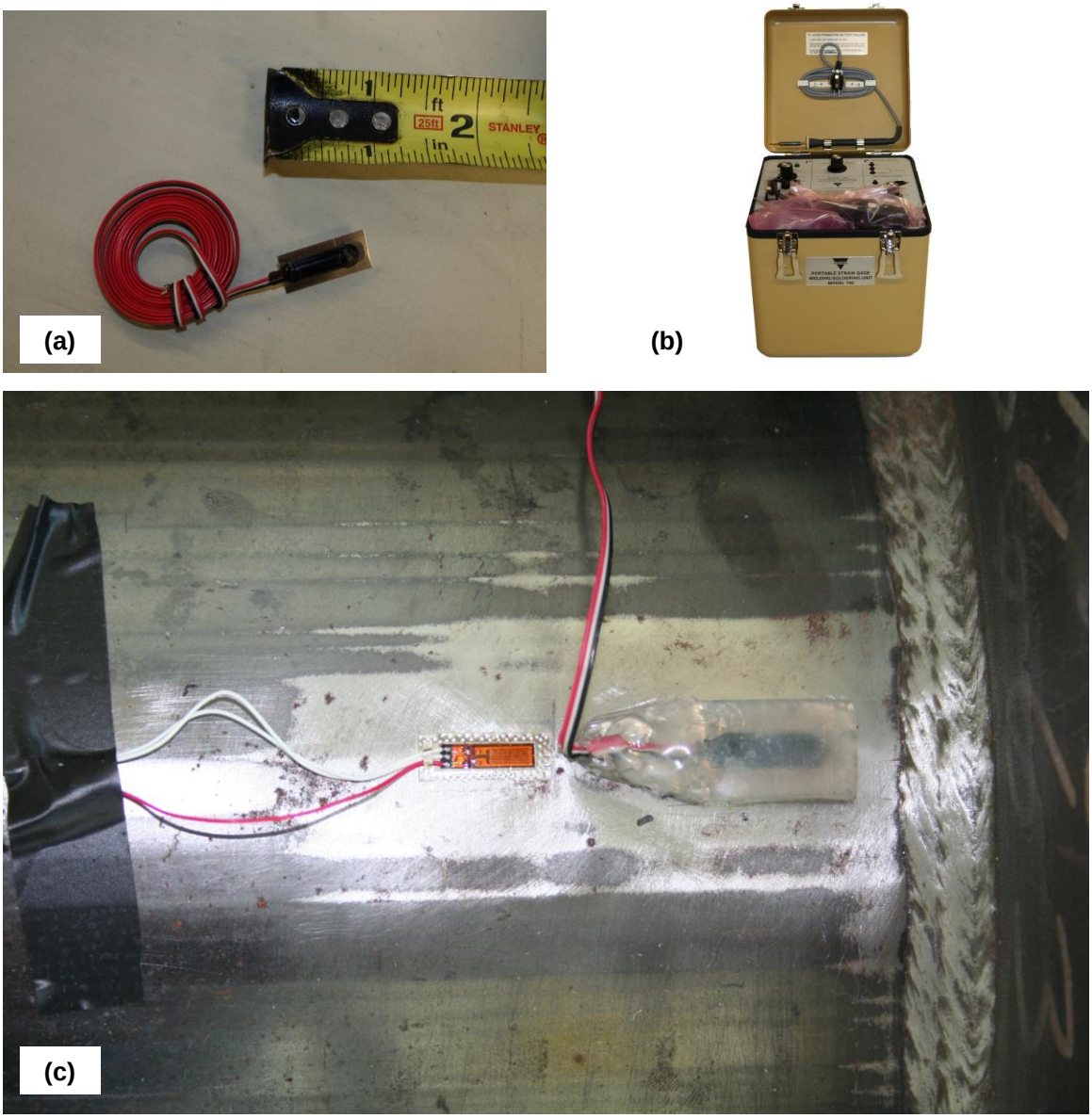

Figure 3.3. Strain Gaging: (a) Vishay strain gage, (b) Vishay spot welder, and (c) round specimen with strain gage installed.

The reviewed literature on fatigue testing has many variations in the protocols that were followed when conducting full-scale fatigue tests. Some studies simply back-calculated a required actuator loading based upon the desired stress-range magnitude and the section properties present. However, the majority of the prior fatigue tests utilized strain gages to verify that the applied loading was generating the desired stress-range response.

As indicated earlier, stress-range magnitudes close to the limits of the existing fatigue testing results database were the targets utilized in the present fatigue testing, namely 6.0 ksi and 15.0 ksi. The procedure used to achieve the desired stress-range magnitudes will now be discussed.

Figure 3.4 provides the resulting shear and moment diagrams for any given actuator loading applied to the fatigue specimens. Utilizing this diagram and some basic geometry, the magnitude of the moment at any point along each specimen may be determined in terms of the applied actuator loading. In this procedure, four moment values were calculated: one at each strain gage location; and one at each weld-toe location. The moments are labeled in Figure 3.4. Because the beam is simply-supported, the maximum moment resulting from the applied loading can be computed as,

$$M_{MAX} = \frac{P \cdot L}{4} \tag{3.1}$$

M_{AG} and M_{AT} are the strain gage and weld-toe moments on Side A specimens, respectively, while M_{BG} and M_{BT} are the strain gage and weld-toe moments on Side B specimens, respectively. After the maximum moment is found using equation (3.1), the values of M_{AG}, M_{AT}, M_{BG} and M_{BT} can be written in terms of the maximum moment and are expressed as:

$$M_{AG} = L_{AG} \cdot \frac{M_{MAX}}{108"} \tag{3.2}$$

$$M_{AT} = L_{AT} \cdot \frac{M_{MAX}}{108"} \tag{3.3}$$

$$M_{BG} = L_{BG} \cdot \frac{M_{MAX}}{108"} \tag{3.4}$$

$$M_{BT} = L_{BT} \cdot \frac{M_{MAX}}{108"} \tag{3.5}$$

Using elementary beam mechanics, the bending stress (stress normal to the weld toe) at each of the four locations are provided in equations (3.6) through (3.9).

$$\sigma_{AG} = \frac{M_{AG} \cdot y}{I} \tag{3.6}$$

$$\sigma_{AT} = \frac{M_{AT} \cdot y}{I} \tag{3.7}$$

$$\sigma_{BG} = \frac{M_{BG} \cdot y}{I} \tag{3.8}$$

$$\sigma_{BT} = \frac{M_{BT} \cdot y}{I} \tag{3.9}$$

where y is the distance from the neutral axis of bending to the strain gage or weld toe and I is the second moment of area of the cross-section at the strain gage or weld toe.

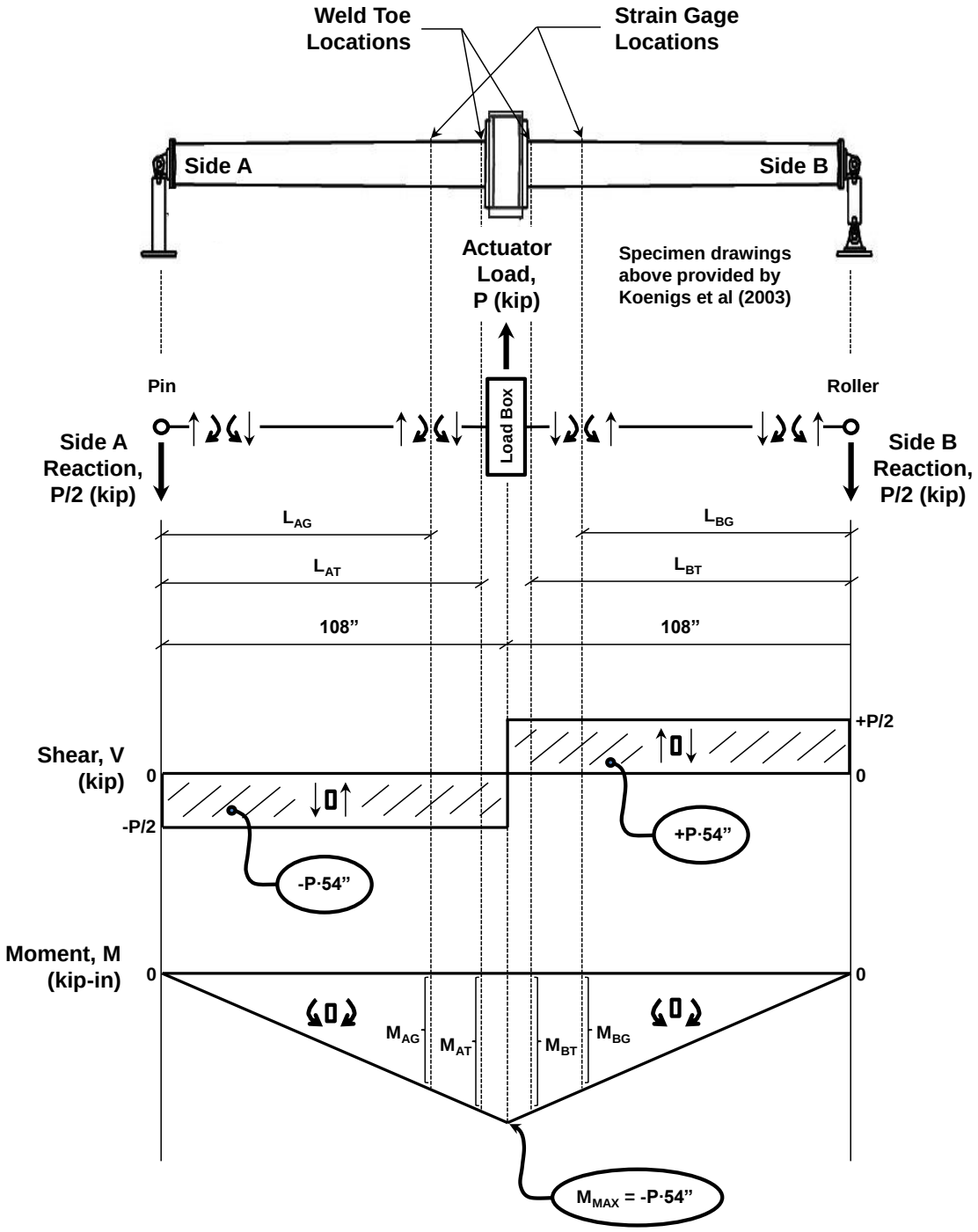

Figure 3.4. Guide for stress-range extrapolation from strain gage to weld toe.

The method used to determine the magnitude of the applied loading for each test will now be discussed in detail. It was felt that the most suitable way of outlining the method was by placing the specific steps taken in the order they occurred:

1) Each test began by applying load via the MTS actuator. The load was increased very slowly (quasi-static) until the pins used at both supports were "seated" to ensure a stable condition was met. The actuator loading which caused the pins to be seated (P = 2,500 lbs) was recorded and used as the minimum actuator loading in the loading cycles for all subsequent fatigue testing.

2) After applying P = 2,500 lbs, the strain readings were zeroed and additional loading was applied (again, at a very slow rate) until an average between strain gages achieved a value, that when converted to stress, would provide the stress-range magnitude desired in the constant amplitude fatigue test (either 6.0 ksi or 15.0 ksi). This loading was then recorded and used as a starting point in terms of target loads input into the MTS controller software (see Figure 3.5). The MTS software requires the operator to input a *Target Setpoint* as well as an *amplitude*. As an example, Figure 3.5 shows the *Target Setpoint* of P = 4,000 lbs with an *amplitude* about the target setpoint equal to 1,500 lbs. In other words, when the test is in operation, the actuator will cycle about a loading of P = 4,000 lbs achieving a minimum value of P = 2,500 lbs and a maximum value of P = 5,500 lbs. It should be noted that the loads listed in this case corresponded to a target stress-range of 6.0 ksi (mean stress = 3.0 ksi and stress amplitude = 3.0 ksi). When the target stress-range was increased to 15.0 ksi, loads were adjusted to achieve a mean stress of 7.5 ksi and stress amplitude of 7.5 ksi.

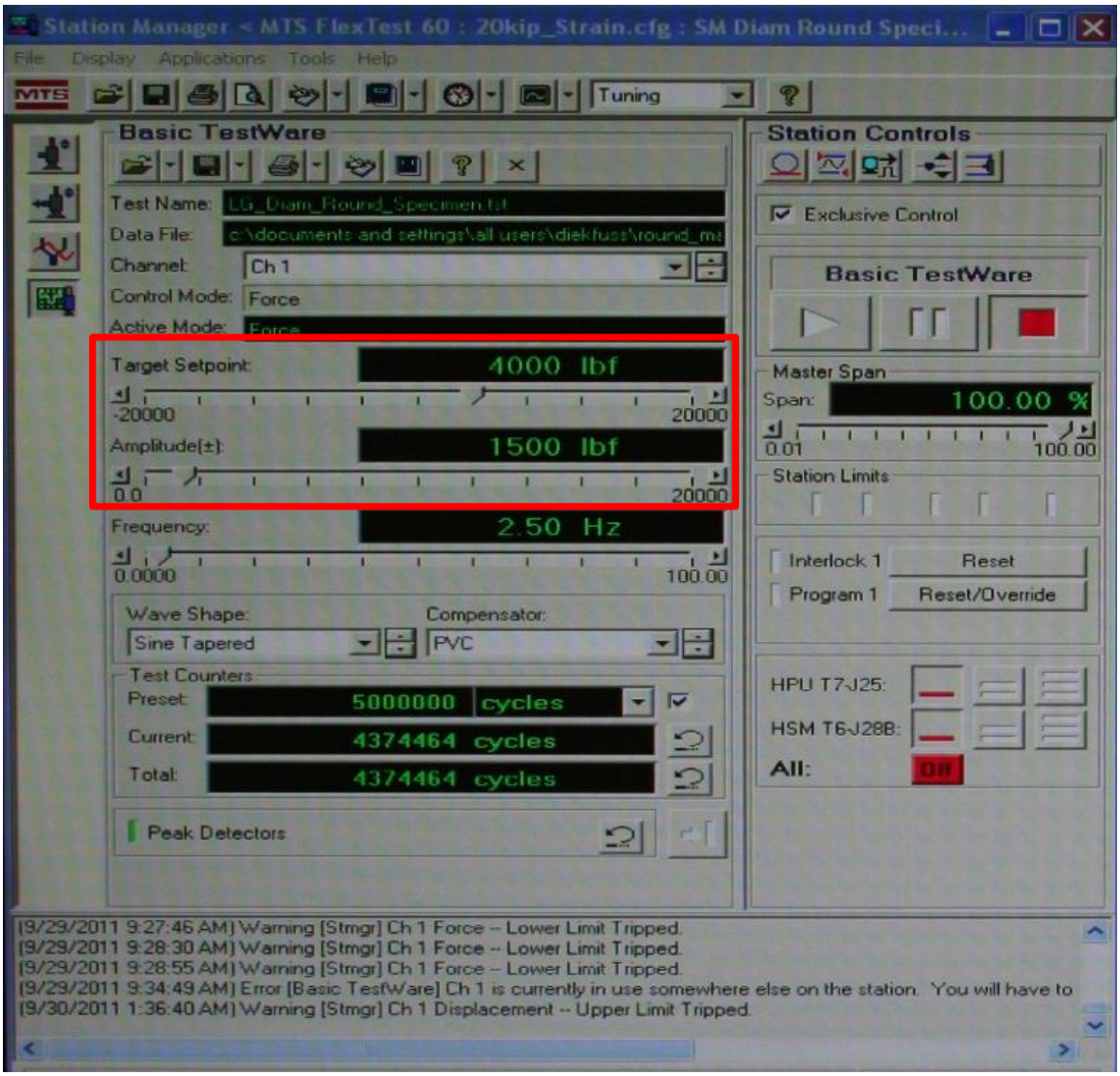

Figure 3.5. Screen-capture of MTS load inputs (note: this particular screenshot shows the load inputs for the MU-R-L-A1 fatigue test).

3) Once the target and amplitude were input for each fatigue test, detection limits for both displacement and force were established and utilized during testing. The MTS detection limits on the application of force were used to prevent overloading of the specimens. The MTS detection limits on vertical displacement of the load application point were used as a secondary means of crack initiation detection. With all material and section properties assumed to be constant, a cracked specimen is more flexible than an un-cracked

specimen. Therefore, barring mechanical malfunction, any increase in displacement without changing the applied loading should indicate that a crack has initiated.

4) The *dynamic* response of the system was anticipated to be different than the *quasi-static* response of the system given the inertial effects that come into play when the rate at which load is applied increases. It should be expected that additional loading (higher magnitude of P) would be required to obtain an equivalent magnitude of strain, at the gages, as was achieved during quasi-static loading. Therefore, the strain readings at the beginning of each fatigue test were monitored closely to determine the extent to which loading must be increased in order to maintain the desired constant amplitude stress-range magnitude. An example screenshot of the Summit Data Viewer (software used in data acquisition system to monitor strain) is provided in Figure 3.6. The strain was recorded in two channels: B1 and B2. Upon initiating the applied loading, approximately 20-30 cycles of loading were carried out, then the fatigue test was paused in order to allow the operator to determine whether or not the recorded strain-ranges were accurate for each test. If the strain-ranges were not at a magnitude that achieved the desired stress-range, both the *Target Setpoint* and *Amplitude* were successively increased by an equivalent amount in order to preserve stability of the overall system by maintaining the minimum loading, P = 2,500 lbs. Testing then resumed and this procedure was carried out until the average value between both gages resulted in the desired stress-range magnitude for each test.

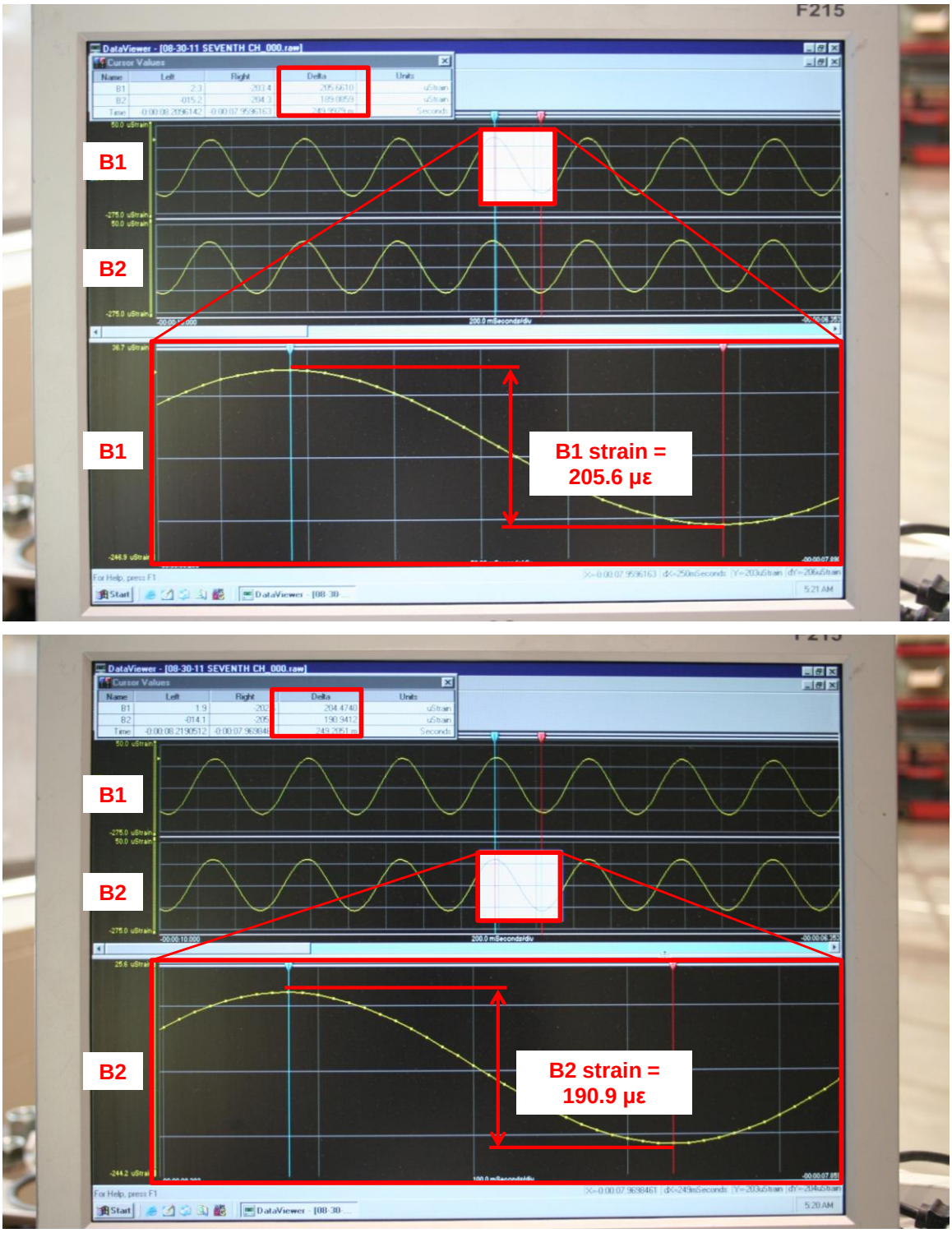

Figure 3.6. Screen-captures of Summit Data Viewer illustrating procedure utilized to determine strain-ranges (note: these particular screenshots show the strain-ranges for one of the checks conducted on the MU-R-L-A1 fatigue test).

5) The primary technique utilized for crack detection was via dye penetrant testing. Each test was paused every 216,000 cycles (approximately) to check if a crack was initiated at the weld toe. This number of cycles was chosen as it is the number of cycles that occurred in a 24-hour period. The loading frequency that provides 216,000 cycles in 24 hours is 2.5 Hz, which was utilized in the tests. The loading frequency was limited to 2.5 Hz to minimize the vibrations in the hoses which ran from the hydraulic service manifold (HSM) to the MTS Actuator. As mentioned in the third step of this testing protocol, a secondary technique utilized for crack detection was via preset detection limits on force and displacement. If a test stopped before the 216,000 cycle mark, the specimens were checked for cracks prior to restarting the test.

Due to the timing of the fatigue testing conducted as part of this research, four of the eight fatigue tests completed were done at the University of Wisconsin-Milwaukee. Midway through testing, the Marquette University Engineering Materials and Structural Testing Laboratory (EMSTL) was opened at which point all remaining fatigue tests were conducted on the Marquette University campus. The results will indicate the location where each test was conducted through the use of a prefix. MU was used to indicate that the test was conducted at Marquette University and UWM was used to indicate that the test was conducted at the University of Wisconsin-Milwaukee.

Other than knowing that strain gages were used to ensure the desired stress-ranges were being achieved, very little information was provided by the sub-contractor as to the protocol that was followed during the fatigue testing conducted in the UWM laboratory. Also, the reader should note that UWM was sub-contracted to complete approximately two million cycles of stress (load) range. Given the limited number of cycles, Miner's equivalent damage rule was employed and tests were conducted with increasing stress-ranges to ensure a crack was initiated within the limited number of cycles.

3.3.4 – Fatigue Testing Results

Eight fatigue tests were conducted. Four of the tests were conducted at MU while the other four tests were conducted at UWM. The results for each test include the stress-range and number of cycles to failure for that stress-range. Failure was classified as crack initiation. Tests where cracking was not achieved are noted. Table 3.1 summarizes all of the fatigue testing results from the present study. Figure 3.7 provides a key for differentiating between the eight tests and Figure 3.8 provides a graphical comparison of the test data by showing their results on a single S_R-N diagram. Also provided on this S_R-N diagram is the AASHTO E' Fatigue Detail Category in order to give reference to the current standards.

Table 3.1. Fatigue testing results from present study (note: mean stress = 0.5 x stress range for all MU tests and unknown for UWM tests).

Specimen Designation	Cycles to Failure	Stress Range (ksi)	Crack Length at Failure (in.)
MU-CSR-R-L-A1-1	4374464	6.00	6.4
UWM-MR-R-S-A1-2 (a)	2246094	5.42	NA
MU-CSR-R-S-A2-3	72660	15.37	7.9
MU-CSR-R-L-B1-4 (a)	4374464	6.00	NA
UWM-MR-R-S-B1-5	2246094	4.80	6.1
MU-CSR-R-S-B2-6 (a)	6893	15.37	NA
UWM-CSR-M-N-A1-7	139000	6.50	10.8
UWM-CSR-M-S-B1-8 (a)	139000	6.50	NA

Notes:

(a) Testing stopped with no failure (no cracks found).

A-B-C-D-E-F		
Testing Location		
A	MU	Marquette University
	UWM	University of Wisconsin-Milwaukee
Stress Range Methodology		
B	CSR	Constant Amplitude Stress Range
	MR	Miner's Cumulative Fatigue Damage Equivalent
Specimen Type		
C	R	Round tube
	M	Multi-sided tube
Specimen Designation - End Tested		
D	If tested at MU:	
	L	Large diameter end tested (d = 11.0 in.)
	S	Small diameter end tested (d = 9.9 in.)
	If tested at UWM:	
	N	North side of specimen tested
	S	South side of specimen tested
Specimen Designation - Top or Bottom		
E	A1	Top of specimen A
	A2	Bottom of specimen A
	B1	Top of specimen B
	B2	Bottom of specimen B
Specimen Serial Number for MU Synthesis		
F	#	

Figure 3.7. Key to testing specimens for the present study.

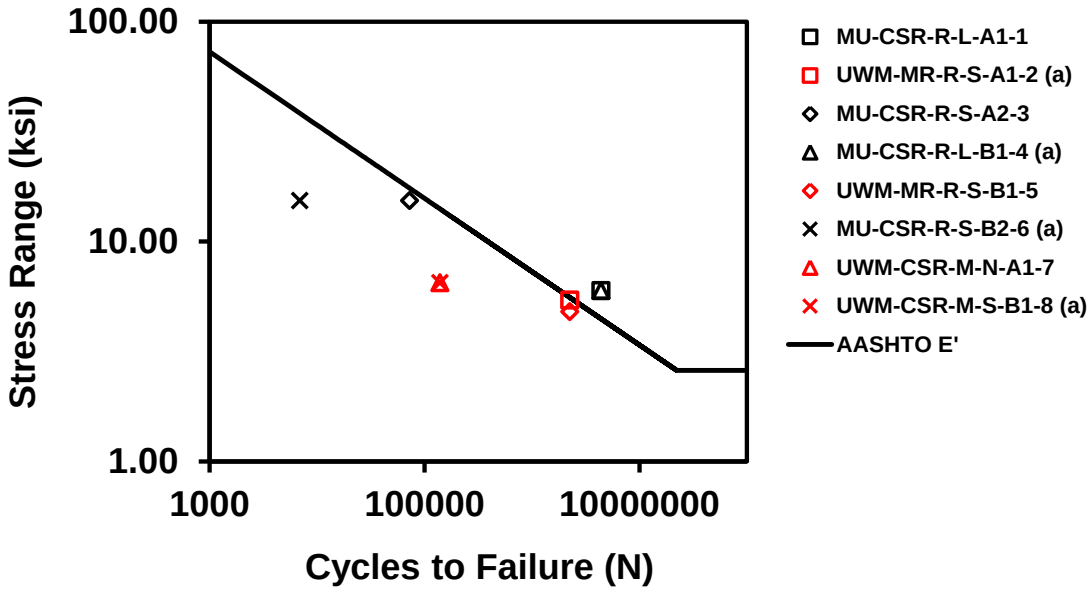

Figure 3.8. Stress-range vs. cycles to fatigue failure for tests conducted in the present study and those completed at the University of Wisconsin-Milwaukee (note: mean stress = 0.5 x stress range for all MU tests and unknown for UWM tests).

Photos of the test specimens in which a crack was initiated are provided in Figures 3.9 through 3.12. Each photo indicates the specimen name, approximate length of crack, crack termination points, as well as the stress-range and number of cycles to failure for that stress-range.

Figure 3.9. Fatigue crack detected after 4,374,464 cycles at 6.0 ksi on MU-CSR-R-L-A1-1.

Figure 3.10. Fatigue crack detected after 72,660 cycles at 15.37 ksi on MU-CSR-R-S-A2-3.

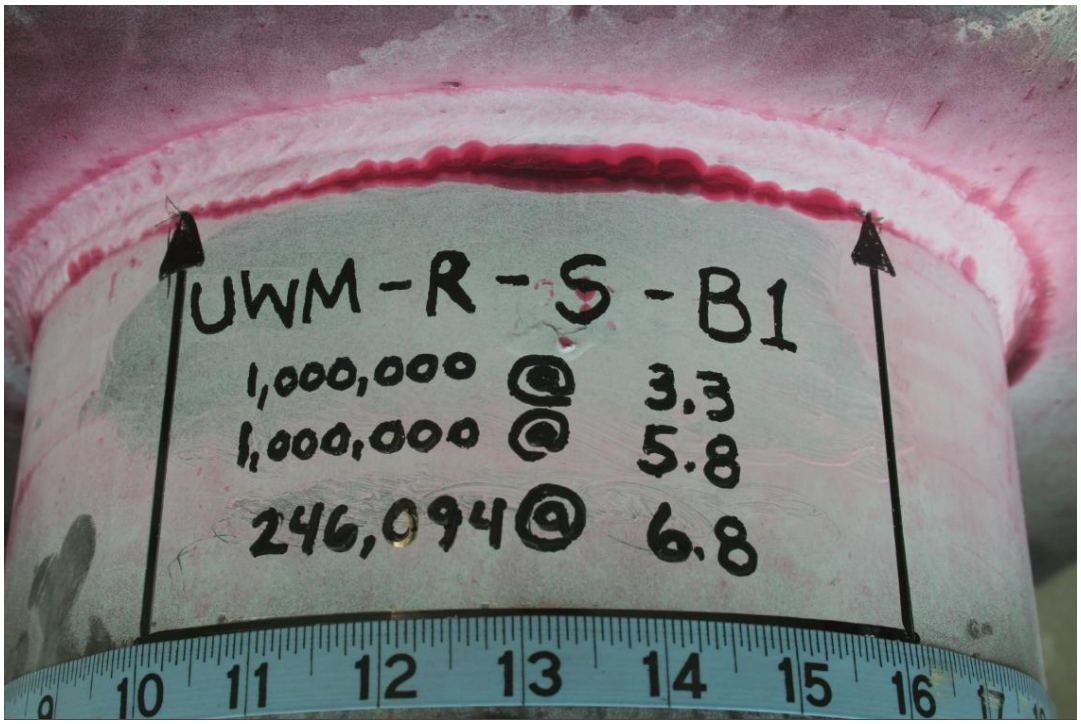

Figure 3.11. Fatigue crack detected after one million cycles at 3.3 ksi, one million cycles at 5.8 ksi and 246,094 cycles at 6.8 ksi on UWM-MR-R-S-B1-5.

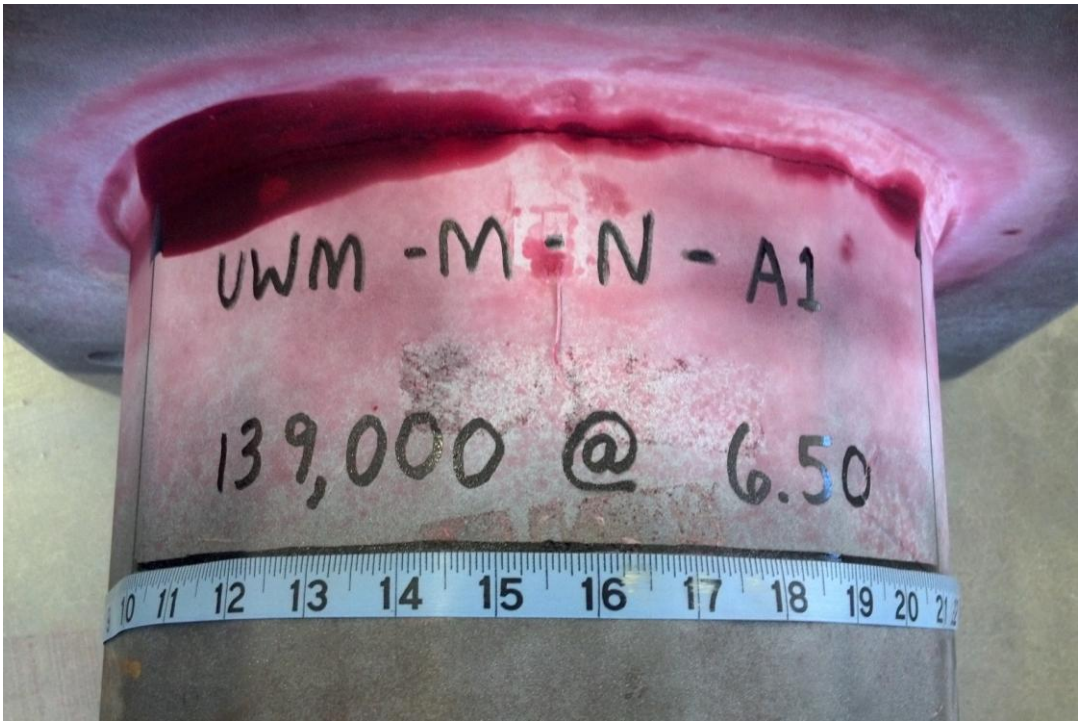

Figure 3.12. Fatigue crack detected after 139,000 cycles at 6.5 ksi on UWM-CSR-M-N-A1-7.

3.4 – Synthesis of Fatigue Testing Database

There has been a lot of fatigue testing on round tubular and faceted tubular shapes conducted in the last three decades. The present research effort includes a detailed synthesis of world-wide fatigue testing done since 1970. The fatigue testing data generated as part of the present research effort was included into this world-wide database prior to synthesis. This section of the chapter will outline the synthesis of fatigue testing data conducted in the present research effort.

3.4.1 – Fatigue Test Data Synthesis

Analysis of fatigue test data for connections used in sign support structures is usually conducted with a goal of determining within which existing fatigue detail category it should reside. This section will outline an approach to synthesizing fatigue test data without the confines of existing detail categories in place. All fatigue test data (relevant to connections considered in the present study) will be looked at holistically. The following is a list of research articles upon which the fatigue test results database is founded:

- Archer and Gurney (1970)
- Fisher et al. (1981)
- South (1997)
- Deschamp (2002)
- Machietto (2002)
- Chen et al. (2003) and Alderson (1999)
- Koenigs (2003) and Koenigs et al. (2003)
- Ocel (2006) and Ocel et al. (2006)
- Rios (2007)
- Anderson (2007)
- Richman (2009)
- Roy et al. (2011)
- Experimental Program from Present Study

Figure 3.13 plots all fatigue test data on a single S_R-N diagram to illustrate the variability among the results. The AASHTO E' detail category S_R-N curve is also present in the figure. The variability in fatigue test data on both sides of this design S_R-N curve is very interesting. It should be noted that all fatigue test data for the mast-arm sign support connections present in this figure fall into the AASHTO E' detail category. One would expect to see all test data lying to the right of this S_R-N curve. The difficulty in accounting for the significant variability in fatigue life is apparent.

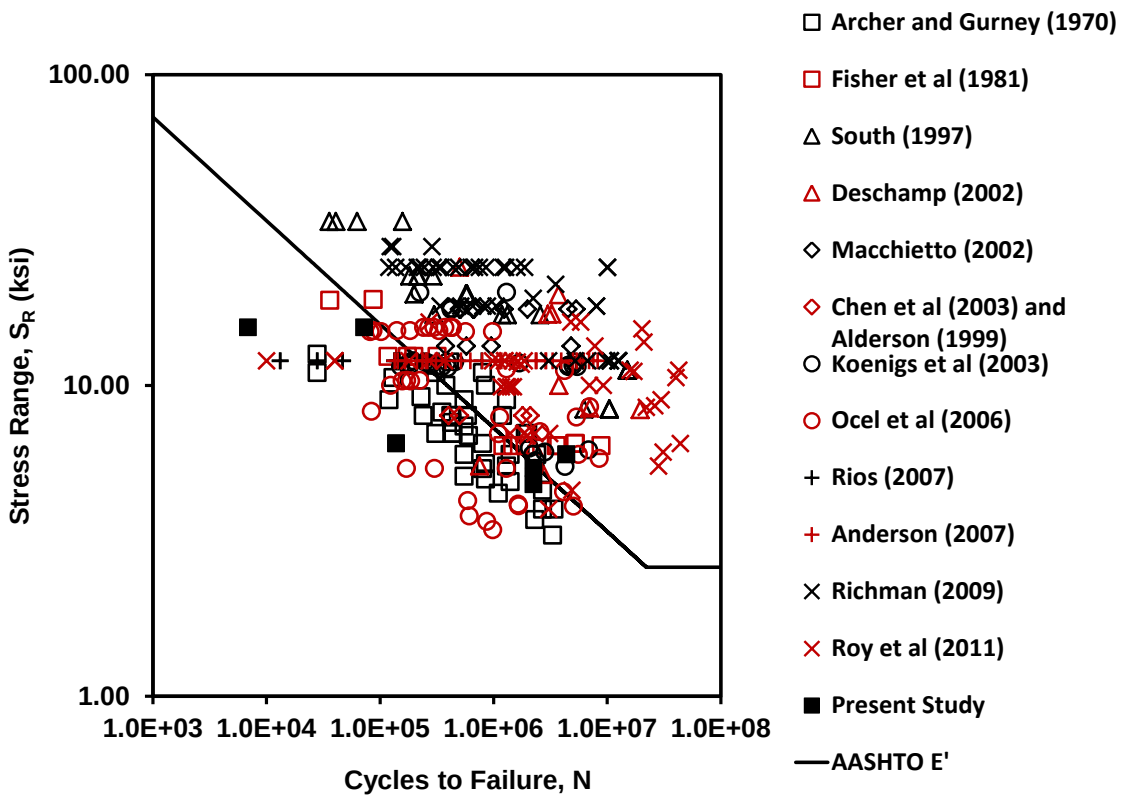

Figure 3.13. S_R-N diagram illustrating variability in fatigue test results.

All fatigue test data were originally considered as the same detail (*i.e.* AASHTO E'). Because of this, a systematic method for segregation of the fatigue test data was needed. The following questions were posed when defining this process: How does one separate the existing fatigue testing results for connections contained within sign support structures? Should they be

separated based on the physical appearance of the details which they contain, or should they be separated by the stress concentration factor present within those details? Both methods were considered. The following sections will describe each method as well as provide the advantages and disadvantages to both methods. The impact that each method has on the subsequent reliability analysis will be provided in chapter six.

The general guidelines that apply to both approaches will be addressed first. The goal of conducting these syntheses was to set baseline fatigue detail categories which will provide the fatigue life parameters required for the subsequent reliability analysis. Therefore, the following bulleted list contains the criteria which disqualified the results of particular fatigue tests from use within either of the two approaches:

- Any test performed on specimens that were already cycled, unless the same stress-range was continued or the specimen was flipped over (*i.e.* testing the reverse side, or the side that was initially in compression);
- Any test that was not conducted using a constant-amplitude stress-range.
- Any test that did not crack, whether they were classified as runout or not;
- Any test that was not strain gaged (or equivalently monitored) to ensure stress-range magnitudes were maintained during testing and were in accordance with target levels;
- Any test that was mechanically (or otherwise) treated (*i.e.* ultra-sonic impact, bristle blaster, etc.).

The database of fatigue test results was sifted based upon the preceding criteria. If any fatigue test met any of these criteria, the test was labeled as an "Unused Test" and it was not included in any of the subsequent statistical analysis.

Wirsching (1983) outlines a procedure for performing statistical analysis on fatigue test data. A modified version of this procedure will be discussed in subsequent sections after both

synthesis approaches are outlined. This is because both methods utilize this procedure to generate the statistical parameters required for the subsequent reliability study. The fatigue test results will be provided in tabular and graphical form after both synthesis approaches are introduced. The results will include where the test was performed, the stress-range and corresponding number of cycles to failure and the newly recommended fatigue detail category.

Synthesis Approach No. 1: Classification by Connection Configuration

This approach is similar to the existing approach presented in AASHTO (2009) which classifies connection details using similarity in appearance. This approach is somewhat simplistic compared to the second approach used in the thesis. All connections were first classified as unreinforced or reinforced (*e.g.* unstiffened or stiffened with welded gusset attachments). The connections were then separated based upon whether or not the tube (mast-arm or pole) was round or multi-sided (faceted). Finally, the connection was classified based upon the type of weld it contained. Thirteen potential fatigue detail configurations were identified in this manner and are listed as follows:

- U1: Unreinforced Round: Socket – Equal Leg Fillet Welds
- U2: Unreinforced Round: Socket – Unequal Leg Fillet Welds
- U3: Unreinforced Round: Flush Fillet Welds
- U4: Unreinforced Round: Full-Penetration Welds
- U5: Unreinforced Multi-Sided: Socket
- U6: Unreinforced Multi-Sided: Flush Fillet Welds
- U7: Unreinforced Multi-Sided: Full-Penetration Welds
- R1: Reinforced Round: Socket
- R2: Reinforced Round: Flush Fillet Welds
- R3: Reinforced Round: Full-Penetration Welds

- R4: Reinforced Multi-Sided: Socket
- R5: Reinforced Multi-Sided: Flush Fillet Welds
- R6: Reinforced Multi-Sided: Full-Penetration Welds

Two hundred sixty-five (265) fatigue tests were used in the first synthesis approach. However, as will be discussed in the subsequent statistical analysis, certain outliers existed in the database. Table 3.2 lists the new fatigue detail categories generated by the first synthesis approach including the corresponding number of contributing fatigue tests for each.

Table 3.2. Number of contributing fatigue tests to each of the new fatigue detail categories developed in Synthesis Approach No. 1.

Fatigue Detail Category	Description	No. of Contributing Fatigue Tests
U1	**Unreinforced Round Socket - Equal Leg**	23
U2	**Unreinforced Round Socket - Unequal Leg**	45
U3	**Unreinforced Round Flush Fillet Weld**	26
U4	**Unreinforced Round Full-Penetration**	2
U5	**Unreinforced Multi-Sided Socket**	38
U6	**Unreinforced Multi-Sided Flush Fillet Weld**	0
U7	**Unreinforced Multi-Sided Full-Penetration**	9
R1	**Reinforced Round Socket**	50
R2	**Reinforced Round Flush Fillet Weld**	0
R3	**Reinforced Round Full-Penetration**	45
R4	**Reinforced Multi-Sided Socket**	4
R5	**Reinforced Multi-Sided Flush Fillet Weld**	0
R6	**Reinforced Multi-Sided Full-Penetration**	23

There are a number of advantages and disadvantages to using this approach as the foundation for quantifying the fatigue life uncertainty. The advantages of Synthesis Approach No. 1 include:

- The fatigue detail category may be specified for a connection by merely knowing what the configuration of the connection looks like.
- There is very little computational effort required.

The disadvantages of this approach include:

- Stress concentration effects may be highly variable within a single connection configuration which may lead to an inappropriate detail selection.
- It is impossible to test all types and variations of connections. Therefore, it may be difficult to decide which fatigue detail category is most appropriate if a unique connection presents itself.
- This approach depends heavily upon engineering judgment and experience to ensure a proper detail category is chosen to represent the connection under consideration.

Synthesis Approach No. 2: Classification by Stress Concentration Factor

There are numerous variations in the geometric configurations of the welded tube-to-transverse-plate connections within sign support structures. It should be expected that the structural response will differ from one to another especially with regard to stress concentrations and, thus, fatigue resistance. It is widely known that, in general, larger stress concentration factors lead to lower fatigue lives. In fact, several studies have performed finite element analyses with very high fidelity (*i.e.* highly detailed) finite element models to gain a better understanding of what the stress concentration factor (*SCF*) is for a given connection-type, where the *SCF* is a maximum on

the cross-section, and the extent to which changing various design parameters like plate thickness, tube thickness, bolt pattern/circle, etc. has on this *SCF* and the resulting fatigue performance (Ocel 2006; Richman 2009; Roy et al. 2011). There is a plethora of connection configurations to choose from with a substantial variation in the magnitude of *SCF*'s and fatigue lives for each.

The most recent study performed on welded tube-to-transverse-plate connections was by Roy et al. (2011). Aside from significantly contributing to the existing database of fatigue test data on typical highway connections, the results of this study provide parametric equations for determining the stress concentration factor contained within these connections. This previous study analyzed finite element models of various connection configurations as cantilevers subjected to concentrated point loads with magnitudes scaled to achieve a nominal reference stress equal to 12 ksi at the most fatigue-critical section. The most fatigue-critical section was defined as the section where fatigue cracking was expected. For example, the most fatigue-critical section for a welded tube-to-transverse plate connection is the section through the weld-toe on the mast-arm tube. The descriptions of each variable used in these equations are provided in Table 3.3. Figure 3.14 provides the resulting parametric equations (Roy et al. 2011).

Table 3.3. Description of variables used in *SCF* parametric equations (Roy et al. 2011).

Variable	Description
D_{BC}	Diameter of circle through the fasteners in the transverse plate
D_{OP}	Diameter of concentric opening in the transverse plate
D_T	External diameter of round tube or outer opposite flat-to-flat distance of a multi-sided tube at top of transverse plate
h_{ST}	Height of longitudinal attachment (stiffener)
N_B	Number of fasteners in the transverse plate
N_{ST}	Number of longitudinal attachments
t_{ST}	Thickness of longitudinal attachments
t_T	Thickness of tube
t_{TP}	Thickness of transverse plate
C_{BC}	D_{BC} / D_T
C_{OP}	D_{OP} / D_T

Section Type	Detail	Location	Stress Concentration Factor (SCF)
Round	Fillet-welded tube-to-transverse plate connections	Fillet weld-toe on tube wall	U.S. Customary Units $SCF = 2.16 + \left(0.908 - 0.924\frac{C_{BC}^{0.0474}}{N_B^{0.0105}}\right)\cdot\left(4.54 + 52.1\cdot t_T\right)\cdot\left(14.6 - 1.17\cdot D_T^{1.15}\right)\cdot t_{TP}^{-2.36}$ (3.10) SI Units $SCF = 2.16 + 207\cdot\left(0.908 - 0.924\frac{C_{BC}^{0.0474}}{N_B^{0.0105}}\right)\cdot\left(4.54 + 2.05\cdot t_T\right)\cdot\left(14.6 - \frac{D_T^{1.15}}{35.3}\right)\cdot t_{TP}^{-2.36}$ (3.11)
Round	Groove-welded tube-to-transverse plate connections	Weld-toe on tube wall	U.S. Customary Units $SCF = 1.35 + \left(0.982 - \frac{C_{BC}^{0.0674}}{N_B^{0.0029}}\right)\cdot\left(1.0 + 17.3\cdot t_T\right)\cdot\left(2.60 - \frac{D_T^{1.12}}{2.24}\right)\cdot\left(\frac{1.0}{C_{OP}^{-0.689} - 0.764}\right)\cdot t_{TP}^{-1.95}$ (3.12) SI Units $SCF = 1.35 + \left(2.63 - 2.68\cdot\frac{C_{BC}^{0.0674}}{N_B^{0.0029}}\right)\cdot\left(12.1 + 8.24\cdot t_T\right)\cdot\left(44.1 - \frac{D_T^{1.12}}{4.93}\right)\cdot\left(\frac{1.0}{C_{OP}^{-0.689} - 0.764}\right)\cdot t_{TP}^{-1.95}$ (3.13)
Round	Fillet-welded tube-to-transverse plate connections stiffened by longitudinal attachments	Weld-toe on tube wall at the end of attachment	U.S. Customary Units $SCF = \left(\frac{4.36\cdot\frac{t_{ST}}{t_T^{0.334}} - 1.0}{2.26\cdot\frac{t_{ST}}{t_T^{0.707}}}\right)\cdot\left(\frac{0.160 + 0.864\cdot h_{ST}}{1.0 + 1.12\cdot h_{ST}}\right)\cdot\left(0.519 + 0.257\cdot\frac{D_T}{N_{ST}^{1.60}\cdot t_T^{1.42}} + \frac{0.870}{t_T^{0.797}} + \frac{0.0293}{t_{ST}^{2.91}}\right)$ (3.14) SI Units $SCF = \left(\frac{\frac{t_{ST}}{t_T^{0.334}} - 1.98}{1.73\cdot\frac{t_{ST}}{t_T^{0.707}}}\right)\cdot\left(\frac{0.160 + \frac{h_{ST}}{29.4}}{1.0 + \frac{h_{ST}}{22.7}}\right)\cdot\left(0.519 + \frac{D_T}{N_{ST}^{1.60}\cdot t_T^{1.42}} + \frac{11.5}{t_T^{0.797}} + \frac{359}{t_{ST}^{2.91}}\right)$ (3.15)
Round	Fillet-welded tube-to-transverse plate connections stiffened by longitudinal attachments	Fillet weld-toe on tube wall	U.S. Customary Units $SCF = \left(9.84 - \frac{D_T}{1.82} + 4.89\cdot\frac{D_T^{1.03}}{N_{ST}^{0.914}}\right)\cdot\left(\frac{0.129}{h_{ST} + 6.56}\right)\cdot\left(0.859 + \frac{2.79}{t_{ST}^{0.631}}\right)\cdot\left(0.802 + \frac{t_{TP}}{12.9}\right)$ (3.16) × SCF as per Equation (4.10) SI Units $SCF = \left(9.84 - \frac{D_T}{46.3} + \frac{D_T^{1.03}}{5.71\cdot N_{ST}^{0.914}}\right)\cdot\left(\frac{1.0}{h_{ST} + 167}\right)\cdot\left(1.0 + \frac{25.0}{t_{ST}^{0.631}}\right)\cdot\left(2.26 + \frac{t_{TP}}{117}\right)$ (3.17) × SCF as per Equation (4.11)
Multi-Sided	As above	As above	Multiply respective SCF above by: U.S. Customary Units $\left[\left(0.186 - \frac{t_T}{8.93}\right)\cdot\left(1.97 + \frac{D_T^{2.44}}{828}\right)\cdot e^{\left(\frac{0.028}{R - 1.01}\right)} + 0.923\right]$ (3.18) SI Units $\left[\left(0.186 - \frac{t_T}{227}\right)\cdot\left(1.97 + \frac{D_T^{2.44}}{2.22\cdot 10^6}\right)\cdot e^{\left(\frac{0.028}{R - 1.01}\right)} + 0.923\right]$ (3.19)

Figure 3.14. Parametric equations used to compute *SCF* in various types of connection configurations (note: the *SCF* is computed for the most fatigue-critical sections within models) (Roy et al. 2011).

The geometric dimensions required to utilize equations (3.10) through (3.19) were unable to be acquired for all fatigue tests within the database. In fact, only 129 of the 265 possible fatigue tests were included in this second synthesis approach due to limited information.

Once the stress concentration factor was determined for each of the applicable connections, they could be categorized based upon their magnitude. In total, three potential fatigue detail categories based upon stress concentration factors were identified and are listed as follows:

- E2: $2.0 \leq SCF < 3.0$
- E3: $3.0 \leq SCF < 4.0$
- E4: $SCF \geq 4.0$

Table 3.4 lists these new fatigue detail categories generated by the second synthesis approach and the number of fatigue tests that fall within each proposed detail category. It should be noted that there are still a significant number of fatigue tests that fall into each of these new detail categories (*e.g.*, 24 to 73 tests).

Table 3.4. Minimum, maximum and average *SCF* as well as number of contributing fatigue tests for each of the new fatigue detail categories developed in Synthesis Approach No. 2.

Fatigue Detail Category	SCF_{MIN}	SCF_{MAX}	SCF_{AVG}	No. of Contributing Fatigue Tests
E2	2.24	2.93	2.57	73
E3	3.08	3.87	3.51	24
E4	4.25	4.66	4.48	31

Similar to the first synthesis approach, there are a number of advantages and disadvantages to using Synthesis Approach No. 2 to generate fatigue curve statistical parameters to be used in the subsequent reliability study. The advantages of this approach include:

- The procedure provides a nearly universal way to estimate the *SCF* in connections typically used in sign support structures.
- The procedure uses a parameter that is more fundamental to the fatigue behavior of connections (*i.e.* the *SCF*) and this parameter may be a better indicator of fatigue life in the connections considered in the present study.
- The procedure removes ambiguity with regard to which fatigue detail category should be specified for a particular connection.

The disadvantages of this approach include:

- The parametric equations are empirically based with a limited number of contributing numerical analyses.
- Unique (unforeseen) connection configurations would require finite element analyses to obtain the *SCF* for appropriate detail specifications.

3.4.2 – Summary of Synthesized Results for Both Syntheses

Tables 3.5 through 3.17 provide all fatigue test results considered in the present study. The tables are separated based upon the research group that conducted the fatigue tests. Each table contains the following:

- Labeled specimens tested by each study
- Resulting fatigue detail category according to both synthesis approaches
- Nominal stress-range magnitude at which each test was conducted

- Number of cycles to failure for each test

It should be noted that only those tests that met the criteria outlined previously will have a fatigue detail category assigned to them. Some tests were able to be assigned using the first synthesis approach but not the second due to insufficient information regarding the geometric dimensions of the connection used within the test. Therefore, to keep the sample size as large as possible for both approaches, rather than labeling these tests as “Unused Test”, “na” was placed in the column for the detail category assigned by the second synthesis approach. Figures 3.15 through 3.26 provide keys for interpreting the labels given to each specimen.

Table 3.5. Fatigue test results and corresponding fatigue detail categories assigned by both synthesis approaches for fatigue data obtained by Archer and Gurney (1970).

Specimen Designation	Synthesis Approach No. 1 Detail Category	Synthesis Approach No. 2 Detail Category	Cycles to Failure	Stress Range (ksi)
AG-F-5/16-W-A-1	U3	na	28000	12.60
AG-F-5/16-W-B-2	U3	na	130000	10.60
AG-F-5/16-W-C-3	U3	na	230000	9.20
AG-F-5/16-W-D-4	U3	na	420000	8.00
AG-F-5/16-W-E-5	U3	na	600000	6.90
AG-F-5/16-W-F-6	U3	na	850000	5.60
AG-F-5/16-W-G-7	U3	na	2700000	4.60
AG-F-7/16-W-A-8	U3	na	550000	7.40
AG-F-7/16-W-B-9	U3	na	1400000	4.90
AG-F-7/16-W-C-10	U3	na	3300000	3.30
AG-F-5/16-RHS-A-11	U3	na	28000	11.00
AG-F-5/16-RHS-B-12	U3	na	120000	9.00
AG-F-5/16-RHS-C-13	U3	na	240000	8.00
AG-F-5/16-RHS-D-14	U3	na	430000	7.00
AG-F-5/16-RHS-E-15	U3	na	550000	6.00
AG-F-5/16-RHS-F-16	U3	na	850000	5.00
AG-F-5/16-RHS-G-17	U3	na	2700000	4.00
AG-F-7/16-RHS-A-18	U3	na	550000	9.00
AG-F-7/16-RHS-B-19	U3	na	1400000	6.00
AG-F-7/16-RHS-C-20	U3	na	3400000	4.00
AG-F-11/16-RHS-A-21	U3	na	800000	11.00
AG-F-11/16-RHS-B-22	U3	na	850000	10.00
AG-F-11/16-RHS-C-23	U3	na	1200000	8.00
AG-F-11/16-RHS-D-24	U3	na	1300000	9.00
AG-F-11/16-RHS-E-25	U3	na	1900000	7.00
AG-F-11/16-RHS-F-26	U3	na	2000000	7.00
AG-S-7/16-W-A-27	U1	na	350000	8.20
AG-S-7/16-W-B-28	U1	na	430000	7.60
AG-S-7/16-W-C-29	U1	na	800000	5.40
AG-S-7/16-W-D-30	U1	na	1100000	4.50
AG-S-9/16-W-A-31	U1	na	310000	7.00
AG-S-9/16-W-B-32	U1	na	550000	5.10
AG-S-9/16-W-C-33	U1	na	2300000	3.70
AG-S-7/16-RHS-A-34	U1	na	380000	10.00
AG-S-7/16-RHS-B-35	U1	na	430000	8.00
AG-S-7/16-RHS-C-36	U1	na	800000	6.50
AG-S-7/16-RHS-D-37	U1	na	1300000	5.50
AG-S-9/16-RHS-A-38	U1	na	310000	11.00
AG-S-9/16-RHS-B-39	U1	na	440000	7.00
AG-S-9/16-RHS-C-40	U1	na	590000	8.00
AG-S-9/16-RHS-D-41	U1	na	2400000	6.00

AG-A-B-C-D-E		
Connection Detail Configuration		
A	S	sleeved connection similar to fillet-welded socket connection
	F	flush fillet welds
Weld Configuration and Size		
B	Weld Size	
	5/16	5/16-in. fillet weld
	7/16	7/16-in. fillet weld
	9/16	9/16-in. fillet weld
	11/16	11/16-in. fillet weld
Failure Location		
C	W	failure in fillet weld
	RHS	failure in round hollow shape wall
Specimen Designation for Series		
D		specimen designation: A, B, C, etc.
Specimen Serial Number for MU Synthesis		
E	#	

Figure 3.15. Key to specimen labels for Archer and Gurney (1970).

Table 3.6. Fatigue test results and corresponding fatigue detail categories assigned by both synthesis approaches for fatigue data obtained by Fisher et al. (1981).

Specimen Designation	Synthesis Approach No. 1 Detail Category	Synthesis Approach No. 2 Detail Category	Cycles to Failure	Stress Range (ksi)
LEH-40-A-45CA-1-1	U1	E2	36100	18.80
LEH-40-A-45CA-2-2	U1	E2	117800	12.40
LEH-40-A-45CA-3-3	U1	E2	1892400	6.40
LEH-40-A-45CA-4-4	U1	E2	174200	12.40
LEH-40-A-45CA-5-5	U1	E2	1208700	6.40
LEH-40-A-45CA-6-6	U1	E2	1472900	6.40
LEH-40-A-34CA-1-7	U2	E2	3751600	6.40
LEH-40-A-34CA-2-8	U2	E2	3573400	6.40
LEH-48-V-28CA-1-9	U2	E2	87000	18.90
LEH-48-V-28CA-2-10	U2	E2	317500	12.40
LEH-48-V-28CA-3-11 (a)	U2	E2	5244000	6.50
LEH-48-V-28CA-4-12	U2	E2	198100	12.40
LEH-48-V-28CA-5-13 (b)	U2	E2	5186500	6.50
LEH-48-V-28CA-6-14 (c)	U2	E2	8832300	6.40

Notes:

(a) Large crack reported in mast-arm, but failure reported in pole at base connection.

(b) Failure in pole at base, but failure seen in mast-arm.

(c) Small crack reported in mast-arm, but no failure in pole.

LEH-A-B-C-D-E		
Mast-Arm and Vertical Pole Seam Weld Location		
A	40	mast arm and vertical column seam welds located at points of tension or compression stress
	48	mast arm and vertical column seam welds located randomly
Mast-Arm and Vertical Pole Material Type		
B	A	ASTM A283 Grade D Steel, galvanized after fabrication
	V	ASTM A595 Grade A Steel, galvanized after fabrication
Fillet Weld Configuration - Contact Angle		
C	45CA	45-degree contact angle
	34CA	34-degree contact angle
	28CA	28-degree contact angle
Specimen Designation for Series		
D		specimen designation: 1, 2, 3, etc.
Specimen Serial Number for MU Synthesis		
E	#	

Figure 3.16. Key to specimen labels for Fisher et al. (1981).

Table 3.7. Fatigue test results and corresponding fatigue detail categories assigned by both synthesis approaches for fatigue data obtained by South (1997).

Specimen Designation	Synthesis Approach No. 1 Detail Category	Synthesis Approach No. 2 Detail Category	Cycles to Failure	Stress Range (ksi)
IDOT-1-1	Unused Test	Unused Test	62565	33.70
IDOT-1-2	Unused Test	Unused Test	216372	22.50
IDOT-1-3	Unused Test	Unused Test	581212	19.70
IDOT-1-4	Unused Test	Unused Test	299657	16.90
IDOT-1-5 (a)	Unused Test	Unused Test	15000000	11.20
IDOT-1-6 (a)	Unused Test	Unused Test	10416673	8.40
IDOT-2-7	Unused Test	Unused Test	157804	33.70
IDOT-2-8	Unused Test	Unused Test	213422	22.50
IDOT-2-9	Unused Test	Unused Test	570601	19.70
IDOT-2-10	Unused Test	Unused Test	2568000	16.90
IDOT-2-11 (a)	Unused Test	Unused Test	15000000	11.20
IDOT-2-12 (a)	Unused Test	Unused Test	10416673	8.40
IDOT-3-13	Unused Test	Unused Test	35629	33.70
IDOT-3-14	Unused Test	Unused Test	291300	22.50
IDOT-3-15	Unused Test	Unused Test	199694	19.70
IDOT-3-16	Unused Test	Unused Test	1322214	16.90
IDOT-3-17 (a)	Unused Test	Unused Test	15000000	11.20
IDOT-3-18 (a)	Unused Test	Unused Test	10416673	8.40
IDOT-4-19	Unused Test	Unused Test	40819	33.70
IDOT-4-20	Unused Test	Unused Test	182166	22.50
IDOT-4-21	Unused Test	Unused Test	581206	19.70
IDOT-4-22	Unused Test	Unused Test	1181967	16.90
IDOT-4-23 (a)	Unused Test	Unused Test	15000000	11.20
IDOT-4-24	Unused Test	Unused Test	6243700	8.40

Notes:

(a) Testing stopped with no failure. Considered runout.

Table 3.8. Fatigue test results and corresponding fatigue detail categories assigned by both synthesis approaches for fatigue data obtained by Deschamp (2002).

Specimen Designation	Synthesis Approach No. 1 Detail Category	Synthesis Approach No. 2 Detail Category	Cycles to Failure	Stress Range (ksi)
WY-IS-S-1.75-4-10.00-1	Unused Test	Unused Test	500000	24.02
WY-IS-S-2.00-6-12.25-2	Unused Test	Unused Test	750000	5.51
WY-IS-FP-2.00-5-11.50-3 (a, b, f)	Unused Test	Unused Test	7000000	8.47
WY-IS-S-1.50-6-12.50-4 (b, e)	Unused Test	Unused Test	2750000	5.17
WY-V-FP-2.00-4-10.00-5 (b, c)	Unused Test	Unused Test	3712687	19.58
WY-V-FP-2.00-4-10.00-6 (b, c)	Unused Test	Unused Test	3750000	10.00
WY-V-FP-2.00-4-10.50-7 (b, c)	Unused Test	Unused Test	3250000	17.00
WY-V-FP-2.00-4-10.50-8 (b, c)	Unused Test	Unused Test	3000000	16.98
WY-V-FP-2.00-4-11.25-9 (b, d)	Unused Test	Unused Test	19500000	8.36
WY-V-FP-2.00-4-12.75-10 (b, d)	Unused Test	Unused Test	2250000	6.39

Notes:

(a) ECASR represents an Equivalent Constant Amplitude Stress Range.

(b) Indicates specimen was considered as a run-out (no cracking found when terminated)

(c) Mast-arm wall thickness rounded up to 4/16-in. (actually 0.239 inches)

(d) Mast-arm wall thickness rounded down to 4/16-in. (actually 0.267 inches)

(e) Indicates an open-box connection configuration (only one in test matrix).

(f) Multi-sided specimen.

WY-A-B-C-D-E-F		
Specimen Designation		
A	IS	in-service specimen
	V	virgin (manufactured) specimen
Mast-Arm Connection Configuration		
B	S	socketed with fillet weld
	FP	full-penetration weld
Mast-Arm Connection Plate Thickness		
C	#	connection plate thickness in inches
Mast-Arm Wall Thickness		
D	#	mast-arm wall thickness in sixteenths of an inch
Mast-Arm Diameter		
E	#	mast-arm diameter in inches
Specimen Serial Number for MU Synthesis		
F	#	

Figure 3.17. Key to specimen labels for Deschamp (2002).

Table 3.9. Fatigue test results and corresponding fatigue detail categories assigned by both synthesis approaches for fatigue data obtained by Machietto (2002).

Specimen Designation	Synthesis Approach No. 1 Detail Category	Synthesis Approach No. 2 Detail Category	Cycles to Failure	Stress Range (ksi)
VAL-R-45FW-A-1	R1	na	575000	13.40
VAL-R-45FW-B-2	R1	na	376740	13.40
VAL-R-15FP-A-3	R3	na	950040	13.40
VAL-R-TCFP-A-4	R3	na	657540	17.60
VAL-R-RFWS-A-5	R1	na	514085	17.60
VAL-R-RFWS-B-6	R1	na	673989	17.60
VAL-U-SFW-A-7 (a)	Unused Test	Unused Test	4808700	13.40
VAL-U-SFW-B-8	U2	na	1240200	17.60
VAL-U-SFW-C-9 (a)	Unused Test	Unused Test	5321160	17.60
VAL-U-SFW-D-10 (a)	Unused Test	Unused Test	1982743	17.60
VAL-U-FP-A-11	U4	na	498960	17.60
VAL-U-FP-B-12	U4	na	4504500	17.60

Notes:

(a) Testing stopped with no failure. Considered runout.

VAL-A-B-C-D		
Reinforcement Configuration		
A	U	unreinforced specimen
	R	reinforced specimen
Connection Detail Configuration		
B	If U-type specimen	
	SFW	socketed connection, unequal-leg fillet welds (long leg on mast-arm)
	FP	full penetration welds, backing ring attached with continuous fillet welds, 1-in. tall backing ring
	If R-type specimen	
	45FW	45-degree gussets, fillet welded, 3.25-in. long
	15FP	15-degree contour gussets, full penetration welds, 6-in. long, weld ground smooth at transition
	TCFP	Tangent-contour gussets, full penetration welds, 5.83-in. long, weld ground smooth at transition
	RFWS	Radial gusset, fillet welds terminated 1/2-in. short of gusset ends, 5.44-in. long
Specimen Designation for Series		
C		specimen designation: A, B, C, etc.
Specimen Serial Number for MU Synthesis		
D	#	

Figure 3.18. Key to specimen labels for Machietto (2002).

Table 3.10. Fatigue test results and corresponding fatigue detail categories assigned by both synthesis approaches for fatigue data obtained by Chen et al. (2002) and Alderson (1999).

Specimen Designation	Synthesis Approach No. 1 Detail Category	Synthesis Approach No. 2 Detail Category	Cycles to Failure	Stress Range (ksi)
UMO-VAL-O-1-1	U1	na	1800000	8.00
UMO-VAL-N-1-2	U2	na	2100000	8.00
UMO-VAL-N-2-3 (a)	U2	na	400000	8.00
UMO-UM-O-1-4 (b)	U1	na	500000	8.00
UMO-JEM-O-1-5 (c)	Unused Test	Unused Test	na	na

Notes:

(a) Lack of fusion noted as potential cause for low cycle count.

(b) NDT using magnetic particle testing indicated a flaw was present in weld.

(c) NDT inspection resulted in weld flaw being detected and no testing conducted.

UMO-A-B-C-D

Fabricator

A	VAL	Valmont
	JEM	Acronym Unknown
	UM	Union Metals

Fillet Weld Configuration

B	O	Standard (equal-leg) fillet weld
	N	New (fatigue-resistant, unequal leg) fillet weld

Specimen Designation for Series

C	specimen designation: 1, 2, 3, etc.

Specimen Serial Number for MU Synthesis

D	#

Figure 3.19. Key to specimen labels for Chen et al. (2002) and Alderson (1999).

Table 3.11. Fatigue test results and corresponding fatigue detail categories assigned by both synthesis approaches for fatigue data obtained by Koenigs et al. (2003).

Specimen Designation	Synthesis Approach No. 1 Detail Category	Synthesis Approach No. 2 Detail Category	Cycles to Failure	Stress Range (ksi)
VAL-U-N-A-1	U2	E2	249446	11.90
VAL-U-N-B-2	U2	E2	453948	11.90
VAL-U-N-C-3	U2	E2	2072592	6.29
VAL-U-N-D-4 (a)	Unused Test	Unused Test	6856881	6.20
TX-U-N-A-5	U2	E2	2199343	6.00
TX-U-N-B-6	U2	E2	2816706	6.10
TX-U-N-C-7	U2	E2	177596	11.80
TX-U-N-D-8	U2	E2	194694	12.00
VALN-U-N-A-9	U2	E2	389428	11.90
VALN-U-N-B-10	U2	E2	265540	11.80
VALN-U2-N-A-11	U2	E2	5144528	11.90
VALN-U2-N-B-12	U2	E2	1683127	11.80
VALN-W-N-A-13	R3	E3	422400	17.71
VALN-W-N-B-14	R3	E3	422400	17.56
VALN-U-P-A-15 (a)	Unused Test	Unused Test	4557126	11.60
VALN-U-P-B-16 (a)	Unused Test	Unused Test	4557126	11.50
VALN-U-P-C-17	Unused Test	Unused Test	1301077	19.95
VAL-U-P-E-18	Unused Test	Unused Test	393767	11.40
VAL-U-P-F-19	Unused Test	Unused Test	353103	11.50
VALN-U-G-A-20	U2	E2	183132	11.60
VALN-U-G-B-21	U2	E2	151679	11.50
VAL-U-GP-A-22	Unused Test	Unused Test	4545952	11.60
VAL-U-GP-B-23	Unused Test	Unused Test	224240	19.91
VALN-U-PG-A-24	Unused Test	Unused Test	277634	11.60
VALN-U-PG-B-25	Unused Test	Unused Test	313727	11.50
VALN-U-P-A-UL-26	Unused Test	Unused Test	5004729	11.60
VALN-U-P-B-UL-27	Unused Test	Unused Test	5440165	11.50
VALN-EC-N-A-28	R1	na	4245460	5.49
VALN-EC-N-B-29	R1	na	2363152	5.73

Notes:

(a) Runout.

(b) Lack of fusion defect detected post-testing.

Possible repeats within data.

Table 3.11. Continued… Fatigue test results and corresponding fatigue detail categories assigned by both synthesis approaches for fatigue data obtained by Koenigs et al. (2003).

Specimen Designation	Synthesis Approach No. 1 Detail Category	Synthesis Approach No. 2 Detail Category	Cycles to Failure	Stress Range (ksi)
VALN-IC-N-A-30	R1	na	227030	10.75
VALN-IC-N-B-31	R1	na	227030	10.68
VAL-3x3/8-P-C-32	Unused Test	Unused Test	393767	11.50
VAL-3x3/8-P-C2-33	Unused Test	Unused Test	353103	11.50
VAL-3x3/8-P-C-LMS-34	Unused Test	Unused Test	1707128	12.10
VAL-3x1/4-N-A-35	R1	E4	476269	11.10
VAL-3x1/4-N-B-36	R1	E4	696326	11.40
VAL-3x1/4-N-C-37	R1	E4	3592372	6.10
TX-3x1/4-N-A-38	R1	E4	616136	11.70
TX-3x1/4-N-B-39	R1	E4	416146	11.80
TX-3x1/4-N-C-LMS-40	R1	E4	523397	11.90
VAL-3x3/8-N-A-41	R1	E3	386253	11.70
VAL-3x3/8-N-B-42	R1	E3	410410	11.60
TX-3x3/8-N-A-43	R1	E3	473735	11.70
TX-3x3/8-N-B-44	R1	E3	657716	11.60
VAL-6x3/8-N-A-45 (b)	R1	E3	242728	11.20
VAL-6x3/8-N-B-46	R1	E3	653392	11.30
VAL-6x3/8-N-C-47	R1	E3	3592372	5.90
TX-6x3/8-N-A-48	R1	E2	783857	11.20
TX-6x3/8-N-B-49	R1	E2	783857	11.30
TX-6x3/8-N-C-50	R1	E2	7503037	5.76
VALN-6x3/8@45-N-A-51	R1	E3	238515	11.96
VALN-6x3/8@45-N-B-52	R1	E3	161843	11.98
VALN-6x3/8@45-N-C-53	R1	E3	6066817	4.30
VALN-6x3/8@45-N-D-54	R1	E3	6066817	4.30
VALN-UR-N-A-55	R1	na	1776724	7.62
VALN-UR-N-B-56	R1	na	950670	7.60
VALN-UR-N-B2-57	R1	na	339152	12.57

Notes:

(a) Runout.

(b) Lack of fusion defect detected post-testing.

Possible repeats within data.

A-B-C-D-E-F		
Mast-Arm Wall Thickness and Manufacturing Entity		
A	VAL	0.179-in. thick, Brenham, TX
	TX	0.239-in. thick, Brenham, TX
	VALN	0.179-in. thick, Valley, NE
Connection Detail Configuration		
B	U	unreinforced, fillet weld, socketed
	U2	unreinforced, fillet weld, socketed, 2-inch plate
	W	reinforced, full-penetration weld with backing ring
	EC	reinforced, external collar
	IC	reinforced, internal collar
	UR	reinforced, U-rib stiffener
	L x t_s	reinforced, triangular stiffener (L - length in inches) (t_s - thickness in inches)
	L x t_s @ 45	reinforced, triangular stiffener at 45-degree orientation
Retrofit Treatment or Specialized Coating		
C	N	no retrofit treatment or galvanizing
	P	ultra-sonic impact treatment (UIT)
	G	galvanized
	PG	UI treated then galvanized
	GP	galvanized then UI treated
Specimen Designation for Series		
D		specimen designation: A, B, C, etc.
Special Notes (no entry indicates no special testing treatment or treatment scenario)		
E	LMS	fatigue testing done at low mean stress
	UL	UIT performed in unloaded state
Specimen Serial Number for MU Synthesis		
F	#	

Figure 3.20. Key to specimen labels for Koenigs et al. (2003).

Table 3.12. Fatigue test results and corresponding fatigue detail categories assigned by both synthesis approaches for fatigue data obtained by Ocel et al. (2006).

Specimen Designation	Synthesis Approach No. 1 Detail Category	Synthesis Approach No. 2 Detail Category	Cycles to Failure	Stress Range (ksi)
MN-P-FR1-IP-N-CSR-5-1.25-1	U5	E4	83806	8.25
MN-P-FR1-IP-N-CSR-5-1.25-2	U5	E4	981490	3.43
MN-P-FR1-IP-N-CSR-5-1.25-3	U5	E4	610124	3.80
MN-P-FR1-OP-N-CSR-5-1.25-4 (a)	Unused Test	Unused Test	5038549	4.09
MN-P-FR1-OP-N-CSR-5-1.25-5	U5	E4	170606	5.41
MN-P-FR1-OP-N-CSR-5-1.25-6 (a)	Unused Test	Unused Test	1292565	5.41
MN-P-FR1-OP-N-CSR-5-1.25-7	U5	E4	301484	5.41
MN-P-FR1-OP-N-CSR-5-1.25-8	U5	E4	2293739	5.41
MN-P-FR2-IP-N-CSR-5-1.25-9	U5	E4	591696	4.26
MN-P-FR2-IP-N-CSR-5-1.25-10	U5	E4	868266	3.65
MN-P-FR2-IP-N-CSR-5-1.25-11	U5	E4	1658906	4.10
MN-P-FR1-IP-HPR-MR-5-1.25-12	Unused Test	Unused Test	4126888	4.55
MN-P-FR2-IP-HPR-CSR-5-1.25-13	Unused Test	Unused Test	1106830	6.99
MN-P-FR2-IP-HP-MR-5-1.25-14	Unused Test	Unused Test	8501877	5.82
MN-P-FR2-IP-HP-MR-5-1.25-15	Unused Test	Unused Test	2558528	7.10
MN-P-FR2-IP-HP-MR-5-1.25-16	Unused Test	Unused Test	124147	10.00
MN-P-FR2-IP-HP-MR-5-1.25-17	Unused Test	Unused Test	5571296	6.00
MN-P-FR2-IP-HPR-MR-5-1.25-18	Unused Test	Unused Test	1131798	7.91
MN-P-FR2-IP-HP-MR-5-1.25-19	Unused Test	Unused Test	5366869	7.91
MN-P-FR2-IP-N-MR-5-2.50-1-20	Unused Test	Unused Test	4222993	11.17
MN-P-FR2-IP-N-CSR-5-2.50-2-21	U5	E4	81924	14.90
MN-P-FR2-IP-HP-CSR-5-2.50-2-22	Unused Test	Unused Test	978382	14.90
MN-P-FR2-IP-N-CSR-5-2.50-1-23	U5	E4	566119	14.90
MN-P-FR2-IP-N-CSR-5-2.50-2-24	U5	E4	101916	14.90
MN-P-FR2-IP-N-CSR-3-2.50-1-25	U5	E4	330137	15.00
MN-P-FR2-IP-N-CSR-3-2.50-2-26	U5	E4	140545	15.00
MN-P-FR2-IP-N-CSR-3-2.50-1-27	U5	E4	183638	15.00
MN-P-FR2-IP-N-CSR-3-2.50-2-28	U5	E4	86888	15.00
MN-MA-FR3-IP-N-CSR-5-1.25-1-29	Unused Test	Unused Test	6997582	8.54
MN-MA-FR3-IP-N-CSR-5-1.25-1-30	U7	E4	420785	15.37
MN-MA-FR3-IP-N-CSR-5-1.25-1-31	U7	E4	434329	15.37
MN-MA-FR3-IP-N-CSR-5-1.25-1-32	U7	E4	242060	15.37
MN-MA-FR3-IP-N-CSR-5-1.25-2-33	U7	E4	420662	15.37
MN-MA-FR3-IP-N-CSR-5-1.25-2-34	U7	E4	372056	15.37
MN-MA-FR3-IP-N-CSR-5-1.25-2-35	U7	E4	298023	15.37
MN-MA-FR3-IP-N-CSR-5-1.25-2-36	U7	E4	267922	15.37
MN-MAG-FR3-IP-N-MR-5-1.25-1-37	Unused Test	Unused Test	1642305	4.15
MN-MAG-FR3-IP-N-MR-5-1.25-1-38	Unused Test	Unused Test	1300949	11.30
MN-MAG-FR3-IP-N-CSR-5-1.25-1-39	R4	E3	171695	10.38
MN-MAG-FR3-IP-N-CSR-5-1.25-1-40	R4	E3	186036	10.33
MN-MAG-FR3-IP-N-CSR-5-1.25-2-41	R4	E3	223987	10.38
MN-MAG-FR3-IP-N-CSR-5-1.25-2-42	R4	E3	157123	10.33

Notes:

(a) Runout.

MN-A-B-C-D-E-F-G-H-I		
Specimen Designation		
A	P	Pole Base Plate Connection
	MA	Unstiffened Mast-Arm Connection - Mast-Arm with full-penetration weld
	MAG	Gusset Stiffened Mast-Arm Connection - Mast-Arm with socket connection and gusset stiffeners
Test Frame Configuration		
B	FR1	Test Frame Configuration 1
	FR2	Test Frame Configuration 2
	FR3	Test Frame Configuration 3
Loading Direction		
C	IP	In-Plane Loading
	OP	Out-of-Plane Loading
Retrofit Treatment Implemented		
D	N	None
	HP	Hammer Peening
	HPR	Hammer Peening with Simulated Dead Load and Crack Present
Stress Range Methodology		
E	CSR	Constant Amplitude Stress Range
	MR	Miner's Cumulative Fatigue Damage Equivalent
Pole or Mast-Arm Tube Wall Thickness		
F	#	Number of sixteenths of an inch (e.g. 5 - indicates 5/16 inch)
Connection Plate Thickness		
G	#	Plate thickness (e.g. 1.25 in. or 2.50 in.)
Test Direction		
H	1	Indicates first side testing
	2	Indicates second side testing
Specimen Serial Number for MU Synthesis		
I	#	

Figure 3.21. Key to specimen labels for Ocel et al. (2006).

Table 3.13. Fatigue test results and corresponding fatigue detail categories assigned by both synthesis approaches for fatigue data obtained by Rios (2007).

Specimen Designation	Synthesis Approach No. 1 Detail Category	Synthesis Approach No. 2 Detail Category	Cycles to Failure	Stress Range (ksi)
UTX-24-1.5-8-S-A-1	U5	E4	13193	12.00
UTX-24-1.5-8-S-B-2	U5	E4	13193	12.00
UTX-24-2.0-8-S-A-3	U5	E3	46772	12.00
UTX-24-2.0-8-S-B-4	U5	E3	46772	12.00
UTX-24-3.0-8-S-A-5	U5	E2	147550	12.00
UTX-24-3.0-8-S-B-6	U5	E2	147550	12.00
UTX-24-1.5-12-S-A-7	U5	E3	27977	12.00
UTX-24-1.5-12-S-B-8	U5	E3	27977	12.00
UTX-24-2.0-12-S-A-9	U5	E2	143214	12.00
UTX-24-2.0-12-S-B-10	U5	E2	143214	12.00
UTX-24-2.0-8-WY-A-11	R3	na	133819	12.00
UTX-24-2.0-8-WY-B-12	R3	na	133819	12.00
UTX-24-3.0-12-TX-A-13	U7	E2	236154	12.00
UTX-24-3.0-12-TX-B-14	U7	E2	327487	12.00
UTX-24-2.0-8-SB-A-15	R1	na	785058	12.00
UTX-24-2.0-8-SB-B-16	R1	na	483314	12.00

UTX-A-B-C-D-E-F		
Pole Diameter		
A	#	pole diameter in inches
Base Plate Thickness in inches		
B	#	
Number of Bolts used in Base Plate		
C	#	
Connection Detail		
D	S	Socketed Connection
	SB	Stool Base
	TX	Texas Full Penetration Weld
	WY	Wyoming Full Penetration Weld
Specimen Designation for Series		
E		specimen designation: A, B, C, etc.
Specimen Serial Number for MU Synthesis		
F	#	

Figure 3.22. Key to specimen labels for Rios (2007).

Table 3.14. Fatigue test results and corresponding fatigue detail categories assigned by both synthesis approaches for fatigue data obtained by Anderson (2007).

Specimen Designation	Synthesis Approach No. 1 Detail Category	Synthesis Approach No. 2 Detail Category	Cycles to Failure	Stress Range (ksi)
S-1.75-10-B-1	U2	E2	142857	12.00
S-1.75-10-B-2 (b)	U2	E2	134197	12.00
S-1.75-10-A-3 (a)	Unused Test	Unused Test	515365	12.00
EC-1.75-10-A-4 (2)	R1	na	2345896	12.00
EC-1.75-10-A-5 (2) (b)	R1	na	2889260	12.00
EC-1.75-10-B-6 (2)	R1	na	5755111	12.00
EC-1.75-10-B-7 (1)	R1	na	3304490	12.00
EC-1.75-10-B-8 (1) (b)	R1	na	2382309	12.00
EC-1.75-10-A-9 (1) (a)	Unused Test	Unused Test	6206754	12.00
S-2.00-10-B-10	U2	E2	165998	12.00
S-2.00-10-A-11	U2	E2	235854	12.00
S-2.00-10-A-12 (2)	U2	E2	210793	12.00
S-2.00-10-A-13 (2) (b)	U2	E2	260700	12.00
S-2.00-10-B-14 (2)	U2	E2	622928	12.00
EC-2.00-10-A-15 (2)	R1	na	3939099	12.00
EC-2.00-10-B-16 (2)	R1	na	6927606	12.00
EC-2.00-10-A-17 (1)	R1	na	5384143	12.00
EC-2.00-10-A-18 (1) (b)	R1	na	2863521	12.00
EC-2.00-10-B-19 (1) (a)	Unused Test	Unused Test	8247664	12.00
WY-2.00-10-A-20	R3	na	4997925	12.00
WY-2.00-10-B-21	R3	na	7527441	12.00
CA-2.00-10-A-22	U2	E2	253657	12.00
CA-2.00-10-B-23	U2	E2	310352	12.00
S-3.00-10-B-24	U2	E2	792576	12.00
S-3.00-10-B-25 (b)	U2	E2	376291	12.00
S-3.00-10-A-26 (a)	Unused Test	Unused Test	1168867	12.00

Notes:

(a) Runout.

(b) Flip side of specimen with a fatigue crack present in the compression zone.

A-B-C-D-E (#)		
Specimen Connection Detail		
A	WY	Full Penetration (Wyoming Detail)
	EC	External Collar
	S	Standard Socket
	CA	California Weld Profile Socket Connection
Base Plate Thickness in inches		
B	#	
Outside Tube Diameter in inches		
C	#	
Specimen Designation for Series		
D		specimen designation: A, B, C, etc.
Specimen Serial Number for MU Synthesis		
E	#	
Weld Quality		
(#)	(1)	Specimen suspected of having unsatisfactory welds.
	(2)	Indicates replicate of specimen suspected of unsatisfactory welds.

Figure 3.23. Key to specimen labels for Anderson (2007).

Table 3.15. Fatigue test results and corresponding fatigue detail categories assigned by both synthesis approaches for fatigue data obtained by Richman (2009).

Specimen Designation	Synthesis Approach No. 1 Detail Category	Synthesis Approach No. 2 Detail Category	Cycles to Failure	Stress Range (ksi)
WY-S-B-P-2-10-A-1	R3	na	6734487	12.00
WY-S-B-P-2-10-B-2	R3	na	5219304	12.00
WY-S-G-V-2-10-A-3 (a)	Unused Test	Unused Test	12602940	12.00
WY-S-G-V-2-10-B-4 (a)	Unused Test	Unused Test	12602940	12.00
WY-S-G-V-2-8-A-5 (a)	Unused Test	Unused Test	12464800	12.00
WY-S-G-V-2-8-B-6 (a)	Unused Test	Unused Test	12464800	12.00
WY-S-G-V-2-8-A-7	R3	na	856122	24.00
WY-S-G-V-2-8-A-8 (b)	R3	na	747510	24.00
WY-S-G-V-2-8-B-9 (a)	Unused Test	Unused Test	1603632	24.00
EC-S-G-V-2-8-A-10	R1	na	512860	18.00
EC-S-G-V-2-8-B-11	R1	na	653208	18.00
WY-S-G-V-2-12-A-12	R3	na	1053554	18.00
WY-S-G-V-2-12-B-13	R3	na	880807	18.00
EC-S-G-V-2-12-A-14 (a)	Unused Test	Unused Test	805991	18.00
EC-S-G-V-2-12-B-15	R1	na	468601	18.00
EC-S-G-V-2-12-B-16 (b)	R1	na	337390	18.00
WY-R-G-V-3-10-A-17 (a)	Unused Test	Unused Test	8037420	18.00
WY-R-G-V-3-10-B-18 (a)	Unused Test	Unused Test	8037420	18.00
WY-R-G-V-3-10-A-19	R3	na	439511	24.00
WY-R-G-V-3-10-B-20	R3	na	343175	24.00
WY-R-B-V-3-10-A-21 (a)	Unused Test	Unused Test	10055123	24.00
WY-R-B-V-3-10-B-22 (a)	Unused Test	Unused Test	10055123	24.00
WY-R-B-V-3-10-A-23	R3	na	2232742	19.07
WY-R-B-V-3-10-A-24 (b)	R3	na	490061	24.00
WY-R-B-V-3-10-B-25	R3	na	3516775	21.14
WY-R-G-A-3-10-A-26	R3	na	222649	24.00
WY-R-G-A-3-10-A-27 (b)	R3	na	212891	24.00
WY-R-G-U-3-10-A-28	R3	na	1873499	24.00
ZZ88734-A-29	Unused Test	Unused Test	677763	24.00
ZZ88734-B-30	Unused Test	Unused Test	633458	24.00
ZZ88735-A-31	Unused Test	Unused Test	286526	28.00
ZZ88735-B-32	Unused Test	Unused Test	123072	28.00
ZZ88735-B-33 (b)	Unused Test	Unused Test	129090	28.00
WY-SR-G-V-2-10-A-34 (a)	Unused Test	Unused Test	9881390	12.00
WY-SR-G-V-2-10-B-35	R3	na	3051996	12.00
EC-SR-G-V-2-10-A-36 (a)	Unused Test	Unused Test	10652284	12.00
EC-SR-G-V-2-10-B-37 (a)	Unused Test	Unused Test	10652284	12.00
WY-R-G-P-3-10-A-38	R3	na	1272665	24.00
WY-R-G-P-3-10-B-39	R3	na	1210499	24.00
EC-R-G-P-2-10-A-40	R1	na	137220	24.00
EC-R-G-P-2-10-B-41	R1	na	244763	24.00
WY-R-G-P-3-12-A-42	R3	na	292468	24.00
WY-R-G-P-3-12-B-43	R3	na	328833	24.00
EC-R-G-P-2-12-A-44	R1	na	169059	24.00
EC-R-G-P-2-12-B-45	R1	na	119289	24.00

Notes:

(a) Runout.

(b) Flip side of specimen with a fatigue crack present in the compression zone.

A-B-C-D-E-F-G-H		
Specimen Connection Detail		
A	WY	Full Penetration (Wyoming Detail)
	EC	External Collar
Base Plate Detail		
B	S	Square Base Plate/Square Bolt Pattern
	R	Rectangular Base Plate/Rectangular Bolt Pattern
	SR	Square Base Plate/Rectangular Bolt Pattern
Galvanizing		
C	G	Galvanized
	B	Not Galvanized (Black)
Manufacturer Identification		
D	A	Ameron
	P	Pelco
	U	Union Metal
	V	Valmont
Base Plate Thickness in inches		
E	#	
Tube Diameter in inches		
F	#	
Specimen Designation for Series		
G		specimen designation: A, B, C, etc.
Specimen Serial Number for MU Synthesis		
H	#	

Figure 3.24. Key to specimen labels for Richman (2009).

Table 3.16. Fatigue test results and corresponding fatigue detail categories assigned by both synthesis approaches for fatigue data obtained by Roy et al. (2011).

Specimen Designation	Synthesis Approach No. 1 Detail Category	Synthesis Approach No. 2 Detail Category	Cycles to Failure	Stress Range (ksi)
LEH-AB-R-I-SF-CSR-1	U2	E2	180000	12.00
LEH-AB-R-I-SF-CSR-2	U2	E2	370000	12.00
LEH-AB-R-I-SF-CSR-3	U2	E2	1260000	12.00
LEH-AB-R-I-SF-CSR-4	U2	E2	2300000	7.00
LEH-AB-R-I-SF-CSR-5	U2	E2	3110000	7.00
LEH-AB-R-I-SF-CSR-6	U2	E2	1400000	7.00
LEH-AB-R-I-SF-CSR-7	U2	E2	1840000	7.00
LEH-PB-R-I-SF-MR-8	Unused Test	Unused Test	4880000	4.60
LEH-PB-R-I-SF-CSR-9	U2	E2	3050000	4.00
LEH-AB-R-II-BP1-CSR-10	R3	na	1610000	11.90
LEH-AB-R-II-BP1-CSR-11	R3	na	1320000	9.90
LEH-AB-R-II-BP1-CSR-12	R3	na	1410000	9.90
LEH-AB-R-II-BP1-CSR-13	R3	na	1170000	9.90
LEH-AB-R-II-BP1-CSR-14	R3	na	1290000	9.90
LEH-AB-R-II-BP1-CSR-15	R3	na	1490000	9.90
LEH-PB-R-II-BP1-CSR-16	R3	na	1980000	6.90
LEH-AB-R-III-BP2-CSR-17	R3	na	980000	12.00
LEH-AB-R-III-BP2-CSR-18	R3	na	1860000	12.00
LEH-AB-R-III-BP2-CSR-19	R3	na	1250000	12.00
LEH-AB-R-III-BP2-MR-20	Unused Test	Unused Test	29830000	9.00
LEH-AB-R-III-BP2-CSR-21	R3	na	6960000	10.00
LEH-AB-R-III-BP2-CSR-22	R3	na	9230000	10.00
LEH-AB-R-III-BP2-MR-23	Unused Test	Unused Test	15920000	11.20
LEH-AB-R-III-BP2-CSR-24	R3	na	5840000	16.00
LEH-AB-R-III-BP2-CSR-25	R3	na	270000	16.00
LEH-AB-R-III-BP2-CSR-26	R3	na	4790000	16.00
LEH-AB-R-IVA-BP2-MR-27	Unused Test	Unused Test	26150000	8.60
LEH-AB-R-IVA-BP2-MR-28	Unused Test	Unused Test	42640000	11.20
LEH-PB-R-IVA-BP2-MR-29	Unused Test	Unused Test	44100000	6.50
LEH-PB-R-IVA-BP2-MR-30	Unused Test	Unused Test	22120000	8.50
LEH-PB-R-V-BP2-CSR-31	R3	na	270000	12.00
LEH-PB-R-V-BP2-CSR-32	R3	na	1100000	12.00
LEH-PB-R-V-BP2-CSR-33	R3	na	1460000	12.00
LEH-PB-R-VI-BP2-MR-34	Unused Test	Unused Test	17200000	11.10
LEH-PB-R-VI-BP2-MR-35	Unused Test	Unused Test	40210000	10.60
LEH-PB-R-VI-BP2-MR-36	Unused Test	Unused Test	21000000	13.80
LEH-PB-R-VI-BP2-MR-37	Unused Test	Unused Test	31020000	6.10
LEH-PB-R-VI-BP2-MR-38	Unused Test	Unused Test	28230000	5.50
LEH-PB-R-VI-BP2-MR-39	Unused Test	Unused Test	20200000	15.20
LEH-PB-R-VI-BP2-MR-40	Unused Test	Unused Test	1750000	11.70
LEH-PB-R-VI-BP2-MR-41	Unused Test	Unused Test	7770000	13.40
LEH-AB-M-VII-SF-CSR-42	U5	E2	40000	12.00
LEH-AB-M-VII-SF-CSR-43	U5	E2	40000	12.00
LEH-AB-M-VII-SF-CSR-44	U5	E2	10000	12.00

Notes:

(a) Failure at stool stiffener.

(b) Failure at tube to stiffener weld toe on the tube wall.

Table 3.16. Continued… Fatigue test results and corresponding fatigue detail categories assigned by both synthesis approaches for fatigue data obtained by Roy et al. (2011).

Specimen Designation	Synthesis Approach No. 1 Detail Category	Synthesis Approach No. 2 Detail Category	Cycles to Failure	Stress Range (ksi)
LEH-AB-M-VII-SF-CSR-45	U5	E2	1030000	4.50
LEH-AB-M-VII-SF-CSR-46	U5	E2	390000	4.50
LEH-AB-M-VII-SF-MR-47	Unused Test	Unused Test	40890000	3.60
LEH-AB-M-VII-SF-CSR-48	U5	E2	70000	2.50
LEH-PB-M-VII-SF-CSR-49	U5	E3	90000	6.60
LEH-PB-M-VII-SF-CSR-50	U5	E3	90000	6.60
LEH-PB-M-VII-SF-CSR-51	U5	E3	100000	6.60
LEH-PB-M-VII-SF-MR-52	Unused Test	Unused Test	20650000	2.60
LEH-PB-M-VII-SF-MR-53	Unused Test	Unused Test	51500000	2.40
LEH-PB-M-VII-SF-MR-54	Unused Test	Unused Test	44620000	2.20
LEH-PB-M-IX-LSS-CSR-55 (a)	R6	na	590000	12.00
LEH-PB-M-IX-LSS-CSR-56 (a)	R6	na	270000	12.00
LEH-PB-M-IX-LSS-CSR-57 (a)	R6	na	510000	12.00
LEH-PB-M-IX-LSS-CSR-58 (a)	R6	na	450000	10.00
LEH-PB-M-IX-LSS-CSR-59 (a)	R6	na	2570000	7.00
LEH-PB-M-IX-LSS-CSR-60 (a)	R6	na	2640000	4.50
LEH-PB-M-IX-LSS-CSR-61 (a)	R6	na	4000000	4.50
LEH-PB-M-IX-LSS-CSR-62 (a)	R6	na	70000	16.00
LEH-PB-M-IX-LSS-CSR-63 (a)	R6	na	130000	16.00
LEH-PB-M-IX-LSS-CSR-64 (a)	R6	na	120000	16.00
LEH-PB-M-X-SF-MR-65	Unused Test	Unused Test	31380000	6.70
LEH-PB-M-X-SF-CSR-66	U5	E2	1750000	8.00
LEH-PB-M-X-SF-CSR-67	U5	E2	680000	8.00
LEH-PB-M-XI-BP1-CSR-68	R6	na	750000	12.00
LEH-PB-M-XI-BP1-CSR-69	R6	na	1560000	12.00
LEH-PB-M-XI-BP1-CSR-70	R6	na	330000	12.00
LEH-PB-M-XI-BP1-MR-71	Unused Test	Unused Test	15350000	7.10
LEH-PB-M-XI-BP1-MR-72	Unused Test	Unused Test	15380000	7.10
LEH-PB-M-XI-BP1-MR-73	Unused Test	Unused Test	15240000	7.10
LEH-PB-M-XI-BP1-MR-74	Unused Test	Unused Test	15200000	7.10
LEH-PB-M-XI-BP1-CSR-75	R6	na	100000	14.00
LEH-PB-M-XI-BP1-CSR-76	R6	na	140000	16.00
LEH-PB-M-XI-BP1-CSR-77	R6	na	60000	16.00
LEH-PB-M-XII-LS-CSR-78 (b)	R6	E2	230000	12.00
LEH-PB-M-XII-LS-CSR-79 (b)	R6	E2	400000	12.00
LEH-PB-M-XII-LS-CSR-80 (b)	R6	E2	580000	12.00
LEH-PB-M-XII-LS-MR-81 (b)	Unused Test	Unused Test	15310000	7.10
LEH-PB-M-XII-LS-MR-82 (b)	Unused Test	Unused Test	19390000	7.70
LEH-PB-M-XII-LS-CSR-83 (b)	R6	E2	4060000	7.00
LEH-PB-M-XII-LS-MR-84 (b)	Unused Test	Unused Test	20940000	7.90
LEH-PB-M-XII-LS-CSR-85 (b)	R6	E2	50000	16.00
LEH-PB-M-XII-LS-CSR-86 (b)	R6	E2	200000	16.00
LEH-PB-M-XII-LS-CSR-87 (b)	R6	E2	50000	16.00

Notes:

(a) Failure at stool stiffener.

(b) Failure at tube to stiffener weld toe on the tube wall.

LEH-A-B-C-D-E-F		
Pole or Mast-Arm		
A	AB	Arm Base
	PB	Pole Base
Specimen Type		
B	R	Round tube
	M	Multi-sided tube
Lehigh Identification Number		
C	#	I,II,III,IV,…X,XI,XII
Conection Detail Identification		
D	BP1	Full-penetration groove-welded round tube-to-transverse plate with backing ring welded to plate and tube
	BP2	Full-penetration groove-welded round tube-to-transverse plate with backing ring welded to plate only
	FPG	Full-penetration groove-welded round tube-to-transverse plate
	SF	Socketed fillet-welded tube-to-transverse plate connections
	LS	Tube-to-transverse plate connection stiffened by welded longitudinal attachments
	LSS	Tube-to-transverse plate connection stiffened by stool type welded longitudinal attachments
Stress Range Methodology		
E	CSR	Constant Amplitude Stress Range
	MR	Miner's Cumulative Fatigue Damage Equivalent
Specimen Serial Number for MU Synthesis		
F	#	

Figure 3.25. Key to specimen labels for Roy et al. (2011).

Table 3.17. Fatigue test results and corresponding fatigue detail categories assigned by both synthesis approaches for fatigue data obtained by the experimental program of this study.

Specimen Designation	Synthesis Approach No. 1 Detail Category	Synthesis Approach No. 2 Detail Category	Cycles to Failure	Stress Range (ksi)
MU-CSR-R-L-A1-1	U2	E2	4374464	6.00
UWM-MR-R-S-A1-2 (a)	Unused Test	Unused Test	2246094	5.42
MU-CSR-R-S-A2-3	U2	E2	72660	15.37
MU-CSR-R-L-B1-4 (a)	Unused Test	Unused Test	4374464	6.00
UWM-MR-R-S-B1-5	Unused Test	Unused Test	2246094	4.80
MU-CSR-R-S-B2-6 (a)	Unused Test	Unused Test	6893	15.37
UWM-CSR-M-N-A1-7	U5	E2	139000	6.50
UWM-CSR-M-S-B1-8 (a)	Unused Test	Unused Test	139000	6.50

Notes:

(a) Testing stopped with no failure (no cracks found).

A-B-C-D-E-F		
Testing Location		
A	MU	Marquette University
	UWM	University of Wisconsin-Milwaukee
Stress Range Methodology		
B	CSR	Constant Amplitude Stress Range
	MR	Miner's Cumulative Fatigue Damage Equivalent
Specimen Type		
C	R	Round tube
	M	Multi-sided tube
Specimen Designation - End Tested		
D	If tested at MU:	
	L	Large diameter end tested (d = 11.0 in.)
	S	Small diameter end tested (d = 9.9 in.)
	If tested at UWM:	
	N	North side of specimen tested
	S	South side of specimen tested
Specimen Designation - Top or Bottom		
E	A1	Top of specimen A
	A2	Bottom of specimen A
	B1	Top of specimen B
	B2	Bottom of specimen B
Specimen Serial Number for MU Synthesis		
F	#	

Figure 3.26. Key to specimen labels for the experimental program of this study.

3.5 – Statistical Analysis of Fatigue Data

Wirsching (1983) summarizes a procedure whereby one may define the relationship between applied constant-amplitude stress-range and resulting cycles to failure for a large number of fatigue test results. The procedure utilizes a least squares regression analysis as the foundation to the approach and recommends use of a lognormal random variable to characterize uncertainty in fatigue life (Wirsching 1983). However, some discussion regarding the appropriateness of this recommendation is warranted.

The lognormal distribution is a widely used probability model in engineering applications; however, many other distribution models are also used. To determine the best possible probabilistic representation of the fatigue data, the Kolmogorov-Smirnov (K-S) *goodness of fit* is performed (Foley et al. 2008; Wirsching 1983). The K-S test (not performed here) is a test that compares the cumulative distribution frequency for a sample with the cumulative distribution function for a particular theoretical probability distribution. In the past, this test has been performed on fatigue test data for typical connections used in offshore structures (Wirsching 1983) and for mast-arm sign connections found in Wisconsin (Foley et al. 2008). Each of these former studies determined that a lognormal distribution provided an acceptable representation of the fatigue-life variability associated with these connections.

The lognormal distribution, like most probability distributions, requires certain parameters to define its shape which ultimately affect the resulting probabilities provided by the distribution. The required parameters in the case of the lognormal distribution are:

$$\lambda_A = \ln \mu_A - \frac{1}{2} \cdot \zeta_A^2 \tag{3.20}$$

$$\zeta_A^2 = \ln\left[1+\left(\frac{\sigma_A}{\mu_A}\right)^2\right] = \ln\left[1+\left(CV_A\right)^2\right] \tag{3.21}$$

where λ_A is the expected value of the random variable *A*, ζ_A^2 is the variance of the random variable *A*, and σ_A is the standard deviation of *A*. Therefore, in order to generate the lognormal distributions necessary to quantify the variability in fatigue life of the connections under consideration, the parameters listed in equations (3.20) and (3.21) must be specified for each fatigue detail category developed in the fatigue syntheses performed in the preceding section. Specifically, this includes determining the mean, μ_A, and coefficient of variation, CV_A, of the lognormal random variable *A*. This will be done using the least-squares regression analysis outlined by Wirsching (1983).

3.5.1 – Least Squares Regression Analysis of Fatigue Data

A least squares regression analysis was performed on each of the fatigue detail categories from both synthesis approaches discussed previously. This section will describe the procedure that was followed.

Determining m, μ_A and CV_A

For clarity and ease of explanation, Figure 3.27 will be referenced in parts of this discussion. The information provided in Figure 3.27 corresponds to the experimental S_R-N data used in developing the E4 fatigue detail category as part of the second synthesis approach.

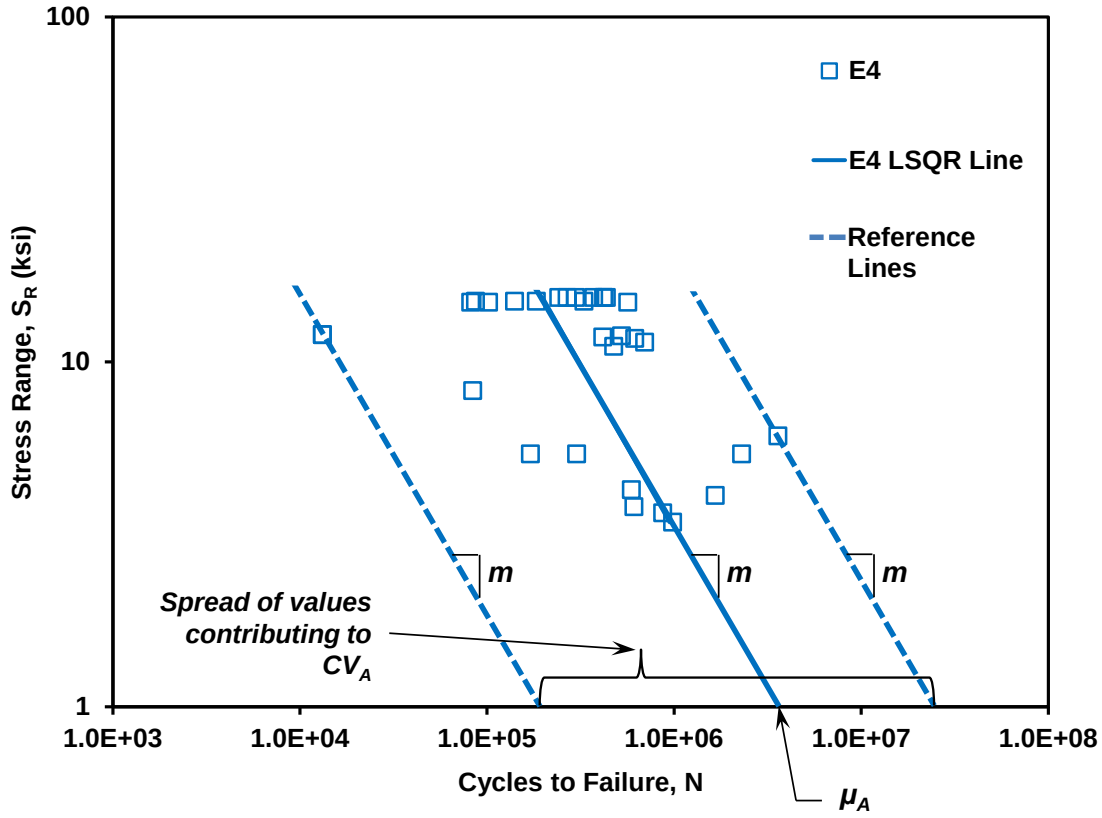

Figure 3.27. Example figure for explanation of statistical analysis (note: this figure also provides real S_R-N data and corresponding regression line for the E4 fatigue detail category).

Consider the group of $n = 31$ fatigue tests plotted in Figure 3.27. Each test contains a constant-amplitude stress-range magnitude, S_{Ri}, and a corresponding number of cycles to fatigue failure, N_i. A single straight line, drawn through the mean of the data and the coefficient of variation are used to characterize the variability in fatigue cycles to failure for the stress-ranges in the data set considered (Wirsching 1983). The analytical form of the typical fatigue life curve is given by,

$$N \cdot S_R^m = A \tag{3.22}$$

where m and A are empirical constants. More specifically, m is the slope of the straight line and A is the value of the x-intercept. Estimates for the values of m and A can be obtained from the

fatigue data being considered. Equation (3.22) can be expressed in a linear form (Wirsching 1983),

$$Y = a + b \cdot X \tag{3.23}$$

where the following are defined (Wirsching 1983),

$$Y = \log N \tag{3.24}$$

$$X = \log S_R \tag{3.25}$$

$$a = \log A \tag{3.26}$$

$$b = -m \tag{3.27}$$

Equations (3.24) through (3.27) convert the measured fatigue test data into log-log space. Equation (3.23) then defines the mean of Y ($\log N$) given X ($\log S_R$) (Wirsching 1983). This procedure assumes that Y has a normal distribution for all X.

The values for a and b are then estimated as follows (Wirsching 1983),

$$\hat{b} = \frac{\sum_{i=1}^{n}\left(X_i - \bar{X}\right)\cdot\left(Y_i - \bar{Y}\right)}{\sum_{i=1}^{n}\left(X_i - \bar{X}\right)^2} \tag{3.28}$$

$$\hat{a} = \bar{Y} - \hat{b} \times \bar{X} \tag{3.29}$$

where $\bar{X}$ and $\bar{Y}$ are the sample means of X and Y, respectively. Also, the estimates $\hat{a}$ and $\hat{b}$ are random variables because Y_i is a random variable (Wirsching 1983). Therefore, the least squares line through all fatigue data under consideration is,

$$\hat{Y} = \hat{a} + \hat{b} \cdot X \tag{3.30}$$

where $\hat{Y}$ is the mean (or expected value) of *Y* given *X*.

In order to determine the coefficient of variation, CV_A, the standard deviation in fatigue life for the samples within the detail category must be determined first. Determining the standard deviation may best be explained in graphical terms. Referencing Figure 3.27, in addition to the least squares (mean) line, two additional lines have been plotted with an equivalent slope, *m*, through test data points. Each line, if continued to the x-axis, will provide a value for *A* that is specific to the test that created that data point. For the sample of fatigue tests considered, the least squares line provides the expected value of *A*, or μ_A, and the two additional lines provide minimum and maximum values of *A*. Continuing this process for all data within the E4 detail category provides values of *A* for each individual fatigue test. A measure of the spread of these values about μ_A is termed the variance of *A* and is determined as (Haldar and Mahadevan 2000),

$$Var(A) = \frac{1}{n-1}\sum_{i=1}^{n}(A_i - \mu_A)^2 \tag{3.31}$$

The standard deviation may then be determined as (Haldar and Mahadevan 2000),

$$\sigma_A = \sqrt{Var(A)} \tag{3.32}$$

and finally, the coefficient of variation for *A* is,

$$CV_A = \frac{\sigma_A}{\mu_A} \tag{3.33}$$

The statistical parameters generated for the detail categories developed in Synthesis Approach No. 1 and Synthesis Approach No. 2 are provided in tabular form within Appendix F for reference. The corresponding S_R-N diagrams illustrating where these fatigue detail categories

land with respect to the existing AASHTO E' detail category are provided in Figures 3.28 through 3.34 for Synthesis Approach No. 1 and in Figures 3.35 through 3.37 for Synthesis Approach No. 2. The least squares lines that represent relationships between stress-range magnitude and cycles to failure for each detail of both synthesis approaches are provided in Figures 3.38 and 3.39. Summaries of the pertinent statistical parameters are provided in Tables 3.18 and 3.19.

It should be noted that in some cases regarding Synthesis Approach No. 1, the statistical parameters were unable to be determined due to an insufficient sample size (U6, R2 and R5), or in other cases, the data for the particular category generated unrealistic results (U4, U7, and R4).

Special Note on New Fatigue Detail Categories

It is clear that the new fatigue detail categories are empirical and based upon a limited number of fatigue tests conducted at a limited number of stress-ranges. Therefore, one should be cautious of extrapolating the use of these curves beyond the stress-range magnitudes used as the empirical foundation for the curves. For example, extrapolating the S_R-N curve of Figure 3.27 (E4 detail) would provide a stress-range magnitude of well over 100 ksi at N = 1000 cycles. A connection cycled at a stress-range of 100 ksi magnitude would certainly fail prior to 1000 cycles. A similar, but opposite argument can be made for low-end stress-ranges. At very low stress-ranges (< 1ksi), these connections are expected to sustain much longer lives than predicted by the new details. In other words, a straight line over all stress-ranges is physically unrealistic. One must be careful when extrapolating the details beyond the range of stress-ranges used during testing.

The present study established unique limits on the range of applicability for the new fatigue detail categories. The curves for each detail category were capped at the maximum stress-range contributing to that detail. The maximum applicable stress-range for each new fatigue detail

category is provided in the far right columns of Tables 3.18 and 3.19. It should be noted that all stress-ranges below the listed maximum applicable magnitudes in the present study contributed to damage accumulation. Therefore, extrapolation of the straight line behavior below the low-end stress-ranges for each new detail was necessary. This can be considered a conservative approach since each detail would perform much better than the curve indicates at very low stress-ranges.

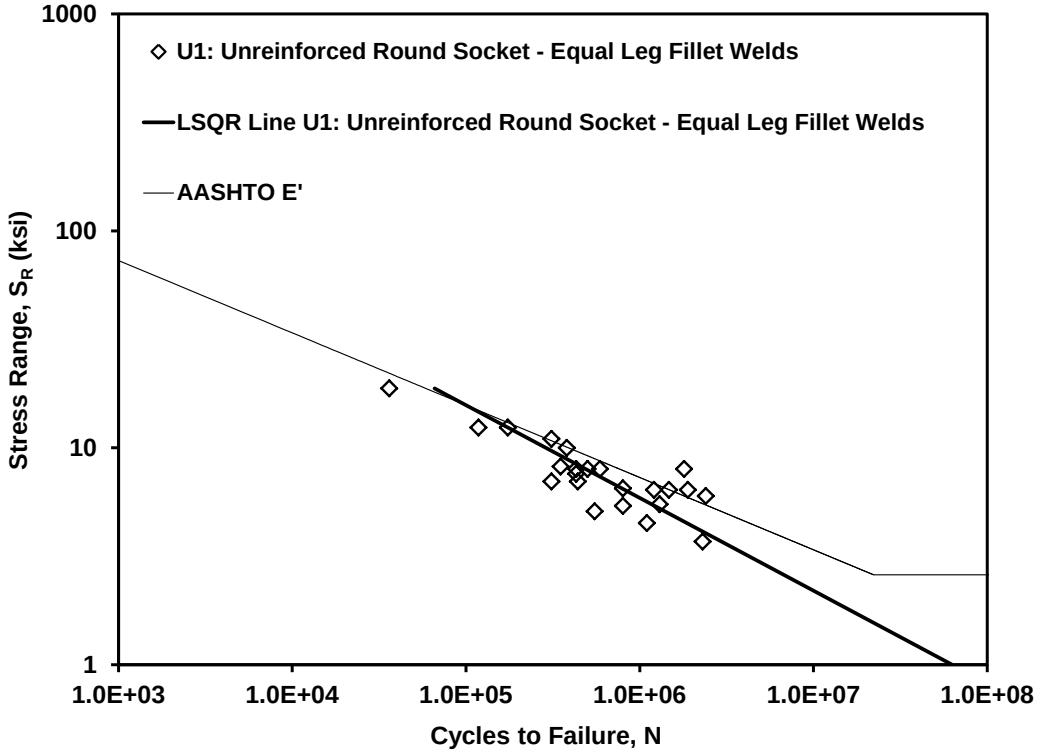

Figure 3.28. S_R-N diagram containing the fatigue tests contributing to the U1 detail category.

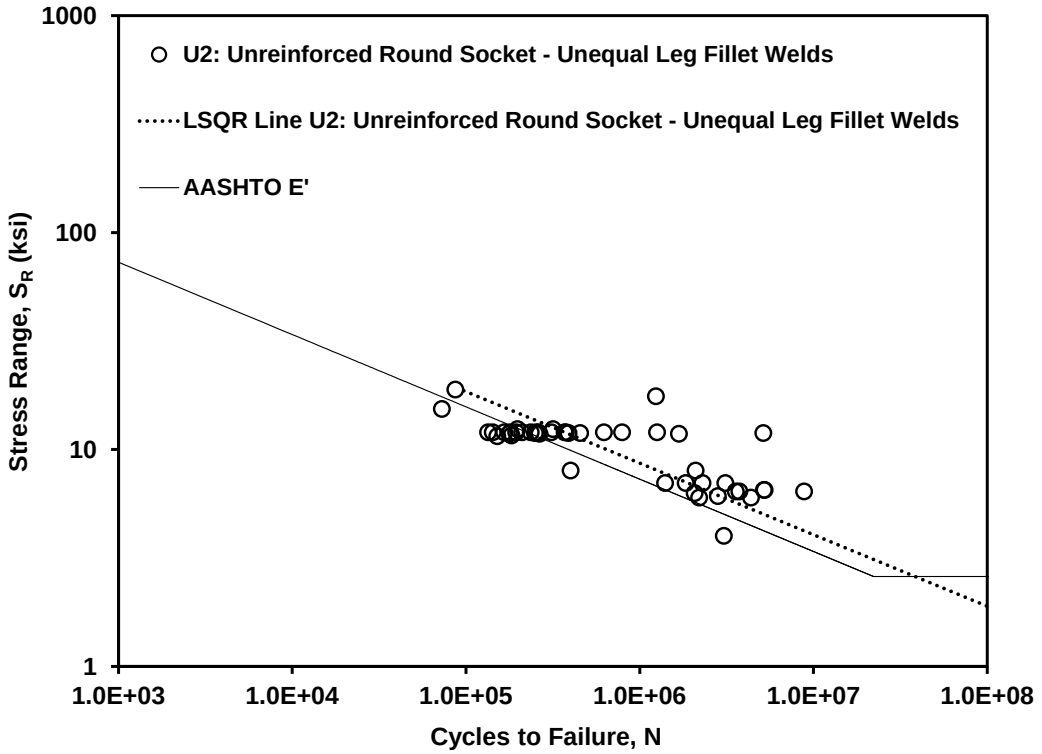

Figure 3.29. S_R-N diagram containing the fatigue tests contributing to the U2 detail category.

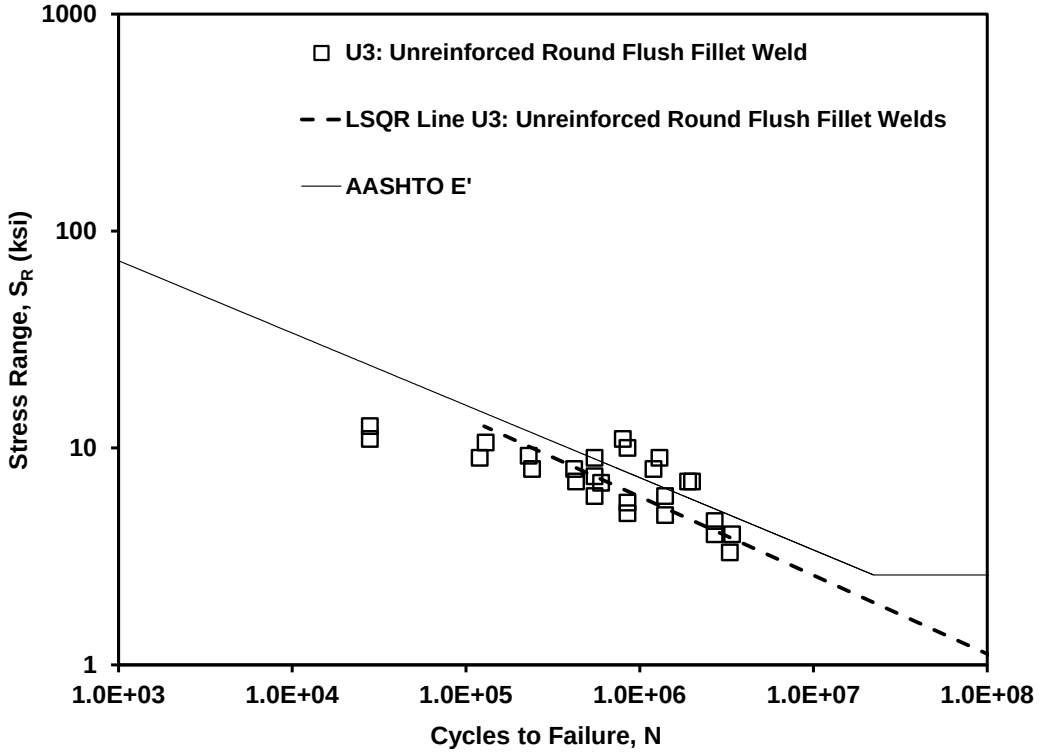

Figure 3.30. S_R-N diagram containing the fatigue tests contributing to the U3 detail category.

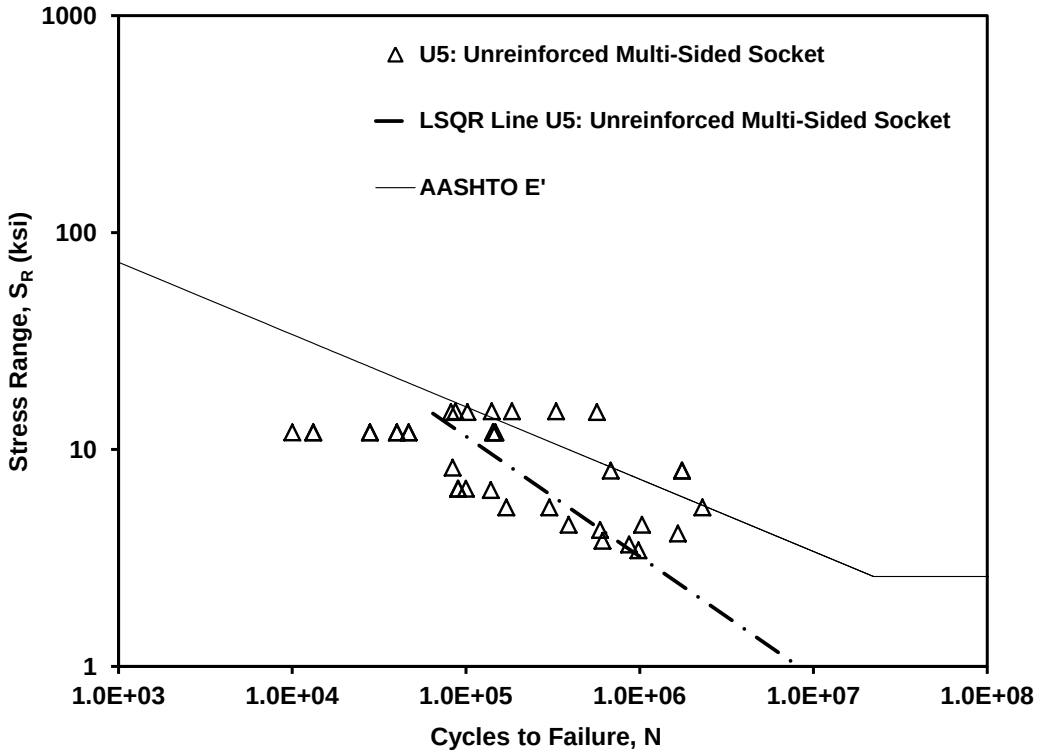

Figure 3.31. S_R-N diagram containing the fatigue tests contributing to the U5 detail category.

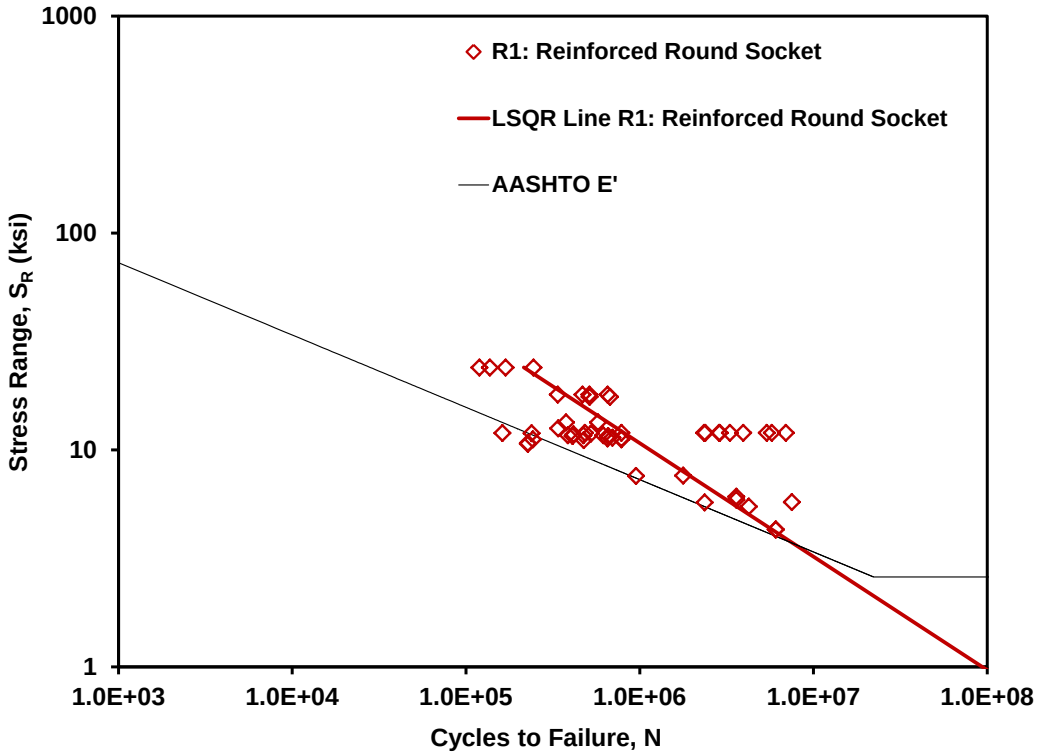

Figure 3.32. S_R-N diagram containing the fatigue tests contributing to the R1 detail category.

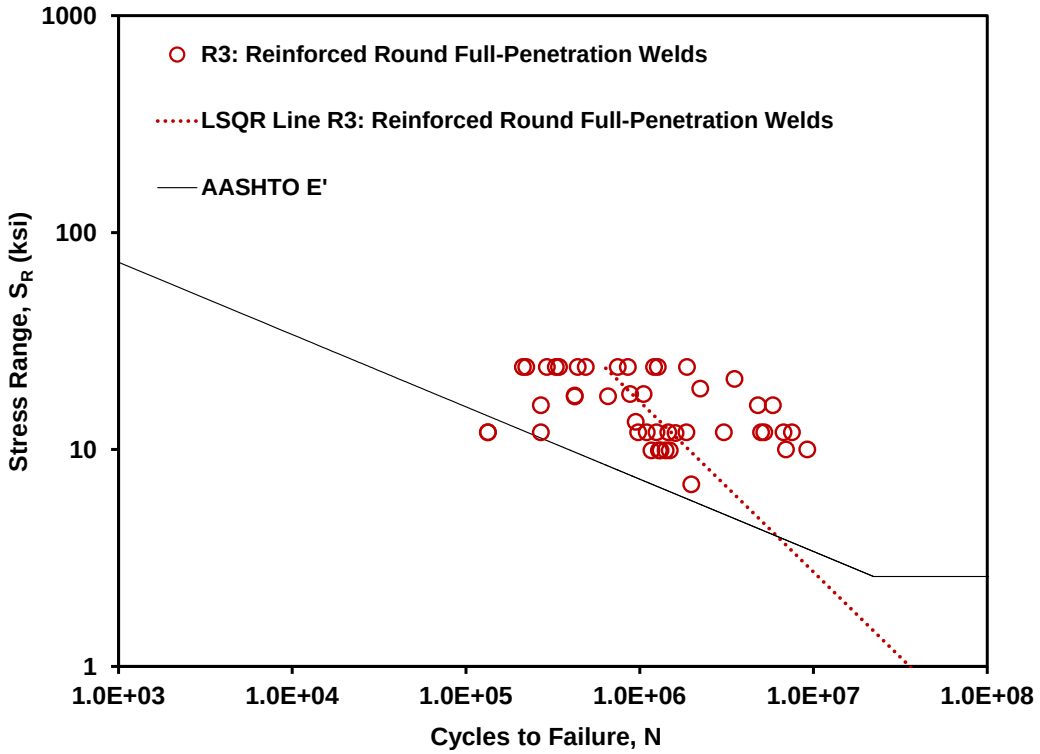

Figure 3.33. S_R-N diagram containing the fatigue tests contributing to the R3 detail category.

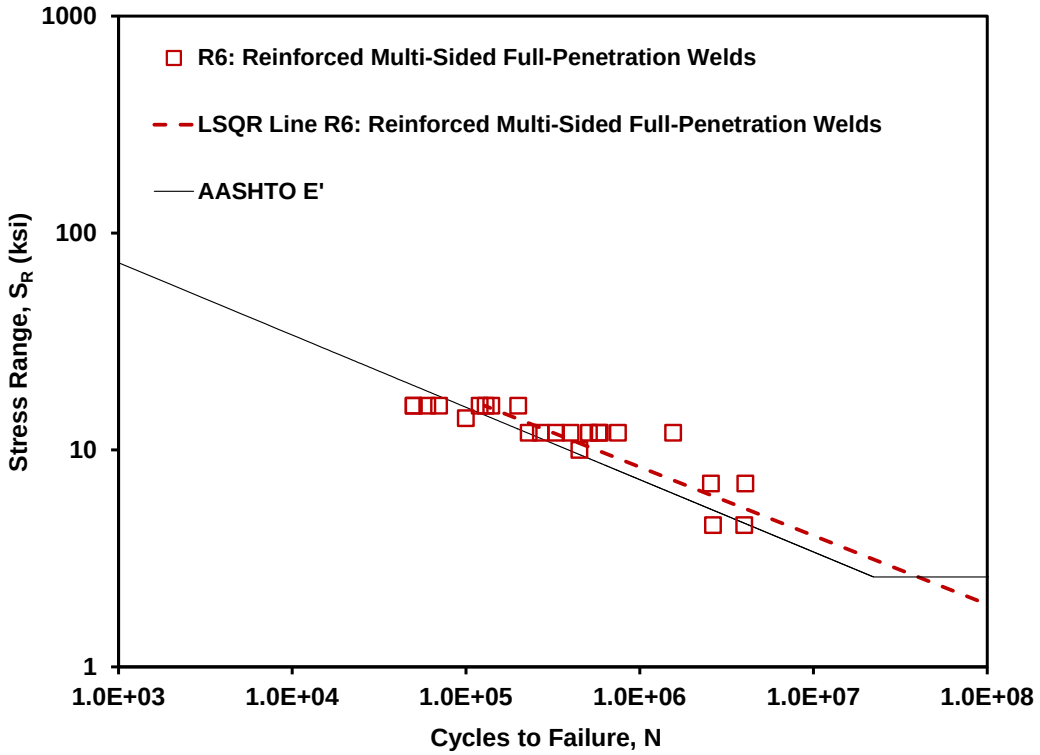

Figure 3.34. S_R-N diagram containing the fatigue tests contributing to the R6 detail category.

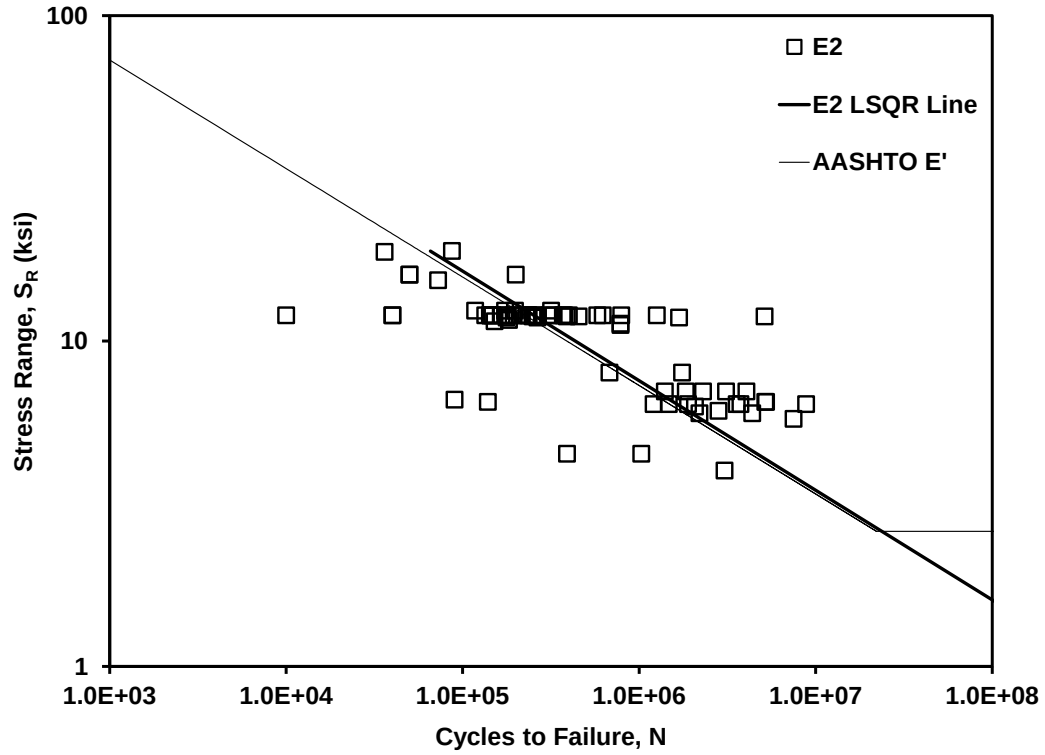

Figure 3.35. S_R-N diagram containing the fatigue tests contributing to the E2 detail category.

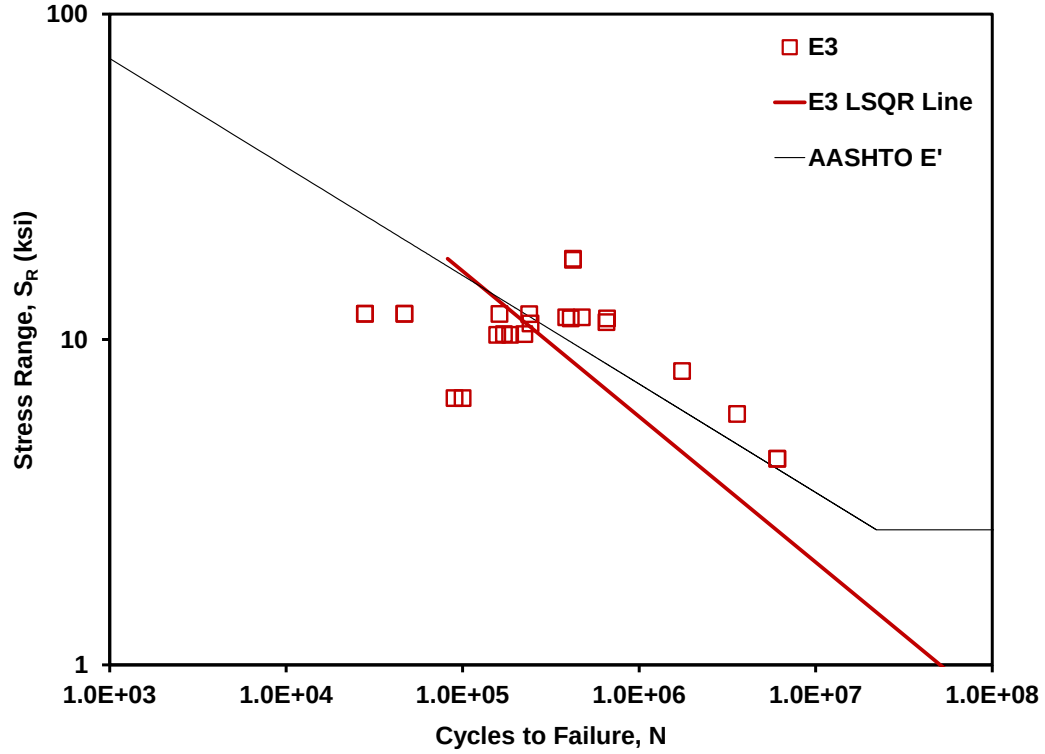

Figure 3.36. S_R-N diagram containing the fatigue tests contributing to the E3 detail category.

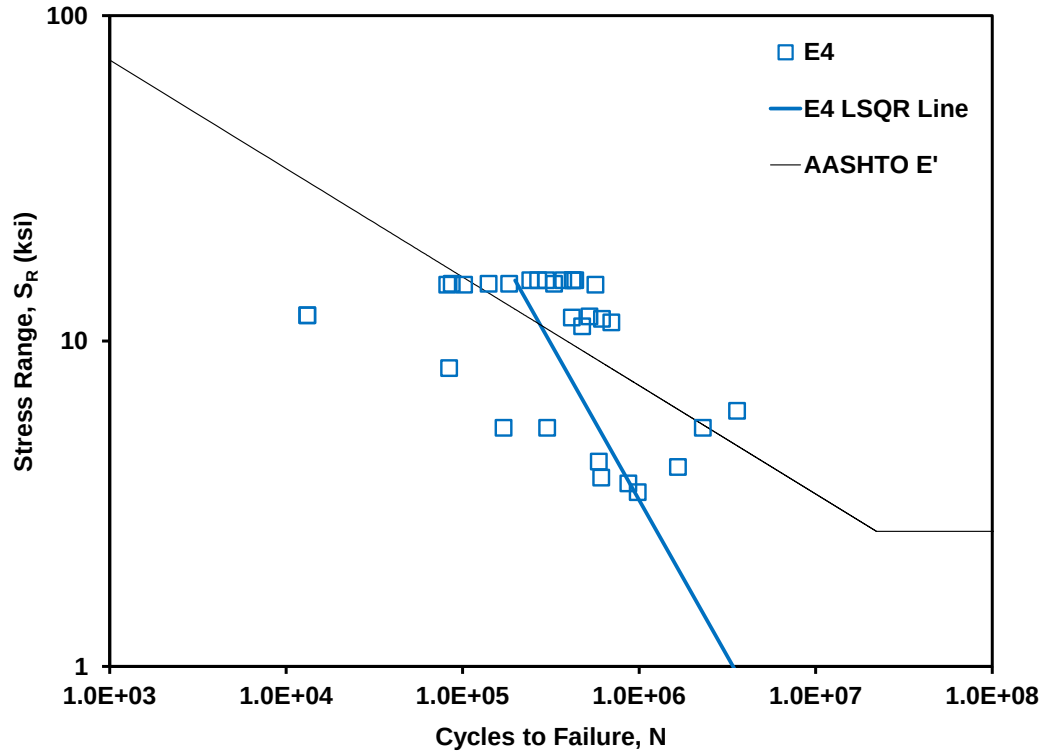

Figure 3.37. S_R-N diagram containing the fatigue tests contributing to the E4 detail category.

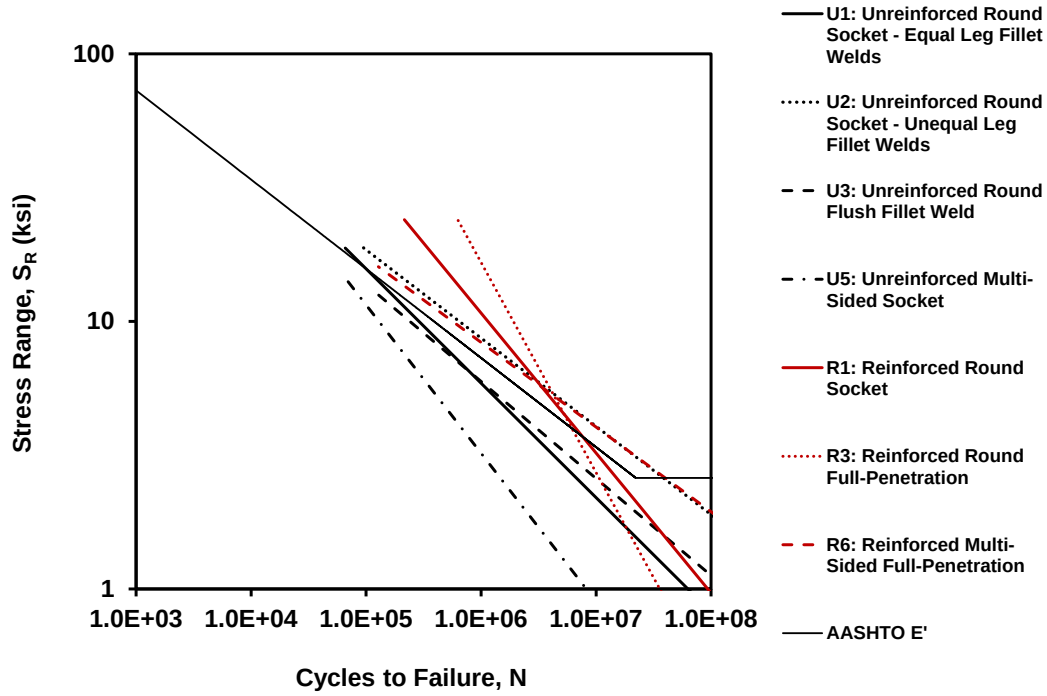

Figure 3.38. S_R-N diagram illustrating variation in least squares regression lines for each detail category generated in Synthesis Approach No. 1.

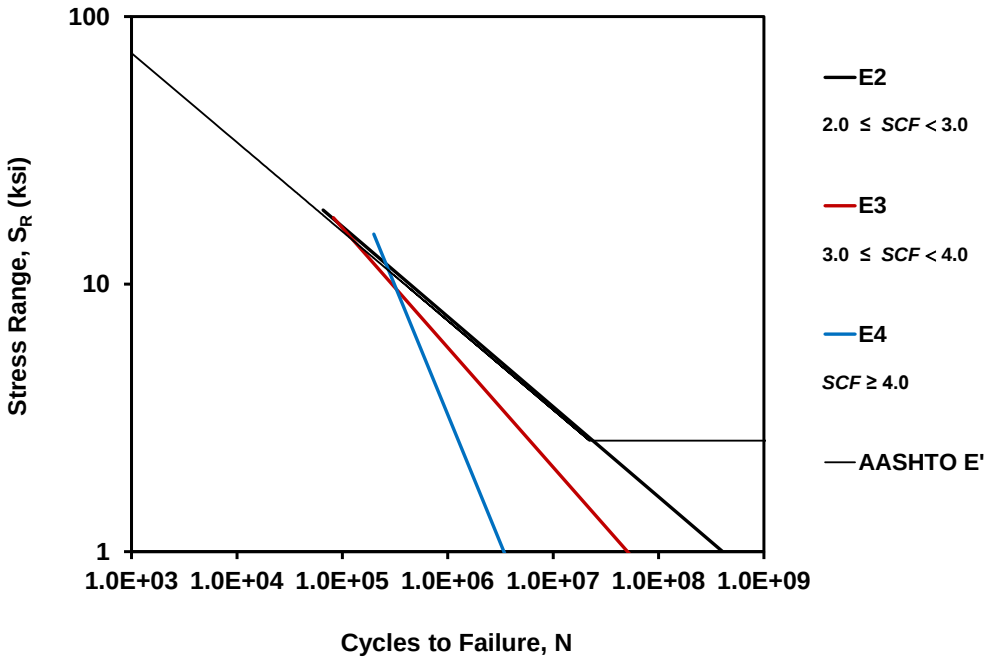

Figure 3.39. S_R-N diagram illustrating variation in least squares regression lines for each detail category generated in Synthesis Approach No. 2.

Table 3.18. Statistical results for Synthesis Approach No. 1.

Fatigue Detail Category		m (1)	μ_A (2)	CV_A	$S_{R,max}$ (ksi)
U1	**Unreinforced Round Socket - Equal Leg**	2.34	7.40E+07	0.66	18.80
U2	**Unreinforced Round Socket - Unequal Leg**	3.03	1.12E+09	1.53	18.90
U3	**Unreinforced Round Flush Fillet Weld**	2.76	1.94E+08	0.87	12.60
U4	**Unreinforced Round Full-Penetration**	na	na	na	na
U5	**Unreinforced Multi-Sided Socket**	1.80	1.58E+07	1.30	15.00
U6	**Unreinforced Multi-Sided Flush Fillet Weld**	na	na	na	na
U7	**Unreinforced Multi-Sided Full-Penetration**	na	na	na	na
R1	**Reinforced Round Socket**	1.91	1.46E+08	1.17	24.00
R2	**Reinforced Round Flush Fillet Weld**	na	na	na	na
R3	**Reinforced Round Full-Penetration**	1.27	5.74E+07	0.98	24.00
R4	**Reinforced Multi-Sided Socket**	na	na	na	na
R5	**Reinforced Multi-Sided Flush Fillet Weld**	na	na	na	na
R6	**Reinforced Multi-Sided Full-Penetration**	3.16	1.03E+09	0.80	16.00

(1) *Deterministic value defining slope of fatigue life curve*

(2) *X-Intercept of fatigue life curve*

Table 3.19. Statistical results for Synthesis Approach No. 2.

Fatigue Detail Category	m (1)	μ_A (2)	CV_A	$S_{R,max}$ (ksi)
E2 (2.0 ≤ *SCF* < 3.0)	2.97	6.73E+08	1.49	18.90
E3 (3.0 ≤ *SCF* < 4.0)	2.24	9.02E+07	0.89	17.71
E4 (*SCF* ≥ 4.0)	1.04	5.22E+06	0.88	15.37

(1) *Deterministic value defining slope of fatigue life curve*

(2) *X-Intercept of fatigue life curve*

3.5.2 – Comparison of Statistical Results

The goal of this chapter was to formulate a method for defining an expected fatigue life, with known variability, for a connection being considered such that a statistical model for fatigue life could be used in a reliability procedure for assessing the expected life of mast-arm sign support structures. Two distinctly different approaches have been presented in order to complete this task. A comparison of these two approaches will now be discussed.

Qualitatively, the results from the statistical analyses of both synthesis approaches seem reasonable. For the first approach (Table 3.18 and Figure 3.38), it appears that reinforced connections tend to perform better than unreinforced connections. For the second approach (Table 3.19 and Figure 3.39), a very clear trend is shown indicating that an increase in *SCF* decreases fatigue performance.

Two very important things to look at when assessing the summary of results provided in Tables 3.18 and 3.19 are the slope of the line defining the expected life for each detail category, m, and the expected value μ_A. For a particular detail category, as the magnitude of m increases, so does the magnitude of μ_A. This is because a larger magnitude of m corresponds to a flattening of the regression line. If the regression line is flattened, its corresponding x-intercept is shifted to the right. In general, a flatter regression line (and right-shifted x-intercept) corresponds to better

fatigue performance and longer life. A steeper regression line (and left-shifted x-intercept) corresponds to poorer fatigue performance and shorter life. However, one must also recognize the relative horizontal location of each curve. If two curves have the same slope but one exists slightly left of the other on the S_R-N diagram, details from the one farther to the left would have poorer fatigue performance compared to details from the one on the right even though their slopes are equivalent. The following discussion will help illustrate this concept within the context of two new fatigue detail categories generated by the first synthesis approach.

Consider two details, U5 and R3, both taken from Synthesis Approach No. 1 with data in Table 3.18 and Figure 3.38. The slope of the regression line for U5 is 1.80 while the slope of the regression line for R3 is 1.27. Clearly, R3 has the steeper slope indicating that this detail should provide poorer fatigue performance compared to the U5 detail. However, comparing the resulting values for μ_A, U5 provides a value of $1.58 \cdot 10^7$ while R3 provides a value of $5.74 \cdot 10^7$. This effect can be seen by looking at the regression lines provided in Figure 3.38. Although the regression line defining the U5 detail category has a flatter slope (*i.e.* higher magnitude *m*) than the R3 detail category, it provides a lower value for μ_A (shorter fatigue life) because of its relative horizontal location residing much further to the left on the same S_R-N diagram. A comparison between the U2 (lower *m*, higher μ_A) and R6 (higher *m*, lower μ_A) detail categories is another example where a slope of lower magnitude provides a larger value for μ_A (longer fatigue life). Again, this can be seen by looking at Figure 3.38 where the R6 regression line resides to the left of the U2 regression line.

3.6 – Concluding Remarks

The results of this chapter indicate that it is reasonable to classify connections based upon the appearance of their configuration and obtain satisfactory statistical information regarding their fatigue performance. However, given the very clear trend illustrated by the regression lines

provided by the second synthesis approach, when sufficient information regarding the dimensions of the connection are known, it is recommended to classify connections based upon the stress concentration factor determined using the equations provided by Roy et al. (2011).

CHAPTER 4 – FE MODELING OF SIGN SUPPORT STRUCTURES

4.1 – Introduction

The successful implementation of the reliability-based fatigue assessment procedure, outlined in chapter one, requires analytical models simulating the structural response of sign support structures. Ginal (2003) outlined a procedure to evaluate the fatigue performance of full-span overhead sign support structures using a purely analytical approach. Such an approach requires a representative group of structures with accurate analytical models for each (Ginal 2003).

To migrate this procedure toward mast-arm sign support structures, a representative test-group of these types of structures is needed. The beginning portions of this chapter discuss the basis on which each structure of the test-group was selected. The remainder of this chapter will provide discussion regarding the development of the numerical models for each structure and a series of comparative studies between these analytical models for determining their adequacy and accuracy within a reliability-based fatigue assessment like that outlined in chapter one.

4.1.1 – Selection of Test-Group Structures

There were two different types of mast-arm sign support structures chosen to be part of the test-group used in the present study. The following discussion will provide a brief description for each structure and the reasoning behind its selection as part of the test-group considered for this study.

Milwaukee Structure: S-40-703

The first structure is designated by WisDOT as S-40-703 and is located in Milwaukee, WI. As indicated in chapter two, S-40-703 was designed and installed in 2004 as part of the Marquette Interchange Project in Milwaukee, WI. This structure supports two traffic signs and represents a typical sign support structure used within the WisDOT infrastructure network.

The first phase of the present study designated S-40-703 as a candidate structure for real-time health-monitoring because of its geographical location. As a result, a significant amount of load and response data exists for this structure. This made S-40-703 an obvious choice for aiding in the quantification of modeling error uncertainty. For convenience, S-40-703 will be referred to as the Milwaukee structure. A photo of the Milwaukee structure is provided in Figure 4.1. Details regarding the mechanical and material properties as well as the overall geometric dimensions for the Milwaukee structure will be provided in later sections of this chapter.

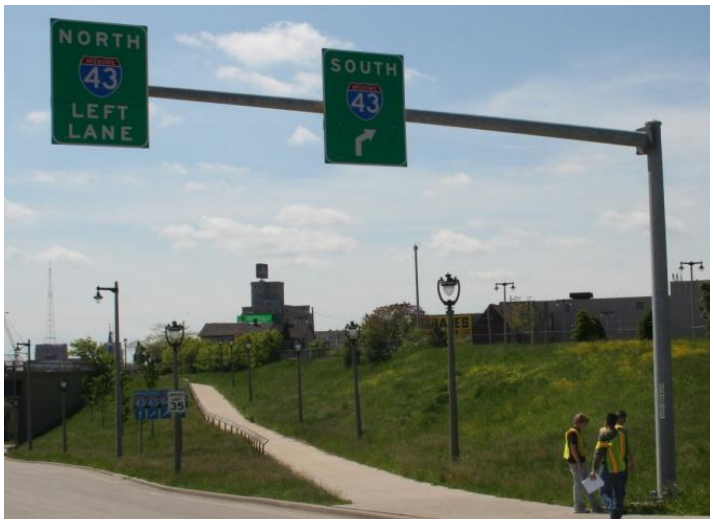

Figure 4.1. Photo of Milwaukee Sign Support Structure: S-40-703 (Smith 2010).

Osseo Structures: S-61-0001 and S-61-0002

In October of 2011, a routine inspection of two mast-arm sign support structures (S-61-0001 and S-61-0002) located in Osseo, WI revealed cracks within their welded connections. Both structures were immediately decommissioned and the welded connections were cut from each of their mast-arms and taken back to the Marquette University Engineering Materials and Structural Testing Laboratory (EMSTL). Comprehensive and exhaustive failure analyses were performed on each of them. Conclusive results from these analyses indicate that the cracks found in S-61-0001 and S-

61-0002 were both fatigue-induced. As indicated earlier, the details regarding the failure analysis for the Osseo structures is provided in Appendix A.

Insofar as the design drawings go, S-61-0001 and S-61-0002 were identical structures designed and installed in 2003. Each of these structures support three traffic signs used to designate turn lanes in the off-ramps of Interstate Highway 94. Because these structures were identically designed, a single analytical model may be used to represent both structures. Therefore, these structures will be referred to as the Osseo structures and will be considered identical moving forward. A photo of one of the Osseo structures is provided in Figure 4.2.

Figure 4.2. Photo of Osseo Sign Support Structure: S-61-0001 (it should be noted that this is also a representative photo of S-61-0002) (Google 2012).

Although as costly and unfortunate as these failures may be, they conveniently serve as tools for evaluating the reliability-based framework developed in this dissertation. With the exception of modeling error uncertainty, all information required to carry out the reliability analysis outlined in chapter one is documented for the Osseo structures. Therefore, these structures were added to the test-group considered in this study in order to evaluate the reliability-based procedure using a real fatigue failure.

Both types of structures within the test-group are classified as mast-arm sign support structures; yet, one of the structures has failed from fatigue while the other has not. Barring vehicular impact, a seven-year service life is not a case in which a structure has performed satisfactorily. In fact, a seven-year service life is alarmingly short and begs the following questions: How could the Osseo structures fail by fatigue so quickly? If both the Milwaukee and Osseo structures were designed and classified in a similar way, and in service for approximately the same length of time, why hasn't the Milwaukee structure failed yet? Should these structures really be classified as having the same fatigue life, or are there significant differences between them which would ultimately lead to defining different fatigue lives?

The main goal of this chapter is to answer the previous list of questions. In order to make the effort tractable, the previous list of questions were synthesized into two main questions:

1. Are there significant differences between the two types of mast-arm sign support structures considered in the test-group? If so, what are they?
2. What level of detail is required in the analytical models for these structures in order to provide accurate predictions of the nominal stress-range at their connections?

The answers to these questions are important as they will shed light on (1) why two structures of seemingly similar configurations yield much different fatigue lives; and (2) the level of effort (in terms of both time and complexity) necessary for moving forward with a reliability-based fatigue assessment of sign support structures.

As evidenced by the results of chapter three, the presence of stress concentrations within the connections of these structures negatively impacts their fatigue performance. Statistically, it was shown that as the *SCF* for a particular connection increased, the resulting fatigue life for that connection decreased. Therefore, to answer the first question, highly detailed (high-fidelity) Finite Element (FE) models for each structure were developed. Highly detailed models can help

distinguish between local stress concentrations generated at the weld-toe of the round tube-to-transverse plate connection for each structure (*i.e.* the typical location of fatigue-induced cracking).

Generating such highly detailed models, however, comes with a steep price. As will be discussed in chapters five and six, the key to successfully implementing the reliability-based procedure is by running time-history analyses with simulated wind pressure in order to determine the resulting number and magnitude of expected stress-ranges caused by various levels of wind loading. Each of the analyses conducted for determining the locations and magnitudes of stress concentrations (discussed in subsequent sections) contained a single load step composed of a single sub-step. The computational run-times took as long as 45 minutes to one hour. This is significant. Each simulation required for the reliability-based procedure contains 3,691 load steps, with four sub-steps in each one. Therefore, running the simulations on the high-fidelity models would be completely impractical.

This leads to the second question that was posed earlier. What level of detail is required in the analytical models for these structures in order to provide accurate predictions of the nominal stress-range at their connections? Obviously, for simulation-based analyses of this length, too much detail is bad because the computational run-time is completely inefficient; however, too little detail is bad because it can lead to inaccurate predictions of structural response (*i.e.* inaccurate stress-ranges). To answer this question, additional models needed to be developed, one for the Milwaukee structure and one for the Osseo structure.

Furthermore, the fatigue synthesis of chapter three provided fatigue detail categories and S_R-N diagrams to specify a number of cycles to failure for a given stress-range (or vice versa). Since these fatigue detail categories are experimentally determined and are assumed to indirectly consider mean stress and stress concentration effects in their curves, there is no need to perform

simulations like the highly detailed FE models. As long as there is a reasonably accurate prediction of the nominal stress-range achieved at a particular detail, the newly developed fatigue detail categories of chapter three may be employed to predict the fatigue life of the connections within each structure.

Therefore, a second set of models were developed for each structure in the test-group. These models were much simpler (lower-fidelity) compared to their higher-fidelity counterparts. They can be thought of as stick-model representations of each structure. Once developed, a series of comparisons between the high- and low-fidelity models of each structure could be conducted. The comparisons were conducted to ensure the analytical results obtained by the lower-fidelity models were appropriate for subsequent stress-range cycle counting.

4.2 – FE Models for Test-Group Sign Support Structures

The accuracy of results obtained by FE models depends heavily on how well the models represent the structural system and the loads to which they are subjected. Discussion regarding the simulation of wind loading will be provided in chapter five. Because FE models are mathematical idealizations of the physical reality of the real structural system, they require the following:

1. Definition of accurate material models and element-types for classifying the material and mechanical properties of each structural component modeled;
2. Discretization of structural components into an appropriately refined FE mesh;
3. Definition of appropriate boundary conditions (*e.g.* supports and external loads) specified within the model.

The following sections will provide the systematic development of two models for each structure considered in the test-group: a high-fidelity model and a low-fidelity model. The difference between high-fidelity and low-fidelity can be attributed to how the bolted connections

between the mast-arm and pole of each structure were modeled. The high-fidelity models contain very detailed renditions of the bolted connections for both structures allowing them to account for any connection-flexibility. The low-fidelity models merely provide stick model representations using rigid connections between the mast-arm and pole.

Outside of the connection, the high- and low-fidelity models for each structure are exactly the same. This allows the dynamic response characteristics for each structure to be quantified at two levels of modeling detail. The high-fidelity models, accounting for flexibility introduced by the bolted connections, will be considered more accurate than the simpler stick model representations provided by the low-fidelity models.

4.2.1 – Development of High-Fidelity FE Models

Before discussing the development of the high-fidelity FE models for the Milwaukee and Osseo structures, it is prudent to define the essential components which constitute a typical mast-arm sign support structure. Both structures within the test-group contained bolted connections classified as unstiffened, socketed, round tube-to-transverse plate connections. A labeled, up-close photo of a typical connection of this type is provided in Figure 4.3. A list of the essential components labeled in Figure 4.3 is as follows:

- Mast-arm
- Pole
- Bolted Connection
    - pretension bolts
- Mast-arm Contribution to Bolted Connection
    - round tube used for mast-arm
    - socketed plate (to be fastened to backing plate with bolts)

- fillet welds used to secure mast-arm to socketed plate

- Pole Contribution to Bolted Connection
  - round tube used for pole
  - backing plate (to be fastened to socketed plate with bolts)
  - connection gussets between pole and backing plate
  - fillet welds used to secure gussets to pole and backing plate

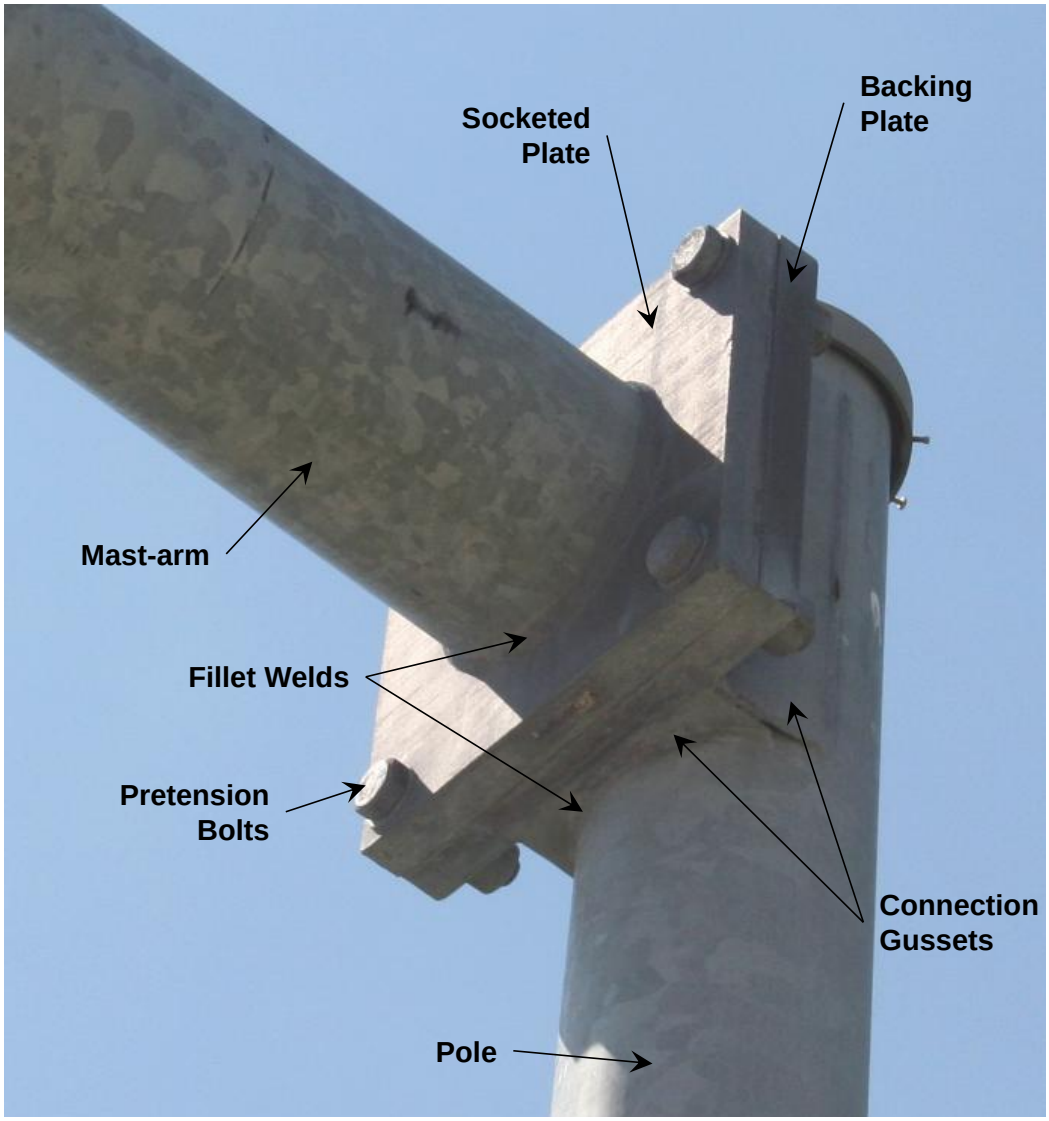

Figure 4.3. Photo of typical unstiffened, socketed, round tube-to-transverse plate connection used within mast-arm sign support structures with key structural components labeled (note: this is an up-close photo of the connection contained within the Milwaukee structure).

For reasons explained throughout the development of the high-fidelity FE models, each of these structural components was systematically generated independently from one another. The following numbered list outlines the multi-step procedure used to generate the high-fidelity FE models:

1. The process began by drawing a cross-sectional area for each structural component. The cross-sectional area chosen for each structural component was selected to provide convenient extrusion from 2-D to 3-D. For some of the components, Boolean addition or subtraction was necessary to obtain an appropriate shape (*e.g.* the socketed plate required Boolean subtraction of five circles from a rectangle for the round mast-arm tube and four pretension bolts to pass through).
2. After each cross-sectional area was generated, the lines containing each of the areas were manually subdivided into segments providing nodes at desired locations within, and around, the perimeter of the area. Some areas required lines to be concatenated to create "source" lines and "target" lines which maintained an equal number of divisions for generating an appropriate mesh.
3. ANSYS provides a MESH200 element which does not contribute to the numerical solution of a given model. As a mesh-only element, MESH200 comes in 12 different configurations and is provided for use within a multi-step procedure such as this. A mesh may be created in 2-D using MESH200 elements and then extruded to 3-D using any solid element. After extrusion is complete, the MESH200 elements may be deleted (cleared) or may be left in place – either way the MESH200 elements will not affect the model in any way (SAS 2013). Each area was meshed using the 4-node quadrilateral configuration of the MESH200 element. As an example, Figure 4.4 shows the base cross-sectional areas for the high-fidelity FE model of the Milwaukee structure. The areas are meshed with MESH200 elements and ready for extrusion using 3-D solid elements.

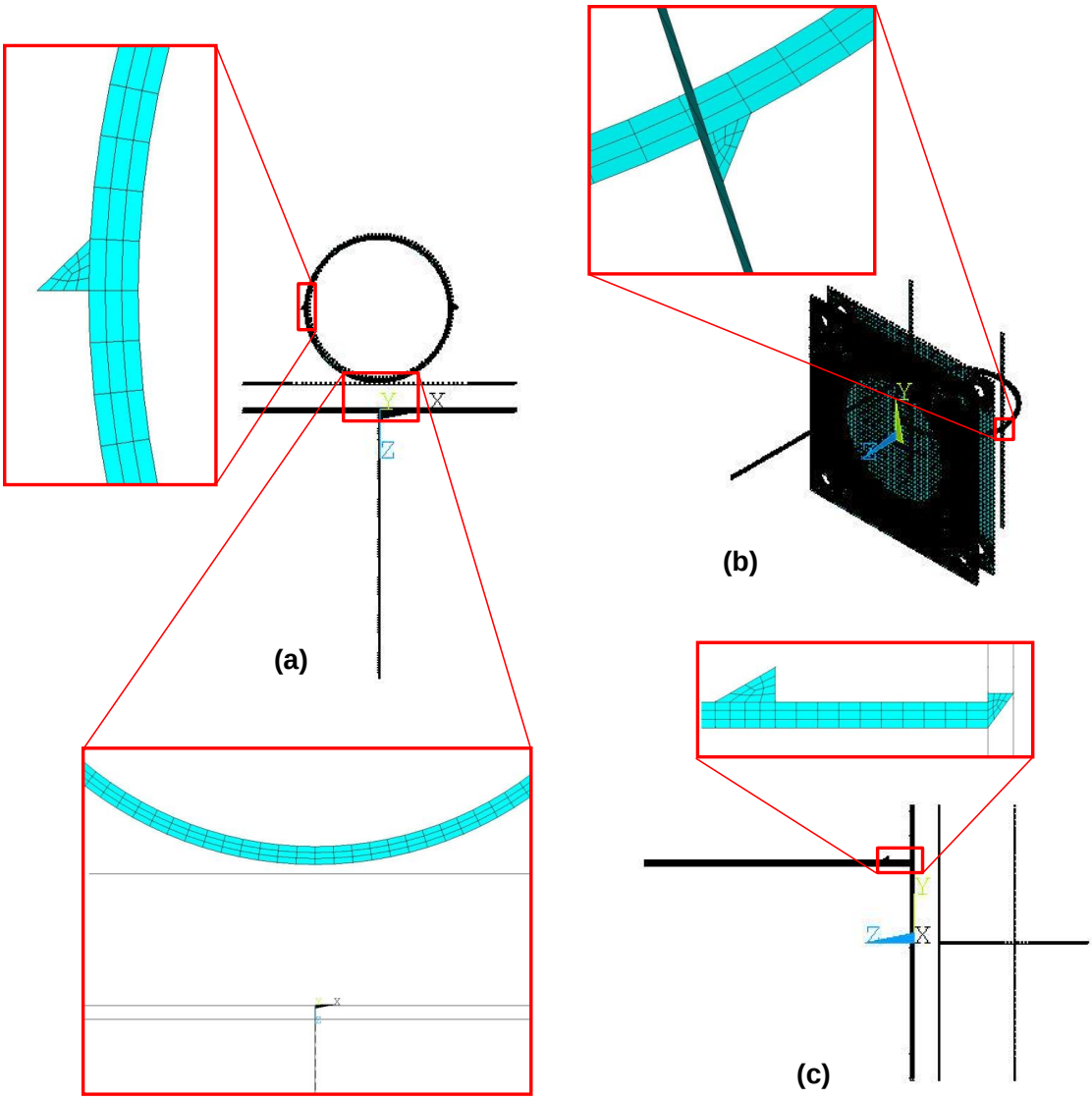

Figure 4.4. Example base areas used for high-fidelity FE model of connection, meshed with MESH200 elements with key geometrical features boxed in red (a) top view; (b) isometric view; and (c) side view.

4. Subsequent to all base areas being meshed; each area was independently extruded along an XYZ offset distance or about an axis. ANSYS provides a number of solid elements for 3-D solid modeling. One of the most recommended elements for solid modeling is the SOLID186 3-D 20-node element because of its quadratic displacement capabilities which enables it to easily take on irregular geometries. However, to save computational power

and run-time, a lower-order version of the SOLID186 element was used. The SOLID185 3-D brick element is defined by eight nodes. Each node contains three degrees of freedom: translations in the x, y and z directions (SAS 2013). This element is capable of degenerating into a prism, tetrahedral or pyramid; however, the tetrahedral and pyramid options are not recommended. This is another important reason for manually subdividing lines in the base areas to maintain 4-node quadrilateral elements. Base areas containing 4-node quadrilateral elements could be easily extruded into 8-node 3-D brick elements.

5. Once the extrusion procedure was completed, the high-fidelity FE model for each structure consisted of independently meshed volumes for each of the structural components listed earlier. At this point, the model for the connection would seem complete; however, each of the independent structural components in their current state had no way of communicating to one another (*i.e.* they were simply occupying adjacent space within the model, but were not connected in any way). The individual components needed to be classified as one of three groups: (1) bolts; (2) mast-arm; or (3) pole. By separating the components into these three groups, two groups of components could be unselected (turned off) so that the shared interfaces between volumes of the remaining selected components could be welded together. Welding various components together was done by simply merging coincident nodes from adjacent elements. The reason for separating the components into three groups was to ensure the nodes on the faying surfaces between the headwasher-to-socket plate, socket plate-to-backing plate and backing plate-to-nutwasher interfaces were not merged since the sign support structures being modeled contained bolted connections between mast-arm and pole, not welded connections (see Figure 4.5).

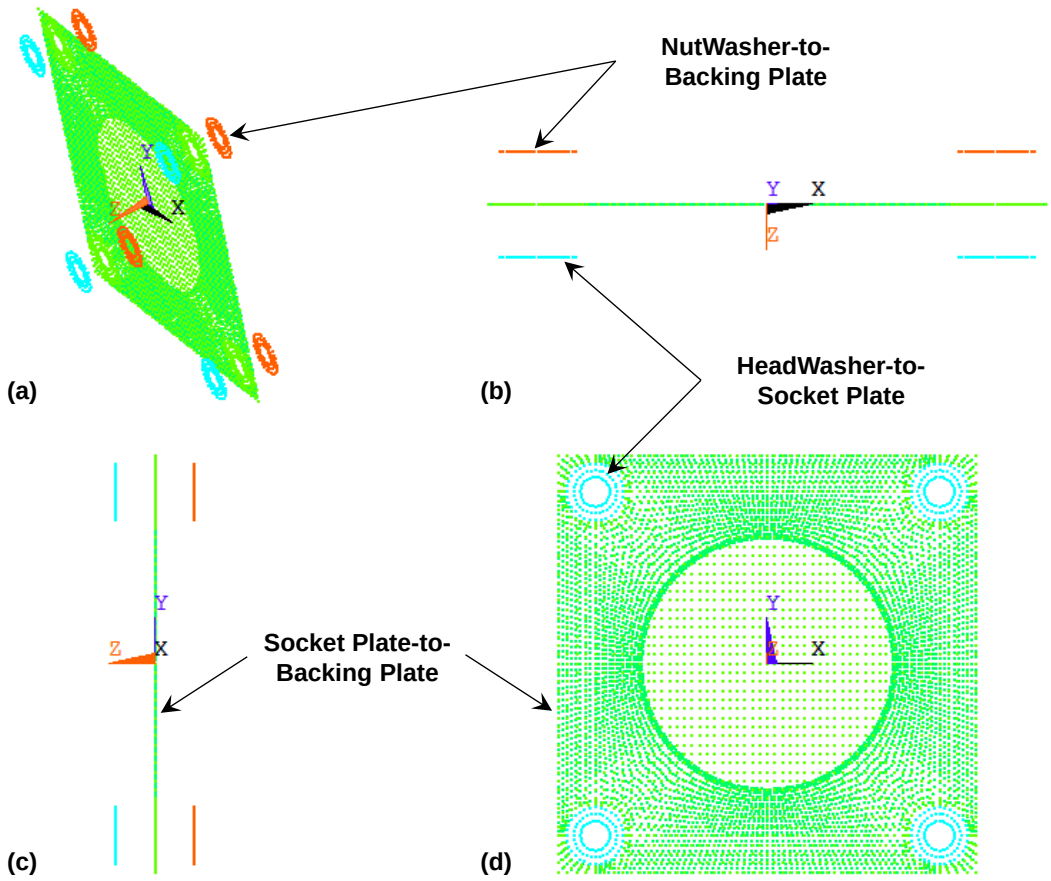

Figure 4.5. Contact surfaces specified at all faying surfaces within high-fidelity FE model (a) isometric view; (b) top view; (c) side view; and (d) front view.

6. In this step, target and contact surfaces were specified at all faying surfaces described in step 5. Both faying surfaces at each interface subject to contact were overlaid with flexible-flexible TARGE170 and CONTA174 elements. Each faying surface required a new "contact pair" of TARGE170 and CONTA174 elements to be specified. Figure 4.5 shows the target and contact surfaces for the Milwaukee high-fidelity FE model.
7. At this point in the procedure, all coincident nodes at weld locations have been merged; however, there is still no connection between the mast-arm and the pole. To make the final connection between the mast-arm and the pole, the PRETS179 element was specified on sections within each of the four pretension bolts. The PRETS179 element allows the user to apply a tensile force only; bending and torsion loads applied to this

element are ignored (SAS 2013). Therefore, the bolts within the models will only have a pretensioned tensile force applied even though they are capable of resisting torsion and bending in the actual connection. The magnitude of the pretensioned force specified for each bolt corresponded to a load which would achieve an internal stress equal to 0.70 times the ultimate tensile strength of the bolts. More information regarding the magnitude of pretensioned force for each model will be provided in subsequent sections.

8. All that remained to be modeled was the mast-arm from the connection to the free end and the pole from the connection to the base. This was done using BEAM188 3-D elements composed of two nodes with six degrees of freedom per node: translations in the x, y and z directions as well as rotations about the x, y and z axes (SAS 2013). This task required lines corresponding to the mast-arm and pole centerlines to be drawn for each model. Some important notes regarding the lines meshed with beam elements include the following:
    a. With the exception of aerodynamic damping (discussed in chapter five), the aluminum signs supported by the Milwaukee and Osseo structures do not contribute to the structural resistance of these systems. Therefore, the supported signs were not included in either of the models. However, these signs do contribute significantly to the bluff area subject to wind loading for each structure. Therefore, the magnitude of applied loading needed to account for the increase in bluff area at the locations where signs would exist if they were modeled.
    b. Wind pressure (ksi) was only applied to the beam elements corresponding to the mast-arm for both high-fidelity FE models. No wind loading was applied to the beam elements corresponding to the pole or any of the solid elements corresponding to the bolted connection of either model.

c. For the mast-arm beam elements, the wind pressure was applied as a line loading (kip/in.). To determine the magnitude of the line loading, the wind pressure was multiplied by the height of the cross-section perpendicular to the direction of applied wind. As indicated in (a), locations where signs existed along the mast-arm needed to account for larger magnitudes of wind loading. Therefore, nodes were placed at the endpoints of sign locations so that the magnitude of wind line loading could be increased over elements that corresponded to sign locations. It should be noted that the centroid of each sign was assumed to be concentric with the centroid of the mast-arm tube. Therefore, no torsional loading on the mast-arm tube was specified. This is consistent with the sign configurations of each test-group structure.

d. Additional discretization was necessary for both the mast-arm and the pole of the Milwaukee model because the Milwaukee structure was composed of tapered sections for both the mast-arm and the pole. To make the modeling procedure tractable, the mast-arm and pole were discretized further to allow for various levels of wind loading along the mast-arm, as well as the definition of changing section properties, for both the mast-arm and pole. The BEAM188 element is capable of tapered sections and a varying line load; however, discretized segments facilitated checking the susceptibility of various portions of the mast-arm to vortex shedding (discussed subsequently).

e. The Osseo model did not require additional discretization beyond accounting for locations of signs because the Osseo structures were composed of prismatic sections.

f. Tables providing the lengths and section properties for the discretized segments of the Milwaukee and Osseo structures are in Appendix G for reference. These

tables also provide totals for length, volume and weight for each mast-arm as well as bluff-area subject to wind loading.

9. After the beam elements of step 8 were meshed, a node existed at the center-points of the solid elements used for the high-fidelity portions of the mast-arm and pole. ANSYS provides the ability to specify constraint equations in the form of rigid regions at such locations. Specifying rigid regions at these locations allows the nodes at the endpoints of the beam elements to interact with the nodes from the solid elements in those regions. This was done by specifying the node from each beam element as the master node and the nodes from the solid elements in those regions as slave nodes. The master node is only allowed to interact through common degrees of freedom between the two element-types contributing to the rigid region. For example, the beam elements provide six degrees of freedom at each node (translations in x, y and z directions and rotations about x, y and z axes), but the solid elements only provide three degrees of freedom at each node (translations in x, y and z directions). Therefore, only translations between the two element-types may interact within the rigid region.
10. The last step in the modeling procedure was to specify the support conditions. Both of these structures are bolted to concrete foundations at the bases of their poles. Because the focus of the present study was on the welded connection between the mast-arm tube and the socketed plate, the high-fidelity portions of the model were limited to the bolted connection between the mast-arm and the pole. Therefore, the foundation for each structure was simply modeled as a fully-fixed support, that is, all translations and rotations at the base of each pole were set equal to zero.

The overall dimensions and layout for each high-fidelity FE model, including lower-fidelity portions, are provided in Figures 4.6 and 4.7. The high-fidelity portions of each model are

provided in Figures 4.8 through 4.11. Summaries of the ANSYS 14.0 input information used to generate the high-fidelity models are provided in Appendix G for reference.

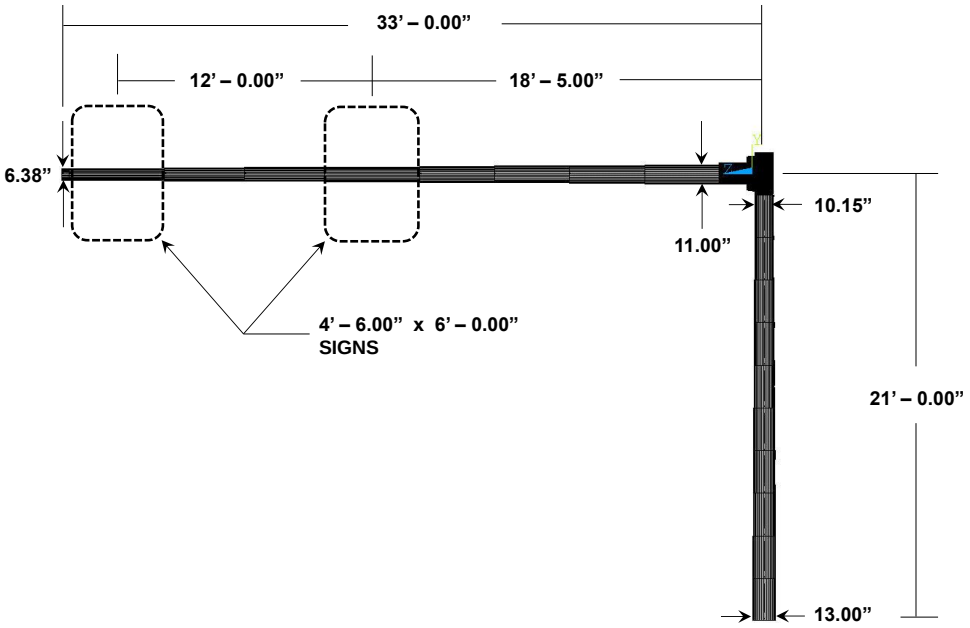

Figure 4.6. Milwaukee structure (S-40-703) – illustrating tapered mast-arm and pole as well as the locations of the supported signs (note: E-SHAPE is turned on for each BEAM188 element).

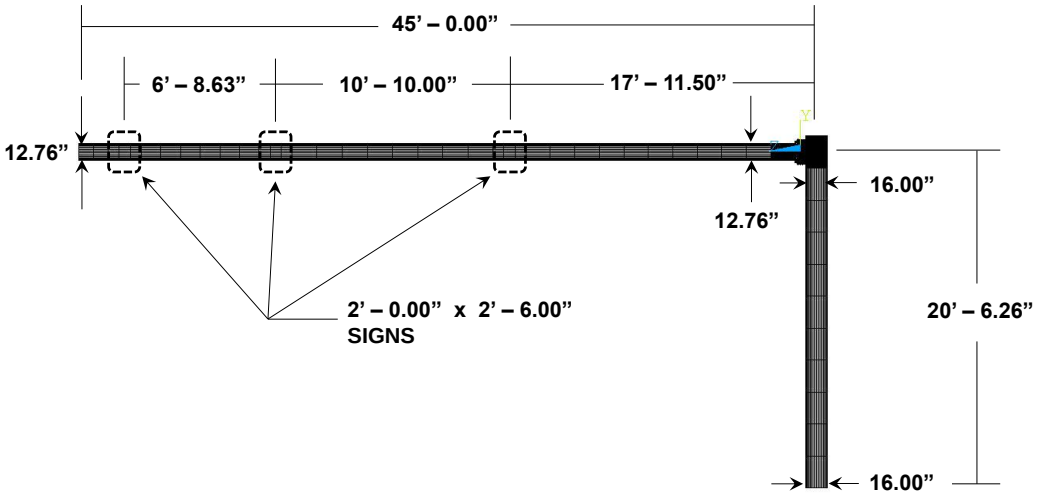

Figure 4.7. Osseo structures (S-61-0001 and S-61-0002) – illustrating non-tapered mast-arm and pole as well as the locations of the supported signs (note: E-SHAPE is turned on for each BEAM188 element).

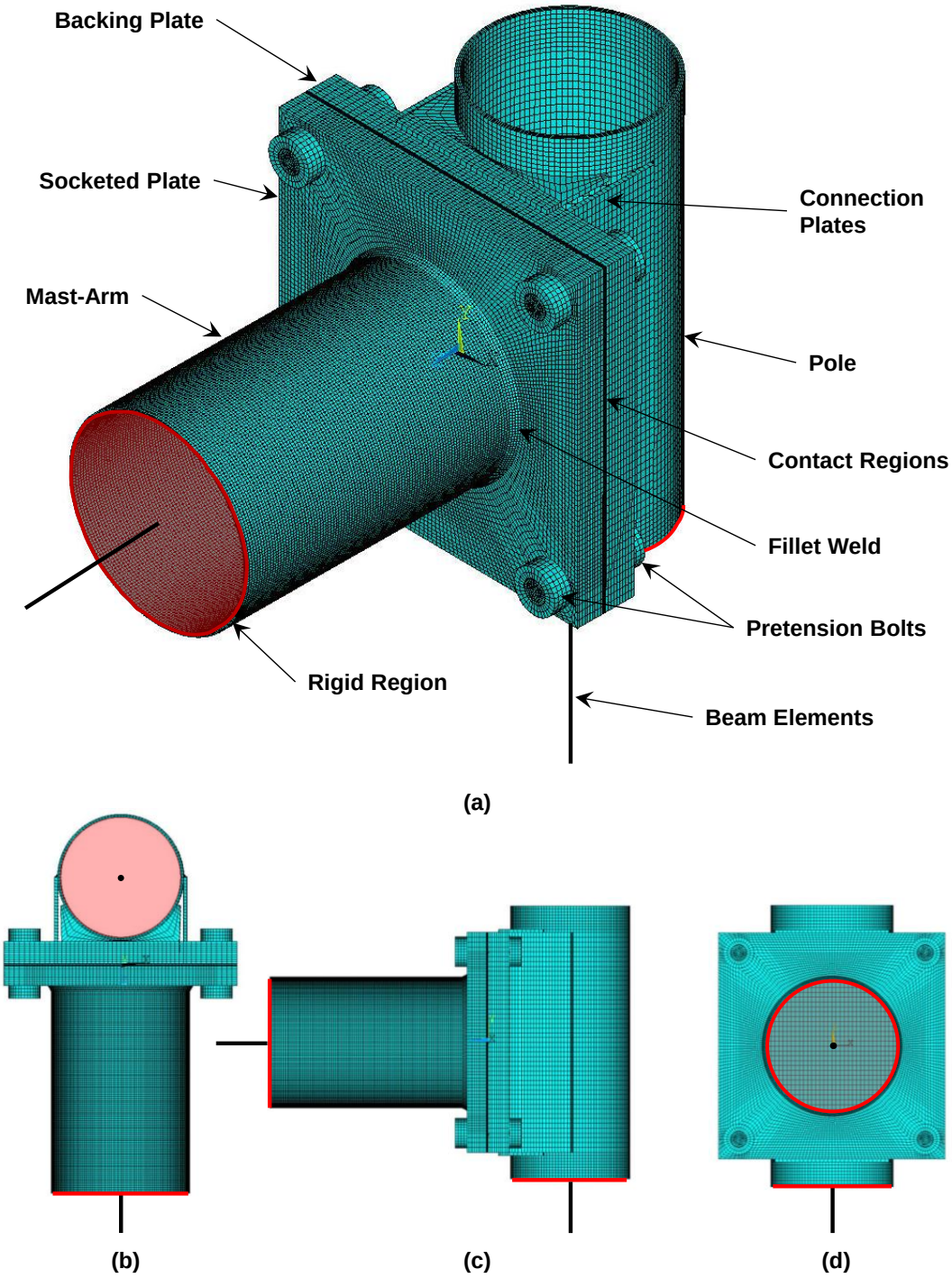

Figure 4.8. Milwaukee structure – detailed views of high-fidelity connection geometry and mesh: (a) labeled isometric view, (b) top view, (c) side view and (d) front view.

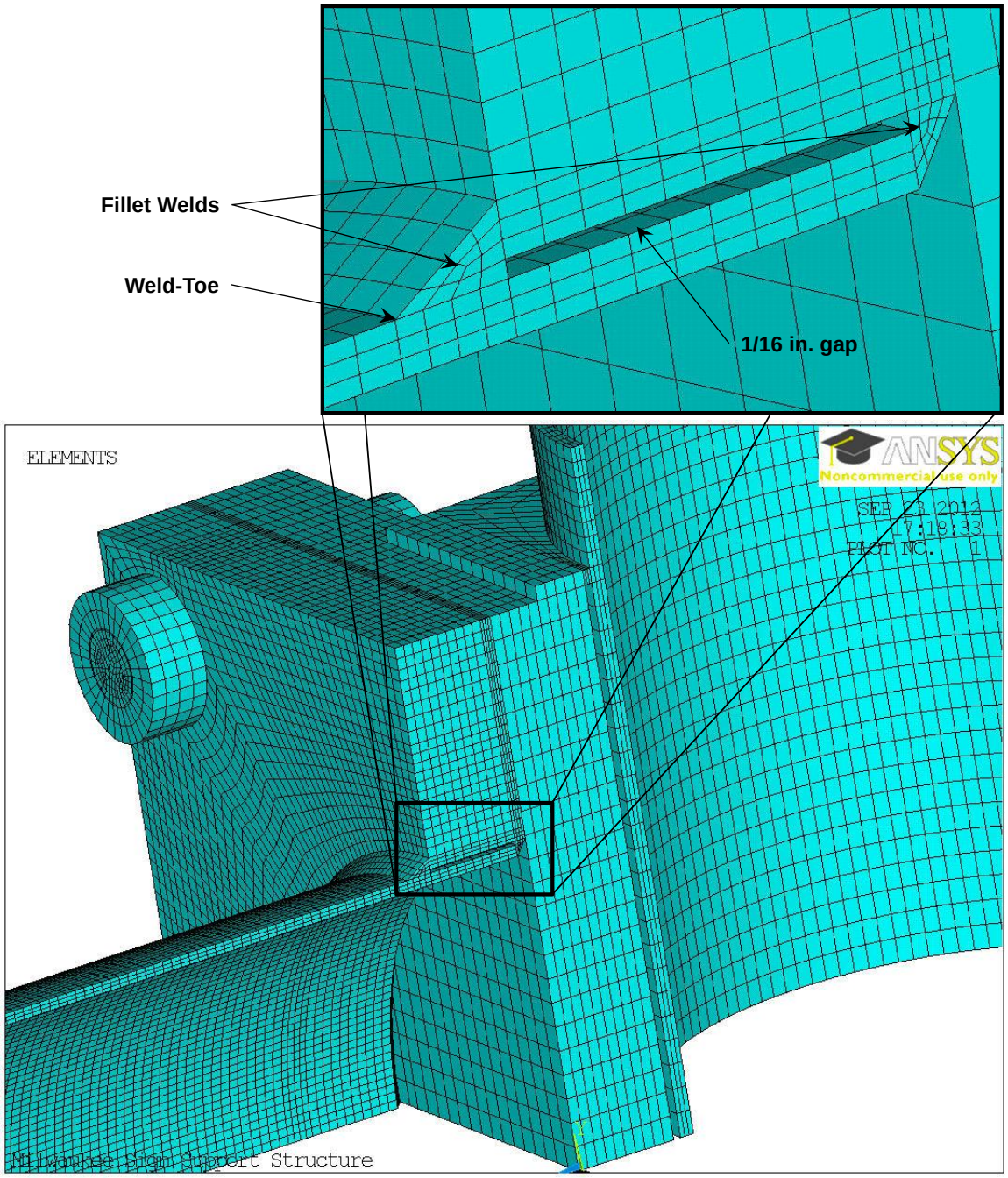

Figure 4.9. Milwaukee structure – up-close view of high-fidelity connection geometry and mesh illustrating fillet welds, weld-toe and 1/16 in. gap.

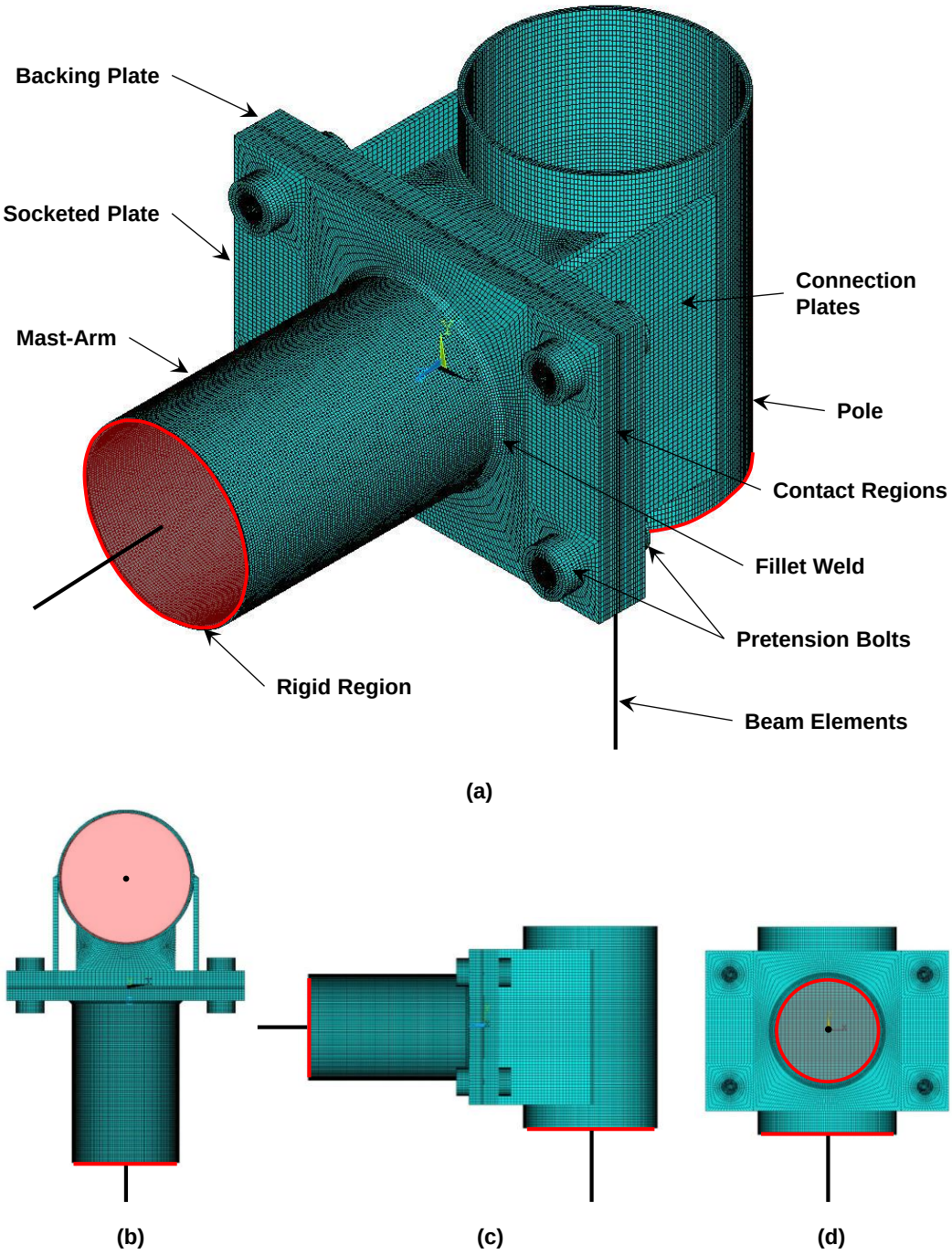

Figure 4.10. Osseo structures – detailed views of high-fidelity connection geometry and mesh: (a) labeled isometric view, (b) top view, (c) side view and (d) front view.

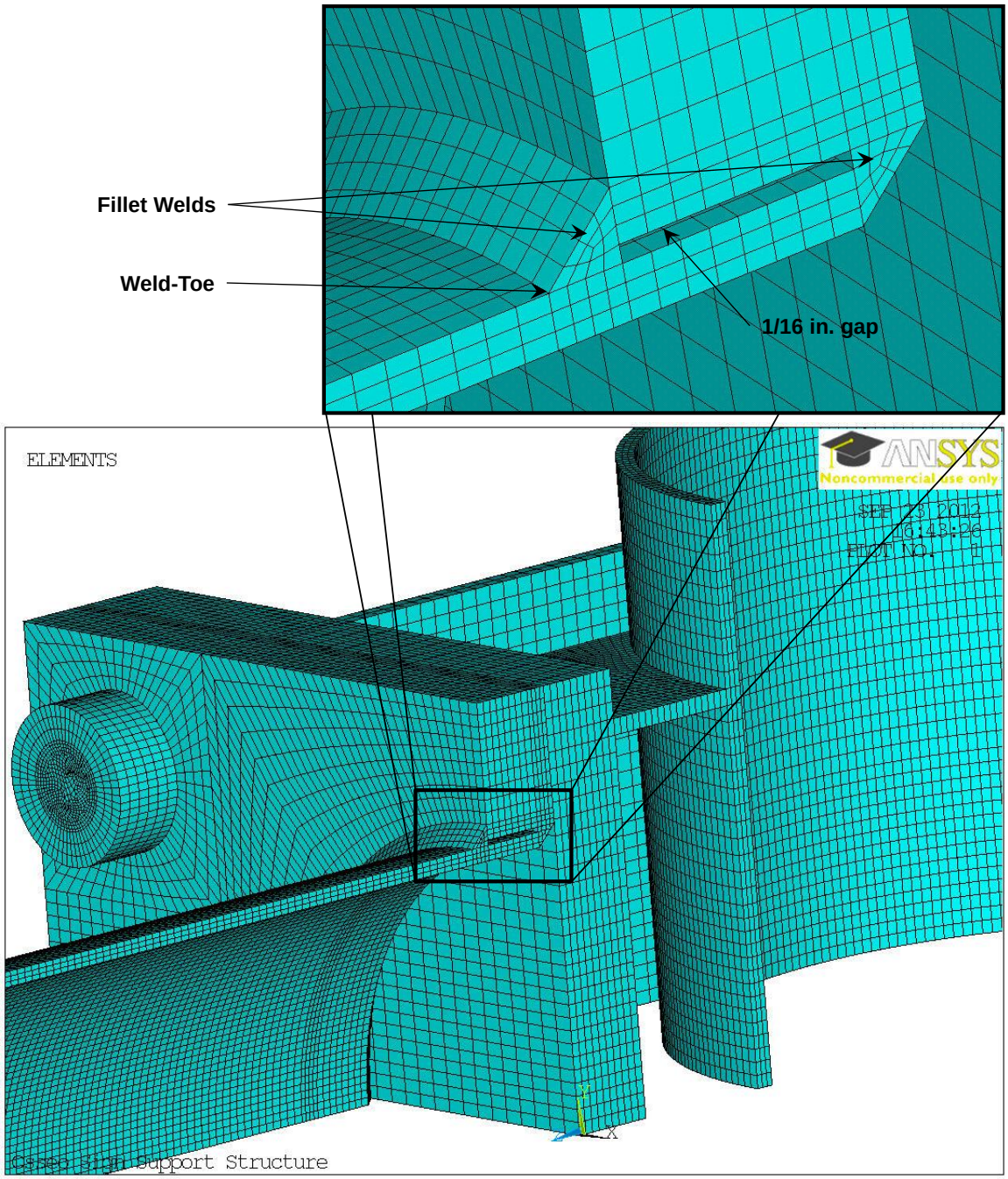

Figure 4.11. Osseo structures – up-close view of high-fidelity connection geometry and mesh illustrating fillet welds, weld-toe and 1/16 in. gap.

4.2.2 – Development of Low-Fidelity FE Models

As indicated earlier, the low-fidelity FE models were exactly the same as the high-fidelity FE models for each structure with the exception of the bolted connection between the mast-arm and

the pole. This made the development of the low-fidelity FE models for each structure very convenient. The procedure for developing the low-fidelity FE model for each structure went as follows:

1. Copies of the high-fidelity FE models for each structure were created.
2. The higher-fidelity portions of each model, in the order they were removed, include the following:
    a. all rigid regions between BEAM188 and SOLID185 elements;
    b. all PRETS179 elements;
    c. all TARGE170 and CONTA174 elements;
    d. all SOLID185 elements

    It should be noted that all types of elements corresponding to those listed above were completely removed from the database. This included the MESH200 element-type even though there were no MESH200 elements present within the model.
3. BEAM188 elements were placed in the void created by step 2. The material and section properties were continued from adjacent BEAM188 elements and the point of intersection between mast-arm and pole was specified as a rigid connection by simply making the adjoining beam elements share the same node.

The low-fidelity FE models of the connections for the Milwaukee and Osseo structures are provided in Figures 4.12 and 4.13. Summaries of the ANSYS 14.0 input information used to generate the low-fidelity FE models for each structure are provided in Appendix G for reference.

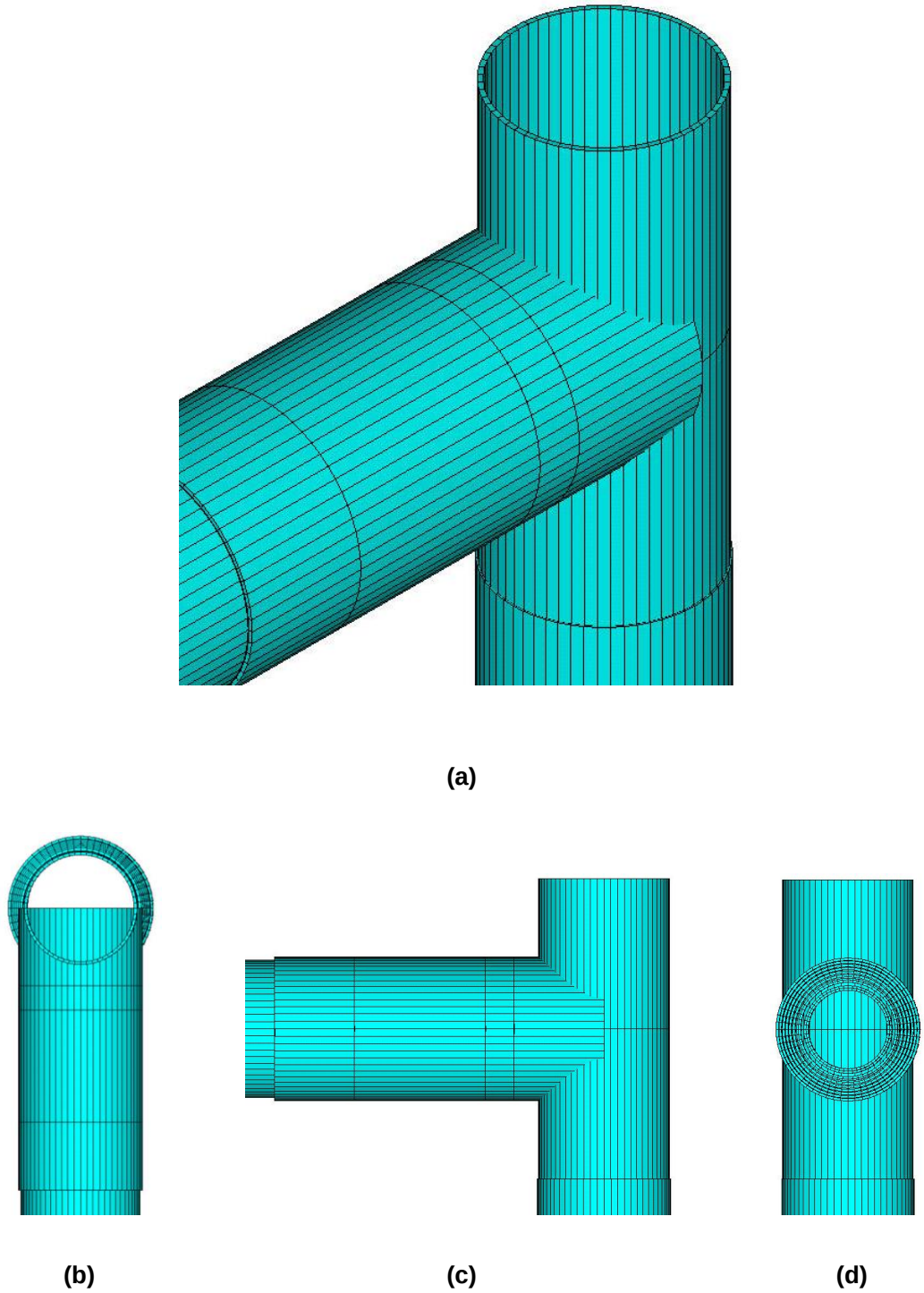

Figure 4.12. Milwaukee Sign Support Structure – detailed views of low-fidelity connection with cross-sectional extrusion generated by ANSYS: (a) isometric view, (b) top view, (c) side view and (d) front view.

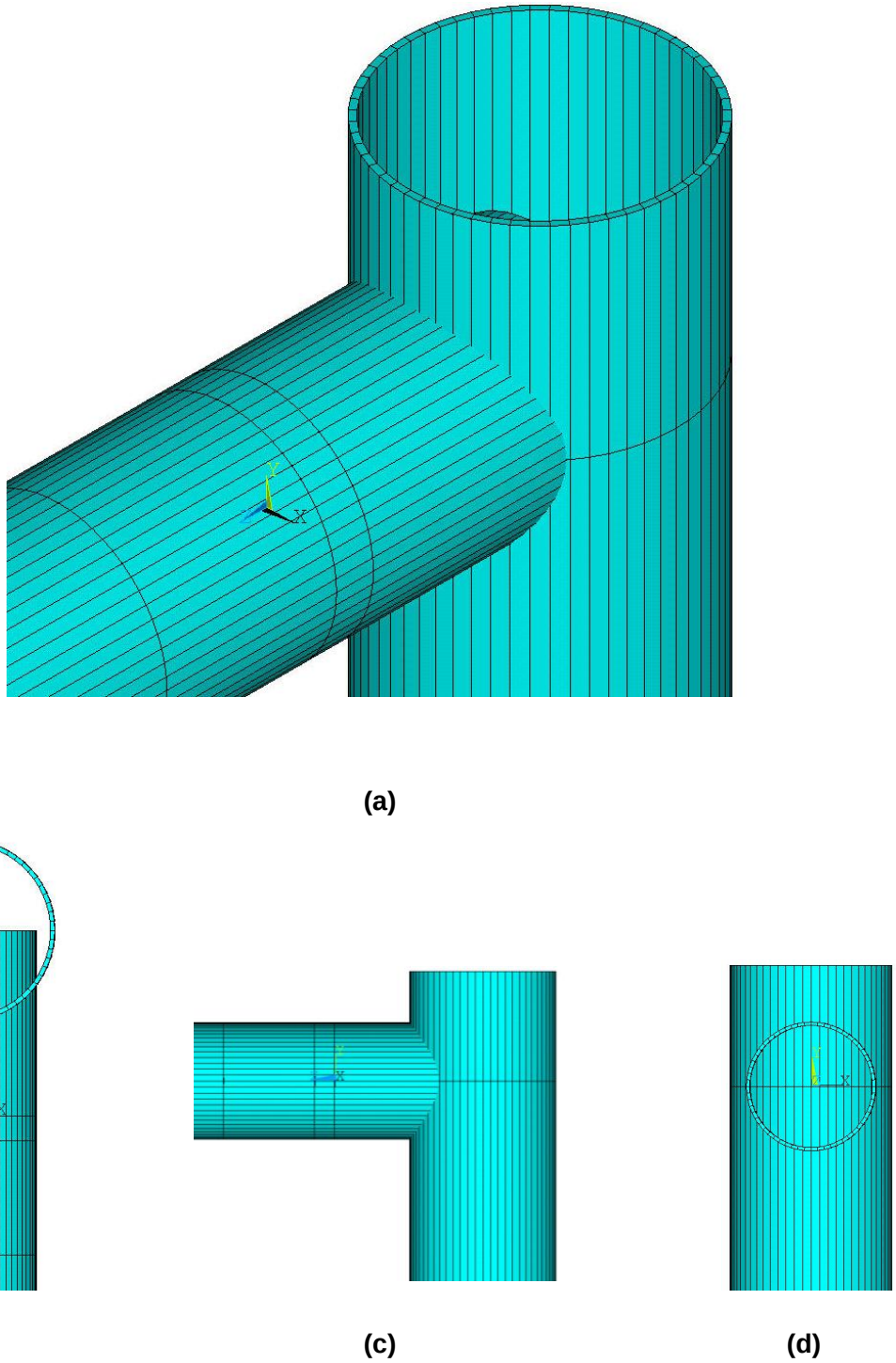

Figure 4.13. Osseo Sign Support Structures – detailed views of low-fidelity connection geometry with cross-sectional extrusion generated by ANSYS: (a) isometric view, (b) top view, (c) side view and (d) front view.

4.3 – Comparative Studies between High- and Low-Fidelity FE Models

Three comparative studies were conducted on results obtained by the FE models developed for both test-group structures. The reasoning behind, and results from, each comparative study will be discussed. The goal of these comparative studies is to answer the questions posed in the introduction to this chapter. For convenience, the questions are restated here:

1. Are there significant differences between the two types of mast-arm sign support structures considered in the test-group? If so, what are they?
2. What level of detail is required in the analytical models for these structures in order to provide accurate predictions of the nominal stress-range at their connections?

The first comparative study (CS1) will focus on the two high-fidelity FE models with a goal in mind of determining the extent to which each structure's connection has on their resulting stress concentrations. As an added benefit, this comparative study will act as an evaluation tool for assessing the parametric *SCF* equations used in *Synthesis Approach No. 2* from chapter three. The second and third comparative studies (CS2 and CS3) will focus on comparing the low-fidelity models of each structure to their high-fidelity counterparts. This will provide some confidence in the efficacy of using low-fidelity models for the ensuing simulation-based reliability study.

4.3.1 – CS1: Stress Concentrations - Milwaukee vs. Osseo Structures

Earlier discussion regarding the development of the high-fidelity FE models for the test-group structures has revealed some significant differences between overall dimensions and geometry for each structure. It is widely known that stress concentrations develop at locations where stress raisers exist. Stress raisers can include a number of possibilities with the most likely cases including concentrated loads over small areas or irregularities in geometry. A mast-arm tube

welded to a socketed plate is most-definitely a stress-raising source and is the culprit in the case of the test-group structures. A discrete connection through various bolting arrangements creates a stress raising behavior as well.

As indicated by the results of chapter three, a slight increase in *SCF* can significantly reduce the expected fatigue life of a connection. This first study compares the magnitude of *SCF* around the circumference of the mast-arm at the weld-toe for both structures. The results from this study will be evaluated against those obtained by the parametric equations for *SCF* provided in chapter three. In this way, the connections within the Milwaukee and Osseo structures can be classified as one of the newly developed fatigue detail categories: E2, E3 or E4. Specifying a fatigue detail category for each structure provides the necessary statistical information for use within the reliability-based procedure outlined in chapter one.

An important aspect to any structural analysis is determining the loads, or combination of loads, which must be resisted by the structure. Two load combinations were considered in the present study:

Load Combination No. 1 (LC1): Bolt Pretension and Gravity

Load Combination No. 2 (LC2): Bolt Pretension, Gravity and Wind Loading

It was felt that these load combinations would provide valuable information regarding where the *SCF* is a maximum on the cross-section – both newly installed (LC1) and in-service (LC2). Some discussion regarding the individual loads, both how they were determined and how they were applied, is provided in the subsequent sections. Figure 4.14 provides both high-fidelity FE models subjected to LC2 for visual reference throughout the subsequent sections.

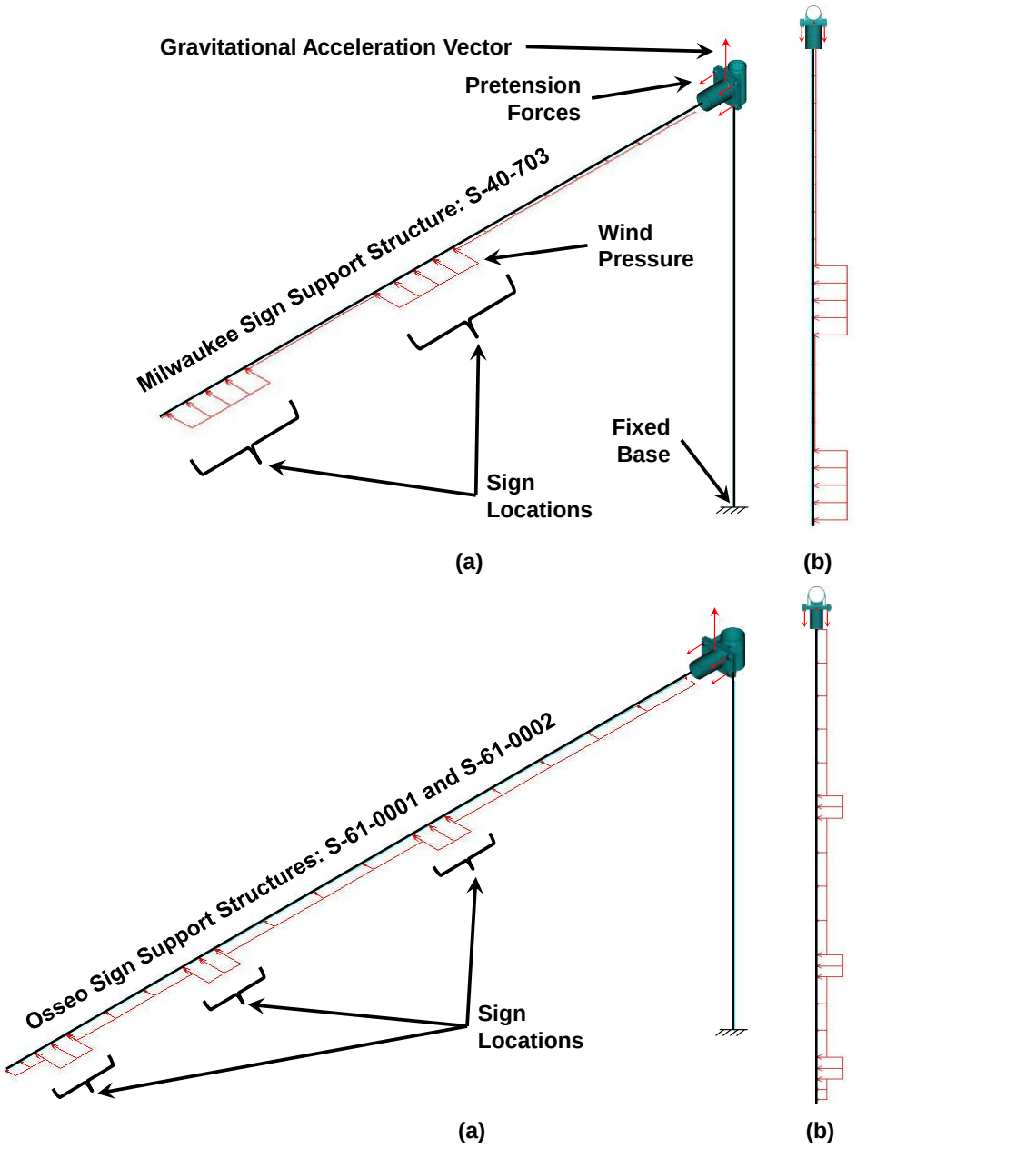

Figure 4.14. Illustration of applied loading for high-fidelity FE models: (a) isometric view and (b) top view.

Bolt Pretension: LC1 and LC2

AASHTO (2009) specifies that the bolted connections used in sign support structures shall be in accordance with the current *Standard Specifications for Highway Bridges*. These specifications require bolt pretension forces to be specified such that internal tensile stresses within each

pretension bolt achieve values approximately equal to 0.70 times their ultimate tensile strength. This corresponded to tensile loads of 71 kip and 177 kip for the bolts within the Milwaukee and Osseo models, respectively.

Gravity: LC1 and LC2

Gravity loading was used to estimate the magnitude of in-service mean stress caused by dead load for each structure. The mean stress is highly variable because the range of lengths and section sizes used for mast-arms varies from one structure to the next. To better distinguish between the two structures currently considered, gravity was applied to determine the structure-specific mean stress for use in later stress-range counting.

Gravity was applied to the models as an inertial load by specifying an acceleration vector in the global y-direction. This was possible because the density for each of the structural components was specified during the development of each high-fidelity FE model. Since all units were consistently defined in kips and inches, the magnitude of the acceleration vector was specified as (+) 386.4 in/s^2.

Wind Loading: LC2 Only

Wind pressure was included in the second load combination because it is the primary loading sustained by sign support structures when they are in-service. By incorporating wind pressure in the load combination, the distribution of *SCF* around the circumference of the mast-arm at the weld-toe may be monitored to determine whether or not there is any migration of the location of maximum *SCF*.

AASHTO (2009) provides the following expression to determine the magnitude of wind pressure acting on a bluff body:

$$P = \frac{1}{2} \cdot \rho \cdot C_d \cdot U^2 \tag{4.1}$$

where: ρ is the density of air $\left(1.146e-10\ kip \cdot s^2 / in^4\right)$; C_d is the drag coefficient; and U is the magnitude of wind speed.

At sign panel locations, C_d depends on the length-to-width $\left(L_{sign} / W_{sign}\right)$ ratio of the supported signs. The Milwaukee structure supported signs with $L_{sign} / W_{sign} = 1.33$ and the Osseo structures supported signs with $L_{sign} / W_{sign} = 1.25$. Therefore, C_d was conservatively taken as 1.19 corresponding to ratios of $L_{sign} / W_{sign} = 2.0$ for both structures (AASHTO 2009). All other locations along the mast-arm for both structures were specified with values of $C_d = 1.10$, which is a conservative value for single cylindrical members (*i.e.* mast-arm tube). It should be noted that a 40 mph wind speed was used in this study. Based on the wind speed probabilities of chapter two, a one-hour average wind speed is not likely to reach this level of magnitude. Nonetheless, a 40 mph wind speed event was arbitrarily selected to represent a "significant" wind load event.

AASHTO (2009) specifies that the natural wind gust pressure shall be applied to exposed surface areas as seen in an elevation view. As noted earlier, the application of wind pressure was limited to the mast-arm only; more specifically, wind pressure was applied only to those portions of the mast-arm modeled using beam elements (*i.e.* the low-fidelity portions). The bluff-area for each segment of mast-arm discretized for each structure can be found in Appendix G.

Special Note on Vortex Shedding

It should be noted that vortex shedding was considered in the present study. The susceptibility of a bluff body (*e.g.* mast-arm) to vortex shedding can be quantified through a dimensionless number called the *Reynolds Number* (Re). The tendency for vortices to be periodically shed

requires subcritical flow ($300 \leq Re \leq 10^5$) and regularly shed vortices requires hypercritical flow ($Re > 3.5x10^6$). Outside of these ranges, irregular (unorganized) vortex shedding occurs (Dyrbye and Hansen 1997; Foley et al. 2004; Liu 1991). Furthermore, previous studies have subscribed to the theory of lock-in velocities defined as a range of wind speeds over which potentially large across-wind vibrations can occur (Dyrbye and Hansen 1997; Foley et al. 2004; Liu 1991; Simiu and Scanlon 1996).

The type of flow and the range of wind speeds over which potentially significant across-wind vibrations were possible were studied for both structures using procedures exhaustively detailed in Foley et al. (2004). It was determined that the magnitude of across wind loading was very, very small (on the order of 30 to 45 lbs total over entire length of mast-arms). As a result, vortex shedding loading was justifiably omitted from the load combinations.

High-Fidelity Model Results

At this point, the models have been developed, the loads have been defined and the results obtained from each high-fidelity model may now be discussed. Figures 4.15 and 4.16 illustrate the results for the nodal solution of longitudinal bending stress from each high-fidelity FE model and for each load combination. Qualitatively, the results from these figures look good. The results for both models subjected to LC1 provide tensile stresses in the top half of the mast-arm and compressive stresses in the bottom half of the mast-arm. Also illustrated by these figures is the apparent stress concentration effect generated at the weld-toe of each connection. Overall, the Osseo structure achieves significantly greater longitudinal bending stresses near its weld-toe compared to the Milwaukee structure. Also, the distribution of longitudinal bending stress in the Milwaukee structure is impacted more extensively by LC2 than is that of the Osseo structure.

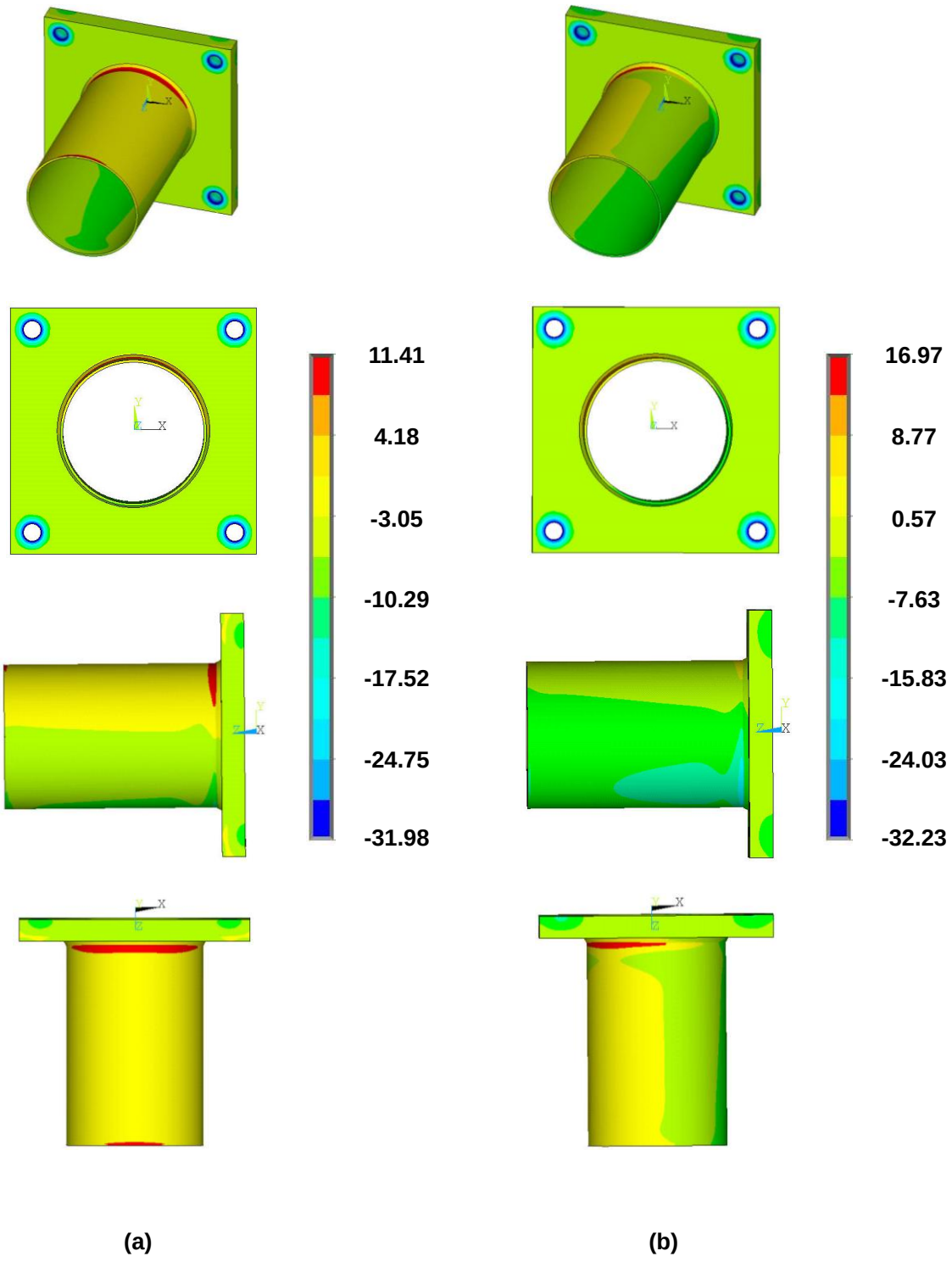

Figure 4.15. Longitudinal bending stress for Milwaukee connection subjected to (a) LC1 and (b) LC2 (all values in units of ksi).

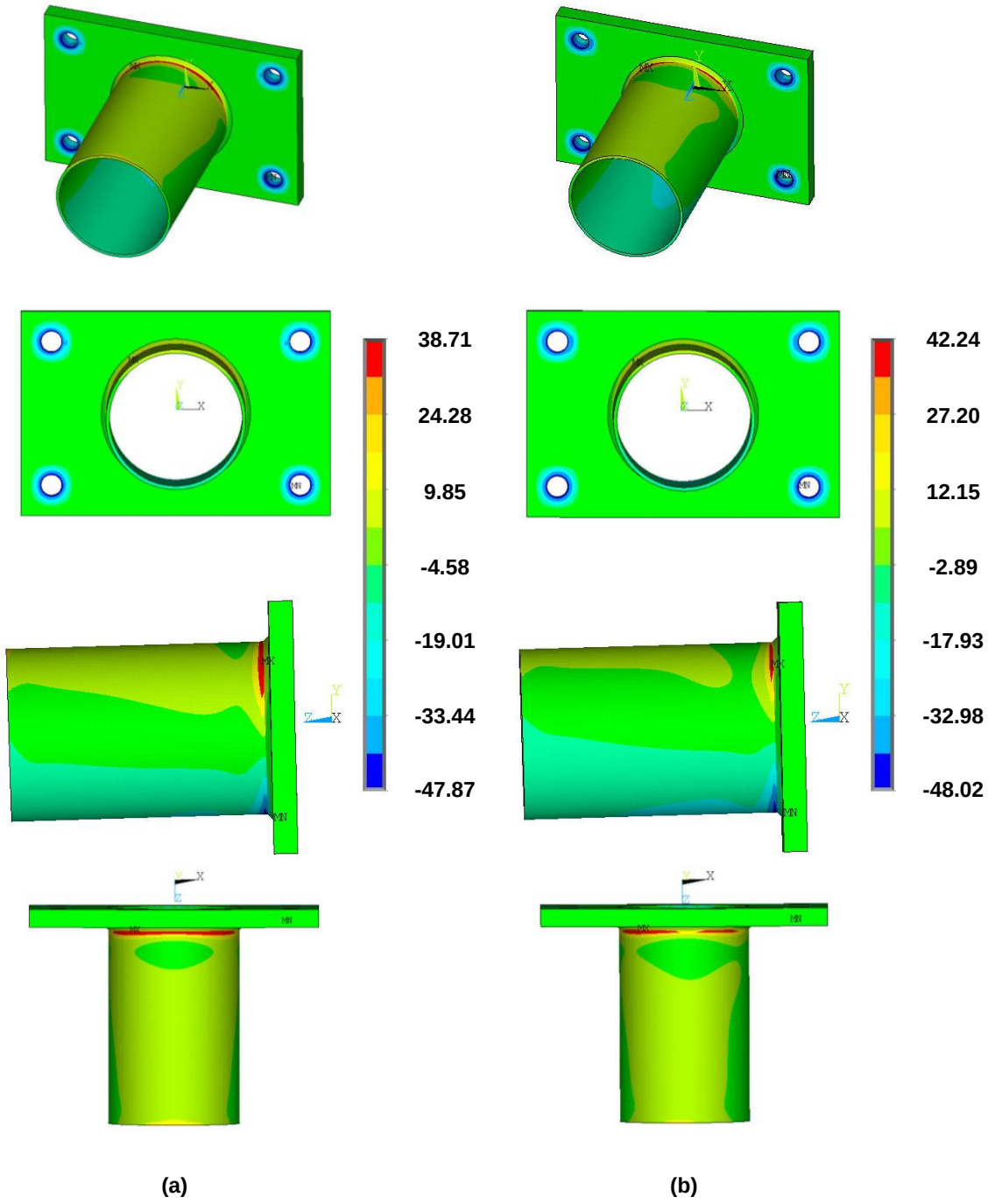

Figure 4.16. Longitudinal bending stress for Osseo connection subjected to (a) LC1 and (b) LC2 (all values in units of ksi).

Figure 4.17 provides the contact status at the socket plate-to-backing plate interface for both models and both load combinations. Some very important information can be gleaned from this figure. This figure indicates that when pretension, gravity and wind pressure is applied to the structures, the faying surfaces of the socketed and backing plates begin to bear against one another to resist the moments that are generated. It is clear from Figure 4.17 that for the same level of wind loading (wind pressure corresponding to a 40 mph wind speed), the Milwaukee structure engages more surface area of each plate indicating that a larger moment is generated in the Milwaukee structure compared to the Osseo structure. The elliptical nature of the contact areas surrounding the bolt holes in the Osseo structure suggests its plate is bending much more than the plate from the Milwaukee structure. This will change the resulting longitudinal bending stress distributions around the circumference of the mast-arm tube. Also, the change in contact status from LC1 to LC2 indicates wind loading significantly affects the Milwaukee structure while the Osseo structure is dominated by gravity loading.

These results make sense because the Milwaukee structure has a smaller and lighter mast-arm providing reduced section properties compared to the Osseo structure. Furthermore, the Milwaukee structure contains larger signs which generate a larger total bluff area subjected to wind pressure. It should be anticipated that a combination of these two effects will generate higher longitudinal bending stresses about the y-axis for the Milwaukee structure compared to the Osseo structure.

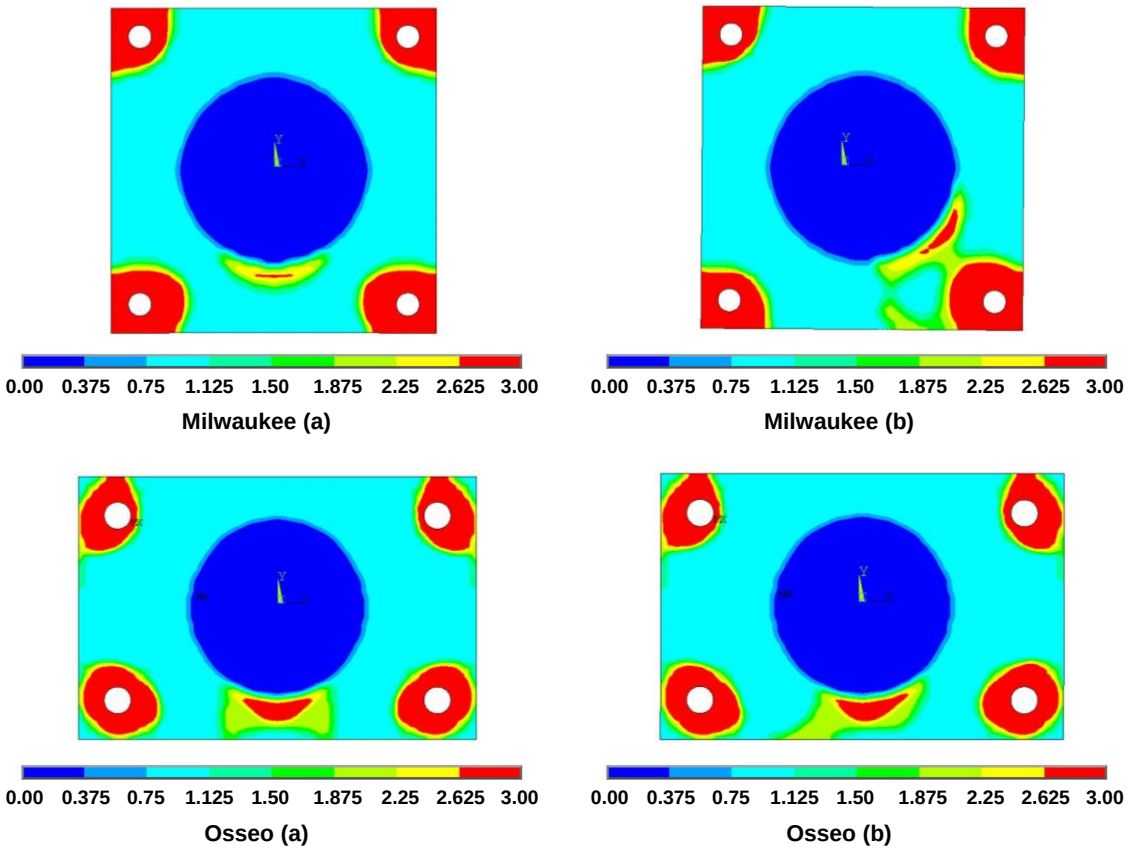

Figure 4.17. Contact status at socket plate to backing plate interface: (a) LC1 and (b) LC2 (0 = open and not near contact; 1 = open but near contact; 2 = closed and sliding; 3 = closed and sticking).

Figure 4.18 provides the contact pressure resulting from the contact status of Figure 4.17. The results for both structures are very comparable; however, they do indicate that larger contact pressures are achieved at the bottom of the cross-section for the Osseo structure. This is a sensible result given the fact that the mast-arm of the Osseo structure is approximately 1.3 times longer and weighs approximately 3.7 times heavier than the mast-arm of the Milwaukee structure.

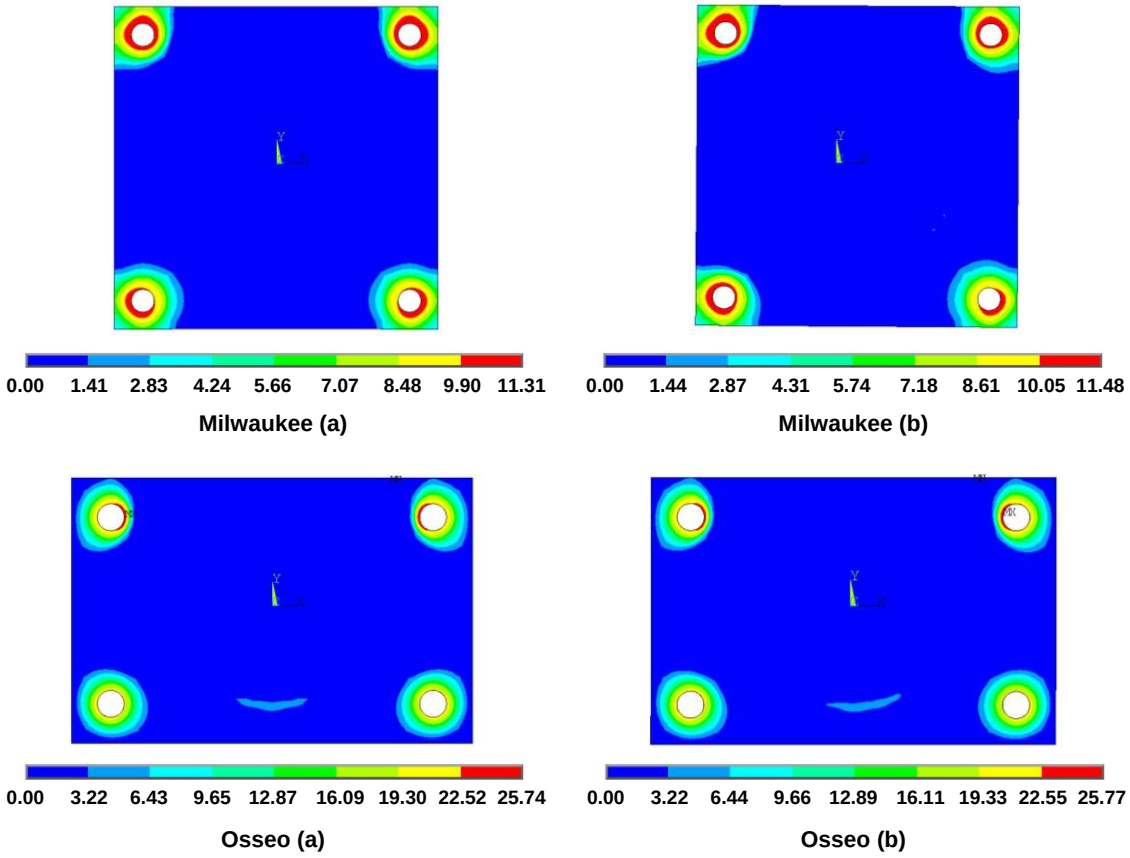

Figure 4.18. Contact pressure at socket plate to backing plate interface: (a) LC1 and (b) LC2 (all values in units of ksi).

As indicated previously, the main goal of this first study was to quantify the differences in *SCF* around the circumference of the mast-arm tube at the weld-toe. To do this, the magnitude of stress around the entire circumference of the mast-arm must be monitored at two distinct locations along its length: (1) at the cross-section corresponding to the weld-toe defining the concentrated stress; and (2) at a cross-section some distance away from the weld-toe defining the nominal stress. It should be noted that the term "stress" actually refers to normal stress in the direction parallel with the axis of the mast-arm tube as this is the direction perpendicular to the likely orientation of fatigue-induced cracks initiating at the weld-toe. This corresponds to the z-direction for both models.

Given the high-fidelity FE models developed for each test-group structure, a simple equation for determining the magnitude of the SCF at any circumferential point around the mast-arm tube at the weld-toe is computed as,

$$SCF(\theta) = \frac{\sigma_{WT}(\theta)}{\sigma_{N}(\theta)} \tag{4.2}$$

where: $\sigma_{WT}(\theta)$ is the magnitude of longitudinal bending stress corresponding to angle θ taken at the weld-toe (*i.e.* weld-toe stress); $\sigma_{N}(\theta)$ is the magnitude of longitudinal bending stress corresponding to angle θ taken at some distance away from the weld-toe stress concentration effects (*i.e.* nominal stress); and θ ranges from 0 to 2π measured counterclockwise from the six o'clock position of the mast-arm tube.

Previous studies have shown that stress concentration effects in similar connections as those modeled in the present study extend approximately five inches from the weld-toe toward the free end of the mast-arm before nominal stress is achieved (Roy et al. 2011). Therefore, the weld-toe stress was taken at nodes corresponding to the weld-toe and the nominal stress was taken at nodes specified ten inches from the weld-toe toward the free end of the mast-arm for each high-fidelity FE model. Ten inches was specified to ensure stress concentrations were not affecting the magnitude used to define the nominal values. Because solid elements were used, it was possible to obtain these values by mapping nodal solutions for longitudinal bending stress onto paths plotted along exterior nodes at these cross-sections.

The path results from each model and each load combination are provided in Figure 4.19. The resulting *SCF*'s at the weld-toe for each point along the circumference of each model computed using equation (4.2) is provided in Figure 4.20. The results provided in these figures are striking. First of all, they indicate that the *SCF* within the connection of the Osseo structure is

much more punishing than that of the Milwaukee structure. In fact, the *SCF* is so great in the connection contained within the Osseo structure that the stress levels at the weld-toe, in some locations, nearly reach the assumed yield stress of the material (50 ksi) for a 40 mph static wind load. The maximum values for longitudinal bending stress for each structure and each load combination is provided in Table 4.1. These results also reiterate the more pronounced impact of wind loading on the Milwaukee structure as compared to the Osseo structure.

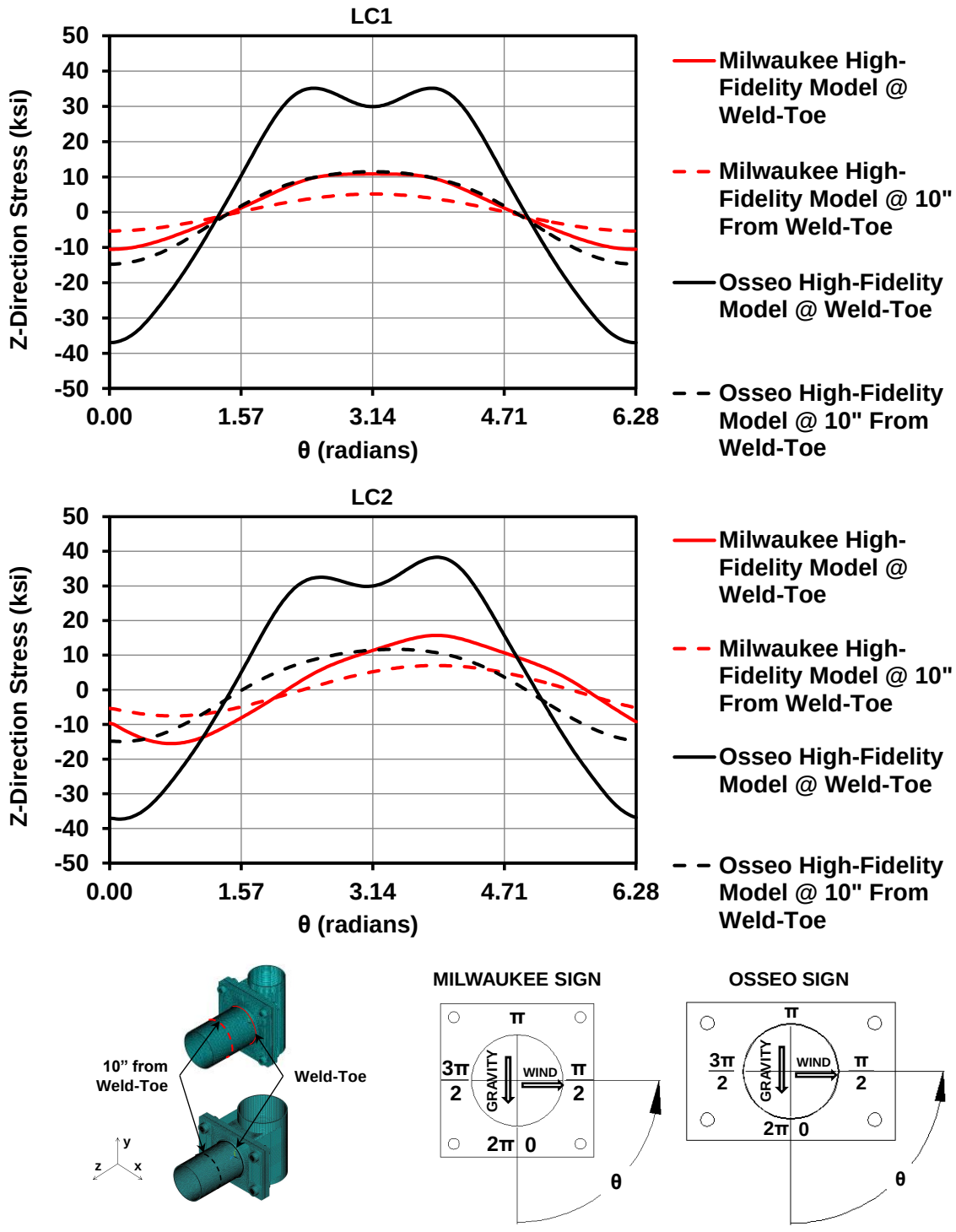

Figure 4.19. Distribution of longitudinal bending stress obtained from path plots at weld-toe and ten inches from weld toe for both high-fidelity models and both load combinations.

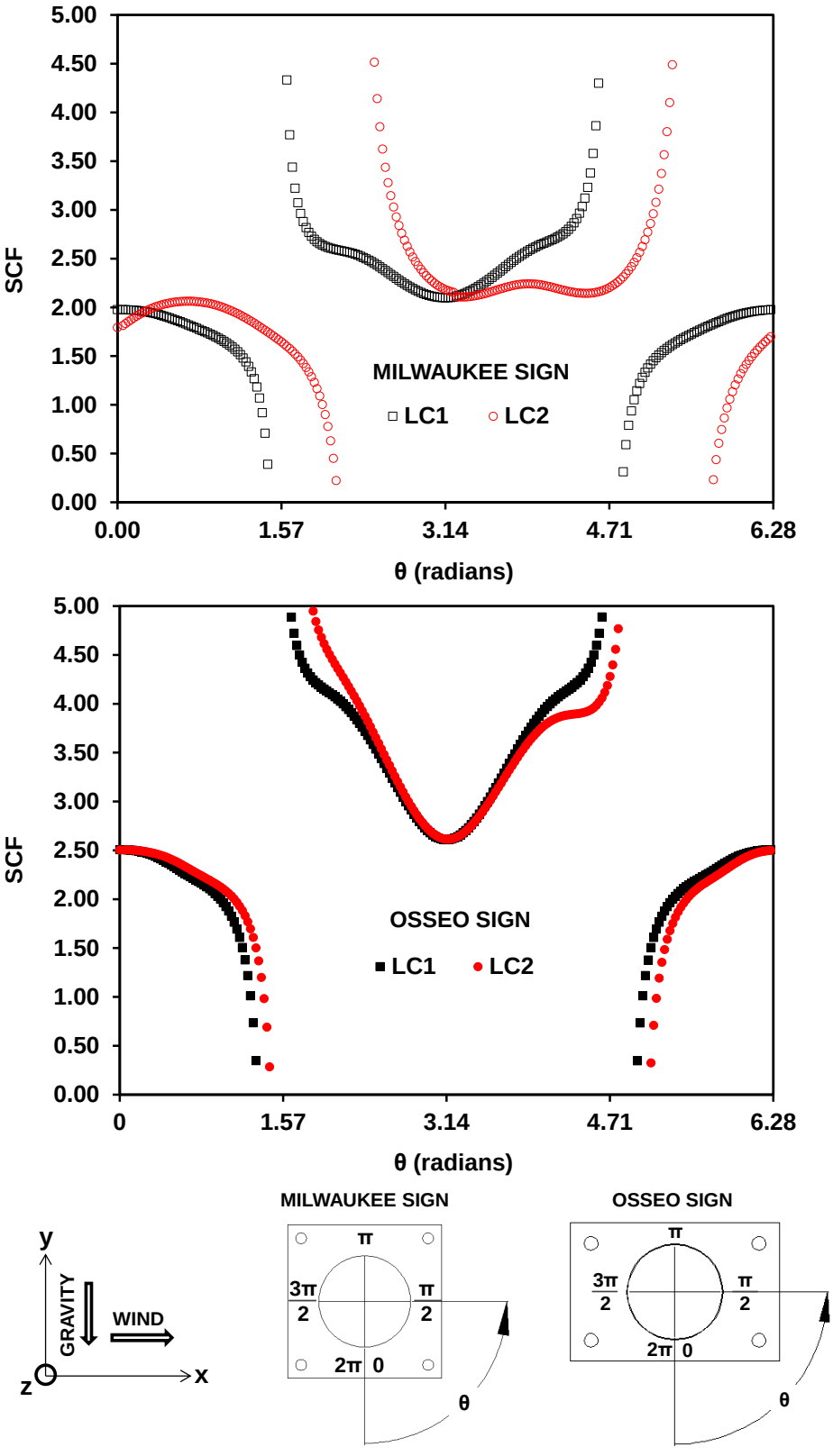

Figure 4.20. Distribution of *SCF* for both structures and both load combinations at weld-toe.

Table 4.1. Maximum values of longitudinal bending stress achieved at the weld-toes of each model and for each load combination (note LC1 is pretension and gravity only and LC2 includes pretension, gravity and a 40 mph static wind load).

Load Combination	Milwaukee Structure	Osseo Structure
	Max. Longitudinal Bending Stress (ksi)	
LC1	10.8	35.2
LC2	15.7	38.3

One last aspect included in the present study was a comparison between the *SCF* results obtained from the high-fidelity FE analytical models and those obtained using the parametric equations discussed in chapter three. To make this comparison, an appropriate parametric equation must be chosen from chapter three. Both structures in this study contain connections composed of round tubes fillet welded to socketed plates. The parametric equation used to determine the *SCF* for this type of connection was presented in chapter three as equation (3.10). For convenience, this equation is restated as,

$$SCF = 2.16 + \left(0.908 - 0.924 \frac{C_{BC}^{0.0474}}{N_B^{0.0105}} \right) \cdot \left(4.54 + 52.1 \cdot t_T \right) \cdot \left(14.6 - 1.17 \cdot D_T^{1.15} \right) \cdot t_{TP}^{-2.36} \quad (4.3)$$

Tables 4.2 and 4.3 provide summaries of the dimensions and parameters required to compute the *SCF* using equation (4.3) and the resulting *SCF* for the Milwaukee and Osseo structures, respectively.

Table 4.2. Summary of parameters used to determine SCF within connection of Milwaukee Sign Support Structure: S-40-703.

S-40-703	
D_T	**11.00**
t_T	**0.18**
N_B	**4**
t_{TP}	**1.75**
D_{BC}	**21.57**
D_{OP}	**11.06**
$C_{BC} = D_{BC} / D_T$	**1.96**
$C_{OP} = D_{OP} / D_T$	**1.01**
SCF	**2.62**

Table 4.3. Summary of parameters used to determine SCF within connection of Osseo Sign Support Structures: S-61-0001 and S-61-0002.

S-61-001 and S-61-002	
D_T	**12.76**
t_T	**0.33**
N_B	**4**
t_{TP}	**1.75**
D_{BC}	**25.99**
D_{OP}	**12.8225**
$C_{BC} = D_{BC} / D_T$	**2.04**
$C_{OP} = D_{OP} / D_T$	**1.00**
SCF	**3.59**

The distribution for *SCF*'s obtained for both models and both load combinations have been summarized in Figure 4.21 with an emphasis on the portions of the cross-section most susceptible to fatigue loading (*i.e.* $\pi/2 < \theta < 3\pi/2$). The *SCF* determined using equation (4.3) and the fatigue detail categories developed by *Synthesis Approach No. 2* from chapter three (E2, E3 and E4) are provided on the left- and right-hand sides of Figure 4.21, respectively. This figure is

indicative of the following: (a) the connection contained within the Osseo structure should be classified as an E3 or E4 detail while the connection contained within the Milwaukee structure should be classified as an E2 or E3 detail and (b) the distribution of *SCF* for each structure are in reasonable agreement with the predictive equations provided by Roy et al. (2011).

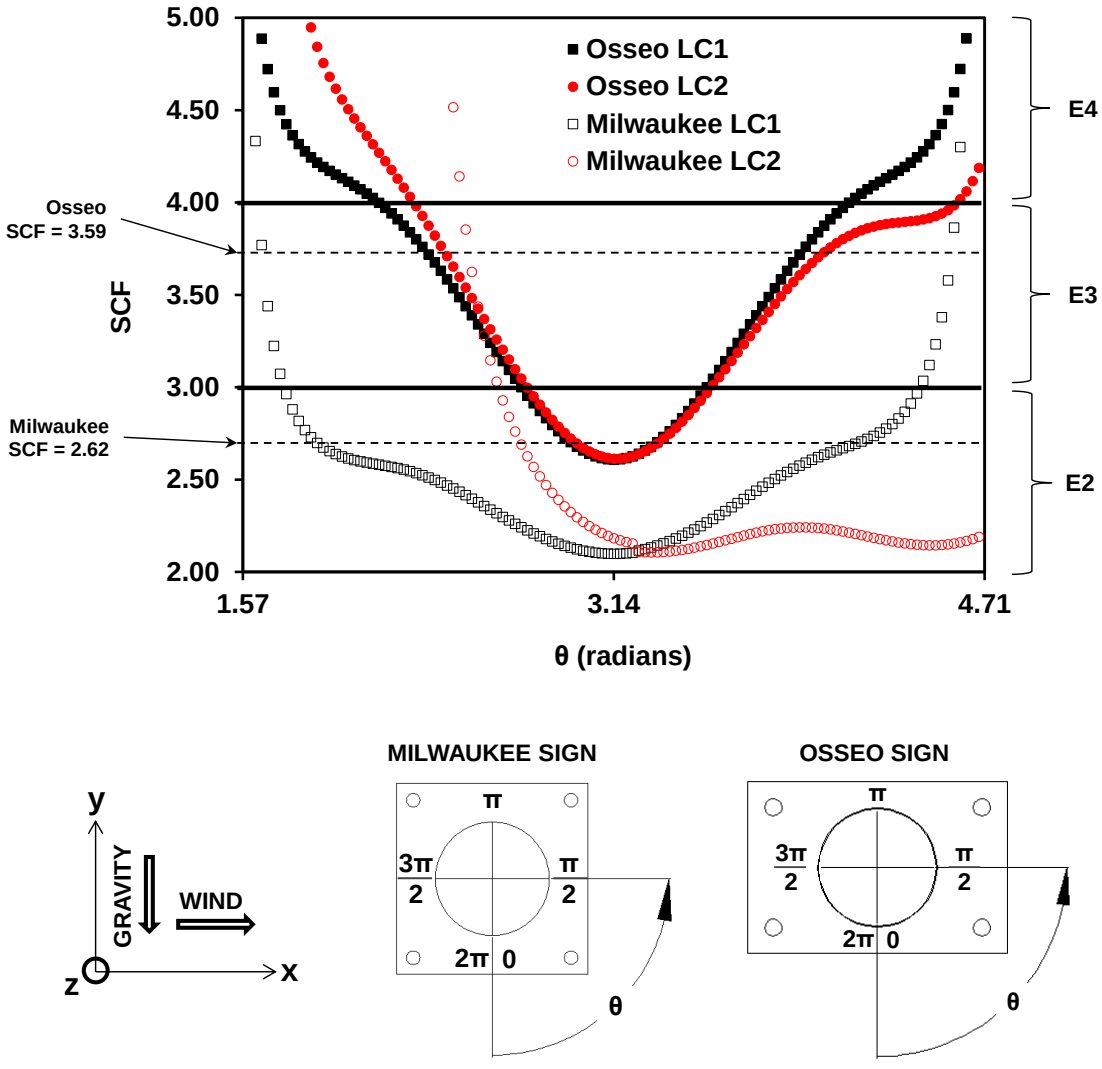

Figure 4.21. Summary of distribution of *SCF*'s and resulting detail classifications from chapter three.

4.3.2 – CS2: High- vs. Low-Fidelity Static Structural Analyses

As indicated previously, the only difference between the high- and low-fidelity models of each structure was the level of detail utilized when modeling the bolted connections between their mast-arms and poles. Because of this, results obtained from both models of each structure, subjected to the same load combinations, could be compared to determine the level of accuracy achieved by the low-fidelity models relative to the high-fidelity models. However, since pretension bolts were not included in the low-fidelity models, the pretension loading was removed from both load combinations. The load combinations utilized in the first comparative study were modified such that LC1 consisted of gravity loading only while LC2 consisted of gravity loading and wind loading generated by a 40 mph wind speed acting perpendicular to the sign faces.

The longitudinal bending stress results from around the circumference of the mast-arm tube at locations corresponding to ten inches from the weld-toe for each modeling approach of each structure were compared in this study. This was a convenient choice because the nodal solution for longitudinal bending stress was already found for the high-fidelity models at these locations.

To make this comparison, the results from the low-fidelity models corresponding to the same locations needed to be obtained. Since the low-fidelity models contained beam elements at these locations, some additional work was required to obtain these results in a similar format as was plotted for the high-fidelity models. Discussion regarding this work and the resulting comparisons will be provided in the following section.

The BEAM188 element is the only element-type used in the low-fidelity models. This element has the ability to provide bending stress, but is limited to providing values for the top, bottom and both sides of the beam cross-section. If appropriate section properties are assigned to

the element, then four values of longitudinal bending stress can be found. However, this would only provide comparisons at four points between each model. Therefore, instead of extracting bending stress from the low-fidelity models, it was decided to extract bending moments. In this way, the bending stress formula from elementary beam theory can be used to determine the magnitude of stress at each point around the circumference of the mast-arm tube. Also, the second load combination considered in the present study generates biaxial loading. Therefore, the bending stress formula used to compute values of longitudinal bending stress at ten inches from the weld-toe can be expressed as,

$$\sigma_z = \frac{M_G \cdot y}{I_{10}} + \frac{M_W \cdot x}{I_{10}} \tag{4.4}$$

where: M_W is the internal moment caused by wind; M_G is the internal moment caused by gravity; x is the distance from the neutral axis of bending to the point of computed stress caused by M_W; y is the distance from the neutral axis of bending to the point of computed stress caused by M_G; and I_{10} is the moment of inertia (all values taken at the cross-section ten inches from the weld-toe).

Given that each mast-arm consisted of a round tube, additional consideration was needed to ensure the same circumferential locations between low- and high-fidelity models were being compared. Figure 4.22 illustrates a procedure which introduces the use of polar coordinates to determine the values for x and y of equation (4.4). Implementing the procedure illustrated in Figure 4.22, the bending stress formula may be restated as,

$$\sigma_z = \frac{M_G \cdot r \cdot \cos(\varphi)}{I_{10}} + \frac{M_W \cdot r \cdot \sin(\varphi)}{I_{10}} \tag{4.5}$$

where:

$$\varphi = \theta - \pi$$

and r is the outside radius of the mast-arm tube at ten inches from the weld-toe.

Figure 4.23 provides longitudinal bending stress results, computed using equation (4.5), and those obtained from each of the high-fidelity models. The results from each modeling approach and for both load combinations look very comparable. This indicates that at ten inches from the weld-toe, the low-fidelity model for each structure provides accurate and appropriate results when subjected to typical loading scenarios that will be used in subsequent analyses.

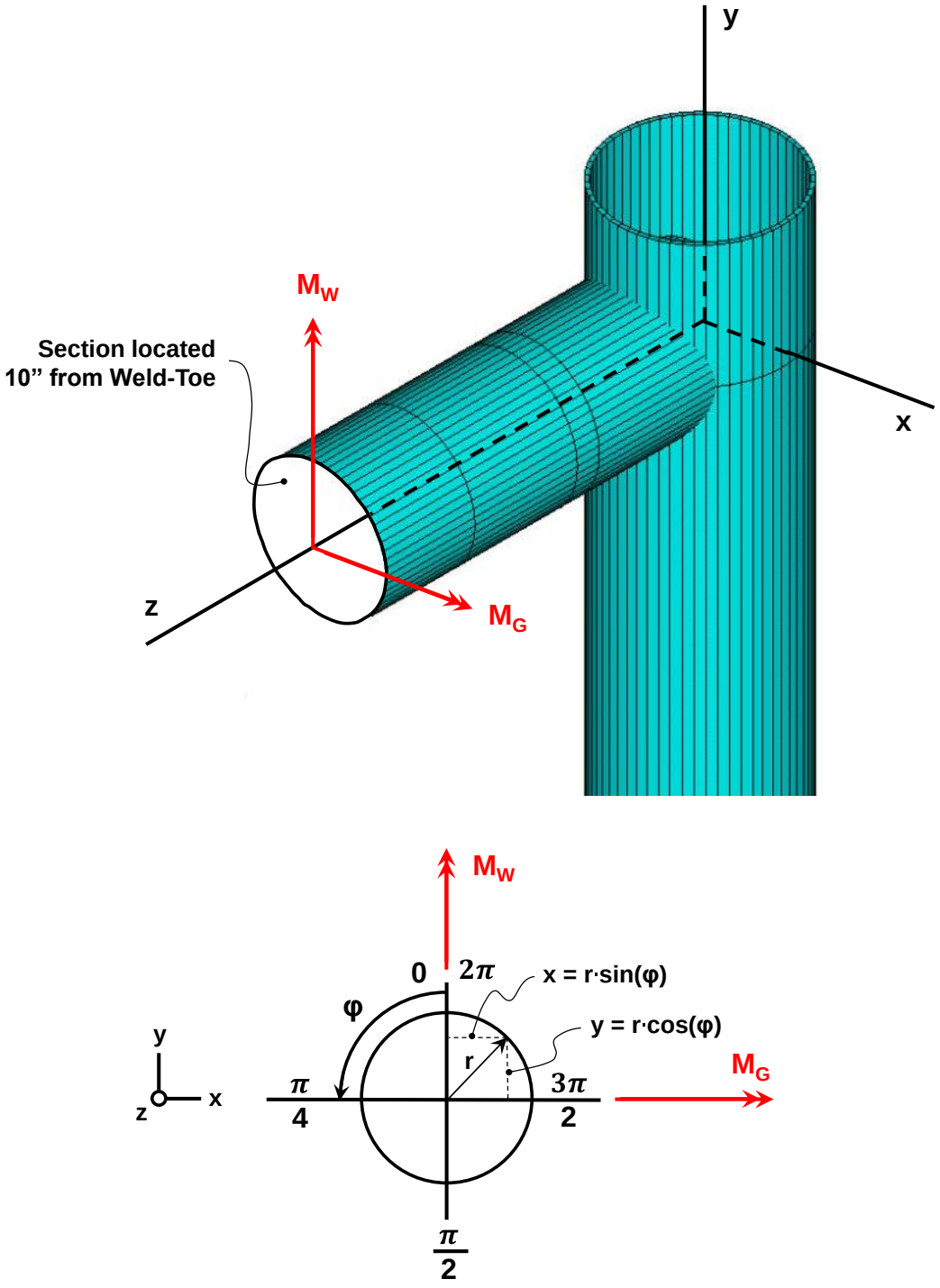

Figure 4.22. Procedure used to determine polar coordinates used in equation (4.5).

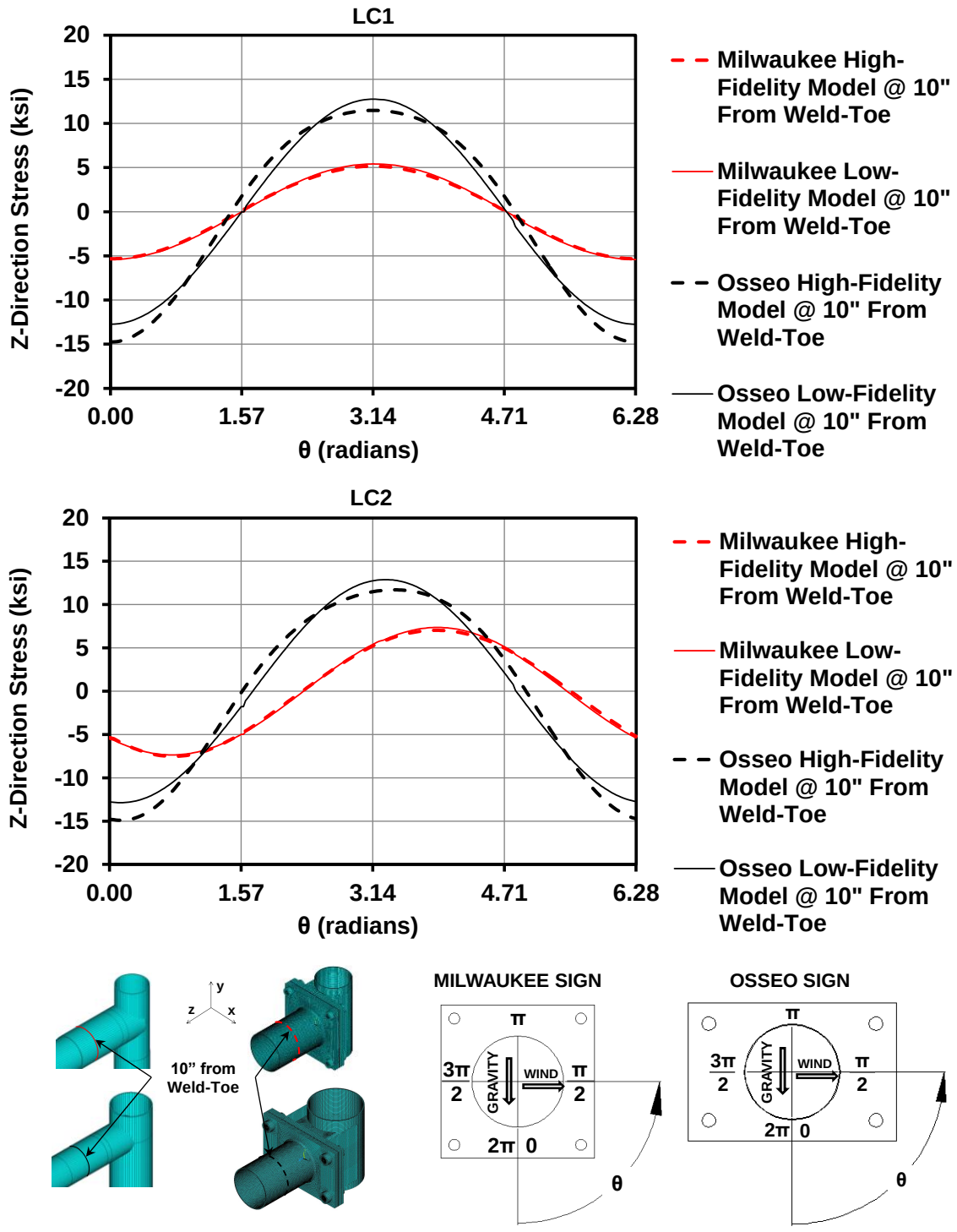

Figure 4.23. Comparison between longitudinal bending stress results obtained at ten inches from the weld-toe from both high- and low-fidelity models and for both load combinations.

4.3.3 – CS3: High- vs. Low-Fidelity Modal Analyses

The previous study compared static results between the high- and low-fidelity models to ensure the lower-fidelity model of each structure provided reasonable longitudinal bending stress results when those results were compared at locations sufficiently far from the connection. The present study will compare dynamic response characteristics to see what effect, if any, happens as a result of not including connection flexibility within the lower-fidelity FE models. To do this, modal analyses were conducted on all four FE models previously developed. The results for the first five dominant modes were extracted from ANSYS in the form of vibrational shapes and natural frequencies. For reference throughout the following discussion, the natural frequencies are provided in Tables 4.4 and 4.5 and corresponding vibrational shapes are provided in Figures 4.24 through 4.27.

Table 4.4. Variation in natural frequencies for dominant modes of vibration for both high- and low-fidelity FE models of the Milwaukee structure.

Milwaukee Sign Support Structure - S-40-703

Vibration Mode	Vibration Shape	High Fidelity Model		Low Fidelity Model		Abs. Diff. (%)
		Frequency (Hz)	Period (sec.)	Frequency (Hz)	Period (sec.)	
1	1st Twist	1.597	0.626	1.608	0.622	0.68
2	1st Hatchet	1.704	0.587	1.751	0.571	2.67
3	2nd Twist	3.863	0.259	4.696	0.213	17.74
4	2nd Hatchet	4.118	0.243	5.158	0.194	20.16
5	3rd Twist	12.047	0.083	12.863	0.078	6.34

Table 4.5. Variation in natural frequencies for dominant modes of vibration for both high- and low-fidelity FE models of the Osseo structure.

Osseo Sign Support Structures - S-61-0001 and S-61-0002

Vibration Mode	Vibration Shape	High Fidelity Model		Low Fidelity Model		Abs. Diff. (%)
		Frequency (Hz)	Period (sec.)	Frequency (Hz)	Period (sec.)	
1	1st Twist	1.143	0.875	1.137	0.879	0.53
2	1st Hatchet	1.220	0.819	1.224	0.817	0.27
3	2nd Hatchet	4.099	0.244	4.447	0.225	7.84
4	2nd Twist	4.563	0.219	5.287	0.189	13.70
5	3rd Hatchet	9.940	0.101	9.945	0.101	0.05

Because the primary loading of the ensuing time-history analyses (discussed in chapters five and six) was natural wind applied horizontal and perpendicular to the mast-arm axes, the first horizontal vibrational mode (pole twisting) was of particular interest in the present study. This mode happened to be the fundamental (*i.e.* most flexible or easiest to excite) vibrational shape for both Milwaukee and Osseo structures. The far-right columns of Tables 4.4 and 4.5 indicate that the low-fidelity models provide natural frequency magnitudes within one percent of those achieved for the fundamental modes of the higher-fidelity models.

Furthermore, the changes in vibrational shape from horizontal motion (twisting-type) in mode one, to vertical motion (hatcheting-type) in mode two, without significant separation in natural frequencies of the two modes, is expected since both structures consist of round mast-arms providing symmetry and equal dimensions about both x- and y-axes. The slight increase in natural frequency between modes one and two for both structures indicates that the poles of each structure provide slightly larger bending stiffness relative to twisting stiffness.

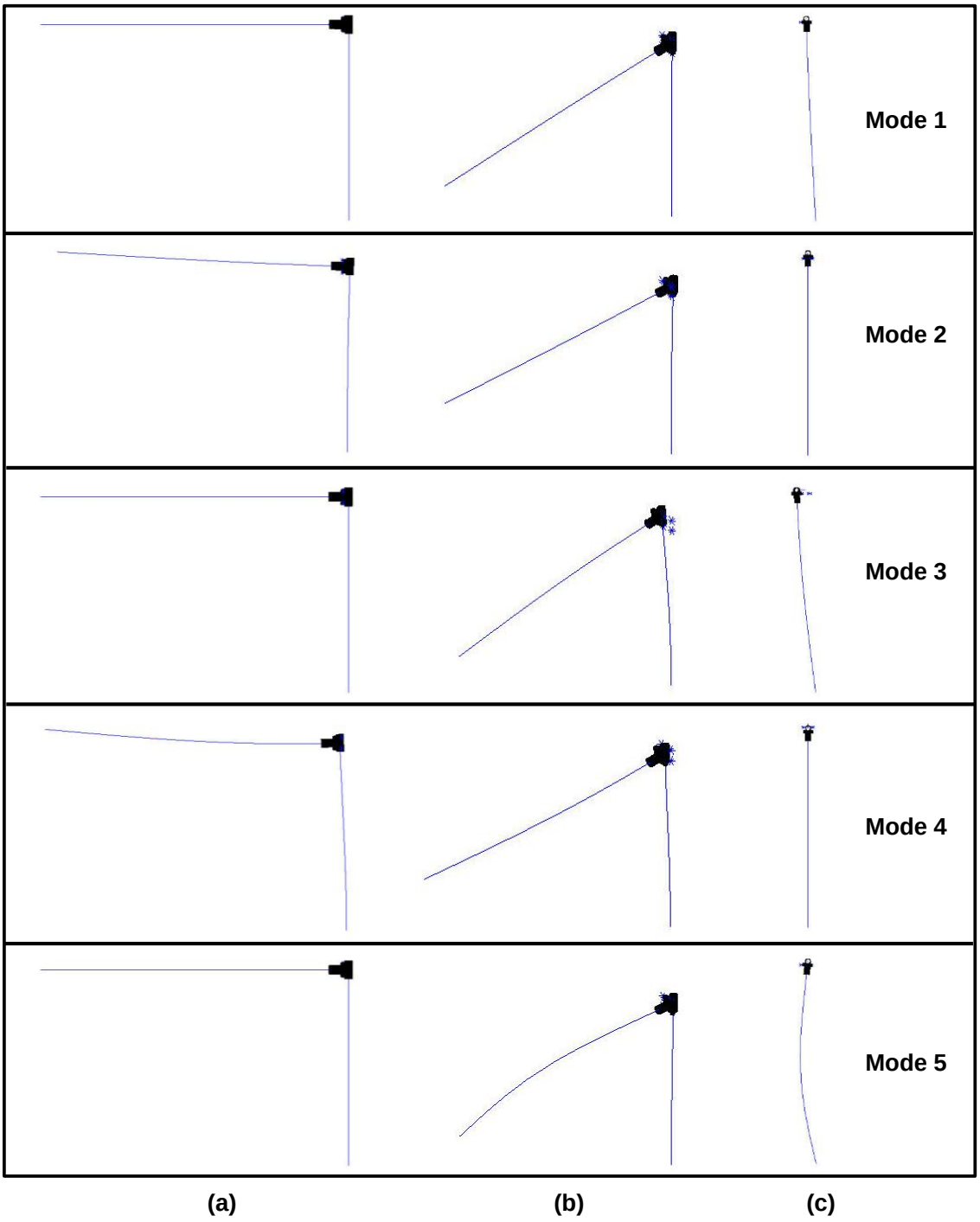

Figure 4.24. First five vibrational mode shapes for high-fidelity FE model of Milwaukee structure: (a) side view; (b) isometric view; and (c) top view.

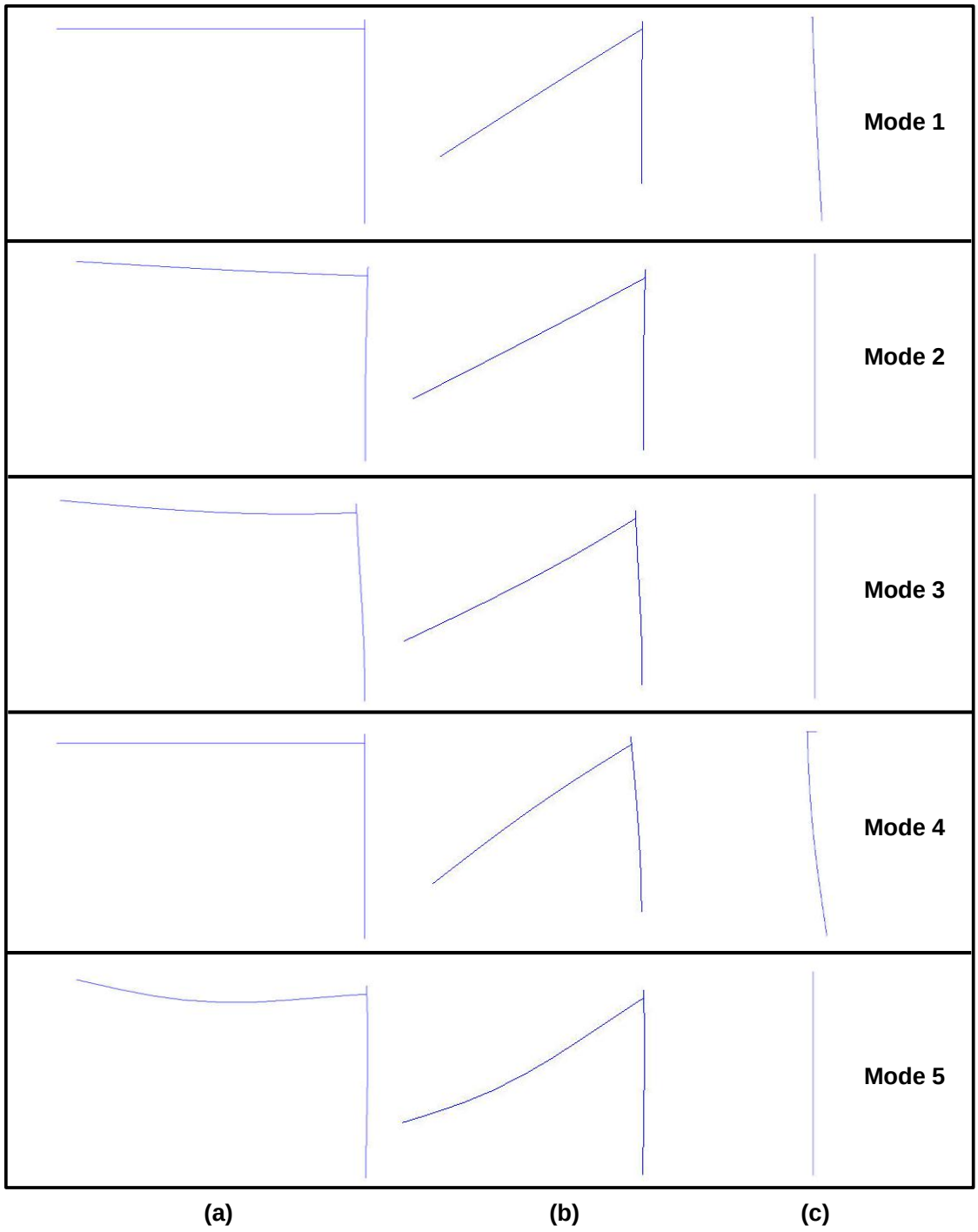

Figure 4.25. First five vibrational mode shapes for low-fidelity FE model of Milwaukee structure: (a) side view; (b) isometric view; and (c) top view.

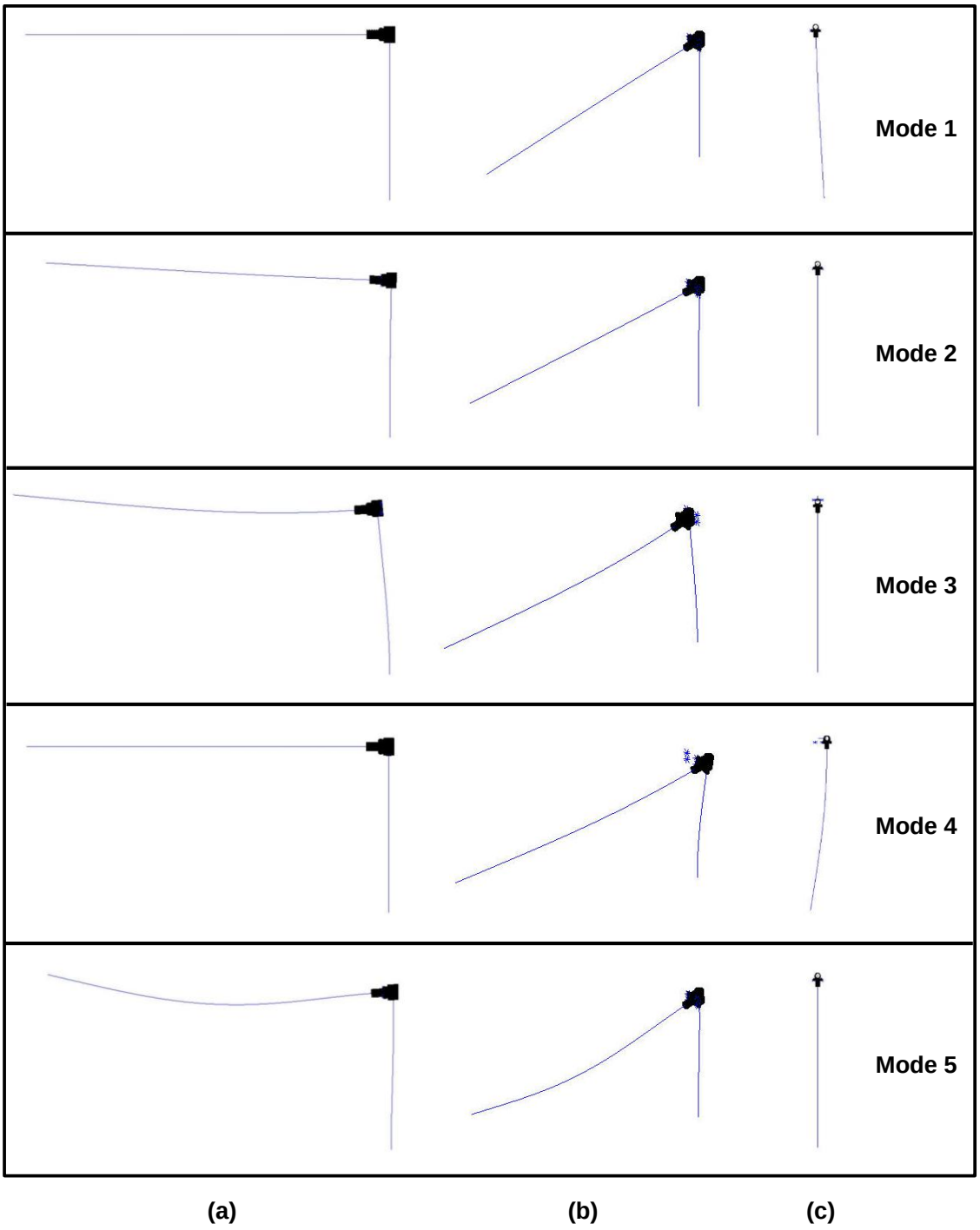

Figure 4.26. First five vibrational mode shapes for high-fidelity FE model of Osseo structure: (a) side view; (b) isometric view; and (c) top view.

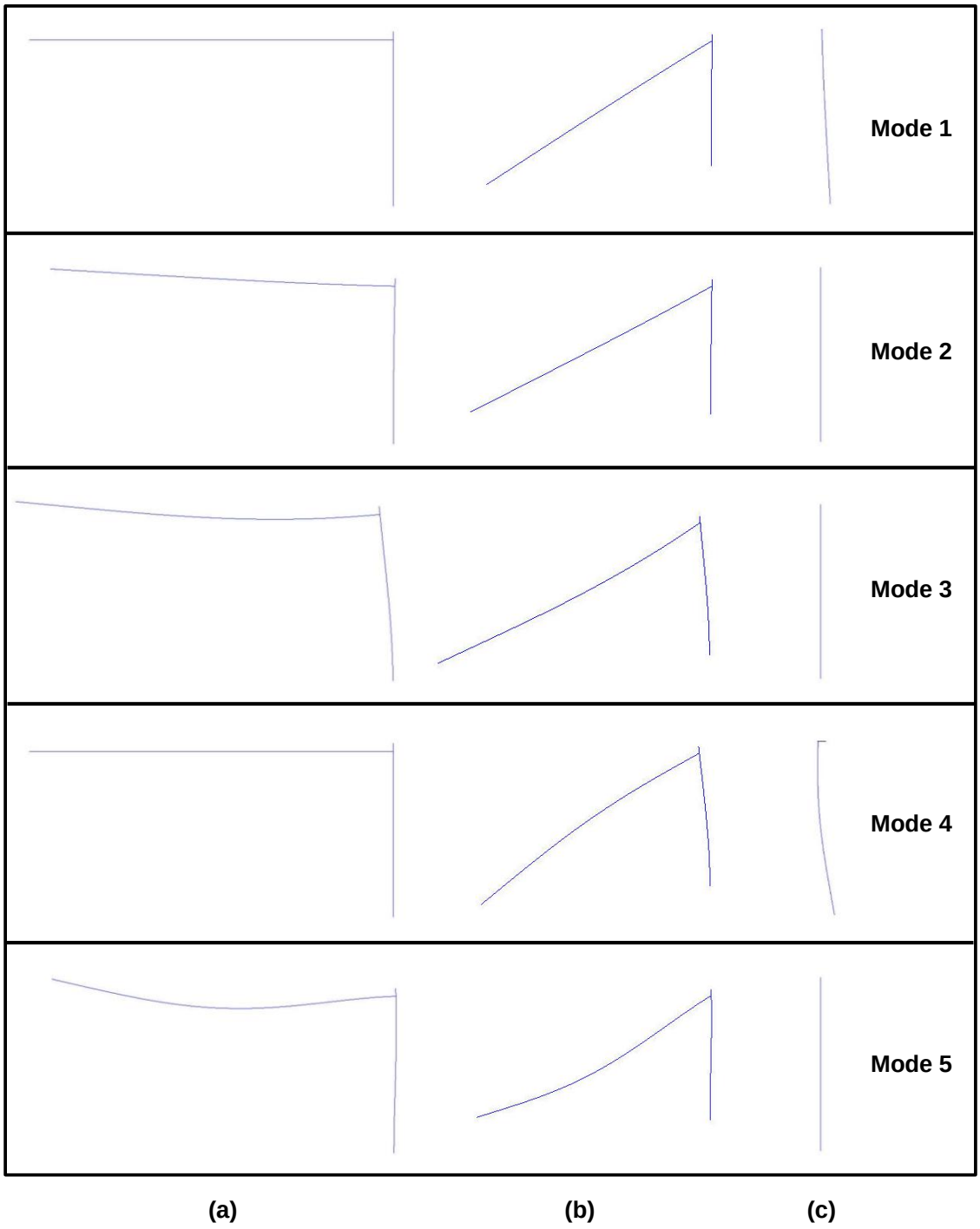

Figure 4.27. First five vibrational mode shapes for low-fidelity FE model of Osseo structure: (a) side view; (b) isometric view; and (c) top view.

A qualitative check on the magnitude of natural frequencies achieved for the first mode of vibration for each structure was conducted to ensure the models were achieving accurate results. To do this, a simple model of a cantilevered beam with lumped mass at its tip was used. The lumped mass approach illustrated in Figure 4.28 is considered a single degree of freedom structure and its natural frequency can be computed as,

$$f = \frac{1}{2\pi}\sqrt{\frac{k}{m}} \tag{4.6}$$

with the following defined as,

$$k = \frac{3EI}{L^3}$$

$$m = 0.25 \cdot V_{ma} \cdot \rho_{st}$$

where: k is the stiffness of the structure; E is the modulus of elasticity of steel; I is taken as the average moment of inertia along the length of the mast-arm, L; m is the contributing mass; V_{ma} is the total volume of steel used in the mast-arm; and ρ_{st} is the density of steel.

It should be noted that the lumped mass approach provided in Figure 4.28 does not include rotational inertia or geometric stiffness effects. Also, it is heavily dependent upon the amount of mass specified in equation (4.6). If additional (less) mass were allocated to the tip of the cantilever, the resulting natural frequencies from equation (4.6) would decrease (increase) accordingly. The fact that a fully-fixed connection was used removes flexibility introduced by bending or twisting of the pole. Therefore, the natural frequencies of Figure 4.28 are higher than expected. With that said, the estimates in Figure 4.28 are definitely in the ballpark of those obtained by the ANSYS modal analyses. Therefore, the low-fidelity FE models developed in this chapter should provide accurate results in the time-history analyses moving forward.

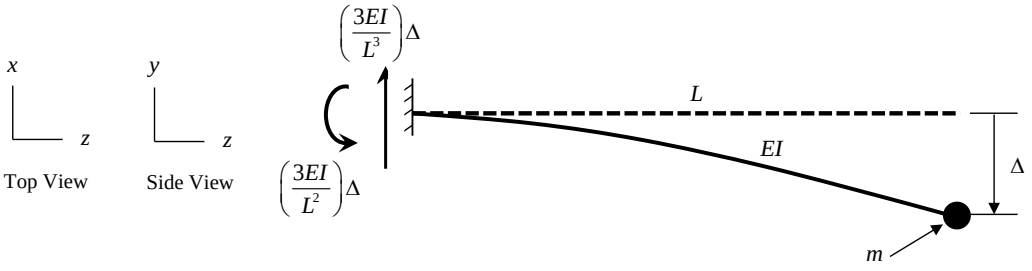

	Milwaukee Structure	**Osseo Structure**
$k = \frac{3EI}{L^3}$	$k = \frac{3 \cdot 29{,}500\ ksi \cdot 47.14\ in^4}{(387.06\ in)^3}$ $k = 0.07194 \frac{kip}{in}$	$k = \frac{3 \cdot 29{,}500\ ksi \cdot 249.75\ in^4}{(542.85\ in)^3}$ $k = 0.13817 \frac{kip}{in}$
$m = 0.5 \cdot V_{ma} \cdot \rho_{st}$	$m = 0.5 \cdot (1764.80\ in^3) \cdot \left(7.405e-7\ \frac{kip \cdot s^2}{in^4}\right)$ $m = 6.534e-4\ \frac{kip \cdot s^2}{in}$	$m = 0.5 \cdot (6536.70\ in^3) \cdot \left(7.405e-7\ \frac{kip \cdot s^2}{in^4}\right)$ $m = 2.420e-3\ \frac{kip \cdot s^2}{in}$
$f = \frac{1}{2\pi}\sqrt{\frac{k}{m}}$	$f = \frac{1}{2\pi}\sqrt{\frac{0.07194\ \frac{kip}{in}}{6.534e-4\ \frac{kip \cdot s^2}{in}}}$ $f = 1.670\ Hz$	$f = \frac{1}{2\pi}\sqrt{\frac{0.13817\ \frac{kip}{in}}{2.420e-3\ \frac{kip \cdot s^2}{in}}}$ $f = 1.202\ Hz$

Figure 4.28. Lumped mass approximation for fundamental natural frequency of both Milwaukee and Osseo structures.

4.4 – Concluding Remarks

The previous discussion has systematically developed FE models of varying levels of detail and provided comparative studies between static and dynamic (modal analysis) results of each. Some conclusions drawn from this chapter include the following:

1. Using the newly developed fatigue detail categories from *Synthesis Approach No. 2* of chapter three, the Osseo structure should be classified as E4 while the Milwaukee structure should be classified as E2.
2. The *SCF* results from the high-fidelity models of each structure indicate that the parametric equations provided by Roy et al. (2011) are suitable for defining the *SCF* within connections for these types of structures.
3. The low-fidelity models of each structure provide reasonable magnitudes of nominal stress in the vicinity of each of their connections. Also, these models accurately represent the dynamic behavior of each structure and are therefore appropriate for use within the ensuing time-history analyses for stress-range cycle counting.

CHAPTER 5 – QUANTIFYING MODELING ERROR UNCERTAINTY

5.1 – Introduction

The reliability-based methodology for assessing risk of fatigue-induced fracture in sign support structures, as outlined in chapter one, is driven by the resulting magnitude and number of stress-ranges obtained from FE models of these types of structures subjected to time histories of various magnitudes of wind loading. It should be anticipated that the results obtained from these FE models will differ from the actual results one may obtain via direct measurement (*e.g.* from the FMS of chapter two). This can be accounted for in the reliability-based methodology by attaching a bias factor, *B*, to the simulated results obtained from the FE models. In other words, the bias factor accounts for any modeling error introduced in the procedure.

Given the variability associated with the primary loading sustained by these structures (*i.e.* natural wind), it was expected that the amount of modeling error would not be constant, but rather, vary depending on the magnitude of wind loading. This is why *B* was left as a random variable within the reliability-based methodology. There is a need to quantify the extent to which modeling error increases or decreases for each magnitude of wind loading considered in this study (*i.e.* 5, 10, 15, 20, 25, 30, 35, 40, 45 and 50 mph). This will be done by comparing expected stress-ranges from simulated results obtained by FE models to expected stress-ranges from measured results obtained by the FMS. As previously indicated, the magnitude of *B* will be dependent upon the level of wind demand being considered. To determine the magnitude of *B*, the following expression was used,

$$B_i = \frac{\left(S_{RE,s}\right)_i}{\left(S_{RE,m}\right)_i} \tag{5.1}$$

where: $\left(S_{RE,s}\right)_i$ is the expected stress-range from a one-hour long simulated stress history and $\left(S_{RE,m}\right)_i$ is the expected stress-range from a one-hour long measured stress history, all values correspond to a one-hour averaged wind speed of magnitude *i*. Computation of the expected stress-ranges provided in equation (5.1) were determined using the rainflow cycle counting technique. Discussion of this technique and the resulting values used in equation (5.1) will be provided in subsequent sections.

Chapter two discussed a field monitoring system which measured wind speed and corresponding direction over a period of six months. Unfortunately, six months of time was not long enough to obtain one-hour long records of wind speed corresponding to all ten mean magnitudes considered in this study. In fact, the maximum mean magnitude achieved using a one-hour averaging time was less than 20 mph. Therefore, *B* was quantified using as many comparable mean wind speed magnitudes measured by the FMS as possible. This resulted in three comparisons using equation (5.1) with *i* approximately equal to 5, 10 and 15 mph.

Since *B* was considered a lognormal random variable, a lognormal distribution quantifying the variation and uncertainty in the magnitude of *B* needed to be defined. Defining this distribution required the expected value (mean value), μ_B, and standard deviation of *B*, σ_B. Once these values were computed, the coefficient of variation of *B*, CV_B, could be determined using the following,

$$CV_B = \frac{\sigma_B}{\mu_B} \tag{5.2}$$

Computation of CV_B using equation (5.2) provided the last remaining piece of information required to carry out the fatigue reliability study presented earlier.

The objective of this chapter is to obtain the values of μ_B and CV_B. This will be done using the Milwaukee structure from the test-group of structures studied in chapter four. The discussion will begin with an explanation of how the measured signals obtained by the FMS were processed into a suitable form for direct comparison with results obtained by the low-fidelity FE model of the Milwaukee structure. Once the measured signals were processed, they served as targets for ensuing simulations of natural wind speed. Discussion regarding the procedure to obtain simulated wind at target magnitudes established by the measured signals will also be provided. This chapter will conclude with comparisons of expected stress-range magnitudes obtained by both measured and simulated results as well as the resulting values for μ_B and CV_B.

5.2 – Signal Processing for Measured Stress Histories

This section of the chapter discusses how FMS-measured signals for wind speed, wind direction and bending strain about horizontal and vertical axes were processed into a suitable form for moving forward with the comparisons using equation (5.1). Manipulation of the measured data was required in order to obtain stress histories that were in a similar form to simulated stress histories acquired from the low-fidelity FE models of chapter four (discussed in subsequent sections). The following 7-step procedure was implemented to obtain one-hour long measured stress-histories for the Milwaukee structure:

1) To begin the process, all bending strain measured by the FMS for the Milwaukee structure was converted to stress. This was done using Hooke's law of elasticity since the magnitude of stress for the Milwaukee structure, even at high levels of wind loading, were much lower than the elastic limit of the material. Therefore, using Hooke's law, the measured bending stress was determined as,

$$\sigma_m = E \cdot \varepsilon_m \tag{5.3}$$

where: E is Young's modulus with an assumed magnitude of 29,500 ksi for steel and ε_m is the bending strain measured by the FMS.

2) Time histories (one hour in length) of wind speed, wind direction and bending strain about both horizontal and vertical axes were processed for the Milwaukee structure. This was done to find one-hour blocks of bending strain corresponding to each of the one-hour averaged wind speeds considered in this study. Since the measured results were eventually going to be compared to simulated results obtained from wind pressure acting perpendicular to the mast-arm of the low-fidelity FE models, the measured data was restricted to only those records corresponding to one-hour averaged wind directions that were perpendicular as well.

3) Given the orientation of the mast-arm for the Milwaukee structure (axis parallel with 50 degrees from true north), all one-hour segments of data corresponding to an average direction equal to 140 degrees (back of sign) or 320 degrees (front of sign) were isolated for further synthesis. This meant that over each isolated, one-hour segment the wind speed was acting out of 140 or 320 degrees on average. The bending strain, however, was *always* measured at the same locations (top, bottom and both sides of the mast arm two inches from the weld-toe). Since the magnitude of bending stress provided by the FE models was determined using perpendicular wind, it was essential that the measured bending strain, converted to bending stress using equation (5.3) was also from perpendicular wind. This required some manipulation of the wind speed magnitudes found in the one-hour blocks of data.

4) Once isolated, the one-hour blocks of data were sorted on the basis of direction from lowest to highest. After sorting the data, the wind speed magnitudes for each entry were adjusted using the following scheme:

$$U_{adj} = U_m \cdot \cos\left(40^o + D_m\right) \qquad \text{for} \quad 0^o < D_m \le 50^o$$

$$U_{adj} = U_m \cdot \cos\left(140^o - D_m\right) \qquad \text{for} \quad 50^o < D_m \le 140^o$$

$$U_{adj} = U_m \cdot \cos\left(D_m - 140^o\right) \qquad \text{for} \quad 140^o < D_m \le 230^o$$

$$U_{adj} = U_m \cdot \cos\left(320^o - D_m\right) \qquad \text{for} \quad 230^o < D_m \le 320^o$$

$$U_{adj} = U_m \cdot \cos\left(D_m - 320^o\right) \qquad \text{for} \quad D_m > 320^o$$

where: U_m is the measured wind speed; D_m is the measured wind direction; and U_{adj} is the adjusted wind speed.

5) After adjusting all wind speeds, the data was placed into its original order. At this point, the one-hour blocks of data now contained averaged wind directions equal to 140 or 320 degrees, averaged wind speed magnitudes adjusted to account for any entries not acting perpendicular and stress records corresponding to measurements taken at two inches from the weld-toe.

6) Before selecting blocks of data to move forward with rainflow cycle counting, one last adjustment needed to be made. Chapter four indicated that stress concentration effects exist within approximately the first five inches of mast-arm, measured longitudinally from the weld-toe toward the free end. Since the strain gages mounted on the Milwaukee structure were placed at two inches from the weld-toe, the measured values needed to be adjusted. Figure 5.1 provides the magnitude of *SCF* along the length of the mast-arm obtained from the high-fidelity FE model of the Milwaukee structure generated in chapter four. This figure indicates that the magnitude of stress two inches from the weld-toe is

actually slightly less than nominal and any values measured at this location need to be increased accordingly. Therefore, all measured values of bending stress were increased by a factor of (1/0.646) or 1.55.

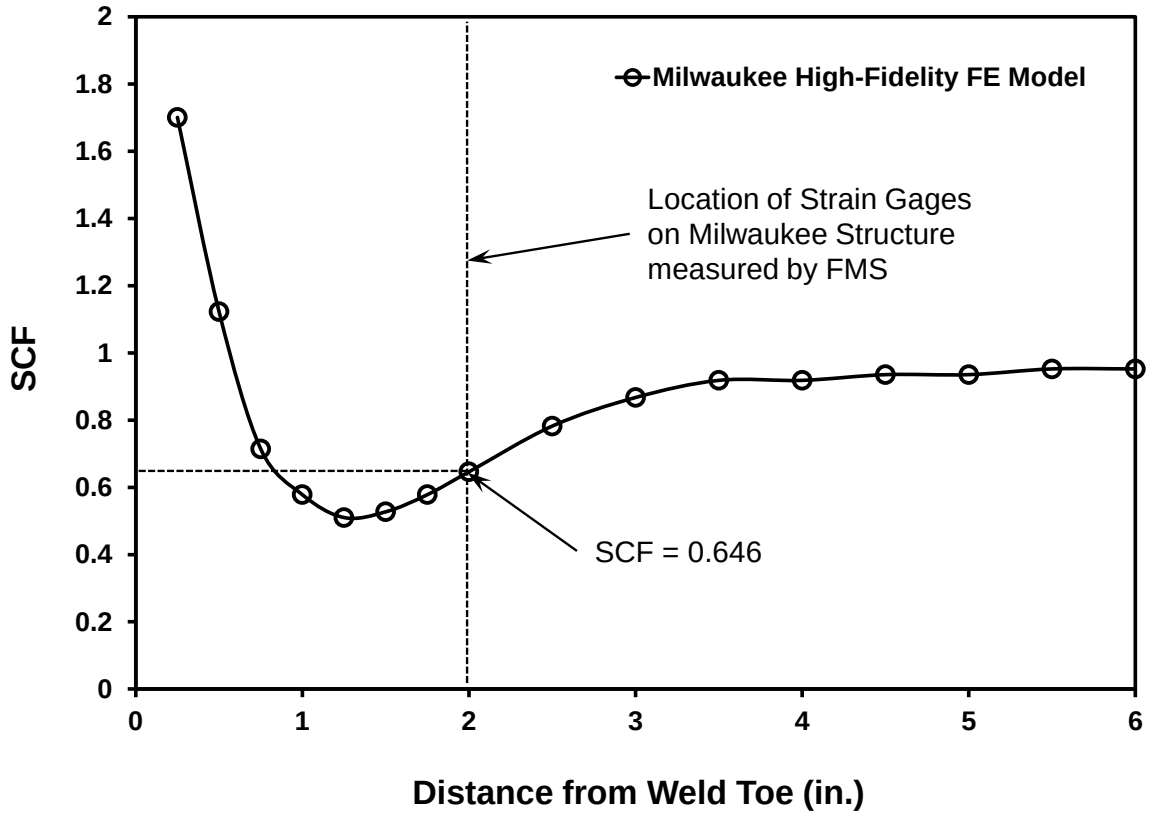

Figure 5.1. *SCF* at top fiber of mast-arm (note: the distance is measured from the weld-toe toward the free end of the mast-arm).

7) At this point in the procedure, all manipulation of measured data was complete and all that was left to do was to select records representative of one-hour averaged wind speeds for 5, 10, 15, 20, 25, 30, 35, 40, 45 and 50 mph. There were many records which met the criteria listed in steps 1 through 6 for one-hour averaged wind speeds equal to 5, 10 and 15 mph; however, there were no such records above the 15 mph mean magnitude. This was anticipated for two reasons: (1) the results of chapter two provided very low combined probabilities of one-hour averaged wind speeds greater than 15 mph; and (2)

the FMS was only operational for six months. It would likely take much longer than six months to achieve a one-hour averaged wind speed larger than 15 mph which also acted from the specified direction of 140 or 320 degrees.

Performing steps 1 through 7 resulted in the selection of three one-hour blocks of measured data. The first, second and third blocks of data corresponded to one-hour averaged wind speeds and directions equal to 5.23 mph and 140 degrees, 10.18 mph and 320 degrees, and 15.97 mph and 140 degrees, respectively. Figure 5.2 provides the time histories for each block of measured data with their corresponding averaged or adjusted data superimposed.

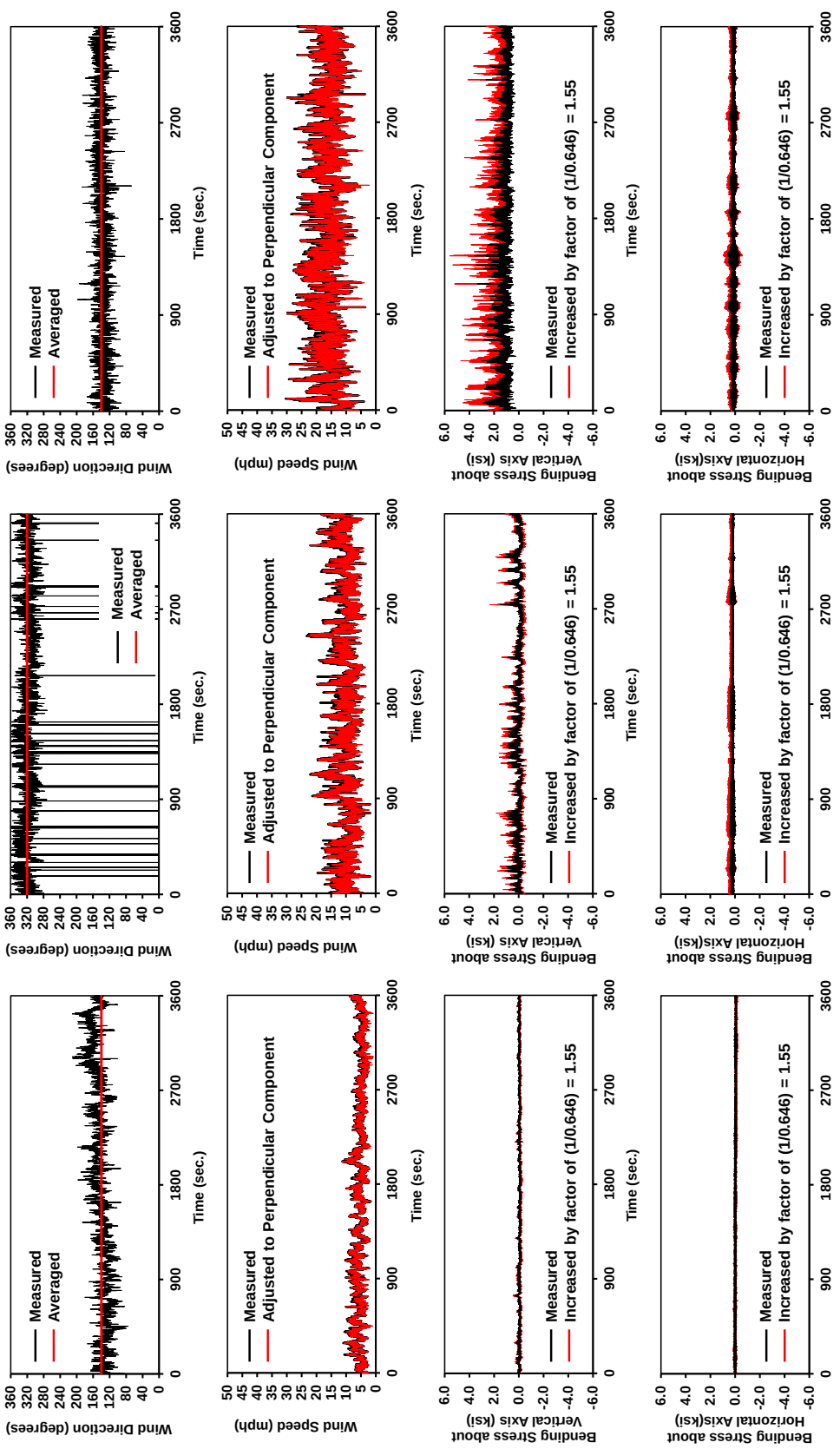

Figure 5.2. One-hour blocks of data from FMS corresponding to (a) 5.22 mph and 140 degrees; (b) 10.18 mph and 320 degrees; and (c) 15.97 mph and 140 degrees.

5.3 – Transient Analyses for Simulated Stress Histories

A number of general modeling considerations need to be addressed before the low-fidelity FE model of the Milwaukee structure could be used to carry out the transient analyses needed for the ensuing reliability study. These considerations include the following: (1) level of damping used in low-fidelity FE model, both inherent structural and aerodynamic, (2) length of time history, and (3) type of results monitored and location where they will be extracted.

5.3.1 – Damping

Ginal (2003) provides a detailed derivation of an expression which estimates the total damping present within sign support structures. The expression contains two components: (1) one which represents inherent structural damping provided by the structure and (2) one which represents aerodynamic damping due to the supported signs moving through the air. The resulting expression for total damping is stated as,

$$c_{tot} = c_s + \rho \cdot C_d \cdot A \cdot U = c_s + c_a \tag{5.4}$$

where: c_s is the inherent structural damping; c_a is the aerodynamic damping; ρ is the density of air; C_d is the drag coefficient; A is the bluff area of the mast-arm and supported signs; and U is the mean wind speed being considered.

Oftentimes, it is convenient to express damping as a percentage of the critical damping ratio. The total damping provided by equation (5.4) may be expressed as a percentage of the critical damping ratio using the following expression (Ginal 2003),

$$\zeta_{tot} = \zeta_s + \zeta_a \tag{5.5}$$

with the following defined as,

$$\zeta_s = \frac{c_s}{c_{cr}} \tag{5.6}$$

$$\zeta_a = \frac{c_a}{c_{cr}} \tag{5.7}$$

$$c_{cr} = 2\sqrt{m \cdot k} \tag{5.8}$$

where: m and k are the effective mass and stiffness of the dynamic structural system, respectively. The present study uses the entire mass of the mast-arm ($m = 1.31e^{-3}\,\frac{kip \cdot s^2}{in}$) to calculate the critical damping ratio. The stiffness was determined by applying a downward force of magnitude 0.10 kip at the tip of the cantilevered mast-arm within the low-fidelity FE model and monitoring the deflection. The resulting stiffness was determined as $k = 0.037\,\frac{kip}{in}$. Therefore, the remaining information required to define the total damping (as a percentage of critical) include the magnitudes of ζ_s and ζ_a. The following sections will discuss each component individually, beginning with inherent structural damping and ending with aerodynamic damping.

For a given structure, inherent structural damping (ζ_s) does not depend on loading – it depends on the natural frequency and vibrational mode shape of the structure. Because a multiple degree of freedom (MDOF) structure consists of multiple natural frequencies and vibrational mode shapes, several magnitudes of inherent structural damping exist. Rather than specifying a different value of ζ_s for each mode of vibration, it is more convenient to set a target damping ratio to be used through all modes of vibration. Experimental tests aimed at exciting various vibrational modes may be performed to estimate the magnitude of inherent structural damping present within a system. The present study did not perform experimental testing on the

Milwaukee structure, but instead relied on experimental results from previous studies conducted on similarly configured sign support structures (Creamer et al. 1979; Edwards and Bingham 1984; Gilani et al. 1997; Johns and Dexter 1998; Kaczinski et al. 1998; South 1994). Table 5.1 provides a summary of these previous efforts.

Table 5.1. Summary of damping ratios for cantilevered sign and signal support structures from past research efforts (Ginal 2003).

Research Effort	Structure Description	Sign Type	Damping Ratio (% of Critical)
Creamer *et al* (1979)	Four chord cantilevered pipe truss supported by monotube upright	Type I	0.40 - 1.11
Edwards and Bingham (1984)	Two- and four-chord cantilevered pipe struss supported by monotube upright	Type I	0.58 - 1.85
South (1994)	Tapered cantilevered monotube mast-arm and upright traffic signal support	NA	0.60
Gilani *et al* (1997)	Monotube cantilevered mast-arm and vertical support	VMS	0.50 - 0.70
Johns and Dexter (1998)	Two-chord cantilevered pipe truss supported by monotube upright	VMS	0.25 - 0.57
Kaczinski *et al* (1998)	Cantilevered sign and signal support structures of varying configurations	Type I	0.12 - 0.62

It should be noted that the experimentally obtained damping ratios provided in Table 5.1 are the results from two modes of vibration. These two modes of vibration conveniently correspond to the first two vibrational shapes of the test-group structures discussed in chapter four: (1) horizontal “twist” mode and (2) vertical “hatchet” mode. Furthermore, the experimentally determined damping ratios include both inherent structural damping and aerodynamic damping. Nonetheless, a target level for the inherent structural damping ratio was set at 0.60 % of critical. This was determined by computing the average of the results obtained by Gilani et al. (1997) and South (1994) as these studies used structures very comparable to the Milwaukee structure (*i.e.* cantilevered mast-arm structures).

The second component contributing to total damping present within equation (5.4) was defined as aerodynamic damping. The magnitude of the aerodynamic damping ratio depends upon the magnitude of the mean wind speed being considered, the total area subject to wind loading, the drag coefficient of the areas considered and the density of air. With the exception of mean wind speed, each of these variables will be held constant through the ensuing simulations. Given the formulation within equation (5.4), it should be expected that as the mean wind speed increases for each simulation, so will the magnitude of aerodynamic damping ratio. Table 5.2 provides the aerodynamic damping ratio (as a percentage of critical) for each of the various mean wind speed magnitudes considered in the present study.

Table 5.2. Summary of aerodynamic damping ratios for various levels of mean wind speed magnitude (note: this table also includes the values for the three wind speed magnitudes used in the comparisons for *B*).

C_d		1.19	
A [in^2]		10154	
ρ [kip-s^2/in^4]		1.15E-10	
m [kip-s^2/in]		1.31E-03	
k [kip/in]		0.037	
Wind Speed [mph]	**Wind Speed [in/sec]**	**Aerodynamic Damping, c_a**	**Aerodymanic Damping Ratio, ζ_a**
5.00	88.00	0.00146	0.00876
5.23	92.01	0.00153	0.00916
10.00	176.00	0.00293	0.01753
10.18	179.08	0.00298	0.01783
15.00	264.00	0.00439	0.02629
15.97	281.15	0.00468	0.02800
20.00	352.00	0.00585	0.03506
25.00	440.00	0.00732	0.04382
30.00	528.00	0.00878	0.05258
35.00	616.00	0.01024	0.06135
40.00	704.00	0.01171	0.07011
45.00	792.00	0.01317	0.07887
50.00	880.00	0.01463	0.08764

When performing transient analyses within ANSYS, users may account for damping using a classical (Rayleigh) formulation. To do this, a damping matrix must first be formulated (Ginal 2003),

$$[C] = \alpha \cdot [M] + \beta \cdot [K] \tag{5.9}$$

where: $[M]$ is the system's mass matrix; $[K]$ is the system's stiffness matrix; α is the mass matrix multiplier; and β is the stiffness matrix multiplier. Defining the damping matrix in this way permits uncoupling of the equations of motion (Tedesco et al. 1999).

The matrix multipliers from equation (5.9) are determined by specifying damping ratios ζ_i and ζ_j from the *i*th and *j*th vibrational modes using the following (Chopra 2001),

$$\frac{1}{2} \cdot \begin{bmatrix} 1/\omega_i & \omega_i \\ 1/\omega_j & \omega_j \end{bmatrix} \cdot \begin{Bmatrix} \alpha \\ \beta \end{Bmatrix} = \begin{Bmatrix} \zeta_i \\ \zeta_j \end{Bmatrix} \tag{5.10}$$

If both vibrational modes are assumed to have the same target damping ratio, then the equations above may be recast into the following set of equations (Chopra 2001),

$$\alpha = \zeta \cdot \frac{2 \cdot \omega_i \cdot \omega_j}{\omega_i + \omega_j} \tag{5.11}$$

$$\beta = \zeta \cdot \frac{2}{\omega_i + \omega_j} \tag{5.12}$$

Because the target damping ratio was partly based upon experimental results obtained from tests conducted on the first two modes of vibration, the *i*th and *j*th frequencies were defined as the first and second natural frequencies for the Milwaukee structure

($\omega_1 = 10.1$ rad / sec and $\omega_2 = 11.0$ rad / sec). The target damping ratio and resulting mass and stiffness matrix multipliers to be used for all ensuing simulations are provided in Table 5.3. The results provided in Table 5.3 indicate that aerodynamic damping significantly increases the amount of total damping present within the dynamic system. These results are consistent with previous studies (Ginal 2003).

Table 5.3. Summary of target damping ratios and matrix multipliers (α and β) for various levels of mean wind speed magnitude (note: this table also includes the values for the three wind speed magnitudes used in the comparisons for *B*).

mode i frequency (1):		***ω_i (rad/sec)***	***10.1***
mode j frequency (2):		***ω_j (rad/sec)***	***11.0***
Mean Wind Speed (mph)	**Target Damping Ratio, ζ**	**Mass Matrix Multiplier, α**	**Stiffness Matrix Multiplier, β**
5.00	0.01476	0.15549	0.00140
5.23	0.01516	0.15970	0.00144
10.00	0.02353	0.24779	0.00223
10.18	0.02383	0.25102	0.00226
15.00	0.03229	0.34009	0.00306
15.97	0.03400	0.35808	0.00322
20.00	0.04106	0.43239	0.00389
25.00	0.04982	0.52469	0.00472
30.00	0.05858	0.61699	0.00555
35.00	0.06735	0.70929	0.00638
40.00	0.07611	0.80159	0.00721
45.00	0.08487	0.89389	0.00804
50.00	0.09364	0.98619	0.00887

5.3.2 – Analytical Modeling of Natural Wind

One of the main goals of this dissertation was to develop a completely simulated modeling procedure for estimating accumulated fatigue damage within sign support structures caused by natural wind. Chapter four provided FE models suitable for performing transient analyses; however, to perform these transient analyses, the primary loading sustained by these structures must be defined. To this end, wind speed time histories needed to be simulated at various levels of mean magnitude. The following sections provide discussion regarding the systematic development of the wind speed simulations used in the ensuing reliability study.

Natural wind speed can be broken down into two components and represented mathematically as (Buchholdt 1997),

$$U(Z,t) = U(Z) + u(Z,t) \tag{5.13}$$

where: $U(Z)$ is defined as the mean wind speed component dependent upon elevation, Z; and $u(Z,t)$ is defined as a fluctuating component that represents wind speed turbulence which is dependent upon both elevation, Z, and time, t.

Mean wind speed can be determined at any elevation above the ground surface using the Power Law. The Power Law is represented mathematically by the following expression (Simiu and Scanlon 1996),

$$U_Z = U_1\left(\frac{Z}{Z_1}\right)^{\alpha} \tag{5.14}$$

where: U_1 is a known wind speed at reference elevation Z_1; and the magnitude of α varies based on the surrounding terrain but is typically defined as 1/7 or 0.143.

If both components are determined at the same elevation, then equation (5.13) can be restated as,

$$U(t) = U + u(t) \tag{5.15}$$

Figure 5.3 provides a typical wind speed record which illustrates the two components of equation (5.15).

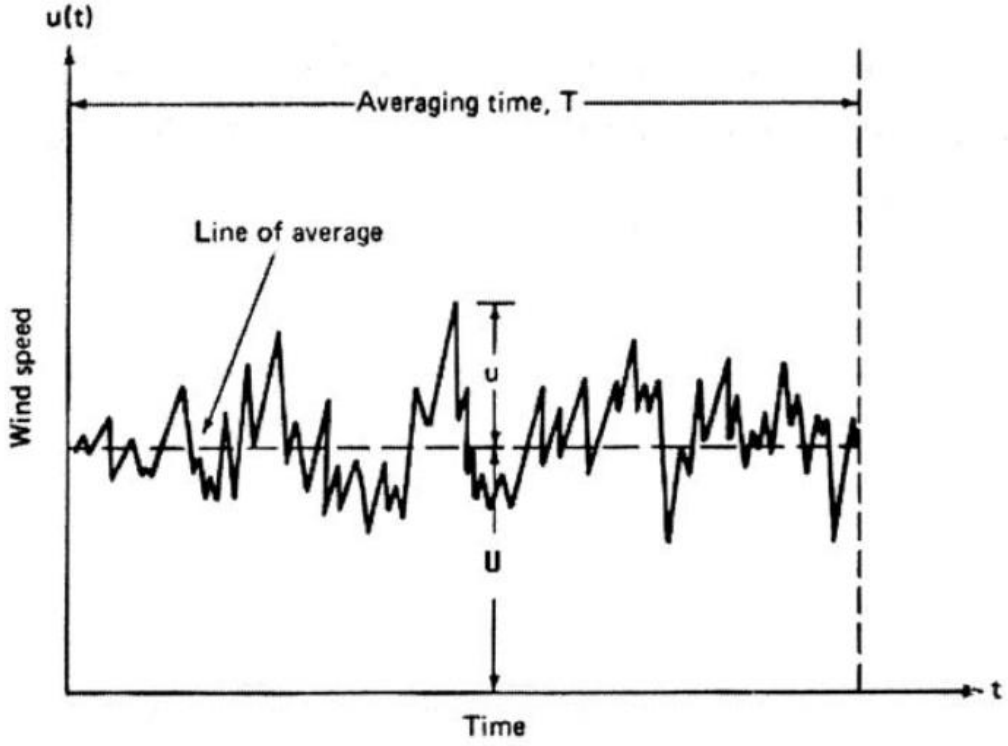

Figure 5.3. Wind speed vs. time (Liu 1991).

Several techniques exist for simulating the fluctuating component of natural wind speed. These techniques rely on target spectra which quantify the turbulent content of natural wind in the frequency domain. If the turbulent content of natural wind at various levels of mean magnitude can be modeled, simulated time histories for the turbulent component of a given mean wind speed

magnitude can be determined using (Iannuzzi and Spinelli 1987; Levy 1996; Shinozuka and Jan 1972),

$$u(t)=\sum_{k=1}^{N}\left[2\cdot S(f_k)\cdot\Delta f\right]^{1/2}\cos(2\cdot\pi\cdot f_k\cdot t+\varphi_k) \tag{5.16}$$

where: N is the number of frequencies considered in the simulation; Δf is the assumed frequency increment; t is the time value in the simulation; φ_k is a randomly generated phase angle distributed uniformly between 0 and 2π; and $S(f_k)$ is the value of the target spectrum used to define the turbulent component of wind speed at a specifically determined frequency, $f_k=k\cdot\Delta f$.

This procedure requires power spectral density (PSD) function models of the turbulent content of natural wind speed. Previous studies have recommended the use of the Kaimal model as the target spectrum for simulating natural wind speed (Ginal 2003). The model is given by (Kaimal 1972),

$$S(f)=\frac{200\cdot U_*^2\cdot Z}{U_Z\left(1+\frac{50\cdot f\cdot Z}{U_Z}\right)^{5/3}} \tag{5.17}$$

where: U_* is the friction (or shear) velocity of the wind; Z is the elevation above the ground surface; U_Z is the mean wind speed at elevation Z; and f is the frequency in Hz. The friction velocity is defined as,

$$U_*=\sqrt{\frac{\sigma_u^2}{6}} \tag{5.18}$$

with σ_u^2 termed as the variance of the turbulent wind component and defined by the following expression,

$$\sigma_u^2 = 6 \cdot K \cdot U_1^2 \tag{5.19}$$

where K is the surface drag coefficient.

The Kaimal model was selected for the following reasons:

1. The model allows structure-height to be accounted for through the use of the Power Law. This is important because wind speed magnitude (and therefore corresponding turbulence) varies with height. Because sign support structures are not uniformly designed, their elevations can vary from one to the next. To provide site-specific wind speed histories, this elevation should be accounted for in the simulation procedure.

2. Previous work has shown that the model accurately predicts the turbulent component of wind at higher frequencies which is typical of the response for most engineered structures (Beaupuits et al. 2004; Ginal 2003; Simiu and Scanlon 1996).

A MATLAB m-file was created to simulate natural wind speed using equation (5.16) with the target spectrum defined as the Kaimal model of equation (5.17). The m-file (*WindHistory.m)* is based upon scripts that have been previously developed (Ginal 2003; Levy 1996) and can be found in Appendix H. A brief explanation regarding the parameters necessary for carrying out the wind speed simulations is provided in the following discussion.

To ensure *WindHistory.m* was performing as expected, simulated time histories of wind speed at all ten mean magnitudes considered in this study were plotted (Figure 5.4) to make a graphical comparison between them. To minimize congestion within the figure, plotting was

limited to the first 120 seconds (two minutes) of the one-hour long simulation. Looking at Figure 5.4, it is clear that the turbulent component of wind speed increases as the magnitude of mean wind speed increases.

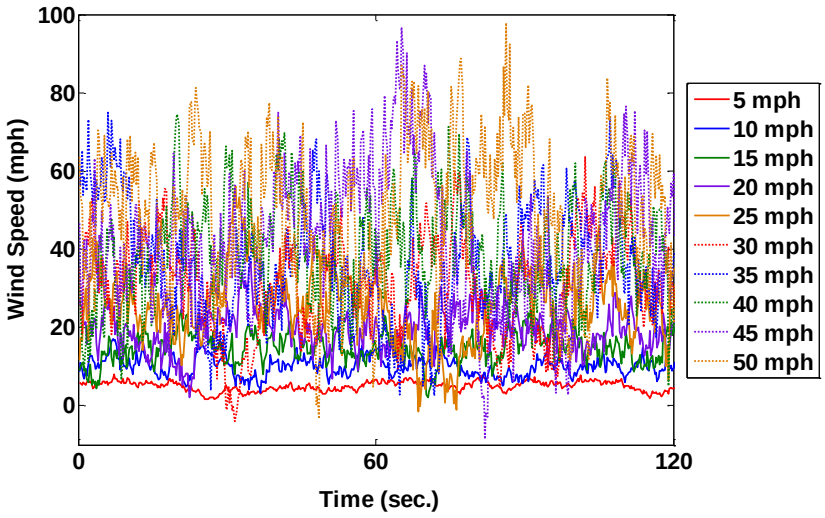

Figure 5.4. Two-minute windows of simulated records for various one-hour averaged wind speed magnitudes.

Additional checks were made on the resulting wind speed simulations. First, the PSD was calculated for each simulation and plotted against the corresponding Kaimal target spectrum. Figure 5.5 provides the PSD for all ten simulations. The results provided illustrate that the simulations are indeed capturing the turbulent content for each of the various mean wind speed magnitudes considered and are closely following the Kaimal model. Second, the turbulent component of the simulated wind was specified to vary about the mean in the form of a Gaussian distribution. Since the variance of the turbulent wind component is a function of mean wind velocity (*e.g.* as mean wind velocity increases, variance increases), it was expected that distributions of the turbulent component of wind speed should consistently widen (*i.e.* variance should increase) as the mean magnitude increases. Figure 5.6 illustrates frequency count histograms of the turbulent wind speed magnitude with corresponding normal distribution curves fit and overlaid validating these expectations.

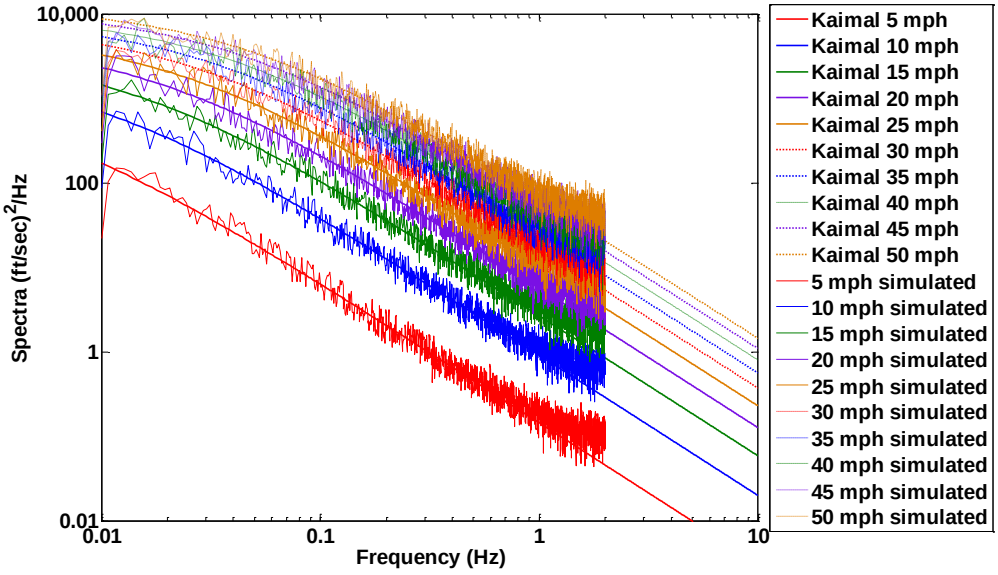

Figure 5.5. Comparison of target Kaimal spectra and spectra obtained using simulated wind histories.

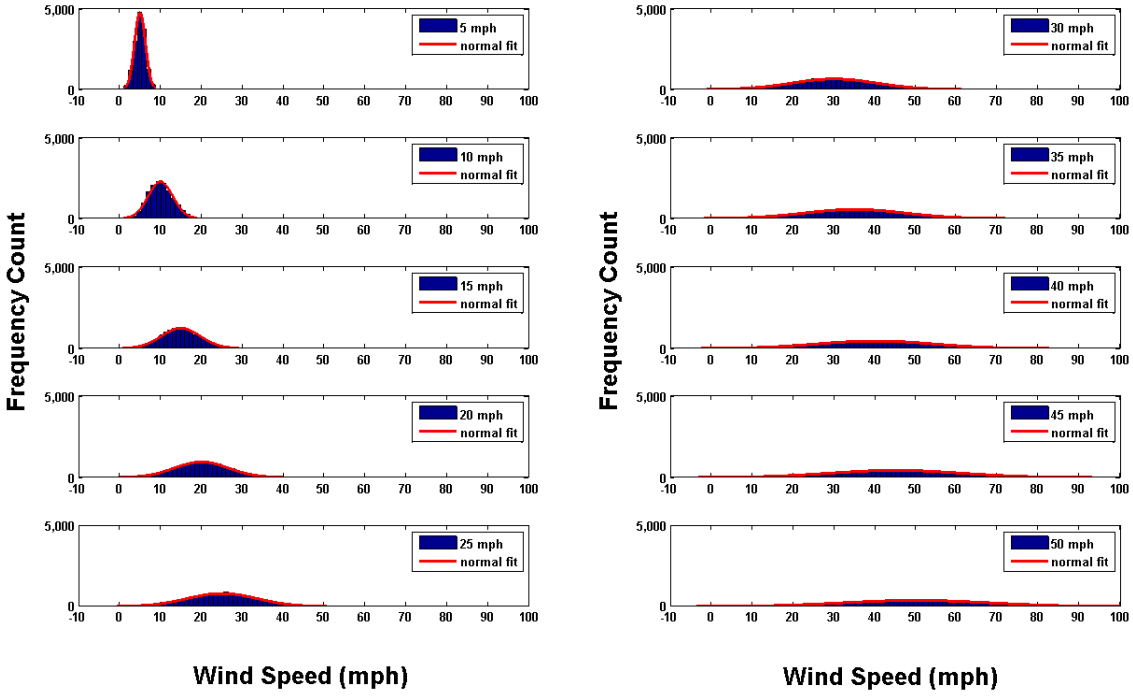

Figure 5.6. Comparison of turbulent wind speed histograms for various magnitudes of one-hour averaged wind speeds (note: each histogram contains a "best-fit" normal distribution).

A final study looked at a comparison between simulated wind speed histories and measured wind speed histories. Figure 5.7 provides graphical comparisons between the simulated and measured results for the wind speed time-histories, their PSD's and their turbulent frequency count histograms (with normal distribution fits for each). As indicated earlier, these comparisons were limited to three mean wind speed magnitudes (5.23, 10.18 and 15.97 mph) because of low probability of occurrence of higher mean wind speeds and limited sampling time for wind speed data collection. It is clear that the simulation procedure implemented is providing very comparable results to site-specific measured wind speed. Therefore, it will be assumed that the simulation procedure is adequately and appropriately mimicking natural wind and is suitable for the ensuing reliability study.

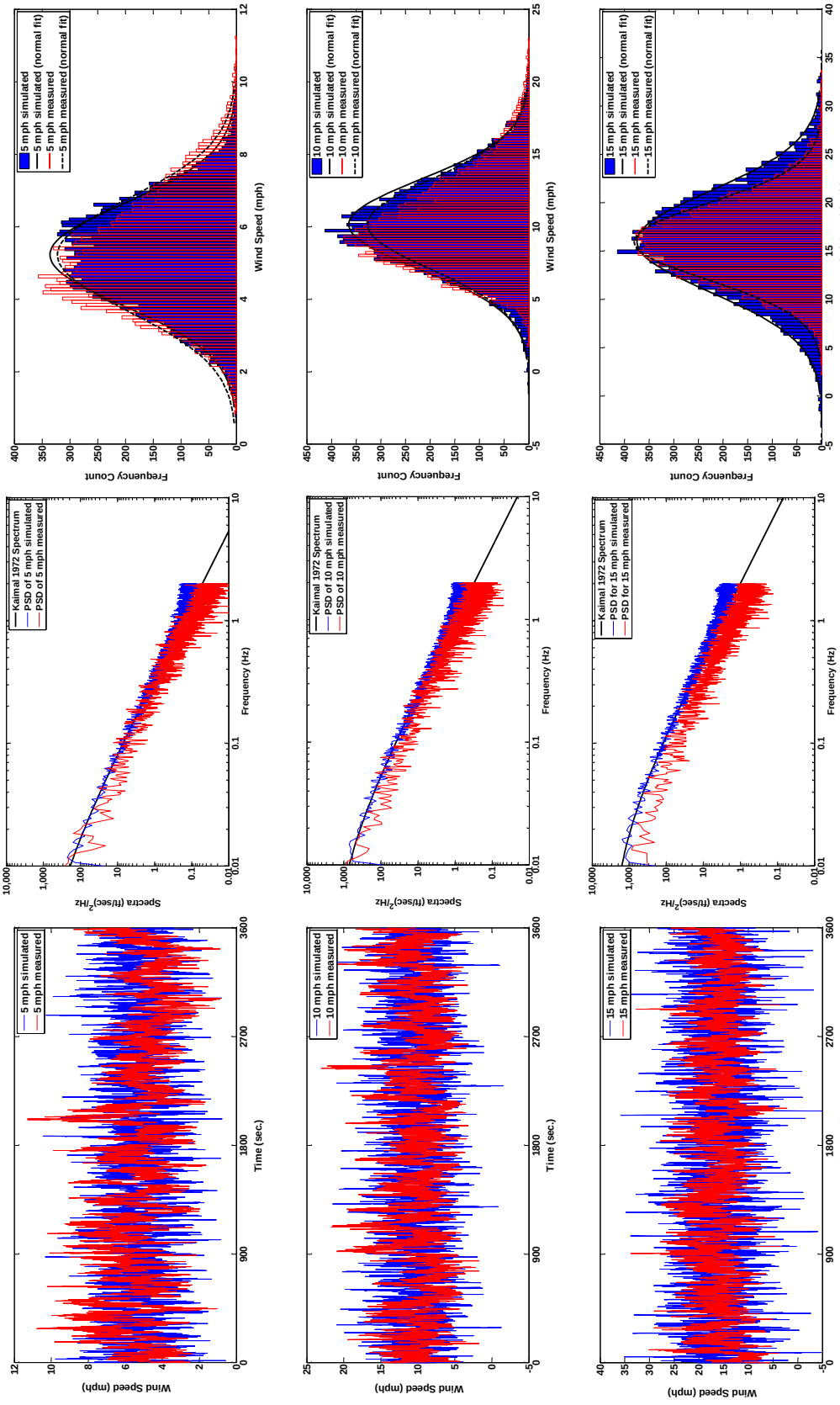

Figure 5.7. Comparison of wind speed histories, power spectral densities and frequency histograms for measured and simulated data.

5.3.3 – Time History Simulation Procedure

This section of the chapter will discuss the procedure used to generate the simulated stress histories. The time history simulation procedure consists of converting the wind speed histories previously developed into wind pressure histories. The wind pressure was computed in a similar way as was done for the static analyses performed in chapter four. For convenience, the AASHTO (2009) expression for converting wind speed to wind pressure provided in chapter four is restated as follows,

$$P = \frac{1}{2} \cdot \rho \cdot C_d \cdot U^2 \tag{5.20}$$

where: ρ is the density of air $\left(1.146e-10\ \ kip \cdot \mathrm{s}^2 / in^4\right)$; C_d is the drag coefficient ($C_d = 1.19$ at sign locations and $C_d = 1.10$ at all non-sign locations along the mast-arm); and U is the magnitude of wind speed (including both mean and turbulent wind speed).

In order to enter the time history simulations for the present study, equation (5.20) must be able to account for all wind speed magnitudes at all times throughout the simulation. Therefore, equation (5.20) was recast into the following form to account for time,

$$P(t) = \frac{1}{2} \cdot \rho \cdot C_d \cdot U^2(t) \tag{5.21}$$

All wind speed simulations were converted to wind pressure using equation (5.21). The remaining discussion will be focused on how the simulations were carried out and how the results were processed for comparison against the measured signals synthesized earlier.

The simulation procedure used in the present study is based upon methods conducted previously (Foley et al. 2004; Ginal 2003). The time history simulations are performed in ANSYS. Given the repetitive nature of the problem, the simulations were conducted using scripts

written in the ANSYS Parametric Design Language (APDL). The scripts used in the present study are modified from versions used previously (Ginal 2003). *MKE_Input_File.txt* is the APDL script used to carry out the time history simulations of the present study. A copy of this script is found in Appendix I for reference throughout the following discussion.

The first step in the time history simulation procedure was to compute the wind pressure histories. This required special attention since the Milwaukee structure contained a tapered mast-arm. Chapter four provided discussion with regard to the discretization of the mast-arm into nine segments for wind load application. Two of these nine segments contained 4.5 ft x 6 ft highway signs while the remaining seven segments represented sign-free mast-arm locations. Because each segment produced a different bluff area subject to wind loading as well as a potentially different drag coefficient depending on the presence of a sign, the magnitude of wind pressure (applied as a line loading in kip/in.) needed to be computed specifically for each segment and for each time increment in the one-hour simulation. An example of the wind pressure histories is provided for the 5.23 mph simulation in Appendix J for reference. It is clear from this table that there is a significant increase in magnitude of wind pressure line loading at the locations where signs exist along the length of the mast-arm. This procedure was conducted for each of the mean wind speed magnitudes. The results for all wind pressure simulations were placed into text files labeled appropriately for later access by *MKE_Input_File.txt*.

Each time history simulation included 3,690 load steps, each composed of four sub-steps. Each load step corresponded to one second of time; thus, if each load step contained four sub-steps, the results would be obtained at 4 Hz resolution. Recall that this is the same resolution at which measured data was acquired. The reason each simulation lasted 3,690 seconds (90 seconds in excess of 1 hour) was to allow any vertical oscillations due to the application of gravity to dampen out in the 90 seconds of the simulation. Therefore, the first wind pressure value (t = 0.00

sec.) in Table 5.4 actually corresponded to t = 90.00 sec in the simulation (*i.e.* the time corresponding to sufficiently decayed vertical oscillations).

The results from each time history simulation were obtained in the form of bending moments about the horizontal and vertical axes of the mast-arm from the cross-section corresponding to ten inches from the weld-toe. Equation (4.5) from chapter four provided the ability to compute longitudinal bending stress at any circumferential point around the perimeter of the mast-arm tube. For convenience, equation (4.5) was recast into the following form to compute the resulting stress histories from each simulation,

$$\sigma_z(t) = \frac{M_G(t) \cdot r \cdot \cos(\varphi)}{I_{10}} + \frac{M_W(t) \cdot r \cdot \sin(\varphi)}{I_{10}} \tag{5.22}$$

where: $\varphi = \theta - \pi$; $M_G(t)$ is the internal moment at time t caused by gravity; $M_W(t)$ is the internal moment at time t caused by wind; $r \cdot \cos(\varphi)$ is the distance from the neutral axis of bending to the point of computed stress caused by $M_G(t)$; $r \cdot \sin(\varphi)$ is the distance from the neutral axis of bending to the point of computed stress caused by $M_W(t)$; r is the outside radius of the mast-arm tube; θ ranges from 0 to 2π measured counterclockwise from the six o'clock position of the mast-arm tube; and I_{10} is the moment of inertia (all values taken at the cross-section ten inches from the weld-toe).

This procedure was conducted for wind pressure simulations corresponding to all ten mean wind speeds considered in the present study as well as the three mean wind speeds used for quantifying *B*. The remaining discussion will be limited to the results obtained from the three mean wind speeds used to quantify *B*. Chapter six will provide the rest of the simulated stress histories as well as discussion regarding their use within the reliability-based methodology discussed earlier.

5.4 – Comparative Study between Simulated and Measured Stress Histories

There are now one-hour long records of both measured and simulated stress histories which corresponded to wind acting perpendicular to the sign face at magnitudes equal to 5.23 mph, 10.18 mph and 15.97 mph. Before jumping into the computation of expected stress-ranges, a graphical comparison was conducted on one-minute long segments of each time history to verify the general response between measured and simulated results were similar. Figures 5.8 through 5.10 provide time histories of wind speed (load) and bending stress (response) for each of the three mean wind speed magnitudes considered in the quantification of *B*. The results from these figures indicate that when wind speed magnitude increases, resulting stress-ranges should also increase. When comparing the measured histories to simulated histories, they look to be achieving similar levels of stress-range magnitude indicating that they are appropriate for quantifying *B*.

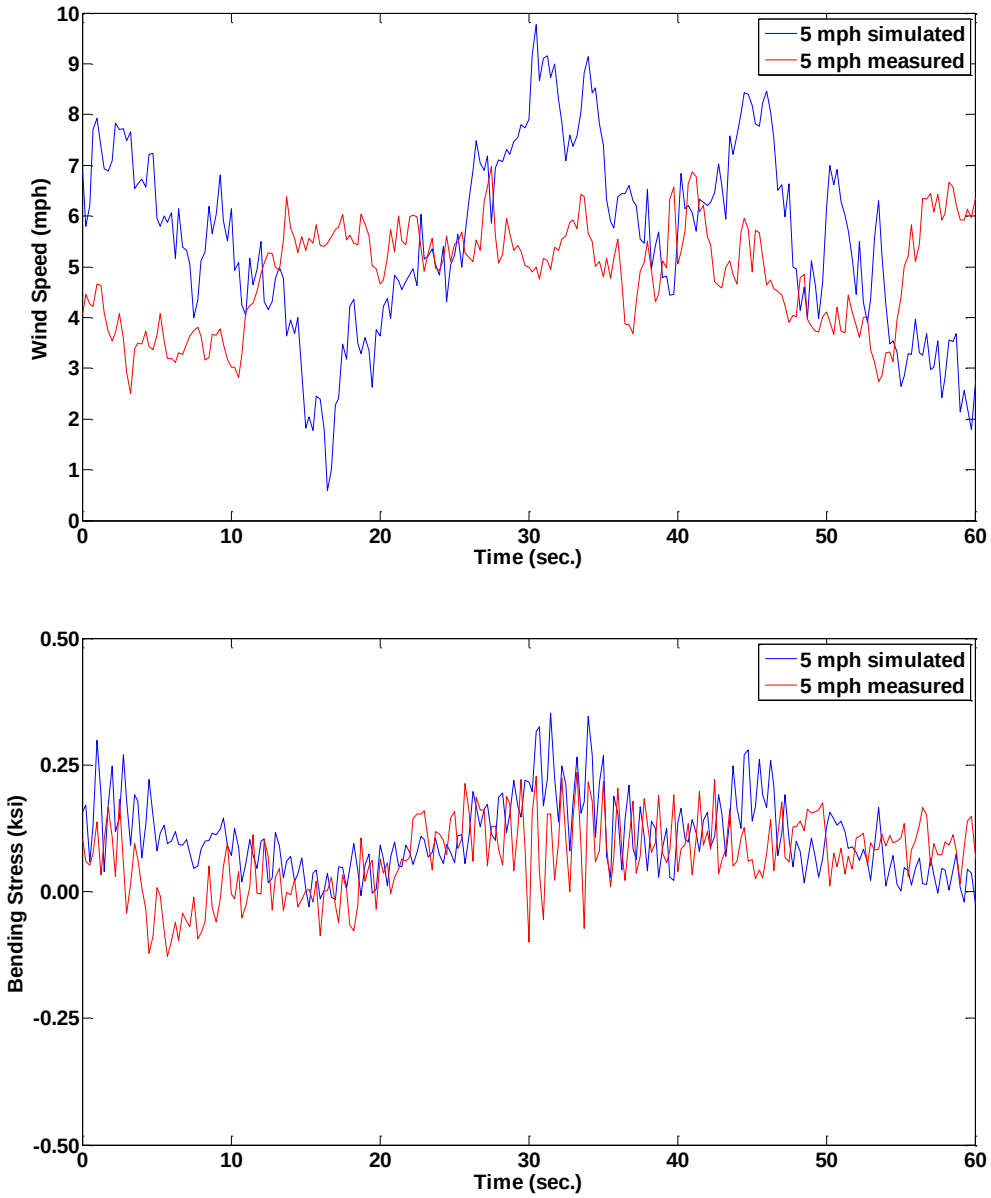

Figure 5.8. Comparison between measured and simulated load and response data for 5 mph one-hour averaged wind speed.

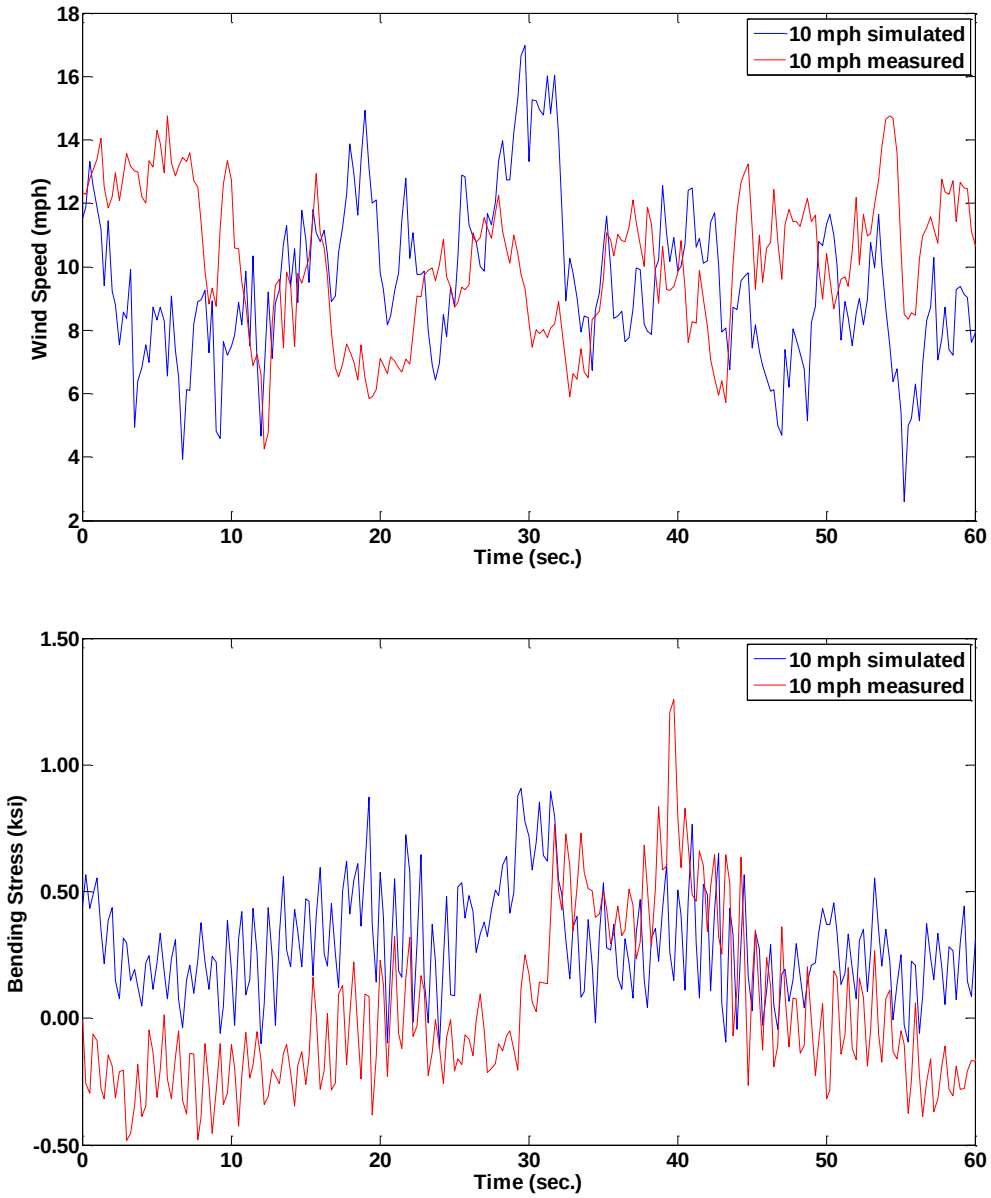

Figure 5.9. Comparison between measured and simulated load and response data for 10 mph one-hour averaged wind speed.

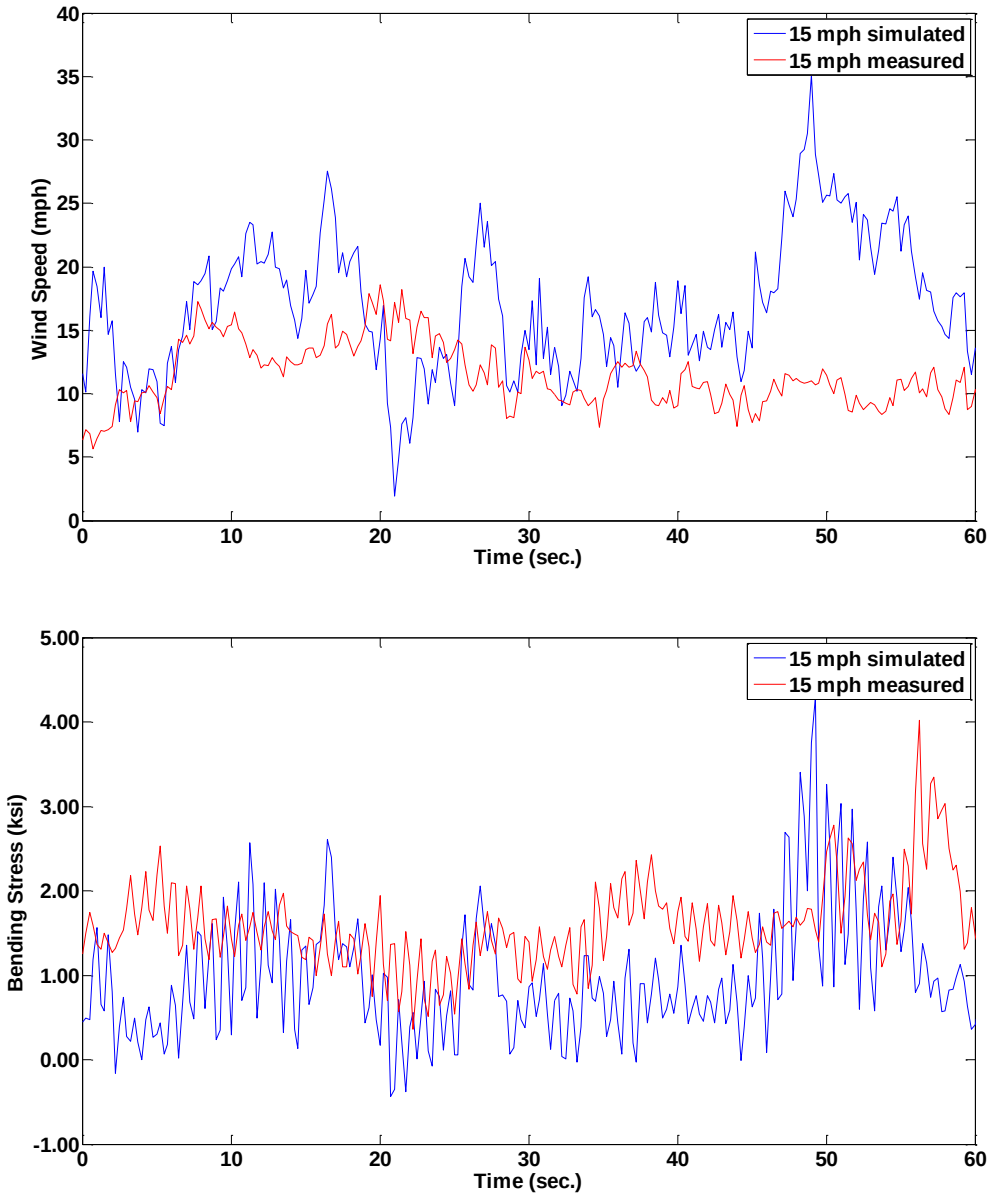

Figure 5.10. Comparison between measured and simulated load and response data for 15 mph one-hour averaged wind speed.

5.4.1 – Rainflow Cycle Counting

In order to obtain the expected stress-ranges used in equation (5.1), the rainflow cycle-counting technique was employed on both the simulated and measured stress histories. The rainflow cycle-counting technique is a method used to count closed hysteresis loops in the stress-strain response

of a material subjected to cyclic loading (Matsuishi and Endo 1968). This technique is very useful because it allows a very complex, variable amplitude stress history to be simplified into a series of constant amplitude stress-ranges. One drawback of this technique is that it requires knowledge of the entire stress history before any stress-ranges may be counted. When considering long stress histories, this becomes very tedious and time intensive. Fortunately, however, MATLAB scripts have been written to automate this procedure (Nieslony 2010). These scripts may be downloaded for free from the MATLAB central file exchange at: http://www.mathworks.com/matlabcentral/fileexchange/3026-rainflow-counting-algorithm.

To ensure the downloaded scripts were performing as expected, they were tested on a short, simple, variable amplitude stress history. To begin this procedure, consider the variable amplitude stress history provided in Figure 5.11. The relative peaks indicating the beginning and ending of cycles or half-cycles are labeled. Figure 5.12 illustrates the procedure used by the rainflow cycle-counting script to determine the number and magnitude of stress-ranges. Table 5.4 provides the stress history in numerical form and Table 5.5 provides the results obtained by the MATLAB scripts.

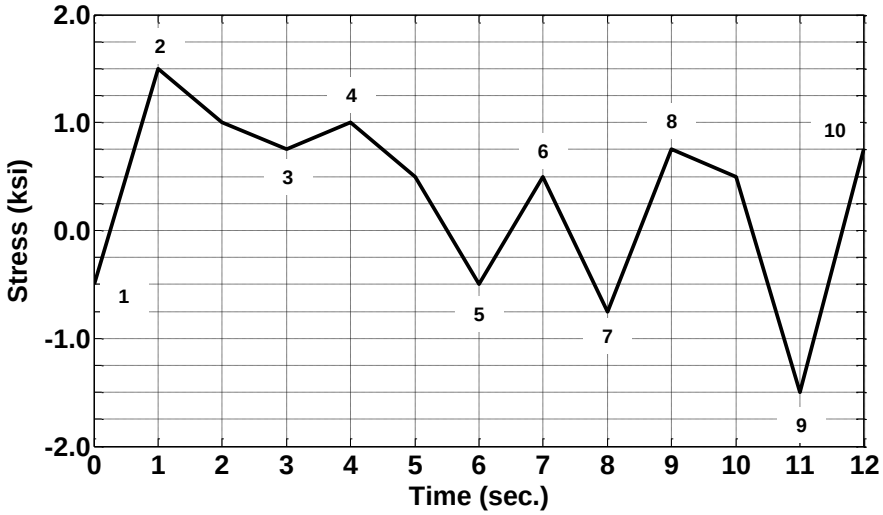

Figure 5.11. Variable amplitude stress history used to validate proper functionality of rainflow cycle-counting scripts (note: relative peaks are numbered 1 through 10).

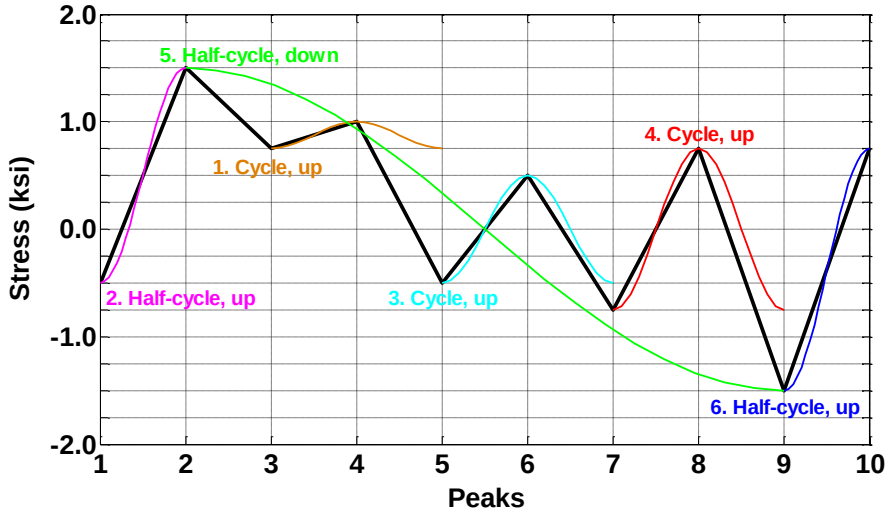

Figure 5.12. Variable amplitude stress history of Figure 5.11 re-plotted in terms of the peaks counted by the rainflow cycle counting script.

Table 5.4. Numerical data for rainflow cycle counting example.

Time (sec.)	Stress (ksi)	Peak No.
0	-0.50	1
1	1.50	2
2	1.00	-
3	0.75	3
4	1.00	4
5	0.50	-
6	-0.50	5
7	0.50	6
8	-0.75	7
9	0.75	8
10	0.50	-
11	-1.50	9
12	0.75	10

Table 5.5. Rainflow cycle counting results from example stress history.

Stress-Range ID No.	1	2	3	4	5	6
Number of Cycles	1.0	0.5	1.0	1.0	0.5	0.5
Stress-Range (ksi)	0.25	2.00	1.00	1.50	3.00	2.25

The results from Table 5.5 enable one to calculate the expected stress-range and total number of cycles that the expected stress-range occurs in the length of time considered (12 seconds in this case). The total number of cycles is simply the sum of all cycles counted (4.5 in this case). The following weighted average approach was used to compute the expected stress-range over the length of time considered,

$$S_{RE} = \frac{\sum_{i=1}^{N} n_{cycles,i} \cdot S_{R,i}}{n_{cycles/time}} \tag{5.23}$$

where: N is the total number of different stress-range magnitudes present in the variable amplitude stress history; $n_{cycles,i}$ is the number of rainflow cycles counted for stress-range magnitude $S_{R,i}$; and $n_{cycles/time}$ is the total number of rainflow cycles counted in the length of time considered. The results for the example variable amplitude stress history using equation (5.23) are provided in Table 5.6. The results in Table 5.5 and 5.6 look reasonable indicating that the MATLAB scripts used are performing as expected.

Table 5.6. Resulting expected stress-range magnitudes and corresponding number of cycle occurrences for example stress history.

S_{RE} (ksi)	1.42
$n_{cycles/12\text{-}sec}$	4.50

5.4.2 – Quantifying *B*

Once the rainflow cycle-counting scripts were validated using simple variable amplitude stress histories, it was time to implement them on the simulated and measured stress histories (six total) used for quantifying *B*. Given the length of each stress history (14,400 data points corresponding to 3,600 seconds), it was not feasible to provide figures labeling the relative peaks. The results of performing the rainflow cycle-counting technique on the one-hour time histories are provided in Figure 5.13. In order to differentiate between the measured and simulated expected stress-ranges, the subscripts *m* and *s* were used for measured and simulated, respectively.

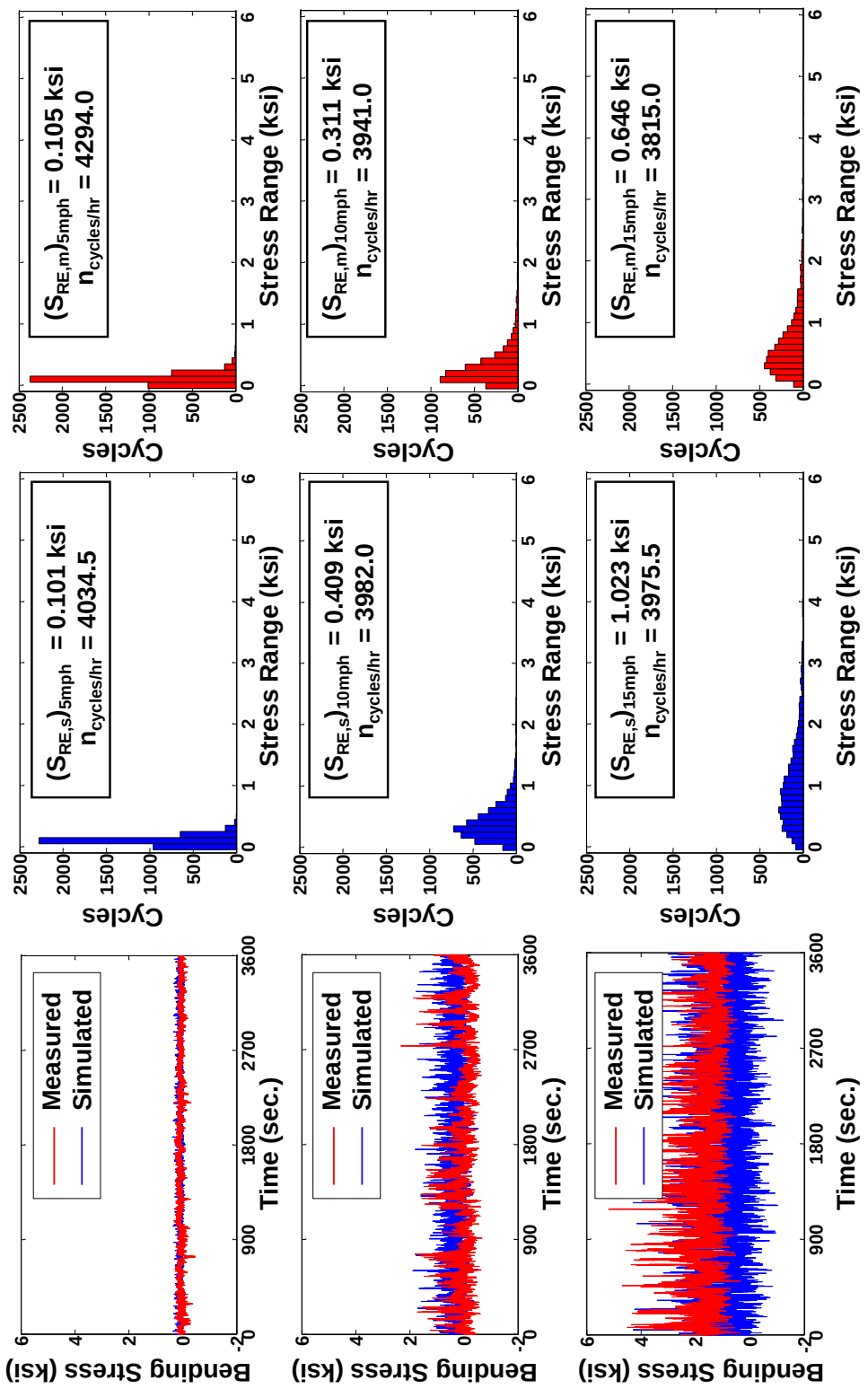

Figure 5.13. Bending stress histories and frequency histograms of stress-range magnitude (note: the expected stress-range and corresponding total number of rainflow cycles counted for each measured or simulated response record is provided in the upper right corner of each histogram).

The comparisons between stress histories provided in Figure 5.13 indicate that there is some variation between the measured and simulated results; however, both the bending stress histories and frequency histograms look very comparable. Employing equation (5.23) provides the expected stress-range magnitudes (S_{RE}) for each of the six stress histories considered. Figure 5.13 also provides the resulting expected stress-range and total number of cycles obtained for each stress history.

The results provided in Figure 5.13 enable the computation of *B*, using equation (5.1), at the three mean wind speed magnitudes considered in the present modeling error study. The resulting *B*-values are provided in Table 5.7. Using Table 5.7 in conjunction with Figure 5.13, it is clear that there is some variation between the measured and simulated results. The comparison made at the 5.23 mph mean wind speed magnitude provided a *B*-value less than 1.0 while comparisons at the other two mean wind speed magnitudes (10.18 mph and 15.97 mph) provided *B*-values greater than 1.0. Ideally, if the modeling procedure was able to simulate the measured stress history exactly, the modeling error would be zero with $\mu_B = 1.0$ and $CV_B = 0$ for all mean wind speeds. More realistically however, none of the simulations are exact, but do provide very comparable results with *B*-values very close to 1.0. It should be noted that the statistical parameters μ_B, σ_B and CV_B are also provided in Table 5.7. Given these statistical parameters, a lognormal distribution can be defined in order to estimate levels of modeling error to be expected at other mean wind speed magnitudes.

Table 5.7. Expected stress-range magnitudes and corresponding number of cycle occurrences for measured and simulated stress histories and resulting values for $B_{5.23mph}$, $B_{10.18mph}$, $B_{15.97mph}$, μ_B, σ_B and CV_B.

Mean Wind Speed Magnitude, i	Simulated Expected Stress-Range (ksi)	Simulated Number of Cycles	Measured Expected Stress-Range (ksi)	Measured Number of Cycles	B-value $(S_{RE,s})_i/(S_{RE,m})_i$
	$(S_{RE,s})_i$	$n_{cycles/hr,i}$	$(S_{RE,m})_i$	$n_{cycles/hr,i}$	
5.23 mph	0.1012	4034.5	0.1050	4294.0	0.964
10.18 mph	0.4090	3982.0	0.3108	3941.0	1.316
15.97 mph	1.0228	3975.5	0.6458	3815.0	1.584

μ_B	**1.288**
σ_B	**0.311**
CV_B	**0.241**

5.5 – Concluding Remarks

As indicated very early in this dissertation, it was expected that modeling error would be present in the procedure used to simulate stress histories and would not be constant throughout all mean wind speed magnitudes. The results of this chapter indicate that this hypothesis was correct. With that said, the results provided in Table 5.7 also indicate that the modeling procedure reasonably estimates the expected stress-range magnitudes and corresponding number of cycle occurrences at the various levels of mean wind speed magnitude considered. Future studies may be able to better quantify the level of modeling error by conducting comparisons at higher mean wind speeds. However, the results of this chapter now provide a known level of uncertainty when trying to employ a completely simulation-based procedure for predicting accumulated fatigue damage in the form of expected stress-range magnitudes and corresponding number of cycle occurrences.

CHAPTER 6 – RELIABILITY-BASED INSPECTION PROTOCOLS

6.1 – Introduction

The reliability-based fatigue assessment procedure for sign support structures includes uncertainty in variables which represent loading demand (wind), resistance (fatigue life), modeling error, and accumulated fatigue damage. In order to quantify the risk of fatigue-induced fracture in these types of structures, one must first quantify the uncertainty associated with these variables. The demand was defined by a stress parameter which summed damage caused by variable-magnitude and variable-direction wind loading; the resistance was defined as the fatigue life (number of cycles to crack-initiation) of a typical welded connection; and modeling error was defined by the ratio of simulated expected stress-ranges to measured expected stress-ranges.

This chapter will begin by providing a synthesized version of the necessary results used to define reliability-based inspection protocols. The major objective is to implement the reliability-based fatigue assessment procedure in order to prescribe inspection frequencies based upon user-defined levels of risk found in typical sign supports used throughout the state of Wisconsin. The protocols will be developed for the test-group structures (*i.e.* the Milwaukee and Osseo structures) situated at various locations throughout the state of Wisconsin.

6.2 – Reliability Framework

The foundation for the reliability-based procedure employed in the present study was described in chapter one of this dissertation. It is founded upon several expressions repeated here for clarity and an outline discussion of the procedure will be provided in the following sections.

6.2.1 – Wind Demand Uncertainty

The primary loading sustained by sign support structures is generated from wind. This loading is highly variable because wind may act out of any direction and at a very wide range of magnitudes. In order to reliably predict the level of wind demand present for a given mast-arm sign support structure, 14 years of wind speed and direction data was collected from NCDC-ASOS sites located at airports from various cities throughout the state of Wisconsin. This data was synthesized and used to generate statistical parameters, and ultimately, combined probabilities of wind speed and wind direction for use within the reliability-based methodology outlined previously.

As indicated in chapter two, not all mast-arm sign support structures are located next to airports. In fact, a significant number of these structures are remotely located at some distance away (or in between) the NCDC-ASOS sites. As a result, it can be difficult to choose a dataset from a single site to use for estimating the level of wind demand expected at the remote location. Therefore, a procedure was developed to interpolate between combined probabilities of wind speed and direction from all NCDC-ASOS sites in order to provide combined probabilities at a virtual weather station (VWS) which will correspond to the remote location. This procedure was discussed in chapter two. The combined probabilities of wind speed and direction required for the interpolation procedure were provided in Tables 2.2 through 2.8. These probabilities will be used in subsequent sections with explanation of how to implement the reliability-based procedure.

The combined probabilities by themselves do not generate demand on a structure. In order to provide demand (*i.e.* damage accumulation), these combined probabilities need to be attached to a number and magnitude of stress-ranges consistent with various magnitudes of wind speed. Chapter two provided a detailed derivation for a semi-deterministic stress parameter given by,

$$\Omega = n_{1-hr/yr} \cdot \sum_i \sum_j \left[P(U = u_i \bigcap D = d_j) \cdot n_{cycles/hr,i}(S_{RE}^m)_i \cdot \cos\theta_j \right] \quad (6.1)$$

where: $n_{1-hr/yr}$ is the number of 1-hour intervals in a year (8,760); $P(U = u_i \cap D = d_j)$ is the probability that a 1-hour averaged wind speed of user-defined magnitude will be intersected with a 1-hour averaged wind direction of user-defined direction (*e.g.* Tables 2.2 through 2.8); $n_{cylces/hr,i}$ is the number of stress-range cycles that occurs in a one hour time interval resulting from application of a wind pressure simulation corresponding to a user-defined 1-hour averaged wind speed, *i*; S_{RE}^m is the expected stress-range cycle magnitude that occurs in a 1-hour simulation history raised to the *m* power where *m* corresponds to the slope of the fatigue detail curve selected; and $\cos\theta_j$ is the angle between the axis of the mast-arm and the centroidal axis of the cardinal wind direction, *j*, being considered.

The number of stress-range cycles and the expected stress-range cycle magnitudes, S_{RE}, are based upon rainflow counting of stress response histories for simulated wind speeds with one-hour averages of 5, 10, 15, 20, 25, 30, 35, 40, 45, and 50 mph. As a result, there are values of Ω corresponding to each of these one-hour wind speed magnitudes. The stress range histories upon which the rainflow counting is conducted are based upon low-fidelity finite element models (stick models) of the sign support structures outlined in chapter four of this dissertation.

Mean Stress and Stress Concentration Effects

Only tensile stress-ranges were monitored during each simulation of the present study. Each structure-type was subjected to each of the ten wind speed simulations. The number and magnitude of expected stress-ranges were obtained at two-degree incremental locations around the tensile portion of the mast-arm tube at ten inches from the weld-toe in order to capture any dead load mean stress effects. Tables 6.1 and 6.2 provide the resulting expected stress-ranges and

number of cycles that occurred during each one-hour simulation. Figure 6.1 provides a graphical depiction of how the expected stress-range varies around the circumference of the mast-arm tube for both types of structures.

Table 6.1. Number and magnitude of expected stress-ranges for one-hour simulated wind records of various magnitudes achieved for the Milwaukee structure.

One-Hour Averaged Wind Speed			5 mph	10 mph	15 mph	20 mph	25 mph	30 mph	35 mph	40 mph	45 mph	50 mph
$n_{cycles/hr}$			4010.00	3971.50	3970.50	3925.00	3916.50	3896.50	3831.50	3813.50	3820.00	3792.50
θ (location on 1/4 section in degrees)	0	S_{RE} (ksi)	0.00000	0.00000	0.00000	0.00000	0.00000	0.00000	0.00000	0.00000	0.00000	0.00000
	2		0.00325	0.01378	0.03179	0.05701	0.09072	0.12350	0.17448	0.22360	0.27431	0.34531
	4		0.00650	0.02755	0.06354	0.11396	0.18133	0.24686	0.34875	0.44693	0.54829	0.69020
	6		0.00974	0.04128	0.09521	0.17077	0.27172	0.36991	0.52260	0.66971	0.82160	1.03426
	8		0.01296	0.05496	0.12677	0.22737	0.36178	0.49251	0.69580	0.89168	1.09390	1.37705
	10		0.01617	0.06857	0.15817	0.28369	0.45139	0.61452	0.86817	1.11256	1.36488	1.71816
	12		0.01937	0.08210	0.18938	0.33966	0.54046	0.73577	1.03947	1.33208	1.63419	2.05718
	14		0.02253	0.09553	0.22035	0.39523	0.62887	0.85613	1.20950	1.54998	1.90151	2.39369
	16		0.02567	0.10884	0.25106	0.45031	0.71651	0.97544	1.37807	1.76600	2.16651	2.72729
	18		0.02878	0.12203	0.28147	0.50484	0.80328	1.09357	1.54495	1.97986	2.42888	3.05756
	20		0.03186	0.13506	0.31153	0.55875	0.88907	1.21036	1.70995	2.19131	2.68828	3.38411
	22		0.03489	0.14793	0.34121	0.61199	0.97378	1.32568	1.87287	2.40009	2.94441	3.70654
	24		0.03788	0.16061	0.37048	0.66448	1.05730	1.43938	2.03351	2.60595	3.19696	4.02445
	26		0.04083	0.17311	0.39929	0.71616	1.13953	1.55133	2.19166	2.80863	3.44560	4.33746
	28		0.04373	0.18539	0.42762	0.76697	1.22038	1.66139	2.34715	3.00789	3.69005	4.64504
	30		0.04657	0.19744	0.45543	0.81684	1.29973	1.76943	2.49978	3.20348	3.93001	4.94681
	32		0.04936	0.20926	0.48268	0.86572	1.37751	1.87531	2.64937	3.39517	4.16517	5.24252
	34		0.05208	0.22082	0.50934	0.91355	1.45360	1.97890	2.79572	3.58273	4.39508	5.53177
	36		0.05475	0.23211	0.53538	0.96026	1.52793	2.08009	2.93867	3.76592	4.61960	5.81414
	38		0.05734	0.24311	0.56078	1.00580	1.60039	2.17874	3.07804	3.94452	4.83844	6.08908
	40		0.05987	0.25383	0.58548	1.05011	1.67091	2.27473	3.21366	4.11832	5.05135	6.35605
	42		0.06232	0.26423	0.60948	1.09315	1.73938	2.36796	3.34536	4.28708	5.25783	6.61470
	44		0.06470	0.27431	0.63273	1.13486	1.80574	2.45829	3.47299	4.45055	5.45763	6.86459
	46		0.06700	0.28406	0.65521	1.17518	1.86990	2.54564	3.59639	4.60846	5.65051	7.10540
	48		0.06922	0.29346	0.67689	1.21407	1.93178	2.62988	3.71539	4.76044	5.83620	7.33668
	50		0.07135	0.30250	0.69775	1.25148	1.99131	2.71088	3.82981	4.90637	6.01437	7.55753
	52		0.07340	0.31117	0.71776	1.28736	2.04841	2.78852	3.93948	5.04677	6.18475	7.76833
	54		0.07535	0.31947	0.73689	1.32168	2.10302	2.86313	4.04400	5.17936	6.34689	7.96861
	56		0.07722	0.32737	0.75513	1.35439	2.15506	2.93378	4.14328	5.30625	6.50044	8.15781
	58		0.07899	0.33488	0.77245	1.38545	2.20448	3.00076	4.23709	5.42520	6.64534	8.33689
	60		0.08066	0.34198	0.78882	1.41482	2.25121	3.06400	4.32528	5.53675	6.78113	8.50274
	62		0.08224	0.34866	0.80423	1.44246	2.29520	3.12337	4.40746	5.64036	6.90731	8.65647
	64		0.08371	0.35492	0.81867	1.46835	2.33638	3.17861	4.48377	5.73577	7.02356	8.79809
	66		0.08509	0.36074	0.83210	1.49245	2.37451	3.22955	4.55365	5.82379	7.12947	8.92751
	68		0.08636	0.36613	0.84453	1.51473	2.40959	3.27589	4.61662	5.90226	7.22460	9.04391
	70		0.08752	0.37107	0.85592	1.53517	2.44168	3.31748	4.67254	5.97251	7.30902	9.14699
	72		0.08858	0.37556	0.86627	1.55372	2.47081	3.35418	4.72133	6.03225	7.38185	9.23689
	74		0.08953	0.37959	0.87557	1.57032	2.49530	3.38591	4.76238	6.08213	7.44467	9.31342
	76		0.09037	0.38315	0.88379	1.58490	2.51532	3.41211	4.79507	6.12172	7.49598	9.37605
	78		0.09111	0.38625	0.89095	1.59724	2.53039	3.43226	4.81914	6.15009	7.53540	9.42513
	80		0.09173	0.38888	0.89688	1.60680	2.53973	3.44461	4.83382	6.16906	7.56284	9.46033
	82		0.09223	0.39104	0.90155	1.61299	2.54201	3.44897	4.83916	6.17745	7.57807	9.48192
	84		0.09263	0.39272	0.90472	1.61297	2.53599	3.44450	4.83453	6.17417	7.58077	9.48930
	86		0.09291	0.39382	0.90370	1.60382	2.51997	3.43068	4.81812	6.15947	7.57050	9.48266
	88		0.09308	0.39284	0.89264	1.58202	2.49240	3.40590	4.79023	6.13263	7.54792	9.46152
	90		0.08929	0.37328	0.86037	1.54331	2.45241	3.36956	4.75129	6.09317	7.51348	9.42582

Table 6.2. Number and magnitude of expected stress-ranges for one-hour simulated wind records of various magnitudes achieved for the Osseo structure.

One-Hour Averaged Wind Speed			5 mph	10 mph	15 mph	20 mph	25 mph	30 mph	35 mph	40 mph	45 mph	50 mph
$n_{cycles/hr}$			3285.00	3276.50	3248.50	3257.00	3240.00	3244.00	3234.50	3224.00	3210.50	3200.50
θ (location on 1/4 section in degrees)	0	S_{RE} (ksi)	0.00000	0.00000	0.00000	0.00000	0.00000	0.00000	0.00000	0.00000	0.00000	0.00000
	2		0.00170	0.00747	0.01734	0.03275	0.05226	0.07601	0.10297	0.13309	0.16561	0.20491
	4		0.00338	0.01494	0.03466	0.06546	0.10446	0.15192	0.20582	0.26601	0.33102	0.40956
	6		0.00507	0.02238	0.05194	0.09809	0.15653	0.22765	0.30841	0.39861	0.49603	0.61372
	8		0.00674	0.02980	0.06915	0.13060	0.20841	0.30310	0.41063	0.53073	0.66043	0.81713
	10		0.00841	0.03718	0.08628	0.16295	0.26003	0.37819	0.51235	0.66220	0.82403	1.01954
	12		0.01007	0.04452	0.10330	0.19511	0.31134	0.45281	0.61344	0.79286	0.98662	1.22071
	14		0.01172	0.05180	0.12020	0.22702	0.36227	0.52688	0.71379	0.92256	1.14802	1.42040
	16		0.01335	0.05902	0.13695	0.25866	0.41275	0.60031	0.81326	1.05113	1.30801	1.61835
	18		0.01496	0.06616	0.15353	0.28998	0.46274	0.67301	0.91175	1.17842	1.46641	1.81433
	20		0.01657	0.07323	0.16993	0.32095	0.51216	0.74488	1.00912	1.30428	1.62302	2.00810
	22		0.01814	0.08021	0.18612	0.35153	0.56096	0.81585	1.10527	1.42854	1.77766	2.19943
	24		0.01970	0.08708	0.20209	0.38168	0.60907	0.88583	1.20007	1.55107	1.93013	2.38807
	26		0.02123	0.09386	0.21780	0.41137	0.65644	0.95473	1.29341	1.67171	2.08025	2.57381
	28		0.02274	0.10052	0.23326	0.44056	0.70301	1.02246	1.38517	1.79031	2.22783	2.75641
	30		0.02422	0.10705	0.24842	0.46920	0.74873	1.08895	1.47524	1.90673	2.37270	2.93565
	32		0.02567	0.11346	0.26329	0.49728	0.79353	1.15411	1.56352	2.02082	2.51468	3.11131
	34		0.02708	0.11972	0.27783	0.52475	0.83737	1.21786	1.64989	2.13246	2.65359	3.28319
	36		0.02847	0.12585	0.29204	0.55158	0.88018	1.28013	1.73425	2.24149	2.78928	3.45106
	38		0.02982	0.13181	0.30589	0.57774	0.92192	1.34085	1.81650	2.34780	2.92156	3.61473
	40		0.03113	0.13762	0.31937	0.60320	0.96254	1.39992	1.89653	2.45124	3.05028	3.77400
	42		0.03241	0.14326	0.33246	0.62792	1.00199	1.45730	1.97426	2.55170	3.17529	3.92867
	44		0.03364	0.14873	0.34514	0.65187	1.04022	1.51289	2.04958	2.64905	3.29643	4.07855
	46		0.03484	0.15401	0.35740	0.67503	1.07718	1.56665	2.12240	2.74317	3.41356	4.22346
	48		0.03599	0.15911	0.36923	0.69737	1.11282	1.61849	2.19264	2.83395	3.52652	4.36322
	50		0.03710	0.16401	0.38061	0.71886	1.14712	1.66836	2.26020	2.92128	3.63519	4.49768
	52		0.03816	0.16871	0.39152	0.73947	1.18001	1.71620	2.32501	3.00504	3.73943	4.62665
	54		0.03918	0.17321	0.40196	0.75919	1.21147	1.76195	2.38699	3.08515	3.83911	4.74998
	56		0.04015	0.17750	0.41191	0.77797	1.24145	1.80556	2.44606	3.16150	3.93411	4.86753
	58		0.04107	0.18157	0.42135	0.79581	1.26991	1.84696	2.50215	3.23399	4.02433	4.97902
	60		0.04194	0.18542	0.43028	0.81268	1.29683	1.88611	2.55519	3.30255	4.10943	5.08440
	62		0.04276	0.18904	0.43869	0.82856	1.32217	1.92297	2.60512	3.36708	4.18940	5.18359
	64		0.04353	0.19243	0.44656	0.84343	1.34590	1.95748	2.65188	3.42751	4.26414	5.27646
	66		0.04424	0.19559	0.45389	0.85728	1.36799	1.98961	2.69540	3.48376	4.33322	5.36279
	68		0.04490	0.19851	0.46067	0.87008	1.38841	2.01931	2.73564	3.53577	4.39656	5.44140
	70		0.04551	0.20119	0.46688	0.88181	1.40715	2.04655	2.77255	3.58347	4.45366	5.51172
	72		0.04606	0.20362	0.47253	0.89248	1.42416	2.07130	2.80608	3.62645	4.50367	5.57301
	74		0.04655	0.20581	0.47760	0.90205	1.43944	2.09353	2.83587	3.66430	4.54676	5.62200
	76		0.04699	0.20774	0.48209	0.91053	1.45297	2.11320	2.86154	3.69590	4.58029	5.65766
	78		0.04737	0.20942	0.48599	0.91790	1.46473	2.13019	2.88249	3.71880	4.60020	5.67416
	80		0.04769	0.21085	0.48930	0.92415	1.47470	2.14432	2.89588	3.72980	4.60192	5.66792
	82		0.04796	0.21202	0.49201	0.92927	1.48250	2.15323	2.89772	3.72302	4.57988	5.63651
	84		0.04816	0.21293	0.49413	0.93327	1.48722	2.15157	2.87734	3.68666	4.52941	5.57167
	86		0.04831	0.21358	0.49564	0.93563	1.48214	2.12601	2.82220	3.61309	4.43833	5.47030
	88		0.04840	0.21397	0.49632	0.92407	1.44002	2.04835	2.71343	3.48864	4.29977	5.32685
	90		0.04328	0.19052	0.43499	0.81495	1.29762	1.88341	2.53214	3.30241	4.11106	5.13918

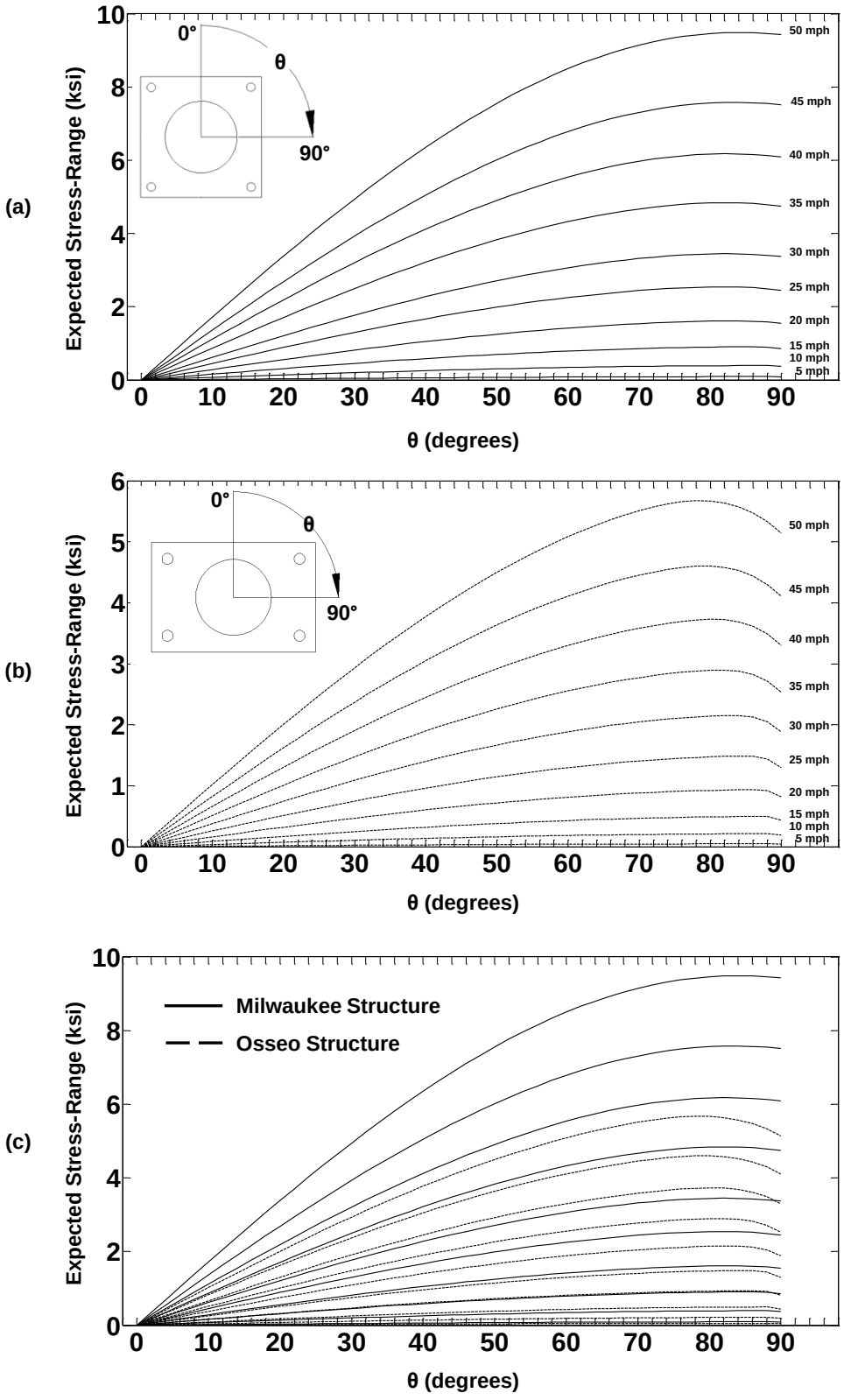

Figure 6.1. Expected stress-range vs. location around mast-arm tube for: (a) Milwaukee structure; (b) Osseo structure; and (c) both structures.

To illustrate the mean stress and stress concentration effects, consider the results from a one-hour simulation corresponding to a one-hour averaged wind speed of 15 mph. Figures 6.2 through 6.4 provide simulated stress histories which correspond to results achieved using equation (5.22) of chapter five and concentrated stress histories which correspond to the same stress histories multiplied by an appropriate *SCF*. The results illustrate that the simulated stress histories generated from variable wind loading creates the largest stress-ranges for both structures in the 70 to 90 degree locations. The opposite is true for the gravity stress histories. The gravity stress is a constant at each location for both structures with maximum values achieved at the top most tension fibers (0 degrees) and minimum values achieved at the neutral axis of the tubes (90 degrees). The stress concentration factor used to compute the concentrated stress histories for all two-degree incremental locations and for each structure-type is provided in Figure 6.5. The results provided in these figures indicate the substantial increase in both mean stress and stress-range for the Osseo structure given its significant self-weight and significant stress concentration effects.

It should be noted that the number and magnitude of expected stress-ranges for each wind speed simulation correspond to the simulated stress histories of the previous figures, not the concentrated stress histories. This study was conducted to illustrate the mean stress and stress concentration effects, to re-iterate the need for different fatigue detail categories when classifying these types of connections and to justify the selections made for the test-group structures considered presently.

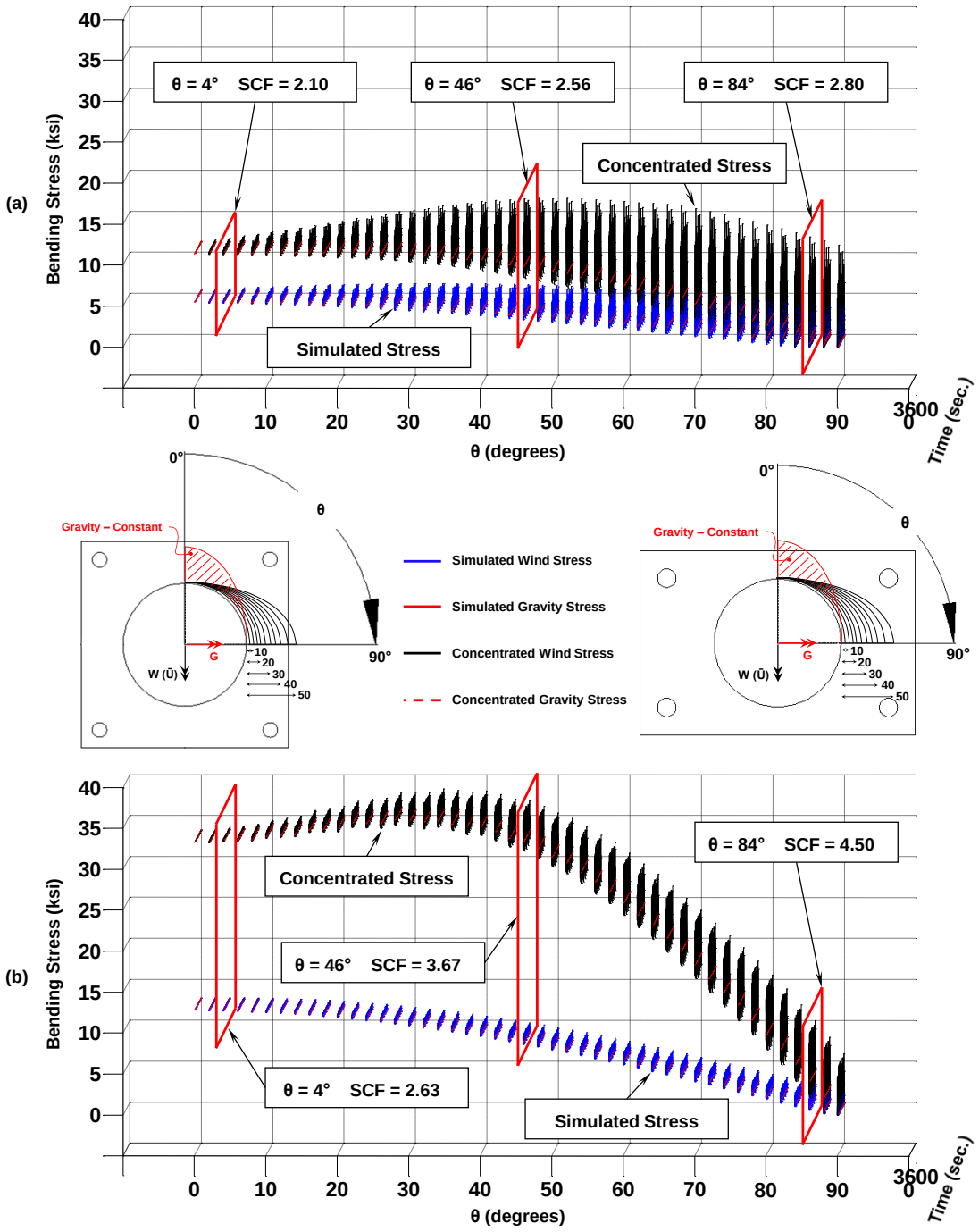

Figure 6.2. Simulated and concentrated stress histories for two-degree incremental locations around mast-arm tube for (a) Milwaukee structure and (b) Osseo structure.

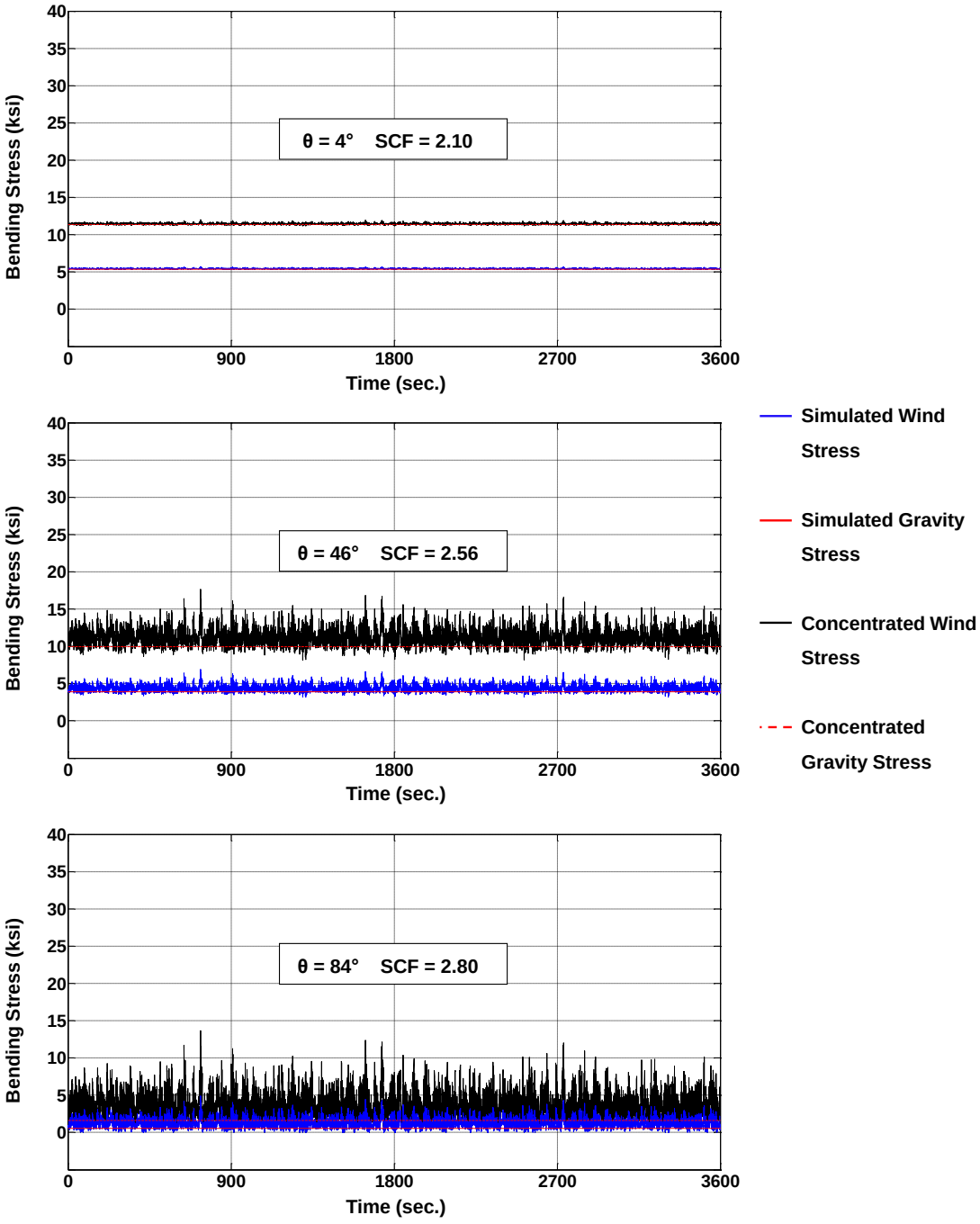

Figure 6.3. Simulated and concentrated stress histories for Milwaukee structure at θ = 4°, 46° and 84°.

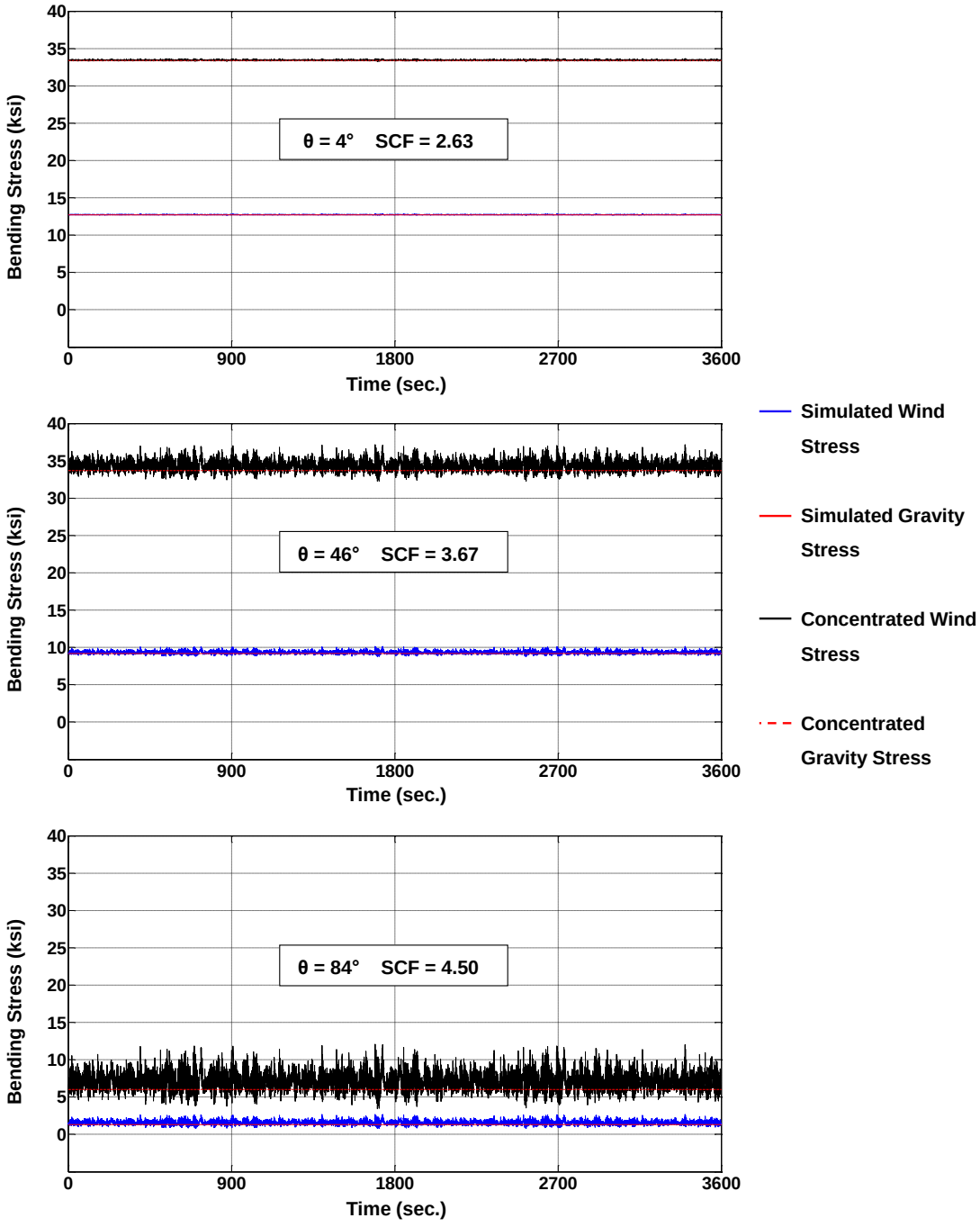

Figure 6.4. Simulated and concentrated stress histories for Osseo structure at θ = 4°, 46° and 84°.

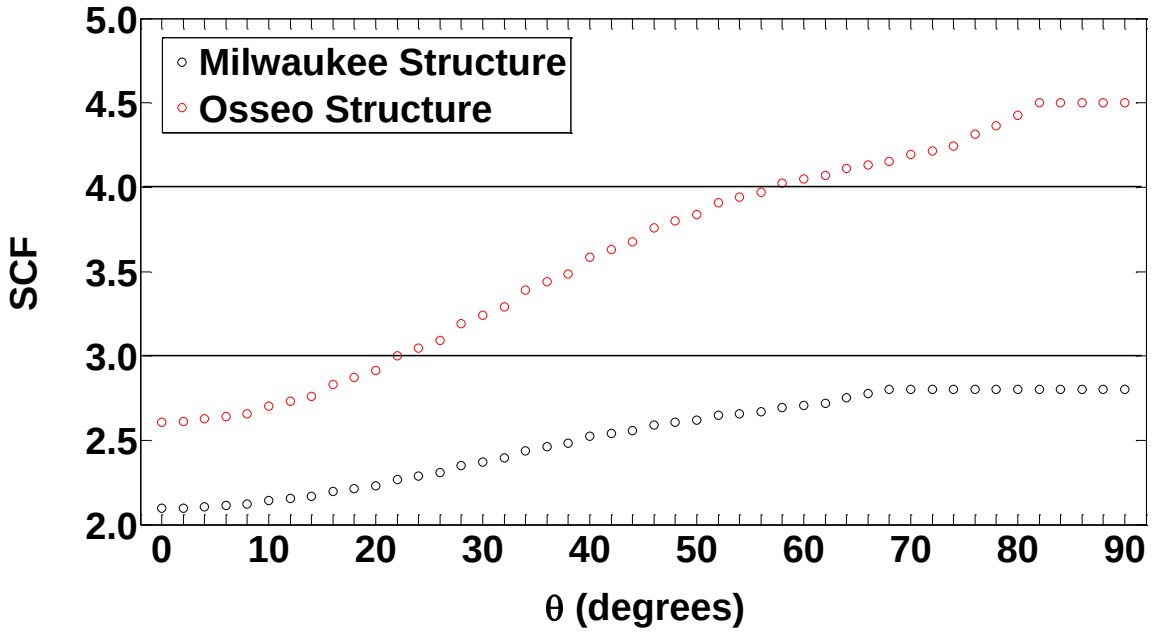

Figure 6.5. Stress concentration factor used at each two-degree incremental location around mast-arm tubes for both structures.

6.2.2 – Fatigue Life Uncertainty

In the present study, resistance was defined as the fatigue life of the connections between the mast-arms and poles of each sign support structure. The parameters needed for modeling uncertainty in fatigue life were described in chapter three of this dissertation. Chapter three provided detailed syntheses of experimental fatigue test data from typical welded connections used within these types of structures. Taxonomy of the test data was based upon the magnitude of the *SCF* present within the connection. As a result, three new fatigue detail categories were developed: E2 ($2.0 \leq SCF < 3.0$), E3 ($3.0 \leq SCF < 4.0$) and E4 ($SCF \geq 4.0$). Figure 3.39 provides the graphical results of this synthesis in the form of stress-range (S_R) versus cycles to failure (N) curves. The statistical parameters generated from these results are provided in Table 3.19.

Clearly, not all sign support structures utilize the same type of connection configuration. To choose a fatigue detail category representative of the connection configuration within the sign support structure of interest, one must employ one of two methods:

1. Perform high-fidelity finite element (FE) analysis of the connection to determine the magnitude of *SCF* at fatigue-critical locations (*e.g.* weld-toe of fillet weld on mast-arm tube – see Figure 6.5).
2. Compute the *SCF* for the connection using equations (3.10) through (3.19) provided in Figure 3.14. It should be noted that the variables used in equations (3.10) through (3.19) were defined in Table 3.3

After a *SCF* is determined for the connection, a fatigue detail representative of that connection may be selected. Once selected, the fatigue detail provides all empirical and statistical information (m , μ_A and CV_A) required to quantify the resistance (*i.e.* fatigue life) of the connection within the mast-arm sign support structure under consideration (see Table 3.19).

6.2.3 – Modeling Error Uncertainty

Uncertainty in modeling error was addressed in chapter five of this dissertation. The lognormal modeling parameters used to model this uncertainty were based upon comparisons of simulated stress histories computed using simulated winds and finite element models that utilized "stick" elements with measured stress histories collected from the field monitoring system designed and deployed in the present research effort. A bias factor, *B*, was then computed as the ratio of simulated expected stress-range to measured expected stress-range at various levels of wind loading. Mathematically, the bias factor was expressed as,

$$B_i = \frac{\left(S_{RE,s}\right)_i}{\left(S_{RE,m}\right)_i} \tag{6.2}$$

where: $S_{RE,s}$ is the expected stress-range from a one-hour long simulated stress history; $S_{RE,m}$ is the expected stress-range from a one-hour long measured stress history; and *i* corresponded to one-hour averaged wind speed magnitudes equal to 5.23 mph, 10.18 mph and 15.97 mph.

Statistical analysis of the modeling error at the three magnitudes of mean wind speed was then used to generate the parameters necessary for quantifying the lognormal modeling error uncertainty. Figure 5.13 provided the frequency histograms for both simulated and measured expected stress-ranges obtained from rainflow cycle counting. Table 5.7 provided the bias factors at each magnitude of wind loading as well as the resulting statistical parameters required in the reliability-based methodology. The modeling parameters synthesized from the measured and simulated response histories used within the reliability assessment are: $\mu_B = 1.288$ and $CV_B = 0.241$.

6.2.4 – Accumulated Damage Uncertainty

Uncertainty in models for accumulated fatigue damage is modeled using existing procedures (Wirsching 1983). The lognormal modeling parameters for uncertainty in accumulated fatigue damage used in the present procedure for defining probabilities of failure are: $\mu_\Delta = 1.00$ and $CV_\Delta = 0.30$.

6.3 – Reliability-Based Fatigue Assessment Process

The probability of a fatigue-induced crack initiating within the connection of a mast-arm sign support structure (*i.e.* probability of failure) is defined using the performance function described in chapter one of this dissertation. The probability of failure can be written as,

$$p_F = P\left[Y \le 1.0\right] = \Phi\left[\frac{\ln(1.0) - \mu_{\ln Y}}{\sigma_{\ln Y}}\right] = \Phi\left[-\frac{\mu_{\ln Y}}{\sigma_{\ln Y}}\right] = \Phi\left[-\beta\right] \tag{6.3}$$

where the reliability index is given by,

$$\beta = \frac{\mu_{\ln Y}}{\sigma_{\ln Y}} \tag{6.4}$$

the mean of the lognormal random variable is computed as,

$$\mu_{\ln Y} = \ln\left(\frac{\mu_A \mu_\Delta}{\mu_B^m}\right) - \frac{1}{2}\ln\left[\frac{\left(1+CV_A^2\right)\left(1+CV_\Delta^2\right)}{\left(1+CV_B^2\right)^m}\right] - \ln\Omega - \ln T \tag{6.5}$$

and the standard deviation of the natural logarithm of the performance function is,

$$\sigma_{\ln Y} = \sqrt{\ln\left[\left(1+CV_A^2\right)\left(1+CV_\Delta^2\right)\left(1+CV_B^2\right)\right]} \tag{6.6}$$

Therefore, the reliability-assessment procedure and subsequent definitions of failure as a function of service life are computed using equations (6.1) and (6.3) through (6.6).

The procedure is outlined in the following. It begins by defining a location of a sign support structure and its orientation relative to North (see Figure 6.6 for reference throughout the following). Thus, a latitude and longitude for the mast-arm sign support is defined and the orientation of the mast-arm is defined: N-S (0° or 180°), NE-SW (45° or 225°), E-W (90° or 270°), and SE-NW (135° or 325°). The mast-arm orientation defines the angle of the mast-arm relative to the "centroidal axis" of each of the eight cardinal wind directions. Once defined, θ_j from equation (6.1) can be established.

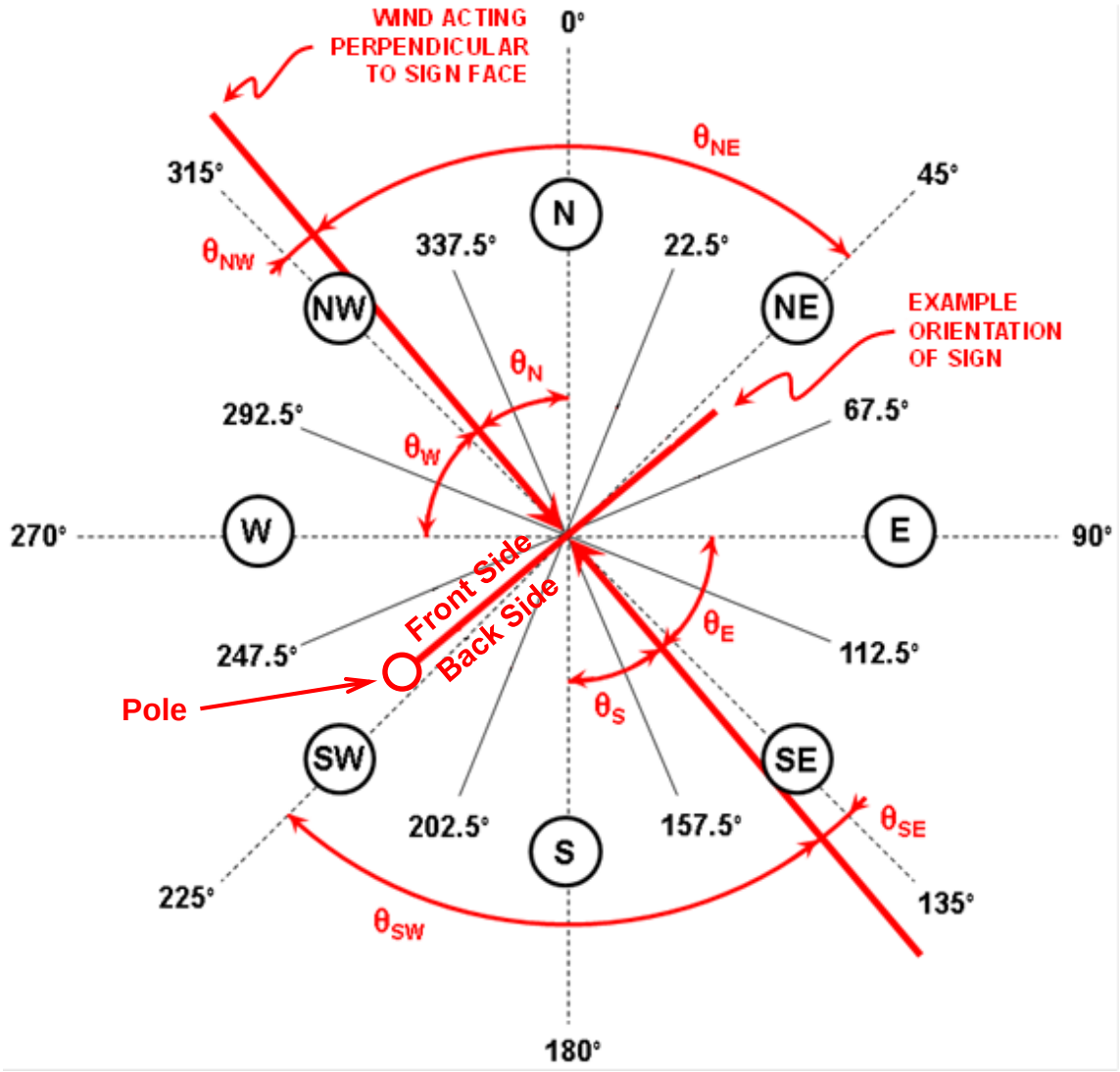

Figure 6.6. Visual reference illustrating centroidal axes of cardinal directions and relative angles to mast-arm of example sign support structure.

A low-fidelity finite element model (composed of one-dimensional finite elements) is then subjected to one-hour averaged wind speed simulations constructed using the Kaimal spectrum as described in chapter five for defined one-hour averaged wind speeds in the following set: 5, 10, 15, 20, 25, 30, 35, 40, 45, and 50 mph. Each of these simulations results in stress histories for critical locations around the circumference of the mast-arm cross-section. Rainflow counting procedures for each wind speed simulation are used to define expected stress-range

magnitudes for that wind speed, S_{RE}, and a number of stress-range cycles for that wind speed in the one-hour averaging window, $n_{cycle/hr,i}$. Equation (6.1) is then used along with combined probabilities of wind speed and direction (*e.g.* Tables 2.2 through 2.8) to compute the stress parameter, Ω, for each one-hour averaged wind speed simulation.

A stress parameter for each wind speed direction generating demand in the mast-arm sign support is computed. In other words, if the sign support is oriented as shown in Figure 6.6, then winds out of the E, SE, S and SW will cause tensile stress-ranges on one side of the mast arm (back) and winds out of the W, NW, N and NE will cause tensile stress-ranges on the opposite side of the mast-arm (front). Both of these scenarios are crucial to defining the fatigue performance of the mast-arm and therefore two stress parameters are computed using equation (6.1). The larger magnitude stress parameter is used in equation (6.5) to facilitate computation of the probability of failure (*i.e.* finding a fatigue-induced crack initiated).

Each of the three detail categories, E2, E3, and E4 has its own unique set of lognormal modeling parameters provided in Table 3.19. These then allow fatigue performance and probabilities of failure to be assessed for each type of detail expected in the mast-arm sign support structure. These parameters are used in equations (6.5) and (6.6) to facilitate computation of the probability of failure for each type of detail.

Uncertainty in accumulated fatigue damage modeling using Miner's rule is included with the single lognormal modeling parameters described earlier and equations (6.5) and (6.6) to allow computation of the probability of fatigue failure.

The assessment process is relatively straightforward, but admittedly computationally intensive when one reflects on all the computations and data needed to execute the procedure. The process is applied in the computation of probabilities of failure for specific sign locations,

specific sign orientations, three different detail types, and two different types of mast-arm sign support structures. The two types of mast-arm configuration considered are an Osseo (non-tapered, heavy wall thickness, relatively small bluff area) and a Milwaukee (tapered, light wall thickness, relatively large bluff area) structural system. Therefore, the procedure developed in this study allows the expected fatigue performance of sign support structures throughout the state of Wisconsin to be evaluated and studied.

6.4 – Mast-Arm Sign Support Structure Service Life Evaluation

The procedure outlined in section 6.3 allows the probabilities of failure (*i.e.* fatigue-induced cracks to initiate) to be defined for various types of sign support structures, in various orientations, with various detail types and in various locations throughout the state of Wisconsin. The procedure was applied to the following scenarios:

Milwaukee-Type Sign Support (tapered, light wall thickness, large bluff area):

Detail Types:	E2, E3, E4 (ranging from square to rectangular four-bolt patterns)
Orientations:	N-S, NE-SW, E-W, SE-NW
Locations:	Milwaukee, Eau Claire, La Crosse, Green Bay, Madison, Oshkosh, Wisconsin Rapids

Osseo-Type Sign Support (non-tapered, heavy wall thickness, small bluff area):

Detail Types:	E2, E3, E4 (ranging from square to rectangular four-bolt patterns)
Orientations:	N-S, NE-SW, E-W, SE-NW
Locations:	Milwaukee, Eau Claire, La Crosse, Green Bay, Madison, Oshkosh, Wisconsin Rapids

Equations (6.3) through (6.6) allow cumulative distribution functions (CDFs) describing the probabilities of fatigue-crack initiation with service life to be defined. These equations and the procedure described earlier were used to generate these CDFs for the sign support types,

detail types, orientations, and cities described above. Figures 6.7 through 6.13 illustrate CDFs for Milwaukee-type sign supports in the seven Wisconsin cities considered and Figures 6.14 through 6.20 illustrate the CDFs for Osseo-type sign supports in these same cities.

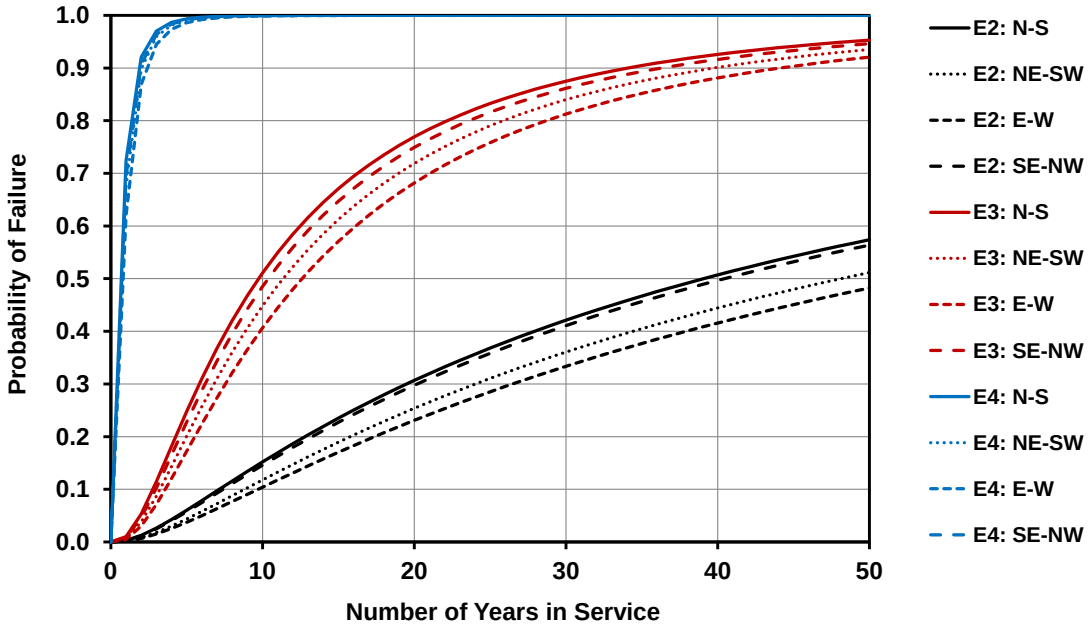

Figure 6.7. Time-zero probabilities of failure for Milwaukee structure located in Milwaukee, Wisconsin.

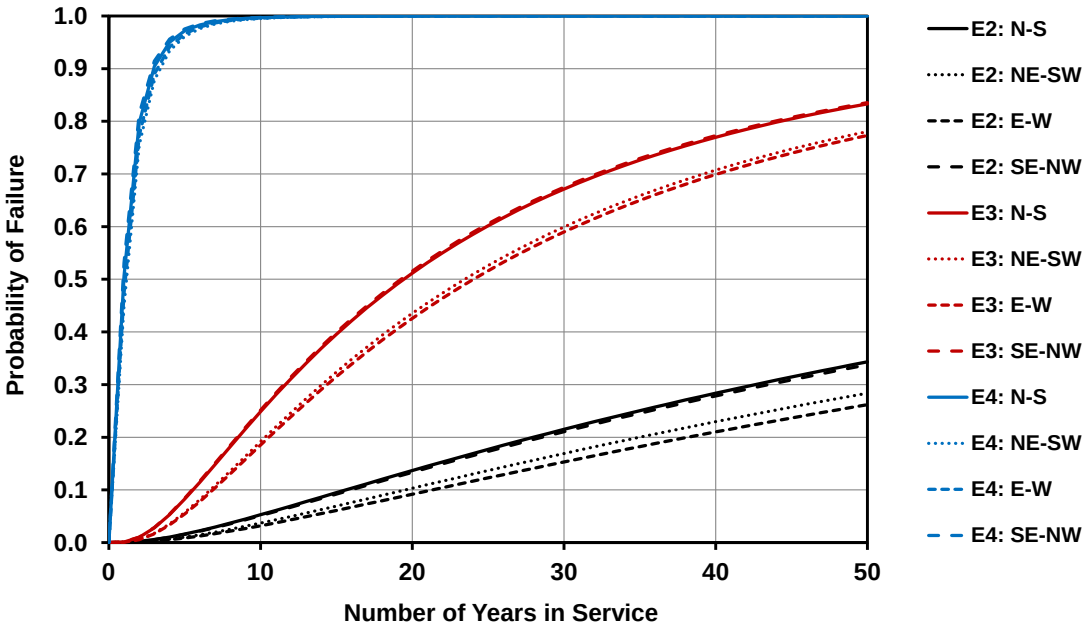

Figure 6.8. Time-zero probabilities of failure for Milwaukee structure located in Eau Claire, Wisconsin.

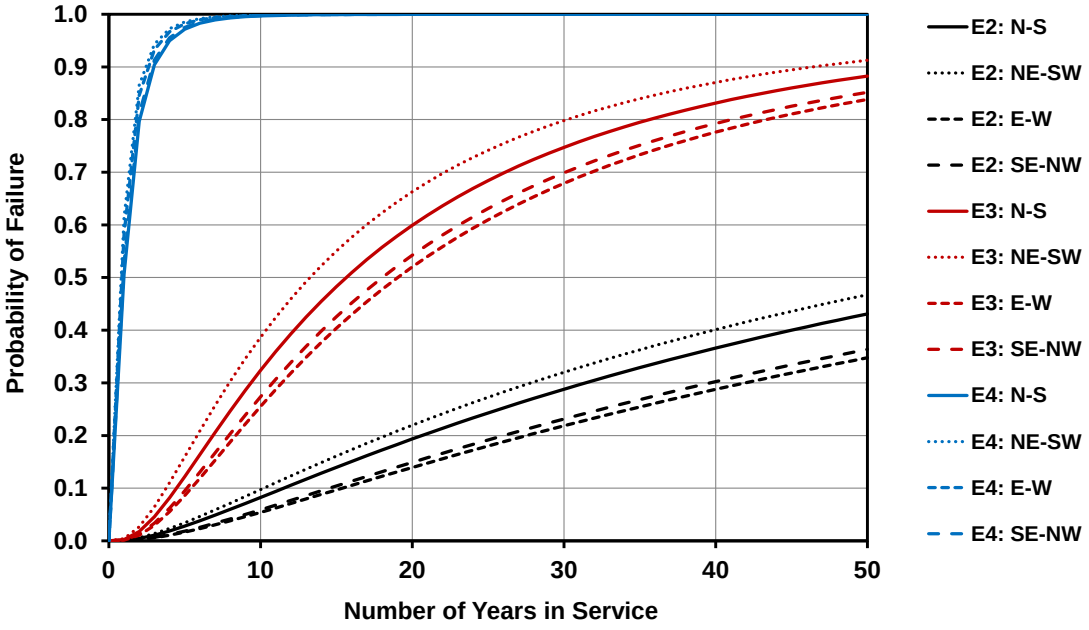

Figure 6.9. Time-zero probabilities of failure for Milwaukee structure located in La Crosse, Wisconsin.

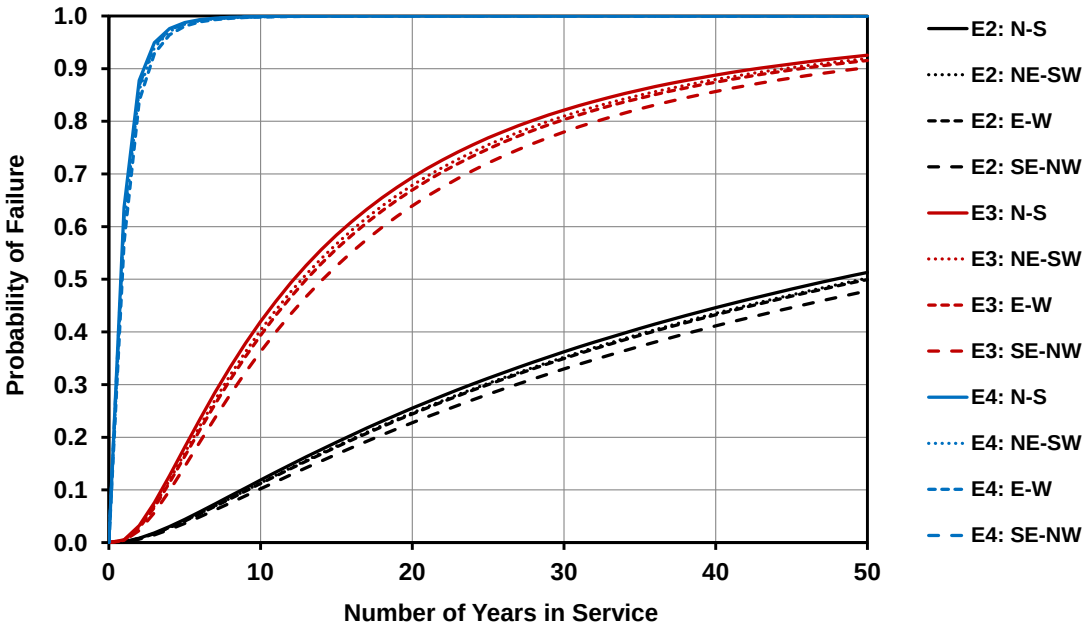

Figure 6.10. Time-zero probabilities of failure for Milwaukee structure located in Green Bay, Wisconsin.

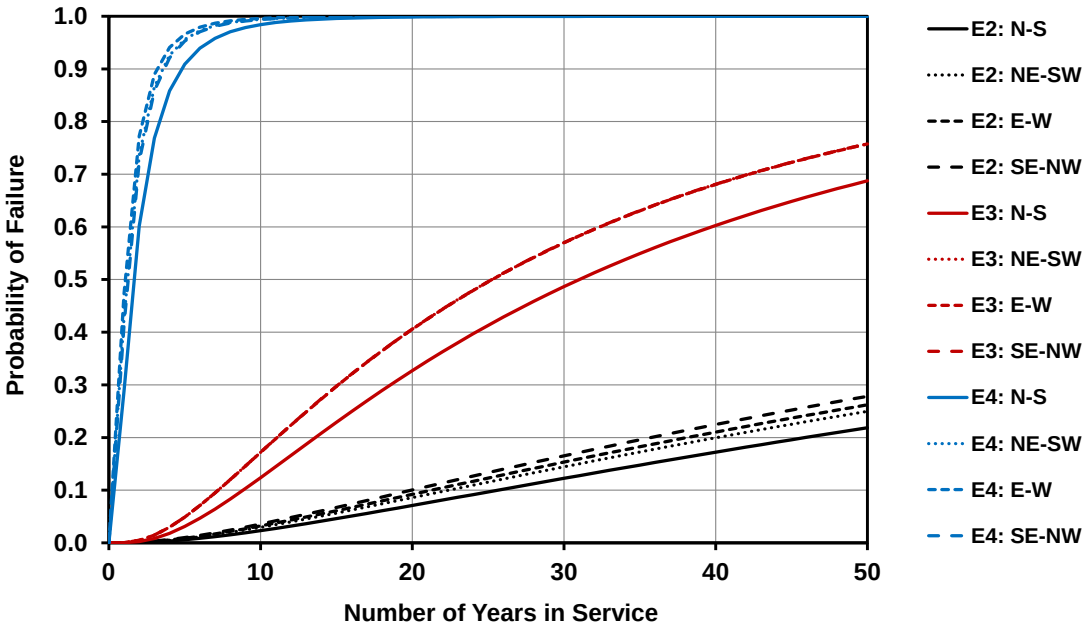

Figure 6.11. Time-zero probabilities of failure for Milwaukee structure located in Madison, Wisconsin.

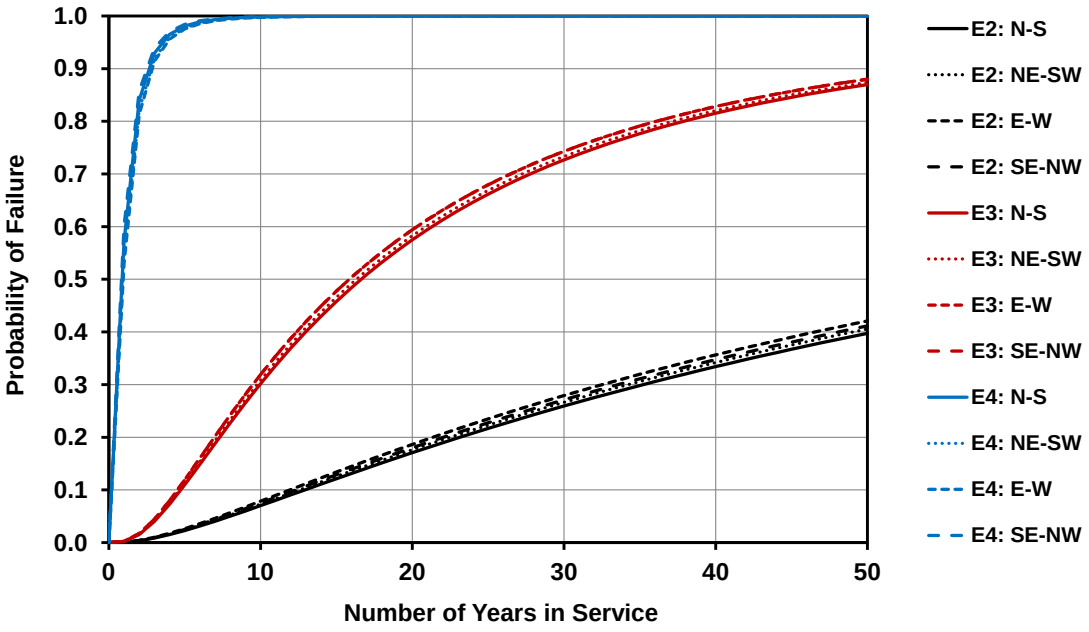

Figure 6.12. Time-zero probabilities of failure for Milwaukee structure located in Oshkosh, Wisconsin.

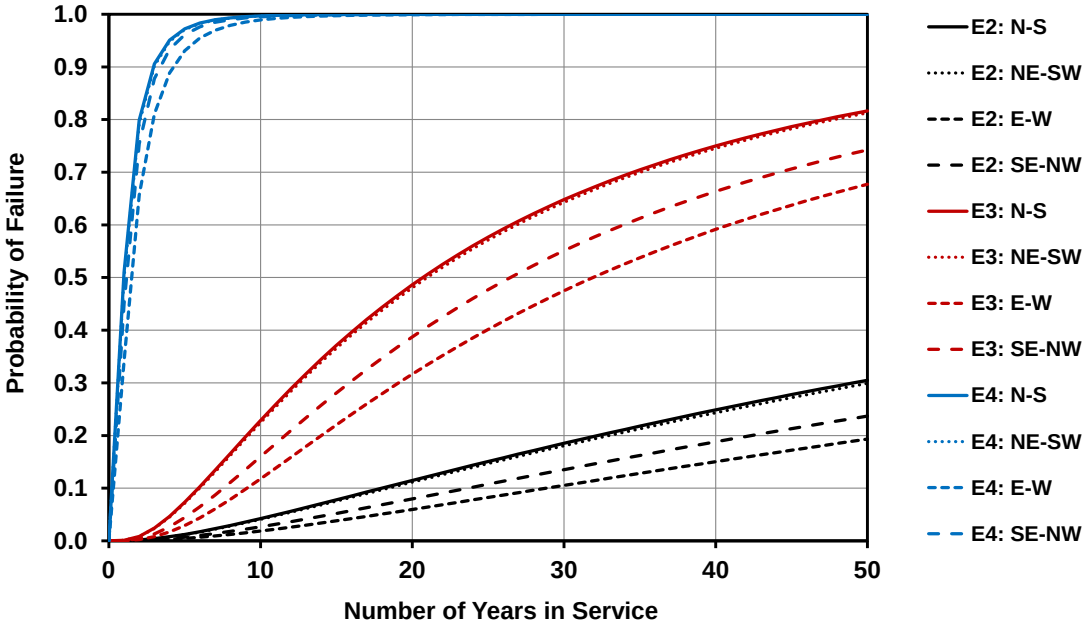

Figure 6.13. Time-zero probabilities of failure for Milwaukee structure located in Wisconsin Rapids, Wisconsin.

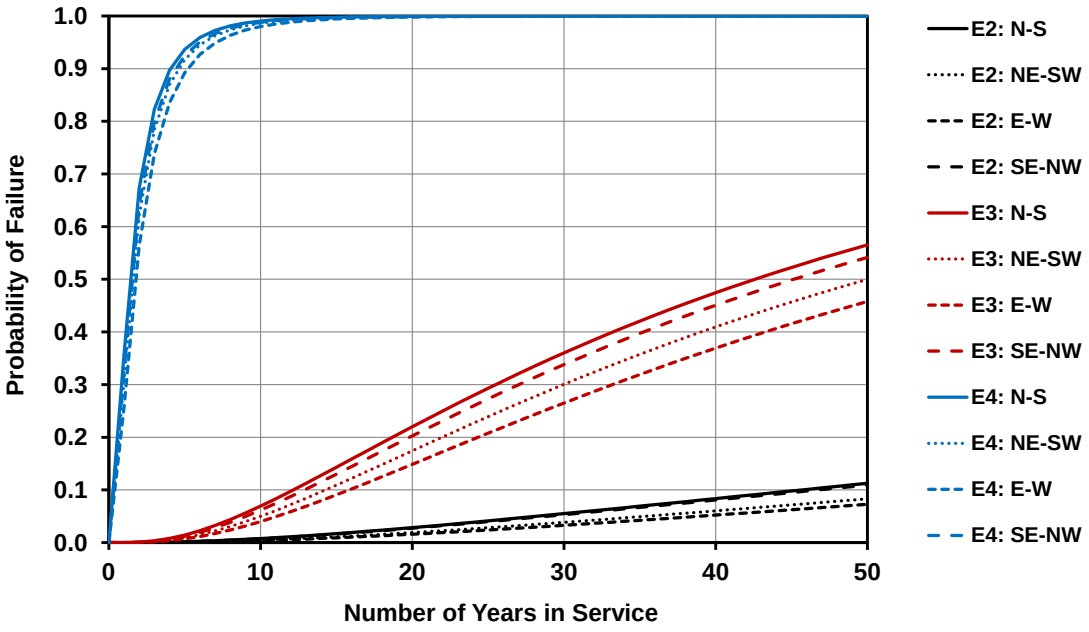

Figure 6.14. Time-zero probabilities of failure for Osseo structure located in Milwaukee, Wisconsin.

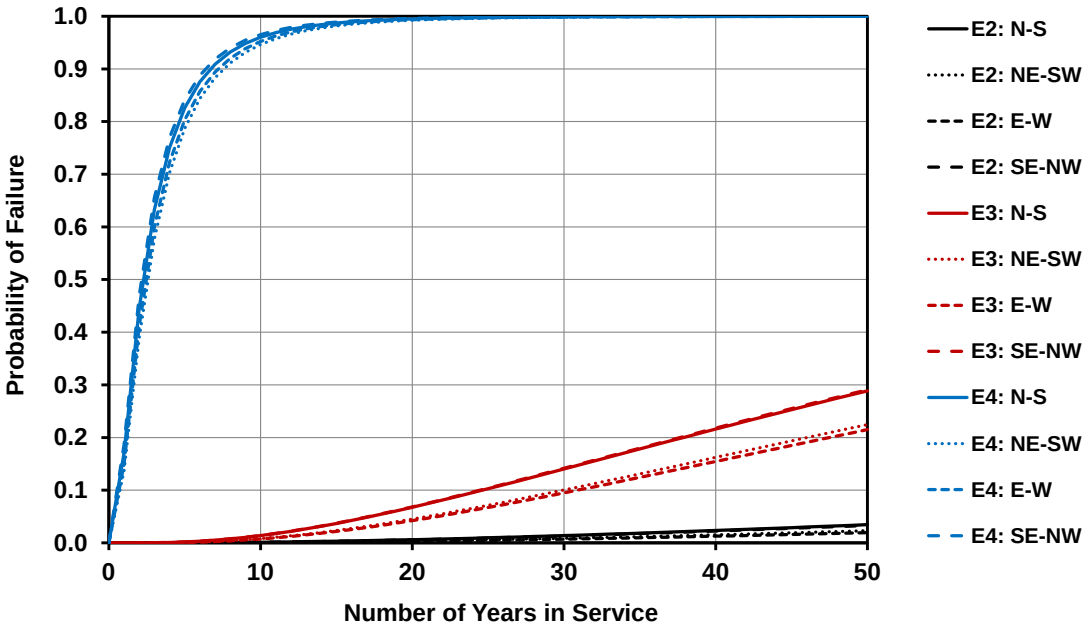

Figure 6.15. Time-zero probabilities of failure for Osseo structure located in Eau Claire, Wisconsin.

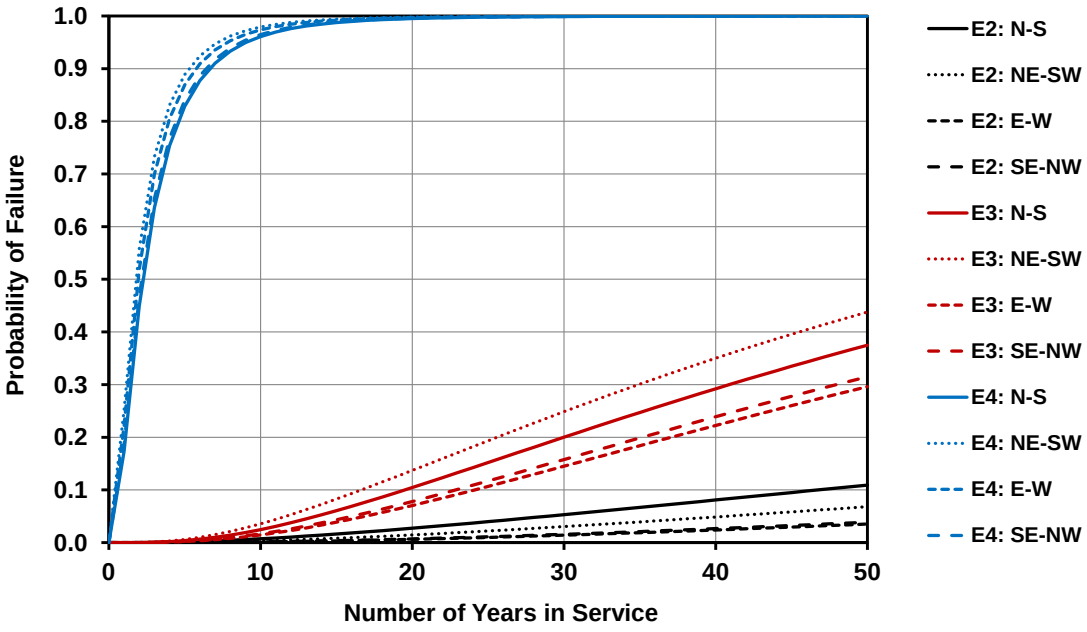

Figure 6.16. Time-zero probabilities of failure for Osseo structure located in La Crosse, Wisconsin.

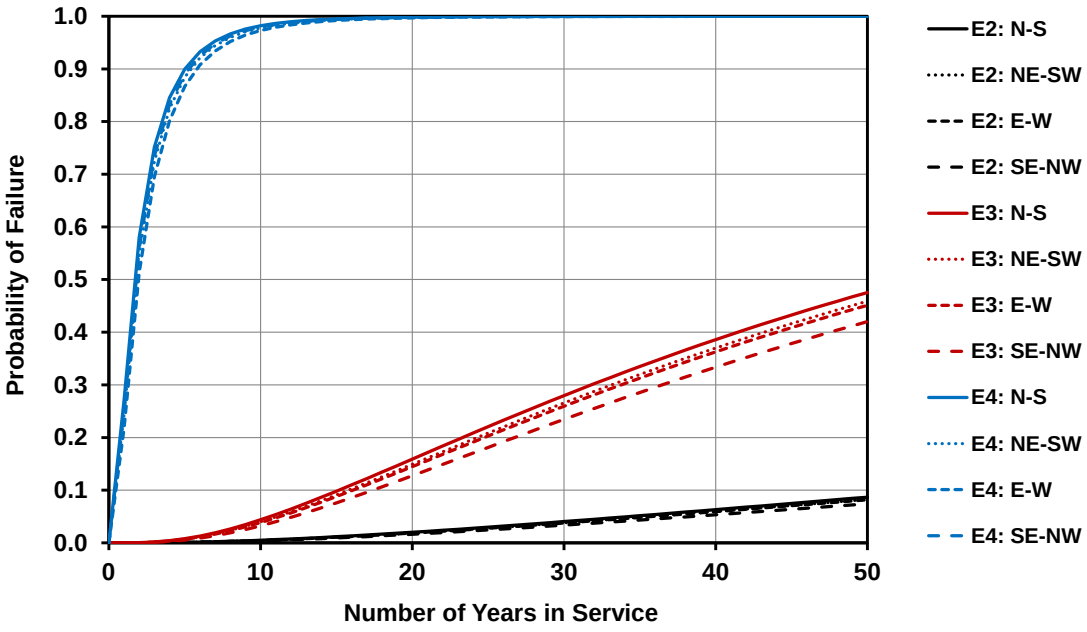

Figure 6.17. Time-zero probabilities of failure for Osseo structure located in Green Bay, Wisconsin.

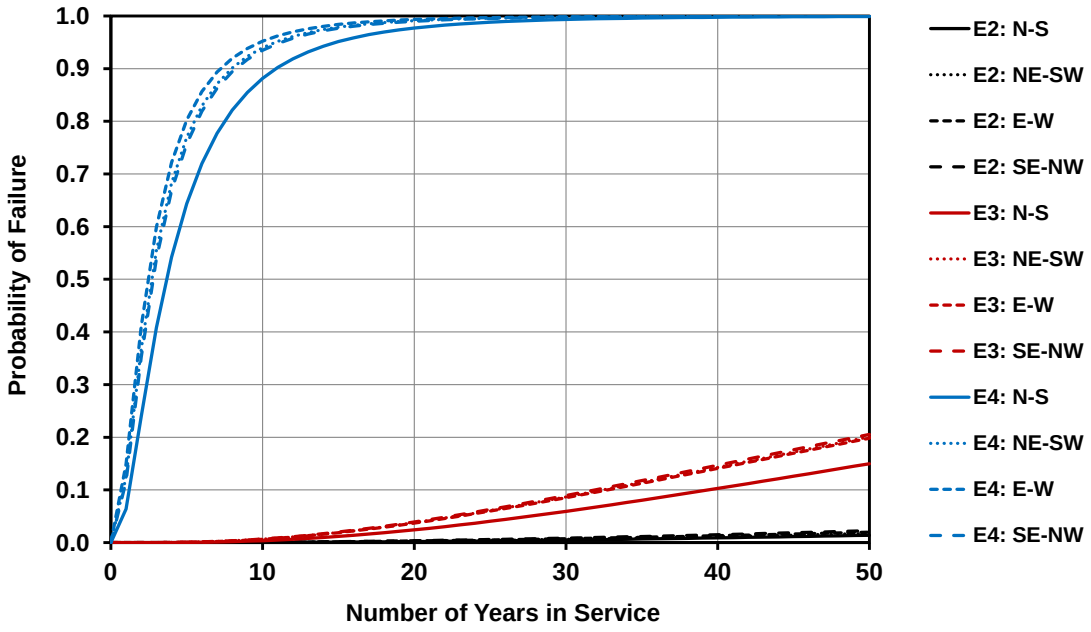

Figure 6.18. Time-zero probabilities of failure for Osseo structure located in Madison, Wisconsin.

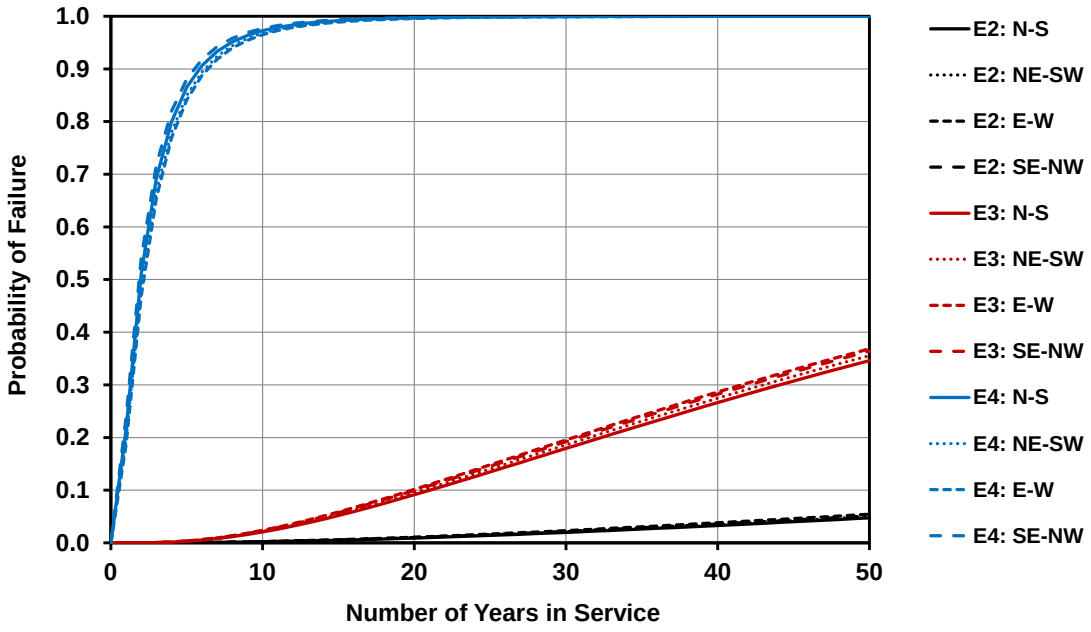

Figure 6.19. Time-zero probabilities of failure for Osseo structure located in Oshkosh, Wisconsin.

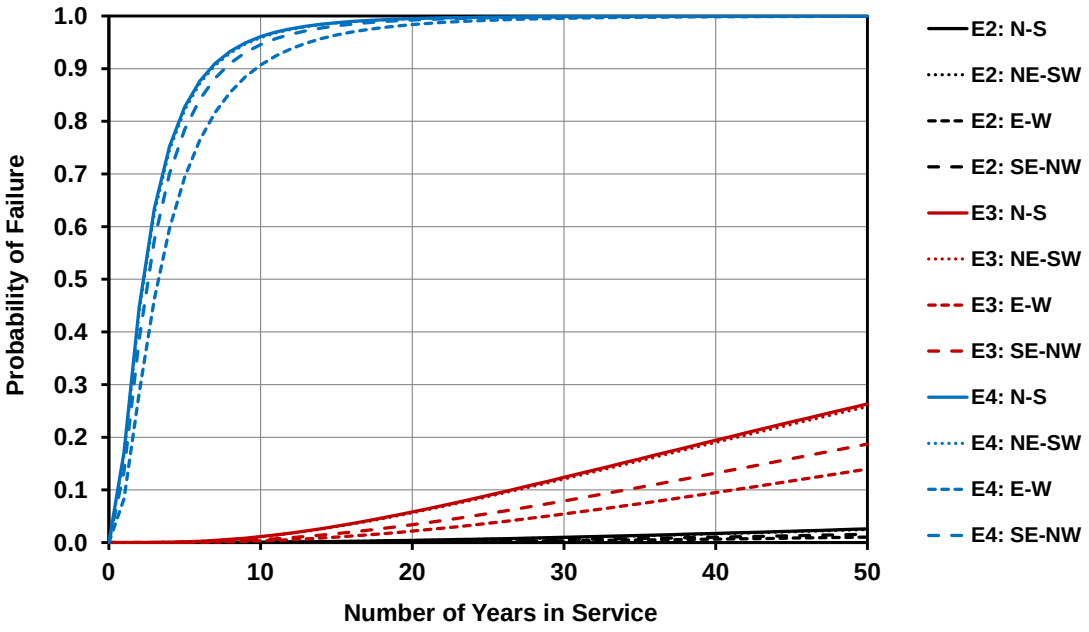

Figure 6.20. Time-zero probabilities of failure for Osseo structure located in Wisconsin Rapids, Wisconsin.

A very useful way to look at Figures 6.7 through 6.20 is to evaluate expected service life (number of years in service) for a single probability of finding a fatigue-induced crack. Service lives expected for a Milwaukee-type structure in Milwaukee, Wisconsin, with three different detail types and four different orientations can be evaluated using Figure 6.7. A 30% probability of finding a fatigue-induced crack can be defined as a threshold for service life expectation. Figure 6.7 illustrates that an E4-type mast-arm connection detail will be expected to have a service life of approximately 1 year with very, very little variability about that one-year life resulting from connection detail behavior and mast-arm orientation. An E3 type detail is expected to have service lives in the range of 5-8 years and this depends, in larger relative extent, to the orientation of the mast arm. The E2 detail type is expected to have service life in the range of 20-28 years depending upon orientation. A holistic view of the information in this figure suggests that one should avoid details that are in the E3 and E4 categories in Milwaukee-type mast arms at this location within the State. The figure also indicates that mast-arms oriented in the N-S

direction will have service lives that are expected to be lower than the other orientations considered.

The effects of mast-arm sign support orientation on the expected service life for a specific detail type (*e.g.* E2) can be studied using these CDFs. As an example, consider the E2 detail type and a Milwaukee-type sign support. Figure 6.8 illustrates that E-W and NE-SW sign orientations in Eau Claire will have substantially similar fatigue life performance. Mast-arms oriented N-S and SE-NW will also have substantially similar performance and will have fatigue lives that are shorter than the mast-arms oriented in the previous two directions. Figure 6.9 illustrates the CDF for the Milwaukee-type sign support in La Crosse, WI. Figure 2.6 (in chapter two) illustrates the wind-speed-direction histograms for La Crosse, WI. It is clear from Figure 2.6 that winds of greater speeds come from the North and South directions. Figure 6.9 illustrates that the service life for a Milwaukee sign support oriented in the NE-SW direction will have the lowest service life in La Crosse. Mast-arms oriented in the E-W direction will have the longest expected service lives. This is clearly consistent with the wind rose histogram in Figure 2.6.

The impact of sign support type (*e.g.* Milwaukee versus Osseo) on the expected fatigue life can be evaluated by examining pairs of CDFs from Figures 6.7 through 6.20. Examination of Figure 6.7 and 6.14 illustrates that the Osseo-type sign support structure with E2 and E3 details will have much better performance than a Milwaukee-type sign when both are located in Milwaukee, Wisconsin. It is interesting to note that E4 details exhibit relatively poor service lives irrespective of sign support type. The expected service performance of the Osseo sign in Eau Claire is also better than a Milwaukee sign type in Eau Claire as illustrated in Figures 6.8 and 6.15 for E2 and E3 detail categories. This behavior is consistent for all cities within Wisconsin. The reason for this is that the Milwaukee-type sign support structure has a much higher state of stress and stress-range magnitudes resulting from wind loading. The Osseo-type sign has a much greater second moment of area and relatively small bluff area subject to wind demand. Therefore,

the stress-ranges are, relatively speaking, much lower. The most important take away from these figures is that the E4 detail type should be avoided in mast-arm sign support structures. Mast-arm-to-pole connections that have bolt holes in a configuration similar to that in the Osseo sign support (*i.e.* rectangular pattern, horizontal orientation, large bolt spacing relative to tube wall) should be avoided.

One characteristic of the CDFs that provides insight with regard to variability in fatigue life is the slope of the CDF. If the slope of the CDF is steep (*e.g.* the E4 detail category in Figures 6.7 and 6.14), it indicates that there will likely be a range of probabilities of failure for a target service life. These two figures indicate that a service life in the range of 1-3 years for the E4 detail category is expected to have probabilities of finding fatigue-induced cracks ranging from 50-75%. This indicates that fatigue-induced cracks are likely to be very difficult to detect during the service of the sign support structure and, in general, should be avoided. The flatter slopes (*i.e.* the E2 and E3 details) indicate that the mast-arm sign support has a better defined probability of failure and greater distinction among different service lives thereby making it easier and more likely for service-life inspection intervals to be lengthened. In the case of Figure 6.7, a service life of 20 years has a probability of fatigue induced crack initiation of 20%, a service life of 25 years has a probability of failure of approximately 30%, and a service life of 30 years has a probability of failure of 35%. The behavior seen in this type of CDF would suggest in-service performance conducive to setting inspection intervals of longer duration than the former E4 detail category.

As longer service lives are reached in the sign support structures, the flattening of the CDF indicates that the limiting service life expectation has been reached. The nearly bilinear nature of the E4 detail CDFs irrespective of location, orientation and sign-type suggests that one should not expect service lives for this type of detail longer than 5 years. In the case of the E2 and E3 detail categories, the service-life limit is more difficult to define because of the flattening of the CDF over longer service life intervals. This suggests that the E2 and E3 details can be

expected to have longer service lives, but that inspection intervals will need to gradually shorten as longer lives are encountered.

These results of this study are reasonable when comparing them to the Osseo fatigue failure described in Appendix A. The significant stress concentration effects generated by the connection configuration within these structures were classified as E4. Figure 6.15 indicates a probability of failure greater than 90% after 8 years of service for an E4 detail, regardless of orientation. With a probability of failure greater than 90%, there is no question as to why cracks were found to have initiated in the connections of both Osseo structures (S-61-001 and S-61-002) after only 8 years of service-life.

6.5 – Reliability-Based Inspection Frequencies

The cumulative distribution functions can be used to establish inspection frequencies for mast-arm sign support structures for various types, various detail configurations, various locations, and various orientations. Inspection protocols can be established in the following manner. All probabilities of failure discussed earlier are based upon time-zero references. In other words, the probabilities of failure are always referenced to an undamaged, un-cracked state at time-zero in the mast-arm's service life. There is no accounting for finding fatigue-induced cracks at a specific time interval and its impact on the service life thereafter. However, the procedure formulated is very valuable as it allows an undamaged sign support installed into service at time-zero to have various probabilities of finding fatigue-induced cracks as the driving parameter defining the inspection interval.

The process begins by defining threshold probabilities for finding fatigue-induced cracks in the mast arm. These threshold probabilities of failure will drive the current discussion and formulations. Two threshold probabilities are defined in the present study: 20% and 50%. Service

lives corresponding to these thresholds can be used to set inspection intervals for mast-arm sign supports. For example, when the probability of finding a fatigue-induced crack is less than 20%, the probability of not finding a crack initiated is 80%. This can be thought of as a lower-threshold that sets the boundary for the first inspection of a mast-arm after installation. The second threshold corresponds to a 50% chance of finding a fatigue-induced crack in the sign support. This, of course, corresponds to a 50% chance of not finding a crack. The 50/50 breakpoint can then be defined as the service-life interval when a traditional four-year inspection cycle might begin. The time interval in between first inspection and four-year inspections can be very wide, or can be very narrow depending upon the detail configuration found in the sign support, its orientation, its location, and its type (*i.e.* Milwaukee-type or Osseo-type).

Tables 6.3 through 6.9 include tabulated time-zero probabilities of finding fatigue induced cracks in mast arm sign supports with the Milwaukee configuration as a function of service life, orientation, location, and detail category type. Tables 6.10 through 6.16 include these same probabilities for Osseo configurations. The 20% and 50% thresholds are used to color service life intervals as green, yellow and red. The green regions suggest that inspections not occur until the yellow regions are encountered at which point it is suggested to tighten the inspection interval somewhat. Finally, it is recommended that sign supports beyond the 50/50 breakpoint be inspected at a minimum of four-year intervals.

Table 6.3. Time-zero probabilities of failure for Milwaukee structure located in Milwaukee, Wisconsin.

Location: Milwaukee							Latitude: 42.9550°					
							Longitude: -87.9044°					
Number of Years in Service	Orientation of Sign: N-S			Orientation of Sign: NE-SW			Orientation of Sign: E-W			Orientation of Sign: SE-NW		
	Probability of Failure			Probability of Failure			Probability of Failure			Probability of Failure		
	E2	E3	E4	E2	E3	E4	E2	E3	E4	E2	E3	E4
0	0.000	0.000	0.000	0.000	0.000	0.000	0.000	0.000	0.000	0.000	0.000	0.000
1	0.003	0.010	0.724	0.002	0.007	0.676	0.001	0.005	0.620	0.003	0.008	0.694
2	0.012	0.053	0.921	0.008	0.038	0.898	0.007	0.030	0.869	0.012	0.046	0.907
3	0.026	0.114	0.970	0.018	0.087	0.960	0.015	0.071	0.945	0.025	0.103	0.964
4	0.043	0.182	0.987	0.030	0.143	0.981	0.026	0.120	0.974	0.040	0.165	0.984
5	0.060	0.248	0.994	0.044	0.201	0.991	0.037	0.172	0.986	0.057	0.228	0.992
6	0.079	0.310	0.997	0.058	0.257	0.995	0.050	0.224	0.992	0.075	0.288	0.996
7	0.097	0.368	0.998	0.073	0.311	0.997	0.063	0.274	0.995	0.093	0.344	0.997
8	0.116	0.421	0.999	0.088	0.360	0.998	0.077	0.321	0.997	0.111	0.396	0.998
9	0.134	0.468	0.999	0.103	0.406	0.999	0.090	0.366	0.998	0.128	0.443	0.999
10	0.152	0.511	1.000	0.118	0.449	0.999	0.104	0.407	0.999	0.146	0.485	0.999
11	0.169	0.550	1.000	0.133	0.487	0.999	0.118	0.445	0.999	0.163	0.524	1.000
12	0.187	0.585	1.000	0.147	0.523	1.000	0.131	0.480	0.999	0.180	0.559	1.000
13	0.203	0.616	1.000	0.162	0.555	1.000	0.144	0.513	1.000	0.196	0.592	1.000
14	0.219	0.645	1.000	0.176	0.585	1.000	0.157	0.543	1.000	0.212	0.621	1.000
15	0.235	0.671	1.000	0.189	0.612	1.000	0.170	0.571	1.000	0.227	0.647	1.000
16	0.250	0.694	1.000	0.203	0.637	1.000	0.183	0.597	1.000	0.242	0.671	1.000
17	0.265	0.716	1.000	0.216	0.660	1.000	0.195	0.620	1.000	0.257	0.693	1.000
18	0.279	0.735	1.000	0.229	0.681	1.000	0.207	0.642	1.000	0.271	0.714	1.000
19	0.293	0.753	1.000	0.242	0.701	1.000	0.219	0.663	1.000	0.284	0.732	1.000
20	0.307	0.769	1.000	0.254	0.719	1.000	0.231	0.682	1.000	0.298	0.749	1.000
21	0.320	0.784	1.000	0.266	0.735	1.000	0.242	0.699	1.000	0.310	0.765	1.000
22	0.332	0.798	1.000	0.277	0.751	1.000	0.253	0.716	1.000	0.323	0.779	1.000
23	0.345	0.810	1.000	0.289	0.765	1.000	0.264	0.731	1.000	0.335	0.792	1.000
24	0.357	0.822	1.000	0.300	0.778	1.000	0.275	0.745	1.000	0.347	0.805	1.000
25	0.368	0.833	1.000	0.311	0.790	1.000	0.285	0.758	1.000	0.358	0.816	1.000
26	0.379	0.842	1.000	0.321	0.802	1.000	0.295	0.771	1.000	0.369	0.826	1.000
27	0.390	0.852	1.000	0.331	0.812	1.000	0.305	0.782	1.000	0.380	0.836	1.000
28	0.401	0.860	1.000	0.341	0.822	1.000	0.315	0.793	1.000	0.391	0.845	1.000
29	0.411	0.868	1.000	0.351	0.831	1.000	0.324	0.803	1.000	0.401	0.853	1.000
30	0.421	0.875	1.000	0.361	0.840	1.000	0.334	0.812	1.000	0.411	0.861	1.000
31	0.431	0.882	1.000	0.370	0.848	1.000	0.343	0.821	1.000	0.420	0.869	1.000
32	0.440	0.888	1.000	0.379	0.855	1.000	0.352	0.830	1.000	0.430	0.875	1.000
33	0.449	0.894	1.000	0.388	0.862	1.000	0.360	0.838	1.000	0.439	0.882	1.000
34	0.458	0.899	1.000	0.397	0.869	1.000	0.369	0.845	1.000	0.448	0.888	1.000
35	0.467	0.905	1.000	0.405	0.875	1.000	0.377	0.852	1.000	0.457	0.893	1.000
36	0.475	0.909	1.000	0.413	0.881	1.000	0.385	0.858	1.000	0.465	0.898	1.000
37	0.484	0.914	1.000	0.421	0.886	1.000	0.393	0.865	1.000	0.473	0.903	1.000
38	0.492	0.918	1.000	0.429	0.892	1.000	0.401	0.870	1.000	0.481	0.908	1.000
39	0.499	0.922	1.000	0.437	0.896	1.000	0.408	0.876	1.000	0.489	0.912	1.000
40	0.507	0.926	1.000	0.444	0.901	1.000	0.416	0.881	1.000	0.497	0.916	1.000
41	0.515	0.929	1.000	0.452	0.905	1.000	0.423	0.886	1.000	0.504	0.920	1.000
42	0.522	0.932	1.000	0.459	0.909	1.000	0.430	0.891	1.000	0.511	0.924	1.000
43	0.529	0.936	1.000	0.466	0.913	1.000	0.437	0.895	1.000	0.518	0.927	1.000
44	0.536	0.938	1.000	0.473	0.917	1.000	0.444	0.899	1.000	0.525	0.930	1.000
45	0.542	0.941	1.000	0.480	0.920	1.000	0.451	0.903	1.000	0.532	0.933	1.000
46	0.549	0.944	1.000	0.486	0.924	1.000	0.457	0.907	1.000	0.539	0.936	1.000
47	0.555	0.946	1.000	0.493	0.927	1.000	0.464	0.911	1.000	0.545	0.939	1.000
48	0.562	0.949	1.000	0.499	0.930	1.000	0.470	0.914	1.000	0.551	0.941	1.000
49	0.568	0.951	1.000	0.505	0.933	1.000	0.476	0.917	1.000	0.558	0.944	1.000
50	0.574	0.953	1.000	0.511	0.935	1.000	0.482	0.921	1.000	0.564	0.946	1.000

Table 6.4. Time-zero probabilities of failure for Milwaukee structure located in Eau Claire, Wisconsin.

Location: Eau Claire							Latitude: 44.8664°					
							Longitude: -91.4878°					
Number of Years in Service	Orientation of Sign: N-S			Orientation of Sign: NE-SW			Orientation of Sign: E-W			Orientation of Sign: SE-NW		
	Probability of Failure			Probability of Failure			Probability of Failure			Probability of Failure		
	E2	E3	E4	E2	E3	E4	E2	E3	E4	E2	E3	E4
0	0.000	0.000	0.000	0.000	0.000	0.000	0.000	0.000	0.000	0.000	0.000	0.000
1	0.000	0.001	0.506	0.000	0.001	0.450	0.000	0.001	0.474	0.000	0.001	0.531
2	0.002	0.010	0.797	0.001	0.006	0.755	0.001	0.006	0.773	0.002	0.010	0.814
3	0.006	0.028	0.904	0.004	0.018	0.878	0.003	0.017	0.890	0.006	0.029	0.915
4	0.010	0.053	0.950	0.007	0.035	0.934	0.005	0.033	0.941	0.010	0.054	0.956
5	0.016	0.083	0.972	0.010	0.057	0.961	0.009	0.054	0.966	0.016	0.084	0.976
6	0.023	0.115	0.983	0.015	0.082	0.976	0.013	0.078	0.979	0.022	0.117	0.985
7	0.030	0.148	0.989	0.020	0.108	0.985	0.017	0.104	0.987	0.029	0.151	0.991
8	0.037	0.182	0.993	0.025	0.136	0.990	0.022	0.131	0.991	0.036	0.185	0.994
9	0.045	0.216	0.995	0.031	0.164	0.993	0.027	0.158	0.994	0.043	0.219	0.996
10	0.053	0.249	0.997	0.037	0.192	0.995	0.032	0.185	0.996	0.051	0.252	0.997
11	0.061	0.280	0.998	0.043	0.220	0.996	0.038	0.212	0.997	0.059	0.284	0.998
12	0.069	0.311	0.998	0.050	0.247	0.997	0.043	0.239	0.998	0.067	0.314	0.999
13	0.078	0.341	0.999	0.056	0.273	0.998	0.049	0.265	0.998	0.076	0.344	0.999
14	0.086	0.369	0.999	0.063	0.299	0.999	0.055	0.291	0.999	0.084	0.372	0.999
15	0.095	0.396	0.999	0.069	0.324	0.999	0.061	0.315	0.999	0.092	0.399	0.999
16	0.103	0.421	0.999	0.076	0.348	0.999	0.067	0.339	0.999	0.101	0.425	1.000
17	0.112	0.446	1.000	0.083	0.371	0.999	0.073	0.362	0.999	0.109	0.449	1.000
18	0.120	0.469	1.000	0.090	0.393	0.999	0.079	0.384	1.000	0.117	0.473	1.000
19	0.128	0.491	1.000	0.096	0.415	1.000	0.086	0.405	1.000	0.125	0.495	1.000
20	0.137	0.512	1.000	0.103	0.435	1.000	0.092	0.426	1.000	0.133	0.516	1.000
21	0.145	0.532	1.000	0.110	0.455	1.000	0.098	0.445	1.000	0.142	0.535	1.000
22	0.153	0.550	1.000	0.117	0.474	1.000	0.104	0.464	1.000	0.150	0.554	1.000
23	0.161	0.568	1.000	0.123	0.492	1.000	0.111	0.482	1.000	0.158	0.572	1.000
24	0.169	0.585	1.000	0.130	0.509	1.000	0.117	0.500	1.000	0.165	0.589	1.000
25	0.177	0.602	1.000	0.137	0.526	1.000	0.123	0.516	1.000	0.173	0.605	1.000
26	0.185	0.617	1.000	0.143	0.542	1.000	0.129	0.532	1.000	0.181	0.621	1.000
27	0.193	0.632	1.000	0.150	0.557	1.000	0.135	0.548	1.000	0.188	0.635	1.000
28	0.200	0.646	1.000	0.156	0.572	1.000	0.141	0.562	1.000	0.196	0.649	1.000
29	0.208	0.659	1.000	0.163	0.586	1.000	0.147	0.576	1.000	0.203	0.662	1.000
30	0.215	0.671	1.000	0.169	0.599	1.000	0.153	0.590	1.000	0.211	0.675	1.000
31	0.222	0.683	1.000	0.175	0.612	1.000	0.159	0.603	1.000	0.218	0.687	1.000
32	0.230	0.695	1.000	0.182	0.625	1.000	0.165	0.615	1.000	0.225	0.698	1.000
33	0.237	0.706	1.000	0.188	0.636	1.000	0.171	0.627	1.000	0.232	0.709	1.000
34	0.244	0.716	1.000	0.194	0.648	1.000	0.177	0.639	1.000	0.239	0.719	1.000
35	0.251	0.726	1.000	0.200	0.659	1.000	0.182	0.650	1.000	0.246	0.729	1.000
36	0.257	0.736	1.000	0.206	0.669	1.000	0.188	0.660	1.000	0.252	0.739	1.000
37	0.264	0.745	1.000	0.212	0.679	1.000	0.194	0.671	1.000	0.259	0.748	1.000
38	0.271	0.753	1.000	0.218	0.689	1.000	0.199	0.680	1.000	0.266	0.756	1.000
39	0.277	0.762	1.000	0.224	0.698	1.000	0.205	0.690	1.000	0.272	0.765	1.000
40	0.284	0.770	1.000	0.230	0.707	1.000	0.210	0.699	1.000	0.279	0.773	1.000
41	0.290	0.777	1.000	0.235	0.716	1.000	0.216	0.708	1.000	0.285	0.780	1.000
42	0.296	0.785	1.000	0.241	0.724	1.000	0.221	0.716	1.000	0.291	0.787	1.000
43	0.302	0.792	1.000	0.246	0.732	1.000	0.226	0.724	1.000	0.297	0.794	1.000
44	0.309	0.798	1.000	0.252	0.740	1.000	0.231	0.732	1.000	0.303	0.801	1.000
45	0.315	0.805	1.000	0.257	0.747	1.000	0.237	0.739	1.000	0.309	0.807	1.000
46	0.320	0.811	1.000	0.263	0.754	1.000	0.242	0.747	1.000	0.315	0.813	1.000
47	0.326	0.817	1.000	0.268	0.761	1.000	0.247	0.754	1.000	0.321	0.819	1.000
48	0.332	0.822	1.000	0.273	0.768	1.000	0.252	0.760	1.000	0.326	0.825	1.000
49	0.338	0.828	1.000	0.279	0.774	1.000	0.257	0.767	1.000	0.332	0.830	1.000
50	0.343	0.833	1.000	0.284	0.780	1.000	0.262	0.773	1.000	0.338	0.835	1.000

Table 6.5. Time-zero probabilities of failure for Milwaukee structure located in La Crosse, Wisconsin.

Location: La Crosse							Latitude: 43.8788°					
							Longitude: -91.2527°					
Number of Years in Service	Orientation of Sign: N-S			Orientation of Sign: NE-SW			Orientation of Sign: E-W			Orientation of Sign: SE-NW		
	Probability of Failure			Probability of Failure			Probability of Failure			Probability of Failure		
	E2	E3	E4	E2	E3	E4	E2	E3	E4	E2	E3	E4
0	0.000	0.000	0.000	0.000	0.000	0.000	0.000	0.000	0.000	0.000	0.000	0.000
1	0.001	0.002	0.506	0.001	0.004	0.614	0.000	0.001	0.581	0.000	0.002	0.528
2	0.005	0.018	0.797	0.006	0.027	0.865	0.002	0.011	0.846	0.003	0.012	0.812
3	0.011	0.046	0.904	0.014	0.064	0.943	0.006	0.029	0.933	0.007	0.033	0.913
4	0.019	0.082	0.950	0.023	0.110	0.973	0.011	0.055	0.967	0.012	0.062	0.955
5	0.028	0.122	0.972	0.034	0.160	0.985	0.017	0.086	0.982	0.018	0.095	0.975
6	0.038	0.164	0.983	0.046	0.209	0.992	0.023	0.119	0.990	0.026	0.131	0.985
7	0.049	0.206	0.989	0.059	0.257	0.995	0.030	0.153	0.994	0.033	0.167	0.991
8	0.060	0.247	0.993	0.072	0.303	0.997	0.038	0.188	0.996	0.042	0.203	0.994
9	0.071	0.286	0.995	0.084	0.346	0.998	0.046	0.222	0.997	0.050	0.239	0.996
10	0.083	0.324	0.997	0.097	0.387	0.999	0.054	0.255	0.998	0.059	0.274	0.997
11	0.094	0.360	0.998	0.110	0.424	0.999	0.063	0.288	0.999	0.068	0.307	0.998
12	0.106	0.393	0.998	0.123	0.460	0.999	0.071	0.319	0.999	0.077	0.339	0.999
13	0.117	0.425	0.999	0.136	0.492	1.000	0.080	0.348	0.999	0.086	0.369	0.999
14	0.128	0.455	0.999	0.149	0.522	1.000	0.088	0.377	1.000	0.095	0.398	0.999
15	0.140	0.483	0.999	0.161	0.550	1.000	0.097	0.404	1.000	0.104	0.426	0.999
16	0.151	0.509	0.999	0.173	0.576	1.000	0.105	0.430	1.000	0.113	0.452	1.000
17	0.162	0.534	1.000	0.185	0.600	1.000	0.114	0.454	1.000	0.122	0.476	1.000
18	0.172	0.557	1.000	0.197	0.623	1.000	0.123	0.477	1.000	0.131	0.500	1.000
19	0.183	0.579	1.000	0.208	0.644	1.000	0.131	0.499	1.000	0.140	0.522	1.000
20	0.193	0.599	1.000	0.220	0.663	1.000	0.139	0.520	1.000	0.149	0.542	1.000
21	0.204	0.618	1.000	0.231	0.681	1.000	0.148	0.540	1.000	0.158	0.562	1.000
22	0.214	0.636	1.000	0.242	0.698	1.000	0.156	0.559	1.000	0.166	0.581	1.000
23	0.224	0.653	1.000	0.252	0.713	1.000	0.164	0.577	1.000	0.175	0.599	1.000
24	0.233	0.669	1.000	0.263	0.728	1.000	0.172	0.594	1.000	0.183	0.615	1.000
25	0.243	0.684	1.000	0.273	0.742	1.000	0.180	0.610	1.000	0.192	0.631	1.000
26	0.252	0.698	1.000	0.283	0.755	1.000	0.188	0.625	1.000	0.200	0.646	1.000
27	0.262	0.712	1.000	0.292	0.766	1.000	0.196	0.640	1.000	0.208	0.660	1.000
28	0.271	0.724	1.000	0.302	0.778	1.000	0.204	0.653	1.000	0.216	0.674	1.000
29	0.279	0.736	1.000	0.311	0.788	1.000	0.211	0.666	1.000	0.224	0.687	1.000
30	0.288	0.747	1.000	0.320	0.798	1.000	0.219	0.679	1.000	0.231	0.699	1.000
31	0.297	0.758	1.000	0.329	0.807	1.000	0.226	0.691	1.000	0.239	0.710	1.000
32	0.305	0.768	1.000	0.338	0.816	1.000	0.233	0.702	1.000	0.246	0.721	1.000
33	0.313	0.777	1.000	0.346	0.824	1.000	0.240	0.713	1.000	0.254	0.732	1.000
34	0.321	0.786	1.000	0.355	0.832	1.000	0.247	0.723	1.000	0.261	0.742	1.000
35	0.329	0.795	1.000	0.363	0.840	1.000	0.254	0.733	1.000	0.268	0.751	1.000
36	0.337	0.803	1.000	0.371	0.846	1.000	0.261	0.743	1.000	0.275	0.760	1.000
37	0.344	0.811	1.000	0.379	0.853	1.000	0.268	0.752	1.000	0.282	0.769	1.000
38	0.352	0.818	1.000	0.386	0.859	1.000	0.275	0.760	1.000	0.289	0.777	1.000
39	0.359	0.825	1.000	0.394	0.865	1.000	0.281	0.768	1.000	0.296	0.785	1.000
40	0.366	0.831	1.000	0.401	0.871	1.000	0.288	0.776	1.000	0.302	0.793	1.000
41	0.373	0.838	1.000	0.408	0.876	1.000	0.294	0.784	1.000	0.309	0.800	1.000
42	0.380	0.844	1.000	0.415	0.881	1.000	0.300	0.791	1.000	0.315	0.807	1.000
43	0.387	0.849	1.000	0.422	0.886	1.000	0.307	0.798	1.000	0.322	0.813	1.000
44	0.393	0.855	1.000	0.429	0.890	1.000	0.313	0.804	1.000	0.328	0.819	1.000
45	0.400	0.860	1.000	0.436	0.894	1.000	0.319	0.810	1.000	0.334	0.825	1.000
46	0.406	0.865	1.000	0.442	0.898	1.000	0.325	0.816	1.000	0.340	0.831	1.000
47	0.413	0.870	1.000	0.449	0.902	1.000	0.331	0.822	1.000	0.346	0.836	1.000
48	0.419	0.874	1.000	0.455	0.906	1.000	0.336	0.828	1.000	0.352	0.842	1.000
49	0.425	0.878	1.000	0.461	0.909	1.000	0.342	0.833	1.000	0.358	0.847	1.000
50	0.431	0.883	1.000	0.467	0.913	1.000	0.348	0.838	1.000	0.364	0.852	1.000

Table 6.6. Time-zero probabilities of failure for Milwaukee structure located in Green Bay, Wisconsin.

Location: Green Bay							Latitude: 44.4794°					
							Longitude: -88.1366°					
Number of Years in Service	Orientation of Sign: N-S			Orientation of Sign: NE-SW			Orientation of Sign: E-W			Orientation of Sign: SE-NW		
	Probability of Failure			Probability of Failure			Probability of Failure			Probability of Failure		
	E2	E3	E4	E2	E3	E4	E2	E3	E4	E2	E3	E4
0	0.000	0.000	0.000	0.000	0.000	0.000	0.000	0.000	0.000	0.000	0.000	0.000
1	0.002	0.005	0.636	0.002	0.005	0.605	0.002	0.004	0.570	0.001	0.003	0.619
2	0.008	0.032	0.878	0.008	0.029	0.860	0.008	0.028	0.839	0.006	0.023	0.868
3	0.018	0.076	0.949	0.017	0.070	0.940	0.017	0.067	0.929	0.015	0.057	0.944
4	0.031	0.127	0.976	0.029	0.119	0.971	0.028	0.114	0.964	0.025	0.099	0.973
5	0.044	0.181	0.987	0.042	0.170	0.984	0.041	0.164	0.981	0.037	0.145	0.986
6	0.059	0.234	0.993	0.055	0.221	0.991	0.055	0.214	0.989	0.049	0.191	0.992
7	0.073	0.285	0.996	0.070	0.271	0.995	0.069	0.263	0.993	0.062	0.237	0.995
8	0.089	0.333	0.997	0.084	0.318	0.997	0.083	0.309	0.996	0.075	0.281	0.997
9	0.104	0.378	0.998	0.099	0.362	0.998	0.098	0.353	0.997	0.089	0.323	0.998
10	0.119	0.420	0.999	0.113	0.403	0.999	0.112	0.394	0.998	0.102	0.363	0.999
11	0.134	0.458	0.999	0.128	0.441	0.999	0.126	0.432	0.999	0.115	0.400	0.999
12	0.148	0.493	0.999	0.142	0.476	0.999	0.141	0.467	0.999	0.129	0.434	0.999
13	0.163	0.526	1.000	0.156	0.509	0.999	0.154	0.499	0.999	0.142	0.467	1.000
14	0.177	0.556	1.000	0.170	0.539	1.000	0.168	0.530	0.999	0.155	0.497	1.000
15	0.191	0.584	1.000	0.183	0.567	1.000	0.182	0.557	1.000	0.168	0.525	1.000
16	0.204	0.609	1.000	0.197	0.593	1.000	0.195	0.583	1.000	0.180	0.551	1.000
17	0.217	0.633	1.000	0.209	0.617	1.000	0.207	0.607	1.000	0.192	0.576	1.000
18	0.230	0.655	1.000	0.222	0.639	1.000	0.220	0.630	1.000	0.204	0.598	1.000
19	0.243	0.675	1.000	0.234	0.659	1.000	0.232	0.650	1.000	0.216	0.620	1.000
20	0.255	0.693	1.000	0.246	0.678	1.000	0.244	0.670	1.000	0.228	0.639	1.000
21	0.267	0.711	1.000	0.258	0.696	1.000	0.256	0.687	1.000	0.239	0.658	1.000
22	0.279	0.727	1.000	0.270	0.712	1.000	0.267	0.704	1.000	0.250	0.675	1.000
23	0.290	0.742	1.000	0.281	0.728	1.000	0.279	0.720	1.000	0.261	0.691	1.000
24	0.301	0.756	1.000	0.292	0.742	1.000	0.289	0.734	1.000	0.271	0.707	1.000
25	0.312	0.768	1.000	0.302	0.755	1.000	0.300	0.748	1.000	0.281	0.721	1.000
26	0.323	0.781	1.000	0.313	0.768	1.000	0.310	0.760	1.000	0.292	0.734	1.000
27	0.333	0.792	1.000	0.323	0.779	1.000	0.321	0.772	1.000	0.301	0.747	1.000
28	0.343	0.802	1.000	0.333	0.790	1.000	0.330	0.783	1.000	0.311	0.758	1.000
29	0.353	0.812	1.000	0.343	0.800	1.000	0.340	0.793	1.000	0.320	0.769	1.000
30	0.362	0.821	1.000	0.352	0.810	1.000	0.350	0.803	1.000	0.330	0.780	1.000
31	0.372	0.830	1.000	0.361	0.819	1.000	0.359	0.812	1.000	0.339	0.790	1.000
32	0.381	0.838	1.000	0.370	0.827	1.000	0.368	0.821	1.000	0.347	0.799	1.000
33	0.389	0.846	1.000	0.379	0.835	1.000	0.376	0.829	1.000	0.356	0.808	1.000
34	0.398	0.853	1.000	0.388	0.843	1.000	0.385	0.837	1.000	0.364	0.816	1.000
35	0.407	0.859	1.000	0.396	0.850	1.000	0.393	0.844	1.000	0.373	0.824	1.000
36	0.415	0.866	1.000	0.404	0.856	1.000	0.402	0.851	1.000	0.381	0.831	1.000
37	0.423	0.872	1.000	0.412	0.863	1.000	0.410	0.857	1.000	0.389	0.838	1.000
38	0.431	0.877	1.000	0.420	0.868	1.000	0.417	0.863	1.000	0.396	0.844	1.000
39	0.439	0.883	1.000	0.428	0.874	1.000	0.425	0.869	1.000	0.404	0.851	1.000
40	0.446	0.888	1.000	0.435	0.879	1.000	0.433	0.874	1.000	0.411	0.857	1.000
41	0.453	0.892	1.000	0.443	0.884	1.000	0.440	0.879	1.000	0.419	0.862	1.000
42	0.461	0.897	1.000	0.450	0.889	1.000	0.447	0.884	1.000	0.426	0.868	1.000
43	0.468	0.901	1.000	0.457	0.894	1.000	0.454	0.889	1.000	0.433	0.873	1.000
44	0.475	0.905	1.000	0.464	0.898	1.000	0.461	0.893	1.000	0.440	0.878	1.000
45	0.481	0.909	1.000	0.471	0.902	1.000	0.468	0.898	1.000	0.446	0.882	1.000
46	0.488	0.913	1.000	0.477	0.906	1.000	0.474	0.901	1.000	0.453	0.887	1.000
47	0.494	0.916	1.000	0.484	0.909	1.000	0.481	0.905	1.000	0.459	0.891	1.000
48	0.501	0.919	1.000	0.490	0.913	1.000	0.487	0.909	1.000	0.466	0.895	1.000
49	0.507	0.922	1.000	0.496	0.916	1.000	0.493	0.912	1.000	0.472	0.898	1.000
50	0.513	0.925	1.000	0.502	0.919	1.000	0.499	0.915	1.000	0.478	0.902	1.000

Table 6.7. Time-zero probabilities of failure for Milwaukee structure located in Madison, Wisconsin.

Location: Madison							Latitude: 43.1405°					
							Longitude: -89.3452°					
Number of Years in Service	Orientation of Sign: N-S			Orientation of Sign: NE-SW			Orientation of Sign: E-W			Orientation of Sign: SE-NW		
	Probability of Failure			Probability of Failure			Probability of Failure			Probability of Failure		
	E2	E3	E4	E2	E3	E4	E2	E3	E4	E2	E3	E4
0	0.000	0.000	0.000	0.000	0.000	0.000	0.000	0.000	0.000	0.000	0.000	0.000
1	0.000	0.000	0.289	0.000	0.000	0.427	0.000	0.000	0.473	0.000	0.000	0.414
2	0.001	0.003	0.602	0.001	0.005	0.736	0.001	0.005	0.773	0.001	0.005	0.725
3	0.002	0.008	0.769	0.003	0.015	0.866	0.003	0.015	0.889	0.003	0.015	0.859
4	0.004	0.018	0.858	0.005	0.030	0.926	0.006	0.030	0.941	0.006	0.030	0.921
5	0.006	0.031	0.909	0.008	0.049	0.956	0.009	0.049	0.966	0.010	0.049	0.953
6	0.009	0.047	0.939	0.011	0.071	0.973	0.013	0.071	0.979	0.014	0.071	0.970
7	0.012	0.064	0.958	0.015	0.095	0.982	0.017	0.095	0.987	0.019	0.095	0.981
8	0.015	0.083	0.970	0.020	0.120	0.988	0.022	0.120	0.991	0.024	0.120	0.987
9	0.019	0.103	0.979	0.024	0.146	0.992	0.027	0.146	0.994	0.030	0.146	0.991
10	0.023	0.124	0.984	0.029	0.172	0.994	0.032	0.172	0.996	0.036	0.172	0.994
11	0.027	0.145	0.988	0.035	0.198	0.996	0.038	0.198	0.997	0.042	0.198	0.995
12	0.032	0.166	0.991	0.040	0.224	0.997	0.043	0.223	0.998	0.048	0.224	0.997
13	0.036	0.187	0.993	0.045	0.249	0.998	0.049	0.249	0.998	0.054	0.249	0.997
14	0.041	0.208	0.995	0.051	0.273	0.998	0.055	0.273	0.999	0.061	0.273	0.998
15	0.046	0.229	0.996	0.057	0.297	0.999	0.061	0.297	0.999	0.067	0.297	0.998
16	0.051	0.249	0.997	0.062	0.321	0.999	0.067	0.320	0.999	0.074	0.321	0.999
17	0.056	0.270	0.997	0.068	0.343	0.999	0.073	0.343	0.999	0.080	0.343	0.999
18	0.061	0.289	0.998	0.074	0.365	0.999	0.080	0.364	1.000	0.087	0.365	0.999
19	0.066	0.308	0.998	0.080	0.386	0.999	0.086	0.385	1.000	0.094	0.386	0.999
20	0.071	0.327	0.998	0.086	0.406	1.000	0.092	0.406	1.000	0.100	0.406	1.000
21	0.076	0.345	0.999	0.092	0.425	1.000	0.098	0.425	1.000	0.107	0.425	1.000
22	0.081	0.363	0.999	0.098	0.444	1.000	0.105	0.444	1.000	0.114	0.444	1.000
23	0.086	0.380	0.999	0.104	0.462	1.000	0.111	0.462	1.000	0.120	0.462	1.000
24	0.092	0.397	0.999	0.110	0.479	1.000	0.117	0.479	1.000	0.127	0.480	1.000
25	0.097	0.413	0.999	0.115	0.496	1.000	0.123	0.496	1.000	0.133	0.496	1.000
26	0.102	0.429	0.999	0.121	0.512	1.000	0.129	0.512	1.000	0.140	0.512	1.000
27	0.107	0.444	1.000	0.127	0.527	1.000	0.135	0.527	1.000	0.146	0.528	1.000
28	0.112	0.459	1.000	0.133	0.542	1.000	0.141	0.542	1.000	0.153	0.542	1.000
29	0.117	0.473	1.000	0.139	0.556	1.000	0.147	0.556	1.000	0.159	0.556	1.000
30	0.123	0.487	1.000	0.144	0.570	1.000	0.153	0.570	1.000	0.165	0.570	1.000
31	0.128	0.500	1.000	0.150	0.583	1.000	0.159	0.583	1.000	0.171	0.583	1.000
32	0.133	0.513	1.000	0.156	0.596	1.000	0.165	0.595	1.000	0.178	0.596	1.000
33	0.138	0.525	1.000	0.161	0.608	1.000	0.171	0.608	1.000	0.184	0.608	1.000
34	0.143	0.538	1.000	0.167	0.620	1.000	0.177	0.619	1.000	0.190	0.620	1.000
35	0.148	0.549	1.000	0.172	0.631	1.000	0.182	0.630	1.000	0.196	0.631	1.000
36	0.153	0.561	1.000	0.178	0.642	1.000	0.188	0.641	1.000	0.202	0.642	1.000
37	0.158	0.572	1.000	0.183	0.652	1.000	0.194	0.652	1.000	0.208	0.652	1.000
38	0.163	0.582	1.000	0.189	0.662	1.000	0.199	0.662	1.000	0.213	0.662	1.000
39	0.167	0.593	1.000	0.194	0.672	1.000	0.205	0.671	1.000	0.219	0.672	1.000
40	0.172	0.603	1.000	0.199	0.681	1.000	0.210	0.681	1.000	0.225	0.681	1.000
41	0.177	0.612	1.000	0.205	0.690	1.000	0.216	0.690	1.000	0.230	0.690	1.000
42	0.182	0.622	1.000	0.210	0.699	1.000	0.221	0.698	1.000	0.236	0.699	1.000
43	0.186	0.631	1.000	0.215	0.707	1.000	0.226	0.707	1.000	0.241	0.707	1.000
44	0.191	0.640	1.000	0.220	0.715	1.000	0.232	0.715	1.000	0.247	0.715	1.000
45	0.196	0.648	1.000	0.225	0.723	1.000	0.237	0.722	1.000	0.252	0.723	1.000
46	0.200	0.657	1.000	0.230	0.730	1.000	0.242	0.730	1.000	0.258	0.730	1.000
47	0.205	0.665	1.000	0.235	0.737	1.000	0.247	0.737	1.000	0.263	0.737	1.000
48	0.210	0.672	1.000	0.240	0.744	1.000	0.252	0.744	1.000	0.268	0.744	1.000
49	0.214	0.680	1.000	0.245	0.751	1.000	0.257	0.751	1.000	0.273	0.751	1.000
50	0.219	0.687	1.000	0.250	0.758	1.000	0.262	0.757	1.000	0.278	0.758	1.000

Table 6.8. Time-zero probabilities of failure for Milwaukee structure located in Oshkosh, Wisconsin.

Location: Oshkosh							Latitude: 43.9844°					
							Longitude: -88.5569°					
Number of Years in Service	Orientation of Sign: N-S			Orientation of Sign: NE-SW			Orientation of Sign: E-W			Orientation of Sign: SE-NW		
	Probability of Failure			Probability of Failure			Probability of Failure			Probability of Failure		
	E2	E3	E4	E2	E3	E4	E2	E3	E4	E2	E3	E4
0	0.000	0.000	0.000	0.000	0.000	0.000	0.000	0.000	0.000	0.000	0.000	0.000
1	0.001	0.002	0.572	0.001	0.002	0.543	0.001	0.002	0.530	0.001	0.002	0.601
2	0.004	0.015	0.840	0.004	0.016	0.822	0.004	0.017	0.813	0.004	0.017	0.858
3	0.009	0.040	0.929	0.009	0.042	0.919	0.010	0.044	0.914	0.009	0.044	0.939
4	0.015	0.073	0.965	0.016	0.075	0.959	0.018	0.080	0.956	0.017	0.080	0.970
5	0.023	0.110	0.981	0.024	0.113	0.977	0.026	0.119	0.975	0.025	0.119	0.984
6	0.031	0.149	0.989	0.033	0.153	0.987	0.036	0.160	0.985	0.034	0.160	0.991
7	0.041	0.188	0.993	0.043	0.194	0.992	0.046	0.202	0.991	0.044	0.202	0.994
8	0.050	0.227	0.996	0.052	0.233	0.995	0.057	0.242	0.994	0.054	0.242	0.997
9	0.060	0.265	0.997	0.063	0.272	0.996	0.068	0.282	0.996	0.065	0.281	0.998
10	0.070	0.302	0.998	0.073	0.308	0.998	0.079	0.319	0.997	0.075	0.319	0.998
11	0.080	0.336	0.999	0.084	0.344	0.998	0.090	0.355	0.998	0.086	0.354	0.999
12	0.091	0.369	0.999	0.094	0.377	0.999	0.101	0.388	0.999	0.097	0.388	0.999
13	0.101	0.401	0.999	0.105	0.408	0.999	0.112	0.420	0.999	0.107	0.420	0.999
14	0.111	0.430	0.999	0.115	0.438	0.999	0.123	0.450	0.999	0.118	0.450	1.000
15	0.121	0.458	1.000	0.126	0.466	0.999	0.134	0.478	0.999	0.129	0.478	1.000
16	0.131	0.484	1.000	0.136	0.492	1.000	0.145	0.504	1.000	0.139	0.504	1.000
17	0.141	0.509	1.000	0.146	0.517	1.000	0.155	0.529	1.000	0.150	0.529	1.000
18	0.151	0.532	1.000	0.156	0.540	1.000	0.166	0.552	1.000	0.160	0.552	1.000
19	0.161	0.554	1.000	0.166	0.562	1.000	0.176	0.574	1.000	0.170	0.573	1.000
20	0.171	0.575	1.000	0.176	0.582	1.000	0.186	0.594	1.000	0.180	0.594	1.000
21	0.180	0.594	1.000	0.186	0.602	1.000	0.197	0.613	1.000	0.190	0.613	1.000
22	0.190	0.613	1.000	0.195	0.620	1.000	0.206	0.631	1.000	0.199	0.631	1.000
23	0.199	0.630	1.000	0.205	0.637	1.000	0.216	0.648	1.000	0.209	0.648	1.000
24	0.208	0.646	1.000	0.214	0.653	1.000	0.226	0.664	1.000	0.218	0.664	1.000
25	0.217	0.662	1.000	0.223	0.669	1.000	0.235	0.679	1.000	0.228	0.679	1.000
26	0.226	0.676	1.000	0.232	0.683	1.000	0.244	0.694	1.000	0.237	0.694	1.000
27	0.234	0.690	1.000	0.241	0.697	1.000	0.253	0.707	1.000	0.245	0.707	1.000
28	0.243	0.703	1.000	0.249	0.710	1.000	0.262	0.720	1.000	0.254	0.720	1.000
29	0.251	0.715	1.000	0.258	0.722	1.000	0.271	0.732	1.000	0.263	0.732	1.000
30	0.259	0.727	1.000	0.266	0.733	1.000	0.279	0.743	1.000	0.271	0.743	1.000
31	0.267	0.738	1.000	0.274	0.744	1.000	0.288	0.754	1.000	0.279	0.754	1.000
32	0.275	0.748	1.000	0.283	0.754	1.000	0.296	0.764	1.000	0.287	0.764	1.000
33	0.283	0.758	1.000	0.290	0.764	1.000	0.304	0.773	1.000	0.295	0.773	1.000
34	0.291	0.768	1.000	0.298	0.774	1.000	0.312	0.782	1.000	0.303	0.782	1.000
35	0.298	0.777	1.000	0.306	0.782	1.000	0.320	0.791	1.000	0.311	0.791	1.000
36	0.306	0.785	1.000	0.313	0.791	1.000	0.327	0.799	1.000	0.318	0.799	1.000
37	0.313	0.793	1.000	0.321	0.799	1.000	0.335	0.807	1.000	0.326	0.807	1.000
38	0.320	0.801	1.000	0.328	0.806	1.000	0.342	0.814	1.000	0.333	0.814	1.000
39	0.327	0.808	1.000	0.335	0.813	1.000	0.349	0.821	1.000	0.340	0.821	1.000
40	0.334	0.815	1.000	0.342	0.820	1.000	0.356	0.828	1.000	0.347	0.828	1.000
41	0.341	0.822	1.000	0.349	0.827	1.000	0.363	0.834	1.000	0.354	0.834	1.000
42	0.348	0.828	1.000	0.356	0.833	1.000	0.370	0.841	1.000	0.361	0.840	1.000
43	0.354	0.834	1.000	0.362	0.839	1.000	0.377	0.846	1.000	0.368	0.846	1.000
44	0.361	0.840	1.000	0.369	0.845	1.000	0.384	0.852	1.000	0.374	0.852	1.000
45	0.367	0.846	1.000	0.375	0.850	1.000	0.390	0.857	1.000	0.381	0.857	1.000
46	0.373	0.851	1.000	0.382	0.855	1.000	0.396	0.862	1.000	0.387	0.862	1.000
47	0.379	0.856	1.000	0.388	0.860	1.000	0.403	0.867	1.000	0.393	0.867	1.000
48	0.386	0.861	1.000	0.394	0.865	1.000	0.409	0.871	1.000	0.399	0.871	1.000
49	0.391	0.865	1.000	0.400	0.870	1.000	0.415	0.876	1.000	0.405	0.876	1.000
50	0.397	0.870	1.000	0.406	0.874	1.000	0.421	0.880	1.000	0.411	0.880	1.000

Table 6.9. Time-zero probabilities of failure for Milwaukee structure located in Wisconsin Rapids, Wisconsin.

Location: Wisconsin Rapids							Latitude: 44.3592°					
							Longitude: -89.8369°					
Number of Years in Service	Orientation of Sign: N-S			Orientation of Sign: NE-SW			Orientation of Sign: E-W			Orientation of Sign: SE-NW		
	Probability of Failure			Probability of Failure			Probability of Failure			Probability of Failure		
	E2	E3	E4	E2	E3	E4	E2	E3	E4	E2	E3	E4
0	0.000	0.000	0.000	0.000	0.000	0.000	0.000	0.000	0.000	0.000	0.000	0.000
1	0.000	0.001	0.510	0.000	0.001	0.501	0.000	0.000	0.341	0.000	0.000	0.450
2	0.002	0.008	0.799	0.002	0.008	0.793	0.000	0.002	0.657	0.001	0.004	0.754
3	0.004	0.024	0.906	0.004	0.023	0.902	0.001	0.008	0.811	0.002	0.013	0.878
4	0.008	0.047	0.951	0.007	0.045	0.948	0.003	0.017	0.888	0.004	0.027	0.933
5	0.012	0.073	0.972	0.012	0.071	0.971	0.005	0.029	0.931	0.007	0.044	0.961
6	0.017	0.103	0.983	0.017	0.100	0.982	0.007	0.044	0.955	0.010	0.065	0.976
7	0.023	0.134	0.990	0.022	0.131	0.989	0.009	0.061	0.970	0.014	0.087	0.985
8	0.029	0.166	0.993	0.028	0.162	0.993	0.012	0.079	0.979	0.018	0.111	0.990
9	0.036	0.197	0.995	0.034	0.194	0.995	0.015	0.098	0.985	0.022	0.135	0.993
10	0.042	0.229	0.997	0.041	0.224	0.997	0.019	0.118	0.989	0.027	0.160	0.995
11	0.049	0.259	0.998	0.047	0.255	0.998	0.022	0.138	0.992	0.032	0.185	0.996
12	0.056	0.289	0.998	0.054	0.284	0.998	0.026	0.159	0.994	0.036	0.209	0.997
13	0.063	0.317	0.999	0.061	0.312	0.999	0.030	0.179	0.995	0.042	0.234	0.998
14	0.071	0.345	0.999	0.068	0.340	0.999	0.034	0.200	0.996	0.047	0.258	0.999
15	0.078	0.371	0.999	0.076	0.366	0.999	0.038	0.220	0.997	0.052	0.281	0.999
16	0.085	0.396	0.999	0.083	0.391	0.999	0.042	0.240	0.998	0.058	0.304	0.999
17	0.093	0.420	1.000	0.090	0.415	1.000	0.046	0.260	0.998	0.063	0.326	0.999
18	0.100	0.443	1.000	0.097	0.438	1.000	0.051	0.279	0.999	0.068	0.347	0.999
19	0.107	0.465	1.000	0.104	0.460	1.000	0.055	0.298	0.999	0.074	0.367	1.000
20	0.115	0.486	1.000	0.111	0.481	1.000	0.060	0.317	0.999	0.080	0.387	1.000
21	0.122	0.506	1.000	0.119	0.500	1.000	0.064	0.335	0.999	0.085	0.407	1.000
22	0.129	0.525	1.000	0.126	0.519	1.000	0.069	0.352	0.999	0.091	0.425	1.000
23	0.136	0.543	1.000	0.133	0.537	1.000	0.073	0.369	0.999	0.096	0.443	1.000
24	0.144	0.560	1.000	0.140	0.555	1.000	0.078	0.386	1.000	0.102	0.460	1.000
25	0.151	0.577	1.000	0.147	0.571	1.000	0.082	0.402	1.000	0.108	0.477	1.000
26	0.158	0.592	1.000	0.154	0.587	1.000	0.087	0.417	1.000	0.113	0.493	1.000
27	0.165	0.607	1.000	0.160	0.602	1.000	0.092	0.432	1.000	0.119	0.508	1.000
28	0.172	0.621	1.000	0.167	0.616	1.000	0.096	0.447	1.000	0.124	0.523	1.000
29	0.178	0.635	1.000	0.174	0.630	1.000	0.101	0.461	1.000	0.130	0.537	1.000
30	0.185	0.648	1.000	0.181	0.643	1.000	0.105	0.475	1.000	0.135	0.551	1.000
31	0.192	0.660	1.000	0.187	0.655	1.000	0.110	0.488	1.000	0.141	0.564	1.000
32	0.198	0.672	1.000	0.194	0.667	1.000	0.114	0.501	1.000	0.146	0.577	1.000
33	0.205	0.683	1.000	0.200	0.678	1.000	0.119	0.514	1.000	0.152	0.589	1.000
34	0.211	0.694	1.000	0.207	0.689	1.000	0.124	0.526	1.000	0.157	0.601	1.000
35	0.218	0.704	1.000	0.213	0.700	1.000	0.128	0.538	1.000	0.162	0.612	1.000
36	0.224	0.714	1.000	0.219	0.710	1.000	0.133	0.549	1.000	0.167	0.623	1.000
37	0.230	0.724	1.000	0.225	0.719	1.000	0.137	0.560	1.000	0.173	0.634	1.000
38	0.237	0.733	1.000	0.231	0.728	1.000	0.142	0.571	1.000	0.178	0.644	1.000
39	0.243	0.741	1.000	0.237	0.737	1.000	0.146	0.581	1.000	0.183	0.654	1.000
40	0.249	0.750	1.000	0.243	0.745	1.000	0.150	0.591	1.000	0.188	0.664	1.000
41	0.255	0.758	1.000	0.249	0.753	1.000	0.155	0.601	1.000	0.193	0.673	1.000
42	0.260	0.765	1.000	0.255	0.761	1.000	0.159	0.611	1.000	0.198	0.682	1.000
43	0.266	0.773	1.000	0.261	0.768	1.000	0.163	0.620	1.000	0.203	0.690	1.000
44	0.272	0.780	1.000	0.266	0.776	1.000	0.168	0.629	1.000	0.208	0.698	1.000
45	0.278	0.786	1.000	0.272	0.782	1.000	0.172	0.637	1.000	0.213	0.706	1.000
46	0.283	0.793	1.000	0.277	0.789	1.000	0.176	0.646	1.000	0.218	0.714	1.000
47	0.289	0.799	1.000	0.283	0.795	1.000	0.181	0.654	1.000	0.223	0.721	1.000
48	0.294	0.805	1.000	0.288	0.801	1.000	0.185	0.662	1.000	0.227	0.729	1.000
49	0.300	0.811	1.000	0.294	0.807	1.000	0.189	0.670	1.000	0.232	0.736	1.000
50	0.305	0.816	1.000	0.299	0.813	1.000	0.193	0.677	1.000	0.237	0.742	1.000

Table 6.10. Time-zero probabilities of failure for Osseo structure located in Milwaukee, Wisconsin.

Location: Milwaukee							Latitude: 42.9550°					
							Longitude: -87.9044°					
Number of Years in Service	Orientation of Sign: N-S			Orientation of Sign: NE-SW			Orientation of Sign: E-W			Orientation of Sign: SE-NW		
	Probability of Failure			Probability of Failure			Probability of Failure			Probability of Failure		
	E2	E3	E4	E2	E3	E4	E2	E3	E4	E2	E3	E4
0	0.000	0.000	0.000	0.000	0.000	0.000	0.000	0.000	0.000	0.000	0.000	0.000
1	0.000	0.000	0.358	0.000	0.000	0.307	0.000	0.000	0.257	0.000	0.000	0.326
2	0.000	0.001	0.674	0.000	0.000	0.622	0.000	0.000	0.564	0.000	0.001	0.642
3	0.000	0.003	0.823	0.000	0.002	0.784	0.000	0.001	0.738	0.000	0.003	0.799
4	0.001	0.008	0.897	0.001	0.005	0.870	0.000	0.004	0.836	0.001	0.007	0.880
5	0.002	0.014	0.937	0.001	0.009	0.917	0.001	0.007	0.892	0.001	0.012	0.925
6	0.002	0.023	0.959	0.001	0.015	0.945	0.001	0.012	0.927	0.002	0.020	0.951
7	0.004	0.032	0.973	0.002	0.022	0.963	0.002	0.017	0.949	0.003	0.028	0.967
8	0.005	0.044	0.981	0.003	0.030	0.974	0.002	0.024	0.963	0.004	0.038	0.977
9	0.006	0.056	0.987	0.004	0.040	0.981	0.003	0.032	0.973	0.006	0.050	0.983
10	0.008	0.069	0.990	0.005	0.050	0.986	0.004	0.040	0.980	0.007	0.062	0.988
11	0.009	0.083	0.993	0.006	0.061	0.990	0.005	0.049	0.985	0.009	0.074	0.991
12	0.011	0.098	0.995	0.007	0.072	0.992	0.006	0.059	0.988	0.011	0.088	0.993
13	0.013	0.113	0.996	0.008	0.084	0.994	0.007	0.069	0.991	0.012	0.102	0.995
14	0.015	0.128	0.997	0.010	0.097	0.995	0.008	0.080	0.993	0.014	0.116	0.996
15	0.017	0.143	0.998	0.011	0.109	0.996	0.009	0.091	0.994	0.016	0.130	0.997
16	0.019	0.159	0.998	0.012	0.122	0.997	0.010	0.102	0.995	0.018	0.144	0.997
17	0.021	0.174	0.998	0.014	0.135	0.998	0.012	0.113	0.996	0.020	0.159	0.998
18	0.024	0.189	0.999	0.016	0.148	0.998	0.013	0.125	0.997	0.023	0.174	0.998
19	0.026	0.205	0.999	0.017	0.161	0.998	0.014	0.137	0.997	0.025	0.188	0.999
20	0.028	0.220	0.999	0.019	0.174	0.999	0.016	0.149	0.998	0.027	0.203	0.999
21	0.031	0.235	0.999	0.021	0.187	0.999	0.017	0.161	0.998	0.030	0.217	0.999
22	0.033	0.250	0.999	0.023	0.201	0.999	0.019	0.172	0.999	0.032	0.231	0.999
23	0.036	0.264	1.000	0.024	0.214	0.999	0.021	0.184	0.999	0.035	0.245	0.999
24	0.039	0.279	1.000	0.026	0.226	0.999	0.022	0.196	0.999	0.037	0.259	0.999
25	0.041	0.293	1.000	0.028	0.239	0.999	0.024	0.208	0.999	0.040	0.273	1.000
26	0.044	0.307	1.000	0.030	0.252	1.000	0.026	0.219	0.999	0.042	0.286	1.000
27	0.047	0.321	1.000	0.032	0.264	1.000	0.027	0.231	0.999	0.045	0.300	1.000
28	0.049	0.334	1.000	0.034	0.277	1.000	0.029	0.242	0.999	0.048	0.313	1.000
29	0.052	0.347	1.000	0.036	0.289	1.000	0.031	0.254	1.000	0.050	0.325	1.000
30	0.055	0.360	1.000	0.038	0.301	1.000	0.033	0.265	1.000	0.053	0.338	1.000
31	0.058	0.373	1.000	0.041	0.312	1.000	0.035	0.276	1.000	0.056	0.350	1.000
32	0.061	0.385	1.000	0.043	0.324	1.000	0.037	0.287	1.000	0.059	0.362	1.000
33	0.063	0.397	1.000	0.045	0.335	1.000	0.038	0.298	1.000	0.061	0.374	1.000
34	0.066	0.409	1.000	0.047	0.347	1.000	0.040	0.309	1.000	0.064	0.386	1.000
35	0.069	0.421	1.000	0.049	0.358	1.000	0.042	0.319	1.000	0.067	0.397	1.000
36	0.072	0.432	1.000	0.051	0.368	1.000	0.044	0.329	1.000	0.070	0.408	1.000
37	0.075	0.443	1.000	0.054	0.379	1.000	0.046	0.340	1.000	0.072	0.419	1.000
38	0.078	0.454	1.000	0.056	0.389	1.000	0.048	0.350	1.000	0.075	0.430	1.000
39	0.081	0.464	1.000	0.058	0.400	1.000	0.050	0.360	1.000	0.078	0.440	1.000
40	0.084	0.474	1.000	0.060	0.410	1.000	0.052	0.369	1.000	0.081	0.451	1.000
41	0.086	0.485	1.000	0.063	0.419	1.000	0.054	0.379	1.000	0.084	0.461	1.000
42	0.089	0.494	1.000	0.065	0.429	1.000	0.056	0.388	1.000	0.087	0.470	1.000
43	0.092	0.504	1.000	0.067	0.439	1.000	0.058	0.397	1.000	0.089	0.480	1.000
44	0.095	0.513	1.000	0.069	0.448	1.000	0.060	0.407	1.000	0.092	0.489	1.000
45	0.098	0.522	1.000	0.072	0.457	1.000	0.062	0.416	1.000	0.095	0.499	1.000
46	0.101	0.531	1.000	0.074	0.466	1.000	0.064	0.424	1.000	0.098	0.508	1.000
47	0.104	0.540	1.000	0.076	0.475	1.000	0.067	0.433	1.000	0.101	0.516	1.000
48	0.107	0.549	1.000	0.079	0.483	1.000	0.069	0.441	1.000	0.104	0.525	1.000
49	0.110	0.557	1.000	0.081	0.492	1.000	0.071	0.450	1.000	0.106	0.533	1.000
50	0.113	0.565	1.000	0.083	0.500	1.000	0.073	0.458	1.000	0.109	0.541	1.000

Table 6.11. Time-zero probabilities of failure for Osseo structure located in Eau Claire, Wisconsin.

Location: Eau Claire							Latitude: 44.8664°					
							Longitude: -91.4878°					
Number of Years in Service	Orientation of Sign: N-S			Orientation of Sign: NE-SW			Orientation of Sign: E-W			Orientation of Sign: SE-NW		
	Probability of Failure			Probability of Failure			Probability of Failure			Probability of Failure		
	E2	E3	E4	E2	E3	E4	E2	E3	E4	E2	E3	E4
0	0.000	0.000	0.000	0.000	0.000	0.000	0.000	0.000	0.000	0.000	0.000	0.000
1	0.000	0.000	0.171	0.000	0.000	0.137	0.000	0.000	0.150	0.000	0.000	0.186
2	0.000	0.000	0.445	0.000	0.000	0.390	0.000	0.000	0.412	0.000	0.000	0.469
3	0.000	0.000	0.633	0.000	0.000	0.578	0.000	0.000	0.600	0.000	0.000	0.655
4	0.000	0.001	0.751	0.000	0.000	0.703	0.000	0.000	0.723	0.000	0.001	0.770
5	0.000	0.002	0.826	0.000	0.001	0.787	0.000	0.001	0.803	0.000	0.002	0.841
6	0.000	0.003	0.876	0.000	0.002	0.844	0.000	0.002	0.857	0.000	0.003	0.888
7	0.000	0.005	0.909	0.000	0.003	0.883	0.000	0.003	0.894	0.000	0.005	0.918
8	0.001	0.008	0.932	0.000	0.004	0.911	0.000	0.004	0.920	0.001	0.008	0.940
9	0.001	0.010	0.948	0.001	0.006	0.931	0.000	0.006	0.939	0.001	0.011	0.954
10	0.001	0.014	0.960	0.001	0.008	0.946	0.001	0.007	0.952	0.001	0.014	0.965
11	0.002	0.018	0.969	0.001	0.011	0.957	0.001	0.010	0.962	0.001	0.018	0.973
12	0.002	0.022	0.975	0.001	0.013	0.966	0.001	0.012	0.970	0.002	0.022	0.979
13	0.002	0.027	0.980	0.001	0.016	0.972	0.001	0.015	0.976	0.002	0.027	0.983
14	0.003	0.032	0.984	0.002	0.020	0.978	0.001	0.018	0.980	0.003	0.032	0.986
15	0.003	0.037	0.987	0.002	0.023	0.982	0.001	0.022	0.984	0.003	0.037	0.989
16	0.004	0.043	0.989	0.002	0.027	0.985	0.002	0.025	0.987	0.004	0.043	0.991
17	0.004	0.048	0.991	0.003	0.031	0.987	0.002	0.029	0.989	0.004	0.049	0.993
18	0.005	0.055	0.993	0.003	0.036	0.989	0.002	0.033	0.991	0.005	0.055	0.994
19	0.005	0.061	0.994	0.003	0.040	0.991	0.003	0.038	0.992	0.005	0.062	0.995
20	0.006	0.068	0.995	0.004	0.045	0.992	0.003	0.042	0.993	0.006	0.068	0.996
21	0.007	0.074	0.996	0.004	0.050	0.993	0.003	0.047	0.994	0.006	0.075	0.996
22	0.007	0.081	0.996	0.004	0.055	0.994	0.004	0.052	0.995	0.007	0.082	0.997
23	0.008	0.088	0.997	0.005	0.060	0.995	0.004	0.057	0.996	0.008	0.089	0.997
24	0.009	0.095	0.997	0.005	0.066	0.996	0.004	0.062	0.996	0.008	0.097	0.998
25	0.010	0.103	0.998	0.006	0.071	0.996	0.005	0.067	0.997	0.009	0.104	0.998
26	0.010	0.110	0.998	0.006	0.077	0.997	0.005	0.072	0.997	0.010	0.111	0.998
27	0.011	0.118	0.998	0.007	0.083	0.997	0.006	0.078	0.998	0.011	0.119	0.999
28	0.012	0.125	0.998	0.008	0.089	0.998	0.006	0.084	0.998	0.011	0.126	0.999
29	0.013	0.133	0.999	0.008	0.094	0.998	0.007	0.089	0.998	0.012	0.134	0.999
30	0.014	0.140	0.999	0.009	0.100	0.998	0.007	0.095	0.998	0.013	0.142	0.999
31	0.015	0.148	0.999	0.009	0.106	0.998	0.008	0.101	0.999	0.014	0.149	0.999
32	0.016	0.155	0.999	0.010	0.113	0.999	0.008	0.107	0.999	0.015	0.157	0.999
33	0.017	0.163	0.999	0.011	0.119	0.999	0.009	0.112	0.999	0.016	0.165	0.999
34	0.017	0.171	0.999	0.011	0.125	0.999	0.009	0.118	0.999	0.017	0.172	0.999
35	0.018	0.178	0.999	0.012	0.131	0.999	0.010	0.124	0.999	0.018	0.180	0.999
36	0.019	0.186	0.999	0.013	0.137	0.999	0.010	0.130	0.999	0.019	0.188	1.000
37	0.020	0.193	0.999	0.013	0.144	0.999	0.011	0.136	0.999	0.020	0.195	1.000
38	0.021	0.201	1.000	0.014	0.150	0.999	0.011	0.142	0.999	0.021	0.203	1.000
39	0.022	0.209	1.000	0.015	0.156	0.999	0.012	0.148	0.999	0.021	0.210	1.000
40	0.023	0.216	1.000	0.015	0.162	0.999	0.013	0.155	1.000	0.022	0.218	1.000
41	0.025	0.224	1.000	0.016	0.169	0.999	0.013	0.161	1.000	0.024	0.225	1.000
42	0.026	0.231	1.000	0.017	0.175	1.000	0.014	0.167	1.000	0.025	0.233	1.000
43	0.027	0.238	1.000	0.018	0.181	1.000	0.015	0.173	1.000	0.026	0.240	1.000
44	0.028	0.246	1.000	0.018	0.187	1.000	0.015	0.179	1.000	0.027	0.248	1.000
45	0.029	0.253	1.000	0.019	0.194	1.000	0.016	0.185	1.000	0.028	0.255	1.000
46	0.030	0.260	1.000	0.020	0.200	1.000	0.017	0.191	1.000	0.029	0.262	1.000
47	0.031	0.267	1.000	0.021	0.206	1.000	0.017	0.197	1.000	0.030	0.269	1.000
48	0.032	0.275	1.000	0.021	0.212	1.000	0.018	0.203	1.000	0.031	0.277	1.000
49	0.033	0.282	1.000	0.022	0.218	1.000	0.019	0.209	1.000	0.032	0.284	1.000
50	0.035	0.289	1.000	0.023	0.225	1.000	0.019	0.215	1.000	0.033	0.291	1.000

Table 6.12. Time-zero probabilities of failure for Osseo structure located in La Crosse, Wisconsin.

Location: La Crosse							Latitude: 43.8788°					
							Longitude: -91.2527°					
Number of Years in Service	Orientation of Sign: N-S			Orientation of Sign: NE-SW			Orientation of Sign: E-W			Orientation of Sign: SE-NW		
	Probability of Failure			Probability of Failure			Probability of Failure			Probability of Failure		
	E2	E3	E4	E2	E3	E4	E2	E3	E4	E2	E3	E4
0	0.000	0.000	0.000	0.000	0.000	0.000	0.000	0.000	0.000	0.000	0.000	0.000
1	0.000	0.000	0.173	0.000	0.000	0.251	0.000	0.000	0.221	0.000	0.000	0.185
2	0.000	0.000	0.449	0.000	0.000	0.557	0.000	0.000	0.518	0.000	0.000	0.467
3	0.000	0.001	0.636	0.000	0.001	0.732	0.000	0.000	0.699	0.000	0.000	0.653
4	0.001	0.002	0.754	0.000	0.003	0.831	0.000	0.001	0.805	0.000	0.001	0.768
5	0.001	0.004	0.828	0.001	0.006	0.889	0.000	0.002	0.869	0.000	0.002	0.840
6	0.002	0.006	0.877	0.001	0.010	0.924	0.000	0.003	0.909	0.000	0.004	0.887
7	0.003	0.010	0.910	0.001	0.015	0.947	0.000	0.005	0.935	0.001	0.006	0.918
8	0.004	0.014	0.933	0.002	0.021	0.962	0.001	0.008	0.953	0.001	0.009	0.939
9	0.006	0.019	0.949	0.003	0.028	0.972	0.001	0.011	0.965	0.001	0.013	0.954
10	0.007	0.025	0.961	0.003	0.036	0.979	0.001	0.015	0.974	0.001	0.017	0.965
11	0.009	0.031	0.970	0.004	0.044	0.984	0.002	0.019	0.980	0.002	0.021	0.973
12	0.011	0.038	0.976	0.005	0.053	0.988	0.002	0.023	0.984	0.002	0.026	0.978
13	0.012	0.045	0.981	0.006	0.063	0.990	0.002	0.028	0.988	0.003	0.032	0.983
14	0.014	0.053	0.985	0.007	0.072	0.992	0.003	0.033	0.990	0.003	0.037	0.986
15	0.016	0.061	0.987	0.008	0.083	0.994	0.003	0.039	0.992	0.004	0.043	0.989
16	0.018	0.069	0.990	0.009	0.093	0.995	0.004	0.045	0.994	0.004	0.050	0.991
17	0.020	0.078	0.991	0.011	0.104	0.996	0.004	0.051	0.995	0.005	0.057	0.992
18	0.023	0.086	0.993	0.012	0.115	0.997	0.005	0.057	0.996	0.006	0.064	0.994
19	0.025	0.095	0.994	0.013	0.126	0.997	0.006	0.064	0.996	0.006	0.071	0.995
20	0.027	0.105	0.995	0.015	0.137	0.998	0.006	0.070	0.997	0.007	0.078	0.996
21	0.030	0.114	0.996	0.016	0.148	0.998	0.007	0.077	0.998	0.008	0.086	0.996
22	0.032	0.123	0.996	0.017	0.160	0.998	0.008	0.085	0.998	0.009	0.093	0.997
23	0.035	0.133	0.997	0.019	0.171	0.999	0.008	0.092	0.998	0.009	0.101	0.997
24	0.037	0.142	0.997	0.021	0.182	0.999	0.009	0.099	0.998	0.010	0.109	0.998
25	0.040	0.152	0.998	0.022	0.193	0.999	0.010	0.107	0.999	0.011	0.117	0.998
26	0.042	0.162	0.998	0.024	0.205	0.999	0.011	0.114	0.999	0.012	0.125	0.998
27	0.045	0.171	0.998	0.025	0.216	0.999	0.012	0.122	0.999	0.013	0.133	0.999
28	0.048	0.181	0.999	0.027	0.227	0.999	0.012	0.130	0.999	0.014	0.141	0.999
29	0.050	0.191	0.999	0.029	0.238	0.999	0.013	0.137	0.999	0.015	0.150	0.999
30	0.053	0.200	0.999	0.030	0.249	1.000	0.014	0.145	0.999	0.016	0.158	0.999
31	0.056	0.210	0.999	0.032	0.259	1.000	0.015	0.153	0.999	0.017	0.166	0.999
32	0.059	0.219	0.999	0.034	0.270	1.000	0.016	0.161	1.000	0.018	0.174	0.999
33	0.061	0.229	0.999	0.036	0.280	1.000	0.017	0.168	1.000	0.019	0.182	0.999
34	0.064	0.238	0.999	0.037	0.291	1.000	0.018	0.176	1.000	0.020	0.191	0.999
35	0.067	0.247	0.999	0.039	0.301	1.000	0.019	0.184	1.000	0.021	0.199	0.999
36	0.070	0.256	0.999	0.041	0.311	1.000	0.020	0.192	1.000	0.022	0.207	1.000
37	0.072	0.265	1.000	0.043	0.321	1.000	0.021	0.199	1.000	0.023	0.215	1.000
38	0.075	0.274	1.000	0.045	0.331	1.000	0.022	0.207	1.000	0.024	0.223	1.000
39	0.078	0.283	1.000	0.047	0.341	1.000	0.023	0.215	1.000	0.025	0.231	1.000
40	0.081	0.292	1.000	0.049	0.350	1.000	0.024	0.222	1.000	0.027	0.239	1.000
41	0.084	0.301	1.000	0.051	0.360	1.000	0.025	0.230	1.000	0.028	0.247	1.000
42	0.087	0.309	1.000	0.052	0.369	1.000	0.026	0.238	1.000	0.029	0.255	1.000
43	0.089	0.318	1.000	0.054	0.378	1.000	0.027	0.245	1.000	0.030	0.262	1.000
44	0.092	0.326	1.000	0.056	0.387	1.000	0.028	0.253	1.000	0.031	0.270	1.000
45	0.095	0.335	1.000	0.058	0.396	1.000	0.030	0.260	1.000	0.033	0.278	1.000
46	0.098	0.343	1.000	0.060	0.404	1.000	0.031	0.267	1.000	0.034	0.285	1.000
47	0.101	0.351	1.000	0.062	0.413	1.000	0.032	0.275	1.000	0.035	0.293	1.000
48	0.104	0.359	1.000	0.064	0.421	1.000	0.033	0.282	1.000	0.036	0.300	1.000
49	0.106	0.367	1.000	0.066	0.430	1.000	0.034	0.289	1.000	0.038	0.308	1.000
50	0.109	0.375	1.000	0.068	0.438	1.000	0.035	0.296	1.000	0.039	0.315	1.000

Table 6.13. Time-zero probabilities of failure for Osseo structure located in Green Bay, Wisconsin.

Location: Green Bay							Latitude: 44.4794°					
							Longitude: -88.1366°					
Number of Years in Service	Orientation of Sign: N-S			Orientation of Sign: NE-SW			Orientation of Sign: E-W			Orientation of Sign: SE-NW		
	Probability of Failure			Probability of Failure			Probability of Failure			Probability of Failure		
	E2	E3	E4	E2	E3	E4	E2	E3	E4	E2	E3	E4
0	0.000	0.000	0.000	0.000	0.000	0.000	0.000	0.000	0.000	0.000	0.000	0.000
1	0.000	0.000	0.270	0.000	0.000	0.244	0.000	0.000	0.218	0.000	0.000	0.254
2	0.000	0.000	0.580	0.000	0.000	0.548	0.000	0.000	0.514	0.000	0.000	0.560
3	0.000	0.002	0.751	0.000	0.001	0.725	0.000	0.001	0.695	0.000	0.001	0.735
4	0.001	0.004	0.845	0.000	0.004	0.825	0.000	0.003	0.802	0.000	0.003	0.833
5	0.001	0.008	0.900	0.001	0.007	0.884	0.001	0.007	0.867	0.001	0.005	0.890
6	0.002	0.013	0.932	0.001	0.012	0.921	0.001	0.011	0.907	0.001	0.009	0.925
7	0.002	0.019	0.953	0.002	0.017	0.944	0.002	0.016	0.934	0.002	0.014	0.948
8	0.003	0.026	0.966	0.003	0.024	0.960	0.003	0.023	0.952	0.002	0.019	0.962
9	0.004	0.035	0.976	0.004	0.032	0.970	0.004	0.030	0.964	0.003	0.025	0.972
10	0.005	0.044	0.982	0.005	0.040	0.978	0.005	0.039	0.973	0.004	0.032	0.979
11	0.006	0.054	0.986	0.006	0.049	0.983	0.006	0.047	0.979	0.005	0.040	0.984
12	0.007	0.064	0.989	0.007	0.059	0.987	0.007	0.057	0.984	0.006	0.048	0.988
13	0.009	0.075	0.992	0.008	0.069	0.990	0.008	0.067	0.987	0.007	0.057	0.991
14	0.010	0.086	0.994	0.009	0.080	0.992	0.009	0.077	0.990	0.008	0.066	0.993
15	0.012	0.098	0.995	0.011	0.091	0.994	0.011	0.088	0.992	0.009	0.076	0.994
16	0.013	0.110	0.996	0.012	0.102	0.995	0.012	0.099	0.993	0.011	0.086	0.995
17	0.015	0.122	0.997	0.014	0.114	0.996	0.014	0.110	0.995	0.012	0.096	0.996
18	0.017	0.134	0.997	0.015	0.126	0.997	0.015	0.122	0.996	0.013	0.106	0.997
19	0.018	0.147	0.998	0.017	0.137	0.997	0.017	0.133	0.996	0.015	0.117	0.997
20	0.020	0.159	0.998	0.019	0.149	0.998	0.019	0.145	0.997	0.016	0.127	0.998
21	0.022	0.171	0.998	0.021	0.161	0.998	0.020	0.156	0.997	0.018	0.138	0.998
22	0.024	0.184	0.999	0.022	0.173	0.998	0.022	0.168	0.998	0.020	0.149	0.999
23	0.026	0.196	0.999	0.024	0.185	0.999	0.024	0.180	0.998	0.021	0.160	0.999
24	0.028	0.208	0.999	0.026	0.197	0.999	0.026	0.191	0.998	0.023	0.171	0.999
25	0.030	0.221	0.999	0.028	0.208	0.999	0.028	0.203	0.999	0.025	0.181	0.999
26	0.032	0.233	0.999	0.030	0.220	0.999	0.030	0.214	0.999	0.026	0.192	0.999
27	0.034	0.245	0.999	0.032	0.232	0.999	0.032	0.226	0.999	0.028	0.203	0.999
28	0.036	0.256	1.000	0.034	0.243	0.999	0.034	0.237	0.999	0.030	0.213	0.999
29	0.038	0.268	1.000	0.036	0.255	0.999	0.036	0.248	0.999	0.032	0.224	1.000
30	0.040	0.280	1.000	0.038	0.266	1.000	0.038	0.259	0.999	0.034	0.235	1.000
31	0.043	0.291	1.000	0.040	0.277	1.000	0.040	0.270	0.999	0.036	0.245	1.000
32	0.045	0.302	1.000	0.042	0.288	1.000	0.042	0.281	1.000	0.037	0.255	1.000
33	0.047	0.313	1.000	0.044	0.299	1.000	0.044	0.292	1.000	0.039	0.265	1.000
34	0.049	0.324	1.000	0.047	0.309	1.000	0.046	0.302	1.000	0.041	0.276	1.000
35	0.052	0.335	1.000	0.049	0.320	1.000	0.048	0.313	1.000	0.043	0.286	1.000
36	0.054	0.345	1.000	0.051	0.330	1.000	0.050	0.323	1.000	0.045	0.295	1.000
37	0.056	0.356	1.000	0.053	0.340	1.000	0.053	0.333	1.000	0.047	0.305	1.000
38	0.058	0.366	1.000	0.055	0.350	1.000	0.055	0.343	1.000	0.049	0.315	1.000
39	0.061	0.376	1.000	0.058	0.360	1.000	0.057	0.353	1.000	0.051	0.324	1.000
40	0.063	0.386	1.000	0.060	0.370	1.000	0.059	0.363	1.000	0.053	0.334	1.000
41	0.065	0.396	1.000	0.062	0.380	1.000	0.062	0.372	1.000	0.055	0.343	1.000
42	0.068	0.405	1.000	0.064	0.389	1.000	0.064	0.382	1.000	0.058	0.352	1.000
43	0.070	0.414	1.000	0.067	0.398	1.000	0.066	0.391	1.000	0.060	0.361	1.000
44	0.073	0.424	1.000	0.069	0.407	1.000	0.068	0.400	1.000	0.062	0.370	1.000
45	0.075	0.433	1.000	0.071	0.416	1.000	0.071	0.409	1.000	0.064	0.378	1.000
46	0.077	0.442	1.000	0.073	0.425	1.000	0.073	0.417	1.000	0.066	0.387	1.000
47	0.080	0.450	1.000	0.076	0.434	1.000	0.075	0.426	1.000	0.068	0.395	1.000
48	0.082	0.459	1.000	0.078	0.442	1.000	0.077	0.435	1.000	0.070	0.404	1.000
49	0.084	0.467	1.000	0.080	0.451	1.000	0.080	0.443	1.000	0.072	0.412	1.000
50	0.087	0.475	1.000	0.083	0.459	1.000	0.082	0.451	1.000	0.074	0.420	1.000

Table 6.14. Time-zero probabilities of failure for Osseo structure located in Madison, Wisconsin.

Location: Madison							Latitude: 43.1405°					
							Longitude: -89.3452°					
Number of Years in Service	Orientation of Sign: N-S			Orientation of Sign: NE-SW			Orientation of Sign: E-W			Orientation of Sign: SE-NW		
	Probability of Failure			Probability of Failure			Probability of Failure			Probability of Failure		
	E2	E3	E4	E2	E3	E4	E2	E3	E4	E2	E3	E4
0	0.000	0.000	0.000	0.000	0.000	0.000	0.000	0.000	0.000	0.000	0.000	0.000
1	0.000	0.000	0.064	0.000	0.000	0.124	0.000	0.000	0.149	0.000	0.000	0.116
2	0.000	0.000	0.239	0.000	0.000	0.367	0.000	0.000	0.411	0.000	0.000	0.352
3	0.000	0.000	0.408	0.000	0.000	0.555	0.000	0.000	0.599	0.000	0.000	0.539
4	0.000	0.000	0.542	0.000	0.000	0.683	0.000	0.000	0.722	0.000	0.000	0.668
5	0.000	0.000	0.643	0.000	0.001	0.769	0.000	0.001	0.802	0.000	0.001	0.757
6	0.000	0.001	0.720	0.000	0.001	0.829	0.000	0.001	0.856	0.000	0.001	0.819
7	0.000	0.001	0.777	0.000	0.002	0.871	0.000	0.002	0.894	0.000	0.002	0.863
8	0.000	0.002	0.821	0.000	0.003	0.901	0.000	0.003	0.920	0.000	0.004	0.894
9	0.000	0.003	0.855	0.000	0.005	0.923	0.000	0.005	0.938	0.000	0.005	0.917
10	0.000	0.004	0.881	0.000	0.006	0.940	0.001	0.006	0.952	0.001	0.007	0.935
11	0.000	0.005	0.902	0.001	0.008	0.952	0.001	0.008	0.962	0.001	0.009	0.948
12	0.001	0.006	0.919	0.001	0.011	0.961	0.001	0.011	0.970	0.001	0.011	0.958
13	0.001	0.008	0.932	0.001	0.013	0.969	0.001	0.013	0.976	0.001	0.014	0.966
14	0.001	0.010	0.943	0.001	0.016	0.974	0.001	0.016	0.980	0.002	0.017	0.972
15	0.001	0.012	0.951	0.001	0.019	0.979	0.002	0.019	0.984	0.002	0.020	0.977
16	0.001	0.014	0.959	0.001	0.023	0.982	0.002	0.022	0.987	0.002	0.023	0.980
17	0.001	0.016	0.964	0.002	0.026	0.985	0.002	0.026	0.989	0.002	0.027	0.984
18	0.001	0.019	0.969	0.002	0.030	0.988	0.002	0.029	0.991	0.003	0.031	0.986
19	0.002	0.021	0.974	0.002	0.034	0.989	0.003	0.033	0.992	0.003	0.035	0.988
20	0.002	0.024	0.977	0.003	0.038	0.991	0.003	0.037	0.993	0.004	0.039	0.990
21	0.002	0.027	0.980	0.003	0.042	0.992	0.003	0.041	0.994	0.004	0.044	0.991
22	0.002	0.030	0.982	0.003	0.047	0.993	0.004	0.046	0.995	0.004	0.048	0.993
23	0.003	0.034	0.985	0.004	0.051	0.994	0.004	0.050	0.996	0.005	0.053	0.994
24	0.003	0.037	0.986	0.004	0.056	0.995	0.005	0.055	0.996	0.005	0.058	0.994
25	0.003	0.040	0.988	0.004	0.061	0.996	0.005	0.060	0.997	0.006	0.063	0.995
26	0.004	0.044	0.989	0.005	0.066	0.996	0.005	0.065	0.997	0.006	0.068	0.996
27	0.004	0.048	0.991	0.005	0.071	0.997	0.006	0.070	0.998	0.007	0.073	0.996
28	0.004	0.052	0.992	0.005	0.076	0.997	0.006	0.075	0.998	0.007	0.079	0.997
29	0.005	0.055	0.993	0.006	0.081	0.997	0.007	0.080	0.998	0.008	0.084	0.997
30	0.005	0.059	0.993	0.006	0.087	0.998	0.007	0.085	0.998	0.008	0.089	0.997
31	0.005	0.063	0.994	0.007	0.092	0.998	0.008	0.091	0.999	0.009	0.095	0.998
32	0.006	0.068	0.995	0.007	0.098	0.998	0.008	0.096	0.999	0.010	0.101	0.998
33	0.006	0.072	0.995	0.008	0.103	0.998	0.009	0.102	0.999	0.010	0.106	0.998
34	0.006	0.076	0.996	0.008	0.109	0.999	0.009	0.107	0.999	0.011	0.112	0.998
35	0.007	0.080	0.996	0.009	0.114	0.999	0.010	0.113	0.999	0.012	0.118	0.999
36	0.007	0.085	0.996	0.009	0.120	0.999	0.011	0.118	0.999	0.012	0.123	0.999
37	0.008	0.089	0.997	0.010	0.126	0.999	0.011	0.124	0.999	0.013	0.129	0.999
38	0.008	0.094	0.997	0.010	0.131	0.999	0.012	0.130	0.999	0.014	0.135	0.999
39	0.009	0.098	0.997	0.011	0.137	0.999	0.012	0.135	0.999	0.014	0.141	0.999
40	0.009	0.103	0.998	0.011	0.143	0.999	0.013	0.141	1.000	0.015	0.147	0.999
41	0.009	0.107	0.998	0.012	0.149	0.999	0.014	0.147	1.000	0.016	0.153	0.999
42	0.010	0.112	0.998	0.013	0.154	0.999	0.014	0.152	1.000	0.016	0.159	0.999
43	0.010	0.117	0.998	0.013	0.160	0.999	0.015	0.158	1.000	0.017	0.164	0.999
44	0.011	0.121	0.998	0.014	0.166	1.000	0.016	0.164	1.000	0.018	0.170	0.999
45	0.011	0.126	0.998	0.014	0.172	1.000	0.016	0.170	1.000	0.019	0.176	0.999
46	0.012	0.131	0.999	0.015	0.178	1.000	0.017	0.175	1.000	0.019	0.182	1.000
47	0.012	0.135	0.999	0.016	0.183	1.000	0.018	0.181	1.000	0.020	0.188	1.000
48	0.013	0.140	0.999	0.016	0.189	1.000	0.018	0.187	1.000	0.021	0.194	1.000
49	0.013	0.145	0.999	0.017	0.195	1.000	0.019	0.192	1.000	0.022	0.200	1.000
50	0.014	0.150	0.999	0.017	0.201	1.000	0.020	0.198	1.000	0.023	0.205	1.000

Table 6.15. Time-zero probabilities of failure for Osseo structure located in Oshkosh, Wisconsin.

Location: Oshkosh							Latitude: 43.9844°					
							Longitude: -88.5569°					
Number of Years in Service	Orientation of Sign: N-S			Orientation of Sign: NE-SW			Orientation of Sign: E-W			Orientation of Sign: SE-NW		
	Probability of Failure			Probability of Failure			Probability of Failure			Probability of Failure		
	E2	E3	E4	E2	E3	E4	E2	E3	E4	E2	E3	E4
0	0.000	0.000	0.000	0.000	0.000	0.000	0.000	0.000	0.000	0.000	0.000	0.000
1	0.000	0.000	0.216	0.000	0.000	0.196	0.000	0.000	0.186	0.000	0.000	0.238
2	0.000	0.000	0.511	0.000	0.000	0.483	0.000	0.000	0.469	0.000	0.000	0.540
3	0.000	0.001	0.693	0.000	0.001	0.668	0.000	0.001	0.655	0.000	0.001	0.718
4	0.000	0.001	0.800	0.000	0.002	0.780	0.000	0.002	0.769	0.000	0.002	0.820
5	0.000	0.003	0.865	0.000	0.003	0.850	0.000	0.004	0.841	0.000	0.003	0.880
6	0.001	0.005	0.906	0.001	0.006	0.894	0.001	0.006	0.887	0.001	0.006	0.918
7	0.001	0.008	0.933	0.001	0.009	0.924	0.001	0.010	0.918	0.001	0.009	0.942
8	0.001	0.012	0.951	0.001	0.012	0.944	0.001	0.014	0.940	0.001	0.013	0.958
9	0.002	0.016	0.964	0.002	0.017	0.958	0.002	0.018	0.954	0.002	0.018	0.969
10	0.002	0.021	0.972	0.002	0.022	0.968	0.002	0.024	0.965	0.002	0.023	0.977
11	0.002	0.026	0.979	0.003	0.028	0.975	0.003	0.030	0.973	0.003	0.029	0.982
12	0.003	0.032	0.983	0.003	0.034	0.980	0.004	0.036	0.979	0.003	0.035	0.986
13	0.004	0.038	0.987	0.004	0.040	0.984	0.004	0.043	0.983	0.004	0.042	0.989
14	0.004	0.045	0.990	0.005	0.047	0.988	0.005	0.051	0.986	0.005	0.050	0.992
15	0.005	0.052	0.992	0.005	0.055	0.990	0.006	0.059	0.989	0.006	0.057	0.993
16	0.006	0.059	0.993	0.006	0.062	0.992	0.007	0.067	0.991	0.006	0.065	0.995
17	0.007	0.067	0.994	0.007	0.070	0.993	0.008	0.075	0.993	0.007	0.073	0.996
18	0.007	0.075	0.995	0.008	0.079	0.994	0.009	0.084	0.994	0.008	0.082	0.996
19	0.008	0.083	0.996	0.009	0.087	0.995	0.010	0.093	0.995	0.009	0.091	0.997
20	0.009	0.091	0.997	0.010	0.096	0.996	0.011	0.102	0.996	0.010	0.099	0.997
21	0.010	0.100	0.997	0.011	0.104	0.997	0.012	0.111	0.996	0.011	0.108	0.998
22	0.011	0.108	0.998	0.012	0.113	0.997	0.013	0.120	0.997	0.012	0.118	0.998
23	0.012	0.117	0.998	0.013	0.122	0.998	0.014	0.129	0.997	0.013	0.127	0.999
24	0.013	0.126	0.998	0.014	0.131	0.998	0.015	0.139	0.998	0.014	0.136	0.999
25	0.014	0.135	0.999	0.015	0.140	0.998	0.017	0.148	0.998	0.016	0.145	0.999
26	0.015	0.144	0.999	0.016	0.149	0.999	0.018	0.158	0.998	0.017	0.155	0.999
27	0.016	0.153	0.999	0.017	0.159	0.999	0.019	0.167	0.999	0.018	0.164	0.999
28	0.018	0.161	0.999	0.019	0.168	0.999	0.021	0.177	0.999	0.019	0.173	0.999
29	0.019	0.170	0.999	0.020	0.177	0.999	0.022	0.186	0.999	0.020	0.183	0.999
30	0.020	0.179	0.999	0.021	0.186	0.999	0.023	0.195	0.999	0.022	0.192	0.999
31	0.021	0.188	0.999	0.022	0.195	0.999	0.025	0.205	0.999	0.023	0.201	1.000
32	0.022	0.197	0.999	0.024	0.204	0.999	0.026	0.214	0.999	0.024	0.211	1.000
33	0.024	0.206	1.000	0.025	0.213	0.999	0.028	0.223	0.999	0.026	0.220	1.000
34	0.025	0.215	1.000	0.026	0.222	0.999	0.029	0.233	0.999	0.027	0.229	1.000
35	0.026	0.224	1.000	0.028	0.231	1.000	0.031	0.242	0.999	0.029	0.238	1.000
36	0.028	0.232	1.000	0.029	0.240	1.000	0.032	0.251	1.000	0.030	0.247	1.000
37	0.029	0.241	1.000	0.031	0.249	1.000	0.034	0.260	1.000	0.031	0.256	1.000
38	0.030	0.249	1.000	0.032	0.258	1.000	0.035	0.269	1.000	0.033	0.265	1.000
39	0.032	0.258	1.000	0.033	0.266	1.000	0.037	0.278	1.000	0.034	0.274	1.000
40	0.033	0.266	1.000	0.035	0.275	1.000	0.038	0.286	1.000	0.036	0.282	1.000
41	0.034	0.275	1.000	0.036	0.283	1.000	0.040	0.295	1.000	0.037	0.291	1.000
42	0.036	0.283	1.000	0.038	0.292	1.000	0.041	0.304	1.000	0.039	0.299	1.000
43	0.037	0.291	1.000	0.039	0.300	1.000	0.043	0.312	1.000	0.040	0.308	1.000
44	0.039	0.299	1.000	0.041	0.308	1.000	0.044	0.320	1.000	0.042	0.316	1.000
45	0.040	0.307	1.000	0.042	0.316	1.000	0.046	0.329	1.000	0.043	0.324	1.000
46	0.042	0.315	1.000	0.044	0.324	1.000	0.048	0.337	1.000	0.045	0.332	1.000
47	0.043	0.323	1.000	0.045	0.332	1.000	0.049	0.345	1.000	0.047	0.341	1.000
48	0.045	0.331	1.000	0.047	0.340	1.000	0.051	0.353	1.000	0.048	0.348	1.000
49	0.046	0.339	1.000	0.048	0.348	1.000	0.053	0.361	1.000	0.050	0.356	1.000
50	0.047	0.346	1.000	0.050	0.355	1.000	0.054	0.369	1.000	0.051	0.364	1.000

Table 6.16. Time-zero probabilities of failure for Osseo structure located in Wisconsin Rapids, Wisconsin.

Location: Wisconsin Rapids							Latitude: 44.3592°					
							Longitude: -89.8369°					
Number of Years in Service	Orientation of Sign: N-S			Orientation of Sign: NE-SW			Orientation of Sign: E-W			Orientation of Sign: SE-NW		
	Probability of Failure			Probability of Failure			Probability of Failure			Probability of Failure		
	E2	E3	E4	E2	E3	E4	E2	E3	E4	E2	E3	E4
0	0.000	0.000	0.000	0.000	0.000	0.000	0.000	0.000	0.000	0.000	0.000	0.000
1	0.000	0.000	0.172	0.000	0.000	0.166	0.000	0.000	0.083	0.000	0.000	0.135
2	0.000	0.000	0.448	0.000	0.000	0.439	0.000	0.000	0.285	0.000	0.000	0.387
3	0.000	0.000	0.635	0.000	0.000	0.626	0.000	0.000	0.463	0.000	0.000	0.575
4	0.000	0.001	0.753	0.000	0.001	0.745	0.000	0.000	0.597	0.000	0.000	0.701
5	0.000	0.001	0.828	0.000	0.001	0.822	0.000	0.000	0.694	0.000	0.001	0.785
6	0.000	0.003	0.877	0.000	0.002	0.872	0.000	0.001	0.765	0.000	0.001	0.842
7	0.000	0.004	0.910	0.000	0.004	0.906	0.000	0.001	0.817	0.000	0.002	0.882
8	0.000	0.006	0.933	0.000	0.006	0.930	0.000	0.002	0.855	0.000	0.003	0.910
9	0.001	0.009	0.949	0.001	0.008	0.947	0.000	0.002	0.885	0.000	0.004	0.931
10	0.001	0.011	0.961	0.001	0.011	0.959	0.000	0.003	0.907	0.000	0.006	0.946
11	0.001	0.015	0.969	0.001	0.014	0.968	0.000	0.004	0.924	0.001	0.007	0.957
12	0.001	0.018	0.976	0.001	0.018	0.974	0.000	0.006	0.938	0.001	0.009	0.965
13	0.002	0.022	0.981	0.001	0.021	0.980	0.000	0.007	0.948	0.001	0.012	0.972
14	0.002	0.026	0.984	0.002	0.026	0.983	0.001	0.009	0.957	0.001	0.014	0.977
15	0.002	0.031	0.987	0.002	0.030	0.987	0.001	0.010	0.964	0.001	0.017	0.981
16	0.003	0.036	0.990	0.002	0.035	0.989	0.001	0.012	0.970	0.001	0.020	0.984
17	0.003	0.041	0.991	0.003	0.040	0.991	0.001	0.014	0.974	0.002	0.023	0.987
18	0.003	0.047	0.993	0.003	0.045	0.992	0.001	0.017	0.978	0.002	0.027	0.989
19	0.004	0.052	0.994	0.004	0.051	0.994	0.001	0.019	0.981	0.002	0.030	0.991
20	0.004	0.058	0.995	0.004	0.056	0.995	0.001	0.022	0.984	0.002	0.034	0.992
21	0.005	0.064	0.996	0.004	0.062	0.995	0.002	0.024	0.986	0.003	0.038	0.993
22	0.005	0.070	0.996	0.005	0.068	0.996	0.002	0.027	0.988	0.003	0.042	0.994
23	0.006	0.077	0.997	0.005	0.075	0.997	0.002	0.030	0.989	0.003	0.046	0.995
24	0.006	0.083	0.997	0.006	0.081	0.997	0.002	0.033	0.991	0.003	0.051	0.996
25	0.007	0.090	0.998	0.006	0.087	0.998	0.002	0.037	0.992	0.004	0.055	0.996
26	0.007	0.096	0.998	0.007	0.094	0.998	0.003	0.040	0.993	0.004	0.060	0.997
27	0.008	0.103	0.998	0.008	0.100	0.998	0.003	0.043	0.994	0.004	0.064	0.997
28	0.009	0.110	0.999	0.008	0.107	0.998	0.003	0.047	0.994	0.005	0.069	0.998
29	0.009	0.117	0.999	0.009	0.114	0.999	0.003	0.051	0.995	0.005	0.074	0.998
30	0.010	0.124	0.999	0.009	0.121	0.999	0.004	0.054	0.996	0.006	0.079	0.998
31	0.011	0.131	0.999	0.010	0.128	0.999	0.004	0.058	0.996	0.006	0.084	0.998
32	0.011	0.138	0.999	0.011	0.134	0.999	0.004	0.062	0.996	0.006	0.089	0.999
33	0.012	0.145	0.999	0.011	0.141	0.999	0.004	0.066	0.997	0.007	0.094	0.999
34	0.013	0.152	0.999	0.012	0.148	0.999	0.005	0.070	0.997	0.007	0.100	0.999
35	0.014	0.159	0.999	0.013	0.155	0.999	0.005	0.074	0.997	0.008	0.105	0.999
36	0.014	0.166	0.999	0.014	0.162	0.999	0.005	0.078	0.998	0.008	0.110	0.999
37	0.015	0.173	1.000	0.014	0.169	0.999	0.006	0.082	0.998	0.009	0.116	0.999
38	0.016	0.180	1.000	0.015	0.176	1.000	0.006	0.086	0.998	0.009	0.121	0.999
39	0.017	0.187	1.000	0.016	0.183	1.000	0.006	0.091	0.998	0.010	0.126	0.999
40	0.017	0.194	1.000	0.017	0.190	1.000	0.007	0.095	0.998	0.010	0.132	0.999
41	0.018	0.201	1.000	0.017	0.197	1.000	0.007	0.099	0.999	0.011	0.137	0.999
42	0.019	0.208	1.000	0.018	0.204	1.000	0.007	0.104	0.999	0.011	0.143	0.999
43	0.020	0.215	1.000	0.019	0.211	1.000	0.008	0.108	0.999	0.012	0.148	1.000
44	0.021	0.222	1.000	0.020	0.218	1.000	0.008	0.113	0.999	0.012	0.154	1.000
45	0.022	0.229	1.000	0.021	0.225	1.000	0.009	0.117	0.999	0.013	0.159	1.000
46	0.022	0.236	1.000	0.021	0.231	1.000	0.009	0.121	0.999	0.014	0.165	1.000
47	0.023	0.243	1.000	0.022	0.238	1.000	0.009	0.126	0.999	0.014	0.170	1.000
48	0.024	0.250	1.000	0.023	0.245	1.000	0.010	0.130	0.999	0.015	0.176	1.000
49	0.025	0.256	1.000	0.024	0.251	1.000	0.010	0.135	0.999	0.015	0.181	1.000
50	0.026	0.263	1.000	0.025	0.258	1.000	0.011	0.140	0.999	0.016	0.187	1.000

An example of how inspection intervals would be set for Milwaukee-type and Osseo-type sign supports in Milwaukee, Wisconsin can be explored using Tables 6.3 and 6.9. Table 6.3 indicates the following for a Milwaukee-type sign support, located in Milwaukee, Wisconsin with an E2-type connection detail. The tabulated data indicates that the first inspection for such a mast-arm need not occur for 13 years when the mast- arm is oriented N-S. The first inspection need not occur for 16 years, 18 years, and 14 years for NE-SW, E-W, and SE-NW orientations, respectively. As a result, one could conservatively say that 13 years can be defined as the first inspection for a Milwaukee-type mast-arm sign support put into service in Milwaukee, Wisconsin. The inspection intervals can then be tightened slightly as the 50% probability of finding a fatigue-induced crack threshold is approached. The 50/50 probability threshold occurs at 40 years, 49 years, greater than 50 years, and 41 years for the N-S, NE-SW, E-W and SE-NW orientations, respectively. Thus, one could say that from 13 years to 40 years, the inspection intervals can be lengthened somewhere between four and seven years for the Milwaukee-type sign support in Milwaukee, Wisconsin.

Table 6.3 also indicates that there is a very short yellow region for E3 type details thereby indicating that a lengthening of inspection intervals is likely not appropriate. Furthermore, the green region is very, very short for the E3 detail when compared to E2 detail configurations. The tabulated data suggests that E3 details used in Milwaukee-type sign supports should have their first inspections after five years, should then be inspected after an additional five years and then at four-year intervals after that. Therefore, the E3 detail configuration will require more inspections during the service life when compared to the E2 detail configuration. The tabulated data in Table 6.3 confirms the previous conclusion that E4 detail configurations should be avoided and will require very, very short inspection intervals.

Table 6.10 can be used in a similar manner as Table 6.3. It is interesting to note that if Osseo-type sign supports (*i.e.* non-tapered, heavy wall thickness, relatively small bluff area) are

used with E2 detail types, these signs would never require inspection in Milwaukee, Wisconsin. When the detail types migrate to E3, the first inspection can be conducted at 19 years. The yellow regions indicate that inspection intervals can increase to 7-year intervals after that until 43 years of service. After 43 years of service with no cracks present, the sign support should be inspected every four years. This results in a significant reduction in inspections when compared to a 50-year service-life with four-year intervals. The tabulated data also indicates that E4 type details with Osseo-type configuration should be avoided in Milwaukee, Wisconsin as fatigue-induced cracking is expected to occur at very short service lives.

The finite element analysis conducted for the Osseo-type mast-arm connection suggests that the Osseo-type mast-arm-to-pole connection tends to behave as an E4 detail type. The reason for this is because the bolt-hole configuration relative to the mast-arm centroidal axis results in stress concentration factors that are consistent with that suggested for the E4 detail types. The tabulated data contained in Table 6.11 indicates that E4 detail types in Osseo-type sign supports located in Eau Claire, Wisconsin have greater than 50% chance of having fatigue-induced cracks after three years of service. The Osseo sign support found with fatigue-induced cracks mentioned in chapter one (and exhaustively studied in Appendix A) was in service for approximately eight years and the reliability-based procedure formulated provides clear indication that this type of sign support would suffer from very, very poor in-service performance. This helps to confirm the ability of the procedure formulated in setting inspection protocols and identifying configurations, locations, and orientations with potential for poor in-service performance.

A summary of the data in Tables 6.3 through 6.16 is given in Table 6.17. This table allows one to gain a feel for how the inspection thresholds described earlier (*i.e.* 20% chance of finding a crack and 50% chance of finding a crack) maps onto all locations throughout the state of Wisconsin for all detail types and all mast-arm configurations. The summary data confirms that E4 details should be avoided throughout the state of Wisconsin. While E3 details do not perform

as well as E2 details, they can be used, but they will likely need relatively short first inspection intervals when compared to E2 detail types. The data also suggests that if an Osseo type configuration can be implemented with E2 detail categories, 50-year service lives should be expected and inspections of these types of sign supports may never need to occur with this service life expectation. In the case of Milwaukee-type mast-arm configurations with E2 detail types, first inspection intervals range from 13-36 years depending upon location with Milwaukee, Wisconsin experiencing the shortest interval. The service life interval to four-year inspection intervals for the E2 detail type ranges from 40 years to greater than 50 years with Milwaukee, Wisconsin again requiring the shortest interval.

Table 6.17. Inspection thresholds for mast-arm sign support structures in Wisconsin as a function of mast-arm type and detail configuration.

Location	Service-Life or Elapsed Time from Time-Zero (years)	Mast-Arm Configuration and Detail Type					
		E2 Detail		E3 Detail		E4 Detail	
		Milwaukee Type	Osseo Type	Milwaukee Type	Osseo Type	Milwaukee Type	Osseo Type
Milwaukee	First Inspection	13	> 50	5	19	1	1
	Four-Year Inspection Interval	40	> 50	10	43	NA	2
Eau Claire	First Inspection	28	> 50	9	38	1	2
	Four-Year Inspection Interval	> 50	> 50	20	> 50	NA	3
La Crosse	First Inspection	19	> 50	6	26	1	2
	Four-Year Inspection Interval	> 50	> 50	14	> 50	NA	3
Green Bay	First Inspection	16	> 50	6	24	1	1
	Four-Year Inspection Interval	48	> 50	13	> 50	NA	2
Madison	First Inspection	36	> 50	12	50	1	2
	Four-Year Inspection Interval	> 50	> 50	26	> 50	2	3
Oshkosh	First Inspection	22	> 50	7	31	1	1
	Four-Year Inspection Interval	> 50	> 50	16	> 50	NA	2
Wisconsin Rapids	First Inspection	33	> 50	10	41	1	2
	Four-Year Inspection Interval	> 50	> 50	21	> 50	NA	3

6.6 – Concluding Remarks

A reliability-based assessment procedure was outlined in the present chapter. The process formulated was applied to compute probabilities of finding fatigue-induced cracks initiating with variation in service life. Cumulative distribution functions describing these failure probabilities were presented for two different mast-arm structure configurations (Milwaukee-type and Osseo-type), with the potential for three different detail categories (E2, E3, E4), located in seven different cities throughout Wisconsin (Milwaukee, Eau Claire, La Crosse, Green Bay, Madison, Oshkosh, Wisconsin Rapids), and four orientations relative to North (N-S, NE-SW, E-W,NW-SE). These cumulative distribution functions were then displayed in tabulated format to define service life intervals and inspection protocols for mast-arm sign supports.

The reliability-based assessment process developed and implemented in this study suggests that E4 detail types be avoided in mast-arm sign support structures. The orientation of the bolt holes relative to the centroidal axis of the mast arm as seen in the Osseo-type mast-arm-to-pole connection results in significant stress concentration factors that approach this detail category. As a result, mast-arm-to-pole connection details that are like the Osseo sign support structure studied in this research effort should be avoided as well. Milwaukee-type connection details are preferable and approach E2 type behavior.

The reliability-based assessment conducted suggests that E2 detail types used in Osseo-type mast-arm configurations are ideal and may never need inspections during their service life. In other words, the Milwaukee-type connection detail is preferable with larger second moments of area used in the mast-arm as seen in the Osseo sign support. The assessment also suggests that Milwaukee-type mast-arm support structures with E2 detail types can have significantly reduced inspections from the regular four-year interval currently used. It is recommended that the first inspection interval for these types of mast arms with E2 connection types be as short as 13 years

and as long as 36 years depending upon location. Sign supports located in Milwaukee should have their first inspection interval set at shorter duration than elsewhere within the State. The time to four-year inspection intervals for these sign types and details can then be after 40 years of service life in Milwaukee and longer elsewhere within the State.

CHAPTER 7 – CONCLUSIONS AND RECOMMENDATIONS

7.1 – Summary

The present research study set out to formulate, apply, and discuss a reliability-based procedure for quantifying the risk of fatigue-induced fracture in mast-arm sign support structures and to generate inspection protocols for these structural systems using this procedure. This procedure was intended to be used to identify mast-arm support structural system configurations that are likely to result in enhanced susceptibility to premature fatigue-induced cracking and poor in-service performance. It was also used to identify regions within the state of Wisconsin that may be more susceptible to having structures with fatigue problems.

The second chapter of this dissertation (Quantifying Wind Demand Uncertainty) provided a detailed development of the information needed to determine the stress parameter that was integral to quantifying demand in the reliability-based formulation. A process through which wind speed and direction data was collected, synthesized and statistically analyzed was described. Individual, conditional, and combined probabilities of one-hour averaged wind speed and one-hour averaged wind direction have been computed for discrete locations throughout the state of Wisconsin and at a field monitoring station designed, constructed and deployed as part of a larger research effort. An interpolation procedure which allows for the computation of combined probabilities at any location throughout the state of Wisconsin has been presented. Data tables defining the probability of one-hour averaged wind speed intersected with cardinal direction, $P\left(U = u_i \bigcap D = d_j\right)$, were developed.

The third chapter of this dissertation (Quantifying Fatigue Life Uncertainty) outlined development of the random variable parameters necessary for defining uncertainty related to fatigue life. A comprehensive synthesis of fatigue testing data, including tests completed as part

of the present research effort, was included within the discussion of this chapter. Random variable fatigue life modeling parameters, μ_A, CV_A, and a best-fit fatigue life exponent, m, were formulated in this chapter for three proposed detail categories: E2, E3, and E4. These new detail categories were synthesized from the myriad of fatigue tests conducted since 1970 on welded connection details that are typical of those seen in mast-arm sign support structures in Wisconsin. These new detail categories are based upon stress concentration factors developed using high-fidelity finite element analysis and are shown in later chapters to successfully predict early fatigue-induced cracking failure of a sign support in Osseo, Wisconsin.

The fourth chapter of this dissertation (FE Modeling of Sign Support Structures) described the development of high- and low-fidelity finite element (FE) models for two structures typically found in Wisconsin (*i.e.* Milwaukee structure and Osseo structure). Three comparative studies between structure-type and model-type were performed to determine the structural response characteristics for each. It was concluded that the Osseo structure contained much higher stress concentration effects from its welded connection compared to the Milwaukee structure. Further, it was determined that low-fidelity modeling approaches may adequately capture the structural response characteristics (as compared to its high-fidelity counterpart) and are appropriate for conducting the simulations necessary to carry out the reliability-based fatigue assessment of mast-arm sign support structures.

The fifth chapter of this dissertation (Quantifying Modeling Error Uncertainty) outlined the formulation of modeling error uncertainty as a lognormal random variable characterized by two parameters: μ_B and CV_B. This random variable model was formulated using data from a field monitoring station located in Milwaukee, Wisconsin and comparison of acquired data with low-fidelity finite element modeling that included simulated wind loading and response histories.

It should be noted that the random variable model for fatigue damage accumulation has not been addressed in the present research effort. Revision to the widely accepted Miner's Rule for fatigue damage accumulation was simply outside the scope of this effort. The present research report utilizes a lognormal random variable for accumulated fatigue damage with parameters given by $\mu_{\Delta} = 1.00$ and $CV_{\Delta} = 0.30$ used by previous researchers (Wirsching 1983; Wirsching 1984; Wirsching 1988).

The sixth chapter of this dissertation (Reliability-Based Inspection Protocols) applied the reliability-based assessment procedure for sign support structures and presented cumulative distribution functions illustrating the variation in probabilities of finding fatigue-induced cracks versus service life for two sign support structure types, three fatigue detail categories, four fundamental orientations of mast-arm relative to North, and seven different cities within Wisconsin. These cumulative distribution functions were displayed in a tabular format that allowed inspection frequencies to be defined and evaluated for these structural systems.

7.2 – Conclusions and Recommendations

The research effort facilitates a significant number of conclusions that may be very useful to WisDOT and the rest of the engineering community for management of mast-arm sign support structures. It also facilitates recommendations that can be used to better understand behavior of mast-arm sign support structures, understanding and characterizing wind load demands, and the susceptibility of these relatively simple structural systems to premature fatigue-induced cracking and poor in-service performance.

A comparison between NCDC-ASOS site data for Milwaukee, Wisconsin and the data acquired at the FMS site indicates that local topography has a significant impact on mean one-hour average wind speed and one-hour wind speed standard deviation, and a minor effect on wind

direction. Based upon the FMS site considered in the present study, a lower mean and standard deviation in the wind speed appears to occur when the sign support structure site is in urban and suburban terrain compared to flat, open terrain like that found at NCDC-ASOS sites. Therefore, use of ASOS sites will result in higher mean wind speeds, greater wind speed variability and likely greater wind loading demand (from a fatigue point of view) than what will likely occur at a sign structure site in the middle of an urban or suburban terrain.

An interpolation procedure for wind speed probability distributions for each of eight cardinal directions was evaluated using NCDC-ASOS site data and the FMS site data. This evaluation indicated that when interpolating combined probability distributions computed from wind speed and direction statistics gathered from NCDC-ASOS sites, the combined probability distributions in each of the eight cardinal directions appear to be conservative. Greater density of higher wind speed magnitudes result when the interpolation procedure is implemented. The wind speed variability is also likely to be slightly larger than the variability that can be expected at the sign structure location.

Three new detail categories for fatigue life modeling founded on the stress concentration factor approach were proposed: E2, E3, and E4. High-fidelity finite element modeling, comparisons with parametric expressions for computing stress concentration factors (*SCF*s) proposed by others (Roy et al. 2011), and synthesis of hundreds of fatigue tests support these new detail categories. It is recommended that mast-arm sign support structures use these alternate detail categories when fatigue-life is being assessed. Furthermore, it is recommended that the E2, E3, and E4 detail categories be used in reliability assessment procedures and be used to formulate design procedures for infinite life-based assessment.

The high- and low-fidelity finite element modal analyses used to evaluate sensitivity of the model in predicting modal frequencies of vibration and mode shapes indicates that low fidelity finite element models are acceptable for dynamic analysis of the structural systems.

The one-hour duration transient wind speed histories generated using the Kaimal turbulence spectrum exhibited expected variability about the mean at all one-hour average wind speeds considered and therefore, the simulation procedure developed is deemed accurate for use in conjunction with the low-fidelity finite element modeling. Comparisons to measured wind speed histories and wind speed variation about the mean indicate that wind speed simulation is a viable procedure for fatigue life estimation.

The lognormal modeling parameters used to quantify modeling error uncertainty in mast-arm sign support systems were found to be consistent with values that have been assumed in past research when conducting reliability analysis of structures in the offshore industry (Wirsching 1983). The present study provides measured data to formalize these types of assumptions upon a foundation that is more realistic and systematic.

The high-fidelity and low-fidelity finite element models for these sign supports used to identify locations around the circumference of the mast-arm tube where fatigue-induced cracks were likely to form first indicates that, while the Milwaukee-type sign support structure is expected to experience larger magnitude expected stress-ranges, the location where these stress-ranges occur are significantly different when compared to the Osseo-type sign support structure. The maximum expected stress-ranges in the Milwaukee sign support tend to form near 80-90 degrees relative to vertical. This location is a significant distance away from the location where peak gravity load tensile stress exists for the Milwaukee sign. In the case of the Osseo sign support structure, the peak expected stress-range magnitudes migrate to locations in the 70-80

degree range from vertical and the stress-range actually reduces at 80-90 degrees from the vertical axis.

The analysis conducted in the present effort indicates that extremely wide spacing of the bolts in the mast-arm-to-pole connection found in the Osseo sign support suggests that there will be a significant tendency for the gravity (dead) load tensile stress-ranges to act in concert with the tensile stress-ranges resulting from the lateral wind loads acting on the sign support. Thus, it is expected that crack initiation is likely to occur in locations lying along a line extending from the centroidal axis of the mast arm to the top bolt in the connection (on either side of the mast arm). This is consistent with the crack locations found in the Osseo sign support (see failure analysis located in Appendix A).

The reliability-based assessment process developed and implemented in this study suggests that E3 and E4 detail types be avoided in mast-arm sign support structures. The orientation of the bolt holes relative to the centroidal axis of the mast arm as seen in the Osseo-type mast-arm-to-pole connection, results in significant stress concentration factors that approach the E4 detail category. As a result, mast-arm-to-pole connection details that are like the Osseo sign support structure studied in this research effort should be avoided as well. Milwaukee-type connection details are preferable and approach E2 type behavior.

The reliability-based assessment conducted suggests that E2 detail types used in Osseo type mast-arm configurations are ideal and may never need inspections during their service life. In other words, the Milwaukee-type connection detail is preferable with larger second moments of area used in the mast-arm as seen in the Osseo sign support. The assessment also suggests that Milwaukee-type mast-arm sign support structures with E2 detail types can have a significantly reduced number of inspections during their service lives when compared to the four-year inspection cycle currently utilized by WisDOT.

It is recommended that the first inspection interval for Milwaukee-type mast-arm supports with E2 type detail category connections can be assigned in the range from 13 years to 36 years depending upon location. Sign supports located in Milwaukee should have their first inspection interval set at shorter duration than elsewhere within the State. The time to four-year inspection intervals for these sign types and details can then be after 40 years of service life in Milwaukee and longer elsewhere within the State. In fact, the study conducted suggests that if service lives for these structures is defined as 30 years, there are locations within the State where these structures need never be inspected.

The procedures developed and employed in the present research effort indicate that implementation of state-of-the-art reliability-based assessment procedures can contribute very valuable procedures for assigning inspection protocols (*i.e.* inspection intervals) that are based upon probabilities of finding fatigue-induced cracking in these structures. The engineering community can use the results of the research effort to design inspection intervals based upon risk and thereby better align inspection needs with fiscal and human resources.

7.3 – Future Work

No comprehensive research effort is complete without recommending additional research efforts to extend the work just completed. This section of the dissertation outlines several recommendations that can be used by WisDOT to improve their mast-arm sign support structure performance, formulate more reliable inspection intervals and perhaps even formulate designs that need never be inspected once put into service. It also provides recommendations for additional research efforts to achieve these goals.

The synthesis of wind speed data conducted indicates that because sign support structures typically exist at locations that are remote from where wind data is measured (*i.e.* NCDC-ASOS

sites), there is a need to develop an accurate methodology for including topographical effects. It is recommended that additional field monitoring systems be deployed throughout the State. This would allow further evaluation, confirmation and modification of the interpolation procedure proposed in this research effort so that combined probabilities of wind speed and wind direction can be accurately computed throughout the State. This would allow much greater understanding of the impact of topography and would facilitate modifications to the interpolation procedure that allow topography to be better incorporated in the procedure.

It is suggested that acceptable levels of risk for finding fatigue-induced cracks be discussed and assigned for these structures. Furthermore, it is recommended that these risk levels (*i.e.* probabilities of a crack initiated) be defined in lieu of service lives after installation. In other words, what is the acceptable probability of a crack initiating in a mast arm after 30 years of service? Is it 50%? Is it 25%? If these probabilities could be established, the reliability assessment procedure could be tailored very easily to directly assign inspection intervals. The results of the present study indicate that these inspection intervals would likely be very long in duration. Inspections in some locations may not even be necessary.

The procedures developed in the present study were unable to consider the impact of crack initiation and propagation on remaining service life. If WisDOT would like to determine how crack initiation and crack growth are expected to impact remaining service life after crack initiation has been identified, then a detailed analysis of crack propagation rates and material toughness for WisDOT standard materials for sign supports would need to be undertaken. This would be a very interesting study because it would give WisDOT (and the rest of the engineering community) a better understanding of how long a typical mast-arm can remain in place with a crack prior to full cross-section fracture. This would allow scheduling for re-design, fabrication, and installation of new sign supports when cracks are found. In other words, the sense of emergency repair/replacement may be able to be avoided.

The syntheses of experimental fatigue testing results in this dissertation were limited to tests conducted on welded connections typically found in sign support structures. It would be very interesting to extend this approach to all fatigue tests conducted on welded steel connections (*i.e.* welded connections typically found in bridge and building details) to date. New fatigue detail categories based upon the magnitude of stress concentration factor present within these connections can be developed. Stress-life (S_R-N) curves can be defined based upon statistical parameters for each detail and expected fatigue life with known variation can be assigned to existing structural configurations.

It is recommended that a study similar to the present be undertaken for high-mast luminaire supports and full-span sign support structures. The reliability-based procedure developed and implemented in the present study would add to the work previously conducted (Foley et al. 2004) for these structural systems. WisDOT would then have the ability to establish inspection protocols for all auxiliary structures in the highway network using the methodology developed in this study.

Finally, it would be interesting to adapt the methodology formulated and implemented in this study to highway bridges in the Wisconsin infrastructure network. A field monitoring program for a typical steel bridge could be developed in a manner analogous to the field monitoring station designed and deployed in this effort. This monitoring system could be used to generate modeling error uncertainty parameters that then could be used directly in a reliability-based assessment of the bridge. Inspection protocols could then be developed for tolerable levels of risk in finding fatigue-induced cracks at critical details in the superstructure of typical steel bridges.

REFERENCES

AASHTO (2009). *Standard Specifications for Structural Supports for Highway Signs, Luminaires and Traffic Signals, 5th Edition with 2010 Interim Revisions*, American Association of State Highway and Transportation Officials, Washington, D.C.

Alderson, J. L. (1999). "Fatigue Study of Cantilevered Traffic Signal Mast Arms."MS Thesis, University of Missouri - Columbia.

Anderson, T. H. (2007). "Fatigue Life Investigation of Traffic Signal Mast-Arm Connection Details."MS Thesis, University of Texas - Austin.

Archer, G., and Gurney, M. (1970). "Fatigue Strength of Mild-Steel Fillet Weld Tube to Plate Joints." *Metal Construction and British Welding Journal*, 2(5), 207-210.

ASCE (1998). *Minimum Design Loads for Buildings and Other Structures (ASCE 7-98)*, American Society of Civil Engineers, Reston, VA.

ASCE (2005). *Minimum Design Loads for Buildings and Other Structures (ASCE 7-05)*, American Society of Civil Engineers, Reston, VA.

ASOS (1998). "Automated Surface Observing System User's Guide."

Assakkaf, I. A., and Ayyub, B. M. (1999). "Reliability-Based Design for Fatigue of Marine Structures."

Atadero, R. A., Goode, J. S., and van de Lindt, J. W. "Development of Lifetime Statistical Distributions of Wind Speed for Fatigue-Based Design." *Proc., 2007 Structures Congress: New Horizons and Better Practices*, American Society of Civil Engineers.

AWS (1999). *Structural Welding Code - Steel, 17th Edition (ANSI/AWS D1.1-98)*, American Welding Society, Miami, FL.

Beaupuits, J. P. P., Otarola, A., Rantakyro, F. T., Rivera, R. C., Radford, S. J. E., and Nyman, L. (2004). "Analysis of Wind Data Gathered at Chajnantor." *ALMA Memo*.

Buchholdt, H. (1997). *Structural Dynamics for Engineers*, Thomas Telford Publications, London, U.K.

Byers, W. G., Marley, M. J., Mohammadi, J., Nielson, R. J., and Sarkarni, S. (1997a). "Fatigue Reliability Reassessment Procedures: State-of-the-Art Paper." *Journal of Structural Engineering*, 123(3), 271-276.

Chen, G., Barker, M., Dharani, L. R., and Ramsay, C. (2003). "Signal Mast Arm Fatigue Failure Investigation." Missouri Department of Transportation, Jefferson City, MO.

Chen, G., Barker, M., MacKenzie, D. S., Ramsay, C., Alderson, J., Dharani, L., and Yu, J. (2002). "Forensic Investigation of Failed Mast Arms of Traffic Signal Supported Structures." *Transportation Research Record, Journal of the Transportation Research Board, No. 1814 - Design of Structures 2002*, 9-16.

Chen, Z. W., Xu, Y. L., and Wang, X. M. (2012). "SHMS-Based Fatigue Reliability Analysis of Multiloading Suspension Bridges." *Journal of Structural Engineering*, 138(3), 299-307.

Chopra, A. K. (2001). *Dynamics of Structures Theory and Applications to Earthquake Engineering*, Prentice-Hall, Inc., Upper Saddle River, NJ.

Chung, H. Y., Manuel, L., and Frank, K. H. "Reliability-Based Optimal Inspection for Fracture-Critical Steel Bridge Members." *Proc., TRB 2003 - 82nd Annual Meeting of the Transportation Research Board*, National Research Council, CD-ROM.

Cook, R. A., Bloomquist, D., Agosta, A. M., and Taylor, K. F. (1996). "Wind Load Data for Variable Message Signs." Florida Department of Transportation, 120.

Creamer, B. M., Frank, K. H., and Klingner, R. E. (1979). "Fatigue Loading of Cantilever Sign Structures from Truck Wind Gusts." Center for Highway Research, University of Texas - Austin, Austin, TX.

Deoliya, R., and Datta, T. K. (2001). "Fatigue Reliability Analysis of Microwave Antenna Towers Due to Wind." *Journal of Structural Engineering*, 127(10), 1221-1229.

DeSantis, P. V., and Haig, P. E. "Unanticipated Loading Causes Highway Sign Failure." *Proc., ANSYS Convention*, ANSYS Inc., 3.99-93.108.

Deschamp, B. (2002). "Fatigue Testing of Traffic Signal Structures."M.S. Thesis, University of Wyoming, Laramie, WY.

Diekfuss, J. A., and Foley, C. M. "Probabilistic Wind Model for Reliability-Based Fatigue Evaluation of Sign Support Structures." *Proc., 3rd International Structural Specialty Conference*, Canadian Society of Civil Engineers, (CD-ROM).

Dyrbye, C., and Hansen, S. O. (1997). *Wind Loads on Structures*, John Wiley & Sons Ltd., Chichester.

Edwards, J. A., and Bingham, W. L. (1984). "Deflection Criteria for Wind Induced Vibrations in Cantilever Highway Sign Structures." Center for Transportation Engineering Studies, North Carolina State University, Rayleigh, NC, 124.

Ellingwood, B. R., and Tekie, P. B. (1999). "Wind Load Statistics for Probability-Based Structural Design." *Journal of Structural Engineering*, 125(4), 453-463.

Fisher, J. W., Kulak, G. L., and Smith, I. F. C. (1998). *A Fatigue Primer for Structural Engineers*, American Institute of Steel Constrution, National Steel Bridge Alliance, Chicago, IL.

Fisher, J. W., Slutter, R. G., and Miki, C. (1981). "Fatigue Behavior of Steel Light Poles." California Department of Transportation, Sacramento, CA.

Foley, C. M., Ginal, S. J., Peronto, J. L., and Fournelle, R. A. (2004). "Structural Analysis of Sign Bridge Structures and Luminaire Supports." Wisconsin Highway Research Program, Madison, WI.

Foley, C. M., Wan, B., Weglarz, M., Hellenthal, M., Komp, J., Smith, A., and Schmidt, J. P. (2008). "Fatigue Risks in the Connections of Sign Support Structures - Phase 1." Wisconsin Highway Research Program, Wisconsin Department of Transportation.

Fouad, F. H., Calvert, E. A., and Nunez, E. (1998). "Structural Supports for Highway Signs, Luminaires, and Traffic Signals." Transportation Research Board, National Research Council, Washington, D.C., 114.

Gilani, A. S., Chavez, J. W., and Whittaker, A. S. (1997). "Fatigue-Life Evaluation of Changeable Message Sign Structures, Volume 1 - As Built Structures." Earthquake Engineering Research Center, University of California, Berkeley, CA.

Ginal, S. J. (2003). "Fatigue Performance of Full-Span Sign Support Structures Considering Truck-Induced Gust and Natural Wind Pressures."MS Thesis, Marquette University, Milwaukee, WI.

Goode, J. S., and van de Lindt, J. W. (2007). "Development of a Semiprescriptive Selection Procedure for Reliability-Based Fatigue Design of High-Mast Lighting Structural Supports." *Journal of Performance of Constructed Facilities*, 21(3), 193-206.

Google. 2012.

Guo, T., Frangopol, D. M., and Chen, Y. (2012). "Fatigue Reliability Assessment of Steel Bridge Details Integrating Weigh-in-Motion Data and Probabilistic Finite Element Analysis." *Computers & Structures*, 245-257.

Haldar, A., and Mahadevan, S. (2000). *Probability, Reliability, and Statistical Methods in Engineering Design*, John Wiley & Sons, Inc., New York, NY.

Iannuzzi, A., and Spinelli, P. (1987). "Artificial Wind Generation and Structural Response." *Journal of Structural Engineering*, 113(12), 2382-2398.

Irwin, H. P., and Peeters, M. (1980). "An Investigation of the Aerodynamic Stability of Slender Sign Bridges, Calgary." National Research Council Canada - Aeronautical Establishment.

Johns, K., and Dexter, R. J. (1998). "Fatigue Related Wind Loads on Highway Support Structures." Center for Advanced Technology for Large Structural Systems, Lehigh University, Bethlehem, PA.

Johns, K. W., and Dexter, R. J. (1998). "The Development of Fatigue Design Load Ranges for Cantilevered Sign and Signal Support Structures." *Journal of Wind Engineering and Industrial Aerodynamics*, 77 & 78(Sep-Dec), 315-326.

Johns, K. W., and Dexter, R. J. "Truck Induced Wind Loads on Highway Sign Support Structures." *Proc., Structural Engineering in the 21st Century, Proceedings of the 1999 Structures Congress*, American Society of Civil Engineers - Structural Engineering Institute, 1103-1106.

Kaczinski, M. R., Dexter, R. J., and Van Dien, J. P. (1998). "Fatigue Resistance Design of Cantilevered Signal, Sign and Light Supports." ATLSS Engineering Research Center, Bethlehem, PA.

Kaimal, J. C. (1972). "Spectral Characteristics of Surface-Layer Turbulence." *Journal of the Royal Meteorological Society*, 98, 563-589.

Koenigs, M. T. (2003). "Fatigue Resistance of Traffic Signal Mast-Arm Connection Details."MS Thesis, University of Texas - Austin, Austin, TX.

Koenigs, M. T., Botros, T. A., Freytag, D., and Frank, K. H. (2003). "Fatigue Strength of Signal Mast Arm Connections." Center for Transportation Research at the University of Texas at Austin, Austin, TX.

Kwon, K., and Frangopol, D. M. (2010). "Bridge Fatigue Reliability Assessment Using Probability Density Functions of Equivalent Stress Range Based on Field Monitoring Data." *International Journal of Fatigue*, 1221-1232.

Kwon, K., Frangopol, D. M., and Soliman, M. (2012). "Probabilistic Fatigue Life Estimation of Steel Bridges by Using a Bilinear S-N Approach." *Journal of Bridge Engineering*, 17(1), 58-70.

Levy, R. (1996). *Structural Engineering of Microwave Antennas*, Institute of Electrical and Electronic Engineers, Inc., New York, NY.

Li, Q., Wang, K. C. P., and Hall, K. D. (2010). "Verification of Virtual Climatic Data in MEPDG Using the LTPP Database." *International Journal of Pavement Research and Technology*, 3(1), 10-15.

Li, X., Whalen, T. M., and Bowman, M. D. "Fatigue Strength and Evaluation of Double-Mastarm Cantilevered Sign Structures." *Proc., TRB 2005 Annual Meeting*, (CD-ROM).

Little, R. E., and Jebe, E. H. (1975). *Statistical Design of Fatigue Experiments*, Applied Science Publishers, Ltd., London, U.K.

Liu, H. (1991). *Wind Engineering: A Handbook for Structural Engineers*, Prentice Hall, Inc., Englewood Cliffs, NJ.

Liu, M., Frangopol, D. M., and Kwon, K. (2012). "Fatigue Reliability Assessment of Retrofitted Steel Bridges Integrating Monitored Data." *Structural Safety*, 77-89.

Machietto, C. "Valmont Fatigue Testing Presentation." *Proc., AASHTO T-12 Committee, November*.

Matsuishi, M., and Endo, T. (1968). "Fatigue of Metals Subjected to Varying Stress." Japan Society of Mechanical Engineers.

McDonald, J. R., Mehta, K. C., Oler, W., and Pulipaka, N. (1995). "Wind Load Effects on Signs, Luminaires and Traffic Signal Structures." Wind Engineering Research Center - Texas Tech University, Lubbock, TX.

Miner, M. A. (1945). "Cumulative Damage in Fatigue." *Transaction of the ASME, Journal of Applied Mechanics*, 67, A159-A164.

Ni, Y. Q., Ye, X. W., and Ko, J. M. (2010). "Monitoring-Based Fatigue Reliability Assessment of Steel Bridges: Analytical Model and Application." *Journal of Structural Engineering*, 136(12), 1563-1573.

Nieslony, A. 2010. Rainflow Counting Algorithm, MATLAB Central File Exchange.

Nowak, A. S., and Collins, K. R. (2000). *Reliability of Structures*, McGraw-Hill, New York, NY.

Ocel, J. M. (2006). "The Behavior of Thin Hollow Structural Section (HSS) to Plate Connections."PhD Thesis, University of Minnesota, Minneapolis, MN.

Ocel, J. M., Dexter, R. J., and Hajjar, J. F. (2006). "Fatigue-Resistant Design for Overhead Signs, Mast-Arm Signal Poles, and Lighting Standards." Minnesota Department of Transportation, St. Paul, MN, 190 pages.

Peterka, J. A. (1992). "Improved Extreme Wind Prediction for the United States." *Journal of Wind Engineering and Industrial Aerodynamics*, 533-541.

Peterka, J. A., and Shahid, S. (1998). "Design Gust Wind Speeds in the United States." *Journal of Structural Engineering*, 124(2), 207-214.

Phares, B. M., Sarkar, P. P., Wipf, T. J., and Chang, B. (2007). "Development of Fatigue Procedures for Slender, Tapered Support Structures for Highway Signs, Luminaires, and Traffic Signals Subjected to Wind-Induced Excitation from Vortex-Shedding and Buffeting."

Puckett, J. A., Erikson, R. G., and Peiffer, J. P. (2010). "Fatigue Testing of Stiffened Traffic Signal Structures." *Journal of Structural Engineering*, 136(10), 1205-1214.

Richman, N. B. (2009). "Fatigue Life Investigation of High Performance Mast Arm Base Plate Connections."MS Thesis, University of Texas - Austin.

Rios, C. A. (2007). "Fatigue Performance of Multi-Sided High-Mast Lighting Towers." M.S. MS Thesis, University of Texas at Austin, Austin, TX.

Roy, S., Park, Y. C., Sause, R., and Fisher, J. W. (2012). "Fatigue Performance of Stiffened Pole-to-Base Plate Socket Connections in High-Mast Structures." *Journal of Structural Engineering*, 138(10), 1203-1213.

Roy, S., Park, Y. C., Sause, R., Fisher, J. W., and Kaufmann, E. J. (2011). "Cost-Effective Connection Details for Highway Sign, Luminaire, and Traffic Signal Structures." ATLSS Center, Bethlehem, PA.

SAS (2013). "ANSYS 14.0 Element Library & Theory Reference."

Schilling, C. G., Klippstein, K. H., Barson, J. M., and Blake, G. T. (1978). "Fatigue of Welded Steel Members Under Variable-Amplitude Loadings." National Cooperative Highway Research Program, Washington, D.C.

Shinozuka, M., and Jan, C. (1972). "Digital Simulation of Random Processes and Its Applications." *Journal of Sound and Vibration*, 25(1), 111-128.

Simiu, E., Changery, M. J., and Filliben, J. J. (1980). "Extreme Wind Speeds at 129 Airport Stations." *Journal of the Structural Division*, 106, 801-817.

Simiu, E., and Scanlon, R. H. (1996). *Wind Effects on Structures: Fundamentals and Applications to Design - 3rd Edition*, John Wiley & Sons, Inc., New York, NY.

Simiu, E., Wilcox, R., Sadek, F., and Filliben, J. J. (2003). "Wind Speeds in ASCE 7 Standard Peak-Gust Map: Assessment." *Journal of Structural Engineering*, 129(4), 427-439.

Smith, A. D. (2010). "Real-Time Health Monitoring System for Mast-Arm Sign Support Structures."MS Thesis, Marquette University, Milwaukee, WI.

Sommer, A. M., Nowak, A. S., and Thoft-Christensen, P. (1993). "Probability-Based Bridge Inspection Strategy." *Journal of Structural Engineering*, 119(12), 3520-3536.

South, J. (1994). "Fatigue Analysis of Overhead Sign and Signal Structures." Illinois Department of Transportation, Springfield, IL.

South, J. (1997). "Fatigue of Tube-to-Plate Fillet Welds and Methods for Their Improvement." Illinois Department of Transportation, Springfield, IL.

Swokowski, E. W. (1979). *Calculus with Analytic Geometry*, Prindle, Weber & Schmidt, Boston, MA.

Tedesco, J. W., MacDougal, W. G., and Ross, C. A. (1999). *Structural Dynamics: Theory and Applications*, Addison Wesley Publishing Company, Inc.

Type, M. (2012). "Movable Type Scripts." <http://www.movable-type.co.uk/scripts/latlong.html>. (May 24, 2012).

van de Lindt, J. W., and Goode, J. S. (2006). "Development of Reliability-Based Design Procedure for High-Mast Lighting Structural Supports in Colorado." Colorado State University.

Wang, C. S., Long, H., and Fu, B. N. (2012). "Fatigue Reliability Updating Evaluation of Existing Steel Bridges." *Journal of Bridge Engineering*, 17(6), 955-965.

Wirsching, P. H. (1983). "Probability-Based Fatigue Design Criteria for Offshore Structures." American Petroleum Institute, Dallas, TX.

Wirsching, P. H. (1984). "Fatigue Reliability for Offshore Structures." *Journal of Structural Engineering*, 110(10), 2340-2356.

Wirsching, P. H. (1988). "Probability-Based Fatigue Design for Marine Structures." *Marine Structures*, 11(1), 23-45.

Ye, X. W. (2010). "Fatigue Reliability Assessment of Steel Bridges Instrumented with Structural Health Monitoring System." PhD, The Hong Kong Polytechnic University, Kowloon, Hong Kong.

Zhao, Z., Haldar, A., and Breen Jr., F. L. (1994a). "Fatigue-Reliability Evaluation of Steel Bridges." *Journal of Structural Engineering*, 120(5), 1608-1623.

Zhao, Z., Haldar, A., and Breen Jr., F. L. (1994b). "Fatigue-Reliability Updating through Inspections of Steel Bridges." *Journal of Structural Engineering*, 120(5), 1624-1642.

APPENDIX A – FAILURE ANALYSIS OF OSSEO STRUCTURES

A.1 - Background

The failed components analyzed in the present failure analysis are from two cantilever sign-support structures. The sign-support structures, S-61-0001 and S-61-0002, were in service in Osseo, Wisconsin from 2003 until 2011. These sign-support structures are two of many found within the Wisconsin Department of Transportation (WisDOT) infrastructure network. Sign-support structures are relatively simple structures and can take on several different geometries.

The failure addressed in this report occurred in the mast arms of the two sign supports, where the tube is welded to the socketed plate. These cantilevered mast arms were 44 feet long and supported three individual 24 inch x 30 inch traffic signs.

Unfortunately, the sign-support structures were decommissioned and scheduled to be replaced immediately after the cracks were detected. As a result, there was no opportunity to photograph the failed components in their service condition. However, Figure A.1 displays a bird's eye view satellite image of the Osseo structures. The structures were located at the exits from Interstate 94 in Osseo, WI. S-61-0001 was located on the southbound exit ramp and S-61-0002 was located on the northbound exit ramp.

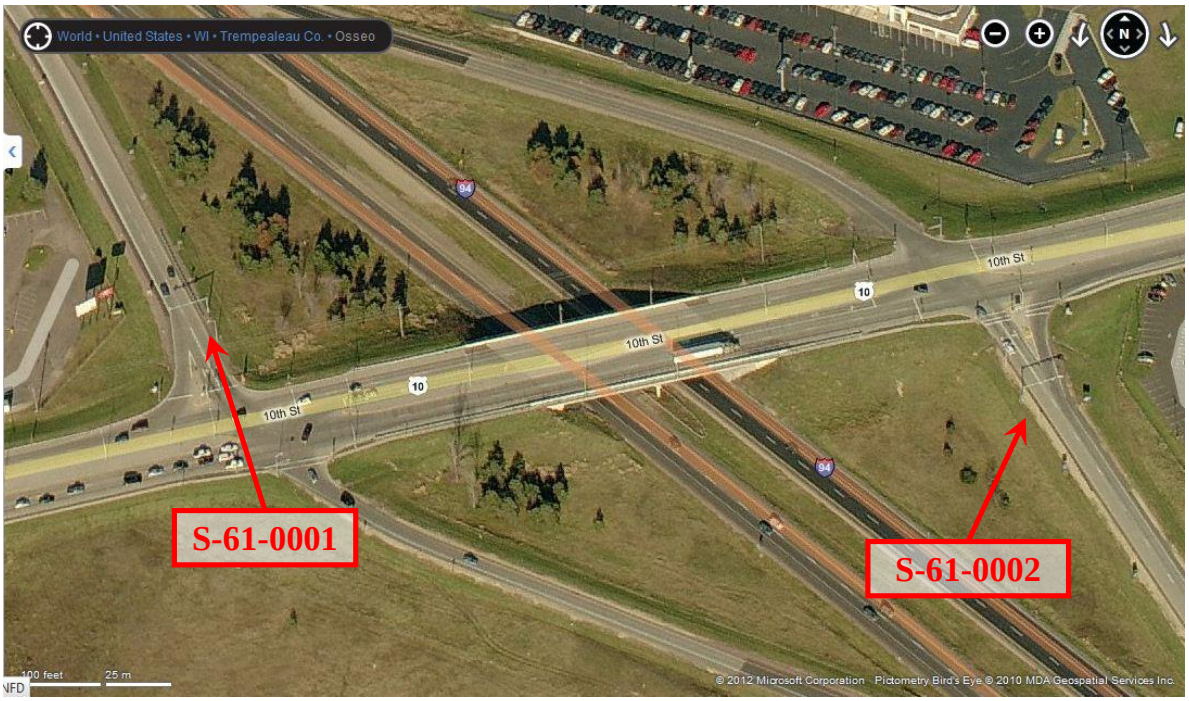

Figure A.1. Satellite bird's eye view of the Osseo, WI exit from I-94 (Bing Maps 2012).

A.2 – Materials Characterization

The first step in characterizing the material used in the fabrication of the Osseo sign structures involved the retrieval of the fabrication drawings and broken pieces. The socketed connections were removed from the rest of the mast-arms via the use of a partner saw and were brought back to the Marquette University Engineering Materials and Structural Testing Laboratory (EMSTL) on October 21, 2011. As shown on the drawings obtained from WisDOT, the tubes used for the poles and mast arms were made from API 5Lx42 steel. The steel plates used for the bolted connections were made from ASTM A36 steel. A photo of the connections obtained from the failed structures is provided in Figure A.2.

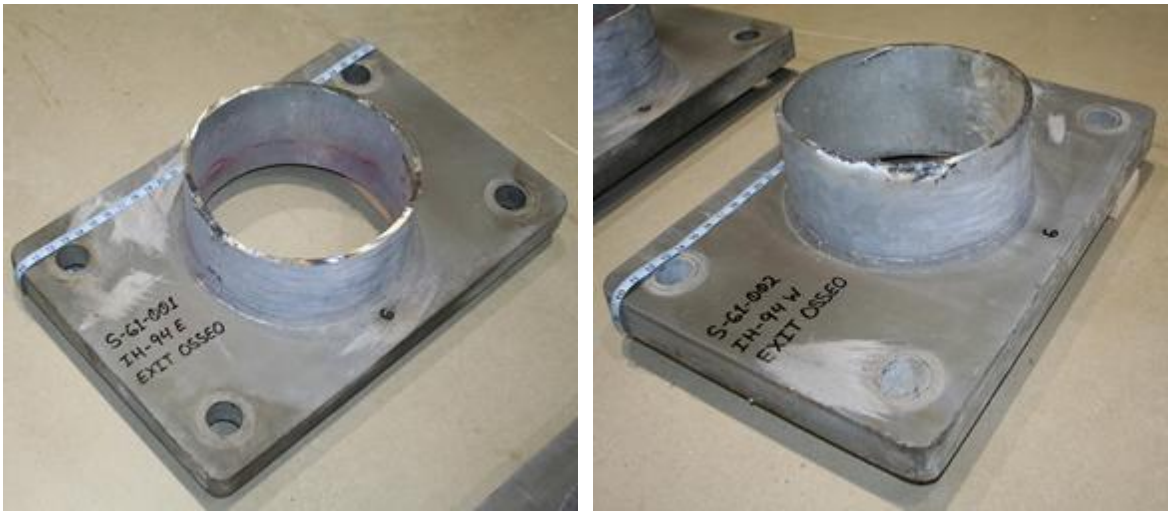

Figure A.2. Failed connections obtained from S-61-0001 and S-61-0002.

After obtaining the failed components of S-61-0001 and S-61-0002, samples were selected from each of them to test their chemical composition. In total, five chemical analyses were conducted on samples taken from the failed components, two samples from S-61-0001 (one from the mast arm tube and one from the socketed plate) and three samples from S-61-0002 (one from the mast arm tube, one from the socketed plate and one from the outside fillet weld). Direct reading optical emission spectroscopy (OES) was conducted on all samples with the exception of the weld. Due to size requirements, inductively coupled plasma OES was performed on the weld specimen. The chemical analyses were performed by Anderson Laboratories, Inc. located in Greendale, WI. The results of the chemical analyses are presented in Table A.1.

Table A.1. Results from chemical analyses performed on steel samples from S-61-0001 and S-61-0002.

	S-61-0001 "East Connection"		S-61-0002 "West Connection"			Industry Specifications	
	Mast Arm Tube (API 5L x 42)	Socket Plate (ASTM A36)	Mast Arm Tube (API 5L x 42)	Socket Plate (ASTM A36)	Outside Fillet Weld (none specified)	Mast Arm Tube (API 5L x 42)	Socket Plate (ASTM A36)
Silicon	0.200	0.250	0.180	0.250	0.480	0.400 max	0.400 max
Sulfur	0.003	< 0.001	0.003	< 0.001	0.004	0.015 max	0.050 max
Phosphorus	0.009	0.006	0.010	0.007	0.030	0.025 max	0.040 max
Manganese	0.990	1.000	1.010	1.000	1.390	1.200 max	-
Carbon	0.070	0.200	0.070	0.200	0.090	0.240 max	0.260 max
Chromium	0.050	0.140	0.050	0.140	0.030	-	-
Nickel	0.020	0.120	0.020	0.120	0.040	-	-
Molybdenum	< 0.010	0.030	< 0.010	0.030	< 0.010	-	-
Copper	0.040	0.210	0.040	0.200	0.060	-	-
Base Metal	Iron	Iron	Iron	Iron	Iron	Iron	Iron
CE	0.284	0.464	0.284	0.464	0.416	-	-

All values are reported in weight percent.

The results provided in Table A.1 indicate that the materials used for both the mast-arm tube (API 5L x 42) and the socketed plate (ASTM A36) meet the typical industry specifications for each material. However, the weight percent of carbon found in the mast arm tube material (0.07) was initially thought to be quite low as compared to the specified maximum (0.24) for API 5L x 42 tubing. Because of this, further investigation was deemed necessary. To this end, the American Welding Society (AWS) D1.1:2000 was referenced to determine whether or not the base materials were suitable to be used in a welded connection such as those found in S-61-0001 and S-61-0002. AWS prescribes a metric, referred to as the carbon equivalent (CE), which provides a measure of the weldability of a particular base metal. The CE value is determined by calculating a sum of the individual weight percentages of various elements which are found via chemical analysis. Equation (A.7) provides the formula used to determine the CE value for both the mast arm tube and socketed plate (AWS 1999).

$$CE = C + \frac{(Mn + Si)}{6} + \frac{(Cu + Ni)}{15} + \frac{(Cr + Mo + V)}{5} \tag{A.7}$$

If the CE value is determined to be less than or equal to 0.5, then the metal is considered to have good weldability. Table A.1 provides the calculated CE values for each base metal of each connection. The CE values are in good standing relative to the prescribed maximum CE values. Therefore, the tubes and plates used as part of S-61-0001 and S-61-0002 have good weldability. This check indicates that the cracks that were found in the mast arm tubes were not likely caused by the welding process.

Hardness testing was performed in order to estimate the tensile strength of the materials used for the tube, plate and fillet weld. Both Rockwell B and Brinell hardness tests were conducted and the subsequent tensile strengths were compared to the specified ranges for each material type. Trials were run across the mast arm tube, the socketed plate and both the inside and outside fillet weld beads. Figure A.3 displays the cross section test locations used for the Rockwell B hardness testing. The results from the Rockwell B hardness test are provided in Table A.2.

Similar to the Rockwell B hardness test, trials were run across the mast arm tube, the socketed plate and both the inside and outside fillet weld beads for a different cross-section from S-61-0002. Figure A.4 displays the cross-section and test locations used for the Brinell hardness testing. The results from the Brinell hardness test are provided in Table A.3.

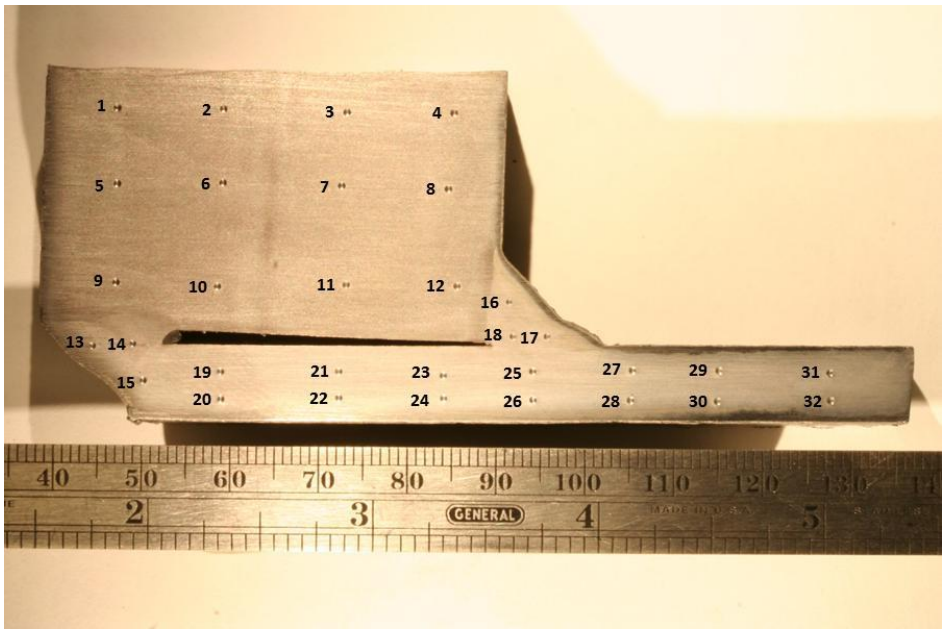

Figure A.3. Rockwell B hardness testing locations on first cross-section from S-61-0002.

Table A.2. Rockwell B hardness test results on first cross-section from S-61-0002.

Cross-Section ID No.	Rockwell B Hardness Test S-61-0002		Cross-Section ID No.	Rockwell B Hardness Test S-61-0002		Cross-Section ID No.	Rockwell B Hardness Test S-61-0002	
	HR_b	Comments		HR_b	Comments		HR_b	Comments
1	72.1	Socketed Plate	13	92.9	Inside Fillet	19	84.0	Mast Arm Tube
2	76.9		14	92.9		20	85.2	
3	75.9		15	86.4		21	83.9	
4	73.8		16	99.1	Outside Fillet	22	85.9	
5	73.5		17	96.1		23	83.4	
6	76.9		18	94.4		24	84.9	
7	77.4					25	84.9	
8	75.5					26	86.5	
9	78.1					27	84.4	
10	81.0					28	85.9	
11	79.8					29	84.2	
12	81.1					30	85.1	
						31	83.8	
						32	84.0	

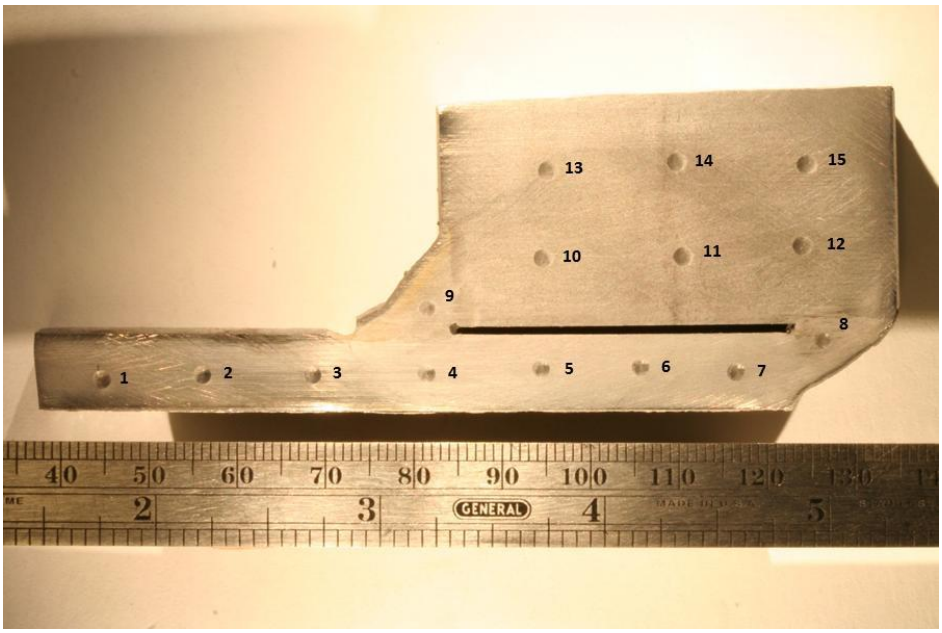

Figure A.4. Brinell hardness testing locations second cross-section from S-61-0002.

Table A.3. Brinell hardness test results on second cross-section from S-61-0002.

Cross-Section ID No.	Brinell Hardness Test S-61-0002		
	Diam. Of Indentation (mm)	HB	Comments
1	2.08	145.5	Mast Arm Tube
2	2.01	156.0	
3	2.01	156.0	
4	2.02	154.4	
5	1.97	162.4	
6	2.00	157.5	
7	2.03	152.9	
8	1.88	178.5	Inside Fillet Weld
9	1.89	176.6	Outside Fillet Weld
10	2.12	140.0	Socketed Plate
11	2.18	132.3	
12	2.20	129.9	
13	2.20	129.9	
14	2.14	137.4	
15	2.27	121.9	

The previous analyses were carried out to verify that the material properties of the failed connections were consistent with the material specifications found on the plans and drawings for these structures. Table A.4 provides a summary of material properties, both plan-specified and experimentally determined. The measured values within Table A.4 represent the average value calculated for each component.

Table A.4. Summary of experimentally-determined and plan-specified tensile strengths.

	Avg. Rockwell B Hardness (HR_B)	Tensile Strength (ksi) Determined from Avg. HR_B	Avg. Brinell Hardness (HB)	Tensile Strength (ksi) Determined from Avg. HB	Tensile Strength (ksi) based on plan specified materials
Mast Arm Tube (API 5L x 42)	85	**81**	155	**78**	**60 - 110**
Socketed Plate (ASTM A36)	77	**67**	132	**66**	**58 - 80**
Fillet Weld (none specified)	94	**98**	178	**89**	**NA**

The resulting tensile strengths for both the tube and plate materials fall well within the ranges specified by API 5L x 42 and ASTM A36 materials, respectively. Unfortunately, there was no material (electrode) specified for the weld filler metal. Therefore, no comparison could be made between the experimentally determined tensile strength and that of a plan-specified value. A relative comparison between the fillet weld and the tube and plate indicates that the weld material has a higher tensile strength. This is consistent with most welded connections.

A.3 – Macroscopic Evaluation

To begin the macroscopic examination, both connections were studied holistically to get an idea as to the extent and location of the cracks. Figures A.5 and A.6 display the failed connections from S-61-0001 and S-61-0002, respectively. These figures display a montage of photos of the connections before and after they were subjected to dye penetrant evaluations.

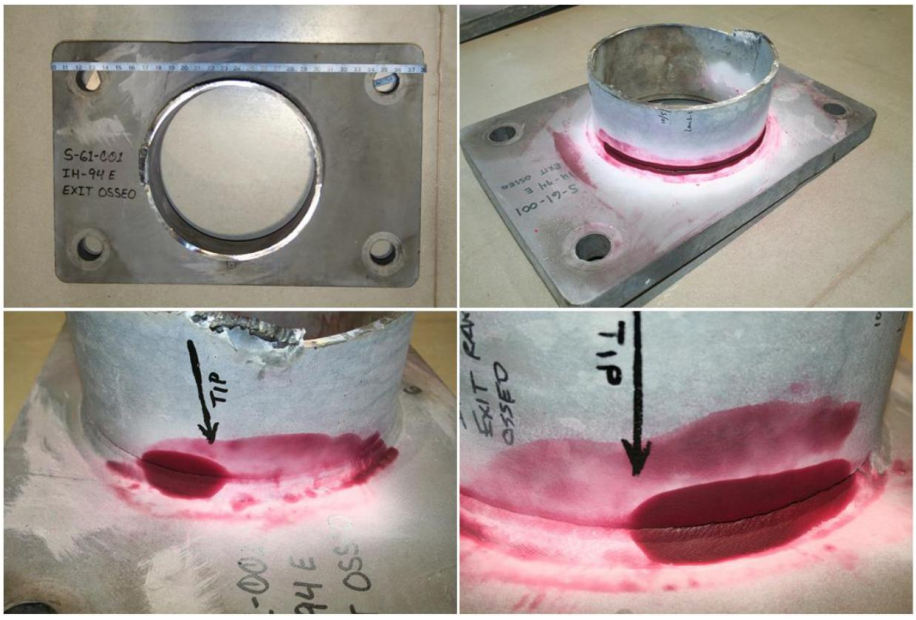

Figure A.5. Photo montage of failed connection from S-61-0001 before and after dye penetrant testing.

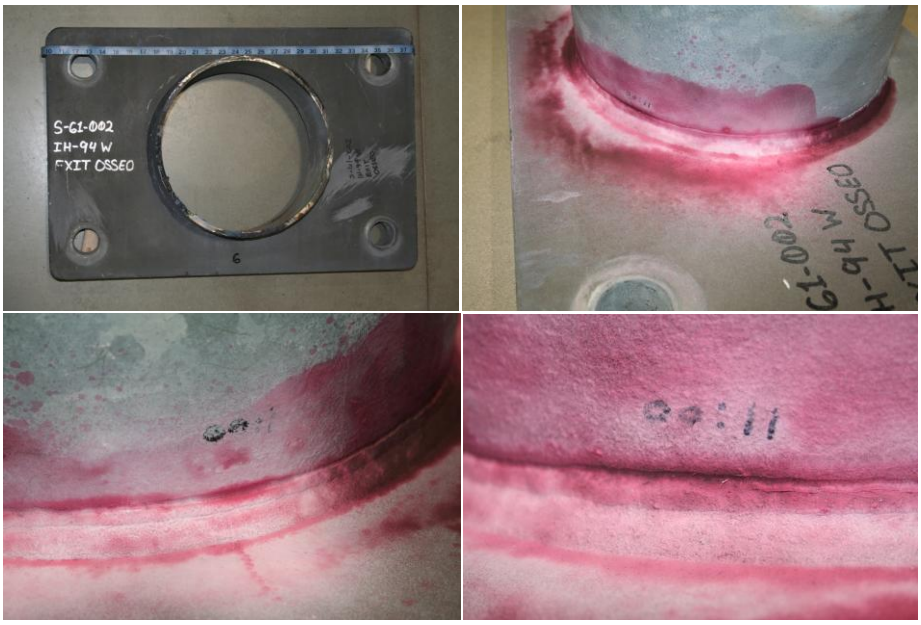

Figure A.6. Photo montage of failed connection from S-61-0002 before and after dye penetrant testing.

It was obvious the failure of S-61-0001 was considerably more severe than that of S-61-0002. The crack in the connection from S-61-0001 was clearly visible with the naked eye whereas

the connection from S-61-0002 appeared structurally sound. However, based on observations made by WisDOT personnel via the use of magnetic particle inspection, the S-61-0002 connection was determined to contain cracks at the eleven o'clock and one o'clock positions. The dye penetrant testing confirmed that both connections did contain cracks as reported. The locations of the crack tips were estimated based upon the dye penetrant test and were used to facilitate proper sectioning of the connections and to continue the macroscopic evaluation.

At this point two different procedures were followed to continue the failure analysis. The first procedure involved separating the cracked portion of the tube (S-61-0001) in order to facilitate a detailed examination of the fracture surface. The second procedure involved generating cross-sections of the tube to plate connection at the WisDOT indicated crack locations (S-61-0002). The cross-sections were used to verify the existence of cracks and to observe the weld joint features.

To examine the fracture surface of the connection from S-61-0001 the tube was cut and separated from the base. The tube half of the fracture surface was then cleaned using replicating tape and acetone. Macroscopic photographs were then taken to document the fracture surface. Figures A.7 and A.8 display macroscopic photographs of the fracture surface from approximately the ten o'clock position. This location was chosen because ratchet marks and beach marks are clearly visible. These fracture features were present along the entire length of the fracture surface. The ratchet marks observed on the surface show crack initiation from the outer surface of the tube while the beach marks indicate progression of the crack radially into the thickness of the material. The presence of ratchet marks at multiple locations indicates multiple crack initiation sites.

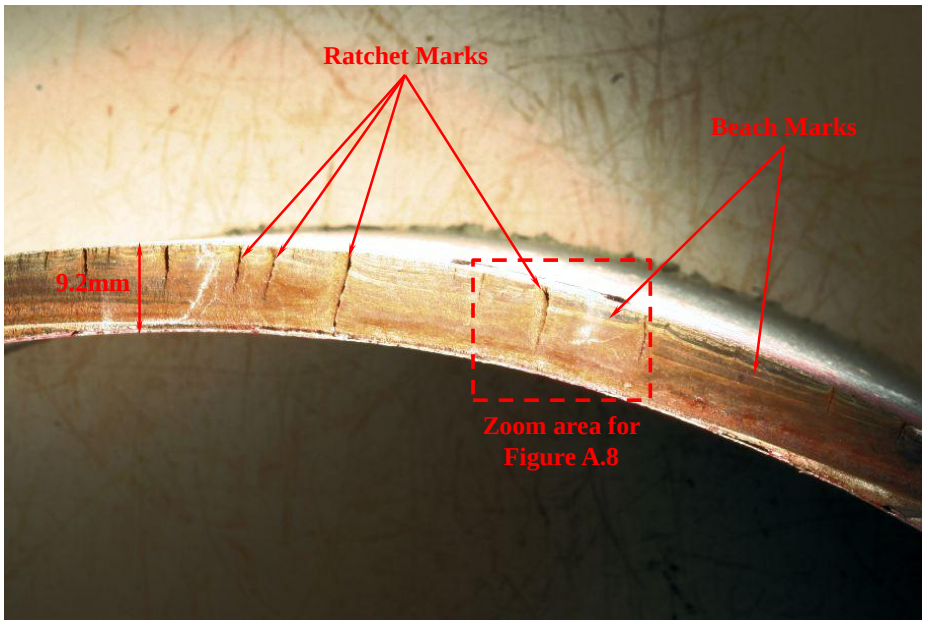

Figure A.7. Macroscopic photograph of fracture surface from S-61-0001 displaying multiple ratchet marks and beach marks.

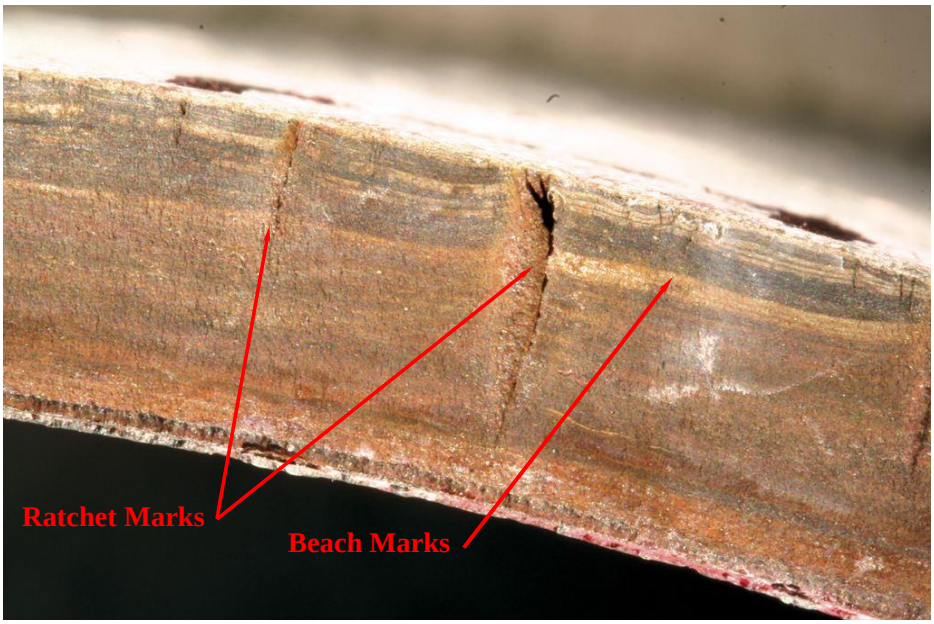

Figure A.8. Zoom area from Figure A.7 displaying fracture surface from S-61-0001.

The cross-sections from S-61-0002 were examined for evidence of cracks. A cross-section from one of the cracked locations was cut to size and mounted in plastic. The section was

progressively ground to 600 grit s/c and then polished with 1.0 and 0.5 micron aluminum oxide, progressively. The polished section was etched using a 3% Nital solution for approximately 10 seconds to reveal and examine the microstructure. Figure A.9 displays a macroscopic photograph of the etched cross-section. From this surface, a crack can be observed initiating at the toe of the weld and propagating through the heat affected zone (HAZ) into the base material of the tube.

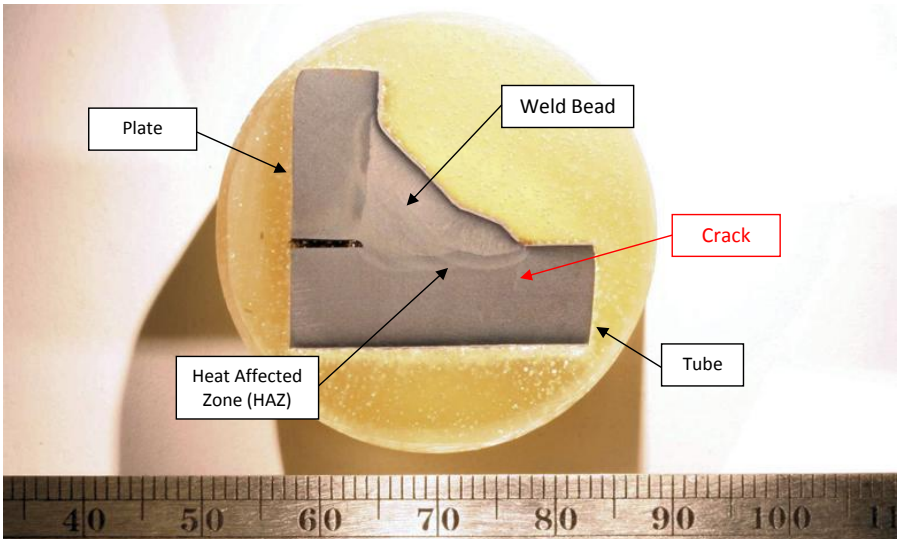

Figure A.9. Macroscopic photograph of cross-section from S-61-0002 displaying the weld bead, HAZ and crack.

Figure A.10 displays the cross section surface with some key weld bead geometric dimensions measured. The measured weld dimensions were then compared to the drawing specification and to some industry recommended fillet weld geometries. Table A.5 shows that the measured weld cross section satisfies the drawing specification for fillet leg length and the weld gap (distance between the two parts being welded). This weld bead cross section also meets all of the recommended dimensions with the exception of weld penetration depth.

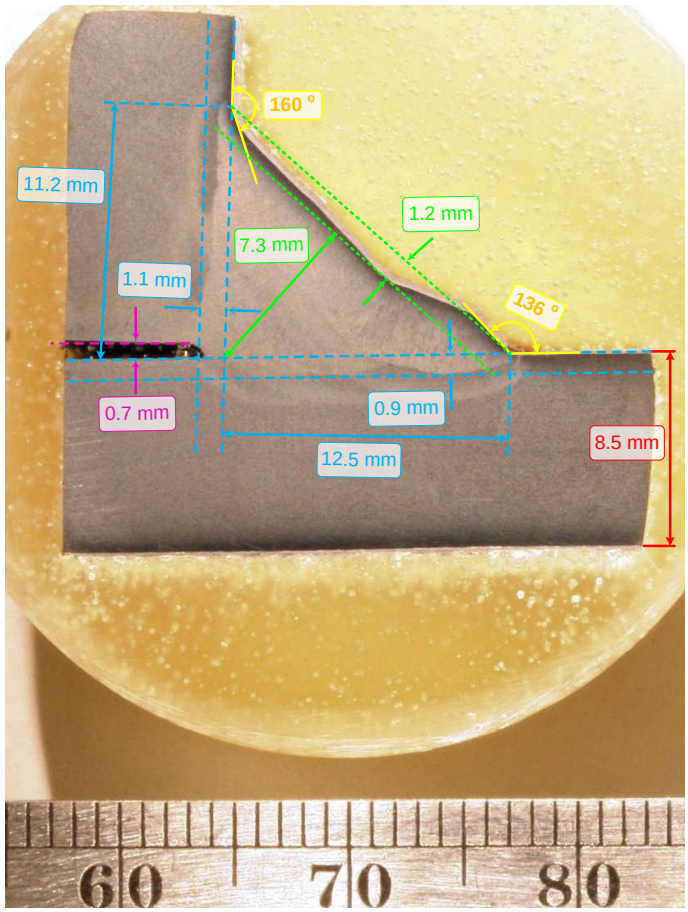

Figure A.10. Macroscopic photograph of cross-section from S-61-0002 displaying the key weld bead geometric dimensions.

Table A.5. Comparison between specified and measured weld bead geometrical features for a fillet welded joint.

	Drawing Specification (mm)	Industry Recommended	Actual Measurement (mm)	Comparison of Actual -vs.- Specified	Comparison of Actual -vs.- Recommend
Thickness "t"	8.4		8.5	+ 0.1	
Leg Length "tube"	9.5		12.5	+ 3	
Penetration leg "tube"		d ≥ 0.2 t	0.9		False
Flank Angle leg "tube"		ψ ≥ 110°	136°		True
Leg Length "plate"	9.5		11.2	+ 1.7	
Penetration leg "plate"		d ≥ 0.2 t	1.1		False
Flank Angle leg "plate"		ψ ≥ 110°	160°		True
Effective Throat		c ≥ 0.8 t	7.3		True
Concavity			1.2		NA for concavity
Weld Gap	1.5 radial *	X ≤ 1.5 t	0.7	- 0.8	True
Undercut **		U ≤ 0.2 t	NA		NA

*Weld Gap per drawing based on Tube OD = 324 mm and Plate Hole ID = 327 mm

**Undercut not measured on this piece, but S-61-0002 "as received" did show signs of significant undercut.

The geometry of a weld including such features as toe angle, throat depth, weld gap, convexity/concavity and depth of penetration work together as a joint within the assembly, transferring load and resisting failure modes. As a result, isolating one feature as the cause of failure is difficult to do unless that characteristic is grossly out of specification. Although the penetration is not ideal in this case, the weld appears to be acceptable overall and is not considered to be the singular root cause for the failure.

S-61-0002 contained a significant undercut at the toe of the weld on the tube side in the "as received" condition. This amount of undercut would be a weld feature considered grossly out of tolerance, but there was no direct evidence that identified this feature to be on the part during service. In fact, there was a lack of galvanized surface treatment present on the undercut and there was no significant corrosion on the undercut surface. This led to the conclusion that these features occurred after decommissioning and therefore should not be considered as part of the cause of failure in this analysis.

A.4 – Microscopic Evaluation

The tube half from S-61-0001 was sectioned to create pieces that could be examined with a scanning electron microscope (SEM). Figure A.11 displays a 20x magnification of the fracture surface from one of the pieces. A large ratchet mark and many smaller ratchet marks can be seen originating at the outer surface of the tube and radiating inward. There were multiple crack initiation sites which is evidence of fatigue failure. Figure A.12 displays a 2000x magnification of the fracture surface; however, because of the presence of oxidization on the fracture surface, no further significant details could be determined from the SEM examination of this piece. Other pieces were looked at but yielded the same images of oxidation being present.

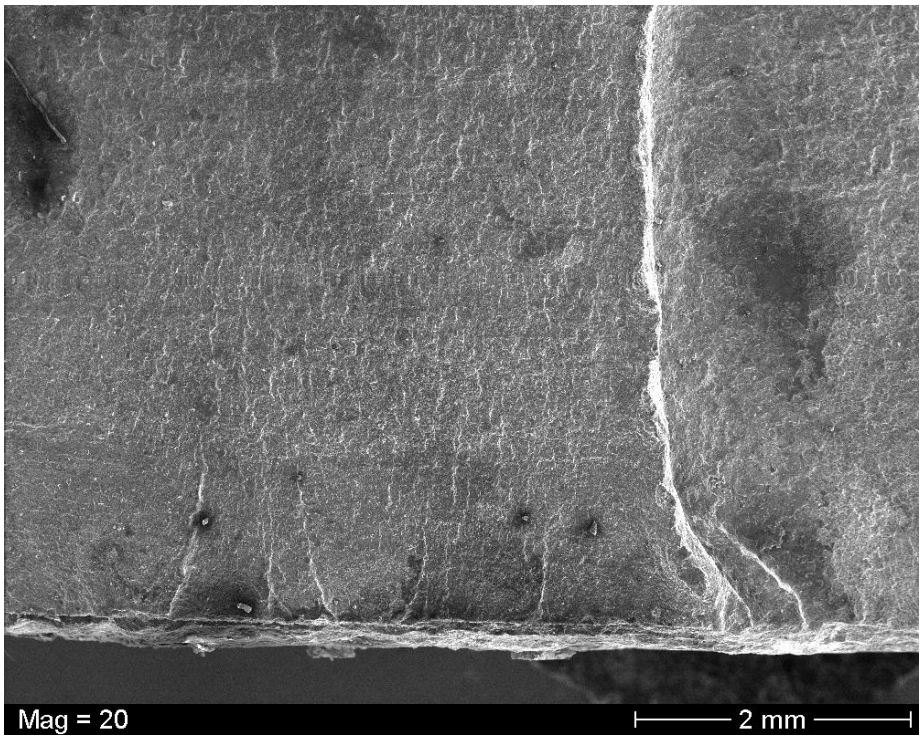

Figure A.11. SEM photograph of fracture surface from S-61-0001 displaying ratchet marks.

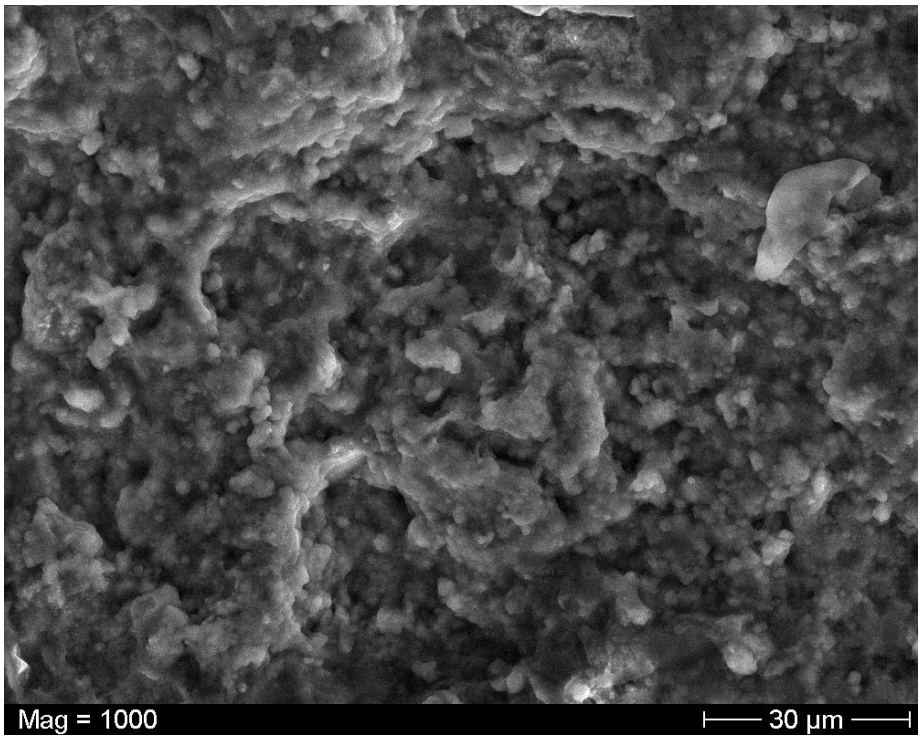

Figure A.12. SEM photograph of fracture surface from S-61-0001 displaying significant oxidation.

The polished and etched section from S-61-0002 was examined using a light optical microscope (LOM). Figure A.13 displays a magnified photograph of the weld cross section and the crack in the tube section. From this view it is evident that the crack is initiating at the toe of the weld in the HAZ of the tube material. The crack appears to propagate in a transgranular fashion directly into the base material of the tube.

Figure A.14 displays magnified views of the base material of the mast arm tube, socketed plate and outside fillet weld. The images from Figure A.14 (a) and (b) show grain structures that are indicative of low carbon structural steel with no gross inclusions or defects. Figure A.14 (c) shows a different grain structure, one that is consistent with typical high strength weld material.

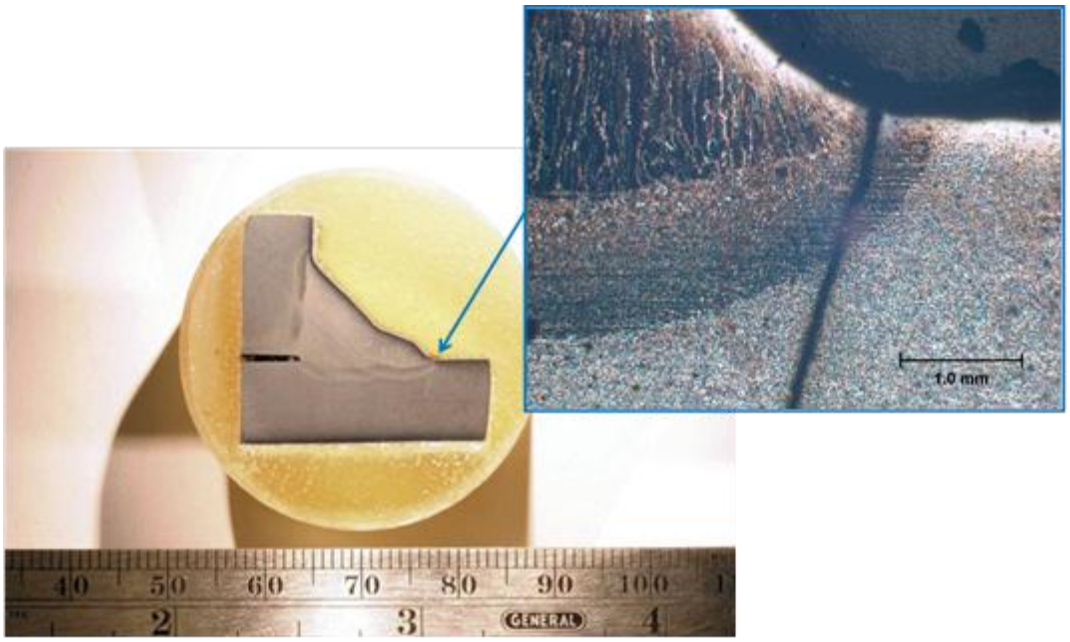

Figure A.13. LOM magnified photograph of crack initiation point on cross-section from S-61-0002.

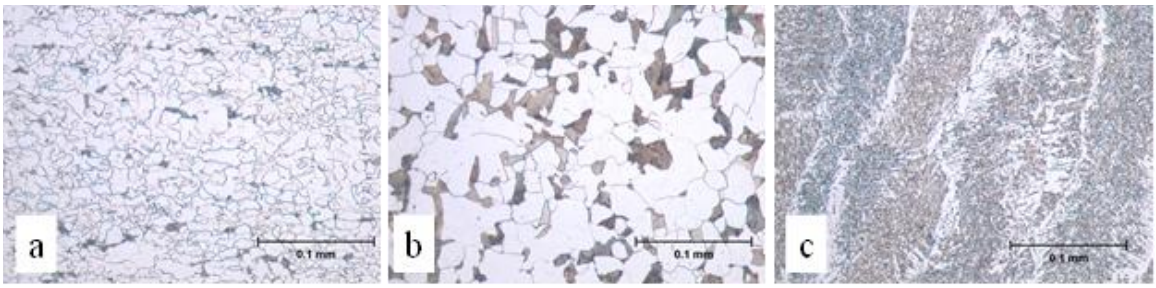

Figure A.14. LOM metallographic photographs of the (a) mast arm tube, (b) socketed plate and (c) weld bead of cross-section from S-61-0002.

To produce a better understanding of the microscopic features of the crack, a section from S-61-0002 was mechanically broken in order reveal the fracture surface from the crack. The sample was examined using the SEM. Figure A.15 displays a 13x magnification of the tube section of the fracture surface. Figure A.16 displays a 1500x magnification of the fracture surface, close to the crack tip. Remnants of striations (a microscopic indicator of fatigue) can be seen as parallel markings within the flat areas of the fracture surface. Since the striations are mostly obscured by oxidation, the ability to use them as a basis for calculating stress-range magnitudes applied to the sign over its service life is not recommended.

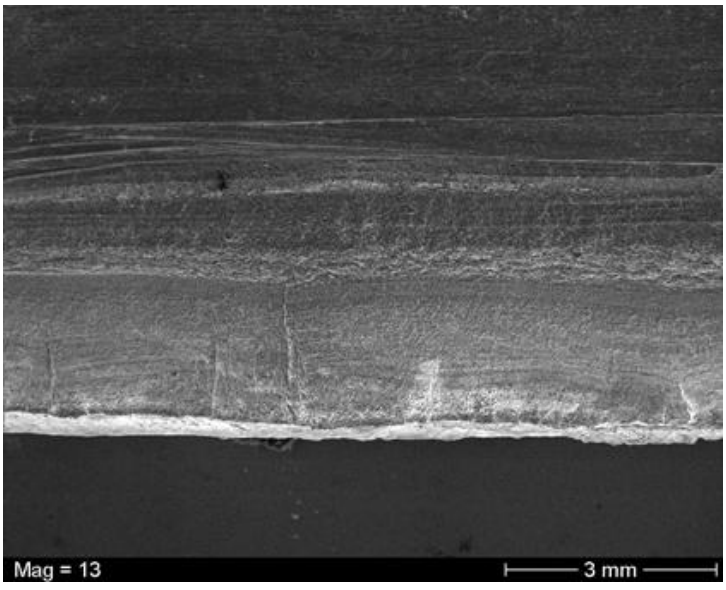

Figure A.15. SEM photograph of cross-section from S-61-0002 displaying ratchet marks and beach marks.

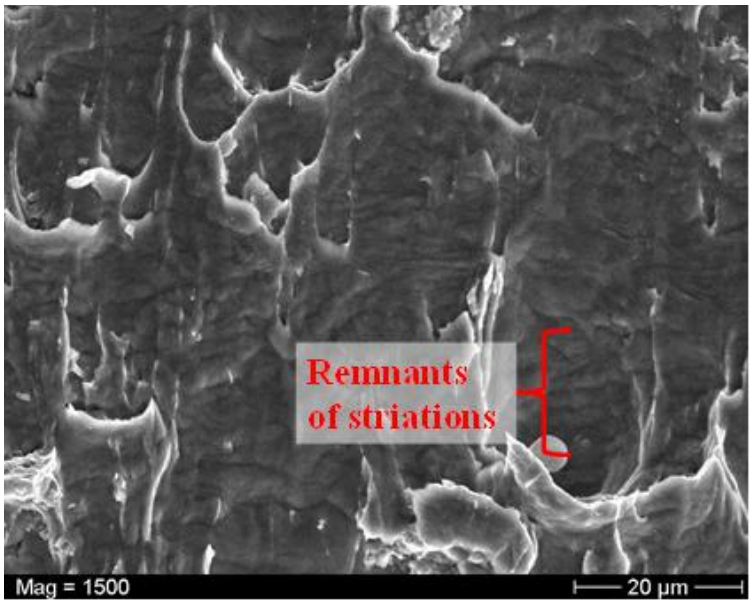

Figure A.16. SEM photograph of cross-section from S-61-0002 displaying remnants of striations.

A.5 – Mechanism of Failure

The results of this failure analysis are indicative of multi-axial bending fatigue. The multiple ratchet mark locations as well as the beach mark features, in conjunction with a lack of visible plastic deformation as seen on the fracture surface of S-61-0001 (see Figures A.7 and A.8), are macroscopic indicators of a multi-axial bending fatigue fracture. The microscopic evaluations of S-61-0002 revealed remnants of striations (see Figure A.16) that result from crack propagation caused by fatigue. Both macroscopic and microscopic evaluations (for both structures) showed signs of oxidation as evidenced in Figures A.7, A.8, A.12 and A.16. The oxidation of the fracture surfaces is evidence of fatigue crack propagation over an extended period of time.

A.6 – Cause of Failure

The presence of multiple ratchet marks and varying beach mark patterns is indication of multiple crack initiation points. This indicates that the applied loading on the sign support structure is variable. This is reasonable considering that the primary loading on the sign structure is wind

which acts from all directions and with significantly varying velocities. The variable load caused by wind, combined with mast arm dead load, produces a peak bending stress that will be generally located between the ten and two o'clock positions at the toe of the weld cross-section. This is consistent with finite element analysis conducted in chapter five of this dissertation.

Studies have shown the theoretical geometric stress concentration factor (*SCF*) for a socketed fillet welded tube to transverse plate connection falls in the range of 2.0 to 4.5 (Roy et al. 2011). In actual practice, welded joint assemblies may be subject to poor weld quality leaving them sensitive to defects in materials or processing which can increase the actual *SCF* which ultimately leads to reduced fatigue performance.

In summary, the likely cause of failure is multi-axial bending fatigue. The key contributing factors for this cause of failure include the location of peak bending stress for a cantilever mast arm, the variable loading conditions inherent in a particular sign structure's environment, the stress concentration caused by the weld in the socketed tube to transverse plate connection, and the potential increase in stress concentrations caused by any weld assembly defects.

A.7 – Recommendations

Given the likely cause of failure for S-61-0001 and S-61-0002 and the key contributing factors previously mentioned, a number of recommendations are warranted. Environmental conditions for the location of these sign structures are likely not going to change. Therefore, the recommendations provided in this section will focus on material specifications, quality of the welded connections, and structural design considerations.

Sensitivity to the weld quality is a critical factor because it is the first key stress riser in the load path for these types of structures. Good weldability of base materials is an essential

property in any welded connection. Although the sign structures examined here were of sufficient quality to be welded, there may be alternative tube materials that are weldable and more resistant to fatigue damage. The material composition and quality should be documented as part of sign structure assembly and commissioning procedure in order to ensure the desired material properties are being achieved for a given assembly. Finally, best practices, including key weld bead geometries, should be specified on the drawings. Suppliers of these sign structures should be able to demonstrate their ability to meet these best practices by either providing sample welds or by demonstrating certification of their welders per an acceptable professional welding society such as American Welding Society.

As previously mentioned, the geometry of a socketed round tube to transverse plate connection inherently gives rise to a geometric *SCF* at the toe of the weld (between the weld bead and mast arm tube) equal to approximately 2.0 to 4.5. It seems reasonable to investigate different connection types to be used in these structures. Implementing a different connection type that has a lower *SCF* would reduce the sensitivity and susceptibility to fatigue induced fracture. If a different connection type is not possible, modifications to the geometry or structure should be considered to either reduce the peak stress caused by multi-axial bending or to better distribute the stress loading away from the weld bead at the socketed joint.

APPENDIX B – MATLAB CODE FOR NCDC WIND DATA SYNTHESIS

B.1 – NCDC_sifter.m

```
function [] = NCDC_sifter()

    clear
    clc

    ExcelFile = 'EAU_WindData.xlsx';
    Sheet = ['EAU'];

    k = 1;
    t = 0;

    for m = 1:3:length(Sheet)

        clc
        t = t + 1;
        Worksheet = Sheet(m:m+2);
        inputArray = xlsread(ExcelFile,Worksheet);

        for i = 1:length(inputArray(:,1))
            SpeedOnly(k,1) = inputArray(i,1);
            DirectionOnly(k,1) = inputArray(i,2);
            SpeedDirection(k,1) = inputArray(i,1);
            SpeedDirection(k,2) = inputArray(i,2);
            k = k + 1;
        end

    end

    OutputFile = 'EAU_matfile_data';
    save(OutputFile,'SpeedOnly','DirectionOnly','SpeedDirection');

end
```

B.2 – NCDC_analysis.m

```
function [] = NCDC_analysis()

    clear
    clc

    InputFile = 'EAU_matfile_data.mat';
    load(InputFile)

    WindData = zeros(17,9);

    N = 1;
    NE = 1;
    E = 1;
    SE = 1;
    S = 1;
    SW = 1;
    W = 1;
    NW = 1;

    for t = 1:length(SpeedDirection)

        % assigns column number based on wind direction

        if SpeedDirection(t,2) == 0
            Dir = 1;
        end

        if SpeedDirection(t,2) > 337.5 || SpeedDirection(t,2) <=
            22.5...
                && SpeedDirection(t,2) ~= 0
            Dir = 2;
            NorthSpeeds(N,1) = SpeedDirection(t,1);
            N = N + 1;
        end

        if SpeedDirection(t,2) > 22.5 && SpeedDirection(t,2) <= 67.5
            Dir = 3;
            NortheastSpeeds(NE,1) = SpeedDirection(t,1);
            NE = NE + 1;
        end

        if SpeedDirection(t,2) > 67.5 && SpeedDirection(t,2) <= 112.5
            Dir = 4;
            EastSpeeds(E,1) = SpeedDirection(t,1);
            E = E + 1;
        end

        if SpeedDirection(t,2) > 112.5 && SpeedDirection(t,2) <= 157.5
            Dir = 5;
            SoutheastSpeeds(SE,1) = SpeedDirection(t,1);
            SE = SE + 1;
```

```
end

if SpeedDirection(t,2) > 157.5 && SpeedDirection(t,2) <= 202.5
    Dir = 6;
    SouthSpeeds(S,1) = SpeedDirection(t,1);
    S = S + 1;
end

if SpeedDirection(t,2) > 202.5 && SpeedDirection(t,2) <= 247.5
    Dir = 7;
    SouthwestSpeeds(SW,1) = SpeedDirection(t,1);
    SW = SW + 1;
end

if SpeedDirection(t,2) > 247.5 && SpeedDirection(t,2) <= 292.5
    Dir = 8;
    WestSpeeds(W,1) = SpeedDirection(t,1);
    W = W + 1;
end

if SpeedDirection(t,2) > 292.5 && SpeedDirection(t,2) <= 337.5
    Dir = 9;
    NorthwestSpeeds(NW,1) = SpeedDirection(t,1);
    NW = NW + 1;
end

% counts occurence of wind speed based on direction

if SpeedDirection(t,1) >= 0 && SpeedDirection(t,1) <= 2.5
    WindData(1,Dir) = WindData(1,Dir) + 1;
end

if SpeedDirection(t,1) > 2.5 && SpeedDirection(t,1) <= 7.5
    WindData(2,Dir) = WindData(2,Dir) + 1;
end

if SpeedDirection(t,1) > 7.5 && SpeedDirection(t,1) <= 12.5
    WindData(3,Dir) = WindData(3,Dir) + 1;
end

if SpeedDirection(t,1) > 12.5 && SpeedDirection(t,1) <= 17.5
    WindData(4,Dir) = WindData(4,Dir) + 1;
end

if SpeedDirection(t,1) > 17.5 && SpeedDirection(t,1) <= 22.5
    WindData(5,Dir) = WindData(5,Dir) + 1;
end

if SpeedDirection(t,1) > 22.5 && SpeedDirection(t,1) <= 27.5
    WindData(6,Dir) = WindData(6,Dir) + 1;
end

if SpeedDirection(t,1) > 27.5 && SpeedDirection(t,1) <= 32.5
    WindData(7,Dir) = WindData(7,Dir) + 1;
```

```
        end

        if SpeedDirection(t,1) > 32.5 && SpeedDirection(t,1) <= 37.5
            WindData(8,Dir) = WindData(8,Dir) + 1;
        end

        if SpeedDirection(t,1) > 37.5 && SpeedDirection(t,1) <= 42.5
            WindData(9,Dir) = WindData(9,Dir) + 1;
        end

        if SpeedDirection(t,1) > 42.5 && SpeedDirection(t,1) <= 47.5
            WindData(10,Dir) = WindData(10,Dir) + 1;
        end

        if SpeedDirection(t,1) > 47.5 && SpeedDirection(t,1) <= 52.5
            WindData(11,Dir) = WindData(11,Dir) + 1;
        end

        if SpeedDirection(t,1) > 52.5 && SpeedDirection(t,1) <= 57.5
            WindData(12,Dir) = WindData(12,Dir) + 1;
        end

        if SpeedDirection(t,1) > 57.5 && SpeedDirection(t,1) <= 62.5
            WindData(13,Dir) = WindData(13,Dir) + 1;
        end

        if SpeedDirection(t,1) > 62.5 && SpeedDirection(t,1) <= 67.5
            WindData(14,Dir) = WindData(14,Dir) + 1;
        end

        if SpeedDirection(t,1) > 67.5 && SpeedDirection(t,1) <= 72.5
            WindData(15,Dir) = WindData(15,Dir) + 1;
        end

        if SpeedDirection(t,1) > 72.5 && SpeedDirection(t,1) <= 77.5
            WindData(16,Dir) = WindData(16,Dir) + 1;
        end

        if SpeedDirection(t,1) > 77.5 && SpeedDirection(t,1) <= 82.5
            WindData(17,Dir) = WindData(17,Dir) + 1;
        end

    end

    disp(WindData)
    ExcelFile = 'EAU_Analysis.xls';
    xlswrite(ExcelFile,WindData,'Sheet1')
    OutputFile = 'EAU_Speeds.mat';

save(OutputFile,'NorthSpeeds','NortheastSpeeds','EastSpeeds','Southeast
Speeds','SouthSpeeds','SouthwestSpeeds','WestSpeeds','NorthwestSpeeds')
;

end
```

B.3 – NCDC_directiononly.m

```
function [] = NCDC_directiononly()

    clear
    clc

    InputFile = 'EAU_matfile_data.mat';
    load(InputFile)
    x = 0:10:360;

    [n,xout] = hist(DirectionOnly,x);
    HiResDir(:,1) = xout;
    HiResDir(:,2) = n;

    WindData = zeros(9,1);

    for t = 1:length(DirectionOnly)

        if DirectionOnly(t) == 0
            WindData(1,1) = WindData(1,1) + 1;
        end

        if DirectionOnly(t) > 337.5 || DirectionOnly(t) <= 22.5...
                && DirectionOnly(t) ~= 0
            WindData(2,1) = WindData(2,1) + 1;
        end

        if DirectionOnly(t) > 22.5 && DirectionOnly(t) <= 67.5
            WindData(3,1) = WindData(3,1) + 1;
        end

        if DirectionOnly(t) > 67.5 && DirectionOnly(t) <= 112.5
            WindData(4,1) = WindData(4,1) + 1;
        end

        if DirectionOnly(t) > 112.5 && DirectionOnly(t) <= 157.5
            WindData(5,1) = WindData(5,1) + 1;
        end

        if DirectionOnly(t) > 157.5 && DirectionOnly(t) <= 202.5
            WindData(6,1) = WindData(6,1) + 1;
        end

        if DirectionOnly(t) > 202.5 && DirectionOnly(t) <= 247.5
            WindData(7,1) = WindData(7,1) + 1;
        end

        if DirectionOnly(t) > 247.5 && DirectionOnly(t) <= 292.5
            WindData(8,1) = WindData(8,1) + 1;
        end

        if DirectionOnly(t) > 292.5 && DirectionOnly(t) <= 337.5
```

```
            WindData(9,1) = WindData(9,1) + 1;
        end

    end

    disp(HiResDir)
    disp(WindData)
    ExcelFile = 'EAU_Direction.xls';
    xlswrite(ExcelFile,WindData,'Sheet1')
    xlswrite(ExcelFile,HiResDir,'Sheet2')

end
```

B.4 – NCDC_speedonly.m

```
function [] = NCDC_speedonly()

    clear
    clc

    InputFile = 'EAU_matfile_data.mat';
    load(InputFile)

    WindData = zeros(17,1);

    for t = 1:length(SpeedOnly)

        if SpeedOnly(t) >= 0 && SpeedOnly(t) <=2.5
            WindData(1,1) = WindData(1,1) + 1;
        end

        if SpeedOnly(t) > 2.5 && SpeedOnly(t) <= 7.5
            WindData(2,1) = WindData(2,1) + 1;
        end

        if SpeedOnly(t) > 7.5 && SpeedOnly(t) <= 12.5
            WindData(3,1) = WindData(3,1) + 1;
        end

        if SpeedOnly(t) > 12.5 && SpeedOnly(t) <= 17.5
            WindData(4,1) = WindData(4,1) + 1;
        end

        if SpeedOnly(t) > 17.5 && SpeedOnly(t) <= 22.5
            WindData(5,1) = WindData(5,1) + 1;
        end

        if SpeedOnly(t) > 22.5 && SpeedOnly(t) <= 27.5
            WindData(6,1) = WindData(6,1) + 1;
        end

        if SpeedOnly(t) > 27.5 && SpeedOnly(t) <= 32.5
            WindData(7,1) = WindData(7,1) + 1;
        end

        if SpeedOnly(t) > 32.5 && SpeedOnly(t) <= 37.5
            WindData(8,1) = WindData(8,1) + 1;
        end

        if SpeedOnly(t) > 37.5 && SpeedOnly(t) <= 42.5
            WindData(9,1) = WindData(9,1) + 1;
        end

        if SpeedOnly(t) > 42.5 && SpeedOnly(t) <= 47.5
            WindData(10,1) = WindData(10,1) + 1;
        end
```

```
        if SpeedOnly(t) > 47.5 && SpeedOnly(t) <= 52.5
            WindData(11,1) = WindData(11,1) + 1;
        end

        if SpeedOnly(t) > 52.5 && SpeedOnly(t) <= 57.5
            WindData(12,1) = WindData(12,1) + 1;
        end

        if SpeedOnly(t) > 57.5 && SpeedOnly(t) <= 62.5
            WindData(13,1) = WindData(13,1) + 1;
        end

        if SpeedOnly(t) > 62.5 && SpeedOnly(t) <= 67.5
            WindData(14,1) = WindData(14,1) + 1;
        end

        if SpeedOnly(t) > 67.5 && SpeedOnly(t) <= 72.5
            WindData(15,1) = WindData(15,1) + 1;
        end

        if SpeedOnly(t) > 72.5 && SpeedOnly(t) <= 77.5
            WindData(16,1) = WindData(16,1) + 1;
        end

        if SpeedOnly(t) > 77.5 && SpeedOnly(t) <= 1000
            WindData(17,1) = WindData(17,1) + 1;
        end

    end

    disp(WindData)
    ExcelFile = 'EAU_Speed.xls';
    xlswrite(ExcelFile,WindData,'Sheet1')

end
```

APPENDIX C – C CODE FOR AVERAGING FMS WIND DATA

C.1 – HourlyAvg.c

```
/*****************************************************************
SECTION 1 - START:

This is where strain data is averaged from 20 Hz to 4 Hz.
*****************************************************************/

#include <stdio.h>
#include <string.h>
#include <stdlib.h>
#include <math.h>

FILE *fpo1,*fpo2,*fpo3,*fpo4,*fpo5,*fpo6,*fpo7 ;
char fno1[200], fno2[200], fno3[200], fno4[200] ;
char fno5[200], fno6[200], fno7[200] ;

int main(int argc, char *argv[]) {

     int   i, j ;
     float sum, a[10], b[10], w[20], n1, n2, avg1, avg2 ;
     char  t1[200], t2[200], t3[200], tt[200] ;

     strcpy(fno1,"/home/diekfusj/Research/HourlyAvgData/Data/") ;
     strcat(fno1,argv[1]) ;
     fpo1 = fopen(fno1,"r") ;  //this opens
     'cRIO_(timestamp).txt'
     if(fpo1==NULL)
        printf("error\n") ;


strcpy(fno2,"/home/diekfusj/Research/HourlyAvgData/RawData/") ;
     strcat(fno2,argv[2]) ;
     fpo2 = fopen(fno2,"w") ;  //this opens
'RawData_(timestamp).txt'

     j   = 0 ;
     sum = 0.0 ;

     while(fgets(tt,200,fpo1)!=NULL) {
          sscanf(tt,"%g %g %g %g %g %g %g %g %g %g %g %g %s %s
                 %s\n",
                &a[0],&a[1],&a[2],&a[3],&a[4],&b[0],&b[1],&b[2],
                &b[3],&b[4],&w[0],&w[1],t1,t2,t3) ;

             sum  = 0 ;
```

```
            for(i=0;i<5;i++) {
               sum  = sum + a[i] ;
            }

               avg1 = sum / 5.0 ;

               sum  = 0 ;

            for(i=0;i<5;i++) {
               sum  = sum + b[i] ;
            }

               avg2 = sum / 5.0 ;

               fprintf(fpo2,"%f %f %f %f\n",avg1,avg2,w[0],w[1]) ;

      }

      fclose(fpo1) ;
      fclose(fpo2) ;

/*****************************************************************
SECTION 1 - END:

This is the end of averaging strain from 20 Hz to 4 Hz.
*****************************************************************/

/*****************************************************************
SECTION 2 - START:

This is where strain offsets are calculated. The offsets are then
applied to the original raw data that is already at 4 Hz. Also,
this
is where the wind direction is adjusted by 6 degrees.
*****************************************************************/

/*     int   n, counta, countb ;
      float atemp, btemp, ctemp, dtemp, adjF1, adjF2, adjWDir ;
      float suma, sumb, offsetF1, offsetF2, threshold, correction;
      char  etemp[100], ftemp[100], gtemp[100] ;

      counta     = 0 ;
      countb     = 0 ;

      suma       = 0.0 ;
      sumb       = 0.0 ;

      threshold  = 1.0 ;
      correction = 6.0 ;

      fpo2 = fopen(fno2,"r") ;
```

```
     i=0;
     while(fgets(tt,200,fpo2)!=NULL) {
          sscanf(tt,"%f %f %f %f\n", &atemp, &btemp, &ctemp,
                &dtemp) ;
                if(ctemp<threshold) {
                  suma = suma + atemp ;
                  sumb = sumb + btemp ;
                  counta++ ;
                  countb++ ;
                }

          offsetF1 = suma / (counta*1.0) ;
          offsetF2 = sumb / (countb*1.0) ;
     }

     fclose(fpo2) ;

     fpo2 = fopen(fno2,"r") ;

     strcpy(fno3,"/home/diekfusj/Research/Avg/AdjData/") ;
     strcat(fno3,argv[3]) ;
     fpo3 = fopen(fno3,"w") ;  //this opens
     'AdjData_(timestamp).txt'

     i=0 ;
     while(fgets(tt,200,fpo2)!=NULL) {
          sscanf(tt,"%f %f %f %f\n", &atemp, &btemp, &ctemp,
                 &dtemp);

          adjF1   = (atemp + offsetF1) ;
          adjF2   = (btemp + offsetF2) ;
          adjWDir = (dtemp + correction) ;

          if(adjWDir > 360) adjWDir = adjWDir - 360 ;

          fprintf(fpo3,"%f %f %f %f\n",adjF1,adjF2,ctemp,adjWDir;
     }

     fclose(fpo2) ;
     fclose(fpo3) ;

/*************************************************************
SECTION 2 - END:

This is the end of the strain and wind adjustments.
*************************************************************/
```

```
/*****************************************************************
SECTION 3.1 - START:  (Using 'RawData_(timestamp).txt')

This is where the one hour averages are calculated using raw
data.
*****************************************************************/

     float atmp[350000], btmp[350000], ctmp[350000], deg[350000];
     float avgF1[30], avgF2[30], avgWSpd[30], avgWDir[30] ;
     float suma, sumb, sumc, sumWx, sumWy ;
     float Wxbar[30], Wybar[30], Wbar_rad[30] ;
     float rad[350000], Wy[350000], Wx[350000] ;

     int   n, rowstart, rowend ;

     fpo2 = fopen(fno2,"r") ;  //open 'RawData_(timestamp).txt'


strcpy(fno4,"/home/diekfusj/Research/HourlyAvgData/AvgStrain/") ;
     strcat(fno4,argv[4]) ;
     fpo4 = fopen(fno4,"w") ;  //open 'AvgStrain_(timestamp).txt'
     if (fpo4==NULL)
        printf("error\n") ;


strcpy(fno5,"/home/diekfusj/Research/HourlyAvgData/AvgWind/") ;
     strcat(fno5,argv[5]) ;
     fpo5 = fopen(fno5,"w") ;  //open file to write daily 1 hr
     avg wind
     if (fpo5==NULL)
        printf("error\n") ;


strcpy(fno6,"/home/diekfusj/Research/HourlyAvgData/Monthly_Avgs/"
) ;
     strcat(fno6,argv[6]) ;
     fpo6 = fopen(fno6,"a") ;  //open file to append monthly 1 hr
avg strain
     if (fpo6==NULL)
        printf("error\n") ;


strcpy(fno7,"/home/diekfusj/Research/HourlyAvgData/Monthly_Avgs/"
) ;
     strcat(fno7,argv[7]) ;
     fpo7 = fopen(fno7,"a") ;  //open file to append monthly 1 hr
avg wind
     if (fpo7==NULL)
        printf("error\n") ;

     i = 0 ;
```

```
     while (fscanf(fpo2,"%f %f %f
%f\n",&atmp[i],&btmp[i],&ctmp[i],&deg[i]) != EOF) {

           //printf("%f\n",deg[i]) ;
           i++ ;
     }

     n        = floor(i/14400) ;
     rowstart = 0 ;

     //printf("%d\n",n);

     for (i=0;i<n;i++) {

         rowend = rowstart + 14379 ;
         suma   = 0.0 ;
         sumb   = 0.0 ;
         sumc   = 0.0 ;
         sumWx  = 0.0 ;
         sumWy  = 0.0 ;

         for (j=rowstart;j<(rowend+1);j++) {

             suma  = suma + atmp[j] ;
             sumb  = sumb + btmp[j] ;
             sumc  = sumc + ctmp[j] ;

             rad[j]  = deg[j]*((M_PI)/180.0) ;
             Wy[j]   = cos ((double)rad[j]) ;

             //printf("%f %f\n",rad[j],Wy[j]);

             if (rad[j] >= M_PI)  Wx[j] = -sqrt(1.0-((pow
                 ((double)Wy[j],2)))) ;
             else Wx[j] = sqrt(1.0-((pow ((double)Wy[j],2)))) ;

             //printf("%f %f\n",Wx[j],Wy[j]);

             sumWx   = sumWx + Wx[j] ;
             sumWy   = sumWy + Wy[j] ;
         }

         //printf("%f %f\n",sumWx,sumWy);

         avgF1[i]   = suma  / (14400.0) ;
         avgF2[i]   = sumb  / (14400.0) ;
         avgWSpd[i] = sumc  / (14400.0) ;
         Wxbar[i]   = sumWx / (14400.0) ;
         Wybar[i]   = sumWy / (14400.0) ;

         //printf("%f %f\n",Wxbar[i],Wybar[i]);
```

```
    if (Wxbar[i] < -0.0001) {

       Wbar_rad[i] = 2*M_PI - acos(Wybar[i]) ;
       //printf("1st if %f %f\n",Wxbar[i],Wybar[i]) ;

    }

    else if (Wxbar[i] > 0.0001) {

       Wbar_rad[i] = acos(Wybar[i]) ;
       //printf("2nd if %f %f\n",Wxbar[i],Wybar[i]) ;

    }

    else {

       //printf("3rd if %f %f\n",Wxbar[i],Wybar[i]) ;

       if (Wybar[i] > 0.0)
          Wbar_rad[i] = 0.0 ;
       else
          Wbar_rad[i] = M_PI ;

    }

    avgWDir[i] = floor(Wbar_rad[i]*180.0/M_PI) ;

    //if (Wxbar[i] < 0.0) Wbar_rad[i] = 2*M_PI -
          acos(Wybar[i]) ;
    //else Wbar_rad[i] = acos(Wybar[i]) ;

    //printf("%f\n",avgWDir[i]) ;

    rowstart   = rowend + 1 ;
}

for (i=0;i<n;i++) {
    fprintf(fpo4,"%f %f\n", avgF1[i],avgF2[i]) ;
}

for (i=0;i<n;i++) {
    fprintf(fpo5,"%f %f\n", avgWSpd[i],avgWDir[i]) ;
}

for (i=0;i<n;i++) {
    fprintf(fpo6,"%f %f\n", avgF1[i],avgF2[i]) ;
}

for (i=0;i<n;i++) {
    fprintf(fpo7,"%f %f\n", avgWSpd[i],avgWDir[i]) ;
}
```

```
     fclose(fpo2) ;
     fclose(fpo4) ;
     fclose(fpo5) ;
     fclose(fpo6) ;
     fclose(fpo7) ;

/*************************************************************
SECTION 3.1 - END:

This is the end of the one hour average calculations.
*************************************************************/

/*************************************************************
SECTION 3.2 - START:  (Using 'AdjData_(timestamp).txt')

This is where the one hour averages are calculated using adjusted
wind directions and zeroed strain values.
*************************************************************/

/*     float atmp[350000], btmp[350000], ctmp[350000],
deg[350000] ;
     float avgF1[730], avgF2[730], avgWSpd[730], avgWDir[730] ;
     float sumc, sumWx, sumWy ;
     float Wxbar[730], Wybar[730], Wbar_rad[730] ;
     float rad[350000], Wy[350000], Wx[350000] ;

     int   rowstart, rowend ;

     fpo3 = fopen(fno3,"r") ;  //this opens
'AdjData_(timestamp).txt'


strcpy(fno4,"/home/diekfusj/Research/Avg/AvgData/AvgStrain/") ;
     strcat(fno4,argv[4]) ;
     fpo4 = fopen(fno4,"w") ;  //open 'AvgStrain_(timestamp).txt'
     if (fpo4==NULL)
        printf("error\n") ;

     strcpy(fno5,"/home/diekfusj/Research/Avg/AvgData/AvgWind/");
     strcat(fno5,argv[5]) ;
     fpo5 = fopen(fno5,"w") ;  //open file to write daily 1 hr
     avg wind
     if (fpo5==NULL)
        printf("error\n") ;

     strcpy(fno6,"/home/diekfusj/Research/Avg/Monthly_Avgs/") ;
     strcat(fno6,argv[6]) ;
     fpo6 = fopen(fno6,"a") ;  //open file to append monthly 1 hr
     avg strain
     if (fpo6==NULL)
        printf("error\n") ;
```

```
strcpy(fno7,"/home/diekfusj/Research/Avg/Monthly_Avgs/") ;
strcat(fno7,argv[7]) ;
fpo7 = fopen(fno7,"a") ;  //open file to append monthly 1 hr
avg wind
if (fpo7==NULL)
   printf("error\n") ;

i = 0 ;
while (fscanf(fpo3,"%f %f %f
       %f\n",&atmp[i],&btmp[i],&ctmp[i],&deg[i]) != EOF) {

      //printf("%f\n",deg[i]) ;
      i++ ;
}

n        = floor(i/480) ;
rowstart = 0 ;

//printf("%d\n",n);

for (i=0;i<n;i++) {

    rowend = rowstart + 479 ;
    suma   = 0.0 ;
    sumb   = 0.0 ;
    sumc   = 0.0 ;
    sumWx  = 0.0 ;
    sumWy  = 0.0 ;

    for (j=rowstart;j<(rowend+1);j++) {

        suma  = suma + atmp[j] ;
        sumb  = sumb + btmp[j] ;
        sumc  = sumc + ctmp[j] ;

        rad[j]  = deg[j]*((M_PI)/180.0) ;
        Wy[j]   = cos ((double)rad[j]) ;

        //printf("%f %f\n",rad[j],Wy[j]);

        if (rad[j] >= M_PI)  Wx[j] = -sqrt(1.0-((pow
            ((double)Wy[j],2)))) ;
        else Wx[j] = sqrt(1.0-((pow ((double)Wy[j],2)))) ;

        //printf("%f %f\n",Wx[j],Wy[j]);

        sumWx   = sumWx + Wx[j] ;
        sumWy   = sumWy + Wy[j] ;
    }

    //printf("%f %f\n",sumWx,sumWy);
```

```
    avgF1[i]   = suma  / (480.0) ;
    avgF2[i]   = sumb  / (480.0) ;
    avgWSpd[i] = sumc  / (480.0) ;
    Wxbar[i]   = sumWx / (480.0) ;
    Wybar[i]   = sumWy / (480.0) ;

    //printf("%f %f\n",Wxbar[i],Wybar[i]);

    if (Wxbar[i] < -0.0001) {

       Wbar_rad[i] = 2*M_PI - acos(Wybar[i]) ;
       //printf("1st if %f %f\n",Wxbar[i],Wybar[i]) ;

    }

    else if (Wxbar[i] > 0.0001) {

       Wbar_rad[i] = acos(Wybar[i]) ;
       //printf("2nd if %f %f\n",Wxbar[i],Wybar[i]) ;

    }

    else {

       //printf("3rd if %f %f\n",Wxbar[i],Wybar[i]) ;

       if (Wybar[i] > 0.0)
          Wbar_rad[i] = 0.0 ;
       else
          Wbar_rad[i] = M_PI ;

    }

    avgWDir[i] = floor(Wbar_rad[i]*180.0/M_PI) ;

    //if (Wxbar[i] < 0.0) Wbar_rad[i] = 2*M_PI -
          acos(Wybar[i]) ;
    //else Wbar_rad[i] = acos(Wybar[i]) ;

    //printf("%f\n",avgWDir[i]) ;

    rowstart   = rowend + 1 ;
}

for (i=0;i<n;i++) {
    fprintf(fpo4,"%f %f\n", avgF1[i],avgF2[i]) ;
}

for (i=0;i<n;i++) {
    fprintf(fpo5,"%f %f\n", avgWSpd[i],avgWDir[i]) ;
}
```

```
     for (i=0;i<n;i++) {
         fprintf(fpo6,"%f %f\n", avgF1[i],avgF2[i]) ;
     }

     for (i=0;i<n;i++) {
         fprintf(fpo7,"%f %f\n", avgWSpd[i],avgWDir[i]) ;
     }

     fclose(fpo3) ;
     fclose(fpo4) ;
     fclose(fpo5) ;
     fclose(fpo6) ;
     fclose(fpo7) ;



/*************************************************************
SECTION 3.2 - END:

This is the end of the 1 hour average calculations.
*************************************************************/

     printf("\n") ;

     return 0 ;
}
```

APPENDIX D – MATLAB CODE FOR FMS WIND DATA SYNTHESIS

D.1 – FMS_sifter.m

```
function [] = FMS_sifter()

    clear
    clc

    ExcelFile = 'FMS_WindData.xlsx';
    Month = ['Mar','Apr','May','Jun','Jul','Aug','Sep'];

    k = 1;
    t = 0;

    for m = 1:3:length(Month)

        clc
        t = t + 1;
        fprintf('Progress: %.0f/7\n',t)
        Worksheet = Month(m:m+2);
        inputArray = xlsread(ExcelFile,Worksheet);

        for i = 1:length(inputArray(:,1))
            SpeedOnly(k,1) = inputArray(i,1);
            DirectionOnly(k,1) = inputArray(i,2);
            SpeedDirection(k,1) = inputArray(i,1);
            SpeedDirection(k,2) = inputArray(i,2);
            k = k + 1;
        end

    end

    OutputFile = 'FMS_matfile_data';
    save(OutputFile,'SpeedOnly','DirectionOnly','SpeedDirection');

end
```

D.2 – FMS_analysis.m

```
function [] = FMS_analysis()

    clear
    clc
    InputFile = 'FMS_matfile_data.mat';
    load(InputFile)

    WindData = zeros(17,9);

    N = 1;
    NE = 1;
    E = 1;
    SE = 1;
    S = 1;
    SW = 1;
    W = 1;
    NW = 1;

    for t = 1:length(SpeedDirection)

        % assigns column number based on wind direction

        if SpeedDirection(t,2) == 0
            Dir = 1;
        end

        if SpeedDirection(t,2) > 337.5 || SpeedDirection(t,2) <=
           22.5...
                && SpeedDirection(t,2) ~= 0
            Dir = 2;
            NorthSpeeds(N,1) = SpeedDirection(t,1);
            N = N + 1;
        end

        if SpeedDirection(t,2) > 22.5 && SpeedDirection(t,2) <= 67.5
            Dir = 3;
            NortheastSpeeds(NE,1) = SpeedDirection(t,1);
            NE = NE + 1;
        end

        if SpeedDirection(t,2) > 67.5 && SpeedDirection(t,2) <= 112.5
            Dir = 4;
            EastSpeeds(E,1) = SpeedDirection(t,1);
            E = E + 1;
        end

        if SpeedDirection(t,2) > 112.5 && SpeedDirection(t,2) <= 157.5
            Dir = 5;
            SoutheastSpeeds(SE,1) = SpeedDirection(t,1);
            SE = SE + 1;
        end
```

```
if SpeedDirection(t,2) > 157.5 && SpeedDirection(t,2) <= 202.5
    Dir = 6;
    SouthSpeeds(S,1) = SpeedDirection(t,1);
    S = S + 1;
end

if SpeedDirection(t,2) > 202.5 && SpeedDirection(t,2) <= 247.5
    Dir = 7;
    SouthwestSpeeds(SW,1) = SpeedDirection(t,1);
    SW = SW + 1;
end

if SpeedDirection(t,2) > 247.5 && SpeedDirection(t,2) <= 292.5
    Dir = 8;
    WestSpeeds(W,1) = SpeedDirection(t,1);
    W = W + 1;
end

if SpeedDirection(t,2) > 292.5 && SpeedDirection(t,2) <= 337.5
    Dir = 9;
    NorthwestSpeeds(NW,1) = SpeedDirection(t,1);
    NW = NW + 1;
end

% counts occurence of wind speed based on direction

if SpeedDirection(t,1) >= 0 && SpeedDirection(t,1) <= 2.5
    WindData(1,Dir) = WindData(1,Dir) + 1;
end

if SpeedDirection(t,1) > 2.5 && SpeedDirection(t,1) <= 7.5
    WindData(2,Dir) = WindData(2,Dir) + 1;
end

if SpeedDirection(t,1) > 7.5 && SpeedDirection(t,1) <= 12.5
    WindData(3,Dir) = WindData(3,Dir) + 1;
end

if SpeedDirection(t,1) > 12.5 && SpeedDirection(t,1) <= 17.5
    WindData(4,Dir) = WindData(4,Dir) + 1;
end

if SpeedDirection(t,1) > 17.5 && SpeedDirection(t,1) <= 22.5
    WindData(5,Dir) = WindData(5,Dir) + 1;
end

if SpeedDirection(t,1) > 22.5 && SpeedDirection(t,1) <= 27.5
    WindData(6,Dir) = WindData(6,Dir) + 1;
end

if SpeedDirection(t,1) > 27.5 && SpeedDirection(t,1) <= 32.5
    WindData(7,Dir) = WindData(7,Dir) + 1;
end
```

```
        if SpeedDirection(t,1) > 32.5 && SpeedDirection(t,1) <= 37.5
            WindData(8,Dir) = WindData(8,Dir) + 1;
        end

        if SpeedDirection(t,1) > 37.5 && SpeedDirection(t,1) <= 42.5
            WindData(9,Dir) = WindData(9,Dir) + 1;
        end

        if SpeedDirection(t,1) > 42.5 && SpeedDirection(t,1) <= 47.5
            WindData(10,Dir) = WindData(10,Dir) + 1;
        end

        if SpeedDirection(t,1) > 47.5 && SpeedDirection(t,1) <= 52.5
            WindData(11,Dir) = WindData(11,Dir) + 1;
        end

        if SpeedDirection(t,1) > 52.5 && SpeedDirection(t,1) <= 57.5
            WindData(12,Dir) = WindData(12,Dir) + 1;
        end

        if SpeedDirection(t,1) > 57.5 && SpeedDirection(t,1) <= 62.5
            WindData(13,Dir) = WindData(13,Dir) + 1;
        end

        if SpeedDirection(t,1) > 62.5 && SpeedDirection(t,1) <= 67.5
            WindData(14,Dir) = WindData(14,Dir) + 1;
        end

        if SpeedDirection(t,1) > 67.5 && SpeedDirection(t,1) <= 72.5
            WindData(15,Dir) = WindData(15,Dir) + 1;
        end

        if SpeedDirection(t,1) > 72.5 && SpeedDirection(t,1) <= 77.5
            WindData(16,Dir) = WindData(16,Dir) + 1;
        end

        if SpeedDirection(t,1) > 77.5 && SpeedDirection(t,1) <= 82.5
            WindData(17,Dir) = WindData(17,Dir) + 1;
        end

    end

    disp(WindData)
    ExcelFile = 'FMS_Analysis.xls';
    xlswrite(ExcelFile,WindData,'Sheet1')
    OutputFile = 'FMS_Speeds.mat';

save(OutputFile,'NorthSpeeds','NortheastSpeeds','EastSpeeds','Southeast
Speeds','SouthSpeeds','SouthwestSpeeds','WestSpeeds','NorthwestSpeeds')
;

end
```

D.3 – FMS_directiononly.m

```
function [] = FMS_directiononly()

    clear
    clc

    InputFile = 'FMS_matfile_data.mat';
    load(InputFile)

    x = 0:10:360;

    [n,xout] = hist(DirectionOnly,x);
    HiResDir(:,1) = xout;
    HiResDir(:,2) = n;
    WindData = zeros(9,1);

    for t = 1:length(DirectionOnly)

        if DirectionOnly(t) == 0
            WindData(1,1) = WindData(1,1) + 1;
        end

        if DirectionOnly(t) > 337.5 || DirectionOnly(t) <= 22.5...
                && DirectionOnly(t) ~= 0
            WindData(2,1) = WindData(2,1) + 1;
        end

        if DirectionOnly(t) > 22.5 && DirectionOnly(t) <= 67.5
            WindData(3,1) = WindData(3,1) + 1;
        end

        if DirectionOnly(t) > 67.5 && DirectionOnly(t) <= 112.5
            WindData(4,1) = WindData(4,1) + 1;
        end

        if DirectionOnly(t) > 112.5 && DirectionOnly(t) <= 157.5
            WindData(5,1) = WindData(5,1) + 1;
        end

        if DirectionOnly(t) > 157.5 && DirectionOnly(t) <= 202.5
            WindData(6,1) = WindData(6,1) + 1;
        end

        if DirectionOnly(t) > 202.5 && DirectionOnly(t) <= 247.5
            WindData(7,1) = WindData(7,1) + 1;
        end

        if DirectionOnly(t) > 247.5 && DirectionOnly(t) <= 292.5
            WindData(8,1) = WindData(8,1) + 1;
        end

        if DirectionOnly(t) > 292.5 && DirectionOnly(t) <= 337.5
```

```
            WindData(9,1) = WindData(9,1) + 1;
        end

    end

    disp(HiResDir)
    disp(WindData)
    ExcelFile = 'FMS_Direction.xls';
    xlswrite(ExcelFile,WindData,'Sheet1')
    xlswrite(ExcelFile,HiResDir,'Sheet2')

end
```

D.4 – FMS_speedonly.m

```
function [] = FMS_speedonly()

    clear
    clc

    InputFile = 'FMS_matfile_data.mat';
    load(InputFile)
    WindData = zeros(17,1);

    for t = 1:length(SpeedOnly)

        if SpeedOnly(t) >= 0 && SpeedOnly(t) <=2.5
            WindData(1,1) = WindData(1,1) + 1;
        end

        if SpeedOnly(t) > 2.5 && SpeedOnly(t) <= 7.5
            WindData(2,1) = WindData(2,1) + 1;
        end

        if SpeedOnly(t) > 7.5 && SpeedOnly(t) <= 12.5
            WindData(3,1) = WindData(3,1) + 1;
        end

        if SpeedOnly(t) > 12.5 && SpeedOnly(t) <= 17.5
            WindData(4,1) = WindData(4,1) + 1;
        end

        if SpeedOnly(t) > 17.5 && SpeedOnly(t) <= 22.5
            WindData(5,1) = WindData(5,1) + 1;
        end

        if SpeedOnly(t) > 22.5 && SpeedOnly(t) <= 27.5
            WindData(6,1) = WindData(6,1) + 1;
        end

        if SpeedOnly(t) > 27.5 && SpeedOnly(t) <= 32.5
            WindData(7,1) = WindData(7,1) + 1;
        end

        if SpeedOnly(t) > 32.5 && SpeedOnly(t) <= 37.5
            WindData(8,1) = WindData(8,1) + 1;
        end

        if SpeedOnly(t) > 37.5 && SpeedOnly(t) <= 42.5
            WindData(9,1) = WindData(9,1) + 1;
        end

        if SpeedOnly(t) > 42.5 && SpeedOnly(t) <= 47.5
            WindData(10,1) = WindData(10,1) + 1;
        end
```

```
        if SpeedOnly(t) > 47.5 && SpeedOnly(t) <= 52.5
            WindData(11,1) = WindData(11,1) + 1;
        end

        if SpeedOnly(t) > 52.5 && SpeedOnly(t) <= 57.5
            WindData(12,1) = WindData(12,1) + 1;
        end

        if SpeedOnly(t) > 57.5 && SpeedOnly(t) <= 62.5
            WindData(13,1) = WindData(13,1) + 1;
        end

        if SpeedOnly(t) > 62.5 && SpeedOnly(t) <= 67.5
            WindData(14,1) = WindData(14,1) + 1;
        end

        if SpeedOnly(t) > 67.5 && SpeedOnly(t) <= 72.5
            WindData(15,1) = WindData(15,1) + 1;
        end

        if SpeedOnly(t) > 72.5 && SpeedOnly(t) <= 77.5
            WindData(16,1) = WindData(16,1) + 1;
        end

        if SpeedOnly(t) > 77.5 && SpeedOnly(t) <= 1000
            WindData(17,1) = WindData(17,1) + 1;
        end

    end

    disp(WindData)
    ExcelFile = 'FMS_Speed.xls';
    xlswrite(ExcelFile,WindData,'Sheet1')

end
```

APPENDIX E – PROBABILITIES OF WIND SPEED AND DIRECTION

Table E.1. Individual probabilities for wind speed and wind direction from Milwaukee NCDC-ASOS site.

Individual Probabilities for Wind Speed – P ($U = u_i$)

One-Hour Averaged Wind Speed (mph)	Frequency of Occurrence	Probability of Occurrence	Probability of Occurrence (%)
0	14723	0.1006	10.06
5	53430	0.3651	36.51
10	52186	0.3566	35.66
15	20726	0.1416	14.16
20	4826	0.0330	3.30
25	385	0.0026	0.26
30	50	0.0003	0.03
35	15	0.0001	0.01
40	0	0.0000	0.00
45	1	0.0000	0.00
50	0	0.0000	0.00
55	0	0.0000	0.00
60	0	0.0000	0.00
65	0	0.0000	0.00
70	0	0.0000	0.00
75	0	0.0000	0.00
80	0	0.0000	0.00
SUM	**146342**	**1.0000**	**100.00**

Individual Probabilities for Wind Direction – P ($D = d_j$) (by cardinal direction)

One-Hour Averaged Wind Direction	Frequency of Occurrence	Probability of Occurrence	Probability of Occurrence (%)
N/A	14723	0.1006	10.06
North	14808	0.1012	10.12
Northeast	13809	0.0944	9.44
East	10154	0.0694	6.94
Southeast	12725	0.0870	8.70
South	16348	0.1117	11.17
Southwest	21366	0.1460	14.60
West	22799	0.1558	15.58
Northwest	19610	0.1340	13.40
SUM	**146342**	**1.0000**	**100.00**

Individual Probabilities for Wind Direction – P ($D = d_j$) (by 10-degree increment)

One-Hour Averaged Wind Direction	Frequency of Occurrence	Probability of Occurrence	Probability of Occurrence (%)
0	14723	0.1006	10.06
10	3159	0.0216	2.16
20	4677	0.0320	3.20
30	4485	0.0306	3.06
40	3571	0.0244	2.44
50	2906	0.0199	1.99
60	2847	0.0195	1.95
70	2079	0.0142	1.42
80	1882	0.0129	1.29
90	1912	0.0131	1.31
100	1926	0.0132	1.32
110	2355	0.0161	1.61
120	3011	0.0206	2.06
130	3483	0.0238	2.38
140	3338	0.0228	2.28
150	2893	0.0198	1.98
160	2707	0.0185	1.85
170	3115	0.0213	2.13
180	2797	0.0191	1.91
190	3223	0.0220	2.20
200	4506	0.0308	3.08
210	4877	0.0333	3.33
220	6038	0.0413	4.13
230	5284	0.0361	3.61
240	5167	0.0353	3.53
250	4713	0.0322	3.22
260	4230	0.0289	2.89
270	4539	0.0310	3.10
280	4438	0.0303	3.03
290	4879	0.0333	3.33
300	6587	0.0450	4.50
310	5478	0.0374	3.74
320	4142	0.0283	2.83
330	3403	0.0233	2.33
340	2778	0.0190	1.90
350	2147	0.0147	1.47
360	2047	0.0140	1.40
SUM	**146342**	**1.0000**	**100.00**

Table E.2. Individual probabilities for wind speed and wind direction from Eau Claire NCDC-ASOS site.

Individual Probabilities for Wind Speed – P ($U = u_i$)

One-Hour Averaged Wind Speed (mph)	Frequency of Occurrence	Probability of Occurrence	Probability of Occurrence (%)
0	25724	0.2008	20.08
5	53762	0.4198	41.98
10	37737	0.2946	29.46
15	9252	0.0722	7.22
20	1491	0.0116	1.16
25	103	0.0008	0.08
30	11	0.0001	0.01
35	0	0.0000	0.00
40	1	0.0000	0.00
45	0	0.0000	0.00
50	0	0.0000	0.00
55	0	0.0000	0.00
60	0	0.0000	0.00
65	0	0.0000	0.00
70	0	0.0000	0.00
75	0	0.0000	0.00
80	0	0.0000	0.00
SUM	**128081**	**1.0000**	**100.00**

Individual Probabilities for Wind Direction – P ($D = d_j$) (by cardinal direction)

One-Hour Averaged Wind Direction	Frequency of Occurrence	Probability of Occurrence	Probability of Occurrence (%)
N/A	25724	0.2008	20.08
North	11534	0.0901	9.01
Northeast	9954	0.0777	7.77
East	9747	0.0761	7.61
Southeast	11110	0.0867	8.67
South	17938	0.1401	14.01
Southwest	13260	0.1035	10.35
West	17473	0.1364	13.64
Northwest	11341	0.0885	8.85
SUM	**128081**	**1.0000**	**100.00**

Individual Probabilities for Wind Direction – P ($D = d_j$) (by 10-degree increment)

One-Hour Averaged Wind Direction	Frequency of Occurrence	Probability of Occurrence	Probability of Occurrence (%)
0	25724	0.2008	20.08
10	2257	0.0176	1.76
20	1988	0.0155	1.55
30	2196	0.0171	1.71
40	2442	0.0191	1.91
50	2709	0.0212	2.12
60	2607	0.0204	2.04
70	1969	0.0154	1.54
80	1849	0.0144	1.44
90	1790	0.0140	1.40
100	1989	0.0155	1.55
110	2150	0.0168	1.68
120	2488	0.0194	1.94
130	2509	0.0196	1.96
140	2838	0.0222	2.22
150	3275	0.0256	2.56
160	3541	0.0276	2.76
170	4064	0.0317	3.17
180	3814	0.0298	2.98
190	3481	0.0272	2.72
200	3038	0.0237	2.37
210	3056	0.0239	2.39
220	3195	0.0249	2.49
230	3494	0.0273	2.73
240	3515	0.0274	2.74
250	3607	0.0282	2.82
260	3729	0.0291	2.91
270	3557	0.0278	2.78
280	3598	0.0281	2.81
290	2982	0.0233	2.33
300	2818	0.0220	2.20
310	2808	0.0219	2.19
320	2940	0.0230	2.30
330	2775	0.0217	2.17
340	2456	0.0192	1.92
350	2443	0.0191	1.91
360	2390	0.0187	1.87
SUM	**128081**	**1.0000**	**100.00**

Table E.3. Individual probabilities for wind speed and wind direction from Green Bay NCDC-ASOS site.

Individual Probabilities for Wind Speed – P ($U = u_i$)

One-Hour Averaged Wind Speed (mph)	Frequency of Occurrence	Probability of Occurrence	Probability of Occurrence (%)
0	22651	0.1433	14.33
5	65772	0.4161	41.61
10	48427	0.3063	30.63
15	16565	0.1048	10.48
20	4099	0.0259	2.59
25	512	0.0032	0.32
30	53	0.0003	0.03
35	5	0.0000	0.00
40	1	0.0000	0.00
45	0	0.0000	0.00
50	0	0.0000	0.00
55	1	0.0000	0.00
60	0	0.0000	0.00
65	0	0.0000	0.00
70	0	0.0000	0.00
75	0	0.0000	0.00
80	0	0.0000	0.00
SUM	**158086**	**1.0000**	**100.00**

Individual Probabilities for Wind Direction – P ($D = d_j$) (by cardinal direction)

One-Hour Averaged Wind Direction	Frequency of Occurrence	Probability of Occurrence	Probability of Occurrence (%)
N/A	22651	0.1433	14.33
North	16548	0.1047	10.47
Northeast	17223	0.1089	10.89
East	8682	0.0549	5.49
Southeast	8577	0.0543	5.43
South	24206	0.1531	15.31
Southwest	19854	0.1256	12.56
West	25477	0.1612	16.12
Northwest	14868	0.0941	9.41
SUM	**158086**	**1.0000**	**100.00**

Individual Probabilities for Wind Direction – P ($D = d_j$) (by 10-degree increment)

One-Hour Averaged Wind Direction	Frequency of Occurrence	Probability of Occurrence	Probability of Occurrence (%)
0	22651	0.1433	14.33
10	3714	0.0235	2.35
20	3022	0.0191	1.91
30	3156	0.0200	2.00
40	5267	0.0333	3.33
50	5309	0.0336	3.36
60	3491	0.0221	2.21
70	2183	0.0138	1.38
80	1836	0.0116	1.16
90	1671	0.0106	1.06
100	1517	0.0096	0.96
110	1475	0.0093	0.93
120	1615	0.0102	1.02
130	1752	0.0111	1.11
140	2359	0.0149	1.49
150	2851	0.0180	1.80
160	2712	0.0172	1.72
170	3597	0.0228	2.28
180	5210	0.0330	3.30
190	5792	0.0366	3.66
200	6895	0.0436	4.36
210	6807	0.0431	4.31
220	5029	0.0318	3.18
230	3919	0.0248	2.48
240	4099	0.0259	2.59
250	3889	0.0246	2.46
260	4499	0.0285	2.85
270	5653	0.0358	3.58
280	6111	0.0387	3.87
290	5325	0.0337	3.37
300	4434	0.0280	2.80
310	3748	0.0237	2.37
320	3505	0.0222	2.22
330	3181	0.0201	2.01
340	3035	0.0192	1.92
350	3142	0.0199	1.99
360	3635	0.0230	2.30
SUM	**158086**	**1.0000**	**100.00**

Table E.4. Individual probabilities for wind speed and wind direction from La Crosse NCDC-ASOS site.

Individual Probabilities for Wind Speed – P ($U = u_i$)

One-Hour Averaged Wind Speed (mph)	Frequency of Occurrence	Probability of Occurrence	Probability of Occurrence (%)
0	19461	0.1516	15.16
5	56344	0.4388	43.88
10	38763	0.3019	30.19
15	11556	0.0900	9.00
20	2098	0.0163	1.63
25	171	0.0013	0.13
30	15	0.0001	0.01
35	2	0.0000	0.00
40	0	0.0000	0.00
45	1	0.0000	0.00
50	0	0.0000	0.00
55	0	0.0000	0.00
60	0	0.0000	0.00
65	0	0.0000	0.00
70	0	0.0000	0.00
75	0	0.0000	0.00
80	0	0.0000	0.00
SUM	**128411**	**1.0000**	**100.00**

Individual Probabilities for Wind Direction – P ($D = d_j$) (by cardinal direction)

One-Hour Averaged Wind Direction	Frequency of Occurrence	Probability of Occurrence	Probability of Occurrence (%)
N/A	19461	0.1516	15.16
North	16693	0.1300	13.00
Northeast	3411	0.0266	2.66
East	9673	0.0753	7.53
Southeast	17085	0.1330	13.30
South	28078	0.2187	21.87
Southwest	6205	0.0483	4.83
West	9639	0.0751	7.51
Northwest	18166	0.1415	14.15
SUM	**128411**	**1.0000**	**100.00**

Individual Probabilities for Wind Direction – P ($D = d_j$) (by 10-degree increment)

One-Hour Averaged Wind Direction	Frequency of Occurrence	Probability of Occurrence	Probability of Occurrence (%)
0	19461	0.1516	15.16
10	1947	0.0152	1.52
20	1331	0.0104	1.04
30	1051	0.0082	0.82
40	764	0.0059	0.59
50	788	0.0061	0.61
60	808	0.0063	0.63
70	1059	0.0082	0.82
80	1382	0.0108	1.08
90	1840	0.0143	1.43
100	2152	0.0168	1.68
110	3240	0.0252	2.52
120	4678	0.0364	3.64
130	4647	0.0362	3.62
140	3935	0.0306	3.06
150	3825	0.0298	2.98
160	4861	0.0379	3.79
170	6668	0.0519	5.19
180	7429	0.0579	5.79
190	5584	0.0435	4.35
200	3536	0.0275	2.75
210	2251	0.0175	1.75
220	1639	0.0128	1.28
230	1329	0.0103	1.03
240	986	0.0077	0.77
250	964	0.0075	0.75
260	1122	0.0087	0.87
270	1796	0.0140	1.40
280	2494	0.0194	1.94
290	3263	0.0254	2.54
300	3645	0.0284	2.84
310	4164	0.0324	3.24
320	4970	0.0387	3.87
330	5387	0.0420	4.20
340	5403	0.0421	4.21
350	4451	0.0347	3.47
360	3561	0.0277	2.77
SUM	**128411**	**1.0000**	**100.00**

Table E.5. Individual probabilities for wind speed and wind direction from Madison NCDC-ASOS site.

Individual Probabilities for Wind Speed – P ($U = u_i$)

One-Hour Averaged Wind Speed (mph)	Frequency of Occurrence	Probability of Occurrence	Probability of Occurrence (%)
0	36602	0.2489	24.89
5	58531	0.3980	39.80
10	40398	0.2747	27.47
15	9870	0.0671	6.71
20	1567	0.0107	1.07
25	86	0.0006	0.06
30	6	0.0000	0.00
35	1	0.0000	0.00
40	1	0.0000	0.00
45	0	0.0000	0.00
50	0	0.0000	0.00
55	0	0.0000	0.00
60	0	0.0000	0.00
65	0	0.0000	0.00
70	0	0.0000	0.00
75	0	0.0000	0.00
80	0	0.0000	0.00
SUM	**147062**	**1.0000**	**100.00**

Individual Probabilities for Wind Direction – P ($D = d_j$) (by cardinal direction)

One-Hour Averaged Wind Direction	Frequency of Occurrence	Probability of Occurrence	Probability of Occurrence (%)
N/A	36602	0.2489	24.89
North	14844	0.1009	10.09
Northeast	9886	0.0672	6.72
East	10243	0.0697	6.97
Southeast	8486	0.0577	5.77
South	25492	0.1733	17.33
Southwest	12522	0.0851	8.51
West	12410	0.0844	8.44
Northwest	16577	0.1127	11.27
SUM	**147062**	**1.0000**	**100.00**

Individual Probabilities for Wind Direction – P ($D = d_j$) (by 10-degree increment)

One-Hour Averaged Wind Direction	Frequency of Occurrence	Probability of Occurrence	Probability of Occurrence (%)
0	36602	0.2489	24.89
10	2675	0.0182	1.82
20	2331	0.0159	1.59
30	2666	0.0181	1.81
40	2701	0.0184	1.84
50	2285	0.0155	1.55
60	2234	0.0152	1.52
70	2308	0.0157	1.57
80	2153	0.0146	1.46
90	1656	0.0113	1.13
100	1892	0.0129	1.29
110	2234	0.0152	1.52
120	2116	0.0144	1.44
130	2161	0.0147	1.47
140	1998	0.0136	1.36
150	2211	0.0150	1.50
160	3676	0.0250	2.50
170	5154	0.0350	3.50
180	6622	0.0450	4.50
190	6088	0.0414	4.14
200	3952	0.0269	2.69
210	3397	0.0231	2.31
220	4034	0.0274	2.74
230	3172	0.0216	2.16
240	1919	0.0130	1.30
250	1171	0.0080	0.80
260	1539	0.0105	1.05
270	2246	0.0153	1.53
280	3258	0.0222	2.22
290	4196	0.0285	2.85
300	3934	0.0268	2.68
310	4426	0.0301	3.01
320	4311	0.0293	2.93
330	3906	0.0266	2.66
340	3790	0.0258	2.58
350	3122	0.0212	2.12
360	2926	0.0199	1.99
Sum	**147062**	**1.0000**	**100.00**

Table E.6. Individual probabilities for wind speed and wind direction from Oshkosh NCDC-ASOS site.

Individual Probabilities for Wind Speed – P ($U = u_i$)

One-Hour Averaged Wind Speed (mph)	Frequency of Occurrence	Probability of Occurrence	Probability of Occurrence (%)
0	17218	0.1362	13.62
5	54725	0.4328	43.28
10	38859	0.3074	30.74
15	12770	0.1010	10.10
20	2611	0.0207	2.07
25	225	0.0018	0.18
30	19	0.0002	0.02
35	3	0.0000	0.00
40	0	0.0000	0.00
45	1	0.0000	0.00
50	0	0.0000	0.00
55	0	0.0000	0.00
60	0	0.0000	0.00
65	0	0.0000	0.00
70	0	0.0000	0.00
75	0	0.0000	0.00
80	0	0.0000	0.00
SUM	**126431**	**1.0000**	**100.00**

Individual Probabilities for Wind Direction – P ($D = d_j$) (by cardinal direction)

One-Hour Averaged Wind Direction	Frequency of Occurrence	Probability of Occurrence	Probability of Occurrence (%)
N/A	17218	0.1362	13.62
North	10303	0.0815	8.15
Northeast	11266	0.0891	8.91
East	10659	0.0843	8.43
Southeast	7267	0.0575	5.75
South	20012	0.1583	15.83
Southwest	16205	0.1282	12.82
West	20306	0.1606	16.06
Northwest	13195	0.1044	10.44
SUM	**126431**	**1.0000**	**100.00**

Individual Probabilities for Wind Direction – P ($D = d_j$) (by 10-degree increment)

One-Hour Averaged Wind Direction	Frequency of Occurrence	Probability of Occurrence	Probability of Occurrence (%)
0	17218	0.1362	13.62
10	1661	0.0131	1.31
20	1615	0.0128	1.28
30	2224	0.0176	1.76
40	3149	0.0249	2.49
50	2976	0.0235	2.35
60	2917	0.0231	2.31
70	2438	0.0193	1.93
80	2218	0.0175	1.75
90	2131	0.0169	1.69
100	2093	0.0166	1.66
110	1779	0.0141	1.41
120	1678	0.0133	1.33
130	1772	0.0140	1.40
140	1931	0.0153	1.53
150	1886	0.0149	1.49
160	2020	0.0160	1.60
170	2529	0.0200	2.00
180	3740	0.0296	2.96
190	5297	0.0419	4.19
200	6426	0.0508	5.08
210	6356	0.0503	5.03
220	4875	0.0386	3.86
230	2870	0.0227	2.27
240	2104	0.0166	1.66
250	2672	0.0211	2.11
260	3346	0.0265	2.65
270	3751	0.0297	2.97
280	4730	0.0374	3.74
290	5807	0.0459	4.59
300	4482	0.0355	3.55
310	3368	0.0266	2.66
320	2786	0.0220	2.20
330	2559	0.0202	2.02
340	2454	0.0194	1.94
350	2473	0.0196	1.96
360	2100	0.0166	1.66
SUM	**126431**	**1.0000**	**100.00**

Table E.7. Individual probabilities for wind speed and wind direction from Wisconsin Rapids NCDC-ASOS site.

Individual Probabilities for Wind Speed – P ($U = u_i$)

One-Hour Averaged Wind Speed (mph)	Frequency of Occurrence	Probability of Occurrence	Probability of Occurrence (%)
0	25390	0.2031	20.31
5	56321	0.4506	45.06
10	33839	0.2707	27.07
15	8192	0.0655	6.55
20	1175	0.0094	0.94
25	65	0.0005	0.05
30	4	0.0000	0.00
35	0	0.0000	0.00
40	0	0.0000	0.00
45	0	0.0000	0.00
50	0	0.0000	0.00
55	0	0.0000	0.00
60	0	0.0000	0.00
65	0	0.0000	0.00
70	0	0.0000	0.00
75	0	0.0000	0.00
80	0	0.0000	0.00
SUM	**124986**	**1.0000**	**100.00**

Individual Probabilities for Wind Direction – P ($D = d_j$) (by cardinal direction)

One-Hour Averaged Wind Direction	Frequency of Occurrence	Probability of Occurrence	Probability of Occurrence (%)
N/A	25390	0.2031	20.31
North	10938	0.0875	8.75
Northeast	6899	0.0552	5.52
East	13727	0.1098	10.98
Southeast	8851	0.0708	7.08
South	16892	0.1352	13.52
Southwest	11305	0.0905	9.05
West	17269	0.1382	13.82
Northwest	13715	0.1097	10.97
SUM	**124986**	**1.0000**	**100.00**

Individual Probabilities for Wind Direction – P ($D = d_j$) (by 10-degree increment)

One-Hour Averaged Wind Direction	Frequency of Occurrence	Probability of Occurrence	Probability of Occurrence (%)
0	25390	0.2031	20.31
10	1704	0.0136	1.36
20	1903	0.0152	1.52
30	1677	0.0134	1.34
40	1544	0.0124	1.24
50	1628	0.0130	1.30
60	2050	0.0164	1.64
70	2507	0.0201	2.01
80	2869	0.0230	2.30
90	3176	0.0254	2.54
100	2736	0.0219	2.19
110	2439	0.0195	1.95
120	2455	0.0196	1.96
130	2312	0.0185	1.85
140	2073	0.0166	1.66
150	2011	0.0161	1.61
160	2190	0.0175	1.75
170	2768	0.0221	2.21
180	3415	0.0273	2.73
190	4104	0.0328	3.28
200	4415	0.0353	3.53
210	3136	0.0251	2.51
220	2932	0.0235	2.35
230	2660	0.0213	2.13
240	2577	0.0206	2.06
250	2724	0.0218	2.18
260	3120	0.0250	2.50
270	3376	0.0270	2.70
280	3865	0.0309	3.09
290	4184	0.0335	3.35
300	4030	0.0322	3.22
310	3572	0.0286	2.86
320	3257	0.0261	2.61
330	2856	0.0229	2.29
340	2568	0.0205	2.05
350	2511	0.0201	2.01
360	2252	0.0180	1.80
SUM	**124986**	**1.0000**	**100.00**

Table E.8. Individual probabilities for wind speed and wind direction from FMS site.

Individual Probabilities for Wind Speed – P ($U = u_i$)

One-Hour Averaged Wind Speed (mph)	Frequency of Occurrence	Probability of Occurrence	Probability of Occurrence (%)
0	453	0.1113	11.13
5	2583	0.6348	63.48
10	894	0.2197	21.97
15	129	0.0317	3.17
20	10	0.0025	0.25
25	0	0.0000	0.00
30	0	0.0000	0.00
35	0	0.0000	0.00
40	0	0.0000	0.00
45	0	0.0000	0.00
50	0	0.0000	0.00
55	0	0.0000	0.00
60	0	0.0000	0.00
65	0	0.0000	0.00
70	0	0.0000	0.00
75	0	0.0000	0.00
80	0	0.0000	0.00
SUM	**4069**	**1.0000**	**100.00**

Individual Probabilities for Wind Direction – P ($D = d_j$) (by cardinal direction)

One-Hour Averaged Wind Direction	Frequency of Occurrence	Probability of Occurrence	Probability of Occurrence (%)
N/A	453	0.1113	11.13
North	348	0.0855	8.55
Northeast	430	0.1057	10.57
East	562	0.1381	13.81
Southeast	452	0.1111	11.11
South	274	0.0673	6.73
Southwest	495	0.1217	12.17
West	672	0.1652	16.52
Northwest	383	0.0941	9.41
SUM	**4069**	**1.0000**	**100.00**

Individual Probabilities for Wind Direction – P ($D = d_j$) (by 10-degree increment)

One-Hour Averaged Wind Direction	Frequency of Occurrence	Probability of Occurrence	Probability of Occurrence (%)
0	453	0.1113	11.13
10	4	0.0010	0.10
20	306	0.0752	7.52
30	162	0.0398	3.98
40	98	0.0241	2.41
50	84	0.0206	2.06
60	86	0.0211	2.11
70	53	0.0130	1.30
80	73	0.0179	1.79
90	103	0.0253	2.53
100	173	0.0425	4.25
110	160	0.0393	3.93
120	150	0.0369	3.69
130	136	0.0334	3.34
140	84	0.0206	2.06
150	82	0.0202	2.02
160	126	0.0310	3.10
170	9	0.0022	0.22
180	0	0.0000	0.00
190	6	0.0015	0.15
200	133	0.0327	3.27
210	146	0.0359	3.59
220	132	0.0324	3.24
230	111	0.0273	2.73
240	106	0.0261	2.61
250	130	0.0319	3.19
260	103	0.0253	2.53
270	125	0.0307	3.07
280	145	0.0356	3.56
290	169	0.0415	4.15
300	154	0.0378	3.78
310	95	0.0233	2.33
320	78	0.0192	1.92
330	56	0.0138	1.38
340	38	0.0093	0.93
350	0	0.0000	0.00
360	0	0.0000	0.00
SUM	**4069**	**1.0000**	**100.00**

Table E.9. Conditional probabilities for wind speed given wind direction from the Milwaukee NCDC-ASOS site – P ($U = u_i \mid D = d_j$).

		One-Hour Averaged Wind Direction - Frequency of Occurrence									
		N/A	**North**	**Northeast**	**East**	**Southeast**	**South**	**Southwest**	**West**	**Northwest**	
One-Hour Averaged Wind Speed (mph)	0	14723	0	0	0	0	0	0	0	0	
	5	0	4622	4882	4621	4831	8773	7583	9690	8428	
	10	0	6282	5998	3531	5598	5742	8605	8746	7684	
	15	0	3019	2368	1486	1926	1544	4002	3457	2924	
	20	0	806	520	467	352	271	1053	809	548	
	25	0	77	34	38	18	15	84	94	25	
	30	0	2	6	3	0	3	32	3	1	
	35	0	0	1	8	0	0	6	0	0	
	40	0	0	0	0	0	0	0	0	0	
	45	0	0	0	0	0	0	1	0	0	
	50	0	0	0	0	0	0	0	0	0	
	55	0	0	0	0	0	0	0	0	0	
	60	0	0	0	0	0	0	0	0	0	
	65	0	0	0	0	0	0	0	0	0	
	70	0	0	0	0	0	0	0	0	0	
	75	0	0	0	0	0	0	0	0	0	
	80	0	0	0	0	0	0	0	0	0	**SUM**
	SUM	14723	14808	13809	10154	12725	16348	21366	22799	19610	**146342**

		One-Hour Averaged Wind Direction - Probability of Occurrence								
		N/A	**North**	**Northeast**	**East**	**Southeast**	**South**	**Southwest**	**West**	**Northwest**
One-Hour Averaged Wind Speed (mph)	0	1.0000	0.0000	0.0000	0.0000	0.0000	0.0000	0.0000	0.0000	0.0000
	5	0.0000	0.3121	0.3535	0.4551	0.3796	0.5366	0.3549	0.4250	0.4298
	10	0.0000	0.4242	0.4344	0.3477	0.4399	0.3512	0.4027	0.3836	0.3918
	15	0.0000	0.2039	0.1715	0.1463	0.1514	0.0944	0.1873	0.1516	0.1491
	20	0.0000	0.0544	0.0377	0.0460	0.0277	0.0166	0.0493	0.0355	0.0279
	25	0.0000	0.0052	0.0025	0.0037	0.0014	0.0009	0.0039	0.0041	0.0013
	30	0.0000	0.0001	0.0004	0.0003	0.0000	0.0002	0.0015	0.0001	0.0001
	35	0.0000	0.0000	0.0001	0.0008	0.0000	0.0000	0.0003	0.0000	0.0000
	40	0.0000	0.0000	0.0000	0.0000	0.0000	0.0000	0.0000	0.0000	0.0000
	45	0.0000	0.0000	0.0000	0.0000	0.0000	0.0000	0.0000	0.0000	0.0000
	50	0.0000	0.0000	0.0000	0.0000	0.0000	0.0000	0.0000	0.0000	0.0000
	55	0.0000	0.0000	0.0000	0.0000	0.0000	0.0000	0.0000	0.0000	0.0000
	60	0.0000	0.0000	0.0000	0.0000	0.0000	0.0000	0.0000	0.0000	0.0000
	65	0.0000	0.0000	0.0000	0.0000	0.0000	0.0000	0.0000	0.0000	0.0000
	70	0.0000	0.0000	0.0000	0.0000	0.0000	0.0000	0.0000	0.0000	0.0000
	75	0.0000	0.0000	0.0000	0.0000	0.0000	0.0000	0.0000	0.0000	0.0000
	80	0.0000	0.0000	0.0000	0.0000	0.0000	0.0000	0.0000	0.0000	0.0000
	SUM	1.0000	1.0000	1.0000	1.0000	1.0000	1.0000	1.0000	1.0000	1.0000

Table E.10. Conditional probabilities for wind speed given wind direction from the Eau Claire NCDC-ASOS site – P ($U = u_i \mid D = d_j$).

		One-Hour Averaged Wind Direction - Frequency of Occurrence									
		N/A	**North**	**Northeast**	**East**	**Southeast**	**South**	**Southwest**	**West**	**Northwest**	
One-Hour Averaged Wind Speed (mph)	0	25724	0	0	0	0	0	0	0	0	
	5	0	7250	6385	4735	5538	8401	8296	8037	5120	
	10	0	3730	2978	3803	4479	7341	3893	6684	4829	
	15	0	515	522	1026	963	1924	881	2209	1212	
	20	0	38	65	179	128	253	167	497	164	
	25	0	1	4	3	1	15	22	42	15	
	30	0	0	0	1	1	4	1	4	0	
	35	0	0	0	0	0	0	0	0	0	
	40	0	0	0	0	0	0	0	0	1	
	45	0	0	0	0	0	0	0	0	0	
	50	0	0	0	0	0	0	0	0	0	
	55	0	0	0	0	0	0	0	0	0	
	60	0	0	0	0	0	0	0	0	0	
	65	0	0	0	0	0	0	0	0	0	
	70	0	0	0	0	0	0	0	0	0	
	75	0	0	0	0	0	0	0	0	0	
	80	0	0	0	0	0	0	0	0	0	**SUM**
	SUM	25724	11534	9954	9747	11110	17938	13260	17473	11341	**128081**

		One-Hour Averaged Wind Direction - Probability of Occurrence								
		N/A	**North**	**Northeast**	**East**	**Southeast**	**South**	**Southwest**	**West**	**Northwest**
One-Hour Averaged Wind Speed (mph)	0	1.0000	0.0000	0.0000	0.0000	0.0000	0.0000	0.0000	0.0000	0.0000
	5	0.0000	0.6286	0.6415	0.4858	0.4985	0.4683	0.6256	0.4600	0.4515
	10	0.0000	0.3234	0.2992	0.3902	0.4032	0.4092	0.2936	0.3825	0.4258
	15	0.0000	0.0447	0.0524	0.1053	0.0867	0.1073	0.0664	0.1264	0.1069
	20	0.0000	0.0033	0.0065	0.0184	0.0115	0.0141	0.0126	0.0284	0.0145
	25	0.0000	0.0001	0.0004	0.0003	0.0001	0.0008	0.0017	0.0024	0.0013
	30	0.0000	0.0000	0.0000	0.0001	0.0001	0.0002	0.0001	0.0002	0.0000
	35	0.0000	0.0000	0.0000	0.0000	0.0000	0.0000	0.0000	0.0000	0.0000
	40	0.0000	0.0000	0.0000	0.0000	0.0000	0.0000	0.0000	0.0000	0.0001
	45	0.0000	0.0000	0.0000	0.0000	0.0000	0.0000	0.0000	0.0000	0.0000
	50	0.0000	0.0000	0.0000	0.0000	0.0000	0.0000	0.0000	0.0000	0.0000
	55	0.0000	0.0000	0.0000	0.0000	0.0000	0.0000	0.0000	0.0000	0.0000
	60	0.0000	0.0000	0.0000	0.0000	0.0000	0.0000	0.0000	0.0000	0.0000
	65	0.0000	0.0000	0.0000	0.0000	0.0000	0.0000	0.0000	0.0000	0.0000
	70	0.0000	0.0000	0.0000	0.0000	0.0000	0.0000	0.0000	0.0000	0.0000
	75	0.0000	0.0000	0.0000	0.0000	0.0000	0.0000	0.0000	0.0000	0.0000
	80	0.0000	0.0000	0.0000	0.0000	0.0000	0.0000	0.0000	0.0000	0.0000
	SUM	1.0000	1.0000	1.0000	1.0000	1.0000	1.0000	1.0000	1.0000	1.0000

Table E.11. Conditional probabilities for wind speed given wind direction from the Green Bay NCDC-ASOS site – P ($U = u_i \mid D = d_j$).

		One-Hour Averaged Wind Direction - Frequency of Occurrence									
		N/A	**North**	**Northeast**	**East**	**Southeast**	**South**	**Southwest**	**West**	**Northwest**	
One-Hour Averaged Wind Speed (mph)	0	22651	0	0	0	0	0	0	0	0	
	5	0	7857	5859	5116	4234	14270	11017	10596	6823	
	10	0	5980	6666	2906	3127	7654	6972	9599	5523	
	15	0	2155	3290	608	1009	1967	1544	3992	2000	
	20	0	479	1221	47	183	300	282	1120	467	
	25	0	65	174	5	23	11	33	150	51	
	30	0	12	13	0	1	3	5	18	1	
	35	0	0	0	0	0	0	1	1	3	
	40	0	0	0	0	0	0	0	1	0	
	45	0	0	0	0	0	0	0	0	0	
	50	0	0	0	0	0	0	0	0	0	
	55	0	0	0	0	0	1	0	0	0	
	60	0	0	0	0	0	0	0	0	0	
	65	0	0	0	0	0	0	0	0	0	
	70	0	0	0	0	0	0	0	0	0	
	75	0	0	0	0	0	0	0	0	0	
	80	0	0	0	0	0	0	0	0	0	**SUM**
	SUM	22651	16548	17223	8682	8577	24206	19854	25477	14868	**158086**

		One-Hour Averaged Wind Direction - Probability of Occurrence								
		N/A	**North**	**Northeast**	**East**	**Southeast**	**South**	**Southwest**	**West**	**Northwest**
One-Hour Averaged Wind Speed (mph)	0	1.0000	0.0000	0.0000	0.0000	0.0000	0.0000	0.0000	0.0000	0.0000
	5	0.0000	0.4748	0.3402	0.5893	0.4936	0.5895	0.5549	0.4159	0.4589
	10	0.0000	0.3614	0.3870	0.3347	0.3646	0.3162	0.3512	0.3768	0.3715
	15	0.0000	0.1302	0.1910	0.0700	0.1176	0.0813	0.0778	0.1567	0.1345
	20	0.0000	0.0289	0.0709	0.0054	0.0213	0.0124	0.0142	0.0440	0.0314
	25	0.0000	0.0039	0.0101	0.0006	0.0027	0.0005	0.0017	0.0059	0.0034
	30	0.0000	0.0007	0.0008	0.0000	0.0001	0.0001	0.0003	0.0007	0.0001
	35	0.0000	0.0000	0.0000	0.0000	0.0000	0.0000	0.0001	0.0000	0.0002
	40	0.0000	0.0000	0.0000	0.0000	0.0000	0.0000	0.0000	0.0000	0.0000
	45	0.0000	0.0000	0.0000	0.0000	0.0000	0.0000	0.0000	0.0000	0.0000
	50	0.0000	0.0000	0.0000	0.0000	0.0000	0.0000	0.0000	0.0000	0.0000
	55	0.0000	0.0000	0.0000	0.0000	0.0000	0.0000	0.0000	0.0000	0.0000
	60	0.0000	0.0000	0.0000	0.0000	0.0000	0.0000	0.0000	0.0000	0.0000
	65	0.0000	0.0000	0.0000	0.0000	0.0000	0.0000	0.0000	0.0000	0.0000
	70	0.0000	0.0000	0.0000	0.0000	0.0000	0.0000	0.0000	0.0000	0.0000
	75	0.0000	0.0000	0.0000	0.0000	0.0000	0.0000	0.0000	0.0000	0.0000
	80	0.0000	0.0000	0.0000	0.0000	0.0000	0.0000	0.0000	0.0000	0.0000
	SUM	1.0000	1.0000	1.0000	1.0000	1.0000	1.0000	1.0000	1.0000	1.0000

Table E.12. Conditional probabilities for wind speed given wind direction from the La Crosse NCDC-ASOS site – P ($U = u_i \mid D = d_j$).

		One-Hour Averaged Wind Direction - Frequency of Occurrence									
		N/A	**North**	**Northeast**	**East**	**Southeast**	**South**	**Southwest**	**West**	**Northwest**	
One-Hour Averaged Wind Speed (mph)	0	19461	0	0	0	0	0	0	0	0	
	5	0	9415	2158	6635	13040	11955	2980	3784	6377	
	10	0	5511	1120	2612	3457	12358	2256	3886	7563	
	15	0	1504	128	376	547	3371	757	1496	3377	
	20	0	253	5	45	39	378	183	422	773	
	25	0	10	0	4	2	15	25	46	69	
	30	0	0	0	0	0	1	2	5	7	
	35	0	0	0	0	0	0	2	0	0	
	40	0	0	0	0	0	0	0	0	0	
	45	0	0	0	1	0	0	0	0	0	
	50	0	0	0	0	0	0	0	0	0	
	55	0	0	0	0	0	0	0	0	0	
	60	0	0	0	0	0	0	0	0	0	
	65	0	0	0	0	0	0	0	0	0	
	70	0	0	0	0	0	0	0	0	0	
	75	0	0	0	0	0	0	0	0	0	
	80	0	0	0	0	0	0	0	0	0	**SUM**
	SUM	19461	16693	3411	9673	17085	28078	6205	9639	18166	**128411**

		One-Hour Averaged Wind Direction - Probability of Occurrence								
		N/A	**North**	**Northeast**	**East**	**Southeast**	**South**	**Southwest**	**West**	**Northwest**
One-Hour Averaged Wind Speed (mph)	0	1.0000	0.0000	0.0000	0.0000	0.0000	0.0000	0.0000	0.0000	0.0000
	5	0.0000	0.5640	0.6327	0.6859	0.7632	0.4258	0.4803	0.3926	0.3510
	10	0.0000	0.3301	0.3283	0.2700	0.2023	0.4401	0.3636	0.4032	0.4163
	15	0.0000	0.0901	0.0375	0.0389	0.0320	0.1201	0.1220	0.1552	0.1859
	20	0.0000	0.0152	0.0015	0.0047	0.0023	0.0135	0.0295	0.0438	0.0426
	25	0.0000	0.0006	0.0000	0.0004	0.0001	0.0005	0.0040	0.0048	0.0038
	30	0.0000	0.0000	0.0000	0.0000	0.0000	0.0000	0.0003	0.0005	0.0004
	35	0.0000	0.0000	0.0000	0.0000	0.0000	0.0000	0.0003	0.0000	0.0000
	40	0.0000	0.0000	0.0000	0.0000	0.0000	0.0000	0.0000	0.0000	0.0000
	45	0.0000	0.0000	0.0000	0.0001	0.0000	0.0000	0.0000	0.0000	0.0000
	50	0.0000	0.0000	0.0000	0.0000	0.0000	0.0000	0.0000	0.0000	0.0000
	55	0.0000	0.0000	0.0000	0.0000	0.0000	0.0000	0.0000	0.0000	0.0000
	60	0.0000	0.0000	0.0000	0.0000	0.0000	0.0000	0.0000	0.0000	0.0000
	65	0.0000	0.0000	0.0000	0.0000	0.0000	0.0000	0.0000	0.0000	0.0000
	70	0.0000	0.0000	0.0000	0.0000	0.0000	0.0000	0.0000	0.0000	0.0000
	75	0.0000	0.0000	0.0000	0.0000	0.0000	0.0000	0.0000	0.0000	0.0000
	80	0.0000	0.0000	0.0000	0.0000	0.0000	0.0000	0.0000	0.0000	0.0000
	SUM	1.0000	1.0000	1.0000	1.0000	1.0000	1.0000	1.0000	1.0000	1.0000

Table E.13. Conditional probabilities for wind speed given wind direction from the Madison NCDC-ASOS site – P ($U = u_i \mid D = d_j$).

		One-Hour Averaged Wind Direction - Frequency of Occurrence									
		N/A	**North**	**Northeast**	**East**	**Southeast**	**South**	**Southwest**	**West**	**Northwest**	
One-Hour Averaged Wind Speed (mph)	0	36602	0	0	0	0	0	0	0	0	
	5	0	8036	4302	5006	4267	11712	7907	7821	9480	
	10	0	4983	3812	3730	3295	10660	4204	3911	5803	
	15	0	1485	1466	1209	799	2726	356	623	1206	
	20	0	311	284	282	119	379	51	54	87	
	25	0	24	21	15	6	15	4	1	0	
	30	0	3	1	1	0	0	0	0	1	
	35	0	1	0	0	0	0	0	0	0	
	40	0	1	0	0	0	0	0	0	0	
	45	0	0	0	0	0	0	0	0	0	
	50	0	0	0	0	0	0	0	0	0	
	55	0	0	0	0	0	0	0	0	0	
	60	0	0	0	0	0	0	0	0	0	
	65	0	0	0	0	0	0	0	0	0	
	70	0	0	0	0	0	0	0	0	0	
	75	0	0	0	0	0	0	0	0	0	
	80	0	0	0	0	0	0	0	0	0	**SUM**
	SUM	36602	14844	9886	10243	8486	25492	12522	12410	16577	**147062**

		One-Hour Averaged Wind Direction - Probability of Occurrence								
		N/A	**North**	**Northeast**	**East**	**Southeast**	**South**	**Southwest**	**West**	**Northwest**
One-Hour Averaged Wind Speed (mph)	0	1.0000	0.0000	0.0000	0.0000	0.0000	0.0000	0.0000	0.0000	0.0000
	5	0.0000	0.5414	0.4352	0.4887	0.5028	0.4594	0.6314	0.6302	0.5719
	10	0.0000	0.3357	0.3856	0.3642	0.3883	0.4182	0.3357	0.3151	0.3501
	15	0.0000	0.1000	0.1483	0.1180	0.0942	0.1069	0.0284	0.0502	0.0728
	20	0.0000	0.0210	0.0287	0.0275	0.0140	0.0149	0.0041	0.0044	0.0052
	25	0.0000	0.0016	0.0021	0.0015	0.0007	0.0006	0.0003	0.0001	0.0000
	30	0.0000	0.0002	0.0001	0.0001	0.0000	0.0000	0.0000	0.0000	0.0001
	35	0.0000	0.0001	0.0000	0.0000	0.0000	0.0000	0.0000	0.0000	0.0000
	40	0.0000	0.0001	0.0000	0.0000	0.0000	0.0000	0.0000	0.0000	0.0000
	45	0.0000	0.0000	0.0000	0.0000	0.0000	0.0000	0.0000	0.0000	0.0000
	50	0.0000	0.0000	0.0000	0.0000	0.0000	0.0000	0.0000	0.0000	0.0000
	55	0.0000	0.0000	0.0000	0.0000	0.0000	0.0000	0.0000	0.0000	0.0000
	60	0.0000	0.0000	0.0000	0.0000	0.0000	0.0000	0.0000	0.0000	0.0000
	65	0.0000	0.0000	0.0000	0.0000	0.0000	0.0000	0.0000	0.0000	0.0000
	70	0.0000	0.0000	0.0000	0.0000	0.0000	0.0000	0.0000	0.0000	0.0000
	75	0.0000	0.0000	0.0000	0.0000	0.0000	0.0000	0.0000	0.0000	0.0000
	80	0.0000	0.0000	0.0000	0.0000	0.0000	0.0000	0.0000	0.0000	0.0000
	SUM	1.0000	1.0000	1.0000	1.0000	1.0000	1.0000	1.0000	1.0000	1.0000

Table E.14. Conditional probabilities for wind speed given wind direction from the Oshkosh NCDC-ASOS site – P ($U = u_i \mid D = d_j$).

		One-Hour Averaged Wind Direction - Frequency of Occurrence									
		N/A	**North**	**Northeast**	**East**	**Southeast**	**South**	**Southwest**	**West**	**Northwest**	
One-Hour Averaged Wind Speed (mph)	0	17218	0	0	0	0	0	0	0	0	
	5	0	4279	4063	5853	4008	10416	8339	12434	5333	
	10	0	4048	4767	3865	2510	6689	5727	6001	5252	
	15	0	1545	1901	832	656	2382	1815	1540	2099	
	20	0	373	500	109	92	480	292	296	469	
	25	0	51	35	0	1	43	22	33	40	
	30	0	7	0	0	0	2	7	2	1	
	35	0	0	0	0	0	0	2	0	1	
	40	0	0	0	0	0	0	0	0	0	
	45	0	0	0	0	0	0	1	0	0	
	50	0	0	0	0	0	0	0	0	0	
	55	0	0	0	0	0	0	0	0	0	
	60	0	0	0	0	0	0	0	0	0	
	65	0	0	0	0	0	0	0	0	0	
	70	0	0	0	0	0	0	0	0	0	
	75	0	0	0	0	0	0	0	0	0	
	80	0	0	0	0	0	0	0	0	0	**SUM**
	SUM	17218	10303	11266	10659	7267	20012	16205	20306	13195	**126431**

		One-Hour Averaged Wind Direction - Probability of Occurrence								
		N/A	**North**	**Northeast**	**East**	**Southeast**	**South**	**Southwest**	**West**	**Northwest**
One-Hour Averaged Wind Speed (mph)	0	1.0000	0.0000	0.0000	0.0000	0.0000	0.0000	0.0000	0.0000	0.0000
	5	0.0000	0.4153	0.3606	0.5491	0.5515	0.5205	0.5146	0.6123	0.4042
	10	0.0000	0.3929	0.4231	0.3626	0.3454	0.3342	0.3534	0.2955	0.3980
	15	0.0000	0.1500	0.1687	0.0781	0.0903	0.1190	0.1120	0.0758	0.1591
	20	0.0000	0.0362	0.0444	0.0102	0.0127	0.0240	0.0180	0.0146	0.0355
	25	0.0000	0.0050	0.0031	0.0000	0.0001	0.0021	0.0014	0.0016	0.0030
	30	0.0000	0.0007	0.0000	0.0000	0.0000	0.0001	0.0004	0.0001	0.0001
	35	0.0000	0.0000	0.0000	0.0000	0.0000	0.0000	0.0001	0.0000	0.0001
	40	0.0000	0.0000	0.0000	0.0000	0.0000	0.0000	0.0000	0.0000	0.0000
	45	0.0000	0.0000	0.0000	0.0000	0.0000	0.0000	0.0001	0.0000	0.0000
	50	0.0000	0.0000	0.0000	0.0000	0.0000	0.0000	0.0000	0.0000	0.0000
	55	0.0000	0.0000	0.0000	0.0000	0.0000	0.0000	0.0000	0.0000	0.0000
	60	0.0000	0.0000	0.0000	0.0000	0.0000	0.0000	0.0000	0.0000	0.0000
	65	0.0000	0.0000	0.0000	0.0000	0.0000	0.0000	0.0000	0.0000	0.0000
	70	0.0000	0.0000	0.0000	0.0000	0.0000	0.0000	0.0000	0.0000	0.0000
	75	0.0000	0.0000	0.0000	0.0000	0.0000	0.0000	0.0000	0.0000	0.0000
	80	0.0000	0.0000	0.0000	0.0000	0.0000	0.0000	0.0000	0.0000	0.0000
	SUM	1.0000	1.0000	1.0000	1.0000	1.0000	1.0000	1.0000	1.0000	1.0000

Table E.15. Conditional probabilities for wind speed given wind direction from the Wisconsin Rapids NCDC-ASOS site – P ($U = u_i \mid D = d_j$).

		One-Hour Averaged Wind Direction - Frequency of Occurrence									
		N/A	**North**	**Northeast**	**East**	**Southeast**	**South**	**Southwest**	**West**	**Northwest**	
One-Hour Averaged Wind Speed (mph)	0	25390	0	0	0	0	0	0	0	0	
	5	0	6234	4210	7459	6595	10548	6358	8899	6018	
	10	0	3709	2254	4834	2068	5311	3990	6203	5470	
	15	0	873	402	1250	182	935	807	1862	1881	
	20	0	117	31	179	6	86	132	290	334	
	25	0	5	2	5	0	9	17	15	12	
	30	0	0	0	0	0	3	1	0	0	
	35	0	0	0	0	0	0	0	0	0	
	40	0	0	0	0	0	0	0	0	0	
	45	0	0	0	0	0	0	0	0	0	
	50	0	0	0	0	0	0	0	0	0	
	55	0	0	0	0	0	0	0	0	0	
	60	0	0	0	0	0	0	0	0	0	
	65	0	0	0	0	0	0	0	0	0	
	70	0	0	0	0	0	0	0	0	0	
	75	0	0	0	0	0	0	0	0	0	
	80	0	0	0	0	0	0	0	0	0	**SUM**
	SUM	25390	10938	6899	13727	8851	16892	11305	17269	13715	**124986**

		One-Hour Averaged Wind Direction - Probability of Occurrence								
		N/A	**North**	**Northeast**	**East**	**Southeast**	**South**	**Southwest**	**West**	**Northwest**
One-Hour Averaged Wind Speed (mph)	0	1.0000	0.0000	0.0000	0.0000	0.0000	0.0000	0.0000	0.0000	0.0000
	5	0.0000	0.5699	0.6102	0.5434	0.7451	0.6244	0.5624	0.5153	0.4388
	10	0.0000	0.3391	0.3267	0.3522	0.2336	0.3144	0.3529	0.3592	0.3988
	15	0.0000	0.0798	0.0583	0.0911	0.0206	0.0554	0.0714	0.1078	0.1371
	20	0.0000	0.0107	0.0045	0.0130	0.0007	0.0051	0.0117	0.0168	0.0244
	25	0.0000	0.0005	0.0003	0.0004	0.0000	0.0005	0.0015	0.0009	0.0009
	30	0.0000	0.0000	0.0000	0.0000	0.0000	0.0002	0.0001	0.0000	0.0000
	35	0.0000	0.0000	0.0000	0.0000	0.0000	0.0000	0.0000	0.0000	0.0000
	40	0.0000	0.0000	0.0000	0.0000	0.0000	0.0000	0.0000	0.0000	0.0000
	45	0.0000	0.0000	0.0000	0.0000	0.0000	0.0000	0.0000	0.0000	0.0000
	50	0.0000	0.0000	0.0000	0.0000	0.0000	0.0000	0.0000	0.0000	0.0000
	55	0.0000	0.0000	0.0000	0.0000	0.0000	0.0000	0.0000	0.0000	0.0000
	60	0.0000	0.0000	0.0000	0.0000	0.0000	0.0000	0.0000	0.0000	0.0000
	65	0.0000	0.0000	0.0000	0.0000	0.0000	0.0000	0.0000	0.0000	0.0000
	70	0.0000	0.0000	0.0000	0.0000	0.0000	0.0000	0.0000	0.0000	0.0000
	75	0.0000	0.0000	0.0000	0.0000	0.0000	0.0000	0.0000	0.0000	0.0000
	80	0.0000	0.0000	0.0000	0.0000	0.0000	0.0000	0.0000	0.0000	0.0000
	SUM	1.0000	1.0000	1.0000	1.0000	1.0000	1.0000	1.0000	1.0000	1.0000

Table E.16. Conditional probabilities for wind speed given wind direction from the FMS site – P ($U = u_i \mid D = d_j$).

		One-Hour Averaged Wind Direction - Frequency of Occurrence									
		N/A	**North**	**Northeast**	**East**	**Southeast**	**South**	**Southwest**	**West**	**Northwest**	
One-Hour Averaged Wind Speed (mph)	0	453	0	0	0	0	0	0	0	0	
	5	0	102	284	469	286	238	431	495	278	
	10	0	160	133	83	156	33	63	176	90	
	15	0	79	10	10	10	3	1	1	15	
	20	0	7	3	0	0	0	0	0	0	
	25	0	0	0	0	0	0	0	0	0	
	30	0	0	0	0	0	0	0	0	0	
	35	0	0	0	0	0	0	0	0	0	
	40	0	0	0	0	0	0	0	0	0	
	45	0	0	0	0	0	0	0	0	0	
	50	0	0	0	0	0	0	0	0	0	
	55	0	0	0	0	0	0	0	0	0	
	60	0	0	0	0	0	0	0	0	0	
	65	0	0	0	0	0	0	0	0	0	
	70	0	0	0	0	0	0	0	0	0	
	75	0	0	0	0	0	0	0	0	0	
	80	0	0	0	0	0	0	0	0	0	**SUM**
	SUM	453	348	430	562	452	274	495	672	383	**4069**

		One-Hour Averaged Wind Direction - Probability of Occurrence								
		N/A	**North**	**Northeast**	**East**	**Southeast**	**South**	**Southwest**	**West**	**Northwest**
One-Hour Averaged Wind Speed (mph)	0	1.0000	0.0000	0.0000	0.0000	0.0000	0.0000	0.0000	0.0000	0.0000
	5	0.0000	0.2931	0.6605	0.8345	0.6327	0.8686	0.8707	0.7366	0.7258
	10	0.0000	0.4598	0.3093	0.1477	0.3451	0.1204	0.1273	0.2619	0.2350
	15	0.0000	0.2270	0.0233	0.0178	0.0221	0.0109	0.0020	0.0015	0.0392
	20	0.0000	0.0201	0.0070	0.0000	0.0000	0.0000	0.0000	0.0000	0.0000
	25	0.0000	0.0000	0.0000	0.0000	0.0000	0.0000	0.0000	0.0000	0.0000
	30	0.0000	0.0000	0.0000	0.0000	0.0000	0.0000	0.0000	0.0000	0.0000
	35	0.0000	0.0000	0.0000	0.0000	0.0000	0.0000	0.0000	0.0000	0.0000
	40	0.0000	0.0000	0.0000	0.0000	0.0000	0.0000	0.0000	0.0000	0.0000
	45	0.0000	0.0000	0.0000	0.0000	0.0000	0.0000	0.0000	0.0000	0.0000
	50	0.0000	0.0000	0.0000	0.0000	0.0000	0.0000	0.0000	0.0000	0.0000
	55	0.0000	0.0000	0.0000	0.0000	0.0000	0.0000	0.0000	0.0000	0.0000
	60	0.0000	0.0000	0.0000	0.0000	0.0000	0.0000	0.0000	0.0000	0.0000
	65	0.0000	0.0000	0.0000	0.0000	0.0000	0.0000	0.0000	0.0000	0.0000
	70	0.0000	0.0000	0.0000	0.0000	0.0000	0.0000	0.0000	0.0000	0.0000
	75	0.0000	0.0000	0.0000	0.0000	0.0000	0.0000	0.0000	0.0000	0.0000
	80	0.0000	0.0000	0.0000	0.0000	0.0000	0.0000	0.0000	0.0000	0.0000
	SUM	1.0000	1.0000	1.0000	1.0000	1.0000	1.0000	1.0000	1.0000	1.0000

Table F.1. Least squares regression analysis for fatigue detail category U1.

U1: Unreinforced Round Socket - Equal Leg Fillet Welds

	Research Group	Specimen Designation	Stress Range	Cycles to Failure	X Log S	Y Log N	$X_i - X_{bar}$	$Y_i - Y_{bar}$	$(X_i - X_{bar})*(Y_i - Y_{bar})$	$(X_i - X_{bar})^2$	Least Squares Line $N_{hat} = A_{hat}S^{-mhat}$	A (m = 2.34)
1	Archer and Gurney (1970)	AG-S-7/16-W-A-27	8.20	350000	0.91	5.54	0.04	-0.22	-0.01	0.00	459313.67	47993263.63
2		AG-S-7/16-W-B-28	7.60	430000	0.88	5.63	0.01	-0.13	0.00	0.00	548638.41	49363263.18
3		AG-S-7/16-W-C-29	5.40	800000	0.73	5.90	-0.14	0.14	-0.02	0.02	1220089.62	41297129.33
4		AG-S-7/16-W-D-30	4.50	1100000	0.65	6.04	-0.22	0.28	-0.06	0.05	1868834.38	37071783.50
5		AG-S-9/16-W-A-31	7.00	310000	0.85	5.49	-0.02	-0.27	0.01	0.00	664987.10	29360948.68
6		AG-S-9/16-W-B-32	5.10	550000	0.71	5.74	-0.16	-0.02	0.00	0.03	1394588.22	24839240.29
7		AG-S-9/16-W-C-33	3.70	2300000	0.57	6.36	-0.30	0.60	-0.18	0.09	2953815.04	49041771.56
8		AG-S-7/16-RHS-A-34	10.00	380000	1.00	5.58	0.13	-0.18	-0.02	0.02	288767.37	82881403.24
9		AG-S-7/16-RHS-B-35	8.00	430000	0.90	5.63	0.03	-0.13	0.00	0.00	486618.92	55654601.21
10		AG-S-7/16-RHS-C-36	6.50	800000	0.81	5.90	-0.06	0.14	-0.01	0.00	790829.18	63713125.60
11		AG-S-7/16-RHS-D-37	5.50	1300000	0.74	6.11	-0.13	0.35	-0.05	0.02	1168839.85	70050292.60
12		AG-S-9/16-RHS-A-38	11.00	310000	1.04	5.49	0.17	-0.27	-0.05	0.03	231070.30	84496587.23
13		AG-S-9/16-RHS-B-39	7.00	440000	0.85	5.64	-0.02	-0.12	0.00	0.00	664987.10	41673604.57
14		AG-S-9/16-RHS-C-40	8.00	590000	0.90	5.77	0.03	0.01	0.00	0.00	486618.92	76363290.03
15		AG-S-9/16-RHS-D-41	6.00	2400000	0.78	6.38	-0.09	0.62	-0.06	0.01	953630.00	158508643.38
16	Chen et al (2003) and Alderson (1999)	UMO-VAL-O-1-1	8.00	1800000	0.90	6.26	0.03	0.49	0.02	0.00	486618.92	232972749.23
17		UMO-UM-O-1-4 (b)	8.00	500000	0.90	5.70	0.03	-0.07	0.00	0.00	486618.92	64714652.56
18	Fisher et al (1981)	LEH-40-A-45CA-1-1	18.80	36100	1.27	4.56	0.40	-1.21	-0.49	0.16	65975.46	34462469.70
19		LEH-40-A-45CA-2-2	12.40	117800	1.09	5.07	0.22	-0.69	-0.15	0.05	174608.46	42491455.58
20		LEH-40-A-45CA-3-3	6.40	1892400	0.81	6.28	-0.06	0.51	-0.03	0.00	820030.24	145346533.97
21		LEH-40-A-45CA-4-4	12.40	174200	1.09	5.24	0.22	-0.52	-0.12	0.05	174608.46	62835412.25
22		LEH-40-A-45CA-5-5	6.40	1208700	0.81	6.08	-0.06	0.32	-0.02	0.00	820030.24	92834683.79
23		LEH-40-A-45CA-6-6	6.40	1472900	0.81	6.17	-0.06	0.40	-0.03	0.00	820030.24	113126669.78
			S_{bar}	N_{bar}	X_{bar}	Y_{bar}	$\sum(X_i - X_{bar})$	$\sum(Y_i - Y_{bar})$	$\sum(X_i - X_{bar})*(Y_i - Y_{bar})$	$\sum(X_i - X_{bar})^2$		
			7.93	856178.26	0.87	5.76	0.00	0.00	-1.27	0.54	Mean	7.40E+07
											Median	6.28E+07
n			b_{hat}	a_{hat}							Standard Deviation	4.89E+07
23			-2.34	7.80							Coefficient of Variation	0.66
			A_{hat}	m_{hat}								
			6.30E+07	2.34								

Table F.2. Least squares regression analysis for fatigue detail category U2.

U2: Unreinforced Round Socket - Unequal Leg Fillet Welds

	Research Group	Specimen Designation	Stress Range	Cycles to Failure	X	Y					Least Squares Line	
					Log S	Log N	$X_i - X_{bar}$	$Y_i - Y_{bar}$	$(X_i - X_{bar})*(Y_i - Y_{bar})$	$(X_i - X_{bar})^2$	$N_{hat} = A_{hat}S^{-mhat}$	A (m = 3.03)
1	Fisher et al (1981)	LEH-40-A-34CA-1-7	6.40	3751600	0.81	6.57	-0.19	0.74	-0.14	0.04	2492857.51	1043788308.97
2		LEH-40-A-34CA-2-8	6.40	3573400	0.81	6.55	-0.19	0.72	-0.14	0.04	2492857.51	994208642.52
3		LEH-48-V-28CA-1-9	18.90	87000	1.28	4.94	0.28	-0.89	-0.25	0.08	93490.82	645421792.42
4		LEH-48-V-28CA-2-10	12.40	317500	1.09	5.50	0.10	-0.33	-0.03	0.01	335552.01	656261977.24
5		LEH-48-V-28CA-3-11 (a)	6.50	5244000	0.81	6.72	-0.18	0.89	-0.16	0.03	2378380.60	1529236610.05
6		LEH-48-V-28CA-4-12	12.40	198100	1.09	5.30	0.10	-0.53	-0.05	0.01	335552.01	409466134.46
7		LEH-48-V-28CA-5-13 (b)	6.50	5186500	0.81	6.71	-0.18	0.89	-0.16	0.03	2378380.60	1512468664.76
8		LEH-48-V-28CA-6-14 (c)	6.40	8832300	0.81	6.95	-0.19	1.12	-0.21	0.04	2492857.51	2457365252.51
9	Machietto (2002)	VAL-U-SFW-B-8	17.60	1240200	1.25	6.09	0.25	0.26	0.07	0.06	116040.34	7412694177.85
10	Chen et al (2003) and Alderson (1999)	UMO-VAL-N-1-2	8.00	2100000	0.90	6.32	-0.09	0.49	-0.04	0.01	1267241.24	1149352788.26
11		UMO-VAL-N-2-3 (a)	8.00	400000	0.90	5.60	-0.09	-0.23	0.02	0.01	1267241.24	218924340.62
12	Koenigs et al (2003)	VAL-U-N-A-1	11.90	249446	1.08	5.40	0.08	-0.43	-0.04	0.01	380152.01	455106044.77
13		VAL-U-N-B-2	11.90	453948	1.08	5.66	0.08	-0.17	-0.01	0.01	380152.01	828213235.78
14		VAL-U-N-C-3	6.29	2072592	0.80	6.32	-0.19	0.49	-0.09	0.04	2627404.40	547117051.97
15		TX-U-N-A-5	6.00	2199343	0.78	6.34	-0.22	0.51	-0.11	0.05	3031674.49	503157270.17
16		TX-U-N-B-6	6.10	2816706	0.79	6.45	-0.21	0.62	-0.13	0.04	2883477.60	677514029.64
17		TX-U-N-C-7	11.80	177596	1.07	5.25	0.08	-0.58	-0.05	0.01	390004.58	315832511.74
18		TX-U-N-D-8	12.00	194694	1.08	5.29	0.09	-0.54	-0.05	0.01	370627.71	364340995.86
19		VALN-U-N-A-9	11.90	389428	1.08	5.59	0.08	-0.24	-0.02	0.01	380152.01	710498612.14
20		VALN-U-N-B-10	11.80	265540	1.07	5.42	0.08	-0.41	-0.03	0.01	390004.58	472230034.28
21		VALN-U2-N-A-11	11.90	5144528	1.08	6.71	0.08	0.88	0.07	0.01	380152.01	9386022587.25
22		VALN-U2-N-B-12	11.80	1683127	1.07	6.23	0.08	0.40	0.03	0.01	390004.58	2993233113.32
23		VALN-U-G-A-20	11.60	183132	1.06	5.26	0.07	-0.57	-0.04	0.01	410752.16	309227232.53
24		VALN-U-G-B-21	11.50	151679	1.06	5.18	0.07	-0.65	-0.04	0.00	421677.96	249481248.70
25	Anderson (2007)	S-1.75-10-B-1	12.00	142857	1.08	5.15	0.09	-0.67	-0.06	0.01	370627.71	267335725.01
26		S-1.75-10-B-2 (b)	12.00	134197	1.08	5.13	0.09	-0.70	-0.06	0.01	370627.71	251129817.16
27		S-2.00-10-B-10	12.00	165998	1.08	5.22	0.09	-0.61	-0.05	0.01	370627.71	310640680.40
28		S-2.00-10-A-11	12.00	235854	1.08	5.37	0.09	-0.46	-0.04	0.01	370627.71	441365841.97
29		S-2.00-10-A-12 (2)	12.00	210793	1.08	5.32	0.09	-0.51	-0.04	0.01	370627.71	394467890.84
30		S-2.00-10-A-13 (2) (b)	12.00	260700	1.08	5.42	0.09	-0.41	-0.04	0.01	370627.71	487861452.43
31		S-2.00-10-B-14 (2)	12.00	622928	1.08	5.79	0.09	-0.03	0.00	0.01	370627.71	1165717525.29
32		CA-2.00-10-A-22	12.00	253657	1.08	5.40	0.09	-0.43	-0.04	0.01	370627.71	474681520.68
33		CA-2.00-10-B-23	12.00	310352	1.08	5.49	0.09	-0.34	-0.03	0.01	370627.71	580777819.28
34		S-3.00-10-B-24	12.00	792576	1.08	5.90	0.09	0.07	0.01	0.01	370627.71	1483188640.30
35		S-3.00-10-B-25 (b)	12.00	376291	1.08	5.58	0.09	-0.25	-0.02	0.01	370627.71	704172895.27
36	Roy et al (2010)	LEH-AB-R-I-SF-CSR-1	12.00	180000	1.08	5.26	0.09	-0.57	-0.05	0.01	370627.71	336843350.36
37		LEH-AB-R-I-SF-CSR-2	12.00	370000	1.08	5.57	0.09	-0.26	-0.02	0.01	370627.71	692400220.18
38		LEH-AB-R-I-SF-CSR-3	12.00	1260000	1.08	6.10	0.09	0.27	0.02	0.01	370627.71	2357903452.50
39		LEH-AB-R-I-SF-CSR-4	7.00	2300000	0.85	6.36	-0.15	0.53	-0.08	0.02	1899743.94	839703810.11
40		LEH-AB-R-I-SF-CSR-5	7.00	3110000	0.85	6.49	-0.15	0.66	-0.10	0.02	1899743.94	1135425586.72
41		LEH-AB-R-I-SF-CSR-6	7.00	1400000	0.85	6.15	-0.15	0.32	-0.05	0.02	1899743.94	511124058.33
42		LEH-AB-R-I-SF-CSR-7	7.00	1840000	0.85	6.26	-0.15	0.44	-0.06	0.02	1899743.94	671763048.09
43		LEH-PB-R-I-SF-CSR-9	4.00	3050000	0.60	6.48	-0.39	0.66	-0.26	0.15	10365827.65	204074721.28
44	Present Study	MJ-CSR-R-L-A1-1	6.00	4374464	0.78	6.64	-0.22	0.81	-0.17	0.05	3031674.49	1000773123.92
45		MJ-CSR-R-S-A2-3	15.37	72660	1.19	4.86	0.19	-0.97	-0.19	0.04	174989.70	287989237.39
			S_{bar}	N_{bar}	X_{bar}	Y_{bar}	$\sum(X_i - X_{bar})$	$\sum(Y_i - Y_{bar})$	$\sum(X_i - X_{bar})*(Y_i - Y_{bar})$	$\sum(X_i - X_{bar})^2$		
			10.39	1519459.69	0.99	5.83	0.00	0.00	-2.94	0.97	Mean	1.12E+09
											Median	6.45E+08
n			b_{hat}	a_{hat}							Standard Deviation	1.71E+09
45			-3.03	8.84							Coefficient of Variation	1.53
			A_{hat}	m_{hat}								
			6.94E+08	3.03								

Table F.3. Least squares regression analysis for fatigue detail category U3.

U3: Unreinforced Round Flush Fillet Welds

	Research Group	Specimen Designation	Stress Range	Cycles to Failure	X	Y					Least Squares Line	
					Log S	Log N	$X_i - X_{bar}$	$Y_i - Y_{bar}$	$(X_i - X_{bar})*(Y_i - Y_{bar})$	$(X_i - X_{bar})^2$	$N_{hat} = A_{hat}S^{-mhat}$	A (m = 2.76)
1	Archer and Gurney (1970)	AG-F-5/16-W-A-1	12.60	28000	1.10	4.45	0.25	-1.35	-0.34	0.06	127040.23	30415160.76
2		AG-F-5/16-W-B-2	10.60	130000	1.03	5.11	0.18	-0.68	-0.12	0.03	204665.85	87653915.41
3		AG-F-5/16-W-C-3	9.20	230000	0.96	5.36	0.12	-0.44	-0.05	0.01	302534.01	104912441.10
4		AG-F-5/16-W-D-4	8.00	420000	0.90	5.62	0.05	-0.18	-0.01	0.00	444877.13	130281445.12
5		AG-F-5/16-W-E-5	6.90	600000	0.84	5.78	-0.01	-0.02	0.00	0.00	669084.99	123749463.62
6		AG-F-5/16-W-F-6	5.60	850000	0.75	5.93	-0.10	0.13	-0.01	0.01	1190189.09	98554468.99
7		AG-F-5/16-W-G-7	4.60	2700000	0.66	6.43	-0.19	0.63	-0.12	0.03	2047946.61	181935938.26
8		AG-F-7/16-W-A-8	7.40	550000	0.87	5.74	0.02	-0.06	0.00	0.00	551639.48	137588047.27
9		AG-F-7/16-W-B-9	4.90	1400000	0.69	6.15	-0.16	0.35	-0.06	0.03	1720347.81	112301391.27
10		AG-F-7/16-W-C-10	3.30	3300000	0.52	6.52	-0.33	0.72	-0.24	0.11	5120222.17	88940280.51
11		AG-F-5/16-RHS-A-11	11.00	28000	1.04	4.45	0.19	-1.35	-0.26	0.04	184782.87	20910753.28
12		AG-F-5/16-RHS-B-12	9.00	120000	0.95	5.08	0.11	-0.72	-0.08	0.01	321447.33	51516314.47
13		AG-F-5/16-RHS-C-13	8.00	240000	0.90	5.38	0.05	-0.42	-0.02	0.00	444877.13	74446540.07
14		AG-F-5/16-RHS-D-14	7.00	430000	0.85	5.63	0.00	-0.16	0.00	0.00	643043.54	92278693.45
15		AG-F-5/16-RHS-E-15	6.00	550000	0.78	5.74	-0.07	-0.06	0.00	0.00	983891.40	77141643.08
16		AG-F-5/16-RHS-F-16	5.00	850000	0.70	5.93	-0.15	0.13	-0.02	0.02	1627080.07	72091383.75
17		AG-F-5/16-RHS-G-17	4.00	2700000	0.60	6.43	-0.25	0.63	-0.16	0.06	3011511.39	123723619.13
18		AG-F-7/16-RHS-A-18	9.00	550000	0.95	5.74	0.11	-0.06	-0.01	0.01	321447.33	236116441.34
19		AG-F-7/16-RHS-B-19	6.00	1400000	0.78	6.15	-0.07	0.35	-0.02	0.00	983891.40	196360546.03
20		AG-F-7/16-RHS-C-20	4.00	3400000	0.60	6.53	-0.25	0.73	-0.18	0.06	3011511.39	155800112.98
21		AG-F-11/16-RHS-A-21	11.00	800000	1.04	5.90	0.19	0.10	0.02	0.04	184782.87	597450093.81
22		AG-F-11/16-RHS-B-22	10.00	850000	1.00	5.93	0.15	0.13	0.02	0.02	240361.28	488008950.30
23		AG-F-11/16-RHS-C-23	8.00	1200000	0.90	6.08	0.05	0.28	0.02	0.00	444877.13	372232700.35
24		AG-F-11/16-RHS-D-24	9.00	1300000	0.95	6.11	0.11	0.32	0.03	0.01	321447.33	558093406.80
25		AG-F-11/16-RHS-E-25	7.00	1900000	0.85	6.28	0.00	0.48	0.00	0.00	643043.54	407743064.08
26		AG-F-11/16-RHS-F-26	7.00	2000000	0.85	6.30	0.00	0.50	0.00	0.00	643043.54	429203225.35
			S_{bar}	N_{bar}	X_{bar}	Y_{bar}	$\sum(X_i - X_{bar})$	$\sum(Y_i - Y_{bar})$	$\sum(X_i - X_{bar})*(Y_i - Y_{bar})$	$\sum(X_i - X_{bar})^2$		
			7.47	1097153.85	0.85	5.80	0.00	0.00	-1.60	0.58	Mean	1.94E+08
											Median	1.24E+08
n			b_{hat}	a_{hat}							Standard Deviation	1.69E+08
26			-2.76	8.14							Coefficient of Variation	0.87
			A_{hat}	m_{hat}								
			1.38E+08	2.76								

Table F.4. Least squares regression analysis for fatigue detail category U5.

U5: Unreinforced Multi-Sided Socket

	Research Group	Specimen Designation	Stress Range	Cycles to Failure	X Log S	Y Log N	$X_i - X_{bar}$	$Y_i - Y_{bar}$	$(X_i - X_{bar})*(Y_i - Y_{bar})$	$(X_i - X_{bar})^2$	Least Squares Line $N_{hat} = A_{hat}S^{-mhat}$	Least Squares Line A (m = 1.80)
1	Ocel et al (2006)	MN-P-FR1-IP-N-CSR-5-1.25-1	8.25	83806	0.92	4.92	-0.02	-0.30	0.01	0.00	182238.49	3777939.29
2		MN-P-FR1-IP-N-CSR-5-1.25-2	3.43	981490	0.54	5.99	-0.40	0.77	-0.31	0.16	888264.47	9077443.38
3		MN-P-FR1-IP-N-CSR-5-1.25-3	3.80	610124	0.58	5.79	-0.36	0.56	-0.20	0.13	738328.18	6788731.42
4		MN-P-FR1-OP-N-CSR-5-1.25-5	5.41	170606	0.73	5.23	-0.20	0.01	0.00	0.04	390278.40	3591201.25
5		MN-P-FR1-OP-N-CSR-5-1.25-7	5.41	301484	0.73	5.48	-0.20	0.25	-0.05	0.04	390278.40	6346140.92
6		MN-P-FR1-OP-N-CSR-5-1.25-8	5.41	2293739	0.73	6.36	-0.20	1.14	-0.23	0.04	390278.40	48282465.86
7		MN-P-FR2-IP-N-CSR-5-1.25-9	4.26	591696	0.63	5.77	-0.31	0.55	-0.17	0.09	600739.79	8091558.89
8		MN-P-FR2-IP-N-CSR-5-1.25-10	3.65	868266	0.56	5.94	-0.37	0.71	-0.27	0.14	793991.82	8983730.83
9		MN-P-FR2-IP-N-CSR-5-1.25-11	4.10	1658906	0.61	6.22	-0.32	0.99	-0.32	0.10	643712.41	21171413.83
10		MN-P-FR2-IP-N-CSR-5-2.50-2-21	14.90	81924	1.17	4.91	0.24	-0.31	-0.07	0.06	62704.65	10733252.69
11		MN-P-FR2-IP-N-CSR-5-2.50-1-23	14.90	566119	1.17	5.75	0.24	0.53	0.13	0.06	62704.65	74169941.40
12		MN-P-FR2-IP-N-CSR-5-2.50-2-24	14.90	101916	1.17	5.01	0.24	-0.22	-0.05	0.06	62704.65	13352499.65
13		MN-P-FR2-IP-N-CSR-3-2.50-1-25	15.00	330137	1.18	5.52	0.24	0.29	0.07	0.06	61952.23	43778131.13
14		MN-P-FR2-IP-N-CSR-3-2.50-2-26	15.00	140545	1.18	5.15	0.24	-0.08	-0.02	0.06	61952.23	18637103.51
15		MN-P-FR2-IP-N-CSR-3-2.50-1-27	15.00	183638	1.18	5.26	0.24	0.04	0.01	0.06	61952.23	24351491.79
16		MN-P-FR2-IP-N-CSR-3-2.50-2-28	15.00	86888	1.18	4.94	0.24	-0.29	-0.07	0.06	61952.23	11521865.95
17	Rios (2007)	UTX-24-1.5-8-S-A-1	12.00	13193	1.08	4.12	0.14	-1.10	-0.16	0.02	92673.66	1169518.83
18		UTX-24-1.5-8-S-B-2	12.00	13193	1.08	4.12	0.14	-1.10	-0.16	0.02	92673.66	1169518.83
19		UTX-24-2.0-8-S-A-3	12.00	46772	1.08	4.67	0.14	-0.55	-0.08	0.02	92673.66	4146193.80
20		UTX-24-2.0-8-S-B-4	12.00	46772	1.08	4.67	0.14	-0.55	-0.08	0.02	92673.66	4146193.80
21		UTX-24-3.0-8-S-A-5	12.00	147550	1.08	5.17	0.14	-0.06	-0.01	0.02	92673.66	13079853.21
22		UTX-24-3.0-8-S-B-6	12.00	147550	1.08	5.17	0.14	-0.06	-0.01	0.02	92673.66	13079853.21
23		UTX-24-1.5-12-S-A-7	12.00	27977	1.08	4.45	0.14	-0.78	-0.11	0.02	92673.66	2480074.91
24		UTX-24-1.5-12-S-B-8	12.00	27977	1.08	4.45	0.14	-0.78	-0.11	0.02	92673.66	2480074.91
25		UTX-24-2.0-12-S-A-9	12.00	143214	1.08	5.16	0.14	-0.07	-0.01	0.02	92673.66	12695480.16
26		UTX-24-2.0-12-S-B-10	12.00	143214	1.08	5.16	0.14	-0.07	-0.01	0.02	92673.66	12695480.16
27	Roy et al (2010)	LEH-AB-M-VII-SF-CSR-42	12.00	40000	1.08	4.60	0.14	-0.62	-0.09	0.02	92673.66	3545876.85
28		LEH-AB-M-VII-SF-CSR-43	12.00	40000	1.08	4.60	0.14	-0.62	-0.09	0.02	92673.66	3545876.85
29		LEH-AB-M-VII-SF-CSR-44	12.00	10000	1.08	4.00	0.14	-1.22	-0.18	0.02	92673.66	886469.21
30		LEH-AB-M-VII-SF-CSR-45	4.50	1030000	0.65	6.01	-0.28	0.79	-0.22	0.08	544161.53	15549962.65
31		LEH-AB-M-VII-SF-CSR-46	4.50	390000	0.65	5.59	-0.28	0.37	-0.10	0.08	544161.53	5887849.94
32		LEH-AB-M-VII-SF-CSR-48	6.60	90000	0.82	4.95	-0.12	-0.27	0.03	0.01	272608.54	2712208.11
33		LEH-PB-M-VII-SF-CSR-49	6.60	90000	0.82	4.95	-0.12	-0.27	0.03	0.01	272608.54	2712208.11
34		LEH-PB-M-VII-SF-CSR-50	6.60	100000	0.82	5.00	-0.12	-0.22	0.03	0.01	272608.54	3013564.57
35		LEH-PB-M-VII-SF-CSR-51	8.00	1750000	0.90	6.24	-0.03	1.02	-0.03	0.00	192645.49	74627546.04
36		LEH-PB-M-X-SF-CSR-66	8.00	1750000	0.90	6.24	-0.03	1.02	-0.03	0.00	192645.49	74627546.04
37		LEH-PB-M-X-SF-CSR-67	8.00	680000	0.90	5.83	-0.03	0.61	-0.02	0.00	192645.49	28998132.18
38	Present Study	UWM-CSR-M-N-A1-7	6.50	139000	0.81	5.14	-0.12	-0.08	0.01	0.02	280224.48	4075010.15
			S_{bar}	N_{bar}	X_{bar}	Y_{bar}	$\sum(X_i - X_{bar})$	$\sum(Y_i - Y_{bar})$	$\sum(X_i - X_{bar})*(Y_i - Y_{bar})$	$\sum(X_i - X_{bar})^2$		
			9.57	418886.74	0.94	5.22	0.00	0.00	-2.95	1.63	Mean	1.58E+07
											Median	8.54E+06
n			b_{hat}	a_{hat}							Standard Deviation	2.04E+07
38			-1.80	6.91							Coefficient of Variation	1.30
			A_{hat}	m_{hat}								
			8.22E+06	1.80								

Table F.5. Least squares regression analysis for fatigue detail category R1.

R1: Reinforced Round Socket

	Research Group	Specimen Designation	Stress Range	Cycles to Failure	X	Y					Least Squares Line	
					Log S	Log N	$X_i - X_{bar}$	$Y_i - Y_{bar}$	$(X_i - X_{bar})*(Y_i - Y_{bar})$	$(X_i - X_{bar})^2$	$N_{hat} = A_{hat}S^{-mhat}$	A (m = 1.91)
1	Machietto (2002)	VAL-R-45FW-A-1	13.40	575000	1.13	5.76	0.06	-0.18	-0.01	0.00	656123.85	82076710.92
2		VAL-R-45FW-B-2	13.40	376740	1.13	5.58	0.06	-0.37	-0.02	0.00	656123.85	53776660.99
3		VAL-R-RFWS-A-5	17.60	514085	1.25	5.71	0.18	-0.23	-0.04	0.03	389618.52	123575752.47
4		VAL-R-RFWS-B-6	17.60	673989	1.25	5.83	0.18	-0.11	-0.02	0.03	389618.52	162013476.05
5	Koenigs et al (2003)	VALN-EC-N-A-28	5.49	4245460	0.74	6.63	-0.32	0.69	-0.22	0.10	3612313.99	110072082.59
6		VALN-EC-N-B-29	5.73	2363152	0.76	6.37	-0.30	0.43	-0.13	0.09	3328618.06	66491421.12
7		VALN-IC-N-A-30	10.75	227030	1.03	5.36	-0.03	-0.59	0.02	0.00	999809.17	21266893.51
8		VALN-IC-N-B-31	10.68	227030	1.03	5.36	-0.03	-0.59	0.02	0.00	1012373.28	21002959.59
9		VAL-3x1/4-N-A-35	11.10	476269	1.05	5.68	-0.02	-0.26	0.00	0.00	940412.50	47432044.32
10		VAL-3x1/4-N-B-36	11.40	696326	1.06	5.84	-0.01	-0.10	0.00	0.00	893673.15	72974617.54
11		VAL-3x1/4-N-C-37	6.10	3592372	0.79	6.56	-0.28	0.61	-0.17	0.08	2953359.70	113920762.12
12		TX-3x1/4-N-A-38	11.70	616136	1.07	5.79	0.01	-0.15	0.00	0.00	850382.16	67857892.24
13		TX-3x1/4-N-B-39	11.80	416146	1.07	5.62	0.01	-0.32	0.00	0.00	836659.34	46583808.00
14		TX-3x1/4-N-C-LMS-40	11.90	523397	1.08	5.72	0.01	-0.22	0.00	0.00	823270.98	59542401.67
15		VAL-3x3/8-N-A-41	11.70	386253	1.07	5.59	0.01	-0.35	0.00	0.00	850382.16	42539819.86
16		VAL-3x3/8-N-B-42	11.60	410410	1.06	5.61	0.00	-0.33	0.00	0.00	864450.78	44464722.36
17		TX-3x3/8-N-A-43	11.70	473735	1.07	5.68	0.01	-0.27	0.00	0.00	850382.16	52174614.99
18		TX-3x3/8-N-B-44	11.60	657716	1.06	5.82	0.00	-0.12	0.00	0.00	864450.78	71258398.52
19		VAL-6x3/8-N-A-45 (b)	11.20	242728	1.05	5.39	-0.01	-0.56	0.01	0.00	924427.17	24591504.41
20		VAL-6x3/8-N-B-46	11.30	653392	1.05	5.82	-0.01	-0.13	0.00	0.00	908852.06	67331538.84
21		VAL-6x3/8-N-C-47	5.90	3592372	0.77	6.56	-0.29	0.61	-0.18	0.08	3147689.44	106887605.93
22		TX-6x3/8-N-A-48	11.20	783857	1.05	5.89	-0.01	-0.05	0.00	0.00	924427.17	79414912.46
23		TX-6x3/8-N-B-49	11.30	783857	1.05	5.89	-0.01	-0.05	0.00	0.00	908852.06	80775855.91
24		TX-6x3/8-N-C-50	5.76	7503037	0.76	6.88	-0.30	0.93	-0.28	0.09	3295556.52	213228988.83
25		VALN-6x3/8@45-N-A-51	11.96	238515	1.08	5.38	0.02	-0.56	-0.01	0.00	815393.97	27395934.92
26		VALN-6x3/8@45-N-B-52	11.98	161843	1.08	5.21	0.02	-0.73	-0.01	0.00	812793.79	18648824.67
27		VALN-6x3/8@45-N-C-53	4.30	6066817	0.63	6.78	-0.43	0.84	-0.36	0.18	5762509.71	98602323.48
28		VALN-6x3/8@45-N-D-54	4.30	6066817	0.63	6.78	-0.43	0.84	-0.36	0.18	5762509.71	98602323.48
29		VALN-UR-N-A-55	7.62	1776724	0.88	6.25	-0.18	0.31	-0.06	0.03	1930232.27	86208149.14
30		VALN-UR-N-B-56	7.60	950670	0.88	5.98	-0.18	0.04	-0.01	0.03	1939953.90	45896154.93
31		VALN-UR-N-B2-57	12.57	339152	1.10	5.53	0.04	-0.41	-0.02	0.00	741428.90	42841315.17
32	Rios (2007)	UTX-24-2.0-8-SB-A-15	12.00	785058	1.08	5.89	0.02	-0.05	0.00	0.00	810206.22	90749468.90
33		UTX-24-2.0-8-SB-B-16	12.00	483314	1.08	5.68	0.02	-0.26	0.00	0.00	810206.22	55869106.25
34	Anderson (2007)	EC-1.75-10-A-4 (2)	12.00	2345896	1.08	6.37	0.02	0.43	0.01	0.00	810206.22	271175908.15
35		EC-1.75-10-A-5 (2) (b)	12.00	2889260	1.08	6.46	0.02	0.52	0.01	0.00	810206.22	333986546.88
36		EC-1.75-10-B-6 (2)	12.00	5755111	1.08	6.76	0.02	0.82	0.01	0.00	810206.22	665267109.85
37		EC-1.75-10-B-7 (1)	12.00	3304490	1.08	6.52	0.02	0.58	0.01	0.00	810206.22	381985423.36
38		EC-1.75-10-B-8 (1) (b)	12.00	2382309	1.08	6.38	0.02	0.44	0.01	0.00	810206.22	275385100.86
39		EC-2.00-10-A-15 (2)	12.00	3939099	1.08	6.60	0.02	0.65	0.01	0.00	810206.22	455343607.99
40		EC-2.00-10-B-16 (2)	12.00	6927606	1.08	6.84	0.02	0.90	0.02	0.00	810206.22	800802698.99
41		EC-2.00-10-A-17 (1)	12.00	5384143	1.08	6.73	0.02	0.79	0.01	0.00	810206.22	622384738.13
42		EC-2.00-10-A-18 (1) (b)	12.00	2863521	1.08	6.46	0.02	0.52	0.01	0.00	810206.22	331011224.57
43	Richman (2009)	EC-S-G-V-2-8-A-10	18.00	512860	1.26	5.71	0.19	-0.23	-0.04	0.04	373235.44	128692690.01
44		EC-S-G-V-2-8-B-11	18.00	653208	1.26	5.82	0.19	-0.13	-0.02	0.04	373235.44	163910413.47
45		EC-S-G-V-2-12-B-15	18.00	468601	1.26	5.67	0.19	-0.27	-0.05	0.04	373235.44	117586716.12
46		EC-S-G-V-2-12-B-16 (b)	18.00	337390	1.26	5.53	0.19	-0.41	-0.08	0.04	373235.44	84661753.07
47		EC-R-G-P-2-10-A-40	24.00	137220	1.38	5.14	0.32	-0.80	-0.26	0.10	215353.71	59676449.83
48		EC-R-G-P-2-10-B-41	24.00	244763	1.38	5.39	0.32	-0.55	-0.18	0.10	215353.71	106446486.58
49		EC-R-G-P-2-12-A-44	24.00	169059	1.38	5.23	0.32	-0.71	-0.23	0.10	215353.71	73523108.38
50		EC-R-G-P-2-12-B-45	24.00	119289	1.38	5.08	0.32	-0.86	-0.28	0.10	215353.71	51878326.95
			S_{bar}	N_{bar}	X_{bar}	Y_{bar}	$\sum(X_i - X_{bar})$	$\sum(Y_i - Y_{bar})$	$\sum(X_i - X_{bar})*(Y_i - Y_{bar})$	$\sum(X_i - X_{bar})^2$		
			12.44	1726264.48	1.06	5.94	0.00	0.00	-2.91	1.52	Mean	1.46E+08
											Median	8.14E+07
n			b_{hat}	a_{hat}							Standard Deviation	1.71E+08
50			-1.91	7.97							Coefficient of Variation	1.17
			A_{hat}	m_{hat}								
			9.37E+07	1.91								

Table F.6. Least squares regression analysis for fatigue detail category R3.

R3: Reinforced Round Full-Penetration Welds

	Research Group	Specimen Designation	Stress Range	Cycles to Failure	X	Y					Least Squares Line	
					Log S	Log N	$X_i - X_{bar}$	$Y_i - Y_{bar}$	$(X_i - X_{bar})*(Y_i - Y_{bar})$	$(X_i - X_{bar})^2$	$N_{hat} = A_{hat}S^{-mhat}$	A (m= 1.27)
1	Machietto (2002)	VAL-R-15FP-A-3	13.40	950040	1.13	5.98	-0.05	-0.07	0.00	0.00	1316291.03	25852844.64
2		VAL-R-TCFP-A-4	17.60	657540	1.25	5.82	0.07	-0.23	-0.02	0.00	930299.29	25317327.07
3	Koenigs et al (2003)	VALN-W-N-A-13	17.71	422400	1.25	5.63	0.07	-0.43	-0.03	0.00	922950.01	16393213.52
4		VALN-W-N-B-14	17.56	422400	1.24	5.63	0.07	-0.43	-0.03	0.00	932997.72	16216670.58
5	Rios (2007)	UTX-24-2.0-8-WY-A-11	12.00	133819	1.08	5.13	-0.10	-0.93	0.09	0.01	1514805.90	3164310.97
6		UTX-24-2.0-8-WY-B-12	12.00	133819	1.08	5.13	-0.10	-0.93	0.09	0.01	1514805.90	3164310.97
7	Anderson (2007)	WY-2.00-10-A-20	12.00	4997925	1.08	6.70	-0.10	0.65	-0.06	0.01	1514805.90	118181939.26
8		WY-2.00-10-B-21	12.00	7527441	1.08	6.88	-0.10	0.82	-0.08	0.01	1514805.90	177995383.09
9	Richman (2009)	WY-S-B-P-2-10-A-1	12.00	6734487	1.08	6.83	-0.10	0.78	-0.08	0.01	1514805.90	159245033.40
10		WY-S-B-P-2-10-B-2	12.00	5219304	1.08	6.72	-0.10	0.66	-0.07	0.01	1514805.90	123416711.59
11		WY-S-G-V-2-8-A-7	24.00	856122	1.38	5.93	0.20	-0.12	-0.02	0.04	626838.91	48921310.23
12		WY-S-G-V-2-8-A-8 (b)	24.00	747510	1.38	5.87	0.20	-0.18	-0.04	0.04	626838.91	42714903.49
13		WY-S-G-V-2-12-A-12	18.00	1053554	1.26	6.02	0.08	-0.03	0.00	0.01	904063.11	41742304.26
14		WY-S-G-V-2-12-B-13	18.00	880807	1.26	5.94	0.08	-0.11	-0.01	0.01	904063.11	34897987.00
15		WY-R-G-V-3-10-A-19	24.00	439511	1.38	5.64	0.20	-0.41	-0.08	0.04	626838.91	25114941.54
16		WY-R-G-V-3-10-B-20	24.00	343175	1.38	5.54	0.20	-0.52	-0.10	0.04	626838.91	19610021.28
17		WY-R-B-V-3-10-A-23	19.07	2232742	1.28	6.35	0.10	0.30	0.03	0.01	839991.82	95209843.12
18		WY-R-B-V-3-10-A-24 (b)	24.00	490061	1.38	5.69	0.20	-0.36	-0.07	0.04	626838.91	28003516.10
19		WY-R-B-V-3-10-B-25	21.14	3516775	1.33	6.55	0.15	0.49	0.07	0.02	736723.21	170985229.14
20		WY-R-G-A-3-10-A-26	24.00	222649	1.38	5.35	0.20	-0.71	-0.14	0.04	626838.91	12722813.81
21		WY-R-G-A-3-10-A-27 (b)	24.00	212891	1.38	5.33	0.20	-0.72	-0.15	0.04	626838.91	12165213.20
22		WY-R-G-U-3-10-A-28	24.00	1873499	1.38	6.27	0.20	0.22	0.04	0.04	626838.91	107057201.88
23		WY-SR-G-V-2-10-B-35	12.00	3051996	1.08	6.48	-0.10	0.43	-0.04	0.01	1514805.90	72168110.94
24		WY-R-G-P-3-10-A-38	24.00	1272665	1.38	6.10	0.20	0.05	0.01	0.04	626838.91	72723793.20
25		WY-R-G-P-3-10-B-39	24.00	1210499	1.38	6.08	0.20	0.03	0.01	0.04	626838.91	69171446.49
26		WY-R-G-P-3-12-A-42	24.00	292468	1.38	5.47	0.20	-0.59	-0.12	0.04	626838.91	16712475.28
27		WY-R-G-P-3-12-B-43	24.00	328833	1.38	5.52	0.20	-0.54	-0.11	0.04	626838.91	18790477.53
28	Roy et al (2010)	LEH-AB-R-II-BP1-CSR-10	11.90	1610000	1.08	6.21	-0.10	0.15	-0.02	0.01	1531028.63	37666991.27
29		LEH-AB-R-II-BP1-CSR-11	9.90	1320000	1.00	6.12	-0.18	0.07	-0.01	0.03	1935121.77	24433405.30
30		LEH-AB-R-II-BP1-CSR-12	9.90	1410000	1.00	6.15	-0.18	0.10	-0.02	0.03	1935121.77	26099319.29
31		LEH-AB-R-II-BP1-CSR-13	9.90	1170000	1.00	6.07	-0.18	0.02	0.00	0.03	1935121.77	21656881.97
32		LEH-AB-R-II-BP1-CSR-14	9.90	1290000	1.00	6.11	-0.18	0.06	-0.01	0.03	1935121.77	23878100.63
33		LEH-AB-R-II-BP1-CSR-15	9.90	1490000	1.00	6.17	-0.18	0.12	-0.02	0.03	1935121.77	27580131.74
34		LEH-PB-R-II-BP1-CSR-16	6.90	1980000	0.84	6.30	-0.34	0.24	-0.08	0.12	3064020.93	23146846.35
35		LEH-AB-R-III-BP2-CSR-17	12.00	980000	1.08	5.99	-0.10	-0.06	0.01	0.01	1514805.90	23173277.00
36		LEH-AB-R-III-BP2-CSR-18	12.00	1860000	1.08	6.27	-0.10	0.22	-0.02	0.01	1514805.90	43981933.91
37		LEH-AB-R-III-BP2-CSR-19	12.00	1250000	1.08	6.10	-0.10	0.04	0.00	0.01	1514805.90	29557751.28
38		LEH-AB-R-III-BP2-CSR-21	10.00	6960000	1.00	6.84	-0.18	0.79	-0.14	0.03	1910522.02	130489497.20
39		LEH-AB-R-III-BP2-CSR-22	10.00	9230000	1.00	6.97	-0.18	0.91	-0.16	0.03	1910522.02	173048571.72
40		LEH-AB-R-III-BP2-CSR-24	16.00	5840000	1.20	6.77	0.02	0.71	0.02	0.00	1050301.98	199166837.77
41		LEH-AB-R-III-BP2-CSR-25	16.00	270000	1.20	5.43	0.02	-0.62	-0.02	0.00	1050301.98	9208055.86
42		LEH-AB-R-III-BP2-CSR-26	16.00	4790000	1.20	6.68	0.02	0.63	0.02	0.00	1050301.98	163357731.66
43		LEH-PB-R-V-BP2-CSR-31	12.00	270000	1.08	5.43	-0.10	-0.62	0.06	0.01	1514805.90	6384474.28
44		LEH-PB-R-V-BP2-CSR-32	12.00	1100000	1.08	6.04	-0.10	-0.01	0.00	0.01	1514805.90	26010821.13
45		LEH-PB-R-V-BP2-CSR-33	12.00	1460000	1.08	6.16	-0.10	0.11	-0.01	0.01	1514805.90	34523453.50
			S_{bar}	N_{bar}	X_{bar}	Y_{bar}	$\sum(X_i - X_{bar})$	$\sum(Y_i - Y_{bar})$	$\sum(X_i - X_{bar})*(Y_i - Y_{bar})$	$\sum(X_i - X_{bar})^2$		
			16.06	2011220.71	1.18	6.05	0.00	0.00	-1.32	1.04	Mean	5.74E+07
											Median	2.80E+07
n			b_{hat}	a_{hat}							Standard Deviation	5.62E+07
45			-1.27	7.55							Coefficient of Variation	0.98
			A_{hat}	m_{hat}								
			3.58E+07	1.27								

Table F.7. Least squares regression analysis for fatigue detail category R6.

R6: Reinforced Multi-Sided Full-Penetration Welds

	Research Group	Specimen Designation	Stress Range	Cycles to Failure	X	Y					Least Squares Line	
					Log S	Log N	$X_i - X_{bar}$	$Y_i - Y_{bar}$	$(X_i - X_{bar})*(Y_i - Y_{bar})$	$(X_i - X_{bar})^2$	$N_{hat} = A_{hat}S^{-mhat}$	A (m = 3.16)
1	Roy et al (2010)	LEH-PB-M-IX-LSS-CSR-55	12.00	590000	1.08	5.77	0.01	0.22	0.00	0.00	317138.32	1517851357.87
2		LEH-PB-M-IX-LSS-CSR-56	12.00	270000	1.08	5.43	0.01	-0.12	0.00	0.00	317138.32	694609943.43
3		LEH-PB-M-IX-LSS-CSR-57	12.00	510000	1.08	5.71	0.01	0.16	0.00	0.00	317138.32	1312041004.26
4		LEH-PB-M-IX-LSS-CSR-58	10.00	450000	1.00	5.65	-0.06	0.11	-0.01	0.00	564252.54	650676225.78
5		LEH-PB-M-IX-LSS-CSR-59	7.00	2570000	0.85	6.41	-0.22	0.86	-0.19	0.05	1741756.05	1203848244.94
6		LEH-PB-M-IX-LSS-CSR-60	4.50	2640000	0.65	6.42	-0.41	0.87	-0.36	0.17	7036794.03	306094154.83
7		LEH-PB-M-IX-LSS-CSR-61	4.50	4000000	0.65	6.60	-0.41	1.06	-0.43	0.17	7036794.03	463779022.47
8		LEH-PB-M-IX-LSS-CSR-62	16.00	70000	1.20	4.85	0.14	-0.70	-0.10	0.02	127768.34	446993001.33
9		LEH-PB-M-IX-LSS-CSR-63	16.00	130000	1.20	5.11	0.14	-0.43	-0.06	0.02	127768.34	830129859.62
10		LEH-PB-M-IX-LSS-CSR-64	16.00	120000	1.20	5.08	0.14	-0.47	-0.07	0.02	127768.34	766273716.57
11		LEH-PB-M-XI-BP1-CSR-68	12.00	750000	1.08	5.88	0.01	0.33	0.00	0.00	317138.32	1929472065.09
12		LEH-PB-M-XI-BP1-CSR-69	12.00	1560000	1.08	6.19	0.01	0.65	0.01	0.00	317138.32	4013301895.39
13		LEH-PB-M-XI-BP1-CSR-70	12.00	330000	1.08	5.52	0.01	-0.03	0.00	0.00	317138.32	848967708.64
14		LEH-PB-M-XI-BP1-CSR-75	14.00	100000	1.15	5.00	0.08	-0.55	-0.04	0.01	194843.83	418735027.48
15		LEH-PB-M-XI-BP1-CSR-76	16.00	140000	1.20	5.15	0.14	-0.40	-0.06	0.02	127768.34	893986002.67
16		LEH-PB-M-XI-BP1-CSR-77	16.00	60000	1.20	4.78	0.14	-0.77	-0.11	0.02	127768.34	383136858.29
17		LEH-PB-M-XII-LS-CSR-78	12.00	230000	1.08	5.36	0.01	-0.19	0.00	0.00	317138.32	591704766.63
18		LEH-PB-M-XII-LS-CSR-79	12.00	400000	1.08	5.60	0.01	0.06	0.00	0.00	317138.32	1029051768.05
19		LEH-PB-M-XII-LS-CSR-80	12.00	580000	1.08	5.76	0.01	0.22	0.00	0.00	317138.32	1492125063.67
20		LEH-PB-M-XII-LS-CSR-83	7.00	4060000	0.85	6.61	-0.22	1.06	-0.23	0.05	1741756.05	1901799172.93
21		LEH-PB-M-XII-LS-CSR-85	16.00	50000	1.20	4.70	0.14	-0.85	-0.12	0.02	127768.34	319280715.24
22		LEH-PB-M-XII-LS-CSR-86	16.00	200000	1.20	5.30	0.14	-0.25	-0.03	0.02	127768.34	1277122860.95
23		LEH-PB-M-XII-LS-CSR-87	16.00	50000	1.20	4.70	0.14	-0.85	-0.12	0.02	127768.34	319280715.24
			S_{bar}	N_{bar}	X_{bar}	Y_{bar}	$\sum(X_i - X_{bar})$	$\sum(Y_i - Y_{bar})$	$\sum(X_i - X_{bar})*(Y_i - Y_{bar})$	$\sum(X_i - X_{bar})^2$		
			12.30	863478.26	1.06	5.55	0.00	0.00	-1.91	0.60	Mean	1.03E+09
											Median	8.30E+08
n			b_{hat}	a_{hat}							Standard Deviation	8.17E+08
23			-3.16	8.91							Coefficient of Variation	0.80
			A_{hat}	m_{hat}								
			8.16E+08	3.16								

Table F.8. Least squares regression analysis for fatigue detail category E2.

E2: SCF in 2.0 Range													
						X	Y					Least Squares Line	
	Research Group	Specimen Designation	Controlling SCF	Stress Range	Cycles to Failure	Log S	Log N	$X_i - X_{bar}$	$Y_i - Y_{bar}$	$(X_i - X_{bar})*(Y_i - Y_{bar})$	$(X_i - X_{bar})^2$	$N_{hat} = A_{hat}S^{-mhat}$	A (m= 2.97)
1	Anderson (2007)	S-3.00-10-B-24	2.24	12	792576	1.08	5.90	0.09	0.24	0.02	0.01	252698.00	1270578356.88
2	Anderson (2007)	S-3.00-10-B-25 (b)	2.24	12	376291	1.08	5.58	0.09	-0.08	-0.01	0.01	252698.00	603231993.51
3	Koenigs et al (2003)	VALN-U2-N-A-11	2.35	11.9	5144528	1.08	6.71	0.08	1.05	0.09	0.01	259056.76	8044757280.59
4	Koenigs et al (2003)	VALN-U2-N-B-12	2.35	11.8	1683127	1.07	6.23	0.08	0.57	0.04	0.01	265631.24	2566847627.36
5	Anderson (2007)	S-2.00-10-B-10	2.37	12	165998	1.08	5.22	0.09	-0.44	-0.04	0.01	252698.00	266111345.90
6	Anderson (2007)	S-2.00-10-A-11	2.37	12	235854	1.08	5.37	0.09	-0.28	-0.02	0.01	252698.00	378097479.34
7	Anderson (2007)	S-2.00-10-A-12 (2)	2.37	12	210793	1.08	5.32	0.09	-0.33	-0.03	0.01	252698.00	337922197.47
8	Anderson (2007)	S-2.00-10-A-13 (2) (b)	2.37	12	260700	1.08	5.42	0.09	-0.24	-0.02	0.01	252698.00	417928094.77
9	Anderson (2007)	S-2.00-10-B-14 (2)	2.37	12	622928	1.08	5.79	0.09	0.14	0.01	0.01	252698.00	998615697.04
10	Anderson (2007)	CA-2.00-10-A-22	2.37	12	253657	1.08	5.40	0.09	-0.25	-0.02	0.01	252698.00	406637463.50
11	Anderson (2007)	CA-2.00-10-B-23	2.37	12	310352	1.08	5.49	0.09	-0.16	-0.01	0.01	252698.00	497525201.64
12	Roy et al (2010)	LEH-AB-R-I-SF-CSR-1	2.37	12	180000	1.08	5.26	0.09	-0.40	-0.03	0.01	252698.00	288557948.06
13	Roy et al (2010)	LEH-AB-R-I-SF-CSR-2	2.37	12	370000	1.08	5.57	0.09	-0.09	-0.01	0.01	252698.00	593146893.23
14	Roy et al (2010)	LEH-AB-R-I-SF-CSR-3	2.37	12	1260000	1.08	6.10	0.09	0.44	0.04	0.01	252698.00	2019905636.40
15	Roy et al (2010)	LEH-AB-R-I-SF-CSR-4	2.37	7	2300000	0.85	6.36	-0.15	0.71	-0.10	0.02	1252517.68	743885881.12
16	Roy et al (2010)	LEH-AB-R-I-SF-CSR-5	2.37	7	3110000	0.85	6.49	-0.15	0.84	-0.12	0.02	1252517.68	1005863082.73
17	Roy et al (2010)	LEH-AB-R-I-SF-CSR-6	2.37	7	1400000	0.85	6.15	-0.15	0.49	-0.07	0.02	1252517.68	452800101.55
18	Roy et al (2010)	LEH-AB-R-I-SF-CSR-7	2.37	7	1840000	0.85	6.26	-0.15	0.61	-0.09	0.02	1252517.68	595108704.90
19	Fisher et al (1981)	LEH-48-V-28CA-1-9	2.39	18.9	87000	1.28	4.94	0.28	-0.72	-0.20	0.08	65571.71	537483412.17
20	Fisher et al (1981)	LEH-48-V-28CA-2-10	2.39	12.4	317500	1.09	5.50	0.10	-0.15	-0.02	0.01	229250.58	561042328.25
21	Fisher et al (1981)	LEH-48-V-28CA-3-11 (a)	2.39	6.5	5244000	0.81	6.72	-0.18	1.06	-0.19	0.03	1560868.00	1361002269.90
22	Fisher et al (1981)	LEH-48-V-28CA-4-12	2.39	12.4	198100	1.09	5.30	0.10	-0.36	-0.04	0.01	229250.58	350055071.58
23	Fisher et al (1981)	LEH-48-V-28CA-5-13 (b)	2.39	6.5	5186500	0.81	6.71	-0.18	1.06	-0.19	0.03	1560868.00	1346078999.40
24	Fisher et al (1981)	LEH-48-V-28CA-6-14 (c)	2.39	6.4	8832300	0.81	6.95	-0.19	1.29	-0.24	0.04	1634417.59	2189137942.57
25	Fisher et al (1981)	LEH-40-A-45CA-1-1	2.44	18.8	36100	1.27	4.56	0.28	-1.10	-0.31	0.08	66612.98	219538510.00
26	Fisher et al (1981)	LEH-40-A-45CA-2-2	2.44	12.4	117800	1.09	5.07	0.10	-0.59	-0.06	0.01	229250.58	208159956.75
27	Fisher et al (1981)	LEH-40-A-45CA-3-3	2.44	6.4	1892400	0.81	6.28	-0.19	0.62	-0.12	0.04	1634417.59	469042564.51
28	Fisher et al (1981)	LEH-40-A-45CA-4-4	2.44	12.4	174200	1.09	5.24	0.10	-0.42	-0.04	0.01	229250.58	307822278.99
29	Fisher et al (1981)	LEH-40-A-45CA-5-5	2.44	6.4	1208700	0.81	6.08	-0.19	0.43	-0.08	0.04	1634417.59	299583464.24
30	Fisher et al (1981)	LEH-40-A-45CA-6-6	2.44	6.4	1472900	0.81	6.17	-0.19	0.51	-0.10	0.04	1634417.59	365067001.30
31	Fisher et al (1981)	LEH-40-A-34CA-1-7	2.44	6.4	3751600	0.81	6.57	-0.19	0.92	-0.17	0.04	1634417.59	929856312.10
32	Fisher et al (1981)	LEH-40-A-34CA-2-8	2.44	6.4	3573400	0.81	6.55	-0.19	0.90	-0.17	0.04	1634417.59	885688385.13
33	Anderson (2007)	S-1.75-10-B-1	2.45	12	142857	1.08	5.15	0.09	-0.50	-0.04	0.01	252698.00	229014015.48
34	Anderson (2007)	S-1.75-10-B-2 (b)	2.45	12	134197	1.08	5.13	0.09	-0.53	-0.05	0.01	252698.00	215131171.97
35	Koenigs et al (2003)	VAL-U-N-A-1	2.53	11.9	249446	1.08	5.40	0.08	-0.26	-0.02	0.01	259056.76	390071261.08
36	Koenigs et al (2003)	VAL-U-N-B-2	2.53	11.9	453948	1.08	5.66	0.08	0.00	0.00	0.01	259056.76	709861328.00
37	Koenigs et al (2003)	VAL-U-N-C-3	2.53	6.29	2072592	0.80	6.32	-0.20	0.66	-0.13	0.04	1720773.40	487924333.56
38	Koenigs et al (2003)	VALN-U-N-A-9	2.53	11.9	389428	1.08	5.59	0.08	-0.07	-0.01	0.01	259056.76	608968157.67
39	Koenigs et al (2003)	VALN-U-N-B-10	2.53	11.8	265540	1.07	5.42	0.08	-0.23	-0.02	0.01	265631.24	404960955.99
40	Koenigs et al (2003)	VALN-U-G-A-20	2.53	11.60	183132	1.06	5.26	0.07	-0.39	-0.03	0.01	279464.76	265460272.65
41	Koenigs et al (2003)	VALN-U-G-B-21	2.53	11.50	151679	1.06	5.18	0.07	-0.48	-0.03	0.00	286743.75	214286018.81
42	Roy et al (2010)	LEH-PB-M-X-SF-CSR-66	2.55	8.00	1750000	0.90	6.24	-0.09	0.59	-0.05	0.01	842478.73	841475443.18
43	Roy et al (2010)	LEH-PB-M-X-SF-CSR-67	2.55	8.00	680000	0.90	5.83	-0.09	0.18	-0.02	0.01	842478.73	326973315.06
44	Koenigs et al (2003)	TX-U-N-A-5	2.61	6.00	2199343	0.78	6.34	-0.22	0.69	-0.15	0.05	1979716.22	450041298.08
45	Koenigs et al (2003)	TX-U-N-B-6	2.61	6.10	2816706	0.79	6.45	-0.21	0.79	-0.17	0.04	1884880.95	605368663.94
46	Koenigs et al (2003)	TX-U-N-C-7	2.61	11.80	177596	1.07	5.25	0.08	-0.41	-0.03	0.01	265631.24	270842230.70
47	Koenigs et al (2003)	TX-U-N-D-8	2.61	12.00	194694	1.08	5.29	0.09	-0.37	-0.03	0.01	252698.00	312113895.22
48	Diekfuss (2012)	MU-CSR-R-L-A1-1	2.63	6.00	4374464	0.78	6.64	-0.22	0.98	-0.21	0.05	1979716.22	895126161.30
49	Diekfuss (2012)	MU-CSR-R-S-A2-3	2.63	15.37	72660	1.19	4.86	0.19	-0.80	-0.15	0.04	121162.83	242934010.94
50	Rios (2007)	UTX-24-3.0-12-TX-A-13	2.66	12.00	236154	1.08	5.37	0.09	-0.28	-0.02	0.01	252698.00	378578409.25
51	Rios (2007)	UTX-24-3.0-12-TX-B-14	2.66	12.00	327487	1.08	5.52	0.09	-0.14	-0.01	0.01	252698.00	524994315.20
52	Roy et al (2010)	LEH-PB-R-I-SF-CSR-9	2.71	4.00	3050000	0.60	6.48	-0.39	0.83	-0.32	0.15	6600245.33	187198387.96

Table F.8. Continued… Least squares regression analysis for fatigue detail category E2.

53	Diekfuss (2012)	UWM-CSR-M-N-A1-7	2.8	6.50	139000	0.81	5.14	-0.18	-0.51	0.09	0.03	1560868.00	36075384.35
54	Roy et al (2010)	LEH-AB-M-VII-SF-CSR-42	2.85	12.00	40000	1.08	4.60	0.09	-1.05	-0.09	0.01	252698.00	64123988.46
55	Roy et al (2010)	LEH-AB-M-VII-SF-CSR-43	2.85	12.00	40000	1.08	4.60	0.09	-1.05	-0.09	0.01	252698.00	64123988.46
56	Roy et al (2010)	LEH-AB-M-VII-SF-CSR-44	2.85	12.00	10000	1.08	4.00	0.09	-1.66	-0.14	0.01	252698.00	16030997.11
57	Roy et al (2010)	LEH-AB-M-VII-SF-CSR-45	2.85	4.50	1030000	0.65	6.01	-0.34	0.36	-0.12	0.12	4652077.43	89691778.07
58	Roy et al (2010)	LEH-AB-M-VII-SF-CSR-46	2.85	4.50	390000	0.65	5.59	-0.34	-0.07	0.02	0.12	4652077.43	33960964.51
59	Roy et al (2010)	LEH-AB-M-VII-SF-CSR-48	2.85	6.60	90000	0.82	4.95	-0.17	-0.70	0.12	0.03	1491676.45	24441633.00
60	Koenigs et al (2003)	TX-6x3/8-N-A-48	2.86	11.20	783857	1.05	5.89	0.06	0.24	0.01	0.00	310160.73	1023793509.83
61	Koenigs et al (2003)	TX-6x3/8-N-B-49	2.86	11.30	783857	1.05	5.89	0.06	0.24	0.01	0.00	302080.09	1051179974.30
62	Koenigs et al (2003)	TX-6x3/8-N-C-50	2.86	5.76	7503037	0.76	6.88	-0.23	1.22	-0.28	0.05	2234878.75	1360020537.79
63	Rios (2007)	UTX-24-2.0-12-S-A-9	2.87	12.00	143214	1.08	5.16	0.09	-0.50	-0.04	0.01	252698.00	229586322.07
64	Rios (2007)	UTX-24-2.0-12-S-B-10	2.87	12.00	143214	1.08	5.16	0.09	-0.50	-0.04	0.01	252698.00	229586322.07
65	Roy et al (2010)	LEH-PB-M-XII-LS-CSR-78	2.87	12.00	230000	1.08	5.36	0.09	-0.29	-0.03	0.01	252698.00	368712933.63
66	Roy et al (2010)	LEH-PB-M-XII-LS-CSR-79	2.87	12.00	400000	1.08	5.60	0.09	-0.05	0.00	0.01	252698.00	641239884.57
67	Roy et al (2010)	LEH-PB-M-XII-LS-CSR-80	2.87	12.00	580000	1.08	5.76	0.09	0.11	0.01	0.01	252698.00	929797832.63
68	Roy et al (2010)	LEH-PB-M-XII-LS-CSR-83	2.87	7.00	4060000	0.85	6.61	-0.15	0.95	-0.14	0.02	1252517.68	1313120294.50
69	Roy et al (2010)	LEH-PB-M-XII-LS-CSR-85	2.87	16.00	50000	1.20	4.70	0.21	-0.96	-0.20	0.04	107536.97	188353864.30
70	Roy et al (2010)	LEH-PB-M-XII-LS-CSR-86	2.87	16.00	200000	1.20	5.30	0.21	-0.36	-0.07	0.04	107536.97	753415457.21
71	Roy et al (2010)	LEH-PB-M-XII-LS-CSR-87	2.87	16.00	50000	1.20	4.70	0.21	-0.96	-0.20	0.04	107536.97	188353864.30
72	Rios (2007)	UTX-24-3.0-8-S-A-5	2.93	12.00	147550	1.08	5.17	0.09	-0.49	-0.04	0.01	252698.00	236537362.42
73	Rios (2007)	UTX-24-3.0-8-S-B-6	2.93	12.00	147550	1.08	5.17	0.09	-0.49	-0.04	0.01	252698.00	236537362.42

		SCF_{MIN}	**2.24**	**S_{bar}**	**N_{bar}**	**X_{bar}**	**Y_{bar}**	**$\sum(X_i - X_{bar})$**	**$\sum(Y_i - Y_{bar})$**	**$\sum(X_i - X_{bar})*(Y_i - Y_{bar})$**	**$\sum(X_i - X_{bar})^2$**		
		SCF_{MAX}	**2.93**	**10.44**	**1225924.74**	**0.99**	**5.66**	0.00	0.00	-5.07	1.71	**Mean**	6.73E+08
		SCF_{AVG}	**2.57**									**Median**	4.07E+08
n				**b_{hat}**	**a_{hat}**							**Standard Deviation**	1.01E+09
73				**-2.97**	**8.61**							**Coefficient of Variation**	1.49
				A_{hat}	**m_{hat}**								
				4.05E+08	**2.97**								

Table F.9. Least squares regression analysis for fatigue detail category E3.

E3: SCF in 3.0 Range

	Research Group	Specimen Designation	Controlling SCF	Stress Range	Cycles to Failure	X Log S	Y Log N	$X_i - X_{bar}$	$Y_i - Y_{bar}$	$(X_i - X_{bar})*(Y_i - Y_{bar})$	$(X_i - X_{bar})^2$	Least Squares Line $N_{hat} = A_{hat}S^{-mhat}$	Least Squares Line A (m = 2.24)
1	Koenigs et al (2003)	VALN-W-N-A-13	3.08	17.71	422400	1.25	5.63	0.25	0.15	0.04	0.06	82214.24	260719541.45
2	Koenigs et al (2003)	VALN-W-N-B-14	3.08	17.56	422400	1.24	5.63	0.25	0.15	0.04	0.06	83792.52	255808733.05
3	Rios (2007)	UTX-24-1.5-12-S-A-7	3.13	12.00	27977	1.08	4.45	0.08	-1.03	-0.08	0.01	196262.67	7233694.59
4	Rios (2007)	UTX-24-1.5-12-S-B-8	3.13	12.00	27977	1.08	4.45	0.08	-1.03	-0.08	0.01	196262.67	7233694.59
5	Roy et al (2010)	LEH-PB-M-VII-SF-CSR-49	3.32	6.60	90000	0.82	4.95	-0.18	-0.52	0.09	0.03	746910.86	6114633.83
6	Roy et al (2010)	LEH-PB-M-VII-SF-CSR-50	3.32	6.60	100000	0.82	5.00	-0.18	-0.47	0.08	0.03	746910.86	6794037.59
7	Roy et al (2010)	LEH-PB-M-VII-SF-CSR-51	3.32	8.00	1750000	0.90	6.24	-0.10	0.77	-0.07	0.01	485845.02	182783509.88
8	Rios (2007)	UTX-24-2.0-8-S-A-3	3.46	12.00	46772	1.08	4.67	0.08	-0.80	-0.06	0.01	196262.67	12093303.91
9	Rios (2007)	UTX-24-2.0-8-S-B-4	3.46	12.00	46772	1.08	4.67	0.08	-0.80	-0.06	0.01	196262.67	12093303.91
10	Koenigs et al (2003)	VAL-6x3/8-N-A-45 (b)	3.54	11.20	242728	1.05	5.39	0.05	-0.09	0.00	0.00	228992.81	53789158.18
11	Koenigs et al (2003)	VAL-6x3/8-N-B-46	3.54	11.30	653392	1.05	5.82	0.05	0.34	0.02	0.00	224487.26	147699433.66
12	Koenigs et al (2003)	VAL-6x3/8-N-C-47	3.54	5.90	3592372	0.77	6.56	-0.23	1.08	-0.25	0.05	959669.73	189957403.88
13	Koenigs et al (2003)	VALN-6x3/8@45-N-A-51	3.54	11.96	238515	1.08	5.38	0.08	-0.09	-0.01	0.01	197733.10	61211501.53
14	Koenigs et al (2003)	VALN-6x3/8@45-N-B-52	3.54	11.98	161843	1.08	5.21	0.08	-0.26	-0.02	0.01	196995.90	41690149.67
15	Koenigs et al (2003)	VALN-6x3/8@45-N-C-53	3.54	4.30	6066817	0.63	6.78	-0.37	1.31	-0.48	0.13	1946475.85	158164348.13
16	Koenigs et al (2003)	VALN-6x3/8@45-N-D-54	3.54	4.30	6066817	0.63	6.78	-0.37	1.31	-0.48	0.13	1946475.85	158164348.13
17	Koenigs et al (2003)	VAL-3x3/8-N-A-41	3.61	11.70	386253	1.07	5.59	0.07	0.11	0.01	0.00	207691.34	94373531.59
18	Koenigs et al (2003)	VAL-3x3/8-N-B-42	3.61	11.60	410410	1.06	5.61	0.07	0.14	0.01	0.00	211715.28	98369949.03
19	Koenigs et al (2003)	TX-3x3/8-N-A-43	3.73	11.70	473735	1.07	5.68	0.07	0.20	0.01	0.00	207691.34	115748084.77
20	Koenigs et al (2003)	TX-3x3/8-N-B-44	3.73	11.60	657716	1.06	5.82	0.07	0.35	0.02	0.00	211715.28	157645986.69
21	Ocel et al (2006)	MN-MAG-FR3-IP-N-CSR-5-1.25-1-39	3.87	10.38	171695	1.02	5.23	0.02	-0.24	0.00	0.00	271419.51	32100611.25
22	Ocel et al (2006)	MN-MAG-FR3-IP-N-CSR-5-1.25-1-40	3.87	10.33	186036	1.01	5.27	0.02	-0.20	0.00	0.00	274365.23	34408412.52
23	Ocel et al (2006)	MN-MAG-FR3-IP-N-CSR-5-1.25-2-41	3.87	10.38	223987	1.02	5.35	0.02	-0.12	0.00	0.00	271419.51	41877280.13
24	Ocel et al (2006)	MN-MAG-FR3-IP-N-CSR-5-1.25-2-42	3.87	10.33	157123	1.01	5.20	0.02	-0.28	0.00	0.00	274365.23	29060789.31
		SCF_{MIN}	3.08	S_{bar}	N_{bar}	X_{bar}	Y_{bar}	$\sum(X_i - X_{bar})$	$\sum(Y_i - Y_{bar})$	$\sum(X_i - X_{bar})*(Y_i - Y_{bar})$	$\sum(X_i - X_{bar})^2$		
		SCF_{MAX}	3.87	10.56	942655.71	1.00	5.47	0.00	0.00	-1.29	0.58	Mean	9.02E+07
		SCF_{AVG}	3.51									Median	5.75E+07
n				b_{hat}	a_{hat}							Standard Deviation	8.07E+07
24				-2.24	7.71							Coefficient of Variation	0.89
				A_{hat}	m_{hat}								
				5.07E+07	2.24								

Table F.10. Least squares regression analysis for fatigue detail category E4.

E4: SCF in 4.0 Range

	Research Group	Specimen Designation	Controlling SCF	Stress Range	Cycles to Failure	X Log S	Y Log N	$X_i - X_{bar}$	$Y_i - Y_{bar}$	$(X_i - X_{bar})*(Y_i - Y_{bar})$	$(X_i - X_{bar})^2$	Least Squares Line $N_{hat} = A_{hat}S^{-mhat}$	A (m = 1.04)
1	Ocel et al (2006)	MN-MA-FR3-IP-N-CSR-5-1.25-1-30	4.25	15.37	420785	1.19	5.62	0.19	0.13	0.02	0.04	198549.87	7223055.58
2	Ocel et al (2006)	MN-MA-FR3-IP-N-CSR-5-1.25-1-31	4.25	15.37	434329	1.19	5.64	0.19	0.14	0.03	0.04	198549.87	7455547.39
3	Ocel et al (2006)	MN-MA-FR3-IP-N-CSR-5-1.25-1-32	4.25	15.37	242060	1.19	5.38	0.19	-0.11	-0.02	0.04	198549.87	4155121.58
4	Ocel et al (2006)	MN-MA-FR3-IP-N-CSR-5-1.25-2-33	4.25	15.37	420662	1.19	5.62	0.19	0.13	0.02	0.04	198549.87	7220944.20
5	Ocel et al (2006)	MN-MA-FR3-IP-N-CSR-5-1.25-2-34	4.25	15.37	372056	1.19	5.57	0.19	0.07	0.01	0.04	198549.87	6386589.75
6	Ocel et al (2006)	MN-MA-FR3-IP-N-CSR-5-1.25-2-35	4.25	15.37	298023	1.19	5.47	0.19	-0.02	0.00	0.04	198549.87	5115763.85
7	Ocel et al (2006)	MN-MA-FR3-IP-N-CSR-5-1.25-2-36	4.25	15.37	267922	1.19	5.43	0.19	-0.07	-0.01	0.04	198549.87	4599060.08
8	Rios (2007)	UTX-24-1.5-8-S-A-1	4.28	12.00	13193	1.08	4.12	0.08	-1.38	-0.12	0.01	256867.42	175051.10
9	Rios (2007)	UTX-24-1.5-8-S-B-2	4.28	12.00	13193	1.08	4.12	0.08	-1.38	-0.12	0.01	256867.42	175051.10
10	Koenigs et al (2003)	VAL-3x1/4-N-A-35	4.51	11.10	476269	1.05	5.68	0.05	0.18	0.01	0.00	278571.35	5827015.47
11	Koenigs et al (2003)	VAL-3x1/4-N-B-36	4.51	11.40	696326	1.06	5.84	0.06	0.34	0.02	0.00	270948.18	8759043.62
12	Koenigs et al (2003)	VAL-3x1/4-N-C-37	4.51	6.10	3592372	0.79	6.56	-0.21	1.06	-0.22	0.04	519329.78	23575905.71
13	Ocel et al (2006)	MN-P-FR1-IP-N-CSR-5-1.25-1	4.58	8.25	83806	0.92	4.92	-0.08	-0.57	0.04	0.01	379329.58	752989.15
14	Ocel et al (2006)	MN-P-FR1-IP-N-CSR-5-1.25-2	4.58	3.43	981490	0.54	5.99	-0.46	0.49	-0.23	0.21	945344.09	3538557.67
15	Ocel et al (2006)	MN-P-FR1-IP-N-CSR-5-1.25-3	4.58	3.80	610124	0.58	5.79	-0.41	0.29	-0.12	0.17	849769.95	2447073.72
16	Ocel et al (2006)	MN-P-FR1-OP-N-CSR-5-1.25-5	4.58	5.41	170606	0.73	5.23	-0.26	-0.27	0.07	0.07	588415.28	988190.49
17	Ocel et al (2006)	MN-P-FR1-OP-N-CSR-5-1.25-7	4.58	5.41	301484	0.73	5.48	-0.26	-0.02	0.00	0.07	588415.28	1746266.97
18	Ocel et al (2006)	MN-P-FR1-OP-N-CSR-5-1.25-8	4.58	5.41	2293739	0.73	6.36	-0.26	0.86	-0.23	0.07	588415.28	13285881.36
19	Ocel et al (2006)	MN-P-FR2-IP-N-CSR-5-1.25-9	4.58	4.26	591696	0.63	5.77	-0.37	0.27	-0.10	0.13	754516.22	2672762.46
20	Ocel et al (2006)	MN-P-FR2-IP-N-CSR-5-1.25-10	4.58	3.65	868266	0.56	5.94	-0.43	0.44	-0.19	0.19	886133.98	3339517.44
21	Ocel et al (2006)	MN-P-FR2-IP-N-CSR-5-1.25-11	4.58	4.10	1658906	0.61	6.22	-0.38	0.72	-0.28	0.15	785175.32	7200877.97
22	Ocel et al (2006)	MN-P-FR2-IP-N-CSR-5-2.50-2-21	4.58	14.90	81924	1.17	4.91	0.18	-0.58	-0.10	0.03	205070.23	1361566.46
23	Ocel et al (2006)	MN-P-FR2-IP-N-CSR-5-2.50-1-23	4.58	14.90	566119	1.17	5.75	0.18	0.26	0.05	0.03	205070.23	9408825.75
24	Ocel et al (2006)	MN-P-FR2-IP-N-CSR-5-2.50-2-24	4.58	14.90	101916	1.17	5.01	0.18	-0.49	-0.09	0.03	205070.23	1693830.95
25	Ocel et al (2006)	MN-P-FR2-IP-N-CSR-3-2.50-1-25	4.58	15.00	330137	1.18	5.52	0.18	0.02	0.00	0.03	203648.00	5525153.63
26	Ocel et al (2006)	MN-P-FR2-IP-N-CSR-3-2.50-2-26	4.58	15.00	140545	1.18	5.15	0.18	-0.35	-0.06	0.03	203648.00	2352152.94
27	Ocel et al (2006)	MN-P-FR2-IP-N-CSR-3-2.50-1-27	4.58	15.00	183638	1.18	5.26	0.18	-0.23	-0.04	0.03	203648.00	3073354.89
28	Ocel et al (2006)	MN-P-FR2-IP-N-CSR-3-2.50-2-28	4.58	15.00	86888	1.18	4.94	0.18	-0.56	-0.10	0.03	203648.00	1454152.51
29	Koenigs et al (2003)	TX-3x1/4-N-A-38	4.66	11.70	616136	1.07	5.79	0.07	0.29	0.02	0.01	263723.63	7962654.20
30	Koenigs et al (2003)	TX-3x1/4-N-B-39	4.66	11.80	416146	1.07	5.62	0.08	0.12	0.01	0.01	261398.70	5425910.25
31	Koenigs et al (2003)	TX-3x1/4-N-C-LMS-40	4.66	11.90	523397	1.08	5.72	0.08	0.22	0.02	0.01	259113.64	6884482.00

		SCF_{MIN}	4.25	S_{bar}	N_{bar}	X_{bar}	Y_{bar}	$\sum(X_i - X_{bar})$	$\sum(Y_i - Y_{bar})$	$\sum(X_i - X_{bar})*(Y_i - Y_{bar})$	$\sum(X_i - X_{bar})^2$		
		SCF_{MAX}	4.66	11.10	575940.42	0.99	5.50	0.00	0.00	-1.69	1.63	Mean	5.22E+06
		SCF_{AVG}	4.49									Median	4.60E+06
n				b_{hat}	a_{hat}							Standard Deviation	4.61E+06
31				-1.04	6.53							Coefficient of Variation	0.88
				A_{hat}	m_{hat}								
				3.41E+06	1.04								

Table G.1. Discretized segments with dimensions and section properties for mast-arm of Milwaukee structure.

Mast-Arm Dimensions for Milwaukee Models										
10 SegmentsTotal including Connection Section	L_{seg} (in)	t_{wall} (in)	D_o (in)	D_i (in)	I (in^4)	Cross-Area (in^2)	Bluff Area (in^2)	Volume (in^3)	Corresponding Element #'s in Low-Fidelity Model For Reference During Simulations	
(Connection Section) MA0	16.06	0.1875	11.00	10.63	93.10	6.37	-	-	22,23,24,25	
MA1	42.25	0.1793	10.55	10.19	78.59	5.84	445.80	246.84	20,21	
MA2	42.25	0.1793	10.05	9.69	67.69	5.56	424.52	234.86	18,19	
MA3	42.25	0.1793	9.54	9.19	57.85	5.28	403.23	222.87	16,17	
MA4	42.25	0.1793	9.04	8.68	49.00	4.99	381.94	210.87	14,15	
MA5	54.00	0.1793	8.47	8.11	40.09	4.67	3888.00	252.08	10,11,12,13	
MA6	45.00	0.1793	7.88	7.52	32.12	4.34	354.43	195.10	8,9	
MA7	45.00	0.1793	7.61	7.25	28.88	4.18	342.35	188.30	6,7	
MA8	54.00	0.1793	6.75	6.39	19.99	3.70	3888.00	199.85	2,3,4,5	
(Free End of Mast Arm) MA9	4.00	0.1793	6.40	6.05	16.99	3.51	25.61	14.02	1	
Totals for Verification of Results:										
Total Mast-Arm Length:	387.06 in	Total Bluff Area:		10153.88 in^2	Total Volume of Mast-Arm:		1764.80 in^3	Mass of Mast-Arm:	1.307e-3 kip-s^2 / in	
Average Moment of Inertia:	47.14 in^4			70.51 ft^2	Density of Steel (ρ_{st}):		7.405e-7 kip-s^2 / in^4	Weight of Mast-Arm:	0.50 kip	
Approximate Dead Load Moment at Section 10" from Weld-Toe: 92.8 kip-in => σ_{10} = 5.45 ksi										

Table G.2. Discretized segments with dimensions and section properties for mast-arm of Osseo structure.

Mast-Arm Dimensions for Osseo Models									
8 Segments Total Including Connection Section	**L_{seg} (in)**	**t_{wall} (in)**	**D_o (in)**	**D_i (in)**	**I (in^4)**	**Cross-Area (in^2)**	**Bluff Area (in^2)**	**Volume (in^3)**	**Corresponding Element #'s in Low-Fidelity Model For Reference During Simulations**
(Connection Section) MA0	37.09	0.3310	12.76	12.10	249.75	12.92	-	-	21,22,23,24
MA1	178.96	0.3310	12.76	12.10	249.75	12.92	2283.53	2312.97	16,17,18,19,20
MA2	24.00	0.3310	12.76	12.10	249.75	12.92	720.00	310.19	14,15
MA3	147.00	0.3310	12.76	12.10	249.75	12.92	1875.72	1899.90	10,11,12,13
MA4	24.00	0.3310	12.76	12.10	249.75	12.92	720.00	310.19	8,9
MA5	86.16	0.3310	12.76	12.10	249.75	12.92	1099.40	1113.58	5,6,7
MA6	24.00	0.3310	12.76	12.10	249.75	12.92	720.00	310.19	3,4
(Free End of Mast-Arm) MA7	21.64	0.3310	12.76	12.10	249.75	12.92	276.13	279.69	1,2
Totals for Verification of Results:									
Mast-Arm Length (L):	**542.85 in**	**Total Bluff Area (A):**		**7694.78 in^2**	**Volume of Mast-Arm (V_{ma}):**		**6536.70 in^3**	**Mass of Mast-Arm:**	**4.840e-3 kip-s^2 / in**
Average Moment of Inertia (I):	**249.75 in^4**			**53.44 ft^2**	**Density of Steel (ρ_{st}):**		**7.405e-7 kip-s^2 / in^4**	**Weight of Mast-Arm:**	**1.85 kip**
Approximate Dead Load Moment at Section 10" from Weld-Toe: 467.8 kip-in => σ_{10} = 11.95 ksi									

Table G.3. Summary of information used to develop high-fidelity FE model within ANSYS 14.0 for Milwaukee structure: S-40-703.

Sign Support Structure: S-40-703

High-Fidelity FE Model Information		
Elements		
Number of Element Types:	**6**	
Elements Used:	**MESH200, SOLID185, BEAM188, PRETS179, TARGE170, CONTA174**	
		No. of Elements:
Element Type 1:	**MESH200**	**15,973 (1)**
Element Type 2:	**SOLID185**	**237,734**
Element Type 3:	**BEAM188**	**19**
Element Type 4:	**PRETS179**	**555**
Element Type 5:	**TARGE170**	**6,285**
Element Type 6:	**CONTA174**	**3,285**
Total No. of Elements:		**247,878**
Material Properties		
Number of Material Models:	**1**	
Material Model Number:	**1**	
Young's Modulus:	**29,500 ksi**	
Poisson's Ratio:	**0.3**	
Density:	**7.405e-7 kip-s^2 / in^4**	
Friction Coefficient:	**0.3**	

NOTES:

(1) MESH200 elements were cleared after base areas were extruded into volumes.

Table G.4. Summary of information used to develop high-fidelity FE model within ANSYS 14.0 for Osseo structures: S-61-0001 and S-61-0002.

Sign Support Structures: S-61-001 and S-61-002

High-Fidelity FE Model Information		
Elements		
Number of Element Types:	**6**	
Elements Used:	**MESH200, SOLID185, BEAM188, PRETS179, TARGE170, CONTA174**	
		No. of Elements:
Element Type 1:	**MESH200**	**31,864 (1)**
Element Type 2:	**SOLID185**	**436,356**
Element Type 3:	**BEAM188**	**44**
Element Type 4:	**PRETS179**	**1,827**
Element Type 5:	**TARGE170**	**7,341**
Element Type 6:	**CONTA174**	**6,621**
Total No. of Elements:		**452,189**
Material Properties		
Number of Material Models:	**1**	
Material Model Number:	**1**	
Young's Modulus:	**29,500 ksi**	
Poisson's Ratio:	**0.3**	
Density:	**7.405e-7 kip-s^2 / in^4**	
Friction Coefficient:	**0.3**	

NOTES:

(1) MESH200 elements were cleared after base areas were extruded into volumes.

Table G.5. Summary of information used to develop low-fidelity FE model within ANSYS 14.0 for Milwaukee structure: S-40-703.

Sign Support Structure: S-40-703

Low-Fidelity FE Model Information		
Elements		
Number of Element Types:	**1**	
Elements Used:	**BEAM188**	
		No. of Elements:
Element Type 1:	**BEAM188**	**37**
Total No. of Elements:		**37**
Material Properties		
Number of Material Models:	**1**	
Material Model Number:	**1**	
Young's Modulus:	**29,500 ksi**	
Poisson's Ratio:	**0.3**	
Density:	**7.405e-7 kip-s^2 / in^4**	
Friction Coefficient:	**N/A**	

Table G.6. Summary of information used to develop low-fidelity FE model within ANSYS 14.0 for Osseo structures: S-61-0001 and S-61-0002.

Sign Support Structures: S-61-001 and S-61-002

Low-Fidelity FE Model Information		
Elements		
Number of Element Types:	**1**	
Elements Used:	**BEAM188**	
		No. of Elements:
Element Type 1:	**BEAM188**	**31**
Total No. of Elements:		**31**
Material Properties		
Number of Material Models:	**1**	
Material Model Number:	**1**	
Young's Modulus:	**29,500 ksi**	
Poisson's Ratio:	**0.3**	
Density:	**7.405e-7 kip-s^2 / in^4**	
Friction Coefficient:	**N/A**	

APPENDIX H – MATLAB CODE USED TO SIMULATE WIND SPEED

H.1 – WindHistory.m

```
% WindHistory(U2,Z) is a program that simulates natural wind using the
% Kaimal (1972) spectrum. This program requires the user to specify U2
% and Z. U2 is the desired mean wind speed for the simulation and
% should be entered in [mph]. Z is the elevation at which the
% simulation will be determined and should be specified in [ft]. The
% reference elevation used in the power law below is set at 33 ft
% (which is typical).


function [Ut_tot_mph,matrix,Sf,f] = WindHistory(U2,Z)

rng('shuffle');  % Set random number seed to shuffle in order to obtain
                 % a distinct random number for every single run

T      = 3600.00;     % Duration of the simulation, [sec]
dt     = 0.25;        % Time increment for the simulation, [sec]
fLow   = 0.01;        % Lower frequency in spectrum, [Hz]
fHigh  = 10.0;        % Higher frequency in spectrum, [Hz]
df     = 0.001;       % Increment in frequency, [Hz]

alpha  = 7.0;      % Constant for Power Law Exponent

K      = 0.0251;  % Surface drag coefficient. Generally ranges from
                  % K = 0.0030 for open coastline exposure
                  %   = 0.0050 for open terrain exposure
                  %   = 0.0150 for urban and suburban exposure
                  %   = 0.0251 for large city exposure

Z1 = 33.0;                  % Conventional reference height, [ft]
U1 = (5280.0/3600.0)*U2;    % Steady (mean) wind speed at a reference
                            % height - Z1, [ft/sec]

sig_usq = 6*K*(U1^2.0);     % Variance in turbulent wind component

Uz = U1*((Z/Z1)^(1/alpha));        % Steady (mean) wind speed at a
                                   % height - Z, [ft/sec]

UStar = ((sig_usq/6)^0.5);         % Friction (or shear) velocity,
                                     [ft/sec]

f = linspace(fLow,fHigh,10000);    % Array of frequency values (1xn)

numerator = 200.0*(UStar^2.0)*Z;  % Numerator of Kaimal (1972) Spectrum

% Compute Kaimal (1972) Spectrum

     for i=1:length(f)
```

```
          denominator(i) = Uz*((1.0+((50.0*f(i)*Z)/Uz))^(5.0/3.0));
          Sf(i) = numerator/denominator(i);
          i = i + 1;
      end

% Create a simulated record of turbulent wind speed vs. time

t = 0.0;
phase = rand(1,length(Sf));

      for k=1:(T/dt)
          for j=1:length(Sf)
              phik(j) = 2*pi*phase(j);
              ut(j) = ((2.0*Sf(j)*df)^0.5)*cos(2*pi*f(j)*t + phik(j));
              j = j+1;
          end
          utsum(k) = sum(ut(:));
          t = t + dt;
          k = k + 1.0;
      end

% Add the mean wind speed to the turbulent wind speed

      for n=1:(T/dt)
          Ut(n) = utsum(n) + Uz;
      end

Ut_tot  = transpose(Ut);          % Total wind speed magnitude both mean
                                  % and turbulent components [ft/sec]

Ut_tot_mph = Ut_tot*3600/5280;    % Total wind speed magnitude both mean
                                  % and turbulent components [mph]

timeref = (dt:dt:T);
time    = transpose(timeref);

% Create a matrix suitable for input into Tom Irvine's PSD.m (a program
% that determines the power spectral density of the wind simulation)

      for x=1:T/dt
          matrix(x,1) = time(x,1);
          matrix(x,2) = Ut_tot(x,1);
          x = x + 1;
      end
```

APPENDIX I – APDL CODE FOR FE SIMULATION PROCEDURE

I.1 – MKE_Input_File.txt

```
  /batch
  resume
  /config,norstgm,1
  /config,noeldw,1
  /config,nres,20000
!
! FINISH CURRENT PROCESSOR
!
  FINISH
!
! ENTER THE PREPROCESSOR
!
  /PREP7
!
! SET THE TIME AT THE END OF THE ZERO LOADING EQUAL TO 1.0 SECONDS.
!
  TIME,1.0
!
! ENTER THE SOLUTION PROCESSOR
!
  /SOLU
!
! SET THE ANALYSIS OPTIONS
!
  ANTYPE,4
! TRANSIENT ANALYSIS
!
  TRNOPT,FULL
! TRNOPT SPECIFIED TRANSIENT ANALYSIS OPTIONS, FULL METHOD (DEFAULT)
!
  LUMPM,1
! LUMPED MASS MATRIX FORMULATION
!
  DELTIM,0.25,0,0
! DELTIM SPECIFIES TIMESTEP SIZES TO BE USED FOR THIS LOAD STEP
! 0.25,0,0 = STEPSIZE,MIN_SIZE,MAX_SIZE
!
! SET THE MASS AND STIFFNESS MATRIX MULTIPLIERS TO REFLECT
! DAMPING OF THE SYSTEM CONSISTENT WITH THE INHERENT STRUCTURAL DAMPING
! (0.006) PLUS THE AERODYNAMIC DAMPING FOR A 5.23 MPH MEAN WIND SPEED
! (0.009163) FOR A TARGET DAMPING RATIO EQUAL TO 0.01516
!
  ALPHAD,0.1596988
  BETAD,0.0014371
!
! SET THE SOLUTION AND LOADING OPTIONS
!
  EQSLV,SPAR
! EQUATION SOLVER, SPARSE SOVLER
!
```

```
  KBC,0
! KBC SPECIFIES STEPPED OR RAMPED LOADING WITHIN A LOAD STEP
! 0 MEANS LINEARLY INTERPOLATED (RAMPED) FOR EACH SUBSTEP
!
  CM,EOUT,ELEM
  ESEL,ALL
!
! SET THE OUTPUT OPTIONS
!
  OUTPR,ALL,NONE
  OUTRES,ALL,NONE
!
  OUTPR,ESOL,ALL,EOUT
  OUTRES,ESOL,ALL,EOUT
!
! SOLVE THE CURRENT LOAD STEP WHICH CONTAINS NO LOADING TO OBTAIN ZERO
! REFERENCE VALUES
!
  SOLVE
!
! SET THE TIME AT THE END OF THE GRAVITY LOADING EQUAL TO 2.0 SECONDS.
!
  TIME,2.0
!
! APPLY THE ACCELERATION DUE TO GRAVITY TO THE MODEL IN THE POSITIVE Y-
! DIRECTION.
!
  ACEL,0,386.4,0
!
! SOLVE THE CURRENT LOAD STEP.
!
  SOLVE
!
! SET UP A LOOP THAT SOLVES THE GRAVITY LOAD ANALYSIS FOR 90 SECONDS
! ONE SECOND AT A TIME.
!
! THIS WILL CREATE 90 LOAD STEPS EACH CONTAINING 4 SUBSTEPS.
!
  *DO,TM,3,90,1
      TIME,TM
      SOLVE
  *ENDDO
!
!
! GRAVITY LOADING APPLICATION IS NOW COMPLETE
!
! SET UP TIME VS. WIND LINE LOADING TABLES FOR EACH SECTION FOR LATER
! ACCESS.
!
! THERE WILL BE A TOTAL OF 9 TABLES CREATED BECAUSE THE MAST ARM WAS
! BROKEN INTO 9 DIFFERENT SECTIONS.
!
! EACH TABLE WILL CONTAIN 2 COLUMNS AND 14401 ROWS. THE FIRST COLUMN
! CONTAINS THE TIME VALUES 0.00 SECONDS THROUGH 3600.00 SECONDS IN
! INCREMENTS OF 0.25 SECONDS.
!
! THE SECOND COLUMN CONTAINS THE WIND PRESSURE LINE LOADING IN [KIP/IN]
```

```
! THAT CORRESPONDS TO THE PARTICULAR SECTION OF INTEREST (e.g. MA1,
! MA2, etc.)
!
! THESE TABLES ARE FILLED WITH DATA SAVED IN FILES CALLED
! MA(xx)_XXmphWindPress.txt
!
!
  *DIM,MA1PRESS,TABLE,14401,1,1,TIME,PRESSURE
  *TREAD,MA1PRESS,MA1_5mphWindPress,txt,,

  *DIM,MA2PRESS,TABLE,14401,1,1,TIME,PRESSURE
  *TREAD,MA2PRESS,MA2_5mphWindPress,txt,,

  *DIM,MA3PRESS,TABLE,14401,1,1,TIME,PRESSURE
  *TREAD,MA3PRESS,MA3_5mphWindPress,txt,,

  *DIM,MA4PRESS,TABLE,14401,1,1,TIME,PRESSURE
  *TREAD,MA4PRESS,MA4_5mphWindPress,txt,,

  *DIM,MA5PRESS,TABLE,14401,1,1,TIME,PRESSURE
  *TREAD,MA5PRESS,MA5_5mphWindPress,txt,,

  *DIM,MA6PRESS,TABLE,14401,1,1,TIME,PRESSURE
  *TREAD,MA6PRESS,MA6_5mphWindPress,txt,,

  *DIM,MA7PRESS,TABLE,14401,1,1,TIME,PRESSURE
  *TREAD,MA7PRESS,MA7_5mphWindPress,txt,,

  *DIM,MA8PRESS,TABLE,14401,1,1,TIME,PRESSURE
  *TREAD,MA8PRESS,MA8_5mphWindPress,txt,,

  *DIM,MA9PRESS,TABLE,14401,1,1,TIME,PRESSURE
  *TREAD,MA9PRESS,MA9_5mphWindPress,txt,,
!
!
! SET UP AN ELEMENT REFERENCE TABLE. THE DATA FOR THIS TABLE IS LOCATED
! IN A FILE CALLED elms.txt.
!
!
  *DIM,ELEMS,TABLE,21,2,1,REF
  *TREAD,ELEMS,elms,txt,,
!
!
  TM = 90.25
  *DO,WTM,0.25,3600.00,0.25
      TIME,(TM + WTM)
      *DO,REF,1,2,1
          ELMNUM = ELEMS(REF,1)
          SURF = ELEMS(REF,2)
          SFBEAM,ELMNUM,SURF,PRES,MA1PRESS(WTM,1)
      *ENDDO
      *DO,REF,3,4,1
          ELMNUM = ELEMS(REF,1)
          SURF = ELEMS(REF,2)
          SFBEAM,ELMNUM,SURF,PRES,MA2PRESS(WTM,1)
      *ENDDO
      *DO,REF,5,6,1
```

```
          ELMNUM = ELEMS(REF,1)
          SURF = ELEMS(REF,2)
          SFBEAM,ELMNUM,SURF,PRES,MA3PRESS(WTM,1)
      *ENDDO
      *DO,REF,7,8,1
          ELMNUM = ELEMS(REF,1)
          SURF = ELEMS(REF,2)
          SFBEAM,ELMNUM,SURF,PRES,MA4PRESS(WTM,1)
      *ENDDO
      *DO,REF,9,12,1
          ELMNUM = ELEMS(REF,1)
          SURF = ELEMS(REF,2)
          SFBEAM,ELMNUM,SURF,PRES,MA5PRESS(WTM,1)
      *ENDDO
      *DO,REF,13,14,1
          ELMNUM = ELEMS(REF,1)
          SURF = ELEMS(REF,2)
          SFBEAM,ELMNUM,SURF,PRES,MA6PRESS(WTM,1)
      *ENDDO
      *DO,REF,15,16,1
          ELMNUM = ELEMS(REF,1)
          SURF = ELEMS(REF,2)
          SFBEAM,ELMNUM,SURF,PRES,MA7PRESS(WTM,1)
      *ENDDO
      *DO,REF,17,20,1
          ELMNUM = ELEMS(REF,1)
          SURF = ELEMS(REF,2)
          SFBEAM,ELMNUM,SURF,PRES,MA8PRESS(WTM,1)
      *ENDDO
      *DO,REF,21,21,1
          ELMNUM = ELEMS(REF,1)
          SURF = ELEMS(REF,2)
          SFBEAM,ELMNUM,SURF,PRES,MA9PRESS(WTM,1)
      *ENDDO
      SOLVE
  *ENDDO
  TM = TM + WTM
!
!
! FINISH THE SOLUTION PROCESSOR.
!
  FINISH

  /POST1
!
!
  ESEL,ALL
  *DIM,MOMTMP,TABLE,1,5,((TM) / 0.25)
  *SET,MSKV
  *DIM,MSKV,,1
!
! SELECT ONLY THE "WANTED" ELEMENTS FOR POSTPROCESSING AND CREATE A
! MASKING VECTOR
!
  ESEL,ELEM,23
!
!
```

```
! CONSTRUCT THE ETABLE FOR EACH 0.25 SEC AND FILL EACH PLANE WITH THE
! RESULTS FROM EACH SUBSTEP OF THE SOLUTION.
!
!
  *CFOPEN,MKE_results,txt,,APPEND
  PLANE = 1
  *DO,TMRES,0.25,TM,0.25
       SET,,,,,TMRES
       ETABLE,MYI,SMISC,2
       ETABLE,MYJ,SMISC,15
       ETABLE,MZI,SMISC,3
       ETABLE,MZJ,SMISC,16
       *VFILL,MOMTMP(1,1,PLANE),RAMP,1,1
       *VGET,MOMTMP(1,2,PLANE),ELEM,23,ETAB,MYI
       *VGET,MOMTMP(1,3,PLANE),ELEM,23,ETAB,MYJ
       *VGET,MOMTMP(1,4,PLANE),ELEM,23,ETAB,MZI
       *VGET,MOMTMP(1,5,PLANE),ELEM,23,ETAB,MZJ

*VWRITE,TMRES,MOMTMP(1,2,PLANE),MOMTMP(1,3,PLANE),MOMTMP(1,4,PLANE),
        MOMTMP(1,5,PLANE)
       (f7.2,' ',f10.3,' ',f10.3,' ',f10.3,' ',f10.3)
       PLANE = PLANE + 1
  *ENDDO

  FINISH

!
! CLOSE THE ABOVE FILE.
!
  *CFCLOS
```

Table J.1. Time history simulations of wind pressure for various discretized mast-arm segments of Milwaukee structure (note: this is an example table illustrating the 5.23 mph mean wind speed magnitude).

			MA1	MA2	MA3	MA4	MA5 - Sign Location	MA6	MA7	MA8 - Sign Location	MA9
Target Mean Wind Speed (mph)		D (in.)	10.55	10.05	9.54	9.04	72.00	7.88	7.61	72.00	6.40
		D (ft)	0.88	0.84	0.80	0.75	6.00	0.66	0.63	6.00	0.53
5.23		C_d	1.10	1.10	1.10	1.10	1.19	1.10	1.10	1.19	1.10
Simulated Wind Speed (mph)	Simulated Wind Speed (ft/sec)	Time (sec.)	Line Loading (kip/in.)	Line Loading (kip/in.)	Line Loading (kip/in.)	Line Loading (kip/in.)	Line Loading (kip/in.)	Line Loading (kip/in.)	Line Loading (kip/in.)	Line Loading (kip/in.)	Line Loading (kip/in.)
0.00	0.00	0.00	0.00000000	0.00000000	0.00000000	0.00000000	0.00000000	0.00000000	0.00000000	0.00000000	0.00000000
6.88	10.09	0.25	0.00000976	0.00000930	0.00000883	0.00000836	0.00007206	0.00000729	0.00000704	0.00007206	0.00000592
5.79	8.49	0.50	0.00000691	0.00000658	0.00000625	0.00000592	0.00005102	0.00000516	0.00000498	0.00005102	0.00000419
6.21	9.11	0.75	0.00000795	0.00000757	0.00000719	0.00000681	0.00005867	0.00000593	0.00000573	0.00005867	0.00000482
7.70	11.29	1.00	0.00001222	0.00001163	0.00001105	0.00001047	0.00009019	0.00000912	0.00000881	0.00009019	0.00000741
7.92	11.62	1.25	0.00001294	0.00001232	0.00001171	0.00001109	0.00009553	0.00000966	0.00000933	0.00009553	0.00000785
7.36	10.80	1.50	0.00001118	0.00001065	0.00001011	0.00000958	0.00008254	0.00000835	0.00000806	0.00008254	0.00000679
6.93	10.16	1.75	0.00000990	0.00000942	0.00000895	0.00000848	0.00007306	0.00000739	0.00000714	0.00007306	0.00000601
6.88	10.10	2.00	0.00000977	0.00000930	0.00000883	0.00000837	0.00007210	0.00000729	0.00000704	0.00007210	0.00000593
7.09	10.39	2.25	0.00001035	0.00000986	0.00000936	0.00000887	0.00007641	0.00000773	0.00000746	0.00007641	0.00000628
7.84	11.49	2.50	0.00001266	0.00001206	0.00001145	0.00001085	0.00009346	0.00000945	0.00000913	0.00009346	0.00000768
			•	•	•	•	•	•	•	•	•
4.68	6.86	3597.00	0.00000451	0.00000430	0.00000408	0.00000387	0.00003332	0.00000337	0.00000325	0.00003332	0.00000274
5.20	7.62	3597.25	0.00000557	0.00000530	0.00000504	0.00000477	0.00004110	0.00000416	0.00000401	0.00004110	0.00000338
5.23	7.67	3597.50	0.00000564	0.00000537	0.00000510	0.00000483	0.00004160	0.00000421	0.00000406	0.00004160	0.00000342
4.95	7.25	3597.75	0.00000504	0.00000480	0.00000456	0.00000432	0.00003722	0.00000376	0.00000364	0.00003722	0.00000306
4.43	6.50	3598.00	0.00000405	0.00000386	0.00000367	0.00000347	0.00002993	0.00000303	0.00000292	0.00002993	0.00000246
3.45	5.06	3598.25	0.00000246	0.00000234	0.00000222	0.00000211	0.00001814	0.00000183	0.00000177	0.00001814	0.00000149
3.94	5.77	3598.50	0.00000320	0.00000304	0.00000289	0.00000274	0.00002359	0.00000239	0.00000230	0.00002359	0.00000194
4.09	6.00	3598.75	0.00000345	0.00000328	0.00000312	0.00000296	0.00002547	0.00000258	0.00000249	0.00002547	0.00000209
4.10	6.02	3599.00	0.00000347	0.00000330	0.00000314	0.00000297	0.00002562	0.00000259	0.00000250	0.00002562	0.00000211
5.04	7.40	3599.25	0.00000524	0.00000499	0.00000474	0.00000449	0.00003869	0.00000391	0.00000378	0.00003869	0.00000318
4.38	6.42	3599.50	0.00000395	0.00000376	0.00000357	0.00000338	0.00002913	0.00000295	0.00000285	0.00002913	0.00000240
4.35	6.39	3599.75	0.00000391	0.00000372	0.00000353	0.00000335	0.00002884	0.00000292	0.00000282	0.00002884	0.00000237
3.33	4.88	3600.00	0.00000228	0.00000217	0.00000206	0.00000195	0.00001684	0.00000170	0.00000164	0.00001684	0.00000138